frontiers | Research Topics

Cellular and molecular targets in epileptogenesis focusing on disease prevention

Edited by
Diana Cunha-Reis, Sandra Henriques Vaz
and Paulo Correia-de-Sá

Published in
Frontiers in Cellular Neuroscience
Frontiers in Neurology
Frontiers in Neuroscience
Frontiers in Aging Neuroscience

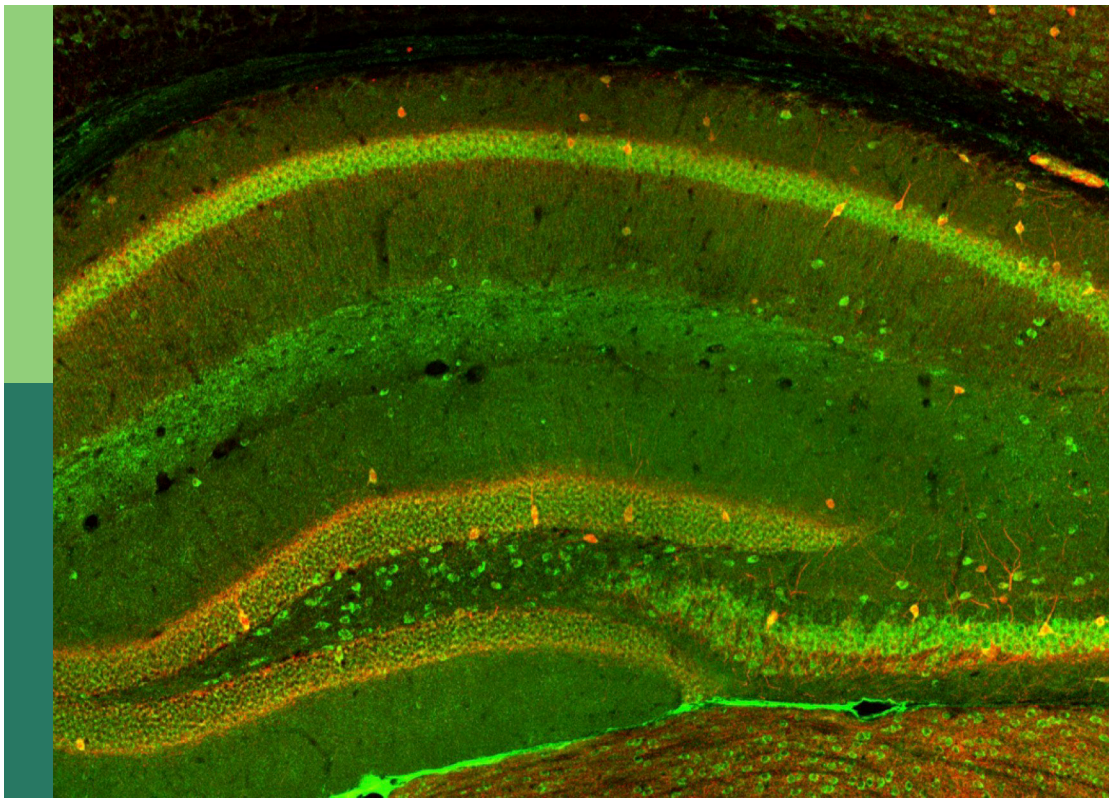

ISSN 1664-8714
ISBN 978-2-8325-3097-9
DOI 10.3389/978-2-8325-3097-9

About Frontiers

Frontiers is more than just an open access publisher of scholarly articles: it is a pioneering approach to the world of academia, radically improving the way scholarly research is managed. The grand vision of Frontiers is a world where all people have an equal opportunity to seek, share and generate knowledge. Frontiers provides immediate and permanent online open access to all its publications, but this alone is not enough to realize our grand goals.

Frontiers journal series

The Frontiers journal series is a multi-tier and interdisciplinary set of open-access, online journals, promising a paradigm shift from the current review, selection and dissemination processes in academic publishing. All Frontiers journals are driven by researchers for researchers; therefore, they constitute a service to the scholarly community. At the same time, the *Frontiers journal series* operates on a revolutionary invention, the tiered publishing system, initially addressing specific communities of scholars, and gradually climbing up to broader public understanding, thus serving the interests of the lay society, too.

Dedication to quality

Each Frontiers article is a landmark of the highest quality, thanks to genuinely collaborative interactions between authors and review editors, who include some of the world's best academicians. Research must be certified by peers before entering a stream of knowledge that may eventually reach the public - and shape society; therefore, Frontiers only applies the most rigorous and unbiased reviews. Frontiers revolutionizes research publishing by freely delivering the most outstanding research, evaluated with no bias from both the academic and social point of view. By applying the most advanced information technologies, Frontiers is catapulting scholarly publishing into a new generation.

What are Frontiers Research Topics?

Frontiers Research Topics are very popular trademarks of the *Frontiers journals series*: they are collections of at least ten articles, all centered on a particular subject. With their unique mix of varied contributions from Original Research to Review Articles, Frontiers Research Topics unify the most influential researchers, the latest key findings and historical advances in a hot research area.

Find out more on how to host your own Frontiers Research Topic or contribute to one as an author by contacting the Frontiers editorial office: frontiersin.org/about/contact

Cellular and molecular targets in epileptogenesis focusing on disease prevention

Topic editors

Diana Cunha-Reis — University of Lisbon, Portugal

Sandra Henriques Vaz — Universidade de Lisboa, Portugal

Paulo Correia-de-Sá — University of Porto, Portugal

Citation

Cunha-Reis, D., Vaz, S. H., Correia-de-Sá, P., eds. (2023). *Cellular and molecular targets in epileptogenesis focusing on disease prevention*. Lausanne: Frontiers Media SA. doi: 10.3389/978-2-8325-3097-9

Table of contents

05 Editorial: Cellular and molecular targets in epileptogenesis focusing on disease prevention
Diana Cunha-Reis, Sandra Henriques Vaz and Paulo Correia-de-Sá

08 The Blood-Brain Barrier Breakdown During Acute Phase of the Pilocarpine Model of Epilepsy Is Dynamic and Time-Dependent
Natália Ferreira Mendes, Aline Priscila Pansani, Elis Regina Ferreira Carmanhães, Poliana Tange, Juliana Vieira Meireles, Mayara Ochikubo, Jair Ribeiro Chagas, Alexandre Valotta da Silva, Glaucia Monteiro de Castro and Luciana Le Sueur-Maluf

21 CK2 Inhibition Prior to Status Epilepticus Persistently Enhances $K_{Ca}2$ Function in CA1 Which Slows Down Disease Progression
Felix Schulze, Steffen Müller, Xiati Guli, Lukas Schumann, Hannes Brehme, Till Riffert, Marco Rohde, Doreen Goerss, Simone Rackow, Anne Einsle, Timo Kirschstein and Rüdiger Köhling

37 Epilepsy miRNA Profile Depends on the Age of Onset in Humans and Rats
Jiri Baloun, Petra Bencurova, Tereza Totkova, Hana Kubova, Marketa Hermanova, Michal Hendrych, Martin Pail, Sarka Pospisilova and Milan Brazdil

51 The Impacts of Surgery and Intracerebral Electrodes in C57BL/6J Mouse Kainate Model of Epileptogenesis: Seizure Threshold, Proteomics, and Cytokine Profiles
Karen Tse, Edward Beamer, Deborah Simpson, Robert J. Beynon, Graeme J. Sills and Thimmasettappa Thippeswamy

73 Altered Expression of Par3, aPKC-λ, and Lgl1 in Hippocampus in Kainic Acid-Induced Status Epilepticus Rat Model
Chen Zhang, Fafa Tian, Zheren Tan, Juan Du and Xiaoyan Long

82 Inflammation Mediated Epileptogenesis as Possible Mechanism Underlying Ischemic Post-stroke Epilepsy
Anna Regina Tröscher, Joachim Gruber, Judith N. Wagner, Vincent Böhm, Anna-Sophia Wahl and Tim J. von Oertzen

92 The Potential of Circulating Cell-Free DNA Methylation as an Epilepsy Biomarker
Ricardo Martins-Ferreira, Bárbara Guerra Leal and Paulo Pinho Costa

100 Role of HMGB1/TLR4 and IL-1β/IL-1R1 Signaling Pathways in Epilepsy
Shaohui Zhang, Feng Chen, Feng Zhai and Shuli Liang

111 Mesial Temporal Lobe Epilepsy (MTLE) Drug-Refractoriness Is Associated With P2X7 Receptors Overexpression in the Human Hippocampus and Temporal Neocortex and May Be Predicted by Low Circulating Levels of miR-22
Bárbara Guerra Leal, Aurora Barros-Barbosa, Fátima Ferreirinha, João Chaves, Rui Rangel, Agostinho Santos, Cláudia Carvalho, Ricardo Martins-Ferreira, Raquel Samões, Joel Freitas, João Lopes, João Ramalheira, Maria Graça Lobo, António Martins da Silva, Paulo P. Costa and Paulo Correia-de-Sá

128 The potential role of DNA methylation as preventive treatment target of epileptogenesis
Toni Christoph Berger, Erik Taubøll and Kjell Heuser

141 Attenuated iron stress and oxidative stress may participate in anti-seizure and neuroprotective roles of xenon in pentylenetetrazole-induced epileptogenesis
Mengdi Zhang, Yao Cheng, Yujie Zhai, Yi Yuan, Haoran Hu, Xianfeng Meng, Xuemeng Fan, Hongliu Sun and Shucui Li

156 Epileptiform activity influences theta-burst induced LTP in the adult hippocampus: a role for synaptic lipid raft disruption in early metaplasticity?
José D. Carvalho-Rosa, Nádia C. Rodrigues, Armando Silva-Cruz, Sandra H. Vaz and Diana Cunha-Reis

frontiers | Frontiers in Cellular Neuroscience

TYPE Editorial
PUBLISHED 12 July 2023
DOI 10.3389/fncel.2023.1251038

OPEN ACCESS

EDITED AND REVIEWED BY
Dirk M. Hermann,
University of Duisburg-Essen, Germany

*CORRESPONDENCE
Diana Cunha-Reis
dcreis@ciencias.ulisboa.pt

RECEIVED 30 June 2023
ACCEPTED 04 July 2023
PUBLISHED 12 July 2023

CITATION
Cunha-Reis D, Vaz SH and Correia-de-Sá P (2023) Editorial: Cellular and molecular targets in epileptogenesis focusing on disease prevention. *Front. Cell. Neurosci.* 17:1251038. doi: 10.3389/fncel.2023.1251038

Editorial: Cellular and molecular targets in epileptogenesis focusing on disease prevention

Diana Cunha-Reis [1,2,3]*, Sandra Henriques Vaz [3,4] and Paulo Correia-de-Sá [5,6]

[1]Biosystems and Integrative Sciences Institute (BioISI), Faculdade de Ciências, Universidade de Lisboa, Lisboa, Portugal, [2]Departamento de Biologia Vegetal, Faculdade de Ciências, Universidade de Lisboa, Lisboa, Portugal, [3]Instituto de Medicina Molecular João Lobo Antunes, Faculdade de Medicina, Universidade de Lisboa, Lisboa, Portugal, [4]Instituto de Farmacologia e Neurociências, Faculdade de Medicina, Universidade de Lisboa, Lisboa, Portugal, [5]Laboratório de Farmacologia e Neurobiologia, Instituto de Ciências Biomédicas de Abel Salazar (ICBAS), Universidade do Porto (UP), Porto, Portugal, [6]Center for Drug Discovery and Innovative Medicines (MedInUP), Porto, Portugal

KEYWORDS

epileptogenesis, miRNA, DNA methylation, synaptic plasticity (LTP/LTD), blood-brain barrier, inflammation, seizures-diagnosis, mesial temporal lobe epilepsy (MTLE)

Editorial on the Research Topic
Cellular and molecular targets in epileptogenesis focusing on disease prevention

Epilepsy is a complex disease characterized by the development of recurrent, unprovoked seizures, often associated with comorbidities, such as cognitive deficits, depression, anxiety and psychiatric disturbances, that worsen the patient's condition and mortality (Devinsky et al., 2018; Vezzani et al., 2019). Temporal lobe epilepsy (TLE) is the most common type of partial epilepsy in adulthood. Its most prevalent mesial form is characterized by seizures originating mostly in the hippocampus, but also in the amygdala and parahippocampal gyrus. Mesial-temporal lobe epilepsy (MTLE) is often accompanied by hippocampal sclerosis (MTLE-HS), commonly associated with antiseizure drug (ASD) resistance (Sloviter, 2005; Thom, 2014; Gambardella et al., 2016). The mechanisms underlying MTLE epileptogenesis are largely unknown, yet associated hereditary and environmental triggering factors, such as trauma, complex febrile seizures, *status epilepticus* (*SE*), inflammatory insults, or ischemia, are frequently detected. Disease onset and progression vary considerably with the putative triggering event and age. Several cellular mechanisms contribute to early epileptogenesis, such as altered synaptic plasticity and neuronal excitability, neuronal death, astrogliosis, and astrocyte dysfunction, neuroinflammation, blood-brain barrier leakage, secondary non-convulsive *SE* and aberrant neurogenesis, yet their pathophysiological relevance is far from being understood. At least one-third of epileptic cases have no available medical treatment. This prompted the focus of research toward the understanding epilepsy etiopathogenesis and to the development of novel therapeutic strategies aiming at epileptogenesis prevention (Pitkänen et al., 2015; Cunha-Reis et al., 2021). This Research Topic highlights the discovery of new circulating biomarkers for early diagnosis and follow-up of epileptic cases and addresses new therapeutic strategies to mitigate early cellular events and the progression of epilepsy to avoid ASD resistance.

Pioneering studies showed that blood-brain barrier (BBB) breakdown generates a vicious cycle favoring epileptic seizures, while seizure-induced BBB disruption is critical to epilepsy onset and progression. Using the pilocarpine-induced *SE* model in the rat, the article by Mendes et al. shows that altered BBB permeability to small molecules occurs within the first 4 h of *SE*, preceding macromolecule leakage in the following 5 h. While BBB leakage of macromolecules disappears within 24h, increased BBB permeability to small molecules persists, adding to brain damage over time. Therefore, the authors propose that there is a critical 24h temporal window of BBB dysfunction after the onset of the *SE,* during the acute phase, where therapeutic approaches should concentrate to prevent BBB damage and epileptogenesis.

Early and delayed BBB disruption leads to leakage of brain contents, which may provide biomarkers for the early diagnosis and progression monitoring of epileptogenesis. The article by Martins-Ferreira et al., reviews the putative role of methylated circulating cell-free DNA generated by neuronal apoptosis as a biomarker of ongoing epileptogenesis. Such an approach, relying on the cell-type specificity of DNA methylation (DNAm) to determine its tissue origin, is not currently used to approach epilepsy. Though it might be interesting, further studies are required to overcome the main limitations, such as the fact that early epileptogenesis depends on the triggering event and might not concur with neuronal apoptosis and cell death (Pitkänen et al., 2015). In line with this, Berger et al. review the role of DNAm changes as a trigger for early epileptogenesis alterations in gene expression (GE), extrapolating mainly on discoveries using the intracortical kainic acid rat model. The authors emphasize the role of glial cell DNAm in controlling early GE alterations involved in the regulation of neuronal death, reactive astrogliosis and brain inflammation and discuss how these processes could be targeted for the early prevention of epileptogenesis through directed epigenetic modifications.

Baloun et al. performed a cross-sectional study using hippocampal tissue from of MTLE-HS patients and from the Li^{2+}-pilocarpine TLE animal model to uncover distinct miRNA profiles depending on the age of epilepsy onset in both patients and animal models. This analysis revealed overlapping miR-142-5p and miR-129-2-3p changes between MTLE-HS patients and rats with adult TLE onset. These miRNAs regulate immunomodulatory agents with convulsive and neuronal growth suppression properties that may be used in diagnosis. The study by Leal et al. extends this concept showing that low serum levels of circulating miRNA-22 correlate with overexpression of the proconvulsant ATP-sensitive ionotropic P2X7 receptor in the hippocampus and neocortex of MTLE-HS patients. These changes, which are more notorious in patients' refractory to three or more ASDs, seem to occur soon after the epileptogenic trigger and are not dependent on the age of onset and gender, making them useful as predictors of drug refractoriness. Interestingly, two P2X7 isotypes were identified in hippocampal and neocortical nerve terminals, being the higher MW (85KDa) isoform the most abundant in brain regions of MTLE-HS patients compared to the naturally occurring 67 kDa receptor. This may denote post-translational protein modifications, which epileptogenesis implications are worth investigating in the future.

Carvalho-Rosa et al., used *in vitro* models of epileptiform activity (EA) to evaluate the time course of long-term potential (LTP) changes occurring within 30 min to 1 h 30 m following EA while characterizing the early modifications in synaptic structure leading to altered synaptic transmission patterns and neuronal excitability that may contribute to early epileptogenesis. The described synaptic molecular alterations in AMPA GluA1/GluA2 levels and AMPA GluA1 phosphorylation likely underlie the observed impaired post-seizure LTP and, notably, were associated modifications in synaptic lipid raft structure. Since lipid raft integrity is required for several molecular mechanisms involved in synaptic metaplasticity these may constitute promising targets for prevention of epileptogenesis.

Zhang C. et al. show that altered expression of Par3, αPKC-λ, and Lgl1 proteins and enzymes participating in neuronal polarity definition and axonal growth during development are correlated with mossy fiber sprouting and neuronal cell loss in the CA3 region of the hippocampus from 3 days after kainic acid (KA)-induced SE in rats. While these findings suggest the involvement of Par3, aPKC-λ, and Lgl1 in early epileptogenesis, their clinical translation requires further investigation. The group of Zhang S. et al. reviewed preclinical studies and clinical evidence concerning the role of two glia-to-neuron signaling pathways, the high mobility group box-1 (HMGB1)/toll-like receptor 4 (TLR4) and interleukin-1beta (IL-1β)/interleukin-1 receptor 1 (IL-1R1) pathways in the neuroinflammatory response contributing to brain injury in epilepsy. Although these signaling pathways were subject to investigation as therapeutic targets through the development of antibodies and inhibitors, the complete upstream and downstream links are still missing.

Finally, the articles by Schulze et al., Tse et al., and Zhang M. et al. go a step further by testing the impact of distinct therapeutic strategies in epileptic animal models. The first paper demonstrates the role of casein kinase 2 (CK2) activity in epileptogenesis in juvenile rats. Inhibition of CK2 activity before SE had a neuroprotective role on seizure onset, disease progression and chronic CA1 neuronal burst firing, by increasing $K_{Ca}2.2$ levels and function, also involving the upregulation of HCN1 and HCN3 channels. Tse et al. demonstrated that surgical implantation of depth electrodes increased brain and plasma molecules involved in epileptogenesis and neuroinflammation while it reduced the threshold for *SE* induced by KA. Implantation chronology aside, this suggests that electrode implantation in TLE patients may contribute to neuroinflammation, neurodegeneration and BBB leakage at the risk of accelerating disease progression. Zhang M. et al. report the neuroprotective role of subclinical anesthetic doses of xenon gas against epileptogenesis in the pentylenetetrazole (PTZ) kindling model of TLE. These actions were evident early in the development of epileptogenesis and were probably due to the reduction of iron and oxidative and iron stress.

Abbreviations: ASDs, antiseizure drugs; BBB, blood-brain barrier; CK2, casein kinase 2; DNAm, DNA methylation; EA, epileptiform activity; GE, gene expression; HMGB1, high mobility group box-1; IL-1β, interleukin-1beta; IL-1R1, interleukin-1 receptor 1; KA, kainic acid; MTLE, mesial temporal lobe epilepsy; SE, status epilepticus; TLR4, toll-like receptor 4.

In summary, this Research Topic puts into evidence multiple targets for the early diagnosis as well as therapeutic interventions directed at epileptogenesis highlighting its benefits, caveats, and hurdles to clinical applications.

Author contributions

DC-R: funding acquisition and writing—original draft, review, and editing. SV and PC-d-S: writing—review and editing. All authors contributed to the article and approved the submitted version.

Funding

This work was supported by national and international funding managed by Fundação para a Ciência e a Tecnologia (FCT, IP), Portugal. Grants: FCT UIDB/04046/2020 and UIDP/04046/2020 to BioISI; FCT/POCTI (PTDC/SAU-PUB/28311/2017) EPIRaft grantto DC-R; International Society for Neurochemistry (Carer Development Grant 2021 to SHV), the European Union (H2020-WIDESPREAD-05-2017-Twinning (EpiEpinet, grant agreement 952455, to SHV), and FCT UIDB/04308/2020 and UIDP/04308/2020 to PC-d-S via MedInUP. Researcher contract: Norma Transitória - DL57/2016/CP1479/CT0044 to DC-R.

Conflict of interest

The authors declare that the research was conducted in the absence of any commercial or financial relationships that could be construed as a potential conflict of interest.

Publisher's note

References

Cunha-Reis, D., Caulino-Rocha, A., and Correia-de-Sá, P. (2021). VIPergic neuroprotection in epileptogenesis: challenges and opportunities. *Pharmacol. Res.* 164, 105356. doi: 10.1016/j.phrs.2020.105356

Devinsky, O., Vezzani, A., O'Brien, T. J., Jette, N., Scheffer, I. E., De Curtis, M., et al. (2018). Epilepsy. *Nat. Rev. Dis. Prim.* 4, 24. doi: 10.1038/nrdp.2018.24

Gambardella, A., Labate, A., Cifelli, P., Ruffolo, G., Mumoli, L., Aronica, E., et al. (2016). Pharmacological modulation in mesial temporal lobe epilepsy: Current status and future perspectives. *Pharmacol. Res.* 113, 421–425. doi: 10.1016/j.phrs.2016.09.019

Pitkänen, A., Lukasiuk, K., Edward Dudek, F., and Staley, K. J. (2015). Epileptogenesis. *Cold Spring Harb. Perspect. Med.* 5, 822. doi: 10.1101/cshperspect.a022822

Sloviter, R. S. (2005). The neurobiology of temporal lobe epilepsy: Too much information, not enough knowledge. *C R. Biol.* 328, 143–153. doi: 10.1016/j.crvi.2004.10.010

Thom, M. (2014). Review: Hippocampal sclerosis in epilepsy: A neuropathology review. *Neuropathol. Appl. Neurobiol.* 40, 520–543. doi: 10.1111/nan.12150

Vezzani, A., Balosso, S., and Ravizza, T. (2019). Neuroinflammatory pathways as treatment targets and biomarkers in epilepsy. *Nat. Rev. Neurol.* 15, 459–472. doi: 10.1038/s41582-019-0217-x

frontiers in Neurology

ORIGINAL RESEARCH
published: 16 April 2019
doi: 10.3389/fneur.2019.00382

The Blood-Brain Barrier Breakdown During Acute Phase of the Pilocarpine Model of Epilepsy Is Dynamic and Time-Dependent

*Natália Ferreira Mendes[1†], Aline Priscila Pansani[2†], Elis Regina Ferreira Carmanhães[1], Poliana Tange[1], Juliana Vieira Meireles[1†], Mayara Ochikubo[1], Jair Ribeiro Chagas[3], Alexandre Valotta da Silva[1], Glaucia Monteiro de Castro[1] and Luciana Le Sueur-Maluf[1]**

[1] Departamento de Biociências, Universidade Federal de São Paulo, Santos, Brazil, [2] Departamento de Neurologia e Neurocirurgia, Universidade Federal de São Paulo, São Paulo, Brazil, [3] Departamento de Psicobiologia, Universidade Federal de São Paulo, São Paulo, Brazil

The maintenance of blood-brain barrier (BBB) integrity is essential for providing a suitable environment for nervous tissue function. BBB disruption is involved in many central nervous system diseases, including epilepsy. Evidence demonstrates that BBB breakdown may induce epileptic seizures, and conversely, seizure-induced BBB disruption may cause further epileptic episodes. This study was conducted based on the premise that the impairment of brain tissue during the triggering event may determine the organization and functioning of the brain during epileptogenesis, and that BBB may have a key role in this process. Our purpose was to investigate in rats the relationship between pilocarpine-induced status epilepticus (SE), and BBB integrity by determining the time course of the BBB opening and its subsequent recovery during the acute phase of the pilocarpine model. BBB integrity was assessed by quantitative and morphological methods, using sodium fluorescein and Evans blue (EB) dyes as markers of the increased permeability to micromolecules and macromolecules, respectively. Different time-points of the pilocarpine model were analyzed: 30 min after pilocarpine injection and then 1, 5, and 24 h after the SE onset. Our results show that BBB breakdown is a dynamic phenomenon and time-dependent, i.e., it happens at specific time-points of the acute phase of pilocarpine model of epilepsy, recovering in part its integrity afterwards. Pilocarpine-induced changes on brain tissue initially increases the BBB permeability to micromolecules, and subsequently, around 5 h after SE, the BBB breakdown to macromolecules occurs. After BBB breakdown, EB dye is captured by damaged cells, especially neurons, astrocytes, and oligodendrocytes. Although the BBB permeability to macromolecules is restored 24 h after the start of SE, the leakage of micromolecules persists and the consequences of BBB degradation are widely disseminated in the brain. Our findings reveal the existence of a temporal window of BBB dysfunction in the acute phase of the pilocarpine model that is important for the development of therapeutic strategies that could prevent the epileptogenesis.

Keywords: epilepsy, blood-brain barrier, pilocarpine, status epilepticus, Evans blue, sodium fluorescein

OPEN ACCESS

Edited by:
Patrick A. Forcelli, Georgetown University, United States

Reviewed by:
João P. Leite, University of São Paulo, Brazil
Ashok K. Shetty, Texas A&M University College of Medicine, United States

****Correspondence:***
Luciana Le Sueur-Maluf
luciana.maluf@unifesp.br; lucianamaluf@gmail.com

†Present Address:
Natália Ferreira Mendes, Faculdade de Enfermagem, Universidade Estadual de Campinas, Campinas, Brazil
Aline Priscila Pansani, Departamento de Ciências Fisiológicas, Universidade Federal de Goiás, Goiânia, Brazil
Juliana Vieira Meireles, Unidade de Cardiologia do Exercício, Hospital Sírio Libanês, São Paulo, Brazil

Specialty section:
This article was submitted to Epilepsy, a section of the journal Frontiers in Neurology

Received: *23 July 2018*
Accepted: *28 March 2019*
Published: *16 April 2019*

Citation:
Mendes NF, Pansani AP, Carmanhães ERF, Tange P, Meireles JV, Ochikubo M, Chagas JR, da Silva AV, Monteiro de Castro G and Le Sueur-Maluf L (2019) The Blood-Brain Barrier Breakdown During Acute Phase of the Pilocarpine Model of Epilepsy Is Dynamic and Time-Dependent. Front. Neurol. 10:382. doi: 10.3389/fneur.2019.00382

INTRODUCTION

The blood-brain barrier (BBB) is a physical and functional interface between blood and brain, essential for providing a suitable environment for neuronal function, regardless of fluctuations in blood composition (1–3). Many of the BBB properties are dependent on a close association among brain capillaries and astrocytes, which contain multiple processes that extend toward neurons and vessels (4, 5). The end-feet of the astrocytes surround about 95% of the abluminal surface of the brain capillaries (6) and are responsible for releasing several factors that induce and maintain the BBB phenotype (7). Besides astrocytes, multiple agents, and cell types including pericytes, neurons, and perivascular microglia are involved in the modulation of BBB permeability. These cells interact with microvessels, regulating the local blood flow and the vascular tone, and altogether make up the concept of a "neurovascular unit" (3, 7, 8).

Due to its anatomic location and its unique physiologic properties, BBB disruption is involved in many central nervous system diseases, including epilepsy (1). The involvement of BBB disruption to epileptic seizures has been studied for 3 decades (9–11). Evidence demonstrates that BBB breakdown may induce epileptic seizures, and conversely, seizure-induced BBB disruption may cause further epileptic episodes (12–14). Although the BBB disruption facilitates seizure onset, long-lasting BBB breakdown can result in long-term cognitive impairment which can be observed through altered electroencephalography (EEG) activity (13, 15).

In the past, BBB was considered a barrier that prevented the entrance of antiepileptic drugs to the central nervous system. Nowadays, studies in BBB and epilepsy have been targeting a therapeutic approach to reduce seizure burden (16–19). However, it is also important to understand the dynamics of BBB breakdown during an early event (in the acute phase of epilepsy), which represents a window of opportunity for therapeutic approaches that could prevent the further development of epilepsy. This study was conducted based on the premise that the impairment of brain tissue during the triggering event may determine the organization and functioning of the brain during epileptogenesis, and that the BBB may have a key role in this process (20). Our purpose was to investigate, in male rats, the relationship between pilocarpine-induced status epilepticus (SE) and BBB integrity by determining the time course of the BBB opening and its subsequent recovery during the acute phase of the pilocarpine model.

BBB integrity was assessed by quantitative and morphological methods. We have used sodium fluorescein (NaFl) and Evans blue (EB) vital dyes as markers of the BBB breakdown and analyzed several brain areas during the acute phase of pilocarpine-induced epilepsy. NaFl dye (MW 376 Da) was used as a marker of micromolecule extravasation through the BBB. It does not bind to plasma proteins and is quickly metabolized and excreted, which hinders a lengthy longitudinal study (21). Conversely, EB dye (MW 961 Da) was used as a marker of macromolecular extravasation through the BBB (22), since it binds to albumin serum forming a complex of 68,500 Da that is not excreted. This allows us to perform a longitudinal study and to determine the time course of the BBB breakdown during the acute phase of pilocarpine model of epilepsy.

MATERIALS AND METHODS

Animal Model

Adult male Wistar rats were obtained from the Federal University of Sao Paulo Experimental Models Development Center (CEDEME/Brazil). All experiments were carried out in accordance with the guidelines of the Brazilian National Council for the Control of Animal Experimentation (CONCEA) and approved by the Ethics Committee for Animal Experimentation of the Federal University of Sao Paulo (UNIFESP—01929/08). Room temperature was controlled (22 ± 1°C) and a light-dark cycle was maintained on a 12-h on-off cycle. Food and water were available *ad libitum* throughout the experimental period.

Study Design

The rats were randomly distributed into two groups: control and pilocarpine-treated. The treated rats received an injection of pilocarpine solution (Pilo; 320–350 mg/Kg *i.p.*) preceded by one dose of methyl-scopolamine 30 min before (1 mg/Kg; *s.c.*) as described by Cavalheiro (23). Rats from the control group were injected with equivalent volumes of saline. For the characterization of the BBB breakdown, different time-points of the pilocarpine model were analyzed: 30 min after pilocarpine injection (group Pilo-30min); and then 1 h (group SE-1h), 5 h (group SE-5h), and 24 h (group SE-24h) after the *status epilepticus* (SE) onset. Additionally, rats from groups SE-5h and SE-24h remained in SE for a period of 3 h, and then the seizures were blocked by diazepam (7–10 mg/Kg *i.p.*).

The Pilo-30 min group was chosen to verify if pilocarpine-induced changes on brain tissue before SE leads to BBB breakdown to micro and macromolecules. The other groups, SE-1h, 5h, and 24h were used to investigate if pilocarpine-induced SE leads to BBB breakdown, and additionally to carry out an investigation about the subsequent closure.

Experiment 1: Assessment of BBB Permeability to Micromolecules

NaFl dye (100 mg/Kg) was injected intravenously in the tail vein of the rats (n = 4–11 rats/group) 30 min before euthanasia. The rats were then deeply anesthetized intraperitoneally with a mixture of Ketamin (100 mg/Kg) and Xylazine (10 mg/Kg), and perfused transcardially with phosphate buffer saline (PBS; 0.1 M pH 7.4). The brains were quickly removed, and specific regions were dissected: hypothalamus, hippocampus, entorhinal/piriform cortex, and neocortex. Samples were homogenized in cold PBS and proteins were precipitated with trichloroacetic acid at final concentration of 30% (Sigma-Aldrich, St. Louis-Mo-USA), and centrifuged for 10 min at 14,000 g. The supernatants were collected and measured in a spectrophotofluorometer

(Spectramax M2; Molecular Devices) at excitation wavelength of 440 nm and emission wavelength of 525 nm (21). The results were expressed in μg of total NaFl obtained from a standard curve and were covariate with the mass of each region.

Experiment 2: Assessment of BBB Permeability to Macromolecules

EB dye (80 mg/Kg) was injected intravenously in the tail vein immediately before pilocarpine injection in the group Pilo-30 min, and at the SE onset in rats of groups SE-1h, SE-5h, and SE-24h (n = 4–12 rats/group). To assess the integrity of BBB 24 h after SE, an additional group was performed (group SE-24h/EB30min; n = 5), in which EB dye was injected 30 min before euthanasia. In the control group, rats received EB dye immediately before saline injection. The brains were quickly removed, photographed for macroscopic analysis, and the specific regions were dissected as described before. The samples were homogenized in cold PBS, protein precipitated with trichloroacetic acid 30% (Sigma-Aldrich, St. Louis-Mo-USA) and then centrifuged for 10 min at 14,000 g. The supernatant was collected and read at 610 nm using a microplate reader (Spectramax M2; Molecular Devices) (24). The results were expressed in μg of total EB obtained from a standard curve and were covariate with the mass of each region.

Morphological Analyses of EB Dye Distribution in Brain Tissue

Based on the results obtained in the macroscopic and quantitative analysis of EB dye, soon after the first clinical signs of SE, EB dye was injected, and the rats were euthanized after 5 and 24 h of dye circulation. Rats from the groups SE-5h and SE-24h were perfused transcardially with PBS followed by 4% paraformaldehyde in PBS (0.1 M, pH 7.4), cryoprotected in 30% sucrose solution, embedded in O.C.T. Compound (Tissue-Tek; Sakura, Alphen aan den Rijn, the Netherlands) and frozen at −80°C. Coronal slices of 30 μm were obtained by cryostat and mounted in a commercial anti-fading agent (Vectashield with DAPI, Vector Labs, Burlingame, CA, USA). The slides were examined and photographed using an Axio Observer D1 fluorescence microscope (Carl Zeiss; Gottingen, Germany). The images were obtained and merged using the multidimensional acquisition tool of Zeiss AxioVision software. Evans blue dye was observed in red (546 nm excitation filter) and nuclear DAPI staining observed in blue (UV filter).

Immunostaining

To determine which cells captured the EB dye, coronal brain slices from the SE-24hEB group were washed with TBS (0.02 M Tris-buffered saline, pH 7.4), and blocked with 5% skimmed milk powder and 0.3% Triton X-100 diluted in TBS for 2 h at room temperature (RT). Slices were incubated overnight at 4°C with primary antibodies diluted in TBS containing 5% skimmed milk powder and 0.1% Triton X-100. The antibodies used were: mouse anti-NeuN (1:150; #MAB377–Millipore) for neuron detection, rabbit anti-GFAP (1:150; #G9269–Sigma Aldrich) for astrocyte labeling, goat anti-OLIG-2 (1:150; #AB9610–Millipore) for oligodendrocyte lineage, and goat anti-IBA-1 (1:150; #AB5076–Abcam) for microglia. Slices were then washed with TBS and incubated with fluorophore-labeled secondary antibody (1:200, Alexa Fluor 488; Thermo Fisher Scientific) in TBS with 0.l% Triton X-100 for 2 h at RT, in the dark. Slides were mounted as described above and were examined and photographed with the same fluorescence microscope mentioned. Evans blue dye was observed in red (546 nm emission filter), immunostained cells in green (488 nm excitation filter), and nuclear DAPI in blue (UV filter).

Statistical Analyses

To verify the Gaussian distribution and homogeneity of data, the Shapiro-Wilk normality test and Levene test were applied. The data were standardized with z-score and the homogeneity submitted to Welch's correction, if necessary. General Linear Model (GLM) using one-way analysis of covariance (ANCOVA), followed by the Sidak *post-hoc* test, was performed for comparison among the groups. A value of $p < 0.05$ indicated statistical significance. The results were expressed as means ± standard error of the mean (SEM). Statistical analyses and graphics were performed using IBM SPSS Statistics 20 and GraphPadPrism 7.0 software.

RESULTS

BBB Breakdown to NaFl Dye in the Acute Phase of Epilepsy Is Quick and Time-Dependent

In *Experiment 1*, we evaluated the permeability of BBB to NaFl dye at different time-points in the acute phase of pilocarpine model of epilepsy. The schematic representation of the experimental design using NaFl dye is depicted in **Figure 1A**. One-way ANCOVA showed a significant increase in the BBB permeability to NaFl dye in the hippocampus [$F_{(4,26)} = 7.101$; $p = 0.001$, $\eta^2 = 0.522$], hypothalamus [$F_{(4,26)} = 5.922$; $p = 0.002$, $\eta^2 = 0.477$], entorhinal/piriform cortex [$F_{(4,26)} = 7.898$; $p = 0.0001$, $\eta^2 = 0.549$], and neocortex [$F_{(4,26)} = 7.241$; $p = 0.0001$, $\eta^2 = 0.527$]. The mass of each region, used as covariate, was not significant. After Sidak *post-hoc*, our quantitative analysis showed that 30 min after PILO injection (Pilo30'NaFl group), an increased amount of NaFl dye was detected only in the hippocampus (**Figure 1B**). One hour after SE onset (SE1hNaFl group), a significant increase in NaFl dye persisted in the hippocampus (**Figure 1B**), and was additionally observed in the hypothalamus (**Figure 1C**). Five hour after SE began (SE5hNaFl group), the areas with higher NaFl dye were the hippocampus, entorhinal/piriform cortex, and neocortex (**Figures 1B,D,E**), but not in the hypothalamus (**Figure 1C**). Twenty-four hour after SE began (SE24hNaFl group), we observed an increase of NaFl dye only in the hippocampus and entorhinal/piriform cortex (**Figures 1B,D**).

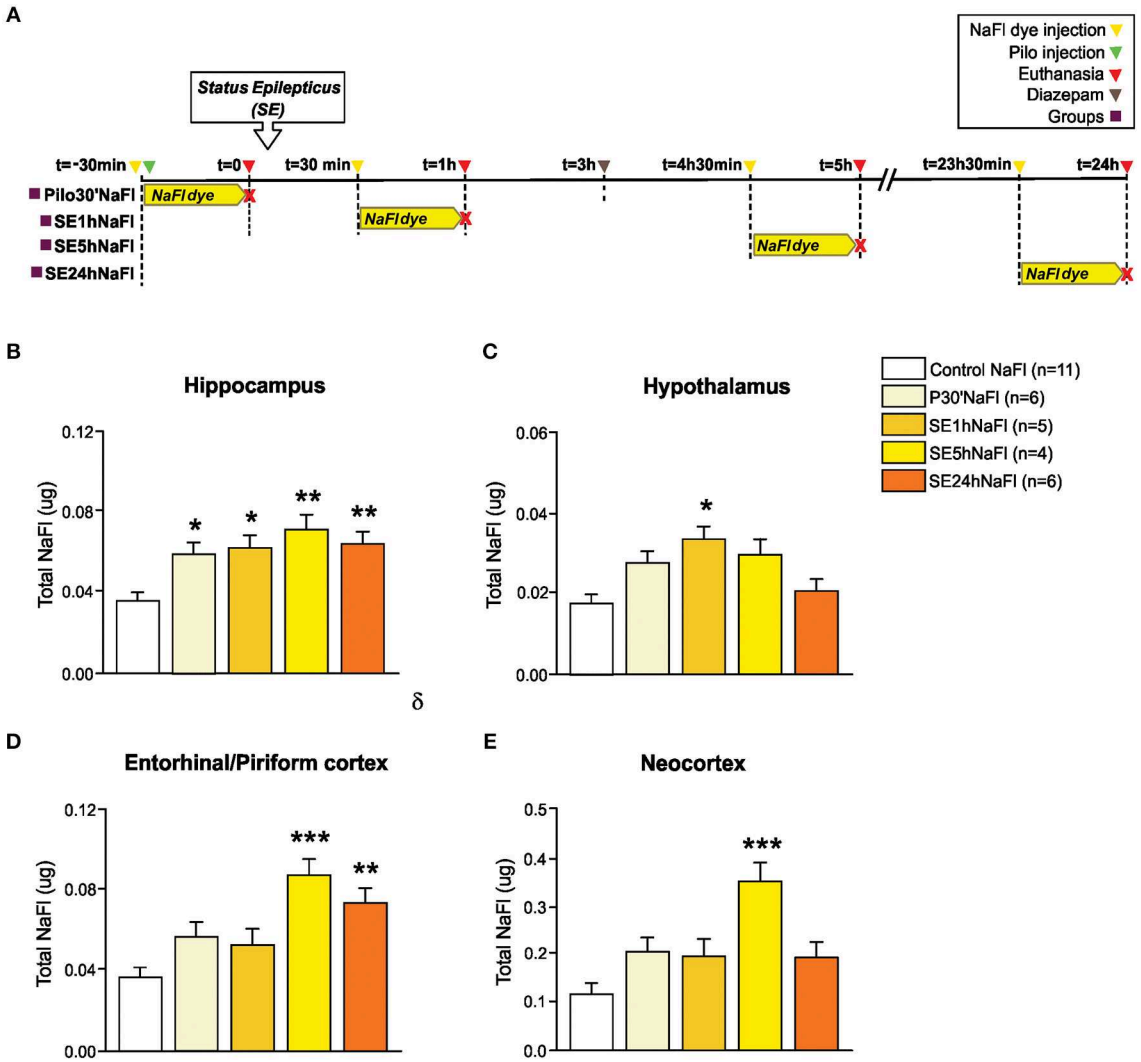

FIGURE 1 | Increased permeability of the BBB to the NaFl dye during the acute phase of the pilocarpine model of epilepsy. In **(A)**, a schematic representation of the experimental design for evaluation of the BBB permeability to micromolecules: in the Pilo30'NaFl group, the NaFl dye was intravenously injected immediately before the pilocarpine (i.p.), and the animals were euthanized 30 min after PILO-injection. In the SE1hNaFl group, the NaFl dye was injected 30 min after the beginning of the *status epilepticus* (SE), and the animals were euthanized 1 h after SE onset. In the SE5hNaFl group, the NaFl dye was injected 4 h 30 min after the beginning of the SE, and the animals euthanized 5 h after SE onset. In the SE24hNaFl group, the NaFl dye was injected at 23 h 30 min after the beginning of the SE, and the animals were euthanized 24 h after SE onset. Note that rats from SE5hNaFl and SE24hNaFl groups had the seizures blocked with diazepam 3 h after SE initiation. In **(B–E)**, quantitative analysis shows that BBB tracer NaFl dye can be detected since the initial periods of the acute phase of the pilocarpine model in the hippocampus **(B)**, hypothalamus **(C)**, entorhinal/piriform cortex **(D)**, and neocortex **(E)**. Data expressed as mean ± SEM. $^{*}p < 0.05$, $^{**}p < 0.01$, $^{***}p < 0.001$ in comparison with control groups by one-way ANCOVA (mass of the region as covariate) and Sidak *post-hoc*.

BBB Breakdown to EB Dye in the Acute Phase of Epilepsy Is Late and Possibly Recoverable

In *Experiment 2*, we evaluated the BBB permeability to EB dye at the same time-points as the NaFl evaluation. The schematic representation of the experimental design using EB dye is depicted in **Figure 2A**. One-way ANCOVA showed a significant increase in the BBB permeability to EB dye in the hippocampus [$F_{(5,33)} = 7.535$; $p = 0.0001$, $\eta^2 = 0.533$], neocortex [$F_{(5,33)} = 9.852$, $p = 0.0001$, $\eta^2 = 0.599$], hypothalamus [$F_{(5,33)} = 5.852$; $p = 0.001$, $\eta^2 = 0.470$], and entorhinal/piriform cortex [$F_{(5,33)} = 10.819$; $p = 0.0001$, $\eta^2 = 0.621$]. The mass of each region, used as covariate, was not significant. After Sidak *post-hoc*, the quantitative analysis carried out 5 h after the SE onset (SE5hEB group) showed a significant increase of EB dye in all brain areas analyzed: hippocampus, hypothalamus, entorhinal/piriform cortex, and neocortex (**Figures 2B–E**). Twenty-four hour after SE began (SE24hEB group), the areas with increased EB dye concentration were the hippocampus, entorhinal/piriform cortex, and neocortex(**Figures 2B,D,E**), but not in the hypothalamus (**Figure 2C**). In the group that received

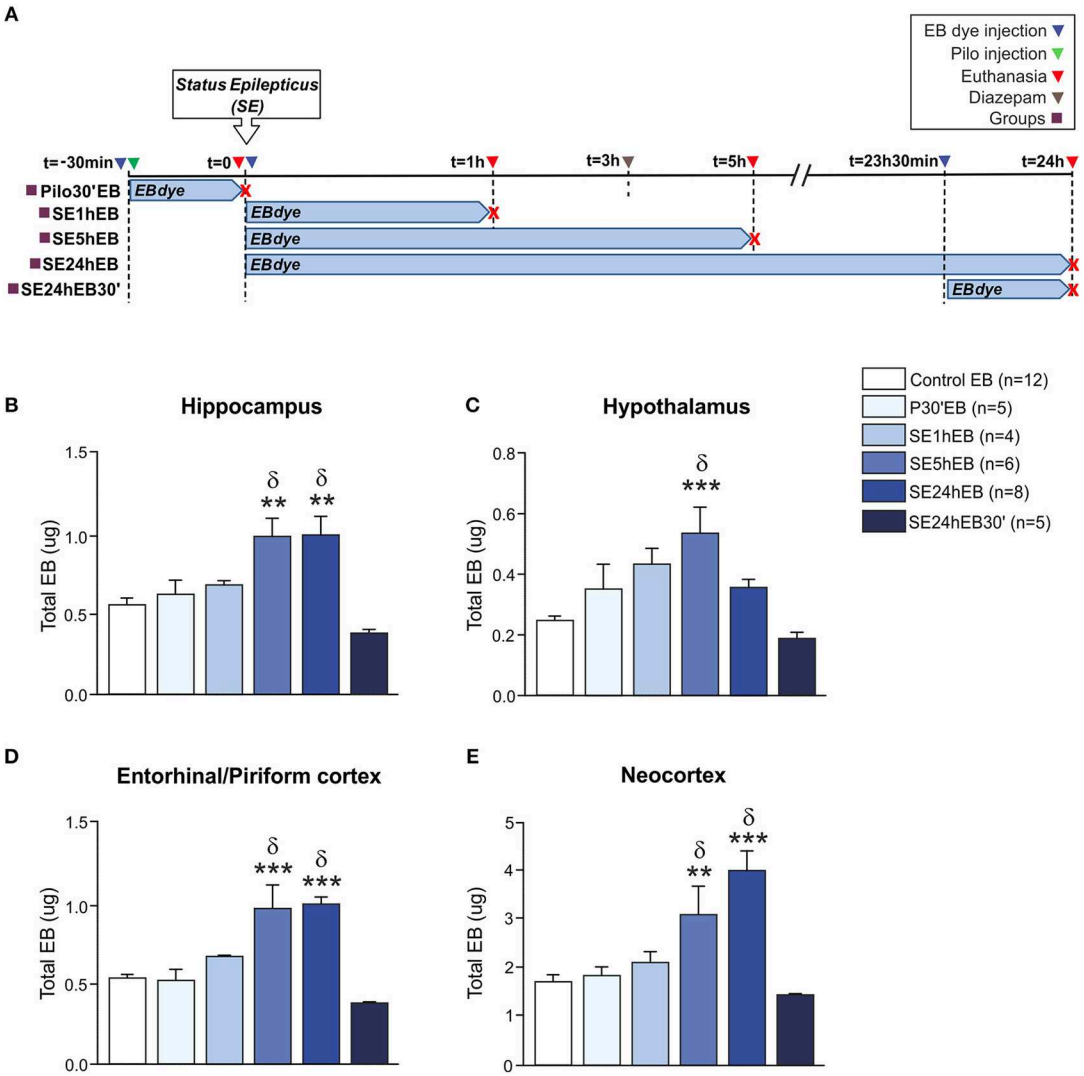

FIGURE 2 | BBB breakdown to the EB dye during the acute phase of the pilocarpine model of epilepsy. In **(A)**, a schematic representation of the experimental design for evaluation of the BBB permeability to macromolecules: in the Pilo30'EB group, Evans blue (EB) dye was intravenously injected immediately before pilocarpine (i.p.), and the animals were euthanized 30 min after PILO injection. In the SE1hEB group, the EB dye was injected at the beginning of the *status epilepticus* (SE), and animals were euthanized 1 h after SE onset. In the SE5hEB group, EB dye was injected at the beginning of the SE, and animals euthanized 5 h after SE onset. In the SE24hEB group, EB dye was injected at the beginning of the SE, and animals were euthanized 24 h after SE onset. In the SE24hEB30' group, EB dye was injected 23 h 30 min after the beginning of the SE, and the animals were euthanized 24 h after SE onset (i.e., EB dye remained in the bloodstream for 30 min). Note that rats from groups SE5hEB, SE24hEB, and SE24hEB30' had seizures blocked with diazepam 3 h after SE initiation. In **(B–E)**, quantitative analysis shows that BBB tracer EB can be detected only between 5 and 24 h after SE beginning in the hippocampus **(B)**, hypothalamus **(C)**, entorhinal/piriform cortex **(D)**, and neocortex **(E)**. Data expressed as mean ± SEM. $^{**}p < 0.01$, $^{***}p < 0.001$ in comparison with control groups and $^{\delta}p < 0.001$ in comparison with SE24hEB30min by one-way ANCOVA (mass of the region as covariate) and Sidak *post-hoc*.

EB dye injection 23h30min after SE began (SE24hEB30' group), we did not observe any increase of EB dye in the regions analyzed.

BBB Breakdown to EB Dye in the Acute Phase of Epilepsy Can Be Seen Macroscopically

Macroscopic analysis of brains from Control, P30'EB, and SE1hEB groups did not show the presence of EB dye (**Figure 3**, first three rows). In the SE5hEB group, we observed that some rats showed EB extravasation to the brain tissue (**Figure 3**, fourth row), whereas in some other animals in the group, this was not observed. In the SE24hEB group, all animals showed diffuse leakage of EB dye to the brain tissue (**Figure 3**, fifth row). The SE24hEB30' group did not show the presence of EB dye in the brain tissue (**Figure 3**, bottom row).

Cells of Brain Tissue Capture EB Dye After BBB Disruption

Microscopic analysis of the SE5hEB and SE24hEB groups confirmed a leakage of EB dye in many brain areas when

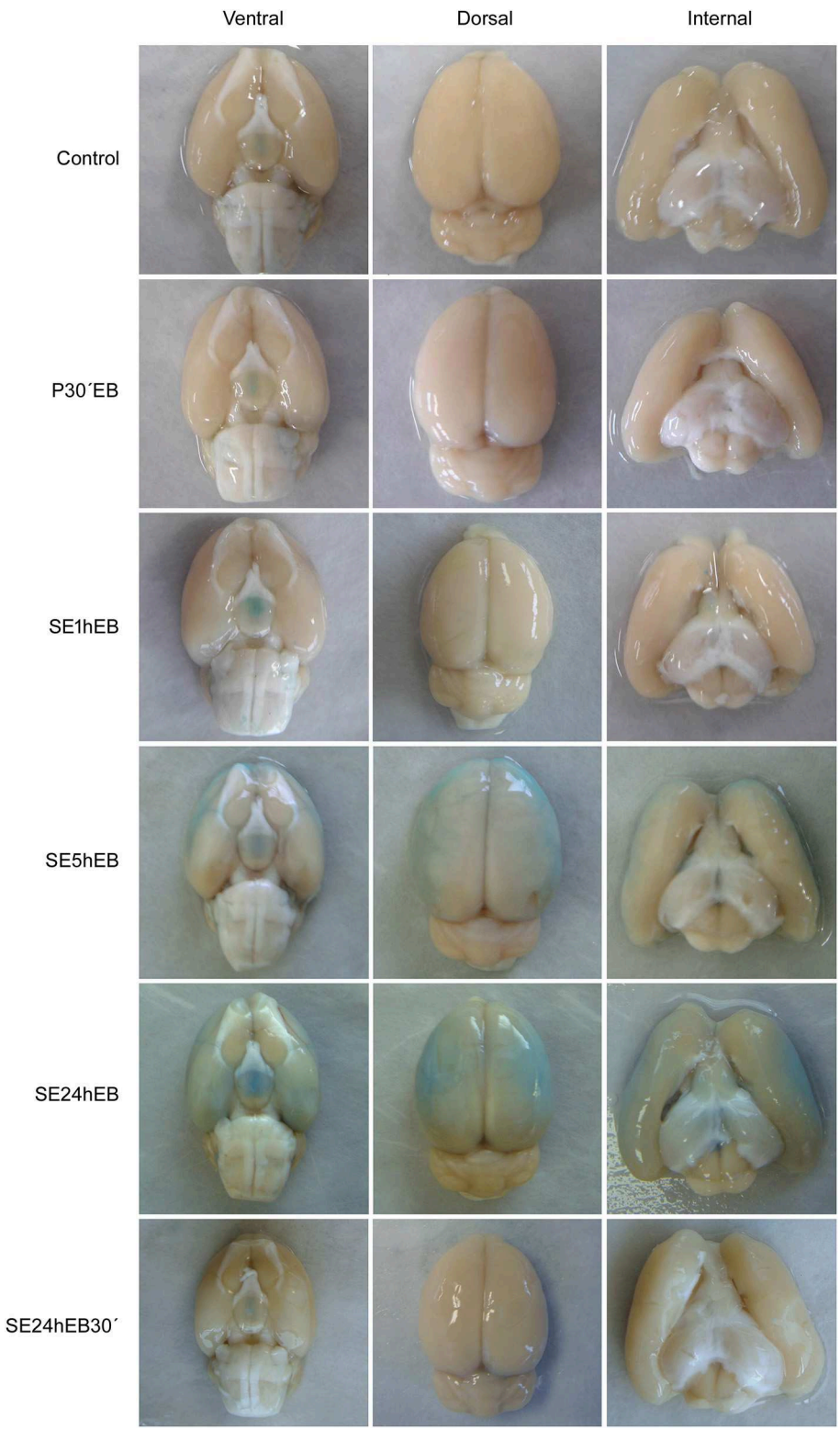

FIGURE 3 | Macroscopic analyses of rats' brains after EB dye injection during the acute phase of the pilocarpine-induced epilepsy model. Representative images of the ventral (left column), dorsal (middle column), and internal (right column) views of the brains after EB injection. Note the EB dye in the neocortex of rats from the SE5hEB group and in the SE24hEB group, the presence of EB dye in the neocortex and entorhinal cortex. In the SE24hEB30' group, note the absence of dye in the brain tissue.

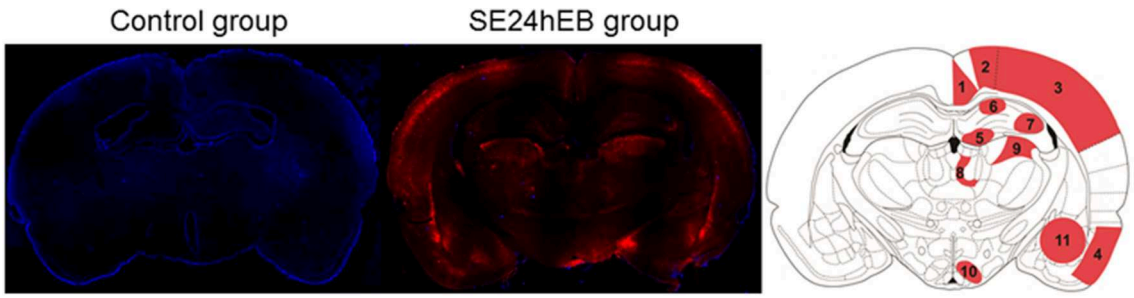

FIGURE 4 | Panoramic view of the brain showing the Evans blue (EB) dye distribution after BBB breakdown. Representative brain slices from Control (left panel) and SE24EB (middle panel) groups obtained by fluorescence microscope. In blue, nuclei of the cells evidenced with DAPI. In red, fluorescence emitted by the EB dye, indicating the sites of BBB breakdown in the SE24hEB group. In the right panel, schematic representation of the main brain areas affected by BBB breakdown in the group SE24hEB: (1) retrosplenial granular cortex (coRSG); (2) motor cortex (coM); (3) somatosensory cortex (coS); (4) piriform cortex (coPir); (5) dentate gyrus (DG); (6) hippocampal CA1 area; (7) hippocampal CA3 area; (8) mediodorsal nucleus of the thalamus; (9) laterodorsal nucleus of the thalamus; (10) ventromedial nucleus of the hypothalamus (VMH); and (11) amygdaloid complex. Bregma−3.14 mm anteroposterior adapted from the rat brain atlas (25). Photomicrographs were taken at a magnification of 100X and panels constructed with Autostitch software (Copyright University of British Columbia).

compared to Control group. The EB dye leakage across the disrupted BBB was captured by cells from the neocortex, hippocampus, and hypothalamus, in addition to the thalamus and amygdala cells (**Figures 4**, **5**, and **Supplementary Figure 1**).

Neurons, Astrocytes, and Oligodendrocytes Capture EB Dye After BBB Disruption

Immunostaining of the brain tissue performed 24 h after SE (SE24hEB group) revealed that cells that captured EB are mainly neurons, astrocytes, and oligodendrocytes. Microglia exhibiting thicker branches suggestive of activated cells were found mainly involving the EB-containing cells, although macrophage-shaped microglia that captured the dye were also found. Detailed photographic documentation of the various brain areas affected are shown in **Figure 6** and **Supplementary Figure 2**.

DISCUSSION

Several exogenous and fluorescent BBB tracers have been used for functional and structural analysis of BBB permeability (26). In our experiments, for evaluating the permeability of BBB to micromolecules during the acute phase of the pilocarpine model, we used NaFl dye as a tracer and observed an increased BBB permeability in the hippocampus, that occurred up to 30 min after pilocarpine injection. BBB permeability to micromolecules in the hypothalamus increased only 1 h after SE onset while in the entorhinal/piriform cortex and in the neocortex it was observed 5 h after SE began. Particularly in the hippocampus and entorhinal/piriform cortex, the BBB leakage of micromolecules persisted until the end of the experimental period (24 h after SE onset). Similar results were found by van Vliet et al. (20), who demonstrated, through MRI and microscopic analysis using fluorescein tracer, BBB leakage 1 day after kainic acid-induced SE in Sprague–Dawley rats. Our results show that increased BBB permeability to micromolecules is a dynamic phenomenon, and that, mostly in the hypothalamus, an adaptive property of BBB can be observed, preventing the breakdown to macromolecules which would cause subsequent brain damage.

Regardless of etiology, BBB disruption has been shown to be associated with epileptogenesis after injury (27, 28) both clinically (29) and experimentally (12, 30, 31). In this context, the early adaptive behavior of BBB damage is important especially because the chemical microenvironment of the synapses and the brain extracellular space play a key role in the generation of seizures (17, 32, 33).

There is evidence that the initial episode, i.e., status epilepticus, can be induced by pilocarpine through a primary peripheral effect on white blood cells, leading to increased serum levels of IL-1β, which alters BBB permeability (34). BBB leakage triggers a complex cascade which includes protein extravasation, impaired potassium buffering, brain inflammation, angiogenesis, and changes in multidrug transporters and metabolic enzymes (17). The ionic imbalance due to potassium accumulation in the extracellular space, induced by BBB disruption, facilitates convulsant activity by stimulation of muscarinic receptors in the brain, leading to neuronal hyperexcitability (35). This has also been demonstrated by electrophysiological investigations performed in cultured endothelium and brain slices in which, even in the presence of cholinergic agonists at high concentrations, the epileptiform activities only occurred in the presence of elevated level of potassium in the extracellular environment (30). Taken together, these findings confirm the hypothesis that BBB disruption during the acute phase of the pilocarpine model of epilepsy may contribute to the triggering and propagation of electrical discharges, and subsequently lead to nervous tissue damage.

Besides increased BBB permeability to micromolecules, our results also demonstrate the existence of a temporal window of BBB breakdown to macromolecules in the acute phase of pilocarpine-induced epilepsy. Our macroscopic and quantitative findings show that while some animals, which were all euthanized 5 h after the commencement of SE, had already had extravasation

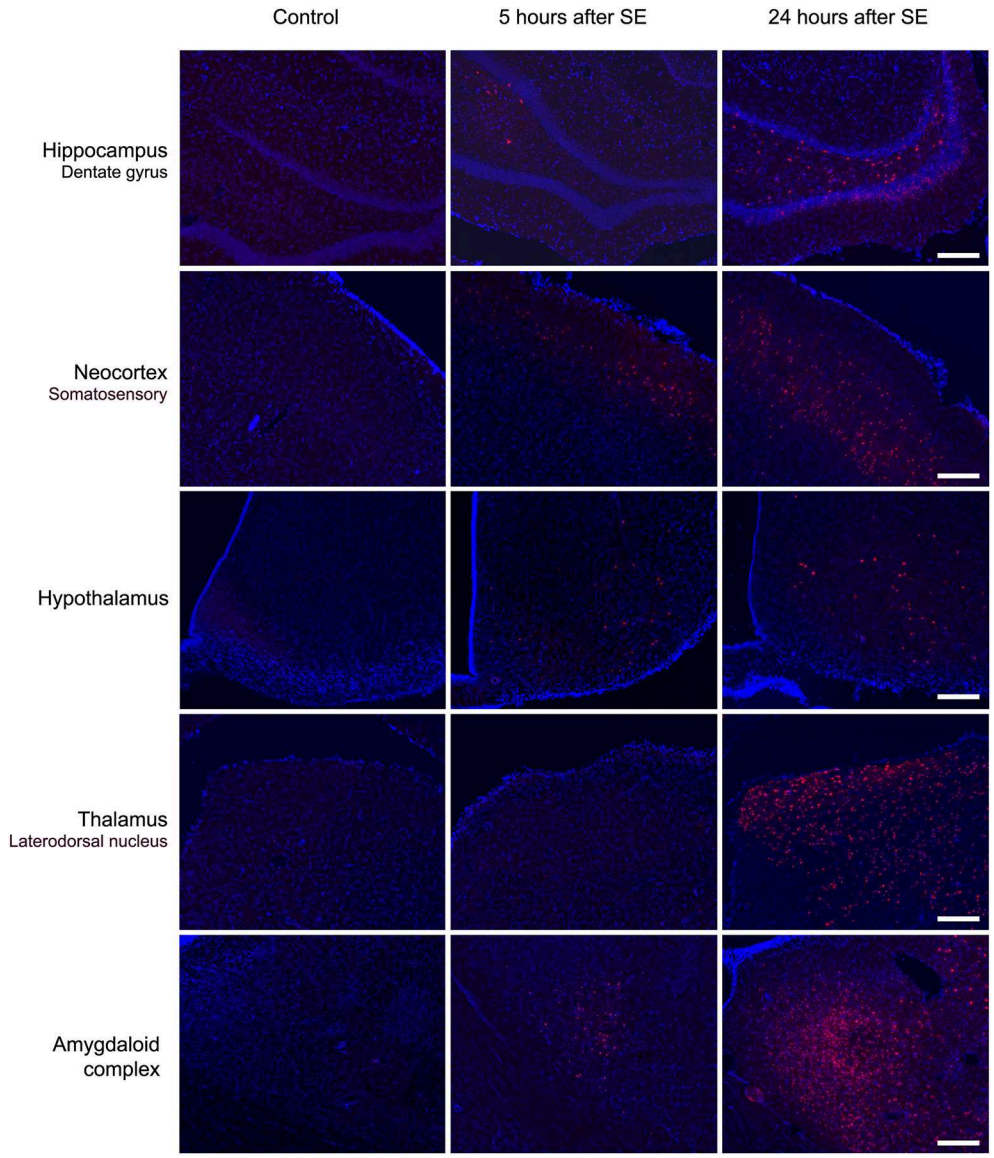

FIGURE 5 | Brain areas affected by BBB breakdown to EB dye in the acute phase of the pilocarpine-induced epilepsy model. Representative photomicrographs obtained under a fluorescence microscope show the main brain areas affected by BBB breakdown: hippocampus, neocortex, hypothalamus, thalamus, and amygdala. Cells containing the Evans blue (EB) fluorescent dye appear as red. Nuclei of the cells evidenced with DAPI are blue. Note that, in the Control group, the cells do not contain EB dye, while in group SE5hEB, there are considerably fewer cells that captured EB than in group SE24hEB, where they are widely distributed into the brain areas analyzed. Magnification: 100X. Bar = 200 μm.

of EB dye; others had not. This variability among animals could be due to different time-dependent responses to the pilocarpine-induced SE, particularly, individual differences in the oxidative stress and neuroinflammation (36, 37), and indicates that BBB breakdown to macromolecules occurs around 5 h after SE onset. Conversely, 24 h after SE onset, all animals showed EB dye in the brain tissue. Results show that even though the BBB function seems to have been restored 24 h after SE started, the consequences of the macromolecules extravasation into the brain tissue, that had occurred earlier, were widely spread in the brain. The animals from SE-24h group, which received EB dye at SE onset and were euthanized 24 h later, showed a significant increase in BBB breakdown and EB dye extravasation in several brain areas (hippocampus, entorhinal cortex, and neocortex). It is noteworthy that animals which received EB dye 23 h 30 min after SE started did not show EB dye extravasation to the nervous tissue. Taken together, this data indicates that during the period between 5 and 24 h after SE onset, there is a BBB breakdown to macromolecules and restoration. Unfortunately, the extensive gap between our experimental periods does not allow us to identify the moment when the BBB restoration happened. Future studies should be conducted in order to elucidate it.

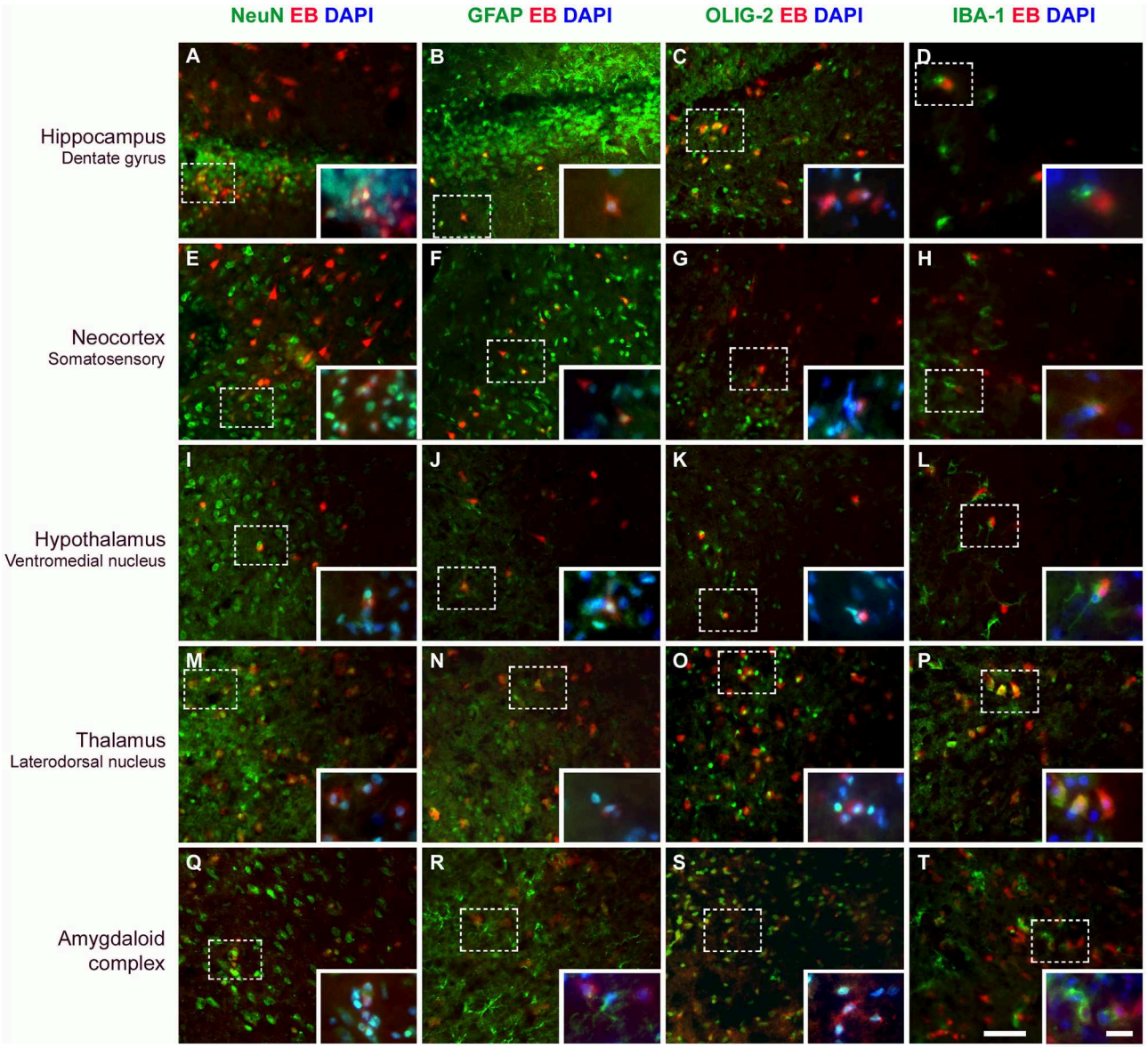

FIGURE 6 | Evans blue (EB) dye is captured by different cell types after BBB breakdown. Immunostaining for detection of neurons (NeuN), astrocytes (GFAP), oligodendrocytes (OLIG-2), and microglia (IBA-1) in various brain areas, 24 h after SE. Positive cells are shown in green. After BBB breakdown, the complex albumin-EB dye enters the brain and is captured by damaged cells (shown in red). Double-staining for the cell types and the EB dye shows that they are mainly neurons, astrocytes, and oligodendrocytes (see in yellow, as a result of red and green fluorescence overlap; larger images). *Inserts* show higher magnification of affected cells (dotted rectangle), with nuclei evidenced with DAPI (shown in blue). White color corresponds to the green, red, and blue fluorescence overlap. The first column of images shows that neurons containing EB are observed in all analyzed areas **(A,E,I,M,Q)**. In the second column, astrocytes are found containing EB **(B,F,J,N)** or involving cells that captured the dye (see amygdaloid complex; **R**). In the third column, oligodendrocytes that captured EB are also observed in all brain areas **(C,G,O,S)**, except in the hypothalamus **(K)**. The fourth column shows that microglia exhibiting thicker branches projections suggestive of activated cells are found involving the EB-containing cells **(D,H,L,T)**, except in the thalamus where macrophage-shaped microglia, are seen containing the dye **(P)**. Magnification: 400X (larger images) and 630X (inserts). Bars = 20 μm (larger images) and 10 μm (inserts).

In agreement with our findings, Marchi et al. (30) demonstrated, by histological assays, points of leakage of fluorescein isothiocyanate (FITC)-labeled albumin in the limbic system of rats during the pilocarpine-induced SE. The authors attribute the onset of seizures to increased BBB permeability in areas sensitive to cholinergic agents. Moreover, our results are also consistent with others who reported that, after pilocarpine-induced SE, these brain areas display the greatest inflammatory response in positron emission tomography (PET) (38, 39).

Some studies have emphasized the potential involvement of a primary lesion of the BBB in the epileptogenesis by exposing

the brain parenchyma to serum albumin (27, 40–42). Here we showed that, after BBB breakdown, the EB-bound albumin enters the brain and is captured mainly by neurons, astrocytes, and oligodendrocytes. These findings are in accordance with literature that has demonstrated that not only neurons, but also astrocytes and microglia can uptake albumin after SE (43–45). In microglia, albumin can be found as a result of a phagocytic activity that protects the brain during SE (12). However, our data show that EB dye was captured mainly by damaged cells, and less by reactive microglia, which was chemoattracted to the injured cells, wrapping them. This can be explained by the fact that, when activated, microglial cells release cytokines, chemokines, growth factors, and other molecules to attenuate or prevent brain damage, besides removing debris by phagocytosis (46). Astrocytes are particularly sensitive to SE-induced brain tissue damage. These cells can uptake albumin through TGF-β receptors, leading to increased intracellular calcium that results in downregulation of inward rectifying potassium (Kir 4.1) and aquaporin-4 (AQP4) channels (47–49), reducing the buffer of extracellular potassium and facilitating NMDA-mediated neuronal hyperexcitability and epileptiform activity (33, 44, 50, 51). Although the presence of albumin in neurons can lead to death (12), it seems that albumin *per se* is not neurotoxic; it can only be captured by damaged neurons (44). In fact, when EB dye is used to evaluate the BBB integrity, it strongly binds to albumin in the bloodstream and forms a complex with high molecular weight. In the case of BBB breakdown, this complex enters the brain and is captured only by cells that have lost their selective permeability of the membrane, but not by cells with an intact membrane (52). Consequently, although using 30 μm thick sections, we were able to detect the distribution of damaged cells after BBB disruption, and then confirm that all cell types are affected during the acute phase of pilocarpine model, with preference for neurons, astrocytes, and oligodendrocytes.

Although the exact moment of BBB opening was not precisely determined, research into pilocarpine-induced SE has already included testing of some new therapies for the prevention of BBB disruption. Fu et al. (53) hypothesized that HMGB1 (high mobility group box-1), a pro-inflammatory cytokine-like molecule, may be involved in the development of epileptogenesis in mice through BBB disruption and induction of inflammatory processes. These authors showed that treatment with anti-HMGB1 decreases the concentration of EB dye in the thalamus and hypothalamus during pilocarpine-induced SE, while the control group did not show any reduction in BBB leakage. On the other hand, injection of recombinant human HMGB1 after pilocarpine, enhanced the leakage of EB dye in an HMGB1 dose-dependent manner. However, the authors injected EB dye 2 h after pilocarpine administration and then waited for only 2 h for the animals' euthanasia. Although they showed the efficacy of the therapy with anti-HMGB1 in preventing BBB disruption, some benefits may have been overlooked due to a lack of knowledge about the time-point of the BBB breakdown in the pilocarpine model. They observed EB dye extravasation only in the thalamus and hypothalamus possibly because, 4 h after pilocarpine injection, the BBB in other areas is still preserved. Although the anti-HMGB1 treatment has been quite successful in epileptogenesis (54), it still needs to be tested after longer periods of SE, and other brain areas should be analyzed.

In recent years, some efforts have been concentrated to develop a quantitative assessment of vascular injury, which could be an important diagnostic, predictive, and pharmacodynamic biomarker for epilepsy. Recently, Bar-Klei et al. (55) proposed a feasible contrast-enhanced modality to detect regions with BBB hyper-permeability in humans throughout two types of T1-weighted MRI sequences. However, further studies are still required to confirm the most sensitive and reliable protocol for BBB imaging, which, in the coming years, will probably be a big step forward for clinical practice.

In conclusion, our findings indicate that BBB breakdown is a dynamic phenomenon and time-dependent, i.e., it happens at specific time-points of the acute phase of pilocarpine model of epilepsy, recovering in part its integrity afterwards (**Figure 7**). We show that pilocarpine-induced changes on brain tissue initially increased the permeability of the BBB to micromolecules, and subsequently, after SE, the BBB breakdown to macromolecules occurred. Although the BBB permeability to macromolecules is restored 24 h after SE, the leakage of micromolecules persists and the consequences of BBB degradation are widely disseminated in the brain, which in turn may induce further episodes of BBB breakdown. Together, our data reveal the existence of a temporal window of BBB dysfunction during the acute phase of the pilocarpine model that is important for the development of therapeutic strategies to prevent the epileptogenesis.

ETHICS STATEMENT

Adult male Wistar rats were obtained from the Federal University of São Paulo Experimental Models Development Center (CEDEME/Brazil). All experiments were carried out in accordance with the guidelines of the Brazilian National Council for the Control of Animal Experimentation (CONCEA) and approved by the Ethics Committee for Animal Experimentation of the Federal University of São Paulo (UNIFESP—01929/08).

AUTHOR CONTRIBUTIONS

NM, EC, PT, JM, MO, GM, and LL carried out the experiments. AP, JC, and AdS contributed to performing the experiments and in the data interpretation. LL designed the study and performed the statistical analyses. NM, GM, and LL interpreted the results and wrote the manuscript. All authors have approved the final manuscript as submitted.

FUNDING

This work was supported by the Fundação de Amparo à Pesquisa do Estado de São Paulo (FAPESP), Brazil (Proc. 2008/06450-0). Scholarships were financed by FAPESP for JM (Proc. 2010/05858-5), and by the Conselho Nacional de Desenvolvimento Científico e Tecnológico (CNPq, Brazil) for NM and EC.

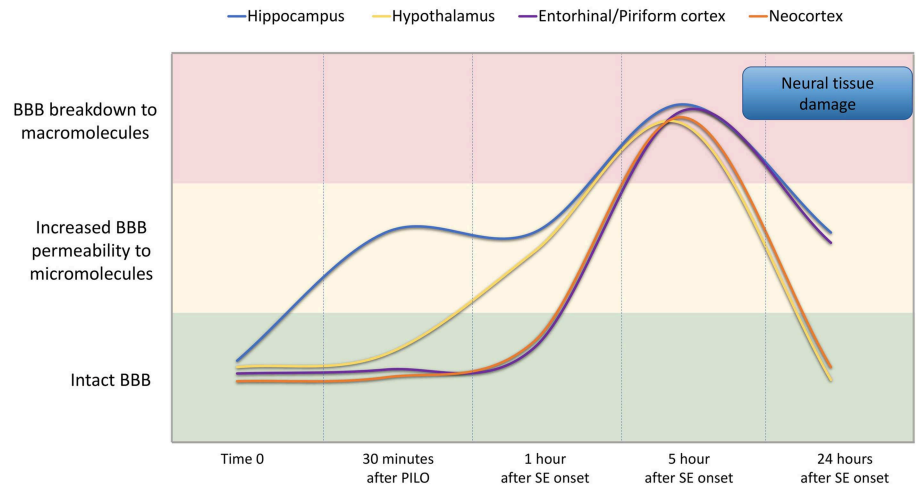

FIGURE 7 | Representation of BBB permeability during the acute phase of the pilocarpine model. The colored bands correspond to the BBB status: intact (green band), increased permeability to micromolecules (yellow band), and breakdown to macromolecules (red band). The lines represent the dynamics of the BBB opening and restoration over time in the regions of the hippocampus (blue line), hypothalamus (yellow line), entorhinal and pyriform cortex (purple line), and neocortex (orange line). Note that increased BBB permeability for micromolecules is observed from 30 min after PILO injection, and the BBB breakdown for macromolecules occurs about 5 h after SE onset. Although the BBB permeability to macromolecules is restored 24 h after SE initiation, the leakage of micromolecules persists and the consequences of BBB degradation on brain tissue are widely disseminated in the brain.

ACKNOWLEDGMENTS

We would like to thank the Full Professor Dr. Esper Abrão Cavalheiro for learning in his laboratory, for his careful and critical reading of this manuscript, and for offering suggestions for improvements. We would like to thank Dr. Altay Alves Lino de Souza for statistical classes, Tony Champion for reviewing the English, and Carlos Eduardo Sydow for technical assistance.

SUPPLEMENTARY MATERIAL

The Supplementary Material for this article can be found online at: https://www.frontiersin.org/articles/10.3389/fneur.2019.00382/full#supplementary-material

Figure S1 | Brain areas affected by BBB breakdown to EB dye in the acute phase of the pilocarpine-induced epilepsy model. Representative photomicrographs obtained under a fluorescence microscope show the main brain areas affected by BBB breakdown: hippocampus, neocortex, hypothalamus, thalamus, and amygdala. Cells containing the Evans blue (EB) fluorescent dye appear as red. Nuclei of the cells evidenced with DAPI are blue. Note that, in the Control group, the cells do not contain EB dye, while in group SE5hEB, there are considerably fewer cells that captured EB than in group SE24hEB, where they are widely distributed into the brain areas analyzed. Magnification: 100X. Bar = 200 μm.

Figure S2 | Evans blue (EB) dye is captured by different cell types after BBB breakdown. Immunostaining for detection of neurons (NeuN), astrocytes (GFAP), oligodendrocytes (OLIG-2), and microglia (IBA-1) in various brain areas, 24 h after SE. Positive cells are shown in green. After BBB breakdown, the complex albumin-EB dye enters the brain and is captured by damaged cells (shown in red). Double-staining for the cell types and the EB dye shows that they are mainly neurons, astrocytes, and oligodendrocytes (see in yellow, as a result of red and green fluorescence overlap; larger images). *Inserts* show higher magnification of affected cells (dotted rectangle), with nuclei evidenced with DAPI (shown in blue). White color corresponds to the green, red, and blue fluorescence overlap. The first column of images shows that neurons containing EB are observed in all analyzed areas **(E,I,M,Q,U)**, except in the CA3 **(A)**. In the second column, astrocytes are found containing EB **(B,F,J,R,V)** or involving cells that captured the dye (see Piriform cortex; **N**). In the third column, oligodendrocytes that captured EB are also observed in all brain areas **(C,G,K,O,S,W)**. The fourth column shows microglia exhibiting thicker branches projections suggestive of activated cells involving the EB-containing cells in all analyzed areas **(D,H,L,P,T,X)**. Magnification: 400X (larger images) and 630X (inserts). Bars = 20 μm (larger images) and 10 μm (inserts).

REFERENCES

1. Zlokovic BV. The blood-brain barrier in health and chronic neurodegenerative disorders. *Neuron.* (2008) 57:178–201. doi: 10.1016/j.neuron.2008.01.003
2. Abbott NJ, Patabendige AA, Dolman DE, Yusof SR, Begley DJ. Structure and function of the blood-brain barrier. *Neurobiol Dis.* (2010) 37:13–25. doi: 10.1016/j.nbd.2009.07.030
3. Neuwelt EA, Bauer B, Fahlke C, Fricker G, Iadecola C, Janigro D, et al. Engaging neuroscience to advance translational research in brain barrier biology. *Nat Rev Neurosci.* (2011) 12:169–82. doi: 10.1038/nrn2995
4. Abbott NJ. Astrocyte-endothelial interactions and blood-brain barrier permeability. *J Anat.* (2002) 200:629–38. doi: 10.1046/j.1469-7580.2002.00064.x
5. Wolburg H, Noell S, Mack A, Wolburg-Buchholz K, Fallier-Becker P. Brain endothelial cells and the glio-vascular complex. *Cell Tissue Res.* (2009) 335:75–96. doi: 10.1007/s00441-008-0658-9
6. Rowland LP, Fink ME, Rubin L. Cerebrospinal fluid: blood-brain barrier, brain edema and hydrocephalus. In: Kandel ER, Schwartz JH, Jessel TM, editors. *Principles of Neural Science.* 3rd ed. New York, NY: Elsevier. (1991). p. 1050–60.
7. Abbott NJ, Rönnbäck L, Hansson E. Astrocyte-endothelial interactions at the blood-brain barrier. *Nat Rev Neurosci.* (2006) 7:41–53. doi: 10.1038/nrn1824

8. Erickson MA, Banks WA. Neuroimmune axes of the blood-brain barriers and blood-brain interfaces: bases for physiological regulation, disease states, and pharmacological interventions. *Pharmacol Rev.* (2018) 70:278–314. doi: 10.1124/pr.117.014647
9. Weissberg I, Reichert A, Heinemann U, Friedman A. Blood-brain barrier dysfunction in epileptogenesis of the temporal lobe. *Epilepsy Res Treat.* (2011) 2011:143908. doi: 10.1155/2011/143908
10. Janigro, D. Blood-brain barrier, ion homeostatis and epilepsy: possible implications towards the understanding of ketogenic diet mechanisms. *Epilepsy Res.* (1999) 37:223–32. doi: 10.1016/S0920-1211(99)00074-1
11. Gorter JA, van Vliet EA, Aronica E. Status epilepticus, blood-brain barrier disruption, inflammation, and epileptogenesis. *Epilepsy Behav.* (2015) 49:13–6. doi: 10.1016/j.yebeh.2015.04.047
12. van Vliet EA, da Costa AS, Redeker S, van Schaik R, Aronica E, Gorter JA. Blood-brain barrier leakage may lead to progression of temporal lobe epilepsy. *Brain.* (2007) 130:521–34. doi: 10.1093/brain/awl318
13. Tomkins O, Shelef I, Kaizerman I, Eliushin A, Afawi Z, Misk A, et al. Blood-brain barrier disruption in post-traumatic epilepsy. *J Neurol Neurosurg Psychiatry.* (2008) 79:774–7. doi: 10.1136/jnnp.2007.126425
14. Raabe A, Schmitz AK, Pernhorst K, Grote A, von der Brelie C, Urbach H, et al. Cliniconeuropathologic correlations show astroglial albumin storage as a common factor in epileptogenic vascular lesions. *Epilepsia.* (2012) 53:539–48. doi: 10.1111/j.1528-1167.2012.03405.x
15. Scott RC. What are the effects of prolonged seizures in the brain? *Epileptic Disord.* (2014) 16:S6–11. doi: 10.1684/epd.2014.0689
16. Marchi N, Granata T, Ghosh C, Janigro D. Blood-brain barrier dysfunction and epilepsy: pathophysiologic role and therapeutic approaches. *Epilepsia.* (2012) 53:1877–86. doi: 10.1111/j.1528-1167.2012.03637.x
17. van Vliet EA, Aronica E, Gorter JA. Role of blood-brain barrier in temporal lobe epilepsy and pharmacoresistance. *Neuroscience.* (2014) 277:455–73. doi: 10.1016/j.neuroscience.2014.07.030
18. van Vliet EA, Aronica E, Gorter JA. Blood-brain barrier dysfunction, seizures, and epilepsy. *Semin Cell Dev Biol.* (2015) 38:26–34. doi: 10.1016/j.semcdb.2014.10.003
19. Aronica E, Mühlebner A. Neuropathology of epilepsy. *Handb Clin Neurol.* (2017) 145:193–216. doi: 10.1016/B978-0-12-802395-2.00015-8
20. van Vliet EA, Otte WM, Gorter JA, Dijkhuizen RM, Wadman WJ. Longitudinal assessment of blood-brain barrier leakage during epileptogenesis in rats. A quantitative MRI study. *Neurobiol Dis.* (2014) 63:74–84. doi: 10.1016/j.nbd.2013.11.019
21. Kaya M, Gurses C, Kalayci R, Ekizoglu O, Ahishali B, Orhan N, et al. Morphological and functional changes of blood-brain barrier in kindled rats with cortical dysplasia. *Brain Res.* (2008) 1208:181–91. doi: 10.1016/j.brainres.2008.02.101
22. Kozler P, Pokorný J. Altered blood-brain barrier permeability and its effect on the distribution of Evans blue and sodium fluorescein in the rat brain applied by intracarotid injection. *Physiol Res.* (2003) 52:607–14.
23. Cavalheiro EA. The pilocarpine model of epilepsy. *Ital J Neurol Sci.* (1995) 16:33–7.
24. Kaya M, Palanduz A, Kalayci R, Kemikler G, Simsek G, Bilgic B, et al. Effects of lipopolysaccharide on the radiation-induced changes in the blood-brain barrier and the astrocytes. *Brain Res.* (2004) 1019:105–12. doi: 10.1016/j.brainres.2004.05.102
25. Paxinos G, Watson C. *The Rat Brain in Stereotaxic Coordinates*. 6th Edn. Sidney: Academic Press (2007).
26. Kaya M, Ahishali B. Assessment of permeability in barrier type of endothelium in brain using tracers: evans blue, sodium fluorescein, and horseradish peroxidase. *Methods Mol Biol.* (2011) 763:369–82. doi: 10.1007/978-1-61779-191-8_25
27. Friedman A, Kaufer D, Heinemann U. Blood-brain barrier breakdown-inducing astrocytic transformation: novel targets for the prevention of epilepsy. *Epilepsy Res.* (2009) 85:142–9. doi: 10.1016/j.eplepsyres.2009.03.005
28. Shlosberg D, Benifla M, Kaufer D, Friedman A. Blood-brain barrier breakdown as a therapeutic target in traumatic brain injury. *Nat Rev Neurol.* (2010) 6:393–403. doi: 10.1038/nrneurol.2010.74
29. Tomkins O, Feintuch A, Benifla M, Cohen A, Friedman A, Shelef I. Blood-brain barrier breakdown following traumatic brain injury: a possible role in posttraumatic epilepsy. *Cardiovasc Psychiatry Neurol.* (2011) 2011:765923. doi: 10.1155/2011/765923
30. Marchi N, Oby E, Batra A, Uva L, De Curtis M, Hernandez N, et al. *In vivo* and *in vitro* effects of pilocarpine: relevance to ictogenesis. *Epilepsia.* (2007) 48:1934–46. doi: 10.1111/j.1528-1167.2007.01185.x
31. Librizzi L, Noé F, Vezzani A, de Curtis M, Ravizza T. Seizure-induced brain-borne inflammation sustains seizure recurrence and blood-brain barrier damage. *Ann Neurol.* (2012) 72:82–90. doi: 10.1002/ana.23567
32. D'Ambrosio R, Maris DO, Grady MS, Winn HR, Janigro D. Impaired K(+) homeostasis and altered electrophysiological properties of post-traumatic hippocampal glia. *J Neurosci.* (1999) 19:8152–62.
33. Ivens S, Kaufer D, Flores LP, Bechmann I, Zumsteg D, Tomkins O, et al. TGF-beta receptor-mediated albumin uptake into astrocytes is involved in neocortical epileptogenesis. *Brain.* (2007) 130:535–47. doi: 10.1093/brain/awl317
34. Marchi N, Fan Q, Ghosh C, Fazio V, Bertolini F, Betto G, et al. Antagonism of peripheral inflammation reduces the severity of status epilepticus. *Neurobiol Dis.* (2009) 33:171–81. doi: 10.1016/j.nbd.2008.10.002
35. Vezzani A. Pilocarpine-induced seizures revisited: what does the model mimic? *Epilepsy Curr.* (2009) 9:146–8. doi: 10.1111/j.1535-7511.2009.01323.x
36. Scorza FA, Arida RM, Naffah-Mazzacoratti MDG, Scerni DA, Calderazzo L, Cavalheiro EA. The pilocarpine model of epilepsy: what have we learned? *Anais Acad Brasil Cienc.* (2009) 81:345–65. doi: 10.1590/S0001-37652009000300003
37. Chwiej J, Kutorasinska J, Janeczko K, Gzielo-Jurek K, Uram L, Appel K, et al. Progress of elemental anomalies of hippocampal formation in the pilocarpine model of temporal lobe epilepsy–an X-ray fluorescence microscopy study. *Anal Bioanal Chem.* (2012) 404:3071–80. doi: 10.1007/s00216-012-6425-5
38. Maeda Y, Oguni H, Saitou Y, Mutoh A, Imai K, Osawa M, et al. Rasmussen syndrome: multifocal spread of inflammation suggested from MRI and PET findings. *Epilepsia.* (2003) 44:1118–21. doi: 10.1046/j.1528-1157.2003.67602.x
39. Dedeurwaerdere S, Callaghan PD, Pham T, Rahardjo GL, Amhaoul H, Berghofer P, et al. PET imaging of brain inflammation during early epileptogenesis in a rat model of temporal lobe epilepsy. *EJNMMI Res.* (2012) 2:60. doi: 10.1186/2191-219X-2-60
40. Nadal A, Fuentes E, Pastor J, McNaughton PA. Plasma albumin is a potent trigger of calcium signals and DNA synthesis in astrocytes. *Proc Natl Acad Sci USA.* (1995) 92:1426–30.
41. Seiffert E, Dreier JP, Ivens S, Bechmann I, Tomkins O, Heinemann U, et al. Lasting blood-brain barrier disruption induces epileptic focus in the rat somatosensory cortex. *J Neurosci.* (2004) 24:7829–36. doi: 10.1523/JNEUROSCI.1751-04.2004
42. Tomkins O, Friedman O, Ivens S, Reiffurth C, Major S, Dreier JP, et al. Blood-brain barrier disruption results in delayed functional and structural alterations in the rat neocortex. *Neurobiol Dis.* (2007) 25:367–77. doi: 10.1016/j.nbd.2006.10.006
43. Braganza O, Bedner P, Hüttmann K, von Staden E, Friedman A, Seifert G, et al. Albumin is taken up by hippocampal NG2 cells and astrocytes and decreases gap junction coupling. *Epilepsia.* (2012) 53:1898–906. doi: 10.1111/j.1528-1167.2012.03665.x
44. Frigerio F, Frasca A, Weissberg I, Parrella S, Friedman A, Vezzani A, et al. Long-lasting pro-ictogenic effects induced *in vivo* by rat brain exposure to serum albumin in the absence of concomitant pathology. *Epilepsia.* (2012) 53:1887–97. doi: 10.1111/j.1528-1167.2012.03666.x
45. Bar-Klein G, Cacheaux LP, Kamintsky L, Prager O, Weissberg I, Schoknecht K, et al. Losartan prevents acquired epilepsy via TGF-β signaling suppression. *Ann Neurol.* (2014) 75:864–75. doi: 10.1002/ana.24147
46. Patel DC, Tewari BP, Chaunsali L, Sontheimer H. Neuron-glia interactions in the pathophysiology of epilepsy. *Nat Rev Neurosci.* (2019). doi: 10.1038/s41583-019-0126-4. [Epubh ahead of print].
47. Heinemann U, Kaufer D, Friedman A. Blood-brain barrier dysfunction, TGFβ signaling, and astrocyte dysfunction in epilepsy. *Glia.* (2012) 60:1251–7. doi: 10.1002/glia.22311
48. Kim SY, Buckwalter M, Soreq H, Vezzani A, Kaufer D. Blood-brain barrier dysfunction-induced inflammatory signaling in brain pathology and epileptogenesis. *Epilepsia.* (2012) 6:37–44. doi: 10.1111/j.1528-1167.2012.03701.x

49. Vega-Zelaya L, Herrera-Peco I, Ortega GJ, Sola RG, Pastor J. Plasma albumin induces cytosolic calcium oscillations and DNA synthesis in human cultured astrocytes. *Biomed Res Int.* (2014) 2014:539140. doi: 10.1155/2014/539140
50. Cacheaux LP, Ivens S, David Y, Lakhter AJ, Bar-Klein G, Shapira M, et al. Transcriptome profiling reveals TGF-beta signaling involvement in epileptogenesis. *J Neurosci.* (2009) 29:8927–35. doi: 10.1523/JNEUROSCI.0430-09.2009
51. Lapilover EG, Lippmann K, Salar S, Maslarova A, Dreier JP, Heinemann U, et al. Peri-infarct blood-brain barrier dysfunction facilitates induction of spreading depolarization associated with epileptiform discharges. *Neurobiol Dis.* (2012) 48:495–506. doi: 10.1016/j.nbd.2012.06.024
52. Yao L, Xue X, Yu P, Ni Y, Chen F. Evans blue dye: a revisit of its applications in biomedicine. *Contrast Media Mol Imaging.* (2018) 22:7628037. doi: 10.1155/2018/7628037
53. Fu L, Liu K, Wake H, Teshigawara K, Yoshino T, Takahashi H, et al. Therapeutic effects of anti-HMGB1 monoclonal antibody on pilocarpine-induced status epilepticus in mice. *Sci Rep.* (2017) 7:1179. doi: 10.1038/s41598-017-01325-y
54. Ravizza T, Terrone G, Salamone A, Frigerio F, Balosso S, Antoine DJ, et al. High mobility group box 1 is a novel pathogenic factor and a mechanistic biomarker for epilepsy. *Brain Behav Immun.* (2018) 72:14–21. doi: 10.1016/j.bbi.2017.10.008
55. Bar-Klein G, Lublinsky S, Kamintsky L, Noyman I, Veksler R, Dalipaj H, et al. Imaging blood-brain barrier dysfunction as a biomarker for epileptogenesis. *Brain.* (2017) 140:1692–705. doi: 10.1093/brain/awx073

Conflict of Interest Statement: The authors declare that the research was conducted in the absence of any commercial or financial relationships that could be construed as a potential conflict of interest.

frontiers in Cellular Neuroscience

ORIGINAL RESEARCH
published: 26 February 2020
doi: 10.3389/fncel.2020.00033

CK2 Inhibition Prior to Status Epilepticus Persistently Enhances $K_{Ca}2$ Function in CA1 Which Slows Down Disease Progression

Felix Schulze[1†], Steffen Müller[1†], Xiati Guli[1], Lukas Schumann[1], Hannes Brehme[1], Till Riffert[1], Marco Rohde[1], Doreen Goerss[2,3], Simone Rackow[1], Anne Einsle[1], Timo Kirschstein[1,4†] and Rüdiger Köhling[1,4*†]*

[1] Oscar Langendorff Institute of Physiology, University of Rostock, Rostock, Germany, [2] Department of Psychosomatic Medicine, Rostock University Medical Center, Rostock, Germany, [3] German Center for Neurodegenerative Diseases (DZNE), Göttingen, Germany, [4] Center of Transdisciplinary Neurosciences Rostock, University of Rostock, Rostock, Germany

OPEN ACCESS

Edited by:
Tycho Hoogland, Erasmus Medical Center, Netherlands

Reviewed by:
Fang Zheng, University of Arkansas for Medical Sciences, United States
Nicholas Poolos, University of Washington, United States

***Correspondence:**
Timo Kirschstein
timo.kirschstein@uni-rostock.de
Rüdiger Köhling
ruediger.koehling@uni-rostock.de

† These authors have contributed equally to this work

Specialty section:
This article was submitted to Cellular Neurophysiology, a section of the journal Frontiers in Cellular Neuroscience

Received: *08 August 2019*
Accepted: *04 February 2020*
Published: *26 February 2020*

Citation:
Schulze F, Müller S, Guli X, Schumann L, Brehme H, Riffert T, Rohde M, Goerss D, Rackow S, Einsle A, Kirschstein T and Köhling R (2020) CK2 Inhibition Prior to Status Epilepticus Persistently Enhances $K_{Ca}2$ Function in CA1 Which Slows Down Disease Progression. Front. Cell. Neurosci. 14:33. doi: 10.3389/fncel.2020.00033

Purpose: Epilepsy therapy is currently based on anti-seizure drugs that do not modify the course of the disease, i.e., they are not anti-epileptogenic in nature. Previously, we observed that *in vivo* casein kinase 2 (CK2) inhibition with 4,5,6,7-tetrabromotriazole (TBB) had anti-epileptogenic effects in the acute epilepsy slice model.

Methods: Here, we pretreated rats with TBB *in vivo* prior to the establishment of a pilocarpine-induced status epilepticus (SE) in order to analyze the long-term sequelae of such a preventive TBB administration.

Results: We found that TBB pretreatment delayed onset of seizures after pilocarpine and slowed down disease progression during epileptogenesis. This was accompanied with a reduced proportion of burst firing neurons in the CA1 area. Western blot analyses demonstrated that CA1 tissue from TBB-pretreated epileptic animals contained significantly less CK2 than TBB-pretreated controls. On the transcriptional level, TBB pretreatment led to differential gene expression changes of $K_{Ca}2.2$, but also of HCN1 and HCN3 channels. Thus, in the presence of the HCN channel blocker ZD7288, pretreatment with TBB rescued the afterhyperpolarizing potential (AHP) as well as spike frequency adaptation in epileptic animals, both of which are prominent functions of $K_{Ca}2$ channels.

Conclusion: These data indicate that TBB pretreatment prior to SE slows down disease progression during epileptogenesis involving increased $K_{Ca}2$ function, probably due to a persistently decreased CK2 protein expression.

Keywords: temporal lobe epilepsy, patch-clamp, intracellular recording, field potential recording, video-EEG monitoring, Timm stain

INTRODUCTION

Temporal lobe epilepsy (TLE) is the most common focal symptomatic epileptic disorder in the adulthood and typically difficult to treat (Kwan and Brodie, 2000; Blümcke et al., 2013). Moreover, all currently available drugs used to treat focal symptomatic epilepsy are merely anti-seizure drugs, i.e., they are anti-ictogenic in nature, but lack any anti-epileptogenic potential

(Schmidt and Sillanpää, 2016). In the last decades, several rodent post-status epilepticus (SE) models such as the pilocarpine animal model have provided valuable insights into the latent period between the initial insult and the subsequent development of chronic TLE (Leite et al., 2002). During this period of epileptogenesis, marked changes in synaptic and intrinsic properties take place that may facilitate the occurrence of seizures—most profoundly and studied at best—within the hippocampal network (Leite et al., 2002).

Among these changes, it appears that channels that are active near the resting membrane potential (RMP) such as K^+ or hyperpolarization-activated cyclic nucleotide-gated non-selective (HCN) channels are particularly intriguing candidates involved in epileptogenesis. With respect to the CA1 area in the pilocarpine model, there is evidence of persistent downregulation of $K_v4.2$ (Bernard et al., 2004), $K_{Ca}2.2$ (Schulz et al., 2012), and HCN1 (Jung et al., 2007, 2010). Importantly, these transcriptional changes partly seem to involve the activation of protein kinases or phosphatases (Bernard et al., 2004; Jung et al., 2010). In turn, protein kinase and/or phosphatase activation also seem to be involved in acute epileptic conditions (Jung et al., 2010; Kernig et al., 2012) suggesting that neuronal hyperactivity may trigger these enzymatic pathways.

Casein kinase 2 (CK2) is a widely expressed enzyme with a substantial number of possible targets; however, one of its major targets is calmodulin (CaM) and $K_{Ca}2.2$ (Bildl et al., 2004; Allen et al., 2007). We recently demonstrated that oral administration of the CK2 blocker 4,5,6,7-tetrabromotriazole (TBB) enhanced K^+ currents mediating the afterhyperpolarizing potential (AHP) in the pilocarpine model, and even more intriguing, blocked the occurrence of spontaneous epileptic activity in the acute slice model with Mg^{2+} removal (Brehme et al., 2014). This compound obviously exerted an anti-epileptogenic potential in the *in vitro* slice preparation, but is not an anti-seizure drug in this model *in vivo* (Bajorat et al., 2018). Therefore, we asked whether TBB might have disease modifying effects in the pilocarpine model *in vivo*, too. To this end, we treated the rats with TBB prior to pilocarpine-induced SE and analyzed the animals in their chronically epileptic stage.

MATERIALS AND METHODS

TBB Pretreatment and Pilocarpine-Induced Chronic Epilepsy

Male Wistar rats (27–30 days; Charles River, Sulzfeld, Germany) were treated with the CK2 inhibitor TBB (Tocris Bioscience, Bristol, United Kingdom or Sigma–Aldrich, Taufkirchen, Germany) 3 days before SE by intraperitoneal (i.p.) injection of 6 μmol/kg body weight [stock solution 6 mmol/l, dissolved in dimethylsulfoxide (DMSO), 1 μl/g body weight]. This was repeated for three times every 24 h (i.e., four consecutive daily injections, **Figure 1A**). The same amount of vehicle (DMSO, 1 μl/g body weight) was injected as control. Allocation of animals to the TBB or vehicle pretreatment group was performed in randomized fashion. Following the last of four injections, the animals were allowed to recover for one hour, before pilocarpine was injected to induce chronic epilepsy. During the TBB pretreatment period, the weight gain was monitored and did not differ significantly between TBB-treated (from 105 ± 18 to 131 ± 19 g, mean ± SD) and vehicle-treated (from 107 ± 19 to 133 ± 18 g, mean ± SD) animals (ANOVA).

Chronic epilepsy was induced by systemic pilocarpine injection 1 h after the last TBB application. As described previously (Kirschstein et al., 2007; Bajorat et al., 2011; Müller et al., 2013), rats received *N*-methyl scopolamine nitrate (1 mg/kg, i.p.) in order to reduce peripheral cholinergic effects, and then pilocarpine hydrochloride (340 mg/kg, i.p.). All pilocarpine-injected animals were carefully monitored to detect spontaneous motor seizures with progression into limbic SE. All stage 4 or 5 seizures (Racine, 1972) were registered for each individual animal to detect the latency to the first stage 4 or 5 seizure after pilocarpine. The onset of SE was determined when an animal had a stage 4 or 5 seizure (Racine, 1972) that was followed by continuous seizure motor activity without showing any reaction to sensory stimuli such as gently touching against the whiskers. SE was terminated after 40 min by administration of diazepam solution (Ratiopharm, Ulm, Germany, 5 mg/ml, i.p.). Finally, the rats were fed with 5% glucose solution for 1 day and kept in separate cages. Experimenters were blinded for all *in vivo* applications and observations, thus were unaware as to whether the animal was pretreated with TBB or vehicle (DMSO) before.

All procedures were performed according to national and international guidelines on the ethical use of animals (European Council Directive 86/609/EEC, approval of local authority LALLF M-V/TSD/7221.3-1.1-013/10 and 7221.3-1.1-019/13), and all efforts were made to minimize animal suffering and to reduce the number of animals used.

Video-EEG Recording and Video Monitoring

Epileptiform potentials in the electroencephalogram (EEG) were recorded using a telemetric system [Neuroscore 2.0, Data Science International (DSI), Arden Hills, MN, United States]. Electrode implantation (TA10EA-F20 or TA11CA-F40 from DSI) was performed as previously described (Bajorat et al., 2011, 2016, 2018). Video-EEG monitoring was performed in three TBB-treated pilocarpine-treated epileptic animals and four vehicle-treated epileptic rats under environmentally controlled conditions (12 h light/dark cycles, lights switched on from 6 a.m. to 6 p.m., 22 ± 2°C, and 40–60% relative humidity in an isolated room). Pilocarpine-treated rats were housed in individual cages and continuous video-EEG monitoring was performed using a telemetric system (Dataquest A.R.T. 4.2., DSI) in combination with a light and dark network camera (Axis 223M, Axis communications, Lund, Sweden). Night recordings were performed with a small blue night light for residual light intensification. The EEG was screened for epileptiform potentials (spikes, sharp waves, spike-and-wave-complexes, sharp-and-slow-wave-complexes) and seizures were detected by concomitant analysis of the video signal (Bajorat et al., 2011, 2016). The EEG experimenter was blinded to the treatment (TBB versus vehicle).

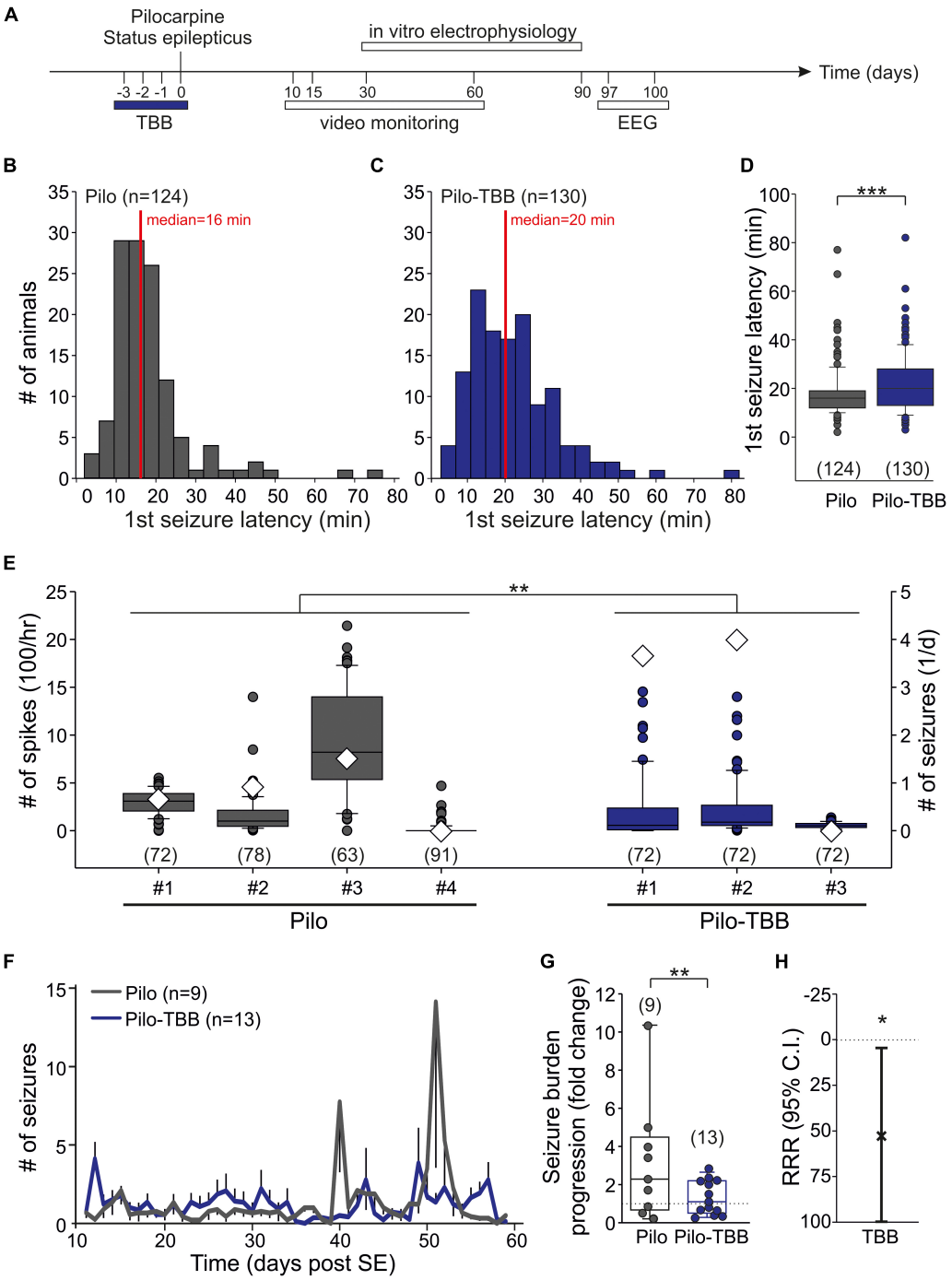

FIGURE 1 | CK2 inhibition exerts disease modifying properties. **(A)** Time frame of the experiment. TBB was administered four times *in vivo* on days "−3" (i.e., 3 days before status epilepticus) through "0" (i.e., day of pilocarpine-induced status epilepticus). All experiments thereafter were performed during the chronic stage of recurrent seizures. **(B–D)** Latency to the first stage 4 or 5 seizure after pilocarpine injection in vehicle-pretreated **(B)** and TBB-pretreated **(C)** rats. The median latency was significantly (***$P < 0.001$, Mann-Whitney U-test) prolonged in the TBB-pretreated group **(D)**. **(E)** Number of interictal spikes per hour (left *y*-axis) in the electroencephalogram (EEG) during 3 days (97–100 post-SE). Note that the number of daily seizures during this period is also depicted (diamonds, right *y*-axis). There was a significant group effect of TBB pretreatment (**$P < 0.01$, two-way ANOVA with Tukey *post hoc* test). **(F)** Number of generalized seizures (at least stage 3) at daylight (from 06:00 to 18:00 h) for both animal groups as grand average for the entire recording period. **(G)** Seizure burden progression as fold change of seizure rates during epileptogenesis. The variability was significantly reduced in TBB-pretreated epileptic animals (**$P < 0.01$, *F*-test). **(H)** Relative risk reduction (RRR) of seizure progression by TBB pretreatment was significant (*$P < 0.05$, *t*-test).

In addition, we performed video analysis in order to detect generalized seizures (13 TBB-treated and nine vehicle-treated epileptic rats) for 7 weeks (10–60 days after pilocarpine-induced SE, i.e., 5–12 weeks of age). All generalized seizures (stage 4–5, Racine, 1972) at daylight (from 6 a.m. to 6 p.m.) were detected in a blinded fashion, i.e., without knowledge about the treatment (TBB versus vehicle). Control animals, i.e., animals that received saline instead of pilocarpine, were repeatedly reported to get no spontaneous seizures at all (Bajorat et al., 2011, 2016) and were therefore not included in these *in vivo* studies. The seizure burden progression was calculated as the ratio of seizure rate day 35–59 over the seizure rate day 11–20. The relative risk reduction (RRR) of seizure burden progression was calculated as 1 – the relative risk (seizure burden progression in the TBB-pretreated animal over the seizure burden progression in the vehicle-pretreated group).

Tissue Preparation

Hippocampal slices were prepared using 8–12-week-old animals (i.e., 4–8 weeks after SE). At this age, chronically epileptic animals show on average 4.5 seizures per day (Bajorat et al., 2011). After deep anesthesia with diethyl ether (Merck, Darmstadt, Germany), rats were decapitated and the brain was rapidly removed and submerged into oxygenated ice-cold dissection solution containing (in mM) 125 NaCl, 26 $NaHCO_3$, 3 KCl, 1.25 NaH_2PO_4, 0.2 $CaCl_2$, 5 $MgCl_2$, and 13 D-glucose (95% O_2, 5% CO_2; pH 7.4; osmolality 306–314 mosmol/kg H_2O). Hippocampal horizontal brain slices (400 μm) were prepared from the brain using a vibratome (Leica VT1200S, Wetzlar, Germany), and these slices were gently transferred into a holding chamber containing artificial cerebrospinal fluid (ACSF) of the following composition: (in mM) 125 NaCl, 26 $NaHCO_3$, 3 KCl, 1.25 NaH_2PO_4, 2.5 $CaCl_2$, 1.3 $MgCl_2$, and 13 D-glucose (95% O_2, 5% CO_2; pH 7.4; osmolality 306–314 mosmol/kg H_2O).

For electrophysiological experiments, hippocampal slices were allowed to recover at room temperature (20–22°C) for at least 1 h before being transferred into recording chamber. For quantitative real-time reverse transcriptase PCR (RT-PCR) analyses, hippocampal slices were immediately dissected into mini-slices. For Timm staining, hippocampal slices were immediately immersed into Na_2S solution.

Electrophysiological Experiments

Extracellular Recordings

After recovery, hippocampal slices were placed into an interface chamber continuously bathed with ACSF at a flow rate of 2 ml/min using a volumetric infusion pump (MCM-500, MC Medicine technique GmbH, Alzenau, Germany). Bath temperature was maintained at 32 ± 1°C by (npi electronic GmbH, Tamm, Germany), and all experiments started after an equilibration time of at least 30 min. Schaffer collateral fibers were stimulated using bipolar platinum wire electrodes connected to an A365 stimulus isolator in constant-current mode (Word Precision Instruments, Friedberg, Germany) and driven by the Master-8 stimulator (A.M.P.I., Jerusalem, Israel). The stimulating electrode was placed into stratum radiatum at the border between CA2 and CA1. Field excitatory postsynaptic potentials (fEPSPs) from the CA1 area were recorded using borosilicate glass pipettes (2–3 MΩ, pulled with PIP5 from HEKA Elektronik, Lambrecht, Germany; filled with ACSF). Data were acquired using a Micro1401 A/D converter and signal 2.16 software (CED, Cambridge Electronic Design, Cambridge, United Kingdom). The fEPSP slope was determined as the local minimum of the differentiated fEPSP curve indicating the maximal negative gradient during its falling phase. With these extracellular recordings, we obtained the input–output curve, the paired-pulse ratio (PPR) with an interstimulus interval of 40 ms and short-term plasticity data.

Patch-Clamp Experiments

Patch pipettes with a tip resistance 3–6 MΩ were pulled from borosilicate glass capillaries (GB150-8P; Science Products GmbH, Hofheim, Germany) using a horizontal electrode puller (P-97 Micropipette Puller; Sutter Instrument Company, Novato, CA, United States) and filled with an intracellular solution (K^+ gluconate 140, $MgCl_2$ 2, HEPES 10, phosphocreatine 10, Na_2-ATP 2, Na_2-GTP 0.4, pH 7.3 adjusted with KOH, osmolality 290–300 mosmol/kg H_2O). Whole-cell patch-clamp recordings from visualized CA1 pyramidal cells were performed in the slice as previously described (Müller et al., 2013) at room temperature using an upright microscope (Nikon Eclipse FN1, Düsseldorf, Germany) and a standard amplifier (ELC-03XS, npi electronic, Tamm Germany, run with signal 2.16 software, CED).

Signals were low-pass filtered at 2 kHz and digitized at a sampling frequency of 4 kHz. Only cells with an RMP of −50 mV or more negative were included in this study. The AHP-mediating K^+ current and charge transfer were measured in the voltage-clamp mode as previously described (Brehme et al., 2014). In brief, the recording solution contained 500 nM tetrodotoxin (TTX) and 1 mM tetraethylammonium (TEA) (both from Tocris Bioscience, Bristol, United Kingdom) to block voltage-activated Na^+ and K^+ channels, respectively. AHP-mediating currents were elicited by a depolarizing voltage command from the holding potential −60 to +60 mV for 100 ms, followed by a step to −120 mV for 2 ms and a return to −60 mV for 2800 ms. The medium AHP (mAHP) was determined as the peak outward current during the first 400 ms following the short hyperpolarizing step to −120 mV (2 ms) and normalized to cell capacitance. The slow component of the AHP (sAHP) was assessed by determining the charge transfer, i.e., the area under the curve (AUC), for the interval between 400 and 2400 ms (i.e., 2000 ms), also normalized to cell capacitance. Low and fast capacitive current transients as well as leak currents were fully compensated and monitored (Cf and Cs). Series resistance ranged from 4 to 15 MΩ and was monitored at regular intervals throughout the experiments.

Intracellular Recordings

Intracellular recordings were performed in CA1 pyramidal cells impaled with borosilicate glass microelectrodes (80–120 MΩ, pulled with Sutter P-97 and filled with 3 M potassium acetate and 0.013 M KCl) using an SEC-10LX amplifier (npi electronic). In these recordings, RMP, membrane

resistance, and membrane time constant were determined. The membrane resistance was calculated as the slope of the steady-state current–voltage curve obtained by hyperpolarizing current injection (ranging from −1.0 to −0.2 nA for 400 ms). The membrane time constant was calculated as the average time constant during the hyperpolarizing steps. Subsequent depolarizing current injection (from + 0.1 to + 0.5 nA) was used to evoke a train of action potentials (400 ms). The AHP following this prolonged depolarization (referred to as train-AHP) was calculated as the difference between the train-AHP peak amplitude and the RMP (for which the last sweep with + 0.5 nA depolarization was used). In addition, burst firing was tested with short depolarizing current steps (duration 3–7 ms, from + 0.5 to + 2.4 nA). Unless otherwise indicated, chemicals were purchased from Sigma–Aldrich (Taufkirchen, Germany).

Quantitative Real-Time Reverse Transcriptase PCR Analyses

Hippocampal horizontal slices were immediately transferred into ice-cold phosphate-buffered saline (PBS, pH = 7.4, PAA Laboratories GmbH, Austria), and the CA1 region was dissected out (referred to as mini-slice) under a binocular microscope (Leica). All mini-slices from one animal (n = 6–8) were pooled and immediately frozen in liquid nitrogen. For mRNA isolation, TRIZOL reagent was used, and total RNA was reverse-transcribed using Moloney murine leukemia virus reverse transcriptase (final concentration [Cf] = 10 U/µl) and RNasin Plus RNase inhibitor (Cf = 2 U/µl, both Promega Corporation, Madison, WI, United States) in the presence of random hexamers (Cf = 0.01 µg/µl) and dNTP Mix (Cf = 0.5 nmol/µl each, Invitrogen, Carlsbad, CA, United States). For the real-time PCR of the target genes (K_{Ca}2.2, HCN1, HCN2, HCN3, and HCN4) as well as three standard reference genes (phosphoglycerate kinase 1, S18 ribosomal protein, 18S rRNA), we used the QuantiFast SYBR Green PCR Kit (concentration as recommended by the manufacturer, Qiagen Inc., Valencia, CA, United States). The mastermix was aliquoted, cDNA (Cf = 0.5 ng/µl) and primers (Cf = 0.5 pmol/µl; TIB Molbiol, Berlin, Germany) were added.

Real-time PCRs were performed using the ep mastercycler (software realplex 2.2, Eppendorf, Hamburg, Germany) with cycling parameters as follows: 95°C for 5 min once, followed by 95°C for 15 s and 60°C for 15 s, with normalized fluorescence read at 68°C (530 nm) for 40 cycles. To confirm single product amplification, melting curve analysis and gel electrophoresis were done. Expression levels of ion channel mRNA were normalized to all three housekeeping genes (TIB Molbiol, Berlin, Germany) and analyzed by $2^{-\Delta\Delta Ct}$ method (i.e., normalized to control levels).

Western Blot

For CK2 western blot analysis, six control and six epileptic TBB-pretreated animals were used at age 133/134 days. Pools of mini-slices, each for CA1, CA3, and DG area from individual animals were subjected to protein extraction with RIPA buffer [50 mM Tris, 150 mM NaCl, 1% (v/v) TritonX-100, 1% (w/v) sodium deoxycholate, 0.1% (w/v) SDS, 1 mM EDTA] in the presence of Complete protease inhibitor cocktail (Roche). After centrifugation at 14,000 g at 4°C for 20 min, 10 µg of total proteins from each sample were separated by 10% SDS-PAGE and blotted onto a PVDF membrane (Immobilon-FL; Millipore). Primary antibody incubation (mouse monoclonal anti-CK2, 1:2000) was done overnight at 4°C and secondary antibody incubation (goat anti-mouse IRDye 680RD, Odyssey, 1:5000) was done for 30 min at room temperature. A single specific protein band was visualized with the Odyssey infrared imaging scanner from Li-cor.

For quantification purposes, GAPDH was used as an internal control for CK2 normalization. Briefly: after CK2 detection, membranes were washed 15 min at 55°C with a buffer (pH 2.2) containing 1.5% glycine, 0.1% SDS, 1% Tween 20 to remove any bound anti-CK2 antibody. Then, according to CK2 immunoreaction, the rabbit monoclonal anti-GAPDH primary antibody (Cell Signaling; 1:5000) and a secondary antibody (goat anti-rabbit IRDye 800CW, Odyssey; 1:5000) was loaded. For each sample, CK2 and GAPDH fluorescence signals were determined with Image Studio lite software (Li-cor) and the ratio between CK2 and GAPDH was calculated.

Mossy Fiber Sprouting Analysis

Timm staining (Timm, 1958) which typically demonstrates the zinc-containing mossy fibers was done for confirmation of mossy fiber sprouting (MFS) using a previously published protocol (Müller et al., 2014). After incubation the brain section in disodium sulfide solution (9.7 mM Na_2S, 19.8 mM NaH_2PO_4, in 500 ml distilled H_2O) the sections were fixed in glutaraldehyde solution (100 ml PBS 0.15 M; 1.2 ml 25% glutaraldehyde) for 10 min and subsequently placed in a 30% sucrose solution at 4°C until the brain pieces sank to the bottom of the chamber. Transversal cryosections were cut at 20 µm using a freezing microtome (Leica CM 3050S, Leica Microsystems, Wetzlar, Germany). After washing for 15 min with PBS, the sections were processed in the dark for 30 min in developer solution (80 ml distilled H_2O; 120 ml gum arabicum; 132.7 mM citric acid; 120.7 mM sodium citrate; 154.4 mM hydroquinone; only in the dark: 0.16 mM $AgNO_3$ in distilled H_2O) and washed with distilled H_2O. After short incubation with the stop solution (63.25 mM $Na_2S_2O_3$ in distilled H_2O), the sections were again washed with distilled H_2O. Finally, the nuclei were counter-stained (8.17 mM toluidine blue and 49.7 mM $Na_2B_4O_7$ in distilled H2O). Following washing, the sections from the hippocampi were dehydrated in alcohol and mounted on slides with slide mounting medium (Fluoromount-G™, Beckman-Coulter, Fullerton, CA, United States).

Mossy fiber sprouting was assessed as previously reported (Müller et al., 2014). Briefly, we used a semi-quantitative classification scheme performed by one investigator (TR) blinded with respect to other data as well as to the vehicle or TBB pretreatment (0 = no staining, 1 = patches of staining in the inner molecular layer, 2 = confluent staining, 3 = massive staining). Second, a morphometric analysis measuring the brownish-colored area within the inner molecular layer (MFS area) normalized to the granule cell area in the same slice to produce an MFS ratio (mean values of three sections per animal).

Statistical Analysis

Unless otherwise indicated, data were expressed as mean values ± the standard error of the mean (SEM). For statistical comparisons, however, data were tested for normal distribution, and then analyses were performed using the appropriate test as indicated. The level of significance was set to $P < 0.05$, and significant differences were indicated with asterisks in all figures ($^{*}P < 0.05$, $^{**}P < 0.01$, $^{***}P < 0.001$).

RESULTS

TBB Exerts Anti-epileptogenic Properties *in vivo*

The aim of this study was to investigate the acute and long-term effect of CK2 inhibition *in vivo* on the pilocarpine-induced SE and the post-SE chronic epilepsy. To this end, we administered TBB three days before pilocarpine-induced SE, i.e., four consecutive injections (**Figure 1A**). One hour after the last TBB injection, we started the pilocarpine procedure. Roughly 85% of the animals developed stage 4 or 5 seizures after a single pilocarpine injection. The proportions of rats developing seizures were not influenced by TBB pretreatment (**Table 1**). In contrast, the median latency of the first stage 4 or 5 seizure after pilocarpine was significantly prolonged from 16 min (**Figure 1B**) in vehicle-pretreated rats to 20 min in TBB-pretreated animals ($P < 0.001$, Mann–Whitney *U*-test; **Figures 1C,D**). Other parameters such as number of seizures before SE, diazepam dose, SE rate, and mortality did not differ between both groups (**Table 1**). Hence, TBB pretreatment prolonged the latency to the first generalized seizure, but did not alter SE rate or mortality.

Next, we asked whether pretreatment with TBB could influence epileptogenesis and thus we analyzed animals in their chronic stages of TLE, i.e., at a time-point of fully established epileptogenesis. To this end, we implanted a telemetric EEG system and counted the number of spikes/hour within 3 days (97–100 days post-SE; see timescale in **Figure 1A**) of four vehicle-pretreated and three TBB-pretreated epileptic animals. Overall, we found 314 ± 25 spikes/hour in vehicle-pretreated rats (in 304 animal hours), which was significantly higher than 168 ± 19 spikes/hour in TBB-pretreated rats (in 216 animal hours; $P < 0.01$, two-way ANOVA followed by Tukey test; **Figure 1E**). During this period, we detected 32 generalized seizures (23 in TBB-pretreated and nine in vehicle-pretreated animals; see diamonds in **Figure 1E**). Hence, the interictal spike counts were quite representative and not taken from a period with increased seizure rate. Since the clinical course of chronic epilepsy in this model is often associated with an increasing seizure rate and also with seizure clustering (Bajorat et al., 2011, 2016, 2018), this short-term analysis of EEG-detected seizures cannot reflect seizure burden and hence is insufficient to study the TBB effect.

Therefore, we performed a long-term video analysis of daytime seizures from nine vehicle-pretreated and 13 TBB-pretreated littermates for 7 weeks covering the full period of epileptogenesis (10–60 days after SE; **Figures 1F–H**). Over this period, vehicle-pretreated animals showed 1.3 ± 1.0 seizures/12 h ($n = 9$) during daylight, i.e., between 6 a.m. and 6 p.m., consistent with previous data (Bajorat et al., 2011, 2016, 2018). TBB-pretreated littermates showed the same overall seizure rates (1.3 ± 1.3 seizures/12 h, $n = 13$), but developed gross changes in seizure rates during the second half of the observation period (**Figure 1F**). Seizure clusters were present in 6/9 vehicle-pretreated animals, but only in 4/13 TBB-pretreated epileptic animals ($P = 0.096$, χ^2 test). Disease progression assessed as the ratio of seizure rate during the second half of observation period over the baseline seizure rate was substantially higher in the vehicle-pretreated group as compared to TBB-pretreated animals (314 ± 99% versus 133 ± 24%, $P = 0.062$, *t*-test). Moreover, and probably more importantly, seizure rate variability was significantly reduced by TBB pretreatment ($P < 0.01$, *F*-test; **Figure 1G**), indicating that the seizure burden was stabilized in the cohort of TBB-treated epileptic rats. Overall, we observed a significant RRR of seizure burden by 58% (95% confidence interval 4–100%, $P < 0.05$, *t*-test, **Figure 1H**) indicating that disease progression following SE was slowed down in TBB-pretreated epileptic animals.

Next, we asked whether this disease modifying effect was associated with a reduced MFS, which is a pathological hallmark of TLE and commonly observed in this model (Schulz et al., 2012). However, MFS in TBB-pretreated epileptic rats did not differ from MFS in vehicle-pretreated epileptic animals (**Figure 2**).

TBB Facilitates Short-Term Synaptic Plasticity in Epileptic Animals

Our data so far indicate that *in vivo* TBB pretreatment affects pilocarpine-induced SE and exerts disease modifying properties during epileptogenesis. Since TBB was not continued after SE, we hypothesized that TBB leads to persistent changes in the epileptic, but probably also in the control tissue. In order to address this issue, we first analyzed extracellular field potentials in control and post-SE tissue, both taken from either vehicle- or TBB-pretreated animals. Basic properties of synaptic transmission such as input–output curves or paired-pulse plasticity were not altered by TBB (**Figures 3A–C**). In contrast, short-term plasticity protocols of five stimuli at increasing frequencies showed significantly higher potentiation in TBB-pretreated epileptic animals as compared to both vehicle-pretreated epileptic tissue as well as tissue from control rats (both comparisons: $P < 0.05$, three-way ANOVA followed by Holm–Sidak test; **Figure 3D**; no significant interaction between stimulus number and animal group or between stimulus number and pretreatment). After delivering the short-term plasticity protocols, the field potentials were significantly increased in tissue from TBB-pretreated epileptic animals ($P < 0.05$ versus baseline, Wilcoxon signed rank test; **Figure 3E**) indicating that some degree of long-term plasticity might have been elicited by these short protocols. Concomitantly with this potentiation, the PPR was significantly reduced ($P < 0.05$, Wilcoxon signed rank test; **Figure 3F**) suggesting presynaptic mechanism for this plasticity-facilitating effect of TBB in tissue from chronically epileptic rats. These

TABLE 1 | Status epilepticus (SE) *in vivo* data in vehicle-pretreated and TBB-pretreated epileptic animals.

	Vehicle-pretreated epileptic rats (Pilo)	TBB-pretreated epileptic rats (Pilo-TBB)
# of stage 4 or 5 seizures before SE	2.4 ± 0.1 (n = 124)	2.5 ± 0.1 (n = 130)
Latency of SE (min)	27.4 ± 1.5 (n = 69)	31.0 ± 1.9 (n = 79)
Diazepam dose (mg)	3.6 ± 0.2 (n = 69)	3.4 ± 0.1 (n = 79)
SE rate	69/146 (47.3%)	79/157 (50.3%)
Died before/during SE	43/146 (29.4%)	36/157 (22.9%)
Non-responder to Pilo	34/146 (23.3%)	42/157 (26.8%)

There were no significant differences between both groups (Mann–Whitney U-test and χ^2 test, respectively).

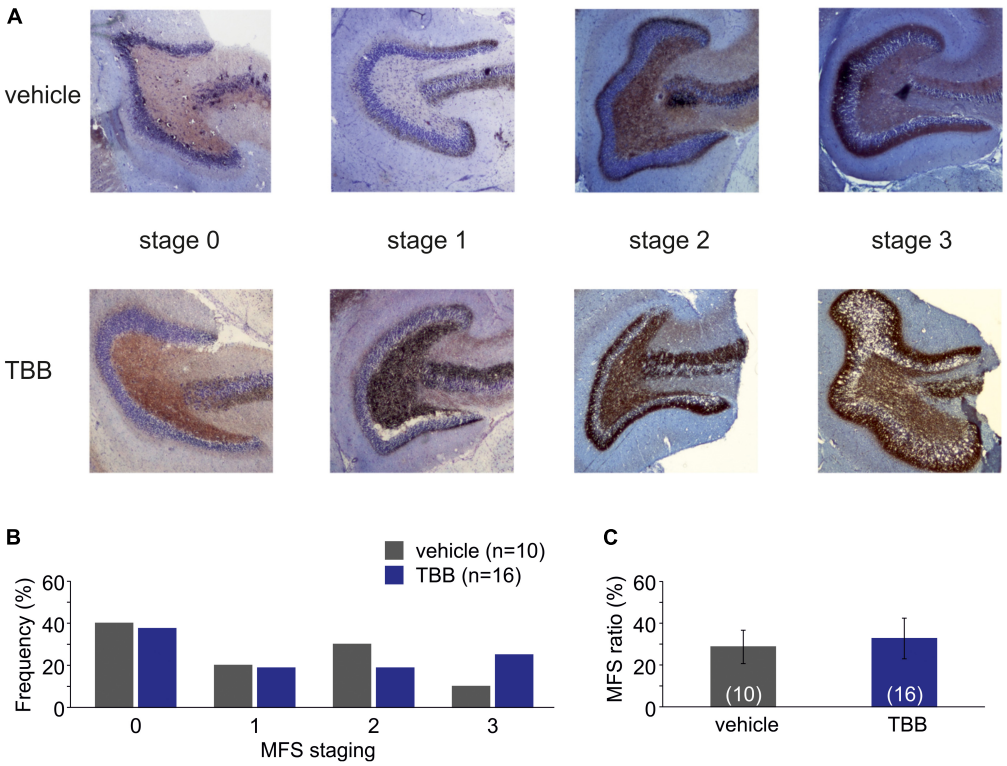

FIGURE 2 | Mossy fiber sprouting (MFS). **(A)** Photomicrographs from vehicle-pretreated epileptic animals (upper row) and TBB-pretreated epileptic animals (lower row) demonstrate the MFS stages 0–3. **(B)** Relative frequencies of MFS stages 0–3 in vehicle- and TBB-pretreated animals. **(C)** MFS ratio (MFS area divided by granule cell area) in both experimental groups.

results demonstrate that TBB may lead to persistent changes in the synaptic network of the CA1 area which may be even more pronounced in epileptic than in control tissue.

TBB Reduces the Number of Burst Firing Neurons in CA1

One hallmark of chronically epileptic tissue is the presence of burst firing neurons, especially in CA1 (Chen et al., 2011). To study this issue in more detail, we performed intracellular recordings from CA1 neurons in vehicle- or TBB-pretreated control and epileptic animals. A typical burst firing behavior is depicted in **Figure 4A**, obtained from a neuron of a vehicle-pretreated animal (upper trace in gray), showing three action potentials for the lowest suprathreshold depolarizing current injection. In contrast, a regular firing behavior is shown in the lower trace in **Figure 4A** (blue trace), taken from a TBB-pretreated animal. Burst firing was observed in 4/9 neurons from vehicle-pretreated epileptic animals, but in 0/7 neurons from TBB-pretreated epileptic animals ($P < 0.05$, χ^2 test; **Figure 4B**). In control rats (either vehicle- or TBB-pretreated), no burst firing neurons were observed (**Figure 4B**).

Bursting behavior may be the consequence of a prolonged afterdepolarizing potential (ADP; Chen et al., 2011). We therefore determined the AUC of the ADP starting at 5 ms after the depolarizing step (**Figure 4C**). The duration of the depolarizing step ("d" in **Figures 4C,D**) was set to 3, 5, and 7 ms, and the ADP was significantly larger in the vehicle-pretreated epileptic group as compared to both TBB-pretreated epileptic and control groups ($P < 0.05$, three-way ANOVA; **Figure 4D**). Taken

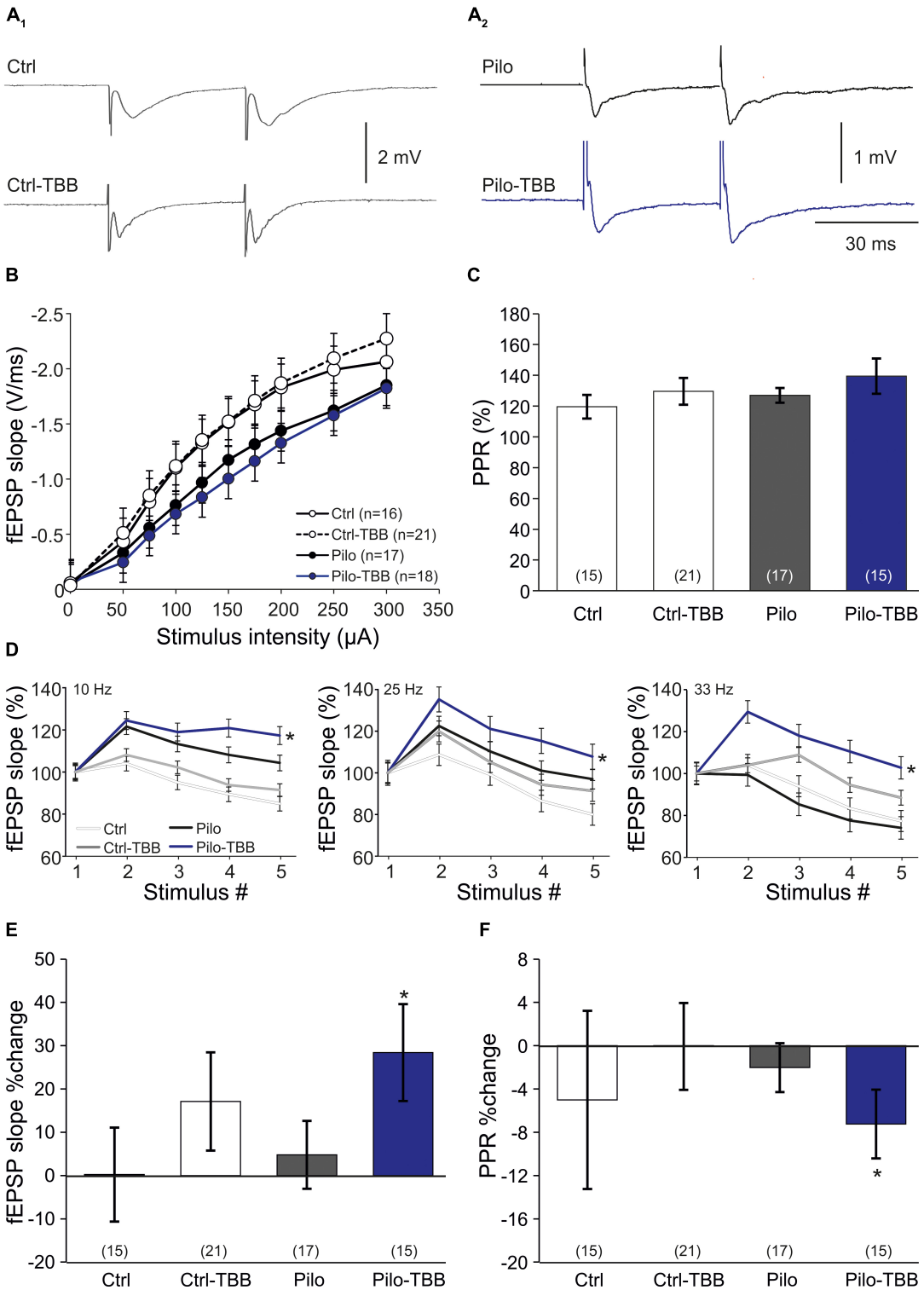

FIGURE 3 | CK2 inhibition facilitates CA1 plasticity. **(A)** Sample traces of CA1 stratum radiatum field excitatory postsynaptic potentials (fEPSP) following Schaffer collateral stimulation in control (A_1) and epileptic animals (A_2). **(B)** Input–output curves of all four groups without significant group differences. **(C)** Paired-pulse ratios (PPRs) were similar among all four experimental groups. Short-term plasticity during five stimuli at frequencies of 10, 25, and 33 Hz **(D)**, and subsequent changes of fEPSP slope **(E)** and PPR **(F)** after this short-term plasticity paradigm. Only slices from the TBB-pretreated epileptic group showed significantly facilitated plasticity. *$P < 0.05$.

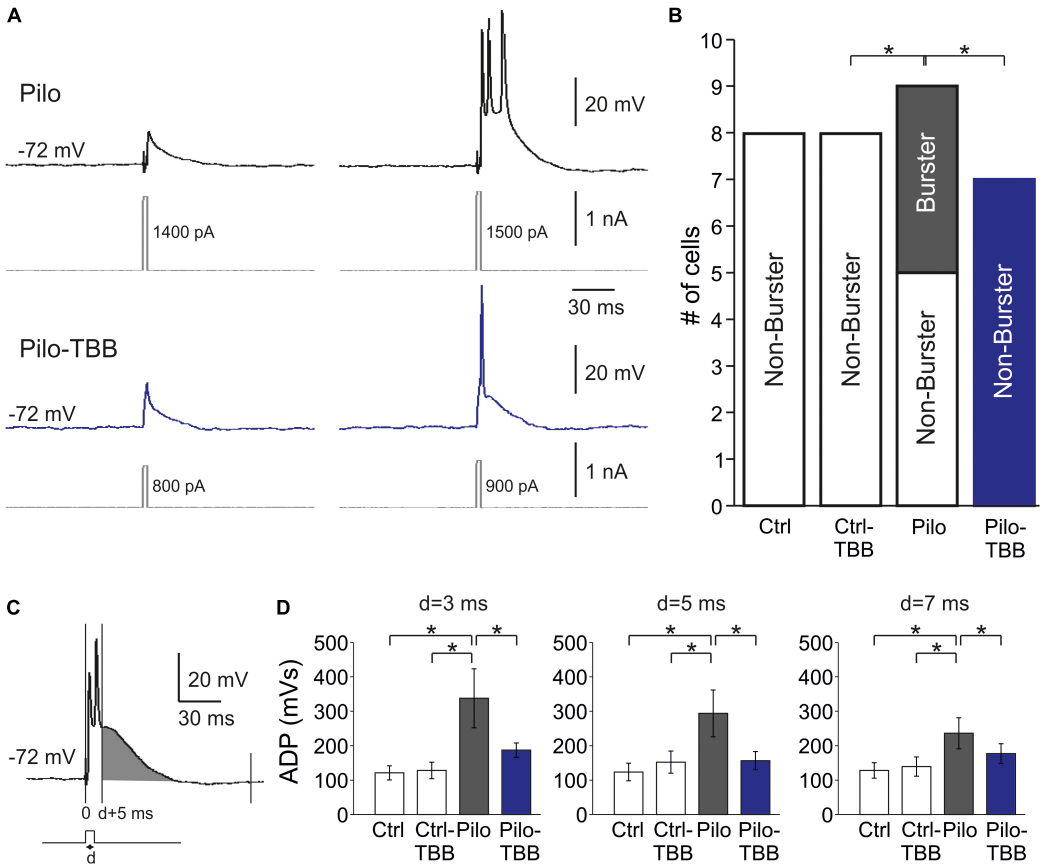

FIGURE 4 | CK2 inhibition reduces bursting in CA1. **(A)** Sample traces of CA1 pyramidal cell intracellular recordings from a vehicle-pretreated epileptic rat (Pilo, black traces) and a TBB-pretreated epileptic rat (Pilo-TBB, blue traces). Note the bursting of the upper traces upon just suprathreshold stimulation. **(B)** Proportions of burster and non-burster neurons in the four experimental groups (*$P < 0.05$). **(C,D)** Afterdepolarizing potential (ADP) with different pulse durations ($d = 3, 5, 7$ ms). The area under curve of the ADP (starting from $d + 5$ ms, indicated in gray in **C**) of cells from vehicle-pretreated epileptic animals (Pilo) was significant against the ADP of all other experimental groups (*$P < 0.05$, three-way ANOVA with Tukey *post hoc* test).

together, pilocarpine-induced SE caused a significant increase in ADP size probably involved in burst firing behavior which in turn was restored by TBB pretreatment *in vivo* prior to SE.

TBB Modifies $K_{Ca}2$ Channel Function

The significant reduction of the number of burst firing neurons in the epileptic CA1 after TBB pretreatment following ADP normalization is an attractive molecular mechanism for the observed disease modifying properties *in vivo*. Since we previously demonstrated that $K_{Ca}2.2$ was downregulated in isolated CA1 neurons from chronically epileptic tissue and TBB administered during chronic epileptic stages enhanced $K_{Ca}2.2$ levels in CA1 from post-SE animals (Schulz et al., 2012; Bajorat et al., 2018), we first performed patch-clamp recordings from visualized CA1 pyramidal neurons in hippocampal slices and confirmed the impaired function of $K_{Ca}2$ by recording the mAHP-mediating current density (0.26 ± 0.06 pA/pF, $n = 7$ versus 1.19 ± 0.38 pA/pF, $n = 4$, $P < 0.05$, unpaired *t*-test, **Figure 5A**) as previously reported in isolated cells (Schulz et al., 2012). Pretreatment with TBB prior to SE significantly enhanced the mAHP current density (0.92 ± 0.18 pA/pF, $n = 14$, $P < 0.05$, unpaired *t*-test; **Figure 5A**) suggesting that TBB might indeed enhance $K_{Ca}2$ function. We next analyzed the sAHP, for which the underlying ion channels are less clearly determined, but do not seem to involve $K_{Ca}2$ (Bond et al., 2004; Villalobos et al., 2004; Pedarzani et al., 2005). Consistent with this, the sAHP charge transfer as assessed by determining the AUC of the sAHP-mediating current density was significantly reduced in CA1 neurons from chronically epileptic rats as compared to control tissue ($P < 0.05$, two-way ANOVA), but without any significant TBB effect (**Figure 5B**).

From these findings so far, it is conceivable that $K_{Ca}2$ function is reduced in chronically epileptic CA1 neurons, and we speculated that TBB might upregulate $K_{Ca}2.2$ gene expression (Bajorat et al., 2018). We, therefore, performed real-time RT-PCR and, as expected, $K_{Ca}2.2$ mRNA was significantly upregulated in TBB-pretreated control animals ($P < 0.05$, ANOVA and Duncan *post hoc* test; **Figure 5C**). More importantly, in TBB-pretreated animals, SE was associated with a significant reduction of $K_{Ca}2.2$ expression as previously observed (Schulz et al., 2012; $P < 0.05$, ANOVA and Duncan *post hoc* test; **Figure 5C**). However, mRNA levels of $K_{Ca}2.2$ were not different between Pilo

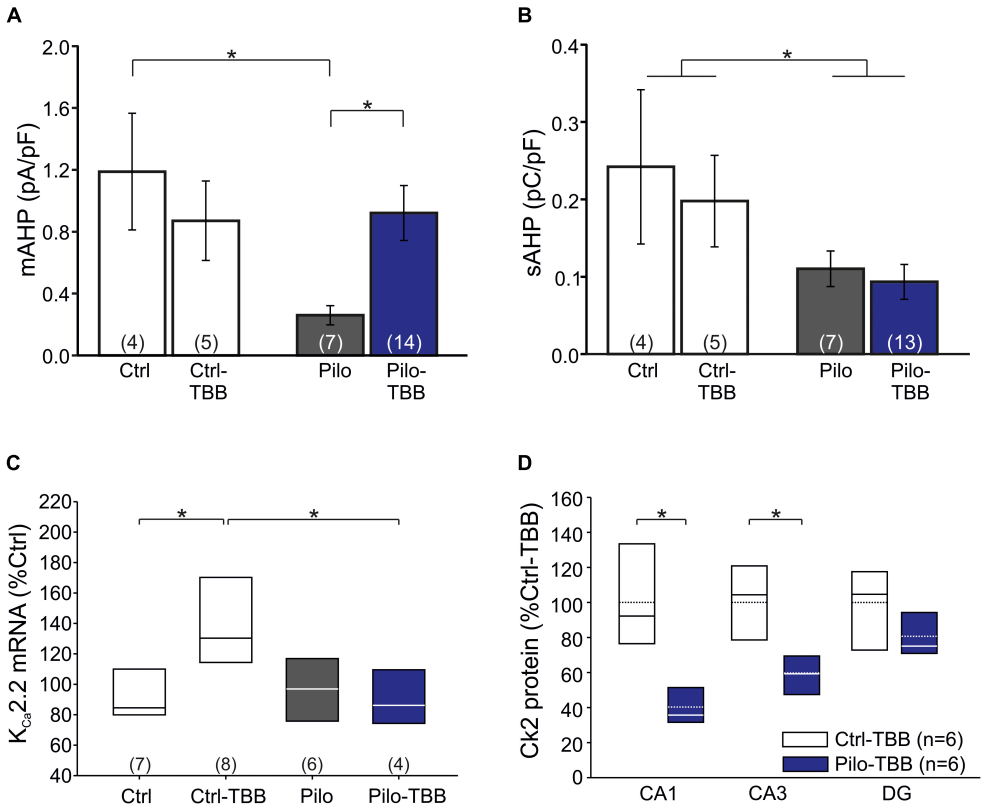

FIGURE 5 | CK2 inhibition modifies KC2 function. **(A)** Bar graph of the mAHP-mediating current in all four experimental groups. CA1 cells from vehicle-pretreated epileptic animals (Pilo) showed significantly less mAHP currents than control cells and cells from TBB-pretreated epileptic animals. **(B)** The sAHP charge transfer is significantly smaller in epileptic animals than in controls. TBB has no effect on the sAHP charge transfer. **(C)** Quantitative RT-PCR analysis of the CA1 subfield reveals that tissue from TBB-pretreated control animals contained significantly more $K_{Ca}2.2$ mRNA than vehicle-pretreated controls and TBB-pretreated epileptic rats. **(D)** Western blot analysis of CK2 protein in TBB-pretreated tissue. Note the region-specific differences between control and epileptic tissues. *$P < 0.05$.

and Pilo-TBB groups. Hence, the TBB effect on the mAHP in epileptic tissue cannot be explained by simple upregulation of $K_{Ca}2.2$ in CA1 neurons. Based on the idea that $K_{Ca}2.2$ function is reduced by CK2 activity (Bildl et al., 2004; Allen et al., 2007), we performed Western blotting of CK2 protein in six control and six epileptic TBB-pretreated animals (**Figure 5D**). These analyses indeed showed a region-specific lack of CK2 protein in epileptic animals which was most pronounced in CA1 (40 ± 5% of Ctrl-TBB tissue, $P < 0.002$, *t*-test; **Figure 5D**) suggesting a persistent downregulation of this enzyme in this area as a potential mechanism for the disease modifying effect.

TBB Modifies HCN Channel Function

The findings so far point to an impaired function of $K_{Ca}2$ in the epileptic CA1 area. Nonetheless, some data appeared inconclusive. Therefore, we asked whether the AHP which is a prominent $K_{Ca}2.2$ function (Hotson and Prince, 1980; Bond et al., 2004) might be altered following SE and TBB pretreatment. To this end, we performed intracellular recordings from CA1 pyramidal cells in vehicle- and TBB-pretreated epileptic and control animals (**Figure 6A**). Basic passive membrane properties such as RMP, membrane resistance and time constant were not different in these four groups (**Table 2**). With respect to the AHP, we found that the AHP following a train of action potentials (train-AHP) was significantly reduced in epileptic CA1 neurons (−4.2 ± 0.6 mV, $n = 10$ versus −6.8 ± 1.0 mV, $n = 9$, $P < 0.05$, two-way ANOVA with Tukey *post hoc* test; **Figures 6A,B**) consistent with a previous report (Schulz et al., 2012). However, TBB pretreatment had no significant effect on these values (**Figure 6B**). Instead, we observed a prominent voltage sag in the individual voltage traces in cells from controls (gray traces in **Figure 6A**) as well as TBB-pretreated epileptic rats (blue traces in **Figure 6A**), but not from vehicle-pretreated epileptic rats (black traces in **Figure 6A**) suggesting that TBB might modify HCN channel function. Indeed, there was a significant enhancement of the voltage sag following TBB pretreatment in both control (3.0 ± 1.4 mV, $n = 10$ versus 2.1 ± 1.0 mV, $n = 10$, $P < 0.05$, two-way ANOVA with Tukey *post hoc* test; **Figure 6B**) and epileptic animals (3.1 ± 2.9 mV, $n = 9$ versus 2.0 ± 2.1 mV, $n = 10$, two-way ANOVA with Tukey *post hoc* test; **Figure 6B**). Thus, we repeated the gene expression analysis with all HCN isoforms (HCN1-4; **Figures 6C–F**). In control animals, TBB led to differential alteration of HCN transcription with a significant upregulation of HCN1 (288 ± 27%, $n = 8$, $P < 0.05$, ANOVA with Duncan *post hoc* test; **Figure 6C**) and concomitantly, a significant downregulation of HCN3 (51 ± 10%, $n = 8$, $P < 0.05$,

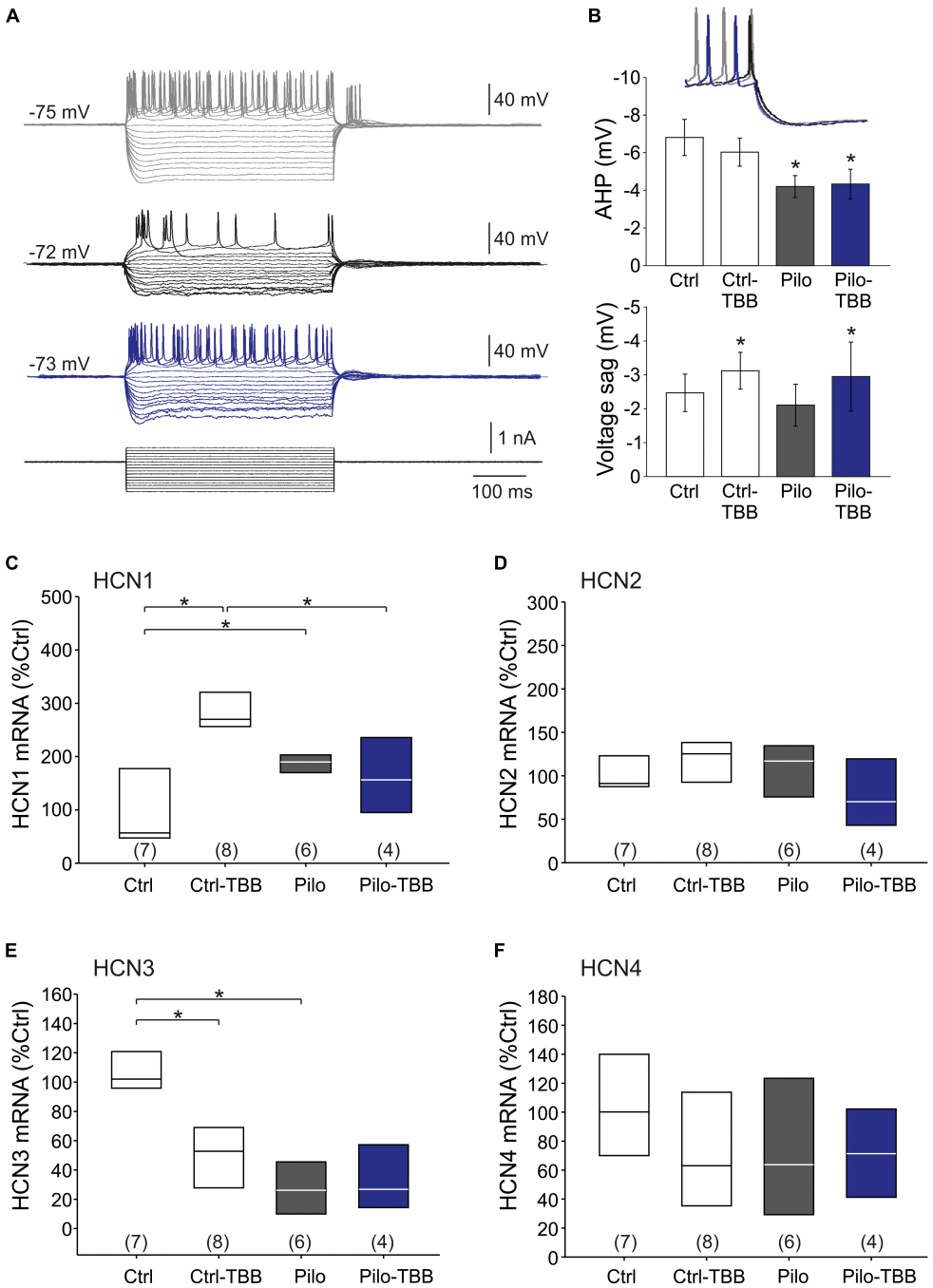

FIGURE 6 | CK2 inhibition modifies HCN channel function. **(A)** Sample traces of the membrane potential following hyperpolarizing and depolarizing pulse steps in intracellular recordings from CA1 neurons (gray: control, black: vehicle-pretreated epileptic, blue: TBB-pretreated epileptic). **(B)** Bar graphs of the train-AHP amplitude and voltage sag obtained from recordings shown in **A**. The train-AHP was significantly smaller in epileptic tissues regardless of the treatment with TBB. In contrast, the voltage sag was enhanced in TBB-pretreated tissue from both control and epileptic animals. Quantitative RT-PCR analysis of the CA1 subfield of all four HCN channel isoforms revealed significant and inverse expression changes for HCN1 **(C)** and HCN3 **(E)**, but no changes for HCN2 **(D)** and HCN4 **(F)**. *$P < 0.05$.

ANOVA with Duncan *post hoc* test; **Figure 6E**). Interestingly, epileptic animals showed similar differential alterations when compared to controls (HCN1 up-regulated to 187 ± 9% and HCN3 downregulated to 28 ± 8%, $n = 6$, $P < 0.05$, ANOVA with Duncan *post hoc* test; **Figures 6C,E**). In epileptic animals, however, TBB pretreatment before SE did not significantly alter HCN1 or HCN3 expression levels (**Figures 6C,E**), and for the other two isoforms, HCN2 and HCN4, no significant changes were observed at all (**Figures 6D,F**). Taken together, this RT-PCR analysis indicates that TBB leads to differential expression

TABLE 2 | Intrinsic cellular parameters.

	Vehicle-pretreated control rats (Ctrl)	TBB-pretreated control rats (Ctrl-TBB)	Vehicle-pretreated epileptic rats (Pilo)	TBB-pretreated epileptic rats (Pilo-TBB)
RMP (mV)	−58.9 ± 1.2 (n = 12)	−60.0 ± 1.2 (n = 12)	−59.3 ± 2.1 (n = 9)	−57.3 ± 2.2 (n = 12)
	−69.6 ± 5.5 (n = 5)*	−72.1 ± 2.1 (n = 5)**	−73.9 ± 4.1 (n = 6)**	−68.1 ± 5.5 (n = 5)
R_m (MΩ)	77.4 ± 9.7 (n = 11)	65.3 ± 7.1 (n = 10)	58.8 ± 8.0 (n = 10)	63.5 ± 5.5 (n = 9)
	81.6 ± 10.6 (n = 5)	95.7 ± 8.8 (n = 5)**	98.5 ± 7.2 (n = 6)*	88.3 ± 11.0 (n = 6)
τ_m (ms)	8.5 ± 1.0 (n = 11)	8.9 ± 0.7 (n = 10)	8.9 ± 0.7 (n = 10)	8.2 ± 0.6 (n = 9)
	11.0 ± 2.0 (n = 5)	25.1 ± 2.6 (n = 5)**	23.2 ± 3.6 (n = 6)**	23.5 ± 3.0 (n = 6)**

*Values obtained in the presence of ZD7288 are given in gray. P-values (*P < 0.05; **P < 0.01) correspond to unpaired t-test or Mann–Whitney U-test, respectively.*

changes of HCN channels which might have contaminated our analyses on $K_{Ca}2$ channel function.

TBB Enhances Train-AHP and Reduces Excitability in HCN-Blocking Conditions

In order to rule out contamination of differential HCN expression changes following TBB pretreatment, we repeated intracellular recordings in the presence of the HCN channel blocker ZD7288 (20 μM, **Figure 7**). Under these conditions, the proportion of burst firing neurons in the epileptic CA1 area was reduced, but still present (two of six cells) and no longer significant when compared to CA1 neurons from TBB-pretreated epileptic rats (zero of six cells, **Figure 7A**) suggesting that both HCN channel and $K_{Ca}2$ function contribute to bursting behavior. However, the power of this analysis is insufficient to dissect a differential TBB effect on those channels with respect to bursting, in particular with respect to other candidate mechanisms such as persistent sodium currents (Chen et al., 2011). Intriguingly, in contrast to the train-AHP analysis above in the absence of ZD7288, prolonged depolarization led to a markedly increased train-AHP in TBB-pretreated epileptic animals under HCN-blocking conditions (see blue traces and blue arrow in **Figure 7B**). On average, the train-AHP in this group was −5.7 ± 1.5 mV (n = 6, blue bar in **Figure 7C**) and thus matched with control levels (−5.8 ± 1.0 mV, n = 5). The statistical comparison by three-way ANOVA revealed a significant animal effect (Ctrl versus Pilo, $P < 0.05$, ANOVA with Holm–Sidak *post hoc* test) and significant pretreatment effect (vehicle versus TBB, $P < 0.05$, ANOVA with Holm–Sidak *post hoc* test), but no significant effect of ZD7288 (**Figure 7C**). However, there was a significant interaction between ZD7288 and pretreatment with TBB or vehicle ($P < 0.05$, three-way ANOVA) indicating that the ZD7288 effect depends on the type of pretreatment. The sample traces in **Figure 7B** also suggested an impaired spike frequency adaptation in CA1 neurons from vehicle-treated epileptic animals when studied in the presence of ZD7288 (black traces in **Figure 7B**). As shown in **Figure 7D**, the mean number of action potentials during the 400 ms pulse was substantially higher in this group, and two-way ANOVA showed a trend effect by animal (Ctrl versus Pilo, $P = 0.08$, indicated by "+," ANOVA with Tukey *post hoc* test) and a significant effect by treatment (vehicle versus TBB, $P < 0.05$, ANOVA with Tukey *post hoc* test). Hence, TBB appears to modify both $K_{Ca}2$ and HCN channel function with partly opposing effects. We conclude that under HCN-blocking conditions, TBB treatment prior to SE leads to persistent increase of the train-AHP amplitude and spike frequency adaptation in epileptic animals, both of which are prominent $K_{Ca}2$ functions.

DISCUSSION

Disease Modification After Transient CK2 Inhibition *in vivo*

In the present study, we investigated the effects of a short-term *in vivo* CK2 inhibition with TBB prior to pilocarpine-induced SE. First, we found that the first generalized seizure after pilocarpine injection was delayed, and moreover, the epileptic phenotype as assessed by EEG spike and video seizure rate analyses was altered in TBB-pretreated epileptic animals. Interestingly, the typical seizure cluster pattern observed in almost half of the chronically epileptic rats in this model (Bajorat et al., 2011, 2016, 2018) was less frequently detected in the TBB-pretreated group, and TBB slowed down disease progression during epileptogenesis. Since TBB was not effective as an anti-seizure drug when administered after epileptogenesis (Bajorat et al., 2018), these data indicate that TBB has potential disease modifying properties. In addition, Western blot analysis demonstrated that CK2 protein abundance was significantly reduced in TBB-pretreated epileptic tissue, especially in CA1. Interestingly, water maze training significantly reduced CK2 activity in the CA1 area, but not in the dentate gyrus (Chao et al., 2007) indicating region-specific regulation of this enzyme. This might be relevant since CA1 long-term potentiation was found to be increased after water maze training (Rehberg et al., 2017).

If CK2 is less abundant, what might be the consequences in the epileptic CA1 neuron? CaM is phosphorylated by CK2 and, in turn, dephosphorylated by protein phosphatase 2A (Bildl et al., 2004; Allen et al., 2007). The phosphomimetic T80D-CaM species decreased Ca^{2+} sensitivity and reduced $K_{Ca}2$ function (Allen et al., 2007). Hence, decreased CK2 activity and concomitantly predominant activity of protein phosphatase 2A would increase $K_{Ca}2$ function without necessarily altering transcription. In the present study, we observed that TBB increased $K_{Ca}2.2$ transcription in control (Bajorat et al., 2018), but not in epileptic animals. This is an intriguing finding probably indicating that epileptogenesis could have reversed the $K_{Ca}2.2$ upregulation. Although we have not performed a serial analysis of $K_{Ca}2.2$ transcription directly after SE as well as during epileptogenesis,

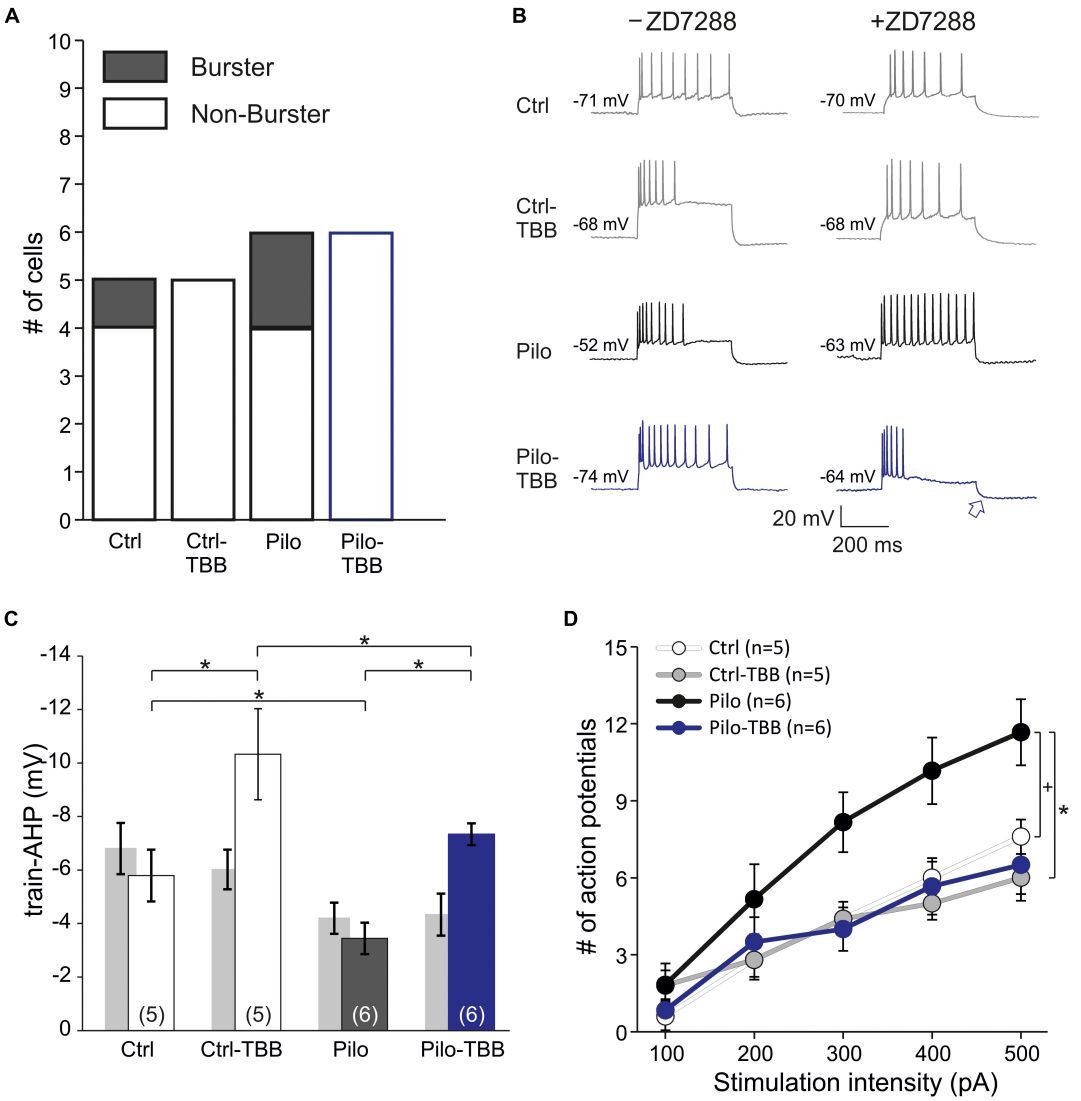

FIGURE 7 | CK2 inhibition enhances train-AHP and reduces excitability in HCN-blocking conditions. **(A)** Proportions of burster and non-burster neurons in the four experimental groups in the presence of the HCN channel blocker ZD7288. **(B)** Sample traces of intracellular recordings following prolonged depolarization (600 ms) used for train-AHP amplitude (e.g., see blue arrow) and number of action potentials. For comparison, sample traces in the absence of ZD7288 were also given (left side). **(C)** Bar graph of the train-AHP amplitude shows a significantly increased train-AHP in cells from TBB-pretreated epileptic rats (blue bar graph). For the sake of clarity, the train-AHP in the absence of ZD7288 (gray bar graphs, values from **Figure 5B**) are also shown. Significant effects were detected between animal groups (Ctrl versus Pilo, $^{*}P < 0.05$) and pretreatment groups (vehicle versus TBB, $^{*}P < 0.05$), but not for the ZD7288 effect by three-way ANOVA with Holm–Sidak *post hoc* tests. However, there was a significant interaction between ZD7288 and pretreatment with TBB or vehicle ($^{*}P < 0.05$). **(D)** Number of action potentials during 600 ms depolarization (from 100 to 500 pA). Two-way ANOVA with Tukey *post hoc* tests showed a trend effect between animal groups (Ctrl versus Pilo, $^{+}P = 0.08$) and a significant effect treatment groups (vehicle versus TBB, $^{*}P < 0.05$).

we assume that ongoing epileptic activity might decrease $K_{Ca}2$ function since chronically epileptic rats have significantly less $K_{Ca}2.2$ protein (Schulz et al., 2012). However, we did not detect a significant transcriptional downregulation of $K_{Ca}2.2$ in vehicle-pretreated epileptic rats as found in our previous paper (Schulz et al., 2012), because we used three different housekeeping genes and averaged the results. Hence, the TBB-induced upregulation of $K_{Ca}2.2$ in control tissue was indeed confirmed (Bajorat et al., 2018), but reduced $K_{Ca}2.2$ protein levels in chronically epileptic tissue (Schulz et al., 2012) are probably due to internalization and degradation observed at potentiated synapses (Lin et al., 2008) as well as after epileptiform activity (Kernig et al., 2012; Müller et al., 2018) rather than transcriptional downregulation. Furthermore, it is important to note that the $K_{Ca}2.3$ isoform which may also be relevant in CA1 and dentate gyrus (Ballesteros-Merino et al., 2014) was not found to be reduced in the chronically epileptic CA1 (Schulz et al., 2012) suggesting that the presumed reduction of CK2 activity should enhance $K_{Ca}2.3$ function as well. Taken together, our findings are consistent with a persistently diminished CK2 activity leading to enhanced $K_{Ca}2$ function

in CA1 as a potentially relevant mechanism for the disease modifying effect of TBB.

Are there alternative molecular pathways for the disease modifying effect of TBB? On the one hand, we found an increased number of burst-spiking neurons in CA1 of vehicle-pretreated, but not in CA1 of TBB-pretreated epileptic rats. The ADP and burst-firing behavior have been recognized as common intrinsic properties of epileptic tissue, especially in the subiculum and CA1 (Magee and Carruth, 1999; Su et al., 2001; Yue and Yaari, 2004; van Welie et al., 2006; Jarsky et al., 2008). Based on this literature, the ADP was demonstrated to be due to persistent Na^+ and Ni^+-sensitive Ca^{2+} currents, rather than Ca^{2+}-activated K^+ currents (Magee and Carruth, 1999; Su et al., 2001). However, pharmacological inhibition of KCNQ/M-type K^+ currents increased spike ADP and burst-spiking in CA1 (Yue and Yaari, 2004) suggesting that K^+ currents can substantially modify these intrinsic firing properties. Thus, the effect of TBB pretreatment to prevent burst-firing behavior might indicate that Ca^{2+}-activated K^+ channels and probably further ion channels have been modified by TBB pretreatment. In this respect, it is noteworthy that functional HCN3 upregulation by phosphatidylinositol-4,5-bisphosphate facilitated low-threshold burst-firing in thalamic neurons (Ying et al., 2011). Hence, one might speculate whether the HCN3 downregulation found in TBB-pretreated epileptic tissue could have exerted the opposite effect and inhibited the development of burst-firing. On the other hand, we observed at least one control burster cell in the presence of ZD7288, and increased excitability has been associated with downregulation of HCN channels in chronically epileptic CA1 (Adams et al., 2009). Nonetheless, there is also uncertainty about the selectivity of TBB which will inhibit other kinases, too (Pagano et al., 2008). CK2 has a pretty large number of substrates (Meggio and Pinna, 2003), and recently, CK2 was demonstrated to phosphorylate histone chaperone Spt6 that is associated with RNA polymerase II and therefore promotes DNA transcription (Dronamraju et al., 2018). Since CK2 is an oncogenic enzyme involved in epigenetic processes (reviewed by Gowda et al., 2019), further targets need to be unraveled. Here, we focused on $K_{Ca}2$ channel-mediated mechanisms.

Increased $K_{Ca}2$ Function as the Relevant Disease Modifying Mechanism

On the network level, we did not observe significant changes of basal synaptic transmission after TBB pretreatment indicating that a potential $K_{Ca}2$-mediated reduction of the EPSP (Hammond et al., 2006) did not occur in our hands because postsynaptic Ca^{2+} increase during basal transmission was quite low. Instead, short-term plasticity was significantly facilitated and PPRs were changed in potentiated synapses in TBB-pretreated epileptic animals. These findings might point to a presynaptic mechanism, but $K_{Ca}2.2$ channels were excluded to have relevant presynaptic functions (Hammond et al., 2006).

Hence, what is the evidence for an enhanced $K_{Ca}2$ function in TBB-pretreated epileptic CA1? Intrinsic cellular properties such as the mAHP and the spike frequency adaptation are well-established $K_{Ca}2$ functions of CA1 neurons (Bond et al., 2004; Pedarzani et al., 2005; Hammond et al., 2006; Schulz et al., 2012). First, we could demonstrate that mAHP-mediating K^+ currents were significantly enhanced by TBB pretreatment in tissue from epileptic animals. On the other hand, the sAHP was also reduced in epileptic CA1 neurons, but not altered by TBB treatment. This is consistent with the view that $K_{Ca}2$ is not involved in sAHP (Stocker et al., 1999; Bond et al., 2004; Villalobos et al., 2004; Pedarzani et al., 2005), but the molecular sAHP-mediating candidates are less clear and may certainly involve HCN channels (Gu et al., 2005; Kaczorowski, 2011). Importantly, we observed that HCN channel function was enhanced in TBB-pretreated epileptic tissue. In addition, the transcriptional analysis revealed HCN1 upregulation and HCN3 downregulation in epileptic CA1. This is in contrast to previous reports showing HCN1 downregulation in the pilocarpine model (Jung et al., 2007, 2010), but more recently, HCN1 immunoreactivity was found be increased, especially in CA1 interneurons (Oh et al., 2012). Moreover, HCN1 upregulation was also found in the epileptic dentate gyrus (Bender et al., 2003; Surges et al., 2012). Hence, HCN isoform expression and protein abundance may depend on the cell type. Nonetheless, since pharmacological HCN channel inhibition by ZD7288 that does not distinguish between HCN isoforms led to an increase of sAHP-mediating currents (Gu et al., 2005), we propose that a net enhancement of HCN channel function by TBB could have antagonized an expected TBB-mediated sAHP increase due to enhanced $K_{Ca}2$ function. In fact, we previously found that the sAHP was increased in control and epileptic tissue when animals were pretreated *in vivo* with TBB (Brehme et al., 2014). On the one hand, this could be simply due to different recording procedures (isolated cells versus slice experiments) that differ with respect to recording from dendritic compartments expressing high levels of HCN1 (Nolan et al., 2004). On the other hand, however, this discrepancy may indicate that enhanced HCN channel function following CK2 inhibition may occur with delayed time course and, probably, activity-dependent (Shin and Chetkovich, 2007). This is an attractive mechanism to be addressed in further studies.

Second, we addressed $K_{Ca}2$ function under HCN channel-blocking conditions. In the presence of the non-selective inhibitor ZD7288, the train-AHP recorded with intracellular electrodes was significantly reduced in vehicle-treated epileptic tissue, but could be enhanced by TBB pretreatment in both control and epileptic animals. This is an important finding, because HCN inhibition shifts the RMP to hyperpolarizing values which should rather decrease the driving force for $K_{Ca}2$ channels. On the other hand, membrane resistance also depends on HCN channel function (Surges et al., 2004), and ZD7288 increased the resistance—and thus could have counteracted the probably reduced K^+ currents. Hence, the enhanced train-AHP recorded intracellularly confirmed the membrane current recordings obtained with the patch-clamp method.

Third, $K_{Ca}2$ channels also play a major role in spike frequency adaptation (Pedarzani et al., 2005). In the present study, we studied spike frequency adaptation in HCN channel-blocking conditions and could demonstrate that this phenomenon was impaired in chronically epileptic tissue confirming previous

results in isolated neurons (Schulz et al., 2012). Moreover, TBB restored spike frequency adaptation in epileptic tissue which can be viewed as an important antiepileptic phenomenon. In summary, our data strongly suggest that CA1 neurons from TBB-pretreated epileptic animals show a significantly enhanced $K_{Ca}2$ function that likely contributes to disease modification.

CONCLUSION

Our experiments demonstrated that TBB pretreatment prior to SE led to reduced epileptogenesis and to differential gene expression changes of $K_{Ca}2.2$, but also of HCN1 and HCN3 channels. Under HCN channel blocking conditions, pretreatment with TBB could significantly enhance $K_{Ca}2$ channel functions such as the AHP and the spike frequency adaptation in epileptic animals, probably due to a persistently decreased CK2 protein abundance.

DATA AVAILABILITY STATEMENT

The datasets generated for this study are available on request to the corresponding author.

ETHICS STATEMENT

The animal study was reviewed and approved by Landesamt für Landwirtschaft, Lebensmittelsicherheit und Fischerei Mecklenburg-Vorpommern (numbers M-V/TSD/7221.3-1.1-013/10 and 7221.3-1.1-019/13).

AUTHOR CONTRIBUTIONS

FS, SM, XG, LS, HB, and TR performed the experiments. FS, TK, and RK contributed to conception and design of the study. FS, SR, AE, and RK organized the database. FS, SM, LS, MR, DG, TK, and RK performed the statistical analysis. TK wrote the first draft of the manuscript. FS, SM, MR, and RK wrote the sections of the manuscript. LS, MR, and DG contributed to manuscript preparation. All authors contributed to manuscript revision and read and approved the final version of this manuscript for submission.

FUNDING

This work was supported by the German Research Foundation (KO 1779/14-1 and KI 1283/5-1) and the Intramural Research Program of the Medical Faculty of the University of Rostock.

ACKNOWLEDGMENTS

The authors wish to thank Tina Sellmann, Katrin Porath, Hanka Schmidt, Bernd Memmener, and Andreas Prestel for their excellent technical assistance.

REFERENCES

Adams, B. E., Reid, C. A., Myers, D., Ng, C., Powell, K., Phillips, A. M., et al. (2009). Excitotoxic-mediated transcriptional decreases in HCN2 channel function increase network excitability in CA1. *Exp. Neurol.* 219, 249–257. doi: 10.1016/j.expneurol.2009.05.030

Allen, D., Fakler, B., Maylie, J., and Adelman, J. P. (2007). Organization and regulation of small conductance Ca2+-activated K+ channel multiprotein complexes. *J. Neurosci.* 27, 2369–2376. doi: 10.1523/jneurosci.3565-06.2007

Bajorat, R., Goerss, D., Brenndörfer, L., Schwabe, L., Köhling, R., and Kirschstein, T. (2016). Interplay between interictal spikes and behavioral seizures in young, but not aged pilocarpine-treated epileptic rats. *Epilepsy Behav.* 57, 90–94. doi: 10.1016/j.yebeh.2016.01.014

Bajorat, R., Porath, K., Kuhn, J., Goßla, E., Goerss, D., Sellmann, T., et al. (2018). Oral administration of the casein kinase 2 inhibitor TBB leads to persistent KCa2.2 channel up-regulation in the epileptic CA1 area and cortex, but lacks anti-seizure efficacy in the pilocarpine epilepsy model. *Epilepsy Res.* 147, 42–50. doi: 10.1016/j.eplepsyres.2018.08.012

Bajorat, R., Wilde, M., Sellmann, T., Kirschstein, T., and Köhling, R. (2011). Seizure frequency in pilocarpine-treated rats is independent of circadian rhythm. *Epilepsia* 52, e118–e122. doi: 10.1111/j.1528-1167.2011.03200.x

Ballesteros-Merino, C., Watanabe, M., Shigemoto, R., Fukazawa, Y., Adelman, J. P., and Luján, R. (2014). Differential subcellular localization of SK3-containing channels in the hippocampus. *Eur. J. Neurosci.* 39, 883–892. doi: 10.1111/ejn.12474

Bender, R. A., Soleymani, S. V., Brewster, A. L., Nguyen, S. T., Beck, H., Mathern, G. W., et al. (2003). Enhanced expression of a specific hyperpolarization-activated cyclic nucleotide-gated cation channel (HCN) in surviving dentate gyrus granule cells of human and experimental epileptic hippocampus. *J. Neurosci.* 23, 6826–6836. doi: 10.1523/jneurosci.23-17-06826.2003

Bernard, C., Anderson, A., Becker, A., Poolos, N. P., Beck, H., and Johnston, D. (2004). Acquired dendritic channelopathy in temporal lobe epilepsy. *Science* 305, 532–535. doi: 10.1126/science.1097065

Bildl, W., Strassmaier, T., Thurm, H., Andersen, J., Eble, S., Oliver, D., et al. (2004). Protein kinase CK2 is coassembled with small conductance Ca(2+)-activated K+ channels and regulates channel gating. *Neuron* 43, 847–858. doi: 10.1016/j.neuron.2004.08.033

Blümcke, I., Thom, M., Aronica, E., Armstrong, D. D., Bartolomei, F., Bernasconi, A., et al. (2013). International consensus classification of hippocampal sclerosis in temporal lobe epilepsy: a task force report from the ILAE commission on diagnostic methods. *Epilepsia* 54, 1315–1329. doi: 10.1111/epi.12220

Bond, C. T., Herson, P. S., Strassmaier, T., Hammond, R., Stackman, R., Maylie, J., et al. (2004). Small conductance Ca2+-activated K+ channel knock-out mice reveal the identity of calcium-dependent afterhyperpolarization currents. *J. Neurosci.* 24, 5301–5306. doi: 10.1523/jneurosci.0182-04.2004

Brehme, H., Kirschstein, T., Schulz, R., and Köhling, R. (2014). In vivo treatment with the casein kinase 2 inhibitor 4,5,6,7- tetrabromotriazole augments the slow afterhyperpolarizing potential and prevents acute epileptiform activity. *Epilepsia* 55, 175–183. doi: 10.1111/epi.12474

Chao, C. C., Ma, Y. L., and Lee, E. H. (2007). Protein kinase CK2 impairs spatial memory formation through differential cross talk with PI-3 kinase signaling: activation of Akt and inactivation of SGK1. *J. Neurosci.* 27, 6243–6248. doi: 10.1523/jneurosci.1531-07.2007

Chen, S., Su, H., Yue, C., Remy, S., Royeck, M., Sochivko, D., et al. (2011). An increase in persistent sodium current contributes to intrinsic neuronal bursting after status epilepticus. *J. Neurophysiol.* 105, 117–129. doi: 10.1152/jn.00184.2010

Dronamraju, R., Kerschner, J. L., Peck, S. A., Hepperla, A. J., Adams, A. T., Hughes, K. D., et al. (2018). Casein kinase II phosphorylation of Spt6 enforces transcriptional fidelity by maintaining Spn1-Spt6 interaction. *Cell Rep.* 25:3476-3489.e5. doi: 10.1016/j.celrep.2018.11.089

Gowda, C., Song, C., Ding, Y., Iyer, S., Dhanyamraju, P. K., McGrath, M., et al. (2019). Cellular signaling and epigenetic regulation of gene expression in leukemia. *Adv. Biol. Regul.* doi: 10.1016/j.jbior.2019.100665 [Epub ahead of print].

Gu, N., Vervaeke, K., Hu, H., and Storm, J. F. (2005). Kv7/KCNQ/M and HCN/h, but not KCa2/SK channels, contribute to the somatic medium after-hyperpolarization and excitability control in CA1 hippocampal pyramidal cells. *J. Physiol.* 566, 689–715. doi: 10.1113/jphysiol.2005.086835

Hammond, R. S., Bond, C. T., Strassmaier, T., Ngo-Anh, T. J., Adelman, J. P., Maylie, J., et al. (2006). Small-conductance Ca2+-activated K+ channel type 2 (SK2) modulates hippocampal learning, memory, and synaptic plasticity. *J. Neurosci.* 26, 1844–1853. doi: 10.1523/jneurosci.4106-05.2006

Hotson, J. R., and Prince, D. A. (1980). A calcium-activated hyperpolarization follows repetitive firing in hippocampal neurons. *J. Neurophysiol.* 43, 409–519.

Jarsky, T., Mady, R., Kennedy, B., and Spruston, N. (2008). Distribution of bursting neurons in the CA1 region and the subiculum of the rat hippocampus. *J. Comp. Neurol.* 506, 535–547. doi: 10.1002/cne.21564

Jung, S., Bullis, J. B., Lau, I. H., Jones, T. D., Warner, L. N., and Poolos, N. P. (2010). Downregulation of dendritic HCN channel gating in epilepsy is mediated by altered phosphorylation signaling. *J. Neurosci.* 30, 6678–6688. doi: 10.1523/JNEUROSCI.1290-10.2010

Jung, S., Jones, T. D., Lugo, J. N. Jr., Sheerin, A. H., Miller, J. W., D'Ambrosio, R., et al. (2007). Progressive dendritic HCN channelopathy during epileptogenesis in the rat pilocarpine model of epilepsy. *J. Neurosci.* 27, 13012–13021. doi: 10.1523/jneurosci.3605-07.2007

Kaczorowski, C. C. (2011). Bidirectional pattern-specific plasticity of the slow afterhyperpolarization in rats: role for high-voltage activated Ca2+ channels and Ih. *Eur. J. Neurosci.* 34, 1756–1765. doi: 10.1111/j.1460-9568.2011.07899.x

Kernig, K., Kirschstein, T., Würdemann, T., Rohde, M., and Köhling, R. (2012). The afterhyperpolarizing potential following a train of action potentials is suppressed in an acute epilepsy model in the rat Cornu Ammonis 1 area. *Neuroscience* 201, 288–296. doi: 10.1016/j.neuroscience.2011.11.008

Kirschstein, T., Bauer, M., Müller, L., Rüschenschmidt, C., Reitze, M., Becker, A. J., et al. (2007). Loss of metabotropic glutamate receptor-dependent long-term depression via downregulation of mGluR5 after status epilepticus. *J. Neurosci.* 27, 7696–7704. doi: 10.1523/jneurosci.4572-06.2007

Kwan, P., and Brodie, M. J. (2000). Early identification of refractory epilepsy. *N. Engl. J. Med.* 342, 314–319. doi: 10.1056/nejm200002033420503

Leite, J. P., Garcia-Cairasco, N., and Cavalheiro, E. A. (2002). New insights from the use of pilocarpine and kainate models. *Epilepsy Res.* 50, 93–103. doi: 10.1016/s0920-1211(02)00072-4

Lin, M. T., Luján, R., Watanabe, M., Adelman, J. P., and Maylie, J. (2008). SK2 channel plasticity contributes to LTP at Schaffer collateral-CA1 synapses. *Nat. Neurosci.* 11, 170–177. doi: 10.1038/nn2041

Magee, J. C., and Carruth, M. (1999). Dendritic voltage-gated ion channels regulate the action potential firing mode of hippocampal CA1 pyramidal neurons. *J. Neurophysiol.* 82, 1895–1901. doi: 10.1152/jn.1999.82.4.1895

Meggio, F., and Pinna, L. A. (2003). One-thousand-and-one substrates of protein kinase CK2? *FASEB J.* 17, 349–368. doi: 10.1096/fj.02-0473rev

Müller, L., Müller, S., Sellmann, T., Groeneweg, L., Tokay, T., Köhling, R., et al. (2014). Effects of oxygen insufflation during pilocarpine-induced status epilepticus on mortality, tissue damage and seizures. *Epilepsy Res.* 108, 90–97. doi: 10.1016/j.eplepsyres.2013.10.017

Müller, L., Tokay, T., Porath, K., Köhling, R., and Kirschstein, T. (2013). Enhanced NMDA receptor-dependent LTP in the epileptic CA1 area via upregulation of NR2B. *Neurobiol. Dis.* 54, 183–193. doi: 10.1016/j.nbd.2012.12.011

Müller, S., Guli, X., Hey, J., Einsle, A., Pfanz, D., Sudmann, V., et al. (2018). Acute epileptiform activity induced by gabazine involves proteasomal rather than lysosomal degradation of KCa2.2 channels. *Neurobiol. Dis.* 112, 79–84. doi: 10.1016/j.nbd.2018.01.005

Nolan, M. F., Malleret, G., Dudman, J. T., Buhl, D. L., Santoro, B., Gibbs, E., et al. (2004). A behavioral role for dendritic integration: HCN1 channels constrain spatial memory and plasticity at inputs to distal dendrites of CA1 pyramidal neurons. *Cell* 119, 719–732. doi: 10.1016/s0092-8674(04)01055-4

Oh, Y. J., Na, J., Jeong, J. H., Park, D. K., Park, K. H., Ko, J. S., et al. (2012). Alterations in hyperpolarization-activated cyclic nucleotidegated cation channel (HCN) expression in the hippocampus following pilocarpine-induced status epilepticus. *BMB Rep.* 45, 635–640. doi: 10.5483/bmbrep.2012.45.11.091

Pagano, M. A., Bain, J., Kazimierczuk, Z., Sarno, S., Ruzzene, M., Di Maira, G., et al. (2008). The selectivity of inhibitors of protein kinase CK2: an update. *Biochem. J.* 415, 353–365. doi: 10.1042/BJ20080309

Pedarzani, P., McCutcheon, J. E., Rogge, G., Jensen, B. S., Christophersen, P., Hougaard, C., et al. (2005). Specific enhancement of SK channel activity selectively potentiates the afterhyperpolarizing current I(AHP) and modulates the firing properties of hippocampal pyramidal neurons. *J. Biol. Chem.* 280, 41404–41411. doi: 10.1074/jbc.m509610200

Racine, R. J. (1972). Modification of seizure activity by electrical stimulation. II. Motor seizure. *Electroencephalogr. Clin. Neurophysiol.* 32, 281–294. doi: 10.1016/0013-4694(72)90177-0

Rehberg, M., Kirschstein, T., Guli, X., Müller, S., Rohde, M., Franz, D., et al. (2017). Functional metaplasticity of hippocampal schaffer collateral-CA1 synapses is reversed in chronically epileptic rats. *Neural Plast.* 2017:8087401. doi: 10.1155/2017/8087401

Schmidt, D., and Sillanpää, M. (2016). Prevention of Epilepsy: Issues and Innovations. *Curr. Neurol. Neurosci. Rep.* 16:95. doi: 10.1007/s11910-016-0695-9

Schulz, R., Kirschstein, T., Brehme, H., Porath, K., Mikkat, U., and Köhling, R. (2012). Network excitability in a model of chronic temporal lobe epilepsy critically depends on SK channel-mediated AHP currents. *Neurobiol. Dis.* 45, 337–347. doi: 10.1016/j.nbd.2011.08.019

Shin, M., and Chetkovich, D. M. (2007). Activity-dependent regulation of h channel distribution in hippocampal CA1 pyramidal neurons. *J. Biol. Chem.* 282, 33168–33180. doi: 10.1074/jbc.m703736200

Stocker, M., Krause, M., and Pedarzani, P. (1999). An apamin-sensitive Ca2+-activated K+ current in hippocampal pyramidal neurons. *Proc. Natl. Acad. Sci. U.S.A.* 96, 4662–4667. doi: 10.1073/pnas.96.8.4662

Su, H., Alroy, G., Kirson, E. D., and Yaari, Y. (2001). Extracellular calcium modulates persistent sodium current-dependent burst-firing in hippocampal pyramidal neurons. *J. Neurosci.* 21, 4173–4182. doi: 10.1523/jneurosci.21-12-04173.2001

Surges, R., Freiman, T. M., and Feuerstein, T. J. (2004). Input resistance is voltage dependent due to activation of Ih channels in rat CA1 pyramidal cells. *J. Neurosci. Res.* 76, 475–480. doi: 10.1002/jnr.20075

Surges, R., Kukley, M., Brewster, A., Rüschenschmidt, C., Schramm, J., Baram, T. Z., et al. (2012). Hyperpolarization-activated cation current Ih of dentate gyrus granule cells is upregulated in human and rat temporal lobe epilepsy. *Biochem. Biophys. Res. Commun.* 420, 156–160. doi: 10.1016/j.bbrc.2012.02.133

Timm, F. (1958). Histochemistry of heavy metals; the sulfide-silver procedure [Zur Histochemie der Schwermetalle. Das Sulfid-Silberverfahren]. *Dtsch. Z. Gesamte Gerichtl. Med.* 46, 706–711.

van Welie, I., Remme, M. W., van Hooft, J. A., and Wadman, W. J. (2006). Different levels of Ih determine distinct temporal integration in bursting and regular-spiking neurons in rat subiculum. *J. Physiol.* 576, 203–214. doi: 10.1113/jphysiol.2006.113944

Villalobos, C., Shakkottai, V. G., Chandy, K. G., Michelhaugh, S. K., and Andrade, R. (2004). SKCa channels mediate the medium but not the slow calcium-activated afterhyperpolarization in cortical neurons. *J. Neurosci.* 24, 3537–3542. doi: 10.1523/jneurosci.0380-04.2004

Ying, S. W., Tibbs, G. R., Picollo, A., Abbas, S. Y., Sanford, R. L., Accardi, A., et al. (2011). PIP2-mediated HCN3 channel gating is crucial for rhythmic burst firing in thalamic intergeniculate leaflet neurons. *J. Neurosci.* 31, 10412–10423. doi: 10.1523/JNEUROSCI.0021-11.2011

Yue, C., and Yaari, Y. (2004). KCNQ/M channels control spike afterdepolarization and burst generation in hippocampal neurons. *J. Neurosci.* 24, 4614–4624. doi: 10.1523/jneurosci.0765-04.2004

Conflict of Interest: The authors declare that the research was conducted in the absence of any commercial or financial relationships that could be construed as a potential conflict of interest.

frontiers in Neuroscience

ORIGINAL RESEARCH
published: 15 September 2020
doi: 10.3389/fnins.2020.00924

Epilepsy miRNA Profile Depends on the Age of Onset in Humans and Rats

*Jiri Baloun[1], Petra Bencurova[1,2], Tereza Totkova[1], Hana Kubova[3], Marketa Hermanova[4], Michal Hendrych[4], Martin Pail[2], Sarka Pospisilova[1] and Milan Brazdil[1,2]**

[1] Central European Institute of Technology, Masaryk University, Brno, Czechia, [2] Brno Epilepsy Center, Department of Neurology, Medical Faculty of Masaryk University, St. Anne's University Hospital, Brno, Czechia, [3] Department of Developmental Epileptology, Institute of Physiology of the Czech Academy of Sciences, Prague, Czechia, [4] First Department of Pathology, Medical Faculty of Masaryk University, St. Anne's University Hospital, Brno, Czechia

Temporal lobe epilepsy (TLE) is a severe neurological disorder accompanied by recurrent spontaneous seizures. Although the knowledge of TLE onset is still incomplete, TLE pathogenesis most likely involves the aberrant expression of microRNAs (miRNAs). miRNAs play an essential role in organism homeostasis and are widely studied in TLE as potential therapeutics and biomarkers. However, many discrepancies in discovered miRNAs occur among TLE studies due to model-specific miRNA expression, different onset ages of epilepsy among patients, or technology-related bias. We employed a massive parallel sequencing approach to analyze brain tissues from 16 adult mesial TLE (mTLE)/hippocampal sclerosis (HS) patients, 8 controls and 20 rats with TLE-like syndrome, and 20 controls using the same workflow and categorized these subjects based on the age of epilepsy onset. All categories were compared to discover overlapping miRNAs with an aberrant expression, which could be involved in TLE. Our cross-comparative analyses showed distinct miRNA profiles across the age of epilepsy onset and found that the miRNA profile in rats with adult-onset TLE shows the closest resemblance to the profile in mTLE/HS patients. Additionally, this analysis revealed overlapping miRNAs between patients and the rat model, which should participate in epileptogenesis and ictogenesis. Among the overlapping miRNAs stand out miR-142-5p and miR-142-3p, which regulate immunomodulatory agents with pro-convulsive effects and suppress neuronal growth. Our cross-comparison study enhanced the insight into the effect of the age of epilepsy onset on miRNA expression and deepened the knowledge of epileptogenesis. We employed the same methodological workflow in both patients and the rat model, thus improving the reliability and accuracy of our results.

Keywords: miRNA, mesial temporal lobe epilepsy, animal model, human, sequencing, cross-comparison study

OPEN ACCESS

Edited by:
Victor Faundez,
Emory University, United States

Reviewed by:
Fei Yin,
Xiangyang Central Hospital, China
Daniel Tarquinio,
Center for Rare Neurological Diseases, United States

***Correspondence:**
Milan Brazdil
milan.brazdil@ceitec.muni.cz;
milan.brazdil@fnusa.cz

Specialty section:
This article was submitted to Neurogenomics, a section of the journal Frontiers in Neuroscience

Received: *31 January 2020*
Accepted: *11 August 2020*
Published: *15 September 2020*

Citation:
Baloun J, Bencurova P, Totkova T, Kubova H, Hermanova M, Hendrych M, Pail M, Pospisilova S and Brazdil M (2020) Epilepsy miRNA Profile Depends on the Age of Onset in Humans and Rats. Front. Neurosci. 14:924. doi: 10.3389/fnins.2020.00924

INTRODUCTION

Temporal lobe epilepsy (TLE) is the most common type of epilepsy—a neurological disorder characterized by recurrent spontaneous seizures. This condition includes several subtypes, of which the most prevalent is mesial TLE (mTLE). The seizures of this subtype originate from the structures in the medial portion of the temporal lobe (such as the hippocampus) and are often associated with a pathological change of the hippocampal tissue—hippocampal sclerosis (HS)

(Thom et al., 2009). The underlying mechanisms of epileptogenesis in TLE are still unclear; hence, a better understanding of involved biological processes is fundamental for novel treatment strategies and therapeutics. Among potential therapeutic targets as well as possible biomarkers of pathological changes in the epileptic brain are microRNAs (miRNAs).

miRNAs are small endogenous noncoding RNAs that act as posttranscriptional regulators of gene expression. Individual miRNAs can target a variety of mRNAs and most commonly inhibit their translation into proteins (Bartel, 2009). Hence, various mechanisms (e.g., methylation hormones and other miRNAs) strictly regulate miRNA expression (review in Gulyaeva and Kushlinskiy, 2016), because their dysregulation can have a profound effect on the cell, and, subsequently, on the whole organism. As a result, the monitoring of miRNA expression might disclose the onset or progression of the disease, making miRNAs a useful biomarker. This relation illustrates the close link between many diseases and altered levels of miRNAs (Srinivasan et al., 2013). The changes in miRNome have been mostly studied in different types of cancer (Li and Kowdley, 2012), but the connection occurs in other conditions, including TLE. Numerous studies of miRNA dysregulation in TLE have provided solid evidence for their importance in the epilepsy pathogenesis (Brennan and Henshall, 2018).

To date, many studies about the role of miRNAs in epilepsy have produced a vast amount of data, however, they also have several drawbacks. Most of them studied epilepsy only in animal models, which have important limitations. Firstly, the animal model is only an approximation of mTLE, which does not correspond perfectly to the biochemistry of this disease in humans. Therefore, the results require cautious interpretation in the context of human mTLE. Moreover, there are fundamental differences between the animal models as each of them implements a different technique to induce epileptic seizures, making it difficult to compare the acquired data (Korotkov et al., 2017). Different experimental protocols can lead to the activation of different pathological pathways. Therefore, the processes involved in epileptogenesis can vary from one model to another. As a result, the affected miRNAs can also be unique to the experimental model and not represent epilepsy in general. Indeed, the results of these studies are often discordant (Korotkov et al., 2017).

Another fraction of the studies focuses on analyzing the miRNome of human brain samples from epilepsy surgeries. This approach has the potential to provide results fully relevant to human mTLE, however, it is not flawless. Unlike TLE patients, controls were not treated with antiepileptic drugs (AEDs) affecting miRNA expression in the brain tissue. Furthermore, some complex factors can never be fully accounted for (such as lifestyle, age, gender, or ethnicity) (Leung and Sharp, 2010; Dluzen et al., 2016; Huan et al., 2018). These factors might affect the miRNA composition of the hippocampal tissue (Crespo et al., 2018) and cause inter-individual variability in both control and patient groups. Another discussed drawback is the origin of control brain tissues, which mostly come from postmortem autopsies, however, previous research discovered virtually unchanged miRNA composition in postmortem tissues within 30 h after death (Kakimoto et al., 2015; Bencurova et al., 2017).

The most promising approach is to compare the data acquired in animal models and human patients and find the intersection. Additionally, the same methodological workflow could enhance reliability and reduce the false negatives in the results. miRNAs identified by this approach are most likely related to epilepsy, rather than to a specific model or the origin of the tissue (surgery or autopsy). To date, only a few studies have used this approach (Roncon et al., 2015; Korotkov et al., 2017); therefore, we compared the miRNomes of patients with mTLE and a rat model of chronic epilepsy from our previous experiments (Bencurova et al., 2017). Moreover, the miRNA expression profile in the brain tissues changes during the development, and seizures might affect the direction of these changes. Our analyses also evaluated the effect of age at the first seizure occurrence on the miRNA profile in the chronic phase of this disease.

MATERIALS AND METHODS

Human Samples

All procedures involving human tissue processing were approved by the Ethical Committee of St. Anne's University Hospital in Brno (approval number 9G/2015-KS). The collection of the hippocampal tissue was performed on a cohort of anteromesial temporal resections at St. Anne's University Hospital in Brno, the Czech Republic, within the period 2007–2016. Patients and controls were previously described in Bencurova et al. (2017). In this study, we focused on a cohort of 16 adult mTLE/HS patients and 8 controls, hippocampal tissues of which were utilized for whole-miRNome analysis by massive parallel sequencing (MPS). All patients (seven men and nine women) were referred to the Department of Neurology at the Brno Epilepsy Center for their medical intractability and fulfilled the diagnostic criteria for mTLE/HS. The diagnosis was made according to the International League Against Epilepsy (ILAE) criteria (Commission on Classification and Terminology of the ILAE, 1989). All of the patients had been routinely investigated, including long-term semi-invasive video-EEG monitoring (using sphenoidal electrodes), high-resolution magnetic resonance imaging (MRI), and neuropsychological testing. The diagnosis of unilateral mTLE in our patients was based on a consonance of history data, ictal and interictal EEG findings, ictal semiology, neuropsychology, and neuroimaging findings (MRI and PET). Unilateral HS concordant with the electroencephalographic lateralization of the epileptogenic zone was confirmed in all cases by visual inspections of the MRI scans by two independent physicians. None of the patients revealed other brain structural lesions on MRI scans or had undergone previous intracranial surgery. Age of TLE onset ranged from 2 to 44 years (mean = 16.9), and the average patient's age at the time of surgery was 40.2 years (range = 25–51). All patients signed informed consent to approve the use of their tissue in this study. Control hippocampal tissue was collected from eight postmortem cases without hippocampal aberrations from the Department of Forensic Medicine at St. Anne's University Hospital. The average

age of these cases at the time of death was 55.6 years (range = 30–72). All procedures to obtain hippocampal control tissue samples were in accordance with the Czech Republic's legislation and ethical standards and with the 1964 Helsinki declaration (revised in 2013). A detailed overview of patients and controls is listed in **Supplementary Table S1**.

The Rat Model of TLE

Protocols involving animals were performed in accordance with ARRIVE guidelines (Kilkenny et al., 2010) and national (Act No 246/1992 Coll.) and international laws and policies (EU Directive 2010/63/EU for animal experiments). The Ethical Committee of the Czech Academy of Sciences approved the experimental protocols (Approval No. 128/2013). Status epilepticus (SE) was induced in male Wistar albino rats aged P12 (P—postnatal day) or P60 as described previously by Kubová et al. (2004). Briefly, all animals were labeled with a unique code and injected intraperitoneally (i.p.) with 127 mg/kg LiCl 24 h prior to pilocarpine/saline injection. Individual animals were tracked throughout the entire project based on the assigned code of each animal. Control and SE groups contained randomly assigned animals, and subjects in the SE group received a single i.p. dose of pilocarpine at P12 (35 mg/ml/kg) or P60 (45 mg/ml/kg); controls were treated with saline. All treated animals were caged separately and continually observed for 3 h. Latency to motor SE characterized by forelimb clonus was registered. Animals were treated with paraldehyde (P12: 0.07 ml/kg and P60: 0.3 ml/kg) approximately 2 h after the onset of convulsive SE in order to decrease mortality. Further experiments included only rats exhibiting behavioral manifestations of seizures progressing to forelimbs clonus for at least 1 h (SE was successfully induced in 100% of P12 and 69% of P60 animals injected with pilocarpine). Twelve P12 and 13 P60 animals were selected for experiments in the chronic stage of epilepsy (3 months after SE), along with 10 control animals per age group. For more details, see **Supplementary Methods** (submitted manuscript).

Monitoring

One week before being sacrificed, animals underwent continuous 24/7 video monitoring with IP infrared Camera Edimax IC-3140W for wireless monitoring. Synology Surveillance Station 7 software was used for both registration and evaluation. An experienced observer evaluated the recordings manually, registering the incidence of motor seizures (Racine stages 3–5). The electrographic analysis was omitted in order to prevent possible inflammatory reactions on EEG electrode implantation and the adverse effect of anesthesia exposure. The remainder of adult-onset animals (n = 10) exhibited similar clonic seizures (frequency summarized in **Supplementary Figure S1**), while animals with SE at P12 and controls did not exhibit motor seizures (submitted manuscript).

Hippocampal Tissue Processing and RNA Isolation

Surgically resected and autopsy tissues from adult mTLE/HS patients and controls were identically treated: fixed in 10% neutral buffered formalin, grossly inspected, carefully oriented, and measured. Hippocampal tissue specimens were dissected into 2–3 mm-thick tissue slices along the anterior–posterior axis and paraffin embedded. Formalin-fixed paraffin-embedded (FFPE) tissue sections were stained with hematoxylin–eosin and evaluated under light microscopy; additionally, the presence of neuronal depletion and gliosis in HS tissue samples was confirmed using NeuN and GFAP immunohistochemistry. The international consensus classification of HS in TLE was applied (Blümcke et al., 2013). For miRNA analysis, paraffin-embedded tissue slices showing the presence of hippocampal complex were selected. Total RNA was isolated from tissue sections using the High Pure miRNA Isolation Kit (Roche) according to the manufacturer's protocol. In order to maximize RNA yield, overnight Proteinase K digestion was used.

Hippocampal tissue was collected from 10 SE and 10 control animals per age group (n = 40) 3 months after SE (chronic stage of epilepsy). Animals were sacrificed by decapitation under the overdose of anesthesia (ether). Brains were immediately dissected, and the entire hippocampus was collected from both hemispheres. Tissues were immediately frozen in dry ice and stored at −80°C until further processing. Total RNA was isolated from frozen hippocampal tissue using the TRI Reagent® (Biotech) according to the manufacturer's protocol. Ceramic beads were used for tissue disruption.

RNA was successfully extracted from all specimens and quantified using NanoDrop ND-1000 (Thermo Fisher Scientific) and Qubit™ dsDNA HS Assay Kit on a Qubit® 2.0 fluorometer (Thermo Fisher Scientific). The 1.1 μg of extracted total RNA was used to prepare small RNA libraries and sequenced on NextSeq 500 (Illumina).

Massive Parallel Sequencing

Libraries for sequencing were prepared from 1.1 μg of total RNA obtained from rat samples (20 SE and 20 controls) and patients (16 mTLE and 8 controls). Libraries were prepared using a NEXTflex Small RNA-Seq Kit v2 for human samples and Kit v3 for rat samples (Bioo Scientific) according to the manufacturer's protocol. After the amplification step, samples were analyzed using a Fragment Analyzer (Advanced Analytical), and specific fragments of the miRNA library (145 bp) were quantified. Samples were equally pooled for each particular sequencing run based on the concentration of miRNA library fragments, which were isolated using the Pippin Prep instrument using the 3% agarose (Sage Science) prior to sequencing. Isolated fragments were quantified using NanoDrop ND-1000 (Thermo Fisher Scientific) and Qubit® 2.0 fluorometer (Thermo Fisher Scientific) and used for sequencing on NextSeq 500 (Illumina) according to the manufacturer's protocol.

MPS Data Processing and Differential Expression Analysis

Human sequencing data were processed as described previously (Bencurova et al., 2017). Adapter trimming, quality control, and miRNA annotation against miRBase v21 were performed using the *Chimira* (Vitsios and Enright, 2015) tool. Further

analyses were performed using *R/Bioconductor* packages (R Core Team, 2020).

MPS data from the rat TLE model were analyzed individually for each age group. Adaptor sequences were scanned and identified by the Kraken package (v15-065) (Davis et al., 2013) and removed with Cutadapt (v1.12) software (Martin, 2011). Only high-quality reads (Phred $\geq$ 10 over at least 85% of the read length) with a length between 16 and 28 bp after adapter trimming were retained as potential miRNA reads. The quality of both raw and processed reads was evaluated using FastQC software (Andrews, 1973). The raw miRNA expression levels were quantified by seqBuster (1.2.4a6) (maximum of one mismatch) with miRBase annotation (v22) (Kozomara and Griffiths-Jones, 2014).

Differential expression analysis was evaluated for both human and rat data by R package DESeq2 (Love et al., 2014). Raw data and annotated sequences of the small RNA libraries can be found in the GEO database (accession numbers GSE99455 and GSE124332).

The expression of miRNA was determined by microRNA quantitative PCR (miQPCR) as described by Benes et al. (2015). Primers were either designed manually or downloaded from the list of miQPCR primers, validated, and optimized for our samples according to the MIQE Guidelines (Bustin et al., 2009). The protocol used for amplification, quantification, and evaluation of miRNA expression using miQPCR was previously described in Bencurova et al. (2017).

miRNA Target Prediction

Target prediction tools were applied to address putative mRNA targets (miRDB - MicroRNA Target Prediction And Functional Study Database) (Wong and Wang, 2015) and pathways (DIANA-mirPath v3) affected by miRNAs with altered regulation in both mTLE/HS patients and the rat model of TLE. Only miRNAs showing the same trend of dysregulation (upregulated/downregulated) in both species were included in target and pathway prediction. Pathway prediction was based on predicted mRNA targets and experimentally validated miRNA interactions from *DIANA-TarBase* (Vlachos et al., 2015). Both MirTarget and DIANA-mirPath analyzed specific miRNA targets for species *Rattus norvegicus* and *Homo sapiens sapiens* individually.

RESULTS

Whole miRNome Sequencing

Our first high-throughput screening focused on profiling the miRNA expression in mTLE/HS patients and controls in order to identify aberrantly expressed miRNAs in this disease (Bencurova et al., 2017). Briefly, we sequenced the hippocampi of 16 patients and eight postmortem controls with median raw reads of 10.8 million per sample. The number of reads after adapter trimming and miRNA mapping dropped to 1.5 million per sample (12% of total) with high quality of sequencing represented by the PHRED-like score above 30 for 98.5% reads. The MPS analyses detected 401 miRNAs with the coverage over 500 reads in all samples together. The total sum of ambiguous base content was below 0.01% of all bases. Prior to the interpretation of differential expression analysis, we conducted additional analysis of gender- and age-related miRNAs in our dataset in order to prevent bias arising from uneven distribution of age and gender in patient and control groups. These analyses did not uncover any gender-specific miRNA with an altered expression level in mTLE/HS within our data, while miR-7110-3p upregulated ($p = 0.028$) in controls $>$ 60 years of age was removed from follow-up analyses (data not shown). In our previous work, we described that miRNA distribution is impartial to the autopsy delay from the death of the subject and that the cellular composition of hippocampi is similar (based on the analysis of miRNAs enriched in specific cell types) in our patients and controls (Bencurova et al., 2017).

Parallel to human MPS, we sequenced rat hippocampi in the chronic stage of epileptogenesis (submitted manuscript). The final median of clean potential miRNA reads was 2.6 million ($\sim$53.91% of the raw reads) after adapter trimming, size selection of the trimmed reads, and removal of possible contaminants. Mapping to *miRBase* (v22) revealed the median content of miRNAs in the samples of 2.3 million (50.45% of the raw reads). Sequencing identified 412 unique miRNA species with read coverage $>$ 500 across all the samples. The average PHRED-like quality score of all samples was above 35, which indicated very high sequencing quality. The total sum of ambiguous base content was $<$ 0.01%. Since all rat individuals were age-matched males, housed under the same conditions, additional correlation analyses were unnecessary.

miRNA Expression in TLE Patients and Model

Principal component analysis (PCA) visualizes variation and uncovers distinct patterns in a dataset. This analysis showed different miRNA production between patients and rats – human individuals clustered separately from rats without any apparent effect of the age of TLE onset on the overall miRNA expression (**Figure 1**). Indeed, analysis of the differential expression using DESeq2 showed that only a fraction of over 400 identified miRNAs reached the threshold of differential expression ($p < 0.05$, fold change of upregulation or downregulation exceeding 1.4 and a minimum of 500 reads) in both human (**Supplementary Table S2**) and rat TLEs (**Supplementary Table S3**).

The basic concept suggests that the presence of seizures in childhood and adolescence could affect the miRNA expression profile and thus potentially introduce a defect in brain development (reviewed in Henshall, 2014; Rao and Pak, 2016). For this reason, we categorized and analyzed patient data in four categories based on their epilepsy onset age: (a) all patients together; (b) the first unprovoked seizure before the age of 10 (childhood); (c) between the 10th and 19th years (adolescent); and (d) at the age of 20 or later (adult onset).

The differential expression analysis of patients without respect to the first seizure was described in our previous study (Bencurova et al., 2017) and was focused on the detection of

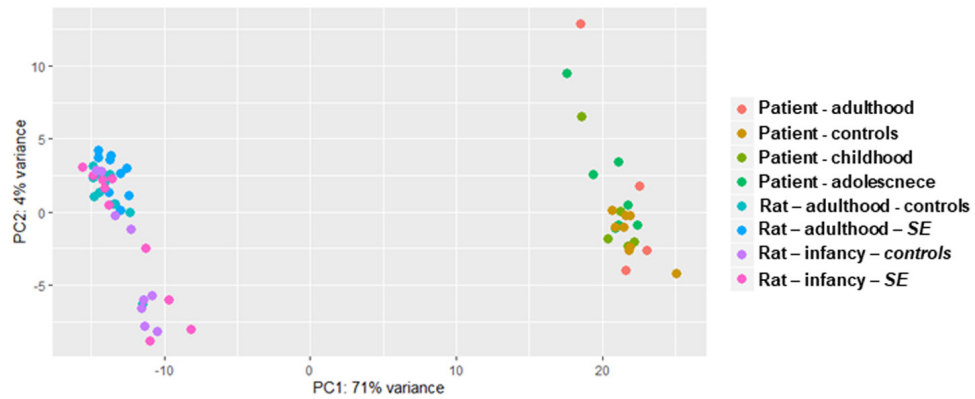

FIGURE 1 | PCA of whole-miRNome expression in rats and humans. The PCA is a transformation technique to describe the variation of miRNA expression (normalized read counts) and thus can detect the correlation and clustering in data. Our PCA plot indicates distinctive miRNA expression between patients and rat models of epilepsy.

dysregulated miRNAs in mTLE/HS patients whose age of the first unprovoked seizure was from 2 to 44 years. This group included mainly miRNAs previously associated with epilepsy, while nine of them have been described in epilepsy for the first time (Bencurova et al., 2017). Next, we searched in our MPS datasets for differentially expressed miRNAs in patients with the TLE onset between the ages of 2 and 9 years and discovered 123 miRNAs significantly dysregulated in patients. In the adolescence-onset category, 130 miRNAs were significantly dysregulated in TLE. The category with onset age above 20 contained 80 dysregulated miRNAs (**Supplementary Table S2**). Of note, 49 miRNAs were significantly dysregulated in all age categories (**Figure 2**).

Since all patients underwent surgery in adulthood, the period between epilepsy onset and sample collection differed among childhood-onset (mean = 33.2 years, *SD* = 10.3), adolescent-onset (mean = 23 years, *SD* = 9.3), and adult-onset (mean = 11 years, *SD* = 11.9) categories. The duration of epilepsy might have affected the expression of detected miRNA, and correlations were found between the expression of miR-142-3p, miR-135a-5p, and miR-484 with the duration of epilepsy, but their effects were low, as displayed in **Supplementary Figures S2, S4**.

DESeq2 analysis of all rat samples combined identified 19 miRNAs differentially expressed in the post-SE rat ($p < 0.05$, minimal fold change of 1.4 with read count over 500 across all samples). When categorized by the onset age, 42 miRNAs showed altered expression in adult-onset and 12 in the infancy-onset model of TLE (**Figure 2**). However, only rno-miR-24-2-5p and miR-135a-5p were upregulated in both age groups (**Supplementary Table S3**; submitted manuscript).

To identify dysregulated miRNAs shared between patients and our animal model, we compared categorized rat miRNA profiles (infancy and adult onset) with data in each onset age category of patients. This comparison showed 19 miRNAs with significantly altered expression in both patients and TLE rats (**Table 1**), but seven of these miRNAs showed the opposite direction of regulation in rats compared with patients (**Table 2**). The overlap between human miRNA profile and the combined ages of onset categories in the rat was minimal. miR-142-3p showed common dysregulation across all patient categories and rat adult-onset group, and miR-135a-5p was dysregulated in rats (both age groups) and patients with epilepsy onset in adulthood (**Table 1**). miR-142-5p was dysregulated in patients with epilepsy onset in infancy, adolescence, and patients without categorization (all onset ages). Altogether, rats with SE in adulthood showed higher similarity with mTLE/HS patients in all categories, while the infancy-onset group corresponded with the human profile only in the case of miR-135a-5p and miR-140-5p (**Figure 2**).

In patient samples, miQPCR validated the dysregulation of miR-129-2-3p and miR-142-3p across all onset categories in patients, and let-7b-3p, miR-135-5p, and miR-140-5p increased in patients with TLE onset in adolescence (**Table 1**). Further, miQPCR confirmed increased expressions of miR-142-5p, miR-193-5p, and miR-203a-3p in one or more onset groups in patients along with the group without onset categorization. In the rat samples, miQPCR validated three out of 12 miRNAs, which overlapped with patients in their altered expression in TLE in our sequencing results: miR-142-5p, miR-484, and miR-539-5p in the adult-onset group.

Putative Targets of Dysregulated miRNAs

The MirTarget search tool (miRDB-MicroRNA Target Prediction And Functional Study Database) produced a list of putative mRNA targets of all identified miRNAs with shared dysregulation in SE animals and mTLE + HS patients. **Table 3** shows brain-function-related targets with a target score of 90 or higher for humans and rats. Among the genes targeted in humans, the most frequent are potassium channels regulated by five miRNAs (miR-130b-3p, miR-135a-5p, miR-129-2-3p, miR-539-5p, and miR-484), followed by semaphorins and solute carriers of various molecules targeted by let-7b-3p and miR-135a-5p, miR-142-5p, and miR-539-5p. Solute carriers stand out also among mRNA

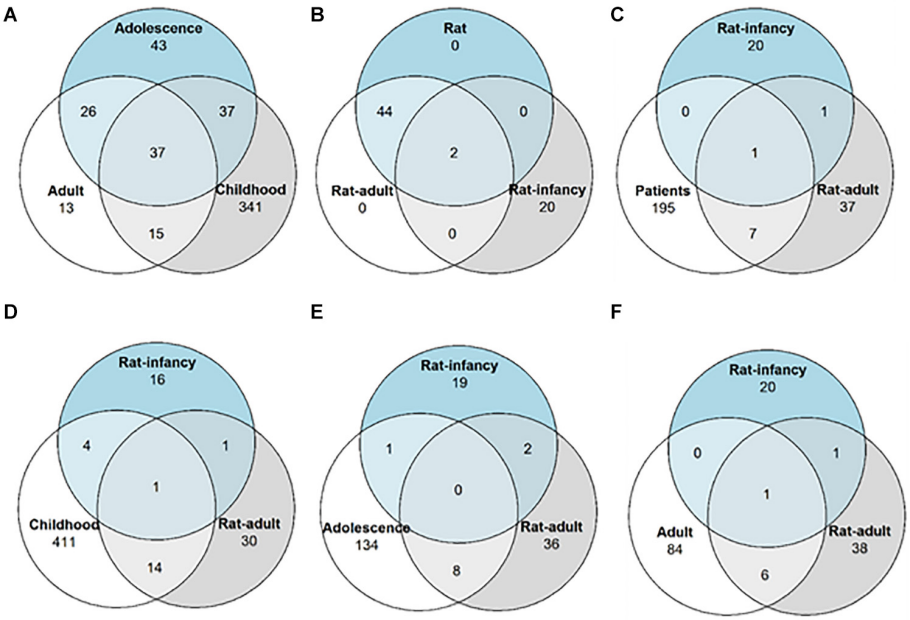

FIGURE 2 | Differentially expressed miRNA distribution across TLE onset stages. Venn diagrams showing the number of overlapping miRNAs with altered expression among **(A)** patients with different epilepsy onset ages; **(B)** both the rat model with different onset age and the rat model without onset age categorization; **(C)** patients without categorization and two rat models with different onset ages; **(D)** patients with epilepsy onset in infancy and both rat models of onset age; **(E)** patients with epilepsy onset in adolescence and both rat models of onset age; and **(F)** patients with epilepsy onset in adulthood and both rat models of onset age.

targets in rats with the same number of miRNAs involved in their regulation (let-7b-3p and miR-135a-5p, miR-142-5p, and miR-203a-3p). Unlike those in humans, calcium and sodium channels occur more frequently among targets than potassium channels, which are regulated only by miR-135a-5p in rats.

Similar to target prediction, humans had more affected pathways identified by *DIANA-mirPath* v3 software (Vlachos et al., 2015) compared with rat prediction data (**Supplementary Table S5**). In both cases, hundreds of genes undergo regulation by the combined force of miRNAs with shared dysregulation in mTLE patients and rats. Pathways common for both species predominantly comprised signaling pathways (Rap1, Ras, TGF-β, ubiquitin, etc.), however, circadian rhythm and gap junctions were also affected. In humans, this set of miRNAs also regulated the expression of genes involved in neurotransmitter synapses (dopaminergic, glutamatergic, and cholinergic) and axon guidance, while affecting the synaptic vesicle trafficking in rats.

DISCUSSION

The analysis of miRNA expression profile in brain tissues increasingly assists in the understanding of the biological processes involved in epileptogenesis and ictogenesis. However, previous comparative studies have explored the miRNA profiles mostly in patient samples affected by pharmacotherapies or models of epilepsy (e.g., cell culture AND animals), which do not correspond to the human biochemistry of the disease exactly. This limitation can be overcome by miRNA profile comparison of patients and model organisms that may reveal specific miRNAs playing an essential role in the onset or development of mTLE. Here, we compared the miRNA profiles of patients and rat models of epilepsy analyzed with the same workflow. This approach reduced technological bias and enhanced the accuracy of discovered miRNAs.

In our analyses of MPS results, we focused on the effect of the onset age on the differential miRNA expression, which seems to be smaller in mTLE/HS patients since 49 miRNAs show altered expression in all onset categories (**Figure 2**). On the contrary, the onset age in the rat model strongly determines the changes in miRNA expression related to post-SE epilepsy, and the profiling study of the animal model revealed only a limited number of dysregulated miRNAs. This difference in miRNA expression between human and model might arise from multiple sources. For instance, tissue samples originated from patients long into their condition (the period from diagnosis to surgery ranges from 1 to 45 years), which means a long and variable progression of the disease (e.g., development of comorbidities or brain damage) and exposure to multiple AEDs. Exposure to AEDs might increase the variability between humans and rats since patients received at the time of surgery on average two AEDs. Levetiracetam and carbamazepine were commonly administered to patients across all age groups. Nevertheless, the inter-individual AED variability might have introduced inconsistency in patient miRNA levels unrelated to onset age (**Supplementary Tables S1, S2**). We also addressed a distinct subpopulation of mTLE patients, which shares similar features—drug resistance and HS. In the rat model,

TABLE 1 | miRNA commonly dysregulated in mTLE/HS patients and TLE-like rats.

		MPS		miQPCR	
miRNA	**Age category**	***p*-value**	**Fold change**	***p*-value**	**Fold change**
(A)					
let-7b-3p	All onset ages	**0.047**	**1.73**	0.070	1.28
	2–9 years (childhood)	0.105	1.68	0.275	1.25
	10–19 years (adolescence)	**0.027**	**2.53**	**0.042**	**1.46**
	≥ 20 years (adult)	0.266	**2.32**	0.794	1.06
miR-129-2-3p	All onset ages	**0.000**	**3.19**	**0.006**	**2.12**
	2–9 years (childhood)	**0.000**	**4.11**	**0.002**	**2.60**
	10–19 years (adolescence)	**0.000**	**4.12**	**0.008**	**2.18**
	≥ 20 years (adult)	**0.000**	**3.10**	**0.034**	**2.34**
miR-130b-3p	All onset ages	**0.005**	**−1..07**	0.053	**1.49**
	2–9 years (childhood)	0.062	**−1..38**	0.166	**1.52**
	10–19 years (adolescence)	0.063	**−1..33**	0.076	**1.62**
	≥ 20 years (adult)	**0.000**	**−1..45**	0.566	1.24
miR-135a-5p	All onset ages	**0.000**	**1.61**	0.114	**1.50**
	2–9 years (childhood)	0.151	**1.42**	0.687	1.13
	10–19 years (adolescence)	0.099	**1.54**	**0.046**	**1.73**
	≥20 years (adult)	**0.026**	**1.75**	0.209	**1.69**
miR-140-5p	All onset ages	0.105	1.05	0.180	1.27
	2–9 years (childhood)	**0.012**	1.38	0.665	1.10
	10–19 years (adolescence)	**0.013**	**1.41**	**0.013**	**1.57**
	≥20 years (adult)	0.889	−1.27	0.872	1.04
miR-142-3p	All onset ages	**0.000**	**3.22**	**0.003**	**2.53**
	2–9 years (childhood)	**0.000**	**2.09**	**0.010**	**2.46**
	10–19 years (adolescence)	**0.000**	**2.42**	**0.010**	**2.46**
	≥20 years (adult)	**0.000**	**2.19**	**0.035**	**2.14**
miR-142-5p	All onset ages	**0.000**	**2.66**	**0.004**	**2.34**
	2–9 years (childhood)	**0.001**	**2.10**	**0.010**	**2.68**
	10–19 years (adolescence)	**0.006**	**1.87**	**0.009**	**2.77**
	≥ 20 years (adult)	**0.002**	**1.90**	**–**	**–**
miR-193a-5p	All onset ages	**0.011**	**1.63**	**0.000**	**2.46**
	2–9 years (childhood)	**0.004**	**1.84**	0.137	**1.56**
	10–19 years (adolescence)	**0.010**	**1.83**	**0.036**	**2.21**
	≥ 20 years (adult)	0.098	**1.59**	0.456	−1.21
miR-203a-3p	All onset ages	**0.003**	**1.79**	**0.000**	**2.20**
	≥ 20 years (adult)	0.302	1.14	0.068	**1.78**
	2–9 years (childhood)	**0.000**	**1.99**	**0.032**	**1.95**
	10–19 years (adolescence)	**0.002**	**1.97**	**0.001**	**2.62**
miR-484	All onset ages	0.013	1.05	0.025	**2.54**
	2–9 years (childhood)	0.004	1.34	0.151	**2.79**
	10–19 years (adolescence)	0.008	**1.40**	0.214	**2.16**
	≥ 20 years (adult)	0.002	**1.46**	0.169	**3.02**
miR-490-5p	All onset ages	0.041	1.07	0.916	1.03
	2–9 years (childhood)	0.103	1.13	0.987	1.01
	10–19 years (adolescence)	0.021	1.38	0.450	1.28
	≥ 20 years (adult)	0.002	**1.44**	0.290	−1.39
miR-539-5p	All onset ages	0.025	**−1..53**	0.182	**2.25**
	2–9 years (childhood)	0.001	**−1..73**	0.378	**2.64**
	10–19 years (adolescence)	0.000	**−1..86**	0.431	**2.07**
	≥ 20 years (adult)	0.433	−1.19	0.537	**2.13**

(Continued)

TABLE 1 | Continued

		MPS		miQPCR	
miRNA	**Age category**	***p*-value**	**Fold change**	***p*-value**	**Fold change**
(B)					
let-7b-3p	All onset ages	0.133	1.39	0.920	**−1..01**
	P12 (infant)	0.948	**−1..01**	0.811	**−1..05**
	P60 (adult)	**0.001**	**1.58**	0.886	1.02
miR-129-2-3p	All onset ages	**0.025**	1.23	0.102	1.13
	P12 (infant)	0.657	1.09	0.177	1.12
	P60 (adult)	**0.005**	**1.66**	0.182	1.15
miR-130b-3p	all onset ages	**0.001**	**−2.07**	0.770	**−1..05**
	P12 (infant)	0.571	**−1..25**	0.664	1.12
	P60 (adult)	**0.002**	**−3.48**	0.120	**−1..24**
miR-135a-5p	All onset ages	**0.000**	**1.50**	0.093	1.23
	P12 (infant)	**0.007**	**1.46**	0.211	**1.49**
	P60 (adult)	**0.001**	**1.58**	0.314	1.16
miR-140-5p	All onset ages	**0.014**	**1.40**	0.722	**−1..02**
	P12 (infant)	**0.018**	**1.42**	0.224	1.11
	P60 (adult)	0.099	1.27	0.100	**−1..17**
miR-142-3p	All onset ages	**0.040**	1.23	0.716	**−1..03**
	P12 (infant)	0.312	1.24	0.742	1.04
	P60 (adult)	**0.040**	**1.54**	0.332	**−1..09**
miR-142-5p	All onset ages	0.075	1.36	–	–
	P12 (infant)	0.989	**−1..00**	0.109	**1.56**
	P60 (adult)	**0.012**	**1.58**	**0.010**	**2.81**
miR-193a-5p	All onset ages	**0.008**	1.24	0.753	**−1..07**
	P12 (infant)	0.152	1.33	**0.000**	**−1..65**
	P60 (adult)	**0.026**	**1.58**	0.145	**1.45**
miR-203a-3p	All onset ages	**0.018**	1.24	0.904	1.01
	P12 (infant)	0.711	**−1..05**	0.630	**−1..09**
	P60 (adult)	**0.000**	**1.57**	0.368	1.11
miR-484	All onset ages	0.057	**1.51**	0.121	1.23
	P12 (infant)	0.754	1.08	0.579	**1.51**
	P60 (adult)	**0.009**	**1.87**	**0.023**	**1.53**
miR-490-5p	All onset ages	0.460	1.09	0.113	**−1..23**
	P12 (infant)	0.471	**−1..27**	**0.001**	**−1..58**
	P60 (adult)	**0.039**	**1.99**	0.733	1.04
miR-539-5p	All onset ages	0.081	**−1..09**	**0.017**	**−1..22**
	P12 (infant)	0.960	1.01	0.563	**−1..06**
	P60 (adult)	**0.028**	**−1..43**	**0.000**	**−1..41**

*List of miRNAs with altered expression determined by MPS and their miQPCR validation in **(A)** mTLE/HS patients and **(B)** rats 3 months after SE. miRNAs are displayed for each analyzed onset age category and all samples per species together (altogether 12 unique miRNAs). p-values below 0.05 are in bold. Fold changes < −1.4 or > 1.4 are in bold. Empty cells indicate impossibility to analyze miRNA expression due to high Ct values (>32) in miQPCR.*

potential bias increasing the influence is suppressed, and hence, the P12 and P60 groups differed solely in the age of SE induction and its consequences. We used age- and gender-matched controls for each age group, animals were not exposed to any medications besides those necessary for the model development, and they lived in a controlled environment. Furthermore, the outcome of SE induction at P12 in rats typically results in a slightly different condition than the model of SE in adult animals. Unlike adults, animals with SE at P12 develop only electrographic seizures at the chronic stage of the disease (motor seizures are not present), and they show a more discrete level of brain damage even though similar structures are affected (Nairismägi et al., 2006; Kubová and Mareš, 2013). On the other hand, induction of SE during brain development results in early manifestations of comorbidities such as impaired learning and memory problems (Rutten et al., 2002; Kubová et al., 2004; Mikulecká et al., 2019). These differences arising from the onset age in our model might explain the difference in miRNA profiles between rats with infant- and adult-onset TLEs.

Our profiling of miRNA expression in brain tissues discovered over a hundred of miRNAs with altered expression in patients with mTLE/HS (Bencurova et al., 2017). Out of these miRNAs,

TABLE 2 | miRNA with opposite dysregulation in mTLE/HS patients and TLE-like rats.

	Human mTLE + HS				Rat 3 months after SE		
First seizure	**miRNA**	***p*-value**	**FC**	**Age at SE**	**miRNA**	***p*-value**	**FC**
All onset ages	miR-22-3p	**	−1.52	All onset ages	miR-187-3p	**	−1.48
	miR-301a-3p	**	2.22		miR-211-5p	**	1.83
2–9 years (childhood)	miR-22-3p	**	−1.81		miR-301a-3p	**	−1.33
	miR-301a-3p	**	1.79		miR-376a-3p	*	−1.34
10–19 years (adolescence)	miR-187-3p	*	1.73		miR-92b-5p	*	−1.37
	miR-211-5p	**	−3.29	P12 (infant)	miR-22-3p	*	1.89
	miR-212-3p	**	−2.22		miR-301a-3p	*	−1.46
	miR-22-3p	**	−1.83	P60 (adult)	miR-187-3p	**	−2.05
	miR-301a-3p	**	1.91		miR-212-3p	**	1.69
≥20 years (adult)	miR-301a-3p	**	2.26				
	miR-211-5p	**	−4.96				
	miR-376a-3p	**	1.97				
	miR-92b-5p	*	2.00				

*List of miRNAs with altered expression (**p-value < 0.01; *p-value < 0.05; fold change over 1.4) with an opposite trend of dysregulation in mTLE/HS patients and rats 3 months after SE screened by MPS. miRNAs are displayed for each analyzed onset age category and all samples per species together (altogether seven unique miRNAs). FC—differential expression fold change.*

10 were also dysregulated in rats with onset in adulthood. In contrast, only miR-140-5p and miR-135a-5p showed concordant dysregulation in rats with onset in infancy (**Table 1** and **Figure 2**). Though the overlap with early-onset TLE in rats is minimal in our data, miR-140-5p shows elevated expression specific for this age group of rats and patients with adolescent-onset mTLE, which would be neglected if compared solely to the adult-onset model. The other reason for the limited overlap of miRNA profiles between the human and early-onset model of TLE might lie in the age difference – even though categorized, human patients underwent surgery with a large delay from the beginning of the disease after extensive medication. Moreover, the resemblance of human and rat with adult-onset miRNA profiles might be partially due to the presence of severe brain damage in these rats, indicating better resemblance of this model to patients with HS in mTLE/HS (Turski et al., 1986). Taken together, although our study showed cardinal differences between human and rat miRNA profiles in hippocampi, the results indicate that miRNA expression changes in mTLE/HS patients are more similar to rats with onset in adulthood than rats with onset in the infancy.

Nevertheless, almost all miRNAs detected by MPS and listed in **Table 1** were previously associated with epilepsy showing the same trend of dysregulation either in both patients and animal models (miR-129-2-3p, miR-135-5p and miR-193a-5p) or in just animal models of epilepsy (miR-140-5p, miR-142-3p, miR-142-5p, miR-203a-3p, and miR-539) (Kan et al., 2012; Risbud and Porter, 2013; Gorter et al., 2014; Kretschmann et al., 2014). In the case of miR-130b-3p, dubious results were previously reported showing both upregulation and downregulation of this miRNA in both patient and animal models of TLE (Liu et al., 2010; McKiernan et al., 2012a,b; Kaalund et al., 2014). let-7b-3p was reported by Risbud and colleagues as downregulated in rats with pilocarpine-induced SE, while miR-484 and miR-490-5p have not been associated with epilepsy so far (**Supplementary Table S6**). Additionally, we found an opposite significant dysregulation of seven miRNAs between patients and rats (**Table 2**). We did not study the reason for these opposite expressions and can only speculate that they arise from a specific reaction of the rat model on TLE onset or the specificity of this animal epilepsy model. The majority of these contradicting miRNAs were previously associated with epilepsy only in animal models. Kan et al. (2012) observed (2012), similarly to our data, the elevation of miR-301a-3p in their study of mTLE patients. On the other hand, miR-187-3p and miR-211-5p were previously identified as downregulated in human patients, which corresponds with the trend of dysregulation we observed in the rat model rather than in patients (McKiernan et al., 2012a; Kaalund et al., 2014).

This cross-comparison study of our previous miRNA profiling analyses showed that the expression of miR-142-5p was significantly dysregulated in the MPS results of patients (in all age groups) and rats with seizure onset in adulthood, but it was validated only in the patient group. To identify the potential targets of this miRNA, we employed miRDB software, which predicts about 300 potential mRNA targets involved in various pathways (e.g., signaling and cell cycle). Literature indicates that these miRNA target genes were included in immunomodulatory pathways. These studies showed in a functional experiment that miR-142-5p negatively regulates the expression of pro-inflammatory agents, interleukin 6 (IL-6), or high mobility group box (HMGB) gene, which are considered pro-convulsive (Kretschmann et al., 2014; Britton, 2016). This evidence supports the idea that autoimmunity plays a significant role in ictogenesis and epileptogenesis and shall be considered in epilepsy management. Besides, ILAE has recognized autoimmune epilepsy as a distinct entity and included it into classification since 2017 (Britton, 2016).

Another miRNA with great influence on TLE might be miR-135a-5p, which was significantly altered in patients and both rat models of mTLE. However, we did not validate this miRNA by miQPCR due to its low amount in samples. Based on the literature, this miRNA mediates the expression of various

TABLE 3 | Predicted targets of miRNA commonly dysregulated in human and rat TLEs.

miRNA	Human		Rat	
	Gene	**Product**	**Gene**	**Product**
let-7b-3p	BDNF	Brain-derived neurotrophic factor	BDNF	Brain-derived neurotrophic factor
	CACNA1C	Calcium voltage-gated channel subunit alpha 1 C	GLS	Glutaminase
	CAMTA1	Calmodulin binding transcription activator 1	NPY1R	Neuropeptide Y receptor Y1
	CARF	calcium responsive transcription factor	SCN7a	Sodium voltage-gated channel alpha subunit 7
	CEPT1	Choline/ethanolamine phosphotransferase 1	SLC18A2	Solute carrier family 18 member A2 (monoamines)
	GABRG1	Gamma-aminobutyric acid type A receptor gamma 1 subunit	SYNGR3	Synaptogyrin 3 (synaptic vesicles)
	GLS	Glutaminase		
	GPR37	G protein-coupled receptor 37		
	GRM5	Glutamate metabotropic receptor 5		
	MNX1	Motor neuron and pancreas homeobox 1		
	NBEA	Neurobeachin (neuron specific post-Golgi membrane traffic)		
	NEUROG2	Neurogenin 2 (differentiation and survival of dopaminergic neurons)		
	NGDN	Neuroguidin (development of nervous system)		
	NLGN1	Neuroligin 1 (formation and remodeling of synapses)		
	NPY	Neuropeptide Y		
	NRP2	Neuropilin 2 (axon guidance)		
	PSD2	Pleckstrin and Sec7 domain containing 2 (endocytosis)		
	SCAMP1	Secretory carrier membrane protein 1		
	SEMA3C	semaphorin 3C		
	SLC18A2	Solute carrier family 18 member A2 (monoamines)		
	SLC6A17	Solute carrier family 6 member 17 (presynaptic uptake of most neurotransmitters)		
	SLC6A4	Solute carrier family 6 member 4 (serotonin)		
	SNCAIP	synuclein alpha interacting protein		
	SYNGR3	Synaptogyrin 3 (synaptic vesicles)		
	TVP23B, C	*Trans*-Golgi network vesicle protein 23 homolog B and C		
	VAPA	VAMP-associated protein A		
miR-129-2-3p	GABRA1	Gamma-aminobutyric acid type A receptor alpha 1 subunit	GABRA1	Gamma-aminobutyric acid (GABA) A receptor, alpha 1
	KCNB1	Potassium voltage-gated channel subfamily B member 1	SCN3B	Sodium channel, voltage-gated, type III, beta
	MPZL1	Myelin protein zero like 1		
	NPTN	Neuroplastin (synaptic membrane Ig)		
	SACS	Sacsin molecular chaperone		
	SCN3B	Sodium voltage-gated channel beta subunit 3		
miR-130b-3p	CLCN3	Chloride voltage-gated channel 3	CLCN3	Chloride voltage-gated channel 3
	CLTC	Clathrin heavy chain	NEUROG1	Neurogenin 1
	GJA1	Gap junction protein alpha 1		
	KCNA4	Potassium voltage-gated channel subfamily A member 4		
	NEUROG1	Neurogenin 1		
	RTN1	Reticulon 1 (neuroendocrine secretion)		
	STON2	Stonin 2 (clathrin-associated)		
	SYBU	Syntabulin (axonal transport)		
miR-135a-5p	CACNA1D	Calcium voltage-gated channel subunit alpha 1 D	CACNA1D	Calcium channel, voltage-dependent, L type, alpha 1D subunit
	CACNA1E	Calcium voltage-gated channel subunit alpha 1 E	CPLX1	Complexin 1 (binding SNARE, synaptic transport)
	CPLX1	Complexin 1 (synaptic vesicles)	KCNAB3	Potassium voltage-gated channel subfamily A regulatory beta subunit 3
	CPLX2	Complexin 2 (synaptic vesicles)	KCND1	Potassium voltage-gated channel subfamily D member 1
	GRIA3	Glutamate ionotropic receptor AMPA type subunit 3	KCNJ6	Potassium voltage-gated channel subfamily J member 6
	GRID2	Glutamate ionotropic receptor delta type subunit 2	KCNS3	Potassium voltage-gated channel, modifier subfamily S, member 3

(Continued)

TABLE 3 | Continued

miRNA	Human		Rat	
	Gene	**Product**	**Gene**	**Product**
	KCNAB3	Potassium voltage-gated channel subfamily A regulatory beta subunit 3	NTNG1	Netrin G1 (axon guidance)
	KCNB1	Potassium voltage-gated channel subfamily B member 1	SLC24A2	Solute carrier family 24 member 2 (calcium/cation antiporter)
	KCNN3	Potassium calcium-activated channel subfamily N member 3	SLC5A7	Solute carrier family 5 (sodium/choline cotransporter), member 7
	KCNQ5	Potassium voltage-gated channel subfamily Q member 5	SLC6A5	Solute carrier family 6 member 5 (glycine)
	KCNS3	Potassium voltage-gated channel modifier subfamily S member 3	SYT3	Synaptotagmin 3
	NTNG1	Netrin G1 (axon guidance)	TNPO1	Transportin 1
	SEMA3A	Semaphorin 3A		
	SLC24A2	Solute carrier family 24 member 2 (calcium/cation antiporter)		
	SLC9A9	Solute carrier family 9 member A9 (sodium/proton exchanger)		
	SV2B	Synaptic vesicle glycoprotein 2B		
	SYT2	Synaptotagmin 2		
	SYT3	Synaptotagmin 3		
miR-140-5p	-		–	
miR-142-3p	CLDN12	Claudin 12 (tight junctions)	–	
	CLOCK	Clock circadian regulator		
	CLTA	Clathrin light chain A		
miR-142-5p	CBLN4	Cerebellin 4 precursor (synapse development)	NEDD1	Neural precursor cell expressed, developmentally downregulated 1
	CNTN1	Contactin 1 (neuronal adhesion)	SEPT2	Septin 2 (axon growth)
	NENF	Neudesin neurotrophic factor	SLC12A1	Solute carrier family 12 (sodium/potassium/chloride transporter), member 1
	SACS	Sacsin molecular chaperone	SLCO1B2	Solute carrier organic anion transporter family, member 1B2
	SLC12A2	Solute carrier family 12 member 2 (sodium, chloride reabsorption)		
	SLC18A2	Solute carrier family 18 member A2 (monoamines)		
	SLC24A2	Solute carrier family 24 member 2 (calcium/cation antiporter)	-	
miR-193a-5p	CLCA2	Chloride channel accessory 2	CACNB4	Calcium voltage-gated channel auxiliary subunit beta 4
	NETO2	Neuropilin and tolloid like 2 (axon guidance)		
miR-203a-3p	CAB39	Calcium binding protein 39	CACNA2D1	Calcium voltage-gated channel auxiliary subunit alpha 2 delta 1
	CLSTN3	Calsyntenin 3 (calcium-mediated postsynaptic signals)	GABARAPL1	GABA type A receptor associated protein like 1
	MYEF2	Myelin expression factor 2	GABRA1	Gamma-aminobutyric acid type A receptor alpha 1 subunit
	NOCT	Nocturnin (circadian rhythm)	SCN2A	Sodium voltage-gated channel alpha subunit 2
	OLFM3	Olfactomedin 3	SEMA5A	Semaphorin 5A (axon guidance)
	PSD3	Pleckstrin and Sec7 domain containing 3 (endocytosis)	SLC12A2	Solute carrier family 12 member 2 (Na/K/2Cl cotransporter)
	SEMA5A	Semaphorin 5A (axon guidance)	SLC9A5	Solute carrier family 9 member A5 (Na^+/H^+)
	SGMS2	Sphingomyelin synthase 2		
miR-484	KCNJ14	Potassium voltage-gated channel subfamily J member 14		
	TNR	Tenascin R (axon growth)		
miR-490-5p	-		-	
miR-539-5p	GABRA4	Gamma-aminobutyric acid type A receptor alpha 4 subunit	NELL2	Neural EGFL like 2
	KCNB1	Potassium voltage-gated channel subfamily B member 1	SEMA3D	Semaphorin 3D (axon guidance)
	KCNG3	Potassium voltage-gated channel modifier subfamily G member 3		
	NAV1	Neuron navigator 1		
	NELL2	Neural EGFL like 2		

(Continued)

TABLE 3 | Continued

miRNA	Human		Rat	
	Gene	Product	Gene	Product
	NEUROD4	Neuronal differentiation 4		
	OPRM1	Opioid receptor mu 1		
	SEMA3A	Semaphorin 3A (axon guidance)		
	SLC1A2	Solute carrier family 1 member 2 (glutamate uptake)		
	SLC2A14	Solute carrier family 2 member 14 (glucose)		
	SLC5A7	Solute carrier family 5 member 7 (choline uptake)		
	SNAP29	Synaptosome-associated protein 29		

Brain physiology-, function-, and development-related predicted targets of miRNAs identified with altered regulation by miRNA sequencing. miRNA targets selected from a list produced by the MirTarget search tool (http://mirdb.org/cgi-bin/search.cgi) individually for humans and rats with a target score above 90 for all miRNAs with common dysregulation in mTLE/HS patients and TLE-like rats (3 months after SE).

proteins included in brain function and neuron development, e.g., serotonin receptor and transporter (Artigas et al., 2018) or complexin 1/2 in the amygdala (Mannironi et al., 2018). It also regulates developmental axon growth and branching, cortical neuronal migration, or regeneration of retinal ganglion cell axons (van Battum et al., 2018). Besides, recent findings revealed that miR-135a-5p affects spontaneous recurrent seizures in the TLE model (Vangoor et al., 2019), which confirms our finding.

Besides, miR-142-5p, miR-142-3p, and miR-129-2-3p have also altered expressions across all patient categories and adult-onset TLE in rats. Functional studies showed that miR-142-3p affects not only immunomodulation via control of IL-1β and IL-10 but also the expression of D1 dopaminergic receptors while suppressing neuronal growth (Tobón et al., 2012; Mandolesi et al., 2017). In the case of miR-129-2-3p, our target prediction indicated regulation of γ-aminobutyric acid receptor 1 (GABRA1) and sodium voltage-gated channel common for both humans and rats (**Table 2**). Previous experiments on cell cultures suggest that miR-129-2-3p represses expression of caspase 6 and spleen tyrosine kinase (SYK) (Huang et al., 2019; Umehara et al., 2019).

Among limitations of this study belongs the age discrepancy between the epilepsy onset and the resection of epileptic foci in patients, which is different from the condition in the rat model of epilepsy. Another potential drawback is patient classification based only on the age onset since different classifications (e.g., etiology based) might yield different results. Due to the small amount of unique patient samples and limited sensitivity of miQPCR, we did not validate discovered miRNAs. Finally, predicted gene targets of discussed miRNAs were generated *in silico*, and they require validation in brain tissues by functional experiments.

In summary, our cross-comparison study compared miRNA profiles of mTLE/HS patients with two different age-onset rat models of TLE. This comparison was focused on both miRNA profiles of all patients and patients categorized based on epilepsy onset age, which plays a substantial role in disorder outcome. These analyses confirmed particular dysregulation of miRNA expression in different onset ages and discovered several miRNAs, which might be truly connected to epileptogenesis and ictogenesis in both patients and animal models. Our analyses also showed that rats with TLE onset in adulthood showed greater resemblance to miRNA profiles of mTLE/HS patients than rats with onset in infancy. Finally, our study enhanced insight into the general knowledge of epilepsy and should be considered in the planning of future epilepsy experiments with animal models.

DATA AVAILABILITY STATEMENT

The datasets generated for this study can be found in the GEO database (accession numbers GSE99455 and GSE124332).

ETHICS STATEMENT

Written informed consent was obtained from the individual(s) and/or minor(s)' legal guardian/next of kin for the publication of any potentially identifiable images or data included in this article. The studies involving human participants were reviewed and approved by the Ethical Committee of St. Anne's University Hospital in Brno (approval number 9G/2015-KS). The patients/participants provided their written informed consent to participate in this study. The animal study was reviewed and approved by the Ethical Committee of the Czech Academy of Sciences (approval number 128/2013).

AUTHOR CONTRIBUTIONS

This manuscript has been read and approved by all named authors and all authors agreed with the order of authors listed in the manuscript. The authors consent to take public responsibility for the content of the manuscript and confirm that the manuscript was prepared following ethical guidelines and regulations of their institutions concerning intellectual property. All authors have had access to all the data in the study and contributed to the study design, data acquisition, data analysis, interpretation, drafting, and revising the manuscript.

FUNDING

This work has received funding from the Czech Science Foundation (Project Nos. GA16-04726S and 19-11931S); the

Ministry of Education, Youth and Sports of the Czech Republic under the National Sustainability Program II project CEITEC 2020 (LQ1601), the support for long-term conceptual development of research organization RVO: 67985823.

ACKNOWLEDGMENTS

We acknowledge the CF Genomics CEITEC MU supported by the NCMG research infrastructure (LM2015091 funded by MEYS CR) for their support with obtaining the scientific data presented in this paper.

SUPPLEMENTARY MATERIAL

The Supplementary Material for this article can be found online at: https://www.frontiersin.org/articles/10.3389/fnins.2020.00924/full#supplementary-material

REFERENCES

Andrews, S. (1973). Babraham bioinformatics - FastQC a quality control tool for high throughput sequence data. *Soil* 5, 47–81. doi: 10.1016/0038-0717(73)90093-X

Artigas, F., Celada, P., and Bortolozzi, A. (2018). Can we increase the speed and efficacy of antidepressant treatments? Part II. Glutamatergic and RNA interference strategies. *Eur. Neuropsychopharmacol.* 28, 457–482. doi: 10.1016/j.euroneuro.2018.01.005

Bartel, D. P. (2009). MicroRNAs: target recognition and regulatory functions. *Cell* 136, 215–233. doi: 10.1016/j.cell.2009.01.002

Bencurova, P., Baloun, J., Musilova, K., Radova, L., Tichy, B., Pail, M., et al. (2017). MicroRNA and mesial temporal lobe epilepsy with hippocampal sclerosis: whole miRNome profiling of human hippocampus. *Epilepsia* 58, 1782–1793. doi: 10.1111/epi.13870

Benes, V., Collier, P., Kordes, C., Stolte, J., Rausch, T., Muckentaler, M. U., et al. (2015). Identification of cytokine-induced modulation of microRNA expression and secretion as measured by a novel microRNA specific qPCR assay. *Sci. Rep.* 5:11590. doi: 10.1038/srep11590

Blümcke, I., Thom, M., Aronica, E., Armstrong, D. D., Bartolomei, F., Bernasconi, A., et al. (2013). International consensus classification of hippocampal sclerosis in temporal lobe epilepsy: a task force report from the ILAE commission on diagnostic methods. *Epilepsia* 54, 1315–1329. doi: 10.1111/epi.12220

Brennan, G. P., and Henshall, D. C. (2018). microRNAs in the pathophysiology of epilepsy. *Neurosci. Lett.* 667, 47–52. doi: 10.1016/j.neulet.2017.01.017

Britton, J. (2016). Autoimmune epilepsy. *Handb. Clin. Neurol.* 133, 219–245. doi: 10.1016/B978-0-444-63432-0.00013-X

Bustin, S. A., Benes, V., Garson, J. A., Hellemans, J., Huggett, J., Kubista, M., et al. (2009). The MIQE guidelines: minimum information for publication of quantitative real-time PCR experiments. *Clin. Chem.* 55, 611–622. doi: 10.1373/clinchem.2008.112797

R Core Team (2020). *R: A Language and Environment for Statistical Computing*. Available online at: http://www.r-project.org/ (accessed June 30, 2020).

Commission on Classification and Terminology of the ILAE (1989). Proposal for revised classification of epilepsies and epileptic syndromes. *Epilepsia* 30, 389–399. doi: 10.1111/j.1528-1157.1989.tb05316.x

Crespo, M. C., Tomé-Carneiro, J., Gómez-Coronado, D., Burgos-Ramos, E., Garciá-Serrano, A., Martín-Hernández, R., et al. (2018). Modulation of miRNA expression in aged rat hippocampus by buttermilk and krill oil. *Sci. Rep.* 8:3993. doi: 10.1038/s41598-018-22148-5

Davis, M. P. A., van Dongen, S., Abreu-Goodger, C., Bartonicek, N., and Enright, A. J. (2013). Kraken: a set of tools for quality control and analysis of high-throughput sequence data. *Methods* 63, 41–49. doi: 10.1016/j.ymeth.2013.06.027

Dluzen, D. F., Noren Hooten, N., Zhang, Y., Kim, Y., Glover, F. E., Tajuddin, S. M., et al. (2016). Racial differences in microRNA and gene expression in hypertensive women. *Sci. Rep.* 6:35815. doi: 10.1038/srep35815

Gorter, J. A., Iyer, A., White, I., Colzi, A., van Vliet, E. A., Sisodiya, S., et al. (2014). Hippocampal subregion-specific microRNA expression during epileptogenesis in experimental temporal lobe epilepsy. *Neurobiol. Dis.* 62, 508–520. doi: 10.1016/j.nbd.2013.10.026

Gulyaeva, L. F., and Kushlinskiy, N. E. (2016). Regulatory mechanisms of microRNA expression. *J. Transl. Med.* 14:143. doi: 10.1186/s12967-016-0893-x

Henshall, D. C. (2014). MicroRNA and epilepsy: profiling, functions and potential clinical applications. *Curr. Opin. Neurol.* 27, 199–205. doi: 10.1097/WCO.0000000000000079

Huan, T., Chen, G., Liu, C., Bhattacharya, A., Rong, J., Chen, B. H., et al. (2018). Age-associated microRNA expression in human peripheral blood is associated with all-cause mortality and age-related traits. *Aging Cell* 17:e12687. doi: 10.1111/acel.12687

Huang, S., Lv, Z., Wen, Y., Wei, Y., Zhou, L., Ke, Y., et al. (2019). miR-129-2-3p directly targets SYK gene and associates with the risk of ischaemic stroke in a Chinese population. *J. Cell. Mol. Med.* 23, 167–176. doi: 10.1111/jcmm.13901

Kaalund, S. S., Venø, M. T., Bak, M., Møller, R. S., Laursen, H., Madsen, F., et al. (2014). Aberrant expression of miR-218 and miR-204 in human mesial temporal lobe epilepsy and hippocampal sclerosis-Convergence on axonal guidance. *Epilepsia* 55, 2017–2027. doi: 10.1111/epi.12839

Kakimoto, Y., Kamiguchi, H., Ochiai, E., Satoh, F., and Osawa, M. (2015). MicroRNA stability in postmortem FFPE tissues: quantitative analysis using autoptic samples from acute myocardial infarction patients. *PLoS One* 10::e0129338. doi: 10.1371/journal.pone.0129338

Kan, A. A., van Erp, S., Derijck, A. A. H. A., de Wit, M., Hessel, E. V. S., O'Duibhir, E., et al. (2012). Genome-wide microRNA profiling of human temporal lobe epilepsy identifies modulators of the immune response. *Cell. Mol. Life Sci.* 69, 3127–3145. doi: 10.1007/s00018-012-0992-997

Kilkenny, C., Browne, W. J., Cuthill, I. C., Emerson, M., and Altman, D. G. (2010). Improving bioscience research reporting: the ARRIVE guidelines for reporting animal research. *PLoS Biol.* 8:e1000412. doi: 10.1371/journal.pbio.1000412

Korotkov, A., Mills, J. D., Gorter, J. A., Van Vliet, E. A., and Aronica, E. (2017). Systematic review and meta- analysis of differentially expressed miRNAs in experimental and human temporal lobe epilepsy. *Sci. Rep.* 7:11592. doi: 10.1038/s41598-017-11510-8

Kozomara, A., and Griffiths-Jones, S. (2014). MiRBase: annotating high confidence microRNAs using deep sequencing data. *Nucleic Acids Res.* 42, D68–D73. doi: 10.1093/nar/gkt1181

Kretschmann, A., Danis, B., Andonovic, L., Abnaof, K., van Rikxoort, M., Siegel, F., et al. (2014). Different microRNA profiles in chronic epilepsy versus acute seizure mouse models. *J. Mol. Neurosci.* 55, 466–479. doi: 10.1007/s12031-014-0368-6

Kubová, H., and Mareš, P. (2013). Are morphologic and functional consequences of status epilepticus in infant rats progressive? *Neuroscience* 235, 232–249. doi: 10.1016/j.neuroscience.2012.12.055

Kubová, H., Mares, P., Suchomelová, L., Brozek, G., Druga, R., and Pitkänen, A. (2004). Status epilepticus in immature rats leads to behavioural and cognitive impairment and epileptogenesis. *Eur. J. Neurosci.* 19, 3255–3265. doi: 10.1111/j.0953-816X.2004.03410.x

Leung, A. K. L., and Sharp, P. A. (2010). MicroRNA functions in stress responses. *Mol. Cell* 40, 205–215. doi: 10.1016/j.molcel.2010.09.027

Li, Y., and Kowdley, K. V. (2012). MicroRNAs in common human diseases. *Genomics Proteomics Bioinforma.* 10, 246–253. doi: 10.1016/j.gpb.2012.07.005

Liu, D. Z., Tian, Y., Ander, B. P., Xu, H., Stamova, B. S., Zhan, X., et al. (2010). Brain and blood microRNA expression profiling of ischemic stroke, intracerebral hemorrhage, and kainate seizures. *J. Cereb. Blood Flow Metab.* 30, 92–101. doi: 10.1038/jcbfm.2009.186

Love, M. I., Huber, W., and Anders, S. (2014). Moderated estimation of fold change and dispersion for RNA-seq data with DESeq2. *Genome Biol.* 15:550. doi: 10.1186/s13059-014-0550-8

Mandolesi, G., De Vito, F., Musella, A., Gentile, A., Bullitta, S., Fresegna, D., et al. (2017). MiR-142-3p is a key regulator of IL-1β-dependent synaptopathy in neuroinflammation. *J. Neurosci.* 37, 546–561. doi: 10.1523/JNEUROSCI.0851-16.2016

Mannironi, C., Biundo, A., Rajendran, S., De Vito, F., Saba, L., Caioli, S., et al. (2018). miR-135a Regulates synaptic transmission and anxiety-like behavior in amygdala. *Mol. Neurobiol.* 55, 3301–3315. doi: 10.1007/s12035-017-0564-9

Martin, M. (2011). Cutadapt removes adapter sequences from high-throughput sequencing reads. *EMBnet. J.* 17, 10–12. doi: 10.14806/ej.17.1.200

McKiernan, R. C., Jimenez-Mateos, E. M., Bray, I., Engel, T., Brennan, G. P., Sano, T., et al. (2012a). Reduced mature microRNA levels in association with dicer loss in human temporal lobe epilepsy with hippocampal sclerosis. *PLoS One* 7:e35921. doi: 10.1371/journal.pone.0035921

McKiernan, R. C., Jimenez-Mateos, E. M., Sano, T., Bray, I., Stallings, R. L., Simon, R. P., et al. (2012b). Expression profiling the microRNA response to epileptic preconditioning identifies miR-184 as a modulator of seizure-induced neuronal death. *Exp. Neurol.* 237, 346–354. doi: 10.1016/j.expneurol.2012.06.029

Mikulecká, A., Druga, R., Stuchlík, A., Mareš, P., and Kubová, H. (2019). Comorbidities of early-onset temporal epilepsy: cognitive, social, emotional, and morphologic dimensions. *Exp. Neurol.* 320, 113005. doi: 10.1016/j.expneurol.2019.113005

Nairismägi, J., Pitkänen, A., Kettunen, M. I., Kauppinen, R. A., and Kubova, H. (2006). Status epilepticus in 12-day-old rats leads to temporal lobe neurodegeneration and volume reduction: a histologic and MRI study. *Epilepsia* 47, 479–488. doi: 10.1111/j.1528-1167.2006.00455.x

Rao, Y. S., and Pak, T. R. (2016). microRNAs and the adolescent brain: filling the knowledge gap. *Neurosci. Biobehav. Rev.* 70, 313–322. doi: 10.1016/j.neubiorev.2016.06.008

Risbud, R. M., and Porter, B. E. (2013). Changes in MicroRNA Expression in the whole hippocampus and hippocampal synaptoneurosome fraction following pilocarpine induced status epilepticus. *PLoS One* 8:e53464. doi: 10.1371/journal.pone.0053464

Roncon, P., Soukupovà, M., Binaschi, A., Falcicchia, C., Zucchini, S., Ferracin, M., et al. (2015). MicroRNA profiles in hippocampal granule cells and plasma of rats with pilocarpine-induced epilepsy – comparison with human epileptic samples. *Sci. Rep.* 5:14143. doi: 10.1038/srep14143

Rutten, A., Van Albada, M., Silveira, D. C., Cha, B. H., Liu, X., Hu, Y. N., et al. (2002). Memory impairment following status epilepticus in immature rats: time-course and environmental effects. *Eur. J. Neurosci.*, 16, 501–513. doi: 10.1046/j.1460-9568.2002.02103.x

Srinivasan, S., Selvan, S. T., Archunan, G., Gulyas, B., and Padmanabhan, P. (2013). MicroRNAs -the next generation therapeutic targets in human diseases. *Theranostics* 3, 930–942. doi: 10.7150/thno.7026

Thom, M., Eriksson, S., Martinian, L., Caboclo, L. O., McEvoy, A. W., Duncan, J. S., et al. (2009). Temporal lobe sclerosis associated with hippocampal sclerosis in temporal lobe epilepsy: neuropathological features. *J. Neuropathol. Exp. Neurol.* 68, 928–938. doi: 10.1097/NEN.0b013e3181b05d67

Tobón, K. E., Chang, D., and Kuzhikandathil, E. V. (2012). MicroRNA 142-3p mediates post-transcriptional regulation of D1 dopamine receptor expression. *PLoS One* 7:e49288. doi: 10.1371/journal.pone.0049288

Turski, L., Cavalheiro, E. A., Sieklucka-Dziuba, M., Ikonomidou-Turski, C., Czuczwar, S. J., and Turski, W. A. (1986). Seizures produced by pilocarpine: neuropathological sequelae and activity of glutamate decarboxylase in the rat forebrain. *Brain Res.* 398, 37–48. doi: 10.1016/0006-8993(86)91247-3

Umehara, T., Mori, R., Mace, K. A., Murase, T., Abe, Y., Yamamoto, T., et al. (2019). Identification of specific miRNAs in neutrophils of type 2 diabetic mice: overexpression of miRNA-129-2-3p accelerates diabetic wound healing. *Diabetes* 68, 617–630. doi: 10.2337/db18-0313

van Battum, E. Y., Verhagen, M. G., Vangoor, V. R., Fujita, Y., Derijck, A. A. H. A., O'Duibhir, E., et al. (2018). An image-based miRNA screen identifies miRNA-135s as regulators of CNS axon growth and regeneration by targeting krüppel-like factor 4. *J. Neurosci.* 38, 613–630. doi: 10.1523/JNEUROSCI.0662-17.2017

Vangoor, V. R., Reschke, C. R., Senthilkumar, K., Van De Haar, L. L., de Wit, M., Giuliani, G., et al. (2019). Antagonizing increased miR-135a levels at the chronic stage of experimental TLE reduces spontaneous recurrent seizures. *J. Neurosci.* 39, 5064–5079. doi: 10.1523/JNEUROSCI.3014-18.2019

Vitsios, D. M., and Enright, A. J. (2015). Chimira: analysis of small RNA sequencing data and microRNA modifications: fig. 1. *Bioinformatics* 31, 3365–3367. doi: 10.1093/bioinformatics/btv380

Vlachos, I. S., Zagganas, K., Paraskevopoulou, M. D., Georgakilas, G., Karagkouni, D., Vergoulis, T., et al. (2015). DIANA-miRPath v3.0: deciphering microRNA function with experimental support. *Nucleic Acids Res.* 43, W460–W466. doi: 10.1093/nar/gkv403

Wong, N., and Wang, X. (2015). miRDB: an online resource for microRNA target prediction and functional annotations. *Nucleic Acids Res.* 43, D146–D152. doi: 10.1093/nar/gku1104

Conflict of Interest: The authors declare that the research was conducted in the absence of any commercial or financial relationships that could be construed as a potential conflict of interest.

frontiers in Neurology

ORIGINAL RESEARCH
published: 12 July 2021
doi: 10.3389/fneur.2021.625017

OPEN ACCESS

Edited by:
Bridgette D. Semple, Monash University, Australia

Reviewed by:
Eugene Golanov, Houston Methodist Hospital, United States
Bevan Scott Main, Georgetown University, United States

***Correspondence:**
Thimmasettappa Thippeswamy
tswamy@iastate.edu

†Present address:
Graeme J. Sills, School of Life Sciences, University of Glasgow, Glasgow, United Kingdom
Thimmasettappa Thippeswamy, Epilepsy Research Laboratory, Department of Biomedical Sciences, College of Veterinary Medicine, Iowa State University, Ames, IA, United States
Karen Tse, GW Pharmaceuticals, Cambridge, United Kingdom
Edward Beamer, Department of Life Sciences, Faculty of Science and Engineering, Manchester Metropolitan University, Manchester, United Kingdom

Specialty section:
This article was submitted to Neurotrauma, a section of the journal Frontiers in Neurology

Received: *02 November 2020*
Accepted: *07 June 2021*
Published: *12 July 2021*

Citation:
Tse K, Beamer E, Simpson D, Beynon RJ, Sills GJ and Thippeswamy T (2021) The Impacts of Surgery and Intracerebral Electrodes in C57BL/6J Mouse Kainate Model of Epileptogenesis: Seizure Threshold, Proteomics, and Cytokine Profiles. Front. Neurol. 12:625017. doi: 10.3389/fneur.2021.625017

The Impacts of Surgery and Intracerebral Electrodes in C57BL/6J Mouse Kainate Model of Epileptogenesis: Seizure Threshold, Proteomics, and Cytokine Profiles

***Karen Tse*[1,2†], *Edward Beamer*[2†], *Deborah Simpson*[3], *Robert J. Beynon*[3], *Graeme J. Sills*[2†] *and Thimmasettappa Thippeswamy*[1*†]**

[1] *Department of Musculoskeletal Biology, Institute of Ageing and Chronic Disease, University of Liverpool, Liverpool, United Kingdom,* [2] *Department of Molecular and Clinical Pharmacology, Institute of Translational Medicine, University of Liverpool, Liverpool, United Kingdom,* [3] *Centre for Proteome Research, Institute of Integrative Biology, University of Liverpool, Liverpool, United Kingdom*

Intracranial electroencephalography (EEG) is commonly used to study epileptogenesis and epilepsy in experimental models. Chronic gliosis and neurodegeneration at the injury site are known to be associated with surgically implanted electrodes in both humans and experimental models. Currently, however, there are no reports on the impact of intracerebral electrodes on proteins in the hippocampus and proinflammatory cytokines in the cerebral cortex and plasma in experimental models. We used an unbiased, label-free proteomics approach to identify the altered proteins in the hippocampus, and multiplex assay for cytokines in the cerebral cortex and plasma of C57BL/6J mice following bilateral surgical implantation of electrodes into the cerebral hemispheres. Seven days following surgery, a repeated low dose kainate (KA) regimen was followed to induce *status epilepticus (SE).* Surgical implantation of electrodes reduced the amount of KA necessary to induce SE by 50%, compared with mice without surgery. Tissues were harvested 7 days post-SE (i.e., 14 days post-surgery) and compared with vehicle-treated mice. Proteomic profiling showed more proteins (103, 6.8% of all proteins identified) with significantly changed expression ($p < 0.01$) driven by surgery than by KA treatment itself without surgery (27, 1.8% of all proteins identified). Further, electrode implantation approximately doubled the number of KA-induced changes in protein expression (55, 3.6% of all identified proteins). Further analysis revealed that intracerebral electrodes and KA altered the expression of proteins associated with epileptogenesis such as inflammation (C1q system), neurodegeneration (cystatin-C, galectin-1, cathepsin B, heat-shock protein 25), blood–brain barrier dysfunction (fibrinogen-α, serum albumin, α2 macroglobulin), and gliosis (vimentin, GFAP, filamin-A). The multiplex assay revealed a significant increase in key cytokines such as TNFα, IL-1β, IL-4, IL-5, IL-6, IL-10, IL12p70,

IFN-γ, and KC/GRO in the cerebral cortex and some in the plasma in the surgery group. Overall, these findings demonstrate that surgical implantation of depth electrodes alters some of the molecules that may have a role in epileptogenesis in experimental models.

Keywords: intracerebral electrodes, traumatic brain injury, neuroinflammation, proinflammatory cytokines, epilepsy, blood-brain barrier, seizure threshold

INTRODUCTION

In some animal models of epilepsy, cranial surgery (drilling burr holes through the skull) is required to implant electrodes for acquiring electroencephalography (EEG) recordings (1–4) and electrical kindling (5, 6) or to implant a cannula for intracerebral administration of drugs (7–9). The incidence of post-craniotomy seizures in humans has been estimated to be 15–20% (10). To our knowledge, no post-operative spontaneous seizures have been reported in rodent models. A study in the rat model, however, revealed abnormal EEG patterns (11), and several other studies in rodent models reported a reduced seizure threshold to chemoconvulsants following cranial surgery (12–15). Implantation of electrodes for kindling causes focal neuronal damage, resembling a penetrating brain injury in humans (12, 13, 16, 17), and it is unclear the extent to which the injury itself contributes to the kindling process (14). Recently, we demonstrated that even epidurally placed electrodes reduce seizure threshold induced by systemic administration of kainate (KA) (15).

KA is widely used as a chemoconvulsant in experimental rodent models for the study of the cellular and molecular mechanisms involved in epileptogenesis (18, 19). Continuous EEG is employed for the detection of the onset and progression of chronic epilepsy, via monitoring of the frequency, duration, and semiology of spontaneous recurrent seizures (SRS) and tracking of other epilepsy-associated electrographic signatures such as interictal spikes (2, 3, 20–26). Acquisition of EEG from experimental models requires the implantation of electrodes on either the *dura mater* or into the brain. It is presumed that the mechanism of epileptogenesis following chemoconvulsant-induced *status epilepticus* (SE) in experimental animals is independent of electrode implantation, but the mechanisms are not completely known. Understanding the differential expression of proteins due to surgical implantation of electrodes alone and subsequent exposure to chemoconvulsant may provide some insight into the mechanism of epileptogenesis. Three proteomics studies have been reported from rodent epilepsy models so far: a C57BL/6J mouse model with intrahippocampal KA approach but without electrodes (27), a rat pilocarpine model without electrodes (28), and an amygdala electrical kindling in female rats (29). There are currently no reports, however, on demonstrating the impact of surgically implanted intracerebral electrodes on protein expression in the hippocampus or cerebral cortical and plasma cytokines levels. Surgical procedure reduce seizure threshold, thereby requiring less KA to induce severe SE (15). This is likely due to associated inflammation in the brain; however, the mechanistic pathways are still largely unknown. To address this, we conducted a proteomics study on the hippocampus and proinflammatory cytokine assay of both cortical tissue and plasma in C57BL/6J mice with and without the implantation of intracerebral electrodes and with and without KA exposure. Proteins that alter due to surgical procedures and KA may facilitate the development of epilepsy and may reveal potential therapeutic targets for disease modification in epileptogenesis.

MATERIALS AND METHODS

Experimental Animals

All experimental procedures in animals were reviewed and approved by the University of Liverpool Ethics Committee as per the Animal (Scientific Procedures) Act, 1986 (UK). All experiments were conducted at the University of Liverpool. Adult male C57BL/6J mice (25–30 g; 8–9 weeks old) were purchased from Charles River, Margate, UK, and habituated for at least 4 days prior to the procedures. All animals had unlimited access to food and water. To determine the effects of intracerebral electrodes on seizure threshold for KA-induced SE, we used 15 mice that had undergone surgery and compared with a large cohort of mice ($n = 187$) without surgery. For the proteomics and Meso Scale Discovery (MSD) multiplex studies, we used a total of eight KA-treated mice (four mice per group; surgery and without surgery). These eight mice were chosen based on similar SE severity i.e., >45 min of convulsive seizures during the 2 h SE period from the first stage 5 seizure to diazepam treatment, and the KA dose of 20–25 mg/kg (4/5 doses of 5 mg/kg). All other mice were euthanized at various time points post-SE, and the tissues were archived for the other studies (not reported here). An additional eight mice (four per group) of the same age from each vehicle-treated (with and without surgery) served as controls for surgery and KA groups. All animals were euthanized at the end of the experiment with pentobarbitone (60 mg/kg, i.p.). The experimental design and experimental groups are illustrated in **Figure 1**. The experiments were designed and reported as per the principles of the ARRIVE guidelines (30).

Surgical Procedure for Intracerebral Electrode Implantation

Eight mice were anesthetized with 3% isoflurane in 2 L/min oxygen until the loss of pinch reflex and maintained at 2% isoflurane during the surgery. The head was shaved and disinfected with Videne. Before surgery, animals were administered with a prophylactic antibiotic, Baytril® (Bayer Health group, Germany, 5 mg/kg, s.c.), and an analgesic, buprenorphine (Vetergesic®, Reckitt Benckiser Healthcare, UK, 0.3 mg/kg, i.m.). An incision was made through the skin, muscle, and connective tissue over the skull, as described previously (31).

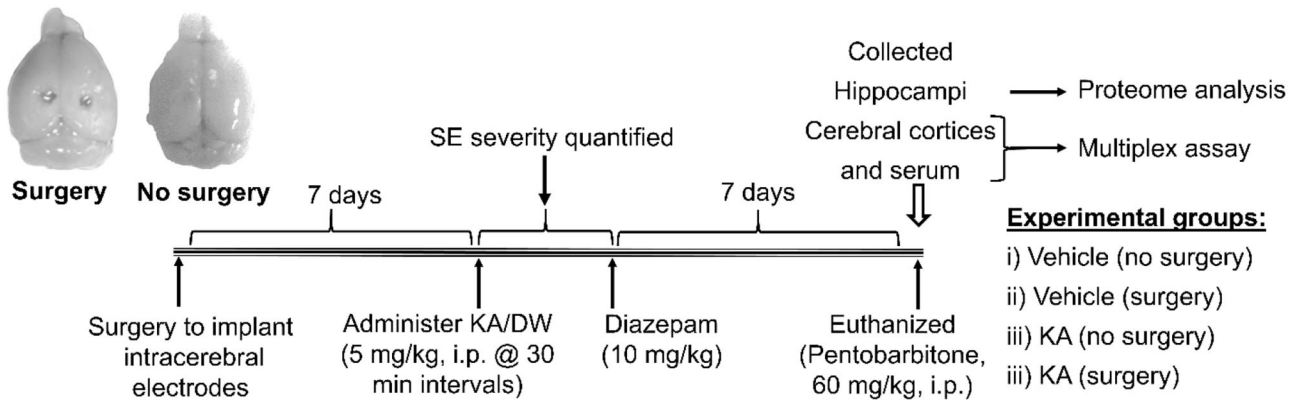

FIGURE 1 | The experimental design. The brain image on the left illustrates the gross impact of the intracerebral electrodes (surgery), and the image on the right is from a mouse with no surgery.

Bilateral burr holes of 1.8 mm diameter were made through the skull corresponding to the cerebral hemispheres and underlying hippocampi (5 mm cranial to lambda and 2 mm lateral to midline over each hemisphere). We used sterile DSI electrode wires (Data Scientific International, USA). The electrodes used were twisted (coiled bifilar) and bipolar, i.e., they measure the voltage between the two leads between the electrode coil in the (+) red insulated lead and the electrode coil in the negative (−) clear insulated lead. Each of the two electrode leads consists of a high-performance nickel cobalt alloy as used in medical implants. The electrode is a coil consisting of two wires (bifilar), but the two wires are electrically common to one another. The diameter of the coil was 0.356 mm. The coil insulation was a medical grade silicone with an outer diameter of 0.94 mm. Following removal of the electrodes' insulation, a V-shaped bend was made in the wire with an extended flat terminal end (∼2 mm). The length/depth of the V-shaped electrode was 2.8 mm, which was enough to penetrate the cortex. The width of the V bend varied from bottom to the top (0.5–2 mm), which was sufficient to pass through the 1.8 mm burr hole. The V-shaped electrode was manually inserted through the burr hole. The flat free terminal end and an insulated wire at the other end of the hole were touching the skull. Electrodes were secured to the skull with dental cement constituted from Alphacryl Rapid Repair and methyl acrylate (National Dental Supplies, Southport, U.K). The incision was sutured using Polysorb 4.0 and reinforced with Vetbond™ Tissue adhesive (3M Animal Care Products, USA). All animals were given subcutaneous injections of saline for rehydration and soft food to facilitate recovery of their body weight, post-surgery.

Repeated Low Doses of KA Administration to Induce SE

KA (Abcam Biochemicals®, Cambridge, UK) was dissolved in sterile distilled water (DW) and administered at 5 mg/kg per dose or an equal volume of DW as the vehicle. Sixteen mice were divided into four groups of four mice each, which were either surgically implanted with intracerebral electrodes or not, and either treated with KA or vehicle (DW), i.p., in a two-by-two trial design [the four groups are vehicle (no surgery), vehicle (surgery), KA (no surgery), and KA (surgery)]. KA-treated animals were scored for seizure severity using a modified Racine scale (32). The stages include stage 1, freezing; stage 2, head nodding; stage 3, rearing; stage 4, rearing and falling; and stage 5, generalized seizures. Repeated doses of KA were given at 30 min intervals until animals reach stage 5 seizures, after which the dosing was discontinued as described previously (32). Each cohort included 8–10 mice since using more animals in a cohort would be difficult to manually quantify initial SE severity, although two experimenters scored SE at the same time. KA-surgery and KA no surgery groups were treated with KA simultaneously. Vehicle-treated animals were matched to KA-treated mice by number of injections. Two hours after the onset of stage 5 seizures, all mice that received KA and their vehicle counterparts were given diazepam (10 mg/kg, i.m., Hameln Pharmaceuticals Ltd, Gloucester, UK) to standardize the duration of behavioral seizures in KA treated animals. The objective of the study was to determine the impact of surgically implanted intracerebral electrodes in the brain on protein and cytokine expression; therefore, EEG was not acquired (dummy telemetry devices were used) during the 7 day post-SE period. Videos, however, were acquired to confirm that the KA-treated mice had SRS during the following 7 days.

Tissue Collection, Sample Preparation, and Protein Estimation

Seven days following the induction of SE with KA, all mice, including the vehicle-treated, were euthanized. Blood samples were collected by cardiac puncture into lithium heparin-coated tubes, centrifuged at 2,000 × *g* for 20 min at 4°C for the isolation of plasma, and stored at −80°C. Brains were removed, and the whole hippocampi and cerebral cortices including the tissue surrounding the electrodes were dissected, collected in cryovials, and snap-frozen in liquid nitrogen. Brain and plasma samples were stored at −80°C until required.

Hippocampi and cortical tissue samples were thawed on ice, dabbed with a sterile tissue paper to remove the water, and weighed before performing assays. Tris lysis buffer containing 1:50 protease inhibitor was added to each sample at a volume of 10 μl/mg of tissue. Samples were then homogenized using a TissueRuptor, sonicated, and centrifuged at 10,000 × *g* for 20 min at 4°C. The resulting supernatants were aliquoted, and protein concentrations were determined using a Bradford assay (Sigma Aldrich, UK). Bovine serum albumin (BSA) standards were prepared using a stock solution containing 4 g/ml BSA. BSA standards were diluted with distilled water to concentrations ranging from 100 to 1,400 μg/ml. A volume of 10 μl of each sample and BSA standards were added in duplicates to a 96-well plate. Bradford reagent (200 μl) was added to each well, and the 96-well plate was incubated at room temperature for 5 min. The maximum absorbance frequency for each sample was measured at 595 nm using a multimode plate reader (DTX 880; Beckman Coulter, USA), and the protein content of samples was determined by comparing to a standard curve generated using a serial dilution of BSA. Tissue supernatants were diluted to 1:50 with distilled water before protein assay. Plasma samples were thawed on ice, vortexed, and centrifuged at 13,000 × *g* for 10 min at 4°C. Hippocampi lysates were used for proteome analysis, and cortical lysates and plasma were used for MSD V-PLEX assay.

Hippocampi Lysate Processing for Proteomics

The hippocampal lysates were processed for proteome analysis, as described previously (33). For digestion, 15 μl (∼100 μg) of homogenate was diluted to 160 μl of ammonium bicarbonate in LoBind tubes. The proteins were denatured using 10 μl of 1% (w/v) RapiGest™ SF surfactant (Waters, Manchester, UK) in 25 mM ammonium bicarbonate followed by incubation at 80°C for 10 min. Samples were reduced by adding 10 μl of 60 mM dithiothreitol and incubated at 60°C for 10 min and alkylated by adding 10 μl of 180 mM iodoacetamide and incubated at room temperature in the dark for 30 min. Trypsin (Sigma, UK) was reconstituted in 50 mM acetic acid to a concentration of 0.2 μg/μl. Digestion was performed by the addition of 10 μl of trypsin to the samples followed by incubation at 37°C overnight. Trifluoroacetic acid (TFA) was added to each sample for acidification, and the samples were incubated at 37°C for 45 min. Samples were centrifuged at 17,000 × *g* for 45 min, and the supernatant was transferred to a LoBind tube. The centrifugation step was repeated, and 10 μl of supernatant was transferred to a total recovery vial for LC-MS analysis. Pre- and post-acidification digest was analyzed by SDS-PAGE to confirm complete digestion.

LC Separation

All peptide separations were carried out using a nanoAcquity UPLC™ system (Waters MS Technologies, Manchester, UK), as previously described (33). For each analysis, 1 μl of sample digest was loaded onto a trapping column (C_{18}, 180 μm × 20 mm, Waters), using partial loop injections for 3 min at 5 μl/min with an aqueous solution containing 0.1% (v/v) TFA and 2% (v/v) acetonitrile. The sample was resolved on an analytical column (nanoAcquity UPLC™ HSS T3 column, C_{18} 150 mm × 75 μm inner diameter, 1.8 μm, Waters) using a mobile gradient phase composed of a cocktail of aqueous (A) and organic (B) solvents. Solvent A contained 0.1% (v/v) formic acid in HPLC grade water, and solvent B contained 0.1% (v/v) formic acid in HPLC grade acetonitrile. Separations were performed by applying a linear gradient of 3 to 40% solvent B over 90 min at 300 nl/min followed by a washing step (5 min at 99% solvent B) and an equilibration step (15 min at 3.8% solvent B). An equivalent to 500 ng of protein for each sample was injected.

Mass Spectrometry

The LTQ-Orbitrap Velos instrument (Thermo Fisher) was operated in the data-dependent mode to switch between full-scan MS and MS/MS acquisition automatically. Survey full-scan MS spectra (m/z 3,350–2,000) were acquired in the Orbitrap with 30,000 resolution (m/z 400) after the accumulation of ions to 1×10^6 target value based on predictive automatic gain control values from the previous full scan. The 20 most intense multiply charged ions ($z \geq 2$) were sequentially isolated and fragmented in the linear ion trap by collision-induced dissociation with a fixed injection time of 100 ms. Dynamic exclusion was set to 20 s. Typical mass spectrometric conditions were as follows: spray voltage, 1.5 kV, no sheath and Auxillary gas flow; heated capillary temperature, 200°C; normalized CID collision energy 35%. The MS/MS ion selection threshold was set to 500 counts, and a 1.2 Da isolation width was set. A metal-coated picotip (New Objective, Presearch, UK) was used in the nanospray assembly and was maintained at a voltage of 1,500 V.

Proteome Identification and Analysis

The hippocampi from all four groups in this study were processed simultaneously for proteomics using the same protocol and the instrument that was used in our previous study (33). We used the vehicle and KA (with no surgery) group's raw data from our recently published study (33) to compare with surgery groups. All four raw data sets were reanalyzed with Proteome Discoverer 2.2.0.388. The data were searched using Mascot 2.2.07 against Uniprot-Mus musculus with quantification using the Minora feature detector. Peptide validation was performed using the Percolator node within Proteome Discoverer. The searches were performed with static modifications of carbamidomethyl (Cys), dynamic modifications of oxidation (Met), and deamidation (Asn, Gun).

Further analysis was performed using the R package MethaboanalystR 2.0 (34), which contains R functions and libraries in the MetaboAnalyst webserver (35). Upon checking the data integrity as satisfactory (i.e., no peptide with more than 50% missing replicates, and positive values for the area), missing value estimation was imputed using the Singular Value Decomposition (SVD) method. Non-informative values that were near-constant throughout the experimental conditions were detected using the interquartile range (IQR) estimation method and deleted. Data were normalized using the Quantile normalization method. Data transformation was performed based on Generalized Logarithm Transformation (glog) to make individual features more comparable. The group samples were

compared by *t*-test for paired groups with the adjusted *p*-value and False Discovery Rate (FDR) set at 0.01. Fold change analysis with a threshold of 2 was performed to compare the absolute value of change between group values (for paired groups). A volcano plot was created to combine the fold change and the two-sample *t*-test analysis. The PCA analysis was performed using the prompt package, and pairwise score plots were created to provide an overview of the various separation patterns among the most significant components. Partial least squared (PLS) regression was then performed using the plsr function provided by the R pls package to predict the continuous and discrete variables. A PLS-DA model was built to classify and cross-validated PLS using the caret package. The uniport protein ids that were altered with the $p < 0.01$ were used to retrieve the corresponding KEGG ids using the "Retrieve/ID mapping" tool of UniProt (accessible at http://www.uniprot.org/uploadlists/). KEGG ids were then used to retrieve the biological pathway association of the proteins. Enrichment analysis was performed using the Database for Annotation, Visualization, and Integrated Discovery (DAVID) 6.8 Tools (36, 37). The one-way analysis of variance (ANOVA) was used to determine whether there were any significant differences between the means ±SEM within four groups. *Post-hoc* analysis was performed with Fisher's Least Significant Difference method. Proteins with FDR values <0.01 were considered significant. Box plots were created for all significantly altered proteins determined by ANOVA (**Supplementary Figure 1**).

Meso Scale Discovery Assay

Reagents Preparation

The standards, antibody detection solution, and read buffer were prepared in accordance with the manufacturer's instructions (MSD Kit # K15048D-1). All reagents were warmed to room temperature before preparation. The multi-analyte lyophilized calibrator, supplied by MSD, contains the highest concentration of all the cytokines and served as the standard stock for the assay. The calibrator was reconstituted in 1,000 μl of Diluent 41 (MSD, USA), mixed by vortexing, and left for 5 min before serial dilution. A series of standards were prepared by serial dilution of the calibrator solution by adding 100 μl of the calibrator to 300 μl of Diluent 41 and vortex-mixed, and the process was repeated five times to generate a total of seven standards. Diluent 41 alone was used as the blank. The kit provided 10 separate detection antibodies, 60 μl of each at 50X stock solution. All detection antibody solutions were combined together (600 μl) and added to 2,400 μl of Diluent 45 (MSD, USA) to achieve 1:50 dilution. Reader buffer T 4X stock solution (MSD, USA) was diluted to 1:2 with distilled water.

Linearity of Dilution for the MSD V-PLEX Kit

The linearity of dilution was first performed on 16 wells of the customized 96-well plate using two cerebral cortices supernatant samples. One sample was from the vehicle (no surgery) group, while the other sample was from KA-treated (surgery). These samples were predicted to have the least and the highest amount of inflammatory changes, respectively, due to the extent of insult to the brain. The cortical supernatants or plasma samples were serially diluted to 1:2, 1:4, 1:8, and 1:16 using Diluent 41 (MSD). The observed values were assessed relative to the standard curve for all 10 inflammatory cytokines. The results were calculated based on the standard curve, and the observed concentration was multiplied by the dilution factor. The criteria for acceptable dilutional linearity were for the corrected observed concentrations to vary no more than 80% to 120% of the theoretical concentration between each serial dilution for each analyte (38).

MSD V-PLEX Assay Protocol

The assay was performed in accordance with the manufacturer's instructions (MSD kit reference K15048D-1). Plasma samples were diluted 1:2 using Diluent 41. The standards, blank, and samples (cortical lysates or plasma) solution were measured in duplicates, with 50 μl of each solution added to an allocated well within the customized 96-well plate. The plate was sealed and incubated at room temperature on a shaker for 2 h. After incubation, the plate was washed three times with wash buffer, and 25 μl of the diluted detection antibody was added to each well, the plate resealed, and incubated at room temperature on a shaker for a further 2 h. After antibody incubation, the plate was washed three times, as previously described, and then 150 μl of 2X read buffer T was added to each well. The plate was then placed on the MSD instrument and read immediately. The reading of the V-Plex plate was performed using the MSD SECTOR Imager 2400, according to the manufacturer's manual (MSD, USA). The plate had an MSD barcode that allowed the SECTOR Imager to detect the type of plate being run. The data generated was automatically analyzed with a template using the Discovery Workbench version 4.0 software. The cytokines levels were expressed in pg/ml for plasma and pg/mg of protein detected in a 100 mg/ml tissue lysate, determined using the Bradford protein assay. One-way ANOVA with Tukey's *post hoc* analysis was performed using the SPSS software.

RESULTS

Intracerebral Electrodes Reduced Seizure Threshold for KA-Induced SE at Day 7 Post-surgery

The rationale for choosing the 7 day time point post-SE, in contrast to the early or later time points, was based on our previous work that demonstrated a significant increase in gliosis, neurodegeneration, and neurogenesis in C57BL/6J mouse KA model at 7 day post-SE (26). KA-induced seizure susceptibility of mice with surgically implanted intracerebral electrodes was compared with no surgery (naïve) animals. We assessed the total amount of KA required to induce stage 5 seizures in both surgery and non-surgery groups at day 7 post-surgery. Electrodes implanted mice required significantly less KA (15.78 ± 1.47 mg/kg; $n = 15$) than non-implanted mice (27.98 ± 0.6 mg/kg; $n = 187$) to induce generalized convulsive seizures ($p < 0.01$; **Figures 2A,B**). We had to use a large cohort of naïve mice to cover a wide range of KA doses to achieve stage 5 seizures. There was a left shift in the KA dose-response curve in the surgery group

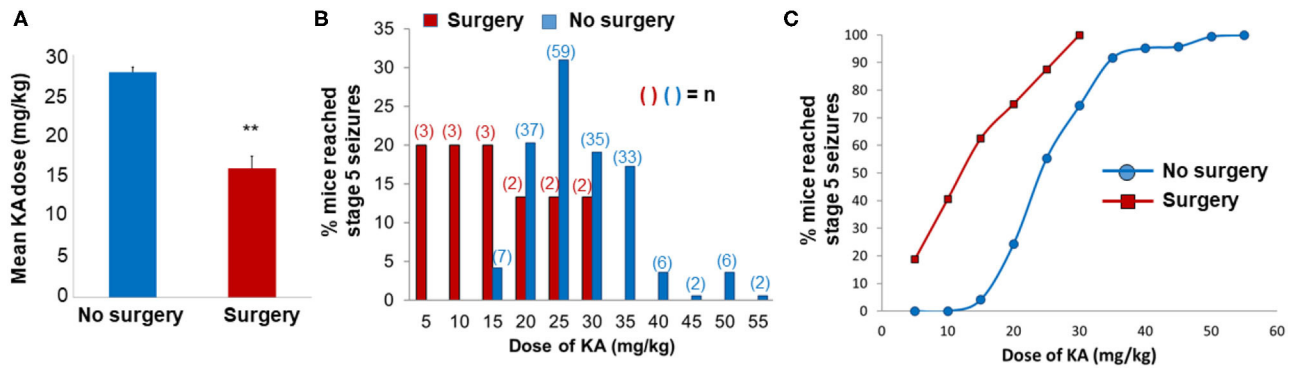

FIGURE 2 | Impact of surgery on seizure threshold in response to kainate (KA). **(A,B)** The mean **(A)** and the total **(B)** KA dose required to induce generalized convulsive seizures (stage 5 on the Racine scale) in C57BL/6J mice that were either implanted with intracerebral electrodes (Surgery, $n = 15$) or not implanted (no surgery, $n = 187$). KA was administered 7 days post-surgery. In graph A, the data are expressed as the mean (±SEM) KA dose (mg/kg) and compared the groups using a two-sample *t*-test (**$p < 0.01$). The data in B are expressed as a percentage of the total number of animals in each group that reached stage 5 seizures at each dose increment. **(C)** The dose-response data for KA are expressed as a cumulative percentage of the total number of animals in each group.

when compared with the group without surgery (**Figure 2C**). The range of total KA doses for post-surgery mice was 5–30 mg/kg, and for mice without surgery, the range was 15–55 mg/kg (**Figure 2B**). After a single dose of 5 mg/kg KA, 18.75% of mice in the post-surgery group experienced generalized seizures (stage 5), whereas no mice that had not previously undergone surgical implantation of electrodes had convulsive seizures (**Figure 2C**). At a total dose of 30 mg/kg KA, all mice that had undergone surgery experienced generalized seizures, compared with 74.4% of naïve mice (**Figure 2C**). Of these, four animals from each group that had similar SE severity (continuous generalized seizures lasting for >45 min) and KA doses (four to five doses of 5 mg/kg) were used for proteomics and cytokine assays. The remaining animals were euthanized at various time-points post-SE and used for other analyses, and not reported here. Video analysis of all eight KA-treated mice used in this proteomics study had a minimum of one SRS during the 7 days post-SE.

After the mice were euthanized, the extent of gross damage (similar in all animals) was confirmed, while the hippocampus was separated from the cerebral cortex under a dissection microscope. Also, clear electrode marks on the cerebral cortices were visible in all animals (an example is shown in **Figure 1**). The hippocampi were used for proteomics and the cortical tissue and serum for cytokine assays.

Overall Changes in Proteins in the Hippocampus in Response to Surgery and KA at 14 Days Post-surgery (i.e., 7 Days Post-SE)

The number of proteins identified from the raw data in which expression was significantly altered ($p < 0.01$) between vehicle and KA-treated mice with or without surgery, as searched for against the UniProt mouse database, is listed in **Table 1**. Data presented as the absolute number of proteins with significant changes (downregulated, upregulated, and total significant) as a percentage of the total number of proteins identified in the study (**Table 1**). The surgery increased higher number of proteins regardless of whether they were subsequently treated with KA or vehicle (A, B in **Table 1**). The impact of surgery alone on the percentage of protein expression was greater than that of KA-induced seizures in mice that had no surgery (103 vs. 27 total significant; 6.8 vs. 1.8%). KA had a greater effect in the surgery group (C, 55 proteins altered; 3.8% of total significant) than in no surgery group (D, 27 proteins altered; 1.8% of total significant) (**Table 1**). We also investigated whether any of the endogenous resolving proteins were altered in response to surgery and/or KA induced brain trauma. We detected leukotriene A-4 hydrolase (FDR, 0.92; $p = 0.89$, but interestingly, not the leukotriene B4, a chemoattractant at an early phase of insult) and prostaglandin E synthase (FDR, 0.46, $p = 0.26$), but there were no significant differences. Also, our search did not yield any lipoxins or resolvins.

Differential Expression of Proteins in the Hippocampus in Response to Surgery Alone or KA (With or Without Surgery) at 14 Days Post-surgery (i.e., 7 Days Post-KA)

One-way ANOVA with Fisher's *post-hoc* analysis of all four groups revealed a significant increase in the proteins that have role in neuroinflammation including gliosis [C1q system, glial fibrillary acidic protein (GFAP), and vimentin] and neurodegeneration (cystatin-C and galectin-1) in both surgery groups treated with KA or vehicle, and in KA-treated group without surgery. The Ras and Rab related proteins (Rab6a and Rras2) and calcium/calmodulin-dependent protein kinase IIa (CaMKIIα that have a role in neuronal plasticity were significantly reduced in all three groups (**Table 2**, **Supplementary Figure 1**). In KA groups, with or without surgery, glypican-1, heat shock protein beta-1 (HSP25), unconventional myosin-Va, neurosecretory protein VGF (VGF-derived peptide TLQP-62), and EF-hand domain-containing protein D2 (Swiprosin-1) were significantly upregulated, while the voltage dependent GABA A transporter (GAT-1) and glutamine synthase (GS) were downregulated (**Table 2**, **Supplementary Figure 1**). In addition to the above listed

TABLE 1 | Comparison of the changes in the expression of proteins in the hippocampus between treatment groups are reported as absolute numbers and percentage of total identified proteins.

Treatment groups	Downregulated	Upregulated	Total significant	% significant of all proteins identified
(A) Vehicle: Surgery vs. no surgery	59	44	103	6.80%
(B) KA: Surgery vs. no surgery	47	35	82	5.40%
(C) Surgery: KA vs. vehicle	32	23	55	3.60%
(D) No surgery: KA vs. vehicle	16	11	27	1.80%

Treatment groups ($n = 4$) comprised animals that had undergone surgery for the implantation of intracerebral electrodes or no surgery and that subsequently received KA to induce seizures or vehicle as a control. Data reports proteins with significantly altered between groups (t-test, $p < 0.01$), either as absolute numbers or as percent significant of all identified proteins.

proteins, the proteins that were up- or downregulated in surgery groups (with or without KA) are listed in **Table 2** and box plots for each protein are illustrated in **Supplementary Figure 1**.

Differential Expression of Proteins in the Hippocampus in Response to Surgically Implanted Intracerebral Electrodes (Without KA)

A large number of proteins were altered in mice with intracerebral electrodes compared with the mice without surgery and electrodes (103 proteins, $p < 0.01$; **Tables 1**, **3**, **Supplementary Table 2**). An overview of the variation of all proteins between surgery and without surgery groups is illustrated in volcano plot, PCA, and heatmap (**Figures 3A,B**, **4A**). The proteins associated with the innate immune system such as complement components C1q a, b, and c were increased by 3.34-fold ($p = 0.0003$) in the surgery group. Astroglia cytoskeletal proteins such as vimentin and GFAP were also upregulated in the surgery group (>2-fold, $p < 0.0001$). The other key proteins that were upregulated by >2-fold ($p < 0.001$) were F-box and leucine-rich repeat protein 8 (FBXL8), solute carrier family 12 member 2 (basolateral Na-K-Cl symporter), and dehydrogenase/reductase SDR family member 1 (DHRS1). The KEGG pathway enrichment analysis revealed a significant increase in proteins involved in the process of neurodegeneration, neuroinflammation, and oxidative stress (for example, prion disease pathway proteins—C1qs and Stip1; Chagas disease pathway proteins—serine/threonine-protein phosphatase 2A (PP2A) related proteins; glutathione pathway proteins such as glutathione S-transferase and peroxiredoxin-6) (**Supplementary Table 4**, **Supplementary Figure 2**). FDR for the proteins in prion disease and ribosome pathways were ≤1, while the other pathways were >9 (**Supplementary Table 4**).

Differential Expression of Proteins in the Hippocampus in Response to KA in Surgically Implanted Intracerebral Electrodes vs. KA Without Surgery at 14 Days Post-surgery (i.e., 7 Days Post-SE)

We analyzed the impact of KA-induced SE on protein levels in mice that had surgery and without surgery. The volcano plot, PCA, and heatmap represent an overview of the variation in protein expression between the treatment groups (**Figures 3C–E**, **4B**). The proteins that were significantly increased by >2-fold ($p < 0.01$) in response to KA in surgery group when compared with no surgery group were BBB function-related proteins such as fibrinogen-α (aids as an adhesive substrate for platelets, endothelial cells, and leukocytes), pregnancy zone protein (α2 macroglobulin), serum albumin, serotransferrin (transferrin/β1 metal-binding globulin), and α1-antitrypsin 1–4 (α1 protease inhibitor 4, a serum glycoprotein) (**Table 4**). FBXL8 and C1qb were also increased. A cation-coupled chloride transporter (Na-K-Cl symporter/SCL12A), a core cycle regulator (sister chromatid cohesion protein PDS5 homolog A), and a cytoskeletal protein Filamin-A (FLN-A/actin-binding protein 280) were significantly increased in KA-treated mice in the surgery group (**Table 4**, **Supplementary Table 3**). The list of KEGG pathways and the proteins altered are listed in **Supplementary Table 5**. The most striking KEGG pathway proteins affected in the surgery group in response to KA, with <1% FDR, were the synaptic vesicle cycle pathway proteins. If we consider $p \leq 0.05$, however, specific proteins involved in the regulation of actin cytoskeleton, prion diseases (neurodegeneration and neuroinflammation), endocytosis, phosphatidylinositol, and neurotrophin signaling pathways, Legionellosis (inflammation-related), glioma, and long-term potentiation were significantly affected in pathway enrichment analysis (**Supplementary Table 5**, **Supplementary Figure 3**).

Multiplex Assay to Determine Differential Expression of Cytokines in Cortical Tissue and Plasma

We used the MSD multiplex kit since it had cytokines/chemokines relevant to epilepsy/seizures and trauma (references are included in the summary **Table 6**). The other advantages of this kit over the other commercial multiplex kits are as follows: (i) it requires small volume of analyte (25 μl, in contrast to 50 μl), therefore suitable for mouse tissue; (ii) it is compatible for both plasma and brain lysate; and (iii) it measures both high and low abundance analytes with a 5-Log+ dynamic range.

Linearity of Dilution Assessment and Detection Ranges of Cytokines in 1:2 Diluted Test Samples

A serial dilution of mouse cortex supernatant was conducted to determine the optimum dilution required for the MSD assay for each cytokine. Two cortical supernatants were used: one from without surgery and KA (no surgery + vehicle) that was expected

TABLE 2 | The impact of intracerebral electrode implants (surgery) and KA or vehicle on altered protein expression in the hippocampus.

Uniprot ID	Protein names	Gene names	*f*-value	*p*-value	Neg $log_{10}(p)$	FDR	Abundance on a log scale			
							Veh-NoSurg	Veh-Surg	KA-NoSurg	KA-Surgery
Proteins upregulated in surgery vehicle and both KA groups										
P03995	Glial fibrillary acidic protein (GFAP)	Gfap	31.792	5.43E-06	5.265	0.00138	25.55244	27.025413	26.87475	27.968345
P20152	Vimentin	Vim	20.7	4.91E-05	4.3091	0.00361	23.70164	25.16986	24.87103	26.487395
P98086	Complement C1qa	C1qa	15.099	0.000224	3.6494	0.00901	17.52368	19.70244	18.78533	19.755233
P14106	Complement C1qb su	C1qb	25.31	1.78E-05	4.7495	0.00191	19.04926	20.753115	19.97015	21.130523
Q02105	Complement C1q subunit C	C1qc C1qg	16.908	0.000131	3.8812	0.00633	18.60421	20.583218	19.43826	20.605043
P16045	Galectin-1 (Gal-1/Galaptin)	Lgals1 Gbp	23.294	2.72E-05	4.566	0.00244	18.55418	19.299368	19.29811	20.263458
P21460	Cystatin-C (Cystatin-3)	Cst3	15.395	0.000205	3.6888	0.00869	21.29772	21.565828	21.74042	22.158848
P62301	40S ribosomal protein S13	Rps13	20.655	4.96E-05	4.3044	0.00361	21.70742	21.852868	21.85315	21.976885
Proteins downregulated in surgery vehicle and both KA groups										
P35279	Ras-related protein Rab-6A (Rab-6)	Rab6a	18.567	8.37E-05	4.077	0.00553	21.63157	21.371815	21.51557	21.370305
P62071	Ras-related protein R-Ras2	Rras2	17.853	0.000101	3.9946	0.00576	20.50515	20.053165	20.35101	19.987185
P11798	Calcium/calmodulin-dependent protein kinase IIa (CaMK-IIa)	Camk2a	24.743	0.00002	4.6992	0.00191	28.23778	28.094555	28.03671	27.681833
Proteins upregulated in both KA groups (with or without surgery)										
Q9QZF2	Glypican-1 [Cleaved into: Secreted glypican-1]	Gpc1	33.445	4.15E-06	5.3816	0.00138	19.79506	19.762235	20.0398	20.213773
P14602	Heat shock protein beta-1 (HspB1/HSP 25)	Hspb1 Hsp25/27	26.34	1.45E-05	4.8385	0.00191	18.34595	18.024863	20.10053	21.608808
Q99104	Unconventional myosin-Va	Myo5a Dilute	17.692	0.000106	3.9756	0.00576	23.74006	23.75106	23.87258	23.905998
Q0VGU4	Neurosecretory protein VGF (VGF-derived peptide TLQP-62)	Vgf	17.569	0.000109	3.961	0.00576	20.14906	19.824463	20.7232	21.123153
Q9D8Y0	EF-hand domain-containing protein D2 (Swiprosin-1)	Efhd2 Sws1	17.443	0.000113	3.946	0.00576	23.16364	23.261423	23.45649	23.668985
Proteins downregulated in both KA groups (with or without surgery)										
P31648	Sodium- and chloride-dependent GABA transporter 1 (GAT-1)	Slc6a1 Gabt1 Gat-1	17.805	0.000103	3.9889	0.00576	23.44462	23.413773	23.06983	22.927308
P15105	Glutamine synthetase (GS)	Glul Gln s	14.75	0.00025	3.6022	0.00969	26.8151	26.797415	26.51625	26.618135
Protein upregulated in both surgery groups (vehicle and KA)										
Q8VHL1	Histone-lysine N-methyltransferase SETD7 (SET7/9)	Setd7 Set7 Set9	66.863	9.25E-08	7.0337	0.00014	21.23233	21.911073	21.15768	21.993103
Q9D0M5	Dynein light chain 2, cytoplasmic (DLC8)	Dynll2 Dlc2	58.2	2.02E-07	6.6954	0.00015	22.21056	21.12811	22.18282	21.00142
Q6A026	Sister chromatid cohesion protein PDS5 A	Pds5a Kiaa0648	36.452	2.62E-06	5.5812	0.00134	19.8724	20.885968	19.80909	20.84635
P03995	Glial fibrillary acidic protein (GFAP)	Gfap	31.792	5.43E-06	5.265	0.00138	25.55244	27.025413	26.87475	27.968345
Q8ClG9	F-box/LRR-repeat protein 8 (F-box protein FBL8)	Fbxl8 Fbl8	32.684	4.69E-06	5.3286	0.00138	19.18971	20.350538	18.93956	20.272563
Q6PB66	Leucine-rich PPR motif-containing protein, mitochondrial (LRP 130)	Lrpprc Lrp130	29.347	8.27E-06	5.0823	0.0018	21.12106	21.556105	21.02334	21.506653

(Continued)

TABLE 2 | Continued

Uniprot ID	Protein names	Gene names	*f*-value	*p*-value	Neg $log_{10}(p)$	FDR	Abundance on a log scale			
							Veh-NoSurg	Veh-Surg	KA-NoSurg	KA-Surgery
Q3URK3	Methylcytosine dioxygenase TET1 (CXXC-type zinc finger protein 6)	Tet1 Cxxc6 Kiaa1676	27.562	1.15E-05	4.9404	0.00181	19.20219	20.01175	18.97767	19.870405
P55012	Solute carrier family 12 member 2 (Basolateral Na-K-Cl symporter)	Slc12a2 Nkcc1	27.452	1.17E-05	4.9313	0.00181	21.57142	22.651055	21.59296	22.838318
P10605	Cathepsin B/B1)	Ctsb	15.512	0.000198	3.7042	0.00868	21.24294	21.535165	21.29265	21.835295
P14602	Heat shock protein beta-1 (HspB1/ HSP 25)	Hspb1 Hsp25/27	26.34	1.45E-05	4.8385	0.00191	18.34595	18.024863	20.10053	21.608808
Q5SSL4	Active breakpoint cluster region-related protein	Abr	24.9	1.94E-05	4.7132	0.00191	21.39741	22.032938	21.47865	22.021938
P16045	Galectin-1 (Gal-1/Galaptin)	Lgals1 Gbp	23.294	2.72E-05	4.566	0.00244	18.55418	19.299368	19.29811	20.263458
Q9WVA3	Mitotic checkpoint protein BUB3	Bub3	22.904	2.96E-05	4.5289	0.00251	19.26223	19.585013	19.20765	19.39816
Q02105	Complement C1qc	C1qc C1qg	16.908	0.000131	3.8812	0.00633	18.60421	20.583218	19.43826	20.605043
P20152	Vimentin	Vim	20.7	4.91E-05	4.3091	0.00361	23.70164	25.16986	24.87103	26.487395
P62301	40S ribosomal protein S13	Rps13	20.655	4.96E-05	4.3044	0.00361	21.70742	21.852868	21.85315	21.976885
Q9CQJ6	Density-regulated protein (DRP)	Denr	19.443	6.69E-05	4.1749	0.00464	19.67067	20.136073	19.63894	20.130675
P02468	Laminin subunit gamma-1 (Laminin B2 chain)	Lamc1 Lamb-2	18.078	9.53E-05	4.0209	0.00576	18.75928	19.305835	18.70097	19.563578
P21460	Cystatin-C (Cystatin-3)	Cst3	15.395	0.000205	3.6888	0.00869	21.29772	21.565828	21.74042	22.158848
P98086	Complement C1qa	C1qa	15.099	0.000224	3.6494	0.00901	17.52368	19.70244	18.78533	19.755233
Proteins downregulated in both surgery groups (vehicle and KA)										
P32037	Solute carrier family 2-(Glucose transporter type 3, brain) (GLUT-3)	Slc2a3 Glut3	24.736	0.00002	4.6986	0.00191	22.52552	22.390868	22.63737	22.245415
Q62283	Tetraspanin-7 (Tspan-7/CD antigen CD231)	Tspan7 Mxs1	21.247	4.31E-05	4.3654	0.00347	19.89033	19.44267	19.63764	19.222073
Q8C0E2	Vacuolar protein sorting-associated protein 26B	Vps26b	27.386	1.19E-05	4.926	0.00181	21.77001	21.464778	21.70237	21.46987
Q8CBW3	Abl interactor 1 (Abelson interactor 1) (Abi-1)	Abi1 Ssh3bp1	18.428	8.69E-05	4.0612	0.00553	21.26101	20.738385	21.16048	20.689868
P35279	Ras-related protein Rab-6A (Rab-6)	Rab6a Rab6	18.567	8.37E-05	4.077	0.00553	21.63157	21.371815	21.51557	21.370305
P62071	Ras-related protein R-Ras2	Rras2	17.853	0.000101	3.9946	0.00576	20.50515	20.053165	20.35101	19.987185
P31648	Sodium- and chloride-dependent GABA transporter 1 (GAT-1)	Slc6a1 Gat-1	17.805	0.000103	3.9889	0.00576	23.44462	23.413773	23.06983	22.927308
Q9D8Y0	EF-hand domain-containing protein D2 (Swiprosin-1)	Efhd2 Sws1	17.443	0.000113	3.946	0.00576	23.16364	23.261423	23.45649	23.668985
P39053	Dynamin-1 (EC 3.6.5.5)	Dnm1 Dnm	16.874	0.000133	3.8771	0.00633	27.24975	27.13156	27.22933	26.941998
Q9QYB8	Beta-adducin (Add97)	Add2	15.586	0.000193	3.7139	0.00868	23.79847	23.675545	23.77589	23.580043
Q62188	Dihydropyrimidinase-related protein 3 (DRP-3)	Dpysl3 Drp3 Ulip	15.49	0.000199	3.7014	0.00868	24.70239	24.31222	24.70526	24.134963
P61161	Actin-related protein 2 (Actin-like protein 2)	Actr2 Arp2	15.215	0.000216	3.665	0.00893	24.06893	23.887608	24.00868	23.72985
P15105	Glutamine synthetase (GS)	Glul Gln	14.75	0.00025	3.6022	0.00969	26.8151	26.797415	26.51625	26.618135

The numbers in the abundance column are the abundances normalized and averaged for four animals (two technical replicates/animal) in each group, and represented on a log scale. All four groups were compared using one-way ANOVA and Fisher's post-hoc test. The proteins that were significantly altered by $p < 0.01$ and FDR < 0.01, and relevant to epileptogenesis/epilepsy are only listed in the table. Box plots for these proteins are included in ***Supplementary Figure 1****. All other proteins are included in the (****Supplementary Table 1****).*

TABLE 3 | The impact of intracerebral electrode implants on altered protein expression in the hippocampus.

Uniprot ID	Protein names	Gene names	KEGG-ID (mmu)	Fold change	log_2(FC)	*P*-value	neg $log_{10}(p)$
P98086	Complement C1q subcomponent subunit A	C1qa	12,259	4.7473	2.2471	0.000337	3.4723
Q02105	Complement C1q subcomponent subunit C	C1qc C1qg	12,262	4.2034	2.0715	0.000383	3.4169
P14106	Complement C1q subcomponent subunit B	C1qb	12,260	3.4434	1.7838	0.000235	3.6293
P20152	Vimentin	Vim	22,352	2.8094	1.4903	0.00067	3.174
P03995	Glial fibrillary acidic protein (GFAP)	Gfap	14,580	2.7743	1.4721	3.33E-06	5.4779
Q8ClG9	F-box and leucine-rich repeat protein 8	Fbxl8 Fbl8	50,788	2.3142	1.2105	0.000804	3.095
P55012	Solute carrier family 12 member 2 (Basolateral Na-K-Cl symporter)	Slc12a2 Nkcc1	20,496	2.1188	1.0833	6.57E-05	4.1824
Q99L04	Dehydrogenase/reductase SDR family member 1	Dhrs1 D14ertd484e	52,585	2.0032	1.0023	0.000742	3.1294

The groups compared were between the surgery vs. no surgery treated with vehicle (distilled water). The proteins that were significantly altered by $p < 0.01$ and >2-fold are only listed in the table. All other proteins are included in ***Supplementary Table 2****.*

to have the lowest cytokine concentrations and one from an electrode implanted and KA-treated mouse (surgery + KA) that was anticipated to have the highest cytokine concentrations. Based on the linearity of dilution results, 1:2 was considered to be the optimum dilution for the quantification of inflammatory cytokines using the MSD kit. We also determined whether the cytokine levels in a 1:2 dilution of cortical supernatants lie within the detectable (dynamic) range of the MSD assay. Six out of 10 cytokines showed concentrations within the anticipated dynamic range for both samples (**Table 5**), suggesting the reliability of the assay kit.

Cytokine Levels in Cortical Samples

We used cortical tissue to perform the cytokine assay. Surgical implantation of intracerebral electrodes caused a significant increase in the concentrations of proinflammatory cytokines IFN-γ, IL-1β, IL-5, IL-6, IL-12p70, and TNFα irrespective of the vehicle or KA treatment post-surgery (**Figure 5**). Likewise, interestingly, the pleiotropic anti-inflammatory cytokines IL-4 and IL-10 were also increased in the mice that had intracerebral electrodes irrespective of the vehicle or KA treatment post-surgery (**Figures 5I,J**). KC/GRO was the only proinflammatory cytokine that was increased in KA-treated group (naïve animals without surgery). KC/GRO, however, was also upregulated in surgery group treated with the vehicle but not with KA (**Figure 5G**). In summary, surgery caused a significant increase in all cytokine levels tested, except IL-2, irrespective of the vehicle or KA treatment post-surgery.

Plasma Cytokine Levels

The effect of surgery and KA-induced seizures on the cytokine profile was also investigated in plasma samples. Surgical implantation of intracerebral electrodes caused a significant increase in the plasma concentrations of proinflammatory cytokines IL-1β, IL-5, IL-6, KC/GRO, and TNFα in the vehicle-treated group (**Figure 6**). KA treatment, post-surgery, had no effect on any of the plasma cytokines tested. However, KA in naive animals (without surgery) increased IL-2 and KC/GRO plasma levels (**Figures 6C,G**). The pleiotropic anti-inflammatory cytokine IL-10 was increased in the mice that had intracerebral electrodes and treated with the vehicle, but not KA, post-surgery (**Figure 6J**). There were no significant effects of either surgery or KA on plasma IFN-γ, IL-12p70, and IL-4 levels (**Figures 6A,F,I**).

It is unknown why there was increased plasma IL-1β in the vehicle surgery group but not in the KA group (Fig. 6B). However, in both KA groups, compared with the vehicle (no surgery), there was an increase in IL-1β but the differences were not statistically significant. The levels of IL-6 increased in both surgery groups (with or without KA) in the hippocampus (**Figure 5E**). In the plasma, we did observe increase of IL-6 in surgery group without KA, and an increase in KA without surgery, but the differences in the latter were not significant (**Figure 6E**). However, it is also unclear why there was no increase of IL-6 and KC/GRO levels in KA+surgery group, though either KA or surgery on their own caused an increase.

A summary of proteins that are relevant to epileptogenesis/epilepsy/trauma, detected by proteomics and cytokines/chemokines by multiplex assay, and the references are tabulated in **Table 6**.

DISCUSSION

Intracranial Surgical Procedure Can Compromise Seizure Threshold for Chemoconvulsants

In this study, we observed a significant difference in KA sensitivity for inducing generalized convulsive seizures in animals that had intracerebral electrodes and without electrodes, suggesting that surgical procedure and intracerebral electrodes can impact seizure threshold in experimental models. This finding is consistent with our previous observation in both rat and mouse telemetry models in which the electrodes were placed epidurally (2, 15, 25, 26). Both hippocampal proteomics and cortical MSD cytokine analyses indicate that cellular processes involved in neuroinflammation (including gliosis and proinflammatory cytokines release), neurodegeneration, synaptic plasticity, and reduced blood–brain barrier integrity

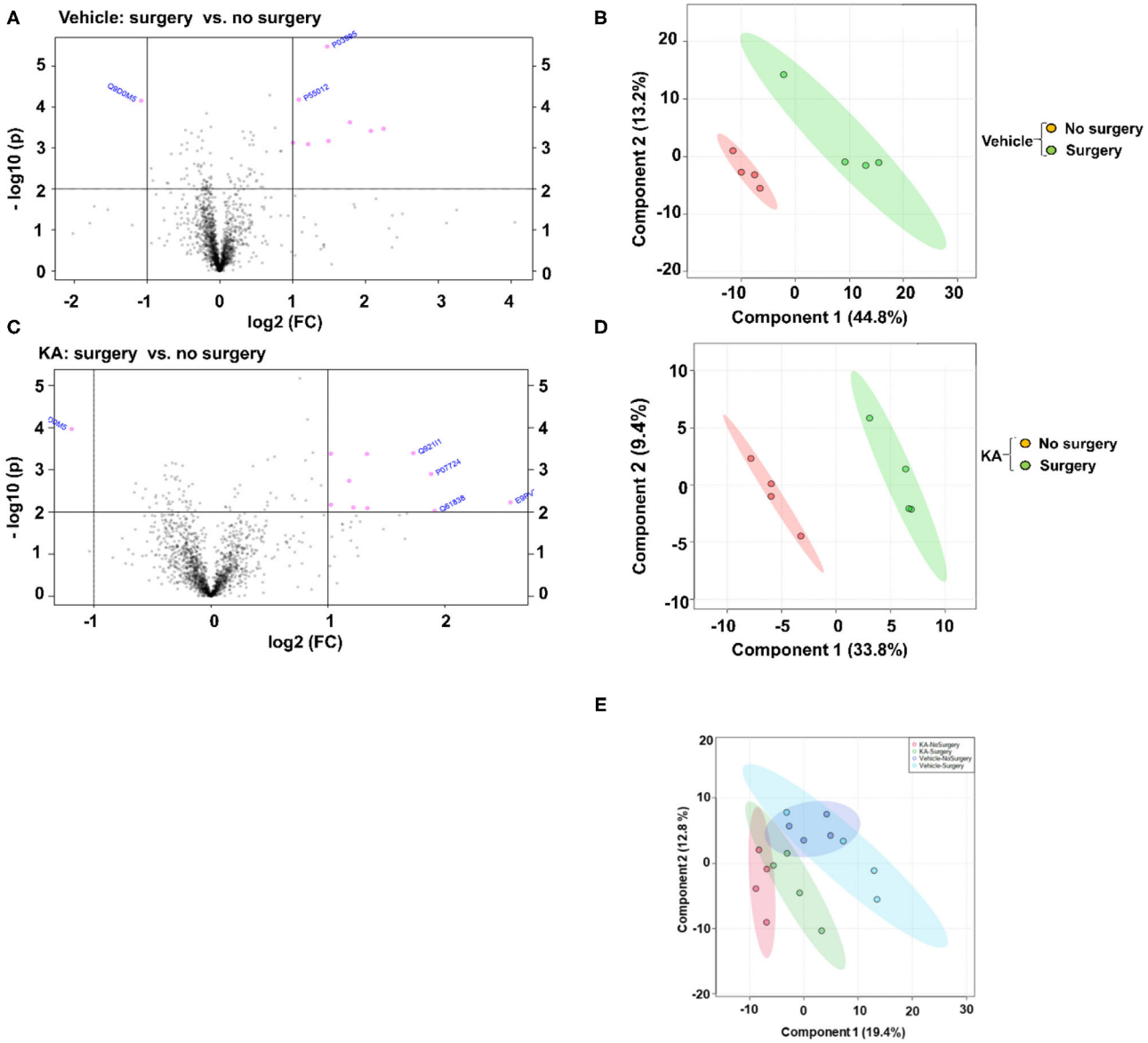

FIGURE 3 | Fold change (FC) analysis of the vehicle or KA treated groups, with or without surgery, with a threshold of 2 was performed to compare the absolute change between group values. The Volcano plots **(A,C)** were created to show both the fold change and the two-sample *t*-test analysis. The PCA analysis was performed using the prccomp package, and pairwise score plots **(B,D)** and all four-way plot **(E)** represent an overview of the various separation patterns among the most significant components.

were significantly altered as a consequence of the surgery and implanted intracerebral electrodes.

Several studies have reported results from RNA microarrays from both experimental models of epilepsy and human samples, highlighting the role of certain genes in the development of epilepsy (78–84). Sampling transcription, however, cannot account for the numerous levels of post-transcriptional control, which continue to emerge (85). Proteomics studies, therefore, may offer a better insight into the molecular mechanisms of the development of epilepsy. The first proteomics study was from a C57BL/6J mouse model of epileptogenesis induced by intrahippocampal KA injection (27). They compared the proteins at 1, 3, and 30 days post-SE (27). Although their model involves intracranial surgery for KA injection, and the same strain of mouse as ours, intracerebral electrodes were not implanted in their study. Furthermore, intrahippocampal KA does not necessarily affect the cortex at an early stage of epileptogenesis, as in the intraperitoneal KA approach (25, 26, 86–88). Our recent proteomics on interventional studies in epileptogenesis in the C57BL/6J mouse model, too, did not use intracerebral

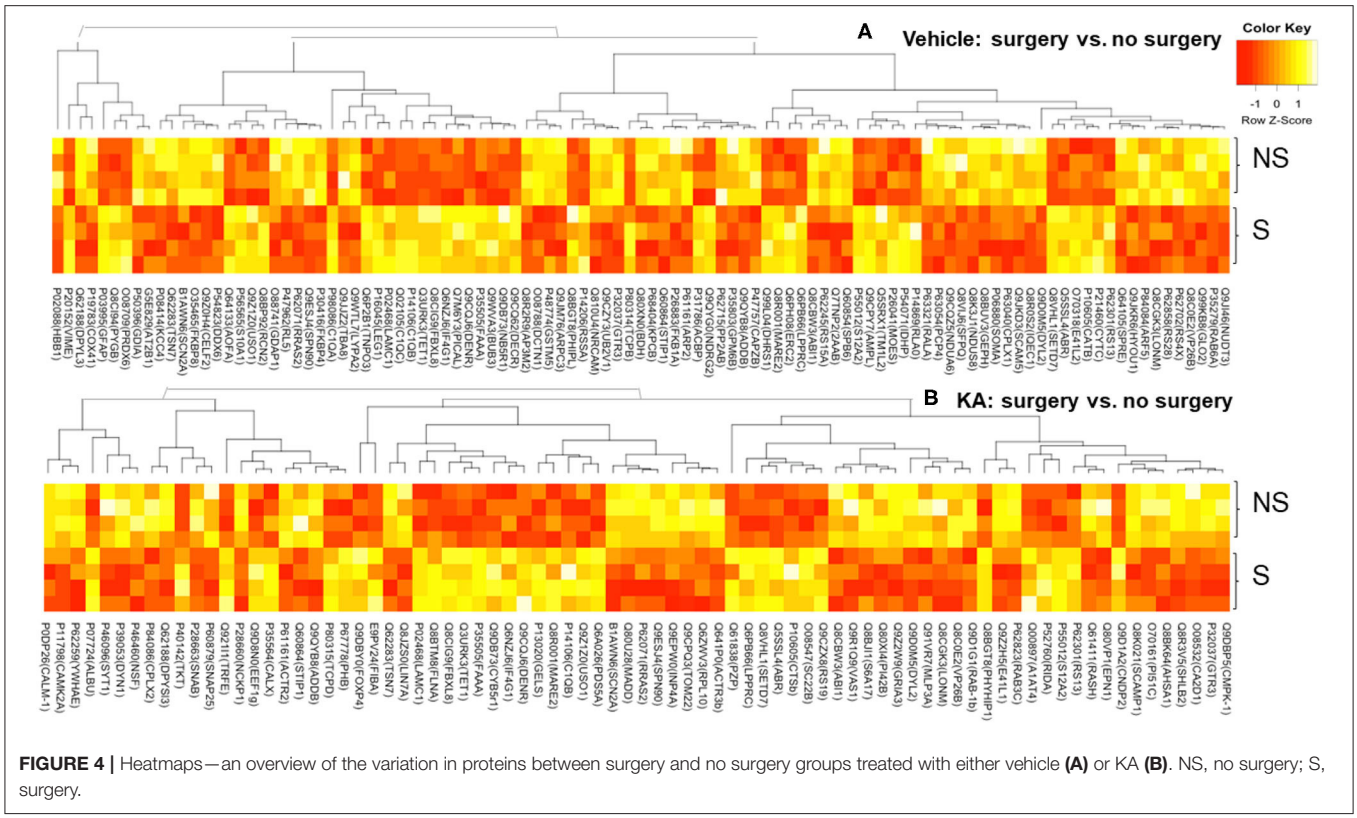

FIGURE 4 | Heatmaps—an overview of the variation in proteins between surgery and no surgery groups treated with either vehicle **(A)** or KA **(B)**. NS, no surgery; S, surgery.

TABLE 4 | The impact of KA-induced SE in intracerebral electrode implanted animals on the expression of proteins in the hippocampus.

Uniprot ID	Protein names	Gene names	KEGG-ID (mmu)	Fold change	log_2(FC)	*P*-value	neg $log_{10}(p)$
E9PV24	Fibrinogen alpha chain	Fga	14,161	5.9018	2.5612	0.005928	2.2271
Q61838	Pregnancy zone protein (Alpha-2-macroglobulin)	Pzp A2m		3.7671	1.9135	0.009382	2.0277
P07724	Serum albumin	Alb Alb-1 Alb1	11,657	3.6877	1.8827	0.001262	2.899
Q921I1	Serotransferrin (Transferrin) (Beta-1 metal-binding globulin)	Tf Trf	22,041	3.3186	1.7306	0.000404	3.3938
Q00897	Alpha-1-antitrypsin 1-4 (α-1 protease inhibitor 4)	Serpina1d Dom4 Spi1-4	20,703	2.5277	1.3378	0.008136	2.0896
Q8CIG9	F-box/LRR-repeat protein 8	Fbxl8 Fbl8	50,788	2.521	1.334	0.000421	3.3757
P14106	Complement C1q subcomponent subunit B	C1qb	12,260	2.3267	1.2183	0.007832	2.1061
P55012	Solute carrier family 12 member 2 (Na-K-Cl symporter)	Slc12a2 Nkcc1	20,496	2.2689	1.182	0.001829	2.7379
Q6A026	Sister chromatid cohesion protein PDS5 homolog A	Pds5a Kiaa0648		2.0361	1.0258	0.000415	3.3817
Q8BTM8	Filamin-A (FLN-A) (Actin-binding protein 280)	Flna Fln Fln1	192,176	2.0359	1.0257	0.006744	2.1711

The groups compared were between surgery vs. no surgery treated with KA. The proteins that were significantly altered by $p < 0.01$ and >2-fold are only listed in the table. All other proteins are included in ***Supplementary Table 3****.*

electrodes (33). Another study on proteomics used an electric kindling in the amygdala of female rats to induce epilepsy (29). It is important to note that in this study, the electrodes penetrated the cerebral hemispheres (**Figure 1**), and the KA was administered as repeated low doses at 30 min intervals *via* the intraperitoneal route, 7 days after surgery, and the proteins were analyzed a further 7 days later.

The Hippocampal Proteins That Mediate Neurodegeneration

Comparing across all four groups, using one-way ANOVA and Fisher's *post-hoc* test, we found a significant increase in some of the common proteins that have a role in neuroinflammation and neurodegeneration, the two important hallmarks of epileptogenesis associated with brain trauma or

TABLE 5 | The linearity of dilution assessment and detection ranges of cytokines in 1:2 diluted test samples using the MSD assay kit.

MSD cytokines tested	Expected dynamic range (pg/ml)	Detected conc. in 1:2 dilution (no surgery+ vehicle) (pg/ml)	Detected conc. In 1:2 dilution (surgery + KA) (pg/ml)
IFN-γ	0.0471–815	321	346
IL-10	0.742–2,540	1,016	1,590
IL-12p70	7.98–22,900	429	422
IL-1	0.123–1,470	617	2,367
IL-2	0.259–2,110	441	581
IL-4	0.120–1,320	753	886
IL-5	0.0667–821	123	131
IL-6	0.830–3,490	846	3,838
KC/GRO	0.208–1,540	3,032	18,048
TNFα	0.127–507	866	1,124

Two cortical supernatants were used: one from a non-implanted, non-KA mouse (no surgery + vehicle) that was expected to have the lowest cytokine concentrations and one from an electrode implanted and KA-treated mouse (surgery + KA) that was predicted to have the highest cytokine concentrations.

exposure to chemoconvulsants (2, 3, 15, 25, 26, 89, 90). Galectin-1 (Gal-1) was significantly increased in response to surgery with or without KA, but surgery seems to potentiate the KA effects on Gal-1 expression (**Supplementary Figure 1**). It binds to β-galactoside moieties present in cell surface glycoproteins of neurons and astrocytes in the brain (91, 92). It is a member of lectin family and a downstream effector of low affinity nerve growth factor receptor, $p75^{NTR}$, and regulates apoptosis and axonal growth (93). A selective proapoptotic role of Gal-1 in a subpopulation of GABAergic interneurons has been demonstrated in a pilocarpine model of epilepsy (56). Gal-1 inhibits CD45 protein phosphatase and dephosphorylates Lyn kinase, a member of the Src tyrosine kinase family (94, 95). Interestingly, we also observed a significant reduction of another member of Src kinase, Abl interactor 1 (Abi-1), in surgery group with or without KA (**Table 3**). Abi-1 interacts with CaMKIIα and regulates dendritic growth and spine maturation (96, 97). CD45, a common leukocyte antigen, expression increases in epileptic brain due to leaky BBB and infiltrated leukocytes (98). We also demonstrated a significant increase in phosphorylated Src kinases in a mouse model of epileptogenesis (2), suggesting a role for galectin–CD45–Src kinase signaling pathway in epilepsy. Ras and Rab related proteins, and CaMKIIα control neuronal plasticity by coordinating dendritic filopodial motility and AMPA receptor turnover (96, 97). In our proteomics study, Ras-related proteins Rab-6A and R-Ras2, and CaMKIIα were significantly decreased in surgery groups with or without KA, and with KA on its own (without surgery) (**Table 2**, **Supplementary Figure 1**), implying that the aberrant neurite growth and excitatory receptor activity could exacerbate during epileptogenesis.

Cystatin-C (CysC) is an endogenous inhibitor of cysteine protease such as cathepsin B (CatB) (99, 100). Interestingly, we observed a significant increase of both CysC and CatB in surgery groups with or without KA, but KA on its own did not increase CatB (**Table 2**, **Supplementary Figure 1**). CysC modulates both neurodegeneration and neurogenesis, during epileptogenesis and in the established epilepsy (4). The increased expression of CysC was observed in glial cells in the molecular layer of the dentate gyrus and associated with granule cell dispersion in both rat model and human patients with TLE (4). High levels of CatB were reported in serum of human patients with surgically resected temporal lobes (59) and in glial cells of progressive myoclonic epilepsies (57), suggesting that CatB can be a potential therapeutic target for certain epilepsies (58).

The Hippocampal Proteins Involved in BBB Integrity

KA-induced SE in intracerebral electrodes mice significantly increased the number of proteins related to BBB integrity. BBB dysfunction occurs within hours of the insult in traumatic brain injury patients and persists for days to weeks (101–104). Leaky BBB has also been reported as a frequent event in post-traumatic patients with epilepsy (105–107). BBB integrity is compromised in response to KA-induced SE in experimental models (25, 26, 108). The fibrinogen alpha chain (FAC), a plasma glycoprotein, was increased by 5.9-fold ($p = 0.005$) in the hippocampus in the surgery+KA group when compared with no surgery+KA group (**Table 4**). FAC protein infiltrates into the brain through a leaky BBB and promotes neuroinflammation (60, 61). FAC aids as an adhesive substrate for platelets, endothelial cells, and leukocytes including brain infiltrated monocytes and further increases vascular permeability by activating the extracellular signal-regulated kinase 1/2 (ERK1/2) pathways in traumatic brain injury (61, 90, 109). The significant increase of the other serum glycoproteins in the hippocampus, such as serum albumin, α2 macroglobulin, serotransferrin, and α1 protease inhibitor 4 (α1 antitrypsin), further confirms the compromised BBB integrity due to the brain trauma caused by intracerebral electrodes and subsequent exposure to KA. The brain infiltrated serum albumin binds to astrocytic transforming growth factor-beta (TGF-β) receptors, phosphorylates SMAD-2/3, increases the cytoskeletal proteins, and induces inflammatory signaling, thus causing reactive gliosis (25, 26, 110–115). Indeed, we observed a significant increase in three key cytoskeletal proteins: GFAP (2.7-fold, $p = 0.0003$), vimentin (2.8-fold, $p = 0.0007$), and filamin A (actin-binding protein 280, >2-fold, $p = 0.006$) in surgery groups. Immunohistochemistry of mice brain sections from the 7 day post-KA of electrode implanted animals confirmed the increased reactive astrogliosis (25, 26). In a model of acquired epilepsy with BBB dysfunction, serum albumin has been shown to induce excitatory synaptogenesis through astrocytic TGF-β/ALK5 signaling pathway (116). There are reports of filamin A pathology, as astrocytic inclusions, in human patients with epilepsy (43, 44).

Glia-Related Proteins and Synaptic Plasticity in the Hippocampus

We observed a significant increase in heat shock protein 25 (HSPβ1 or HSP25) in KA treated animals with or without surgery (**Table 2**). HSP25 functions as a molecular chaperone

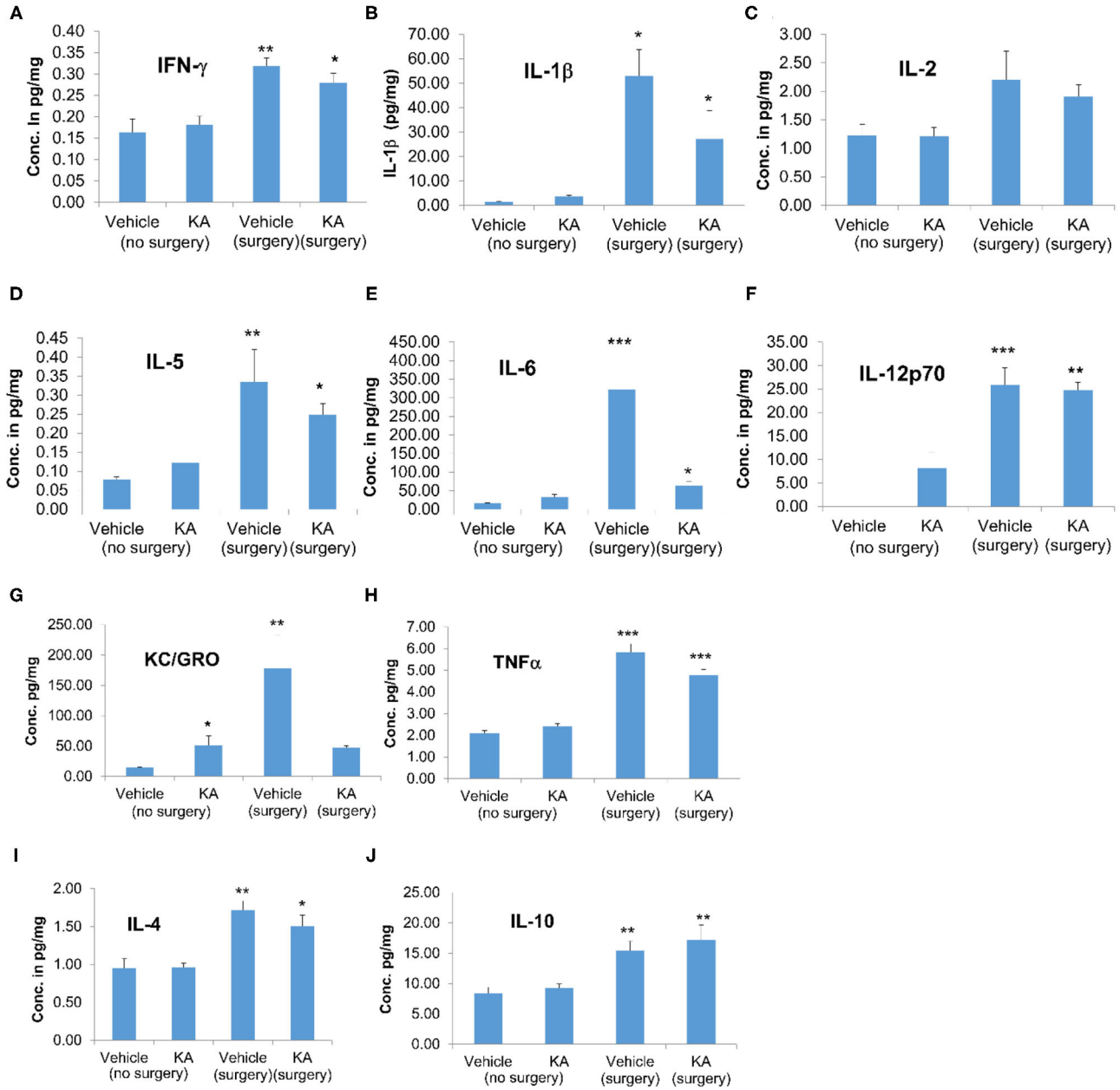

FIGURE 5 | The effects of the vehicle or KA treatment in mice that had surgery for implantation of intracerebral electrodes or without surgery on inflammatory cytokines in the cerebral cortex. The following cytokines were measured and represented in the graphs: **(A)** interferon-γ (IFN-γ), **(B)** interleukin-1β (IL-1β), **(C)** interleukin-2 (IL-2), **(D)** interleukin-5 (IL-5), **(E)** interleukin-6 (IL-6), **(F)** interleukin-12p70 (IL-12p70), **(G)** keratinocyte-derived cytokine/growth-related oncogene (KC-GRO), **(H)** tumor necrosis factor-α (TNF-α), **(I)** interleukin-4 (IL-4), **(J)** interleukin-10 (IL-10). The data are expressed as the mean (± SEM) cytokine concentration in pg/mg protein. The values were compared across all four groups using one-way ANOVA with Tukey's *post-hoc* test ($n = 4$, $^{*}p < 0.05$; $^{**}p < 0.01$; $^{***}p < 0.001$).

and regulates phosphorylation and the axonal transport of neurofilament proteins (117). HSP25 was upregulated in astrocytes and persisted for a long term in the hippocampus after the induction of SE in a rat pilocarpine model (45). The glutamine synthase (GS) and voltage-dependent GABA-A transporter (GAT-1, encoded by SLC6A1) proteins were significantly decreased in KA groups with or without surgery (both, FDR < 0.01). GS was predominantly expressed in astrocytes and required for the synthesis of glutamate and ammonia in the brain. GS deficiency causes epilepsy in both humans and animal models (46, 47). In a recent study, a selective deletion of GS in the mouse cerebral cortex induced glial dysfunction and vascular impairment (leaky BBB) that preceded the onset of epilepsy and neurodegeneration (118). Gat-1 is one

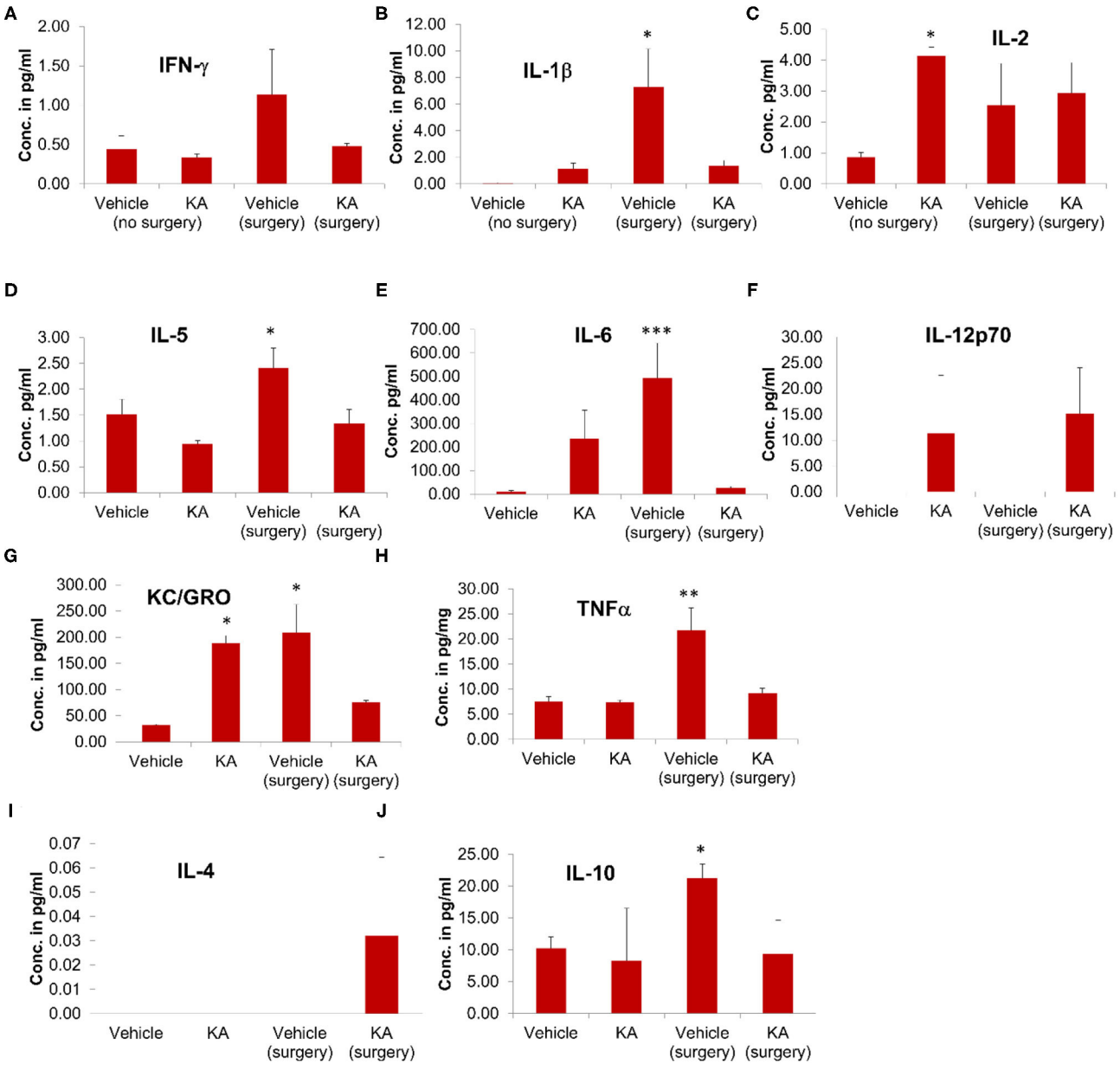

FIGURE 6 | The effects of the vehicle or KA treatment in the mice that had surgical implantation of EEG electrodes or without surgery on inflammatory cytokines in the plasma from the same animals that were used for proteomics (hippocampi) and multiplex assay (cerebral cortices). The following inflammatory cytokines were measured and represented in the graphs: **(A)** interferon-γ (IFN-γ), **(B)** interleukin-1β (IL-1β), **(C)** interleukin-2 (IL-2), **(D)** interleukin-5 (IL-5), **(E)** interleukin-6 (IL-6), **(F)** interleukin-12p70 (IL-12p70), **(G)** keratinocyte-derived cytokine/growth-related oncogene (KC-GRO), **(H)** tumor necrosis factor-α (TNF-α), **(I)** interleukin-4 (IL-4), **(J)** interleukin-10 (IL-10). The data are expressed as the mean (± SEM) cytokine concentration in pg/ml of plasma. The values were compared statistically using one-way ANOVA with Tukey's *post-hoc* test ($n = 4$, $^{*}p < 0.05$; $^{**}p < 0.01$; $^{***}p < 0.001$).

of the major GABA transporters in the brain and is responsible for re-uptake of GABA by astrocytes at the synapses. The studies in human patients revealed GAT-1 mutation/polymorphism in febrile seizures, myoclonic-atonic seizures, and TLE (48, 49).

The activation of astrocytes and the induction of excitatory synaptogenesis exacerbates the hyperexcitability of neurons, which we had previously shown this phenomenon as an increased epileptiform spiking during the first week of epileptogenesis (2, 25, 26, 31). Activated astrocytes compromise extracellular buffering at synapses by downregulating Kir1.4 ion channels (25, 26). In this study, we also found a significant change in the synaptic vesicle cycle and glutathione metabolism pathways (**Supplementary Table 5**). We have recently shown that activated astrocytes after

TABLE 6 | Summary of altered hippocampal proteins and cortical and plasma proinflammatory cytokines and chemokines between groups.

Protein/cytokine/chemokine	No surgery		Surgery		References related to epilepsy/seizure/trauma
	Vehicle	KA	Vehicle	KA	
Gliosis related proteins					
GFAP	++	++++	+++	+++++	(25, 26, 39, 40)
Vimentin	++	++++	+++	+++++	(41, 42)
Filamin A	++	++	+++	+++	(43, 44)
Heat shock protein beta-1 (HSP 25)	++	++++	++	+++++	(45)
Glutamine synthase	++++	++	+++	++	(46, 47)
GAT-1	++++	++	+++	++	(48, 49)
Complement C1qa	+	+++	++++	++++	(50–55)
Complement C1qb	++	+++	++++	++++	
Complement C1qc	++	+++	++++	++++	
Neurodegeneration related proteins					
Galectin-1	++	+++	+++	+++++	(56)
Cystatin-C (Cystatin-3)	++	+++	++	+++	(4)
Cathepsin B	++	+++	++	++++	(57–59)
BBB integrity related proteins					
Fibrinogen alpha chain	++	++++	+	+++	(60, 61)
Alpha 2 macroglobulin	++	+++	++++	++++	(62)
Transferrin	++	+++	++++	++++	(63)
α1 antitrypsin	++	++	+++	++++	(64)
Cytokines and chemokines [+ for cortical lysate and + for plasma; – (the minus sign) indicates undetected]					
Interferon-γ	++ ++	++++ ++	++ ++++	++++ ++	(65, 66)
Interleukin-1β	+ +	++ ++	++++ ++++	+++ ++	(67–69)
Interleukin-2	++ ++	++ ++++	++++ +++	++++ +++	(70)
Interleukin-4	++ –	++ –	++++ –	++++ +	(71, 72)
Interleukin-5	+ +++	++ ++	++++ +++	++++ +++	(72)
Interleukin-6	+ +	++ +++	+++++ +++++	+++ ++	(66, 69, 73)
Interleukin-10	++ ++	++ ++	++++ ++++	++++ ++	(66, 68, 74)
Interleukin-12p70	– –	++ ++	+++++ –	+++++ +++	(71, 75)
KC/GRO (CX_3CL)	+ +	+++ ++++	+++++ +++++	+++ +++	(76, 77)
Tumor necrosis-α	++ ++	++ ++	++++ ++++	++++ +++	(66, 68, 69)

Relative abundance in each group is indicated by a plus sign.

SE induction produce complement C and chemokines, which attract microglia at the synaptic terminals/neurons (3, 23). In this study, we found a significant increase in C1q related proteins in the surgery group with or without KA exposure, suggesting the role of these proteins in neuroinflammation and epileptogenesis. Several studies have demonstrated both astrogliosis and microgliosis during epileptogenesis and epilepsy (2, 3, 39, 40). A significant increase in GFAP, vimentin, filamin A, and C1q proteins in this study confirms that the proteomics method and the analysis are reliable and reiterate the plausible role of the identified proteins in the process of onset of spontaneous recurrent seizures/epileptogenesis.

The Cortical and Peripheral Cytokines in Response to Surgery and/or KA

Reactive astrocytes and microglia produce proinflammatory cytokines (39, 40). The cytokine assay of the cerebral cortex and the plasma from the same animals in our study showed a significant increase in some of the key proinflammatory

cytokines in the surgery group with or without KA when compared with the group without surgery (**Figures 5**, **6**). Proinflammatory cytokines are well-known to lower the seizure threshold (39, 40). Both hippocampus and cortex were affected in both human and animal models of temporal lobe epilepsy (25, 26, 86, 119–121). The epileptogenic network that involves the initiation and propagation of seizures has been well-defined in both humans and experimental models of epilepsy (115, 122, 123). Our previous work in the C57BL/6J mouse KA model, focused on the hippocampus, the entorhinal cortex, and the amygdala, suggested that the hippocampal gliosis and neurodegenerative changes were maximally affected at 7 days post-KA but beginning to decrease thereafter in contrast to the rat KA model of progressive epilepsy (25, 26). Interestingly, cortical changes persisted. Continuous video-EEG monitoring from these mice revealed persistent non-convulsive seizures (26). Therefore, in this study, we used the hippocampus for protein profiling and the cerebral cortex, where the electrodes penetrated the brain, for cytokine assay at 7 days post-KA (and plasma from the same animals). It has been demonstrated that the localized electrode-induced trauma causes localized gliosis (124–126). We were also interested in determining whether the impact of surgery and KA-induced SE or KA, on its own, would change cytokine profiles in the plasma, which may serve as a biomarker for epileptogenesis in experimental models. Indeed, we observed a significant increase in pro-inflammatory cytokines IFN-γ, IL-1β, IL-5, 1L-6, IL-10, IL-12p70, KC/GRO (also known as CXCL1), and TNFα in the cerebral cortex in the surgery group, and some in KA, suggesting the occurrence of neuroinflammation due to implanted electrodes and/or KA. Appropriate references with respect to the roles of these cytokines in epilepsy/seizure/trauma are included in **Table 6**. In the plasma of KA-induced SE in animals without surgery, only IL-2 and KC/GRO were upregulated. Interestingly, IL-2 was unaffected in the cerebral cortex, implying the peripheral effects. Although there is no literature on either plasma/serum or cerebral tissue cytokines at 14 days post-trauma, there are reports on early time-points demonstrating upregulation of some of these cytokines (89, 127). Therefore, the plausible reason for the reduced seizure threshold in the mice that had surgery could be due to localized cerebral inflammation, which seems to have persisted for a further 7 days as a result of the implanted electrodes.

The occurrence of seizures immediately prior to euthanasia could affect some of the cytokine levels. In this study, we did not monitor the animals for seizures throughout. Once a spontaneous seizure was confirmed in a mouse, the recording was stopped. An important variable in this study and Ravizza et al. (128) is the model (pilocarpine rat model vs. KA mouse model). The rat pilocarpine model is a progressive epilepsy model, while C57BL/6J mouse KA model is a regressive model (convulsive seizures are infrequent) (129).

The Limitations of This Study

The proteins discussed in this study, focused on the effects of surgery and KA on the development of epilepsy, are based on the literature. We have investigated the hippocampus only for proteomes and the cortex only for cytokines at 7 day post-KA (only one time-point), and the other epileptogenic areas and the time-points were not investigated. It has been suggested that the endogenous proresolving molecules such as lipoxins, resolvins, protectins, and maresins synthesis occur within hours to days of insult (130). In this study, none of the proresolving endogenous mediators of inflammation were significantly altered in any groups. Since we did proteomics at 14 days post-surgery or 7 days post-SE, it is likely that the resolution phase has passed. For example, the brain infiltrated monocytes and leucocytes persist only during the first 3 days of chemoconvulsant-induced SE (131). The altered levels of proteins or cytokines/chemokines alone do not necessarily affect the brain function *per se*. In this context, further studies are needed to determine the cell types and the receptor subtype expression in different regions of the brain at various time points post-SE to determine the functional outcome.

A summary of proteins identified in this study with a known role in seizures/epilepsy/trauma are listed in **Table 6**. In addition to the proteins discussed, there are many other proteins that may have a role in epileptogenesis that were not detected in this study due to single time point analysis. However, a few other proteins that were altered due to surgery and/or KA are briefly mentioned here. VGF, a BDNF-inducible peptide precursor, regulates fear-associated memory formation in hippocampus (132–134). Glypican-1, a member of the heparin sulfate proteoglycans, mediates phosphatidylinositol glycan signal propagation and receptor activation in the brain. Although glypican-4 has been demonstrated in the brains of epileptic patients and epileptic animals (135), the role of glypican-1 in epileptogenesis is yet unknown. Unconventional myosin-Va is required for neuronal plasticity, motor learning, oligodendrocyte morphogenesis, and myelination (136, 137), but its role in epileptogenesis is also unknown. Further mining of the proteomics data can yield other molecular mechanisms that may be affected by surgery and KA. The raw data and analyzed data are available at https://github.com/ISUgenomics/2020_Thippeswamy_Surgery-Proteomics/tree/ or *via* ProteomeXchange (Project doi: 10.6019/PXD021554). The results of this study did not show significant changes in the other proteins of certain pathways such as glutamate receptor activation, immunomodulating effects, or calcium homeostasis; however, the identified proteins having a significant role in inflammation, neurodegeneration, BBB integrity, and gliosis support the hypotheses of the potential impact of intracerebral electrodes on brain pathology and electrical activity. Surgery and intracerebral electrodes can alter chemoconvulsants' sensitivity in animals and appear to have a higher impact on altering the expression of proteins involved in epilepsy than KA itself. Thus, it can be misleading to assume that the development of epilepsy observed in EEG will reflect what occurs in brains without electrodes. These findings should give insights into the impact of intracranial surgery on epilepsy development and should be considered in the design of epilepsy studies and the interpretation of data arising from models in which intracranial procedures have been used. It should be noted that the sample size used in this study is small ($n = 4$) as in the rat pilocarpine model (28). However, a combination of proteomics and multiplex

assay from two different brain regions, and the plasma assay, revealed the altered key proteins in trauma and/or KA-induced brain injury.

In conclusion, surgery and intracerebral electrodes reduce seizure threshold and increase the key proteins that regulate the BBB function, neuroinflammation, and neurodegeneration as revealed by the proteomics at 7 days post-KA. The cytokine assay from the cerebral cortex and plasma suggest that the intracerebral electrode-induced proinflammatory cytokine responses may partly contribute to the decreased seizure threshold but not necessarily promote epileptogenesis, which was not tested in this study. It should also be noted that some of the inflammatory molecules (IL-6, IL-1beta, KC/GRO) reported in this study are inconsistent and require further investigation. The transient inflammatory responses evoked by surgery and electrodes procedures (persistent responses at different time-points were not tested in this study) unlikely have an impact on the development of epilepsy; otherwise, it is difficult to extrapolate the refined experimental models of SE induction by electrical stimulation in which only a small percentage of animals develop epilepsy (138). Our past EEG studies in the C57BL/6J mice did not show epileptiform spikes in their baseline EEG during the first 10 days of continuous (24/7) EEG monitoring post-surgery before KA challenge, suggesting that mere electrode implantation *per se* unlikely initiates epileptogenesis (129). However, the surgical procedure decreases the seizure threshold; therefore, to reduce mortality in KA models, irrespective of rodent species, a repeated low-dose method of administering KA would be advantageous (32, 139).

DATA AVAILABILITY STATEMENT

The datasets presented in this study can be found in online repositories. The names of the repository/repositories and accession number(s) can be found at: ProteomeXchange, http://www.proteomexchange.org/, PXD021554.

ETHICS STATEMENT

The animal study was reviewed and approved by The University of Liverpool Ethics Committee as per the Animal (Scientific Procedures) Act, 1986 (U.K).

AUTHOR CONTRIBUTIONS

TT conceived the idea and secured funding in collaboration with GS. TT and RB designed experiments. KT and EB conducted *in vivo* experiments. KT performed MSD assay. KT and GS analyzed the data. DS, KT, and RB conducted proteomics experiments. TT wrote the manuscript. KT wrote the Methods section and some of the Introduction. EB edited and proof-read the first manuscript. All authors contributed to the article and approved the submitted version.

FUNDING

This research was funded in 2011 (TT and GS) by the Center for Integrative Mammalian Biology and Biotechnology (The University of Liverpool, UK) and Biological Sciences Research Center, UK. Maryam Sayadi and Andrew Severin at Genomics Facility, Iowa State University, USA, reanalyzed and revalidated the proteomics data and uploaded the data on ProteomeXchange platform. The CVM Dean's Faculty Fellowship (TT) funded the reanalysis and validation of the proteome data at the Iowa State University.

SUPPLEMENTARY MATERIAL

The Supplementary Material for this article can be found online at: https://www.frontiersin.org/articles/10.3389/fneur.2021.625017/full#supplementary-material

Supplementary Figure 1 | Box plots for all 40 significant proteins identified by one-way ANOVA.

Supplementary Figure 2 | The schematic diagrams of KEGG pathways (vehicle: surgery vs. no surgery).

Supplementary Figure 3 | The schematic diagrams of KEGG pathways (KA: surgery vs. no surgery).

Supplementary Table 1 | List of all proteins identified by comparing all four groups using one-way ANOVA.

Supplementary Table 2 | The impact of intracerebral electrode implants on the expression of proteins in the hippocampus. The groups compared were between surgery vs. no surgery treated with vehicle (distilled water), and all the proteins that were significantly altered by $p > 0.01$ are listed and the proteins with >2-fold change are highlighted.

Supplementary Table 3 | The impact of KA-induced SE in intracerebral electrode implanted animals on the expression of proteins in the hippocampus. The groups compared were between surgery vs. no surgery treated with KA, and all the proteins that were significantly altered by $p > 0.01$ are listed and the proteins with >2-fold change are highlighted.

Supplementary Table 4 | The list of KEGG pathways and the key proteins of the pathways affected by intracerebral electrode implants. The groups compared were between surgery vs. no surgery and treated with the vehicle (distilled water).

Supplementary Table 5 | The list of KEGG pathways and the key proteins of the pathways affected by intracerebral electrode implants and KA-induced SE. The groups compared were between surgery vs. no surgery and treated with KA.

REFERENCES

1. Galanopoulou AS, Mowrey WB, Liu W, Li Q, Shandra O, Mosh,é SL. Preclinical screening for treatments for infantile spasms in the multiple hit rat model of infantile spasms: an update. *Neurochem Res.* (2017) 42:1949–61. doi: 10.1007/s11064-017-2282-0
2. Sharma S, Carlson S, Puttachary S, Sarkar S, Showman L, Putra M, et al. Role of the Fyn-PKCδ signaling in SE-induced neuroinflammation and epileptogenesis in experimental models of temporal lobe epilepsy. *Neurobiol Dis.* (2018) 110:102–21. doi: 10.1016/j.nbd.2017.11.008
3. Putra M, Gage M, Sharma S, Gardner C, Gasser G, Anantharam V, et al. Diapocynin, an NADPH oxidase inhibitor, counteracts diisopropylfluorophosphate-induced long-term neurotoxicity in the rat model. *Ann N Y Acad Sci.* (2020) 1479:75–93. doi: 10.1111/nyas.14314
4. Wu X, Kuruba R, Reddy DS. Midazolam-Resistant seizures and brain injury following acute intoxication of diisopropylfluorophosphate, an

organophosphate pesticide and surrogate for nerve agents. *J Pharmacol Exp Ther.* (2018) 367:302–21. doi: 10.1124/jpet.117.247106
5. Potschka H, Friderichs E, Löscher W. Anticonvulsant and proconvulsant effects of tramadol, its enantiomers and its M1 metabolite in the rat kindling model of epilepsy. *Br J Pharmacol.* (2000) 131:203–12. doi: 10.1038/sj.bjp.0703562
6. Nolte MW, Löscher W, Herden C, Freed WJ, Gernert M. Benefits and risks of intranigral transplantation of GABA-producing cells subsequent to the establishment of kindling-induced seizures. *Neurobiol Dis.* (2008) 31:342–54. doi: 10.1016/j.nbd.2008.05.010
7. Rashid K, Van der Zee CE, Ross GM, Chapman CA, Stanisz J, Riopelle RJ, et al. A nerve growth factor peptide retards seizure development and inhibits neuronal sprouting in a rat model of epilepsy. *Proc Natl Acad Sci USA.* (1995) 92:9495–9. doi: 10.1073/pnas.92.21.9495
8. Gasior M, Tang R, Rogawski MA. Long-Lasting attenuation of amygdala-kindled seizures after convection-enhanced delivery of botulinum neurotoxins A and B into the amygdala in rats. *J Pharmacol Exp Ther.* (2013) 346:528–34. doi: 10.1124/jpet.113.205070
9. Rattka M, Brandt C, Löscher W. The intrahippocampal kainate model of temporal lobe epilepsy revisited: epileptogenesis, behavioral and cognitive alterations, pharmacological response, and hippoccampal damage in epileptic rats. *Epilepsy Res.* (2013) 103:135–52. doi: 10.1016/j.eplepsyres.2012.09.015
10. Greenhalgh J, Weston J, Dundar Y, Nevitt SJ, Marson AG. Antiepileptic drugs as prophylaxis for postcraniotomy seizures. *Cochrane Database Syst Rev.* (2018) 5:CD007286. doi: 10.1002/14651858.CD007286.pub4
11. Taylor JA, Rodgers KM, Bercum FM, Booth CJ, Dudek FE, Barth DS. Voluntary control of epileptiform spike-wave discharges in awake rats. *J Neurosci Off J Soc Neurosci.* (2017) 37:5861–9. doi: 10.1523/JNEUROSCI.3235-16.2017
12. Löscher W, Hörstermann D, Hönack D, Rundfeldt C, Wahnschaffe U. Transmitter amino acid levels in rat brain regions after amygdala-kindling or chronic electrode implantation without kindling: evidence for a pro-kindling effect of prolonged electrode implantation. *Neurochem Res.* (1993) 18:775–81. doi: 10.1007/BF00966772
13. Löscher W, Wahnschaffe U, Hönack D, Rundfeldt C. Does prolonged implantation of depth electrodes predispose the brain to kindling? *Brain Res.* (1995) 697:197–204. doi: 10.1016/0006-8993(95)00843-F
14. Löscher W, Brandt C. Prevention or modification of epileptogenesis after brain insults: experimental approaches and translational research. *Pharmacol Rev.* (2010) 62:668–700. doi: 10.1124/pr.110.003046
15. Sharma S, Puttachary S, Thippeswamy A, Kanthasamy AG, Thippeswamy T. Status epilepticus: behavioral and electroencephalography seizure correlates in kainate experimental models. *Front Neurol.* (2018) 9:7. doi: 10.3389/fneur.2018.00007
16. Niespodziany I, Klitgaard H, Margineanu DG. Chronic electrode implantation entails epileptiform field potentials in rat hippocampal slices, similarly to amygdala kindling. *Epilepsy Res.* (1999) 36:69–74. doi: 10.1016/S0920-1211(99)00027-3
17. Löscher W. Animal models of epilepsy for the development of antiepileptogenic and disease-modifying drugs. A comparison of the pharmacology of kindling and post-status epilepticus models of temporal lobe epilepsy. *Epilepsy Res.* (2002) 50:105–23. doi: 10.1016/S0920-1211(02)00073-6
18. Ben-Ari Y, Cossart R. Kainate, a double agent that generates seizures: two decades of progress. *Trends Neurosci.* (2000) 23:580–7. doi: 10.1016/S0166-2236(00)01659-3
19. Brandt C, Potschka H, Löscher W, Ebert U. N-methyl-D-aspartate receptor blockade after status epilepticus protects against limbic brain damage but not against epilepsy in the kainate model of temporal lobe epilepsy. *Neuroscience.* (2003) 118:727–40. doi: 10.1016/S0306-4522(03)00027-7
20. Chang P, Hashemi KS, Walker MC. A novel telemetry system for recording EEG in small animals. *J Neurosci Methods.* (2011) 201:106–15. doi: 10.1016/j.jneumeth.2011.07.018
21. Beamer E, Otahal J, Sills GJ, Thippeswamy T. N w-Propyl-l-arginine (L-NPA) reduces status epilepticus and early epileptogenic events in a mouse model of epilepsy: behavioural, EEG and immunohistochemical analyses. *Eur. J. Neurosci.* (2012) 36:3194–203. doi: 10.1111/j.1460-9568.2012.08234.x
22. Gage M, Golden M, Putra M, Sharma S, Thippeswamy T. Sex as a biological variable in the rat model of diisopropylfluorophosphate-induced long-term neurotoxicity. *Ann N Y Acad Sci.* (2020) 1479:44–64. doi: 10.1111/nyas.14315
23. Putra M, Sharma S, Gage M, Gasser G, Hinojo-Perez A, Olson A, et al. Inducible nitric oxide synthase inhibitor, 1400W, mitigates DFP-induced long-term neurotoxicity in the rat model. *Neurobiol Dis.* (2020) 133:104443. doi: 10.1016/j.nbd.2019.03.031
24. White A, Williams PA, Hellier JL, Clark S, Dudek FE, Staley KJ. EEG spike activity precedes epilepsy after kainate-induced status epilepticus. *Epilepsia.* (2010) 51:371–83. doi: 10.1111/j.1528-1167.2009.02339.x
25. Puttachary S, Sharma S, Verma S, Yang Y, Putra M, Thippeswamy A, et al. 1400W, a highly selective inducible nitric oxide synthase inhibitor is a potential disease modifier in the rat kainate model of temporal lobe epilepsy. *Neurobiol Dis.* (2016) 93:184–200. doi: 10.1016/j.nbd.2016.05.013
26. Puttachary S, Sharma S, Thippeswamy A, Thippeswamy T. Immediate epileptogenesis: impact on brain in C57BL/6J mouse kainate model. *Front Biosci Elite Ed.* (2016) 8:390–411. doi: 10.2741/e775
27. Bitsika V, Duveau V, Simon-Areces J, Mullen W, Roucard C, Makridakis M, et al. High-Throughput LC–MS/MS proteomic analysis of a mouse model of mesiotemporal lobe epilepsy predicts microglial activation underlying disease development. *J Proteome Res.* (2016) 15:1546–62. doi: 10.1021/acs.jproteome.6b00003
28. Marques-Carneiro JE, Persike DS, Litzahn JJ, Cassel JC, Nehlig A, Fernandes MJDS. Hippocampal proteome of rats subjected to the li-pilocarpine epilepsy model and the effect of carisbamate treatment. *Pharmaceuticals.* (2017) 10:67. doi: 10.3390/ph10030067
29. Keck M, Androsova G, Gualtieri F, Walker A, von Rüden EL, Russmann V, et al. A systems level analysis of epileptogenesis-associated proteome alterations. *Neurobiol Dis.* (2017) 105:164–78. doi: 10.1016/j.nbd.2017.05.017
30. Kilkenny C, Browne WJ, Cuthill IC, Emerson M, Altman DG. Improving bioscience research reporting: the arrive guidelines for reporting animal research. *PLoS Biol.* (2010) 8:e1000412. doi: 10.1371/journal.pbio.1000412
31. Puttachary S, Sharma S, Tse K, Beamer E, Sexton A, Crutison J, et al. Immediate epileptogenesis after kainate-induced status epilepticus in C57BL/6J mice: evidence from long term continuous video-EEG telemetry. *PLoS ONE.* (2015) 10:e0131705. doi: 10.1371/journal.pone.0131705
32. Tse K, Puttachary S, Beamer E, Sills GJ, Thippeswamy T. Advantages of repeated low dose against single high dose of kainate in C57BL/6J mouse model of status epilepticus: behavioral and electroencephalographic studies. *PLoS ONE.* (2014) 9:e96622. doi: 10.1371/journal.pone.0096622
33. Tse K, Hammond D, Simpson D, Beynon RJ, Beamer E, Tymianski M, et al. The impact of postsynaptic density 95 blocking peptide (Tat-NR2B9c) and an iNOS inhibitor (1400W) on proteomic profile of the hippocampus in C57BL/6J mouse model of kainate-induced epileptogenesis. *J Neurosci Res.* (2019) 97:1378–92. doi: 10.1002/jnr.24441
34. Chong J, Yamamoto M, Xia J. MetaboAnalystR 2.0: from raw spectra to biological insights. *Metabolites.* (2019) 9:57. doi: 10.3390/metabo9030057
35. Chong J, Soufan O, Li C, Caraus I, Li S, Bourque G, et al. MetaboAnalyst 4.0: towards more transparent and integrative metabolomics analysis. *Nucleic Acids Res.* (2018) 46:W486–94. doi: 10.1093/nar/gky310
36. Huang DW, Sherman BT, Lempicki RA. Bioinformatics enrichment tools: paths toward the comprehensive functional analysis of large gene lists. *Nucleic Acids Res.* (2009) 37:1–13. doi: 10.1093/nar/gkn923
37. Huang DW, Sherman BT, Lempicki RA. Systematic and integrative analysis of large gene lists using DAVID bioinformatics resources. *Nat. Protoc.* (2009) 4:44–57. doi: 10.1038/nprot.2008.211
38. Ray CA, Bowsher RR, Smith WC, Devanarayan V, Willey MB, Brandt JT, et al. Development, validation, and implementation of a multiplex immunoassay for the simultaneous determination of five cytokines in human serum. *J Pharm Biomed Anal.* (2005) 36:1037–44. doi: 10.1016/j.jpba.2004.05.024
39. Vezzani A, French J, Bartfai T, Baram TZ. The role of inflammation in epilepsy. *Nat Rev Neurol.* (2011) 7:31–40. doi: 10.1038/nrneurol.2010.178
40. Devinsky O, Vezzani A, Najjar S, Lanerolle NCD, Rogawski MA. Glia and epilepsy: excitability and inflammation. *Trends Neurosci.* (2013) 36:174–84. doi: 10.1016/j.tins.2012.11.008
41. Stringer JL. Repeated seizures increase GFAP and vimentin in the hippocampus. *Brain Res.* (1996) 717:147–53. doi: 10.1016/0006-8993(96)00059-5

42. Berger TC, Vigeland MD, Hjorthaug HS, Etholm L, Nome CG, Taubøll E, et al. Neuronal and glial DNA methylation and gene expression changes in early epileptogenesis. *PLoS ONE.* (2019) 14:e0226575. doi: 10.1371/journal.pone.0226575
43. Hazrati LN, Kleinschmidt-DeMasters BK, Handler MH, Smith ML, Ochi A, Otsubo H, et al. Astrocytic inclusions in epilepsy: expanding the spectrum of filaminopathies. *J Neuropathol Exp Neurol.* (2008) 67:669–76. doi: 10.1097/NEN.0b013e31817d7a06
44. Adam J, Polivka M, Kaci R, Godfraind C, Gray F. Hyaline astrocytic inclusions in pediatric epilepsy: report of two cases. *Clin Neuropathol.* (2010) 29:246–53. doi: 10.5414/NPP29246
45. Kim JE, Hyun HW, Min SJ, Kang TC. Sustained HSP25 expression induces clasmatodendrosis via ER stress in the rat hippocampus. *Front Cell Neurosci.* (2017) 11:47. doi: 10.3389/fncel.2017.00047
46. Eid T, Tu N, Lee TSW, Lai JCK. Regulation of astrocyte glutamine synthetase in epilepsy. *Neurochem Int.* (2013) 63:670–81. doi: 10.1016/j.neuint.2013.06.008
47. Papageorgiou IE, Valous NA, Lahrmann B, Janova H, Klaft Z.-J, et al. Astrocytic glutamine synthetase is expressed in the neuronal somatic layers and down-regulated proportionally to neuronal loss in the human epileptic hippocampus. *Glia.* (2018) 66:920–33. doi: 10.1002/glia.23292
48. Carvill GL, McMahon JM, Schneider A, Zemel M, Myers CT, Saykally J, et al. Mutations in the GABA transporter SLC6A1 cause epilepsy with myoclonic-atonic seizures. *Am J Hum Genet.* (2015) 96:808–15. doi: 10.1016/j.ajhg.2015.02.016
49. Schijns OE, Bisschop J, Rijkers K, Dings J, Vanherle S, Lindsey P, et al. GAT-1 (rs2697153) and GAT-3 (rs2272400) polymorphisms are associated with febrile seizures and temporal lobe epilepsy. *Epileptic Disord Int Epilepsy J Videotape.* (2020) 22:176–82. doi: 10.1684/epd.2020.1154
50. Aronica E, Boer K, van Vliet EA, Redeker S, Baayen JC, Spliet WG, et al. Complement activation in experimental and human temporal lobe epilepsy. *Neurobiol Dis.* (2007) 26:497–511. doi: 10.1016/j.nbd.2007.01.015
51. Wyatt SK, Witt T, Barbaro NM, Cohen-Gadol AA, Brewster AL. Enhanced classical complement pathway activation and altered phagocytosis signaling molecules in human epilepsy. *Exp Neurol.* (2017) 295:184–93. doi: 10.1016/j.expneurol.2017.06.009
52. Kopczynska M, Zelek WM, Vespa S, Touchard S, Wardle M, Loveless S, et al. Complement system biomarkers in epilepsy. *Seizure.* (2018) 60:1–7. doi: 10.1016/j.seizure.2018.05.016
53. Andoh M, Ikegaya Y, Koyama R. Synaptic pruning by microglia in epilepsy. *J Clin Med.* (2019) 8:2170. doi: 10.3390/jcm8122170
54. Brewster AL. Human microglia seize the chance to be different. *Epilepsy currents.* (2019) 19:190–2. doi: 10.1177/1535759719843299
55. Schartz ND, Wyatt-Johnson SK, Price LR, Colin SA, Brewster AL. Status epilepticus triggers long-lasting activation of complement C1q-C3 signaling in the hippocampus that correlates with seizure frequency in experimental epilepsy. *Neurobiol Dis.* (2018) 109(Pt A):163–73. doi: 10.1016/j.nbd.2017.10.012
56. Bischoff V, Deogracias R, Poirier F, Barde Y.-A. Seizure-induced neuronal death is suppressed in the absence of the endogenous lectin Galectin-1. *J Neurosci Off J Soc Neurosci.* (2012) 32:15590–600. doi: 10.1523/JNEUROSCI.4983-11.2012
57. Houseweart MK, Pennacchio LA, Vilaythong A, Peters C, Noebels JL, Myers RM. Cathepsin B but not cathepsins L or S contributes to the pathogenesis of unverricht-lundborg progressive myoclonus epilepsy (EPM1). *J Neurobiol.* (2003) 56:315–27. doi: 10.1002/neu.10253
58. Hook G, Jacobsen JS, Grabstein K, Kindy M, Hook V. Cathepsin B is a new drug target for traumatic brain injury therapeutics: evidence for E64d as a promising lead drug candidate. *Front Neurol.* (2015) 6:178. doi: 10.3389/fneur.2015.00178
59. Simões PSR, Zanelatto AO, Assis MC, Varella PPV, Yacubian EM, Carrete H, et al. Plasma kallikrein-kinin system contributes to peripheral inflammation in temporal lobe epilepsy. *J Neurochem.* (2019) 150:296–311. doi: 10.1111/jnc.14793
60. Davalos D, Akassoglou K. Fibrinogen as a key regulator of inflammation in disease. *Semin Immunopathol.* (2012) 34:43–62. doi: 10.1007/s00281-011-0290-8
61. Muradashvili N, Lominadze D. Role of fibrinogen in cerebrovascular dysfunction after traumatic brain injury. *Brain Inj.* (2013) 27:1508–15. doi: 10.3109/02699052.2013.823562
62. Keren-Aviram G, Dachet F, Bagla S, Balan K, Loeb JA, Dratz EA. Proteomic analysis of human epileptic neocortex predicts vascular and glial changes in epileptic regions. *PLoS ONE.* (2018) 13:e0195639. doi: 10.1371/journal.pone.0195639
63. Jang HN, Yoon HS, Lee EH. Prospective case control study of iron deficiency and the risk of febrile seizures in children in South Korea. *BMC Pediatr.* (2019) 19:309. doi: 10.1186/s12887-019-1675-4
64. Lolin YI, Ward AM. Alpha-1-antitrypsin phenotypes and associated disease patterns in neurological patients. *Acta Neurol Scand.* (1995) 91:394–8. doi: 10.1111/j.1600-0404.1995.tb07027.x
65. Getts DR, Matsumoto I, Müller M, Getts MT, Radford J, Shrestha B, et al. Role of IFN-gamma in an experimental murine model of West Nile virus-induced seizures. *J Neurochem.* (2007) 103:1019–30. doi: 10.1111/j.1471-4159.2007.04798.x
66. Gao F, Gao Y, Zhang SJ, Zhe X, Meng FL, Qian H, et al. Alteration of plasma cytokines in patients with active epilepsy. *Acta Neurol Scand.* (2017) 135:663–9. doi: 10.1111/ane.12665
67. Balosso S, Maroso M, Sanchez-Alavez M, Ravizza T, Frasca A, Bartfai T, et al. A novel non-transcriptional pathway mediates the proconvulsive effects of interleukin-1beta. *Brain.* (2008) 131 (Pt. 12):3256–65. doi: 10.1093/brain/awn271
68. Vieira ÉLM, de Oliveira GNM, Lessa JMK, Gonçalves AP, Oliveira ACP, Bauer ME, et al. Peripheral leukocyte profile in people with temporal lobe epilepsy reflects the associated proinflammatory state. *Brain Behav Immun.* (2016) 53:123–30. doi: 10.1016/j.bbi.2015.11.016
69. Vezzani A, Viviani B. Neuromodulatory properties of inflammatory cytokines and their impact on neuronal excitability. *Neuropharmacology.* (2015) 96 (Pt. A):70–82. doi: 10.1016/j.neuropharm.2014.10.027
70. Zhou H, Wang N, Xu L, Huang H, Yu C. The efficacy of gastrodin in combination with folate and vitamin B12 on patients with epilepsy after stroke and its effect on HMGB-1, IL-2 and IL-6 serum levels. *Exp Ther Med.* (2017) 14:4801–6. doi: 10.3892/etm.2017.5116
71. Benson MJ, Manzanero S, Borges K. Complex alterations in microglial M1/M2 markers during the development of epilepsy in two mouse models. *Epilepsia.* (2015) 56:895–905. doi: 10.1111/epi.12960
72. Mathieu O, Picot MC, Gelisse P, Breton H, Demoly P, Hillaire-Buys D. Effects of carbamazepine and metabolites on IL-2, IL-5, IL-6, IL-10 and IFN-γ secretion in epileptic patients: the influence of co-medication. *Pharmacol Rep.* (2011) 63:86–94. doi: 10.1016/S1734-1140(11)70402-9
73. Nowak M, Bauer S, Haag A, Cepok S, Todorova-Rudolph A, Tackenberg B, et al. Interictal alterations of cytokines and leukocytes in patients with active epilepsy. *Brain Behav Immun.* (2011) 25:423–8. doi: 10.1016/j.bbi.2010.10.022
74. Li G, Bauer S, Nowak M, Norwood B, Tackenberg B, Rosenow F, et al. Cytokines and epilepsy. *Seizure.* (2011) 20:249–256. doi: 10.1016/j.seizure.2010.12.005
75. Choi J, Nordli DR Jr, Alden TD, DiPatri A Jr. Cellular injury and neuroinflammation in children with chronic intractable epilepsy. *J Neuroinflammation.* (2009) 6:38. doi: 10.1186/1742-2094-6-38
76. Ahl M, Avdic U, Skoug C, Ali I, Chugh D, Johansson UE, et al. Immune response in the eye following epileptic seizures. *J Neuroinflammation.* (2016) 13:155. doi: 10.1186/s12974-016-0618-3
77. Liang LP, Pearson-Smith JN, Huang J, McElroy P, Day BJ, Patel M. Neuroprotective effects of AEOL10150 in a rat organophosphate model. *Toxicol Sci.* (2018) 162:611–1. doi: 10.1093/toxsci/kfx283
78. Hunsberger JG, Bennett AH, Selvanayagam E, Duman RS, Newton SS. Gene profiling the response to kainic acid induced seizures. *Brain Res Mol Brain Res.* (2005) 141:95–112. doi: 10.1016/j.molbrainres.2005.08.005
79. Gorter JA, van Vliet EA, Aronica E, Breit T, Rauwerda H, Lopes da Silva FH, et al. Potential new antiepileptogenic targets indicated by microarray analysis in a rat model for temporal lobe epilepsy. *J Neurosci Off J Soc Neurosci.* (2006) 26:11083–110. doi: 10.1523/JNEUROSCI.2766-06.2006
80. Sharma AK, Searfoss GH, Reams RY, Jordan WH, Snyder PW, Chiang AY, et al. Kainic acid-induced F-344 rat model of mesial temporal lobe epilepsy:

gene expression and canonical pathways. *Toxicol Pathol.* (2009) 37:776–89. doi: 10.1177/0192623309344202
81. Okamoto OK, Janjoppi L, Bonone FM, Pansani AP, da Silva AV, Scorza FA, et al. Whole transcriptome analysis of the hippocampus: toward a molecular portrait of epileptogenesis. *BMC Genomics.* (2010) 11:230. doi: 10.1186/1471-2164-11-230
82. Motti D, Le Duigou C, Eugène E, Chemaly N, Wittner L, Lazarevic D, et al. Gene expression analysis of the emergence of epileptiform activity after focal injection of kainic acid into mouse hippocampus. *Eur J Neurosci.* (2010) 32:1364–79. doi: 10.1111/j.1460-9568.2010.07403.x
83. Venugopal AK, Sameer Kumar GS, Mahadevan A, Selvan LDN, Marimuthu A, Dikshit JB, et al. Transcriptomic profiling of medial temporal lobe epilepsy. *J Proteomics Bioinform.* (2012) 5:1000210. doi: 10.4172/jpb.1000210
84. Laurén HB, Lopez-Picon FR, Brandt AM, Rios-Rojas CJ, Holopainen IE. Transcriptome analysis of the hippocampal CA1 pyramidal cell region after kainic acid-induced status epilepticus in juvenile rats. *PLoS ONE.* (2010) 5:e10733. doi: 10.1371/journal.pone.0010733
85. Kan AA, van Erp S, Derijck AA, de Wit M, Hessel EV, O'Duibhir E, et al. Genome-wide microRNA profiling of human temporal lobe epilepsy identifies modulators of the immune response. *Cell Mol Life Sci.* (2012) 69:3127–45. doi: 10.1007/s00018-012-0992-7
86. Bouilleret V, Ridoux V, Depaulis A, Marescaux C, Nehlig A, Le Gal La Salle G. Recurrent seizures and hippocampal sclerosis following intrahippocampal kainate injection in adult mice: electroencephalography, histopathology and synaptic reorganization similar to mesial temporal lobe epilepsy. *Neuroscience.* (1999) 89:717–29. doi: 10.1016/S0306-4522(98)00401-1
87. Riban V, Bouilleret V, Pham,-Lê BT, Fritschy J.-M, Marescaux C, et al. Evolution of hippocampal epileptic activity during the development of hippocampal sclerosis in a mouse model of temporal lobe epilepsy. *Neuroscience.* (2002) 112:101–11. doi: 10.1016/S0306-4522(02)00064-7
88. Heinrich C, Nitta N, Flubacher A, Müller M, Fahrner A, Kirsch M, et al. Reelin deficiency and displacement of mature neurons, but not neurogenesis, underlie the formation of granule cell dispersion in the epileptic hippocampus. *J Neurosci Off J Soc Neurosci.* (2006) 26:4701–13. doi: 10.1523/JNEUROSCI.5516-05.2006
89. Bell MJ, Kochanek PM, Doughty LA, Carcillo JA, Adelson PD, Clark RS, et al. Interleukin-6 and interleukin-10 in cerebrospinal fluid after severe traumatic brain injury in children. *J Neurotrauma.* (1997) 14:451–7. doi: 10.1089/neu.1997.14.451
90. Agoston DV, Kamnaksh A. Protein biomarkers of epileptogenicity after traumatic brain injury. *Neurobiol Dis.* (2019) 123:59–68. doi: 10.1016/j.nbd.2018.07.017
91. Sakaguchi M, Shingo T, Shimazaki T, Okano HJ, Shiwa M, Ishibashi S, et al. A carbohydrate-binding protein, galectin-1, promotes proliferation of adult neural stem cells. *Proc Natl Acad Sci USA.* (2006) 103:7112–7. doi: 10.1073/pnas.0508793103
92. Imaizumi Y, Sakaguchi M, Morishita T, Ito M, Poirier F, Sawamoto K, et al. Galectin-1 is expressed in early-type neural progenitor cells and down-regulates neurogenesis in the adult hippocampus. *Mol Brain.* (2011) 4:7. doi: 10.1186/1756-6606-4-7
93. Sakaguchi M, Okano H. Neural stem cells, adult neurogenesis, and galectin-1: from bench to bedside. *Dev Neurobiol.* (2012) 72:1059–67. doi: 10.1002/dneu.22023
94. Fouillit M, Joubert-Caron R, Poirier F, Bourin P, Monostori E, Levi-Strauss M, et al. Regulation of CD45-induced signaling by galectin-1 in burkitt lymphoma B cells. *Glycobiology.* (2000) 10:413–9. doi: 10.1093/glycob/10.4.413
95. Park GB, Kim DJ, Kim YS, Lee K, Kim CW, Hur DY, et al. Silencing of galectin-3 represses osteosarcoma cell migration and invasion through inhibition of FAK/Src/Lyn activation and β-catenin expression and increases susceptibility to chemotherapeutic agents. *Int J Oncol.* (2015) 46:185–94. doi: 10.3892/ijo.2014.2721
96. Park E, Chi S, Park D. Activity-dependent modulation of the interaction between CaMKIIα and abi1 and its involvement in spine maturation. *J Neurosci.* (2012) 32:13177–88. doi: 10.1523/JNEUROSCI.2257-12.2012
97. Szíber Z, Liliom H, Morales COO, Ignácz A, Rátkai AE, Ellwanger K, et al. Ras and Rab interactor 1 controls neuronal plasticity by coordinating dendritic filopodial motility and AMPA receptor turnover. *Mol Biol Cell.* (2017) 28:285–5. doi: 10.1091/mbc.E16-07-0526
98. Zattoni M, Mura ML, Deprez F, Schwendener RA, Engelhardt B, Frei K, et al. Brain infiltration of leukocytes contributes to the pathophysiology of temporal lobe epilepsy. *J Neurosci.* (2011) 31:4037–50. doi: 10.1523/JNEUROSCI.6210-10.2011
99. Bernstein HG, Kirschke H, Wiederanders B, Pollak KH, Zipress A, Rinne A. The possible place of cathepsins and cystatins in the puzzle of Alzheimer disease: a review. *Mol Chem Neuropathol.* (1996) 27:225–47. doi: 10.1007/BF02815106
100. Turk V, Stoka V, Turk D. Cystatins: biochemical and structural properties, medical relevance. *Front Biosci J Virtual Libr.* (2008) 13:5406–20. doi: 10.2741/3089
101. Abbott NJ, Friedman A. Overview and introduction: the blood-brain barrier in health and disease. *Epilepsia.* (2012) 53 (Suppl. 6):1–6. doi: 10.1111/j.1528-1167.2012.03696.x
102. Cunningham AS, Salvador R, Coles JP, Chatfield DA, Bradley PG, Johnston AJ, et al. Physiological thresholds for irreversible tissue damage in contusional regions following traumatic brain injury. *Brain J Neurol.* (2005) 128:1931–42. doi: 10.1093/brain/awh536
103. Rosenberg GA. Neurological diseases in relation to the blood-brain barrier. *J Cereb Blood Flow Metab.* (2012) 32:1139–51. doi: 10.1038/jcbfm.2011.197
104. Shlosberg D, Benifla M, Kaufer D, Friedman A. Blood-brain barrier breakdown as a therapeutic target in traumatic brain injury. *Nat Rev Neurol.* (2010) 6:393–403. doi: 10.1038/nrneurol.2010.74
105. Raabe A, Schmitz AK, Pernhorst K, Grote A, von der Brelie C, Urbach H, et al. Cliniconeuropathologic correlations show astroglial albumin storage as a common factor in epileptogenic vascular lesions. *Epilepsia.* (2012) 53:539–48. doi: 10.1111/j.1528-1167.2012.03405.x
106. Schmitz AK, Grote A, Raabe A, Urbach H, Friedman A, von Lehe M, et al. Albumin storage in neoplastic astroglial elements of gangliogliomas. *Seizure.* (2013) 22:144–50. doi: 10.1016/j.seizure.2012.10.014
107. Tomkins O, Shelef I, Kaizerman I, Eliushin A, Afawi Z, Misk A, et al. Blood-brain barrier disruption in post-traumatic epilepsy. *J Neurol Neurosurg Psychiatry.* (2008) 79:774–7. doi: 10.1136/jnnp.2007.126425
108. Löscher W, Friedman A. Structural, molecular, and functional alterations of the blood-brain barrier during epileptogenesis and epilepsy: a cause, consequence, or both? *Int J Mol Sci.* (2020) 21:591. doi: 10.3390/ijms21020591
109. Montagne A, Toga AW, Zlokovic BV. Blood-Brain barrier permeability and gadolinium: benefits and potential pitfalls in research. *JAMA Neurol.* (2016) 73:13–4. doi: 10.1001/jamaneurol.2015.2960
110. Seiffert E, Dreier JP, Ivens S, Bechmann I, Tomkins O, Heinemann U, et al. Lasting blood-brain barrier disruption induces epileptic focus in the rat somatosensory cortex. *J Neurosci Off J Soc Neurosci.* (2004) 24:7829–36. doi: 10.1523/JNEUROSCI.1751-04.2004
111. Ivens S, Kaufer D, Flores LP, Bechmann I, Zumsteg D, Tomkins O, et al. TGF-beta receptor-mediated albumin uptake into astrocytes is involved in neocortical epileptogenesis. *Brain J Neurol.* (2007) 130:535–47. doi: 10.1093/brain/awl317
112. David Y, Cacheaux LP, Ivens S, Lapilover E, Heinemann U, Kaufer D, et al. Astrocytic dysfunction in epileptogenesis: consequences of altered potassium and glutamate homeostasis? *J Neurosci Off J Soc Neurosci.* (2009) 29:10588–99. doi: 10.1523/JNEUROSCI.2323-09.2009
113. Cacheaux LP, Ivens S, David Y, Lakhter AJ, Bar-Klein G, Shapira M, et al. Transcriptome profiling reveals TGF-beta signaling involvement in epileptogenesis. *J Neurosci Off J Soc Neurosci.* (2009) 29:8927–35. doi: 10.1523/JNEUROSCI.0430-09.2009
114. Braganza O, Bedner P, Hüttmann K, von Staden E, Friedman A, Seifert G, et al. Albumin is taken up by hippocampal NG2 cells and astrocytes and decreases gap junction coupling. *Epilepsia.* (2012) 53:1898–906. doi: 10.1111/j.1528-1167.2012.03665.x
115. Bar-Klein G, Cacheaux LP, Kamintsky L, Prager O, Weissberg I, Schoknecht K, et al. Losartan prevents acquired epilepsy via TGF-β signaling suppression. *Ann Neurol.* (2014) 75:864–75. doi: 10.1002/ana.24147
116. Weissberg I, Wood L, Kamintsky L, Vazquez O, Milikovsky DZ, Alexander A, et al. Albumin induces excitatory synaptogenesis through astrocytic TGF-β/ALK5 signaling in a model of acquired epilepsy

following blood-brain barrier dysfunction. *Neurobiol Dis*. (2015) 78:115–25. doi: 10.1016/j.nbd.2015.02.029
117. Huang L, Min JN, Masters S, Mivechi NF, Moskophidis D. Insights into function and regulation of small heat shock protein 25 (HSPB1) in a mouse model with targeted gene disruption. *Genes*. (2007) 45:487–501. doi: 10.1002/dvg.20319
118. Zhou Y, Dhaher R, Parent M, Hu QX, Hassel BP, Yee SP, et al. Selective deletion of glutamine synthetase in the mouse cerebral cortex induces glial dysfunction and vascular impairment that precede epilepsy and neurodegeneration. *Neurochem Int*. (2019) 123:22–33. doi: 10.1016/j.neuint.2018.07.009
119. Coulter DA, McIntyre DC, Löscher W. Animal models of limbic epilepsies: what can they tell us? *Brain Pathol Zurich Switz*. (2002) 12:240–56. doi: 10.1111/j.1750-3639.2002.tb00439.x
120. Scharfman HE. The neurobiology of epilepsy. *Curr Neurol Neurosci Rep*. (2007) 7:348–54. doi: 10.1007/s11910-007-0053-z
121. Liu L, Hamre KM, Goldowitz D. Kainic acid-induced neuronal degeneration in hippocampal pyramidal neurons is driven by both intrinsic and extrinsic factors: analysis of FVB/N↔C57BL/6 chimeras. *J Neurosci Off J Sock Neurosci*. (2012) 32:12093–01. doi: 10.1523/JNEUROSCI.6478-11.2012
122. Lu Y, Zhong C, Wang L, Wei P, He W, Huang K, et al. Optogenetic dissection of ictal propagation in the hippocampal-entorhinal cortex structures. *Nat Commun*. (2016) 7:10962. doi: 10.1038/ncomms12019
123. Bartolomei F, Lagarde S, Wendling F, McGonigal A, Jirsa V, Guye M, et al. Defining epileptogenic networks: contribution of SEEG and signal analysis. *Epilepsia*. (2017) 58:1131–47. doi: 10.1111/epi.13791
124. Goc J, Liu JYW, Sisodiya SM, Thom M. A spatiotemporal study of gliosis in relation to depth electrode tracks in drug-resistant epilepsy. *Eur J Neurosci*. (2014) 39:2151–62. doi: 10.1111/ejn.12548
125. Sillay KA, Ondoma S, Wingeier B, Schomberg D, Sharma P, Kumar R, et al. Long-term surface electrode impedance recordings associated with gliosis for a closed-loop neurostimulation device. *Ann Neurosci*. (2018) 25:289–98. doi: 10.1159/000481805
126. Campbell A, Wu C. Chronically implanted intracranial electrodes: tissue reaction and electrical changes. *Micromachines*. (2018) 9:430. doi: 10.3390/mi9090430
127. Shein SL, Shellington DK, Exo JL, Jackson TC, Wisniewski SR, Jackson EK, et al. Hemorrhagic shock shifts the serum cytokine profile from pro- to anti-inflammatory after experimental traumatic brain injury in mice. *J Neurotrauma*. (2014) 31:1386–95. doi: 10.1089/neu.2013.2985
128. Ravizza T, Gagliardi B, Noé F, Boer K, Aronica E, Vezzani A. Innate and adaptive immunity during epileptogenesis and spontaneous seizures: evidence from experimental models and human temporal lobe epilepsy. *Neurobiol Dis*. (2008) 29:142–60. doi: 10.1016/j.nbd.2007.08.012
129. Tse K, Puttachary S, Beamer E, Sills GJ, Thippeswamy T. Advantages of repeated low dose against single high dose of kainate in C57BL/6J mouse model of status epilepticus: behavioral and electroencephalographic studies. *PLOS ONE*. (2014) 9:e96622.
130. Serhan CN, Levy BD. Resolvins in inflammation: emergence of the pro-resolving superfamily of mediators. *J Clin Invest*. (2018) 128:2657–69. doi: 10.1172/JCI97943
131. Varvel NH, Neher JJ, Bosch A, Wang W, Ransohoff RM, Miller RJ, et al. Infiltrating monocytes promote brain inflammation and exacerbate neuronal damage after status epilepticus. *Proc Natl Acad Sci USA*. (2016) 113:E5665–74. doi: 10.1073/pnas.1604263113
132. Bartolomucci A, Possenti R, Mahata SK, Fischer-Colbrie R, Loh YP, Salton SRJ. The extended granin family: structure, function, biomedical implications. *Endocr Rev*. (2011) 32:755–97. doi: 10.1210/er.2010-0027
133. Ferri GL, Noli B, Brancia C, D'Amato F, Cocco C. VGF: an inducible gene product, precursor of a diverse array of neuro-endocrine peptides and tissue-specific disease biomarkers. *J Chem Neuroanat*. (2011) 42:249–61. doi: 10.1016/j.jchemneu.2011.05.007
134. Lin, W.-J, Jiang C, Sadahiro M, Bozdagi O, Vulchanova L, et al. VGF and its c-terminal peptide TLQP-62 regulate memory formation in hippocampus via a BDNF-TrkB-dependent mechanism. *J Neurosci Off J Sock Neurosci*. (2015) 35:10343–56. doi: 10.1523/JNEUROSCI.0584-15.2015
135. Xiong Y, Zhang Y, Zheng F, Yang Y, Xu X, Wang W, et al. Expression of Glypican-4 in the brains of epileptic patients and epileptic animals and its effects on epileptic seizures. *Biochem Biophys Res Commun*. (2016) 478:241–6. doi: 10.1016/j.bbrc.2016.07.061
136. Miyata M, Kishimoto Y, Tanaka M, Hashimoto K, Hirashima N, Murata Y, et al. A role for myosin Va in cerebellar plasticity and motor learning: a possible mechanism underlying neurological disorder in myosin Va disease. *J Neurosci Off J Soc Neurosci*. (2011) 31:6067–78. doi: 10.1523/JNEUROSCI.5651-10.2011
137. Sloane JA, Vartanian TK. Myosin Va controls oligodendrocyte morphogenesis and myelination. *J Neurosci Off J Soc Neurosci*. (2007) 27:11366–75. doi: 10.1523/JNEUROSCI.2326-07.2007
138. Brandt C, Ebert U, Loscher W. Epilepsy induced by extended amygdala-kindling in rats: lack of clear association between development of spontaneous seizures and neuronal damage. *Epilepsy Res*. (2004) 62:135–56. doi: 10.1016/j.eplepsyres.2004.08.008
139. Hellier JL, Patrylo PR, Buckmaster PS, Dudek FE. Recurrent spontaneous motor seizures after repeated low-dose systemic treatment with kainate: assessment of a rat model of temporal lobe epilepsy. *Epilepsy Res*. (1998) 31:73–84. doi: 10.1016/S0920-1211(98)00017-5

Conflict of Interest: The authors declare that the research was conducted in the absence of any commercial or financial relationships that could be construed as a potential conflict of interest.

frontiers in Neurology

ORIGINAL RESEARCH
published: 08 December 2021
doi: 10.3389/fneur.2021.780042

Altered Expression of Par3, aPKC-λ, and Lgl1 in Hippocampus in Kainic Acid-Induced Status Epilepticus Rat Model

Chen Zhang[1,2], *Fafa Tian*[1,2], *Zheren Tan*[1,2], *Juan Du*[1,2] *and Xiaoyan Long*[1,2]*

[1] Department of Neurology, Xiangya Hospital, Central South University, Changsha, China, [2] National Clinical Research Center for Geriatric Disorders, Xiangya Hospital, Central South University, Changsha, China

Introduction: Mossy fiber sprouting (MFS) is a frequent histopathological finding in temporal lobe epilepsy (TLE) and is involved in the pathology of TLE. However, molecular signals underlying MFS remain unclear. Partitioning defective 3(Par3), atypical protein kinase C-λ(aPKC-λ), and lethal giant larvae 1(Lgl1) were involved in the neuronal polarity and axon growth. The potential roles of those proteins in MFS and epileptogenesis of TLE were investigated.

Material and Methods: The epileptic rat models were established by intracerebroventricular injection of kainic acid (KA). The degree of MFS was measured by using Timm staining, Neuronal loss and the expression aPKC-λ, Par3, and Lgl1 in hippocampus were measured by using immunohistochemistry and western blot analysis.

Results: The neuronal loss in CA3 region was observed from 3 days to 8 weeks, while the neuronal loss in the hilar region was observed from 1 to 8 weeks in experimental group. The Timm score in the CA3 region in experimental group was significantly higher than that in the control group from 2 to 8 weeks. Compared with control group, the expressions of Par3 and Lgl1 were upregulated and the expression of aPKC-λ was downregulated in the experimental groups. Positive correlation between the Par3 expression and Timm scores, and the negative correlation between the aPKC-λ expression and Timm scores in CA3 region were discovered in experimental group.

Conclusion: The findings of the present study indicated that aPKC-λ, Par3, and Lgl1 may be involved in MFS and in the epileptogenesis of temporal lobe epilepsy.

Keywords: temporal lobe epilepsy, atypical protein kinase C, partitioning defective 3, lethal giant larvae 1, mossy fiber sprouting

OPEN ACCESS

Edited by:
Dinesh Upadhya, Manipal Academy of Higher Education, India

Reviewed by:
Carmen Rubio, Manuel Velasco Suárez Instituto Nacional de Neurología y Neurocirugía, Mexico
Binglin Zhu, University at Buffalo, United States

***Correspondence:**
Xiaoyan Long
409685656@qq.com; longxyan@qq.com

Specialty section:
This article was submitted to Epilepsy, a section of the journal Frontiers in Neurology

Received: *20 September 2021*
Accepted: *08 November 2021*
Published: *08 December 2021*

Citation:
Zhang C, Tian F, Tan Z, Du J and Long X (2021) Altered Expression of Par3, aPKC-λ, and Lgl1 in Hippocampus in Kainic Acid-Induced Status Epilepticus Rat Model. Front. Neurol. 12:780042. doi: 10.3389/fneur.2021.780042

INTRODUCTION

Epilepsy is a devastating neurological disorder. There are estimated 30–40% patients with epilepsy fail to get satisfactory response to appropriate administrations of antiepileptic drugs or other treatments (1). One of the most common types of refractory epilepsy that can be found in adults is the temporal lobe epilepsy (TLE) (2). Therefore, a better understanding for the pathogenesis of TLE is urgently needed. Although exact pathogenic mechanisms of TLE are still unknown, it is generally

accepted that the aberrant axonal outgrowth and the synaptic reorganization caused by Mossy Fiber Sprouting (MFS) are the causes of the imbalance between excitatory and inhibitory inputs in hippocampus, which may contribute to the epileptogenesis of TLE (3, 4). Chen et al. discovered that the Repulsive guidance molecule a (RGMa), a protein regulating axonal growth, was significantly decreased in TLE patients, and an overexpression of RGMa in the hippocampus suppresses seizures, MFS and hyperexcitability of hippocampal neurons (5). It was confirmed that a mammalian target of rapamycin (mTOR) pathway was involved in regulating axonal outgrowth (6, 7). Pun et al. selectively removed the mTOR pathway inhibitor phosphatase and tensin homolog (PTEN) gene from an adult-born granule cells, and then a mice without PTEN gene showed spontaneous seizures (8). Based on this finding, LaSarge et al. discovered that PTEN deletion in dentate granule cells resulted in aberrant axonal growth of mossy fiber and enhanced communication between CA3 area and granule cells, thus, resulting to possible promotion of the epileptogenesis of TLE (9). Those findings implicated that axonal growth may be a potential target to attenuate epileptogenesis of TLE.

Numerous studies confirmed that the Partitioning defective 3(Par3) /Partitioning defective 6(Par6)/atypical protein kinase C (aPKC) complex played a determinant role in cell polarity (10–12) and is required for axon–dendrite specification of hippocampal neurons (13–15). The aPKC family has three isoforms: aPKC-ζ, PKM-ζ and aPKC-λ in vertebrate, and Par3 proteins that interacted with aPKC-λ to achieve the function of regulating cell polarity in neuron and in neural progenitors (16–18). In embryonic hippocampal neurons, the aPKC-λ and Par3 complex has localized the presumptive axon (19), which implicated the involvement of aPKC-λ and Par3 in axon specification during the neuronal differentiation. Previous studies had discovered the long-lasting increased of mRNA expression of PKC epsilon in mossy fiber of adult rats, which followed the seizures induced by kainic acid injection (20). Moreover, Gao et al. also discovered that the PAR3 regulates CNTNAP2 spatial localization (21). CNTNAP2 has been considered a prominent disease susceptibility gene associated with epilepsy (22), and seizure was observed in *Cntnap2* knockout rat (23). Those findings implied that Par3 and aPKC-λ have potentiality to be involved in epileptogenesis. However, the functions of aPKC-λ and Par3 in epileptogenesis have not yet been explored.

Lethal giant larvae 1 (Lgl1) was initially known as a tumor suppressor (24) and regulator of polarization processes in variety of cells (25, 26). It has been confirmed that Lgl1 is enriched in developing axons, and upregulation of Lgl1, which has promoted the axonal growth during neuronal morphogenesis (27). Aside from this, Scott et al. found that Lgl1 protein activity is restricted by its phosphorylation by aPKC in the apical neuroblast cortex of flies (28). Nevertheless, this association between Lgl1 and epilepsy has not yet been investigated.

The effects of proteins that were involved in the neuronal polarity are not fully described in epileptogenesis of TLE. By considering the functions of aPKC-λ, Par3, and Lgl1 in neuronal polarity in hippocampal neuron, we also investigated the potential role of those proteins in development of TLE.

MATERIALS AND METHODS

Ethic Statement

All animals were treated humanely. Study design and all animal experimental protocols were done in accordance with the guidelines of the National Institutes of Health, and the study were approved by the Animal Ethics Committee of Central South University (Changsha, China).

Animals and Model Establishing

Male Sprague–Dawley rats, which are between post-natal days 42 and 56, that weighed between 180 and 220 g, were purchased from the Center for Experimental Animals of Central South University (Changsha, China). The animals were housed under controlled conditions (18-25°C; 50-60% humidity; 12 h light/dark cycle) with food pellets and water available *ad libitum*.

A total of 120 rats were randomly divided into model group ($n = 65$) and control group ($n = 55$) and underwent a surgery for intracerebroventricular injection. Rats were anesthetized with ketamine/xylazine (100/10 mg/kg, I.P.). Rats were placed in a stereotaxic apparatus, and a guide cannula was placed into the lateral ventricle (AP = −0.8, ML = 1.4, DV = 3.3). Kainic acid dissolved in normal saline (0.5 μg/μl) was injected intracerebroventricularly (5 μl/kg, i.c.v.) through a guide cannula by a Hamilton microsyringe at an infusion rate of 0.2 μl/min. The injection usually started 1 min after microsyringe insertion, then cannula will be slowly pulled out of the brain 5 min after the drug injection. Rats in the control group were injected intracerebroventricularly with an equal dose of saline.

The KA-treated rats were observed for the occurrence of seizures immediately following the surgery, and the seizure severity was measured using Racine's scale (29). Five rats died in KA-induced SE. KA-treated rats that demonstrated seizure which reached IV levels and evolved into SE were included in the experimental group ($n = 60$). All saline-treated rats survived after surgery. All rats from experimental and control groups ($n = 60$, and 55, respectively) were sacrificed at five-time points after surgery (3 days and 1, 2, 4, 8 weeks post-surgery) for Timm staining, immunohistochemistry, and western blot analysis.

Tissue Processing

At different time points, rats were deeply anesthetized by intraperitoneal injection of ketamine/xylazine (100/10 mg/kg). Rats were perfused intracardially with 300 ml saline for immunohistochemistry or with 200 ml 0.4% sodium sulfide in 0.1 M phosphate buffer (pH 7.3) for Timm staining, then followed by application of 4% paraformaldehyde for perfusion fixation. The brains were removed, were fixed in 4% paraformaldehyde for 24 h, then underwent dehydration using 30% sucrose, then finally were cut into 20 μm coronal sections (frozen cryosections). For western blotting, Hippocampus was separated and was stored at −80°C.

Timm's Staining

In a darkroom, corresponding sections were stained for 90 min in a specific solution which was composed of 100 ml 50% gum arabic, 5 ml citrate buffer (27.2% citric acid and 31% sodium citrate), 15 ml 5.6% hydroquinone, and 0.5 ml 17% silver nitrate. After washing in water, sections were routinely dehydrated, cleaned and mounted with gum. Finally, the corresponding Timm's score for the CA3 region in the hippocampus was analyzed based on the published criteria (30).

Immunohistochemistry

The tissue sections were incubated at room temperature with 3% H_2O_2 solution for 20 min to block the endogenous peroxidase activity. After being washed three times with PBS, the sections were pre-incubated in PBS containing 0.1%Triton X-100 and 5% normal goat-serum for 30 min, then incubated again overnight with the following primary antibodies at 4°C: rabbit anti-aPKC-λ (1:50, Santa cruz), rabbit anti-PAR3(1:300, Abcam), rabbit anti-LGL1(1:40, Santa Cruz), mouse anti- NeuN(1:1,500, Chemicon). After being washed by PBS, the sections were re-incubated with biotin-labeled anti-rabbit or anti-mouse immunoglobulin (Ig) G secondary antibodies which were raised in a goat (1:200, Cwbiotech) at room temperature for 2 h. Afterwards, these were washed in PBS and incubated in avidin-biotin-horseradish peroxidase complex (1:200, Vector laboratories) at room temperature for another 2 h. Finally, the sections were processed with 3,3′-diaminobenzidine tetrahydrochloride solution (Zsbio) for visualization. Following this, the slides were routinely washed, dehydrated, and mounted. Mean optical density (OD) was calculated by Image pro plus 6. The total number of NeuN(+) cells in CA3 and hilar region of five sections, which were randomly selected from every rat, were calculated at 40× magnification of the microscope.

Western Blotting

Proteins were extracted from hippocampal tissues using RIPA lysate buffer (Beyotime), and then concentrations of proteins were measured using bicinchoninic acid (BCA) Protein Assay Kit (Beyotime). Proteins were separated by using sodium dodecyl sulfate polyacrylamide gel electrophoresis (SDS-PAGE) and then transferred to nitrocellulose membranes. Membranes. which had been washed by using Tris Buffered Saline Tween (TBST)

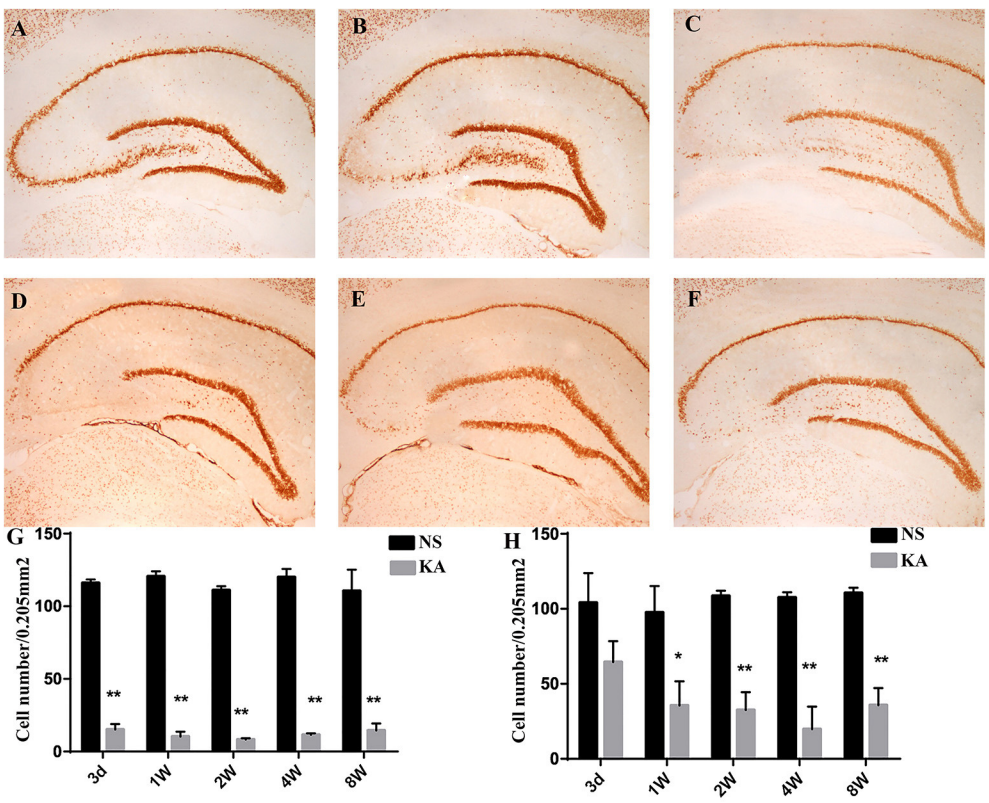

FIGURE 1 | NeuN staining in hippocampus in the control and experimental groups. There is no obvious neuronal loss in control group **(A)**; NeuN staining at five different time points after injection of kainic acid in experimental group: 3 d **(B)**, 1 w **(C)**, 2 w **(D)**, 4 w **(E)**, 8 w **(F)**. The number of NeuN-positive cells measured using NeuN immunohistochemistry in CA3 **(G)** and hilar regions **(H)**. The data are expressed as the mean ± SD. $^*P < 0.05$, compared with the control; and $^{**}P < 0.01$, compared with the control; KA, kainic acid; NS, normal saline.

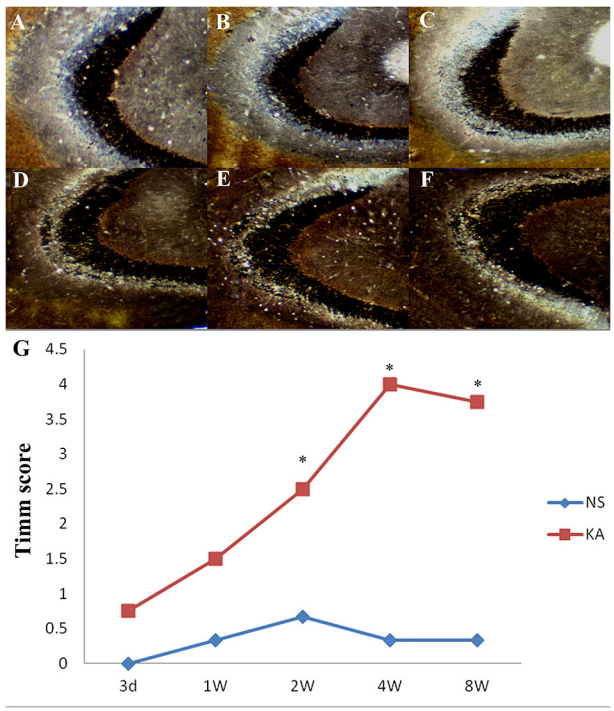

FIGURE 2 | Timm staining in the CA3 region in the control and experimental groups. There is no obvious MFS in control group **(A)**; Timm staining at 5 different time points after injection of kainic acid in experimental group: 3 d **(B)**, 1 w **(C)**, 2 w **(D)**, 4 w **(E)**, 8 w **(F)**. **(G)** Time-dependent changes of Timm scores in the CA3 region in the experimental ($n = 4$ at each time point) and control group ($n = 3$ at each time point). *$P < 0.05$, compared with the control; KA, kainic acid; NS, normal saline.

and had been blocked with 5% skimmed milk in TBST (room temperature, 2 h), were incubated at 4°C overnight with primary antibodies. The primary antibodies included rabbit anti-aPKC-λ (1:1,000, Santa Cruz), rabbit anti-PAR3 (1:1,000, Abcam), rabbit anti-LGL1 (1:100, Santa Cruz), and rabbit anti-GAPDH (1:10,000, Proteintech). Unbound antibodies were washed by TBST, then the membranes were subsequently incubated with HRP-labeled goat antirabbit IgG secondary antibodies (1:200, Beyotime) for 1 h. The immunoreactive bands were visualized by using chemiluminescence (ECL) kit (Beyotime), and the optical density (OD) of these bands were quantified by using the Image J software.

Statistical Analysis

All values were expressed as means ± standard deviations. All statistical analyses were performed using SPSS 21.0 for Windows (SPSS Inc., Chicago, IL, USA). Comparisons between two groups were performed by using two-sample *t* test (parametric) and Mann Whitney *U* test (non-parametric). Multiple comparisons were performed by using one-way analysis of variance and had been followed, respectively, by three more tests; the Least Significant Difference *post-hoc* test (parametric), the Kruskal-Wallis test, and the Bonferroni Procedure (non-parametric). The correlation of MFS severity with expression levels of aPKC-λ, Par3, and Lgl1 were investigated by using Spearman rank correlation coefficient. All tests were two-sided and statistical significance was determined at $p < 0.05$.

RESULTS

KA-Induced SE Lead to Neuronal Loss and MFS in Hippocampus

The number of NeuN-positive cells, which was measured by using NeuN immunohistochemistry in CA3 and hilar regions, was counted to investigate the neuronal death in hippocampus (**Figure 1**). Compared with control group, the number of NeuN-positive cells in CA3 region decreased significantly from 3 days to 8 weeks ($p < 0.001$ for all, **Figure 1G**), and the number of NeuN-positive cells in hilar region decreased significantly from 1 to 8 weeks in experimental group ($p < 0.01$ for all, **Figure 1H**).

Timm staining was used to evaluate the aberrant mossy fiber reorganization in CA3 region (**Figure 2**), which was graded by Timm scores (a scale of 0–5). In control group, extremely slight MFS appeared in CA3 region from 1 to 8 weeks, and there was no significant difference in Timm scores between all time points ($P > 0.05$). Compared with control group, Timm scores increased significantly from 2 to 8 weeks in experimental group ($P < 0.05$ for all, **Figure 2G**).

Expression of aPKC-λ, Par3, and Lgl1 in Hippocampus

There is no significant difference among the all time points with respect to the expression of aPKC-λ, Par3 and Lgl1 in CA3, and hilar region in control group.

Compared with control group, the expression of Par3 in CA3 region decreased significantly in 3 days and increased from 2 weeks to 8 weeks ($p < 0.05$ for all, **Figures 3**, **5A**), while the expression of Par3 in hilar region decreased significantly in 1 week and increased from 2 weeks to 8 weeks in experimental group ($p < 0.01$ for all, **Figures 3**, **5B**).

Compared with control group, the expression of aPKC-λ in CA3 region decreased significantly at all time points ($p < 0.01$ for all, **Figures 3**, **5C**), and the expression of aPKC-λ in hilar region decreased significantly from 2 weeks to 8 weeks in experimental group ($p < 0.01$ for all, **Figures 3**, **5D**).

The expression of Lgl1 was mainly observed in the cytoplasm in the CA3 region in control group, but the expression of Lgl1 mainly appeared in the axon terminal at CA3 region from experimental group. Compared with control group, the expression of LGL1 in CA3 region increased significantly from 3 days to 4 weeks in experimental group ($p < 0.05$ for all, **Figures 3**, **5E**).

The expression of Par3, aPKC-λ, and Lgl1 in hippocampus have been measured by western blot analysis, and multiple comparisons of western blot results were performed (**Figures 4**, **5**). In experimental group, the expression of Par3 in hippocampus increased at 4 weeks ($p < 0.05$, **Figure 5F**); while the expression

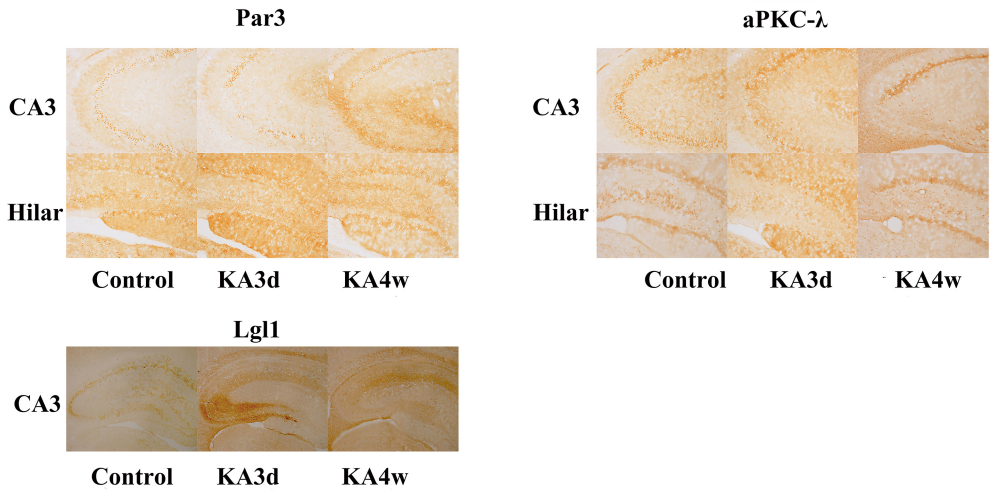

FIGURE 3 | Expression of Par3, aPKC-λ and Lgl1 in the CA3 and hilar region by immunohistochemistry.

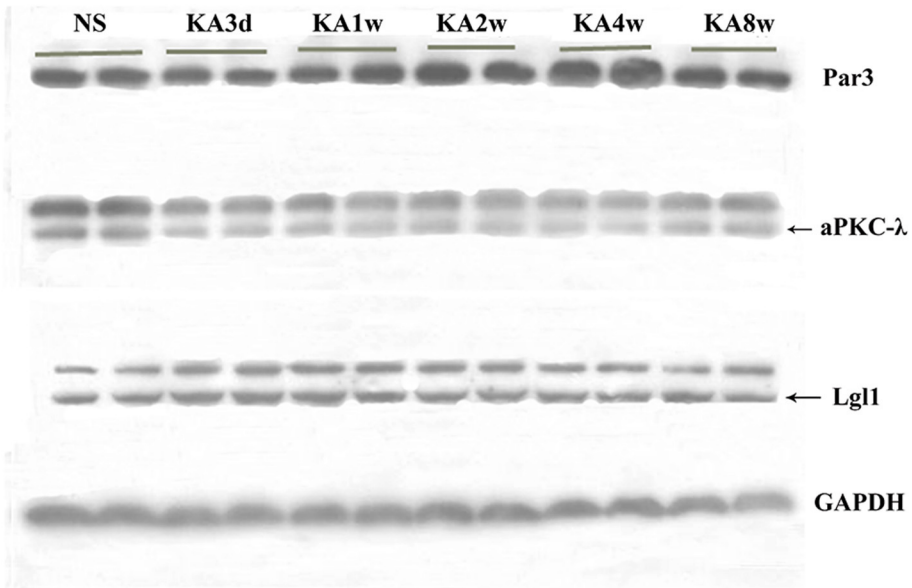

FIGURE 4 | Expression of Par3, aPKC-λ and Lgl1 in hippocampus between experimental and control group by western blot.

of Lgl1 in hippocampus increased significantly from 3 days to 2 weeks ($p < 0.05$ for all, **Figure 5G**), lastly, the expression of aPKC-λ in hippocampus decreased at 4 weeks ($p < 0.05$, **Figure 5H**).

In addition, there is a positive correlation between the expression of Par3 and Timm scores ($r = 0.903$, $P < 0.01$, **Figure 6**) and a negative correlation between the expression of aPKC-λ and Timm scores ($r = -0.785$, $P < 0.01$, **Figure 6**) in CA3 region in the experimental group. No correlation between the expression of Lgl1 and Timm scores ($r = -0.405$, $P > 0.05$) was observed in experimental group.

DISCUSSION

MFS, a frequent histopathological finding in TLE (31), has preceded the appearance of spontaneous seizures in PTZ kindling rat model of epilepsy (32). It has been found that severity of MFS is associated with susceptibility of spontaneous seizures (33, 34). Furthermore, it was confirmed that mTOR pathway was involved in regulating axonal outgrowth (7). In the study conducted by Pun et al., the mice presented MFS and a spontaneous recurrent seizure by deleting PTEN gene that regulates the mTOR pathway (8). All those studies supported the hypothesis that MFS was

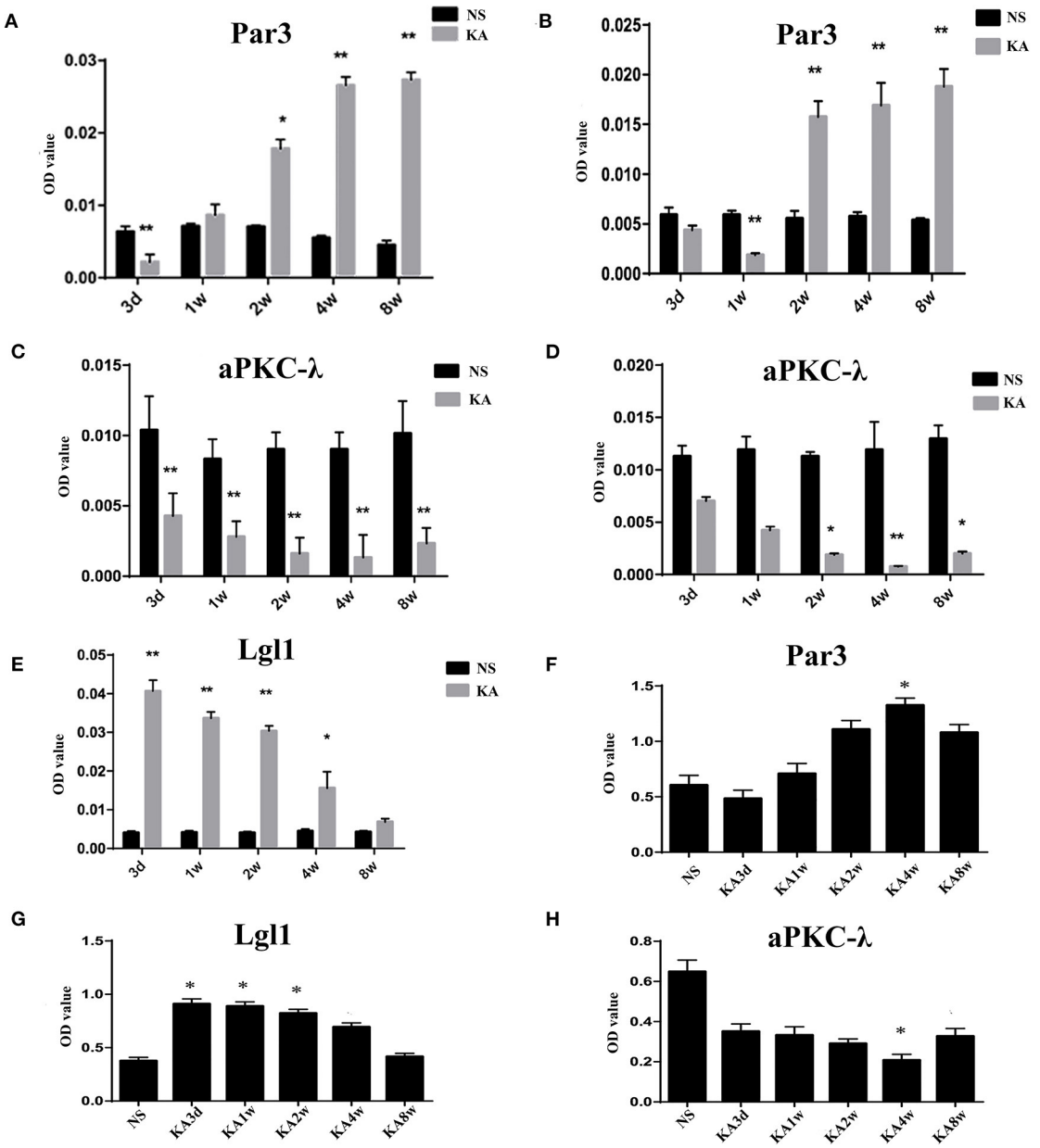

FIGURE 5 | Comparison of Par3, aPKC-λ and Lgl1 in CA3 region **(A,C,E)** and hilar region **(B,D)** between experimental and control group. **(F–H)** Comparison of Par3, aPKC-λ and Lgl1 in hippocampus between experimental and control group.*$P < 0.05$, compared with the control; and **$P < 0.01$, compared with the control; KA, kainic acid; NS, normal saline.

involved in the mechanism of epileptogenesis of TLE (35–37). Moreover, several studies had discovered that severity of MFS and spontaneous seizures could be relieved by regulating the expression of specific proteins involved in axonal growth (5, 38, 39), which means that further studies are required to explore the role of other proteins that are regulating axonal growth in the mechanism of epileptogenesis of TLE.

Numerous studies confirmed that only two kinds of protein, kinase C (aPKC) isoforms (aPKC-λ and PKM-ζ), were expressed in rat hippocampal neurons, and aPKC-λ-Par3 complex promotes the axon specification, while PKM-ζ competes with aPKC-λ for binding to Par3 and PKMζ-PAR3 complex inhibits axon formation (19, 40), and the upregulating of aPKC-λ or the silencing of PKM-ζ has caused supernumerary axon growth in hippocampal neurons (19). On the contrary, Buchser et al. discovered that the overexpression of aPKC-λ has inhibited neuronal growth and axon formation (41). However, Yamanaka et al. observed that Neuronal deletion of aPKC-λ does not affect distribution of neural structures including dendrites, axons and synapses in mouse brain cortex (42). Those findings

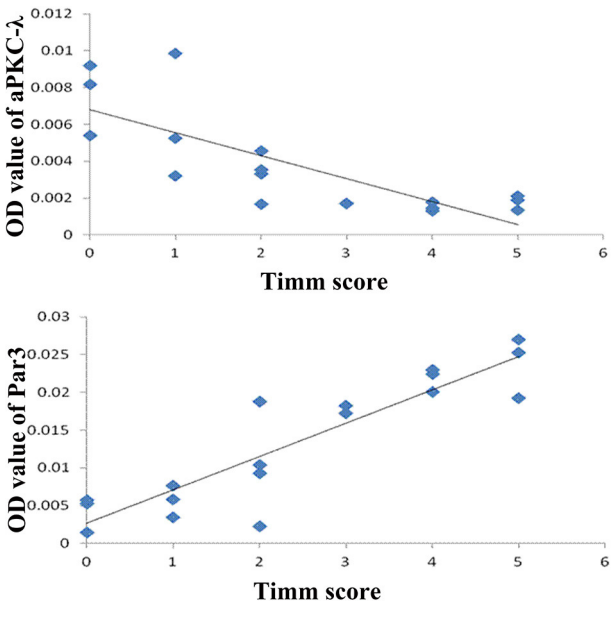

FIGURE 6 | Correlation between Timm score and expression of Par3 and aPKC-λ.

indicated that the function of aPKC-λ in axon formation and its growth in neurons are controversial. In the present study, the decrease in aPKC-λ expression at hippocampus and negative correlation between aPKC-λ expression, and the severity of MFS were observed in experimental group. Those findings imply that the condition-dependent effect of aPKC-λ in morphology of axon and aPKC-λ may suppress axonal formation and growth in hippocampus under certain pathological condition (such as epileptogenesis). Besides, effects of aPKC-λ in MFS and epileptogenesis of TLE are still open to debate and further research.

In the present study, Par3 and Lgl 1 increased during epileptogenesis with presence of MFS. Par3 is established as an interaction partner of full-length aPKC isoforms and is involved in neuronal polarity and axon-dendrite differentiation (10–12). It has been demonstrated that the increase in axonal concentration of Par3 could be induced by nerve growth factor or netrin-1 stimulation, which is known to promote axonal growth (43), and the Par3 complex is localized at the presumptive axon in embryonic hippocampal neurons (19). Those findings indicated Par3 may display facilitative effort on MFS and may aggravate epileptogenesis. Moreover, Par3 may indirectly contribute to epileptogenesis through CNTNAP2, which has been considered a prominent disease susceptibility gene associated with epilepsy (21, 22).

Lgl1 is well-known to be a cytoskeletal protein and regulates establishment of polarity in many cell types. It has been confirmed that Lgl1 is enriched in developing axons, and its upregulation promoted the axonal growth (27), which is consistent with findings in present study.

In the present study, the expression of Par 3 in CA3 decreased at 3 days and increased from 2 weeks, then peaked at 8 weeks following KA administration. Conversely, the expression of Lgl1 in CA3 peaked at 3days and declined from 1 week. It reached the lowest level at 8 weeks following KA administration. Those opposite observations may result from antagonism between Par3 and Lgl1 in a cell polarity. Previous studies have confirmed that Par3 and Lgl1/2 all binded directly to Par6 (28, 44–47). However, the binding of Par3 and Lgl to Par6 appeared to be mutually exclusive in establishing and maintaining cell polarization (45–47). Moreover, Wang et al. found that Par3 and Lgl antagonized each other in modulating myosin II activation during cell–cell contact formation (48). Our finding indicated that increase in Par3 and Lgl1 at different phase of epileptogenesis may promote aberrant axonal growth to form excitatory neural connections and aggravate epileptogenesis.

Numerous studies confirmed Par 3 (46) and Lgl (45, 49) could be phosphorylated by aPKC in many cell types. Bailey et al. found that phosphorylation by aPKC prevented lgl from the apical cell cortex in S2 cell system (49). Yamanaka et al. found that activation of aPKC in the Par6 complex resulted in the phosphorylation of Lgl and its dissociation from the cortex in epithelial cell (50). In addition, it has been proposed that the release of Par3 from the Par6/aPKC complex was a result from aPKC-mediated phosphorylation on Par3 via conserved region 3 (51–53). Those findings indicated that the subcellular localizations of lgl and Par3 were regulated by phosphorylation by aPKC, which may have been a possible reason for the expression of aPKC to change in the opposite direction in CA3 and in hilar regions during epileptogenesis compared with lgl and Par3.

In the present study, the neuronal loss in CA3 and hilar region demonstrated by a significant decrease in the number of NeuN-positive cells is observed in the course of epileptogenesis of TLE, which is consistent with previous studies (54, 55). With the neuronal loss in CA3 and hilar region, the loss of connecting targets resulted in the abnormal growth of mossy fiber, and the positive correlation between the degree of neuron loss and extent of MFS has been confirmed in TLE model and patients (56, 57), which indicated that neuronal loss may promote the effect of MFS in epileptogenesis of TLE.

CONCLUSIONS

The findings of this study indicated, for the first time, that aPKC-λ, Par3, and Lgl1 may be involved in MFS and epileptogenesis of TLE. Further studies are required to explore the effects of those proteins mediating cell polarity in MFS and epileptogenesis of TLE, which may lead to more interventions that can prevent or relieve the recurrent spontaneous seizures.

DATA AVAILABILITY STATEMENT

The raw data supporting the conclusions of this article will be made available by the authors, without undue reservation.

ETHICS STATEMENT

The animal study was reviewed and approved by Research Ethics Committee of the Xiangya Hospital.

AUTHOR CONTRIBUTIONS

CZ, ZT, and XL: conceptualization. ZT and CZ: methodology. CZ, ZT, and JD: investigation. CZ: formal analysis, resources, and writing—original draft. FT and XL: writing—review and editing and supervision. All authors have read and approved the manuscript and had full access to all the data in the study, took responsibility for the integrity of the data, and the accuracy of the data analysis.

FUNDING

This work was supported by Public Health Program of Hunan Provincial Department of Finance, China (Xiangcaishezhi No. 2020-46, Xiangcaiqizhi No. 2015-122, and Xiangcaijiaozhi No. 2010-216).

ACKNOWLEDGMENTS

We would like to thank all staffs of experimental animal facility of Central South University for their assistance.

REFERENCES

1. Laxer KD, Trinka E, Hirsch LJ, Cendes F, Langfitt J, Delanty N, et al. The consequences of refractory epilepsy and its treatment. *Epilepsy Behav.* (2014) 37:59–70. doi: 10.1016/j.yebeh.2014.05.031
2. Falconer MA, Serafetinides EA, Corsellis JA. Etiology and pathogenesis of temporal lobe epilepsy. *Arch Neurol.* (1964) 10:233–48. doi: 10.1001/archneur.1964.00460150003001
3. Godale CM, Danzer SC. Signaling pathways and cellular mechanisms regulating mossy fiber sprouting in the development of epilepsy. *Front Neurol.* (2018) 9:298. doi: 10.3389/fneur.2018.00298
4. Parent JM, Murphy GG. Mechanisms and functional significance of aberrant seizure-induced hippocampal neurogenesis. *Epilepsia.* (2008) 49:19–25. doi: 10.1111/j.1528-1167.2008.01634.x
5. Chen L, Gao B, Fang M, Li J, Mi X, Xu X, et al. Lentiviral vector-induced overexpression of rgma in the hippocampus suppresses seizures and mossy fiber sprouting. *Mol Neurobiol.* (2017) 54:1379–91. doi: 10.1007/s12035-016-9744-2
6. Huang S, Ge X, Yu J, Han Z, Yin Z, Li Y, et al. Increased miR-124-3p in microglial exosomes following traumatic brain injury inhibits neuronal inflammation and contributes to neurite outgrowth via their transfer into neurons. *FASEB J.* (2018) 32:512–28. doi: 10.1096/fj.201700673r
7. Zhu H, Wang Y, Yang X, Wan G, Qiu Y, Ye X, et al. Catalpol improves axonal outgrowth and reinnervation of injured sciatic nerve by activating Akt/mTOR pathway and regulating BDNF and PTEN expression. *Am J Transl Res.* (2019) 11:1311–26.
8. Pun RYK, Rolle IJ, LaSarge CL, Hosford BE, Rosen JM, Uhl JD, et al. Excessive activation of mtor in postnatally generated granule cells is sufficient to cause epilepsy. *Neuron.* (2012) 75:1022–34. doi: 10.1016/j.neuron.2012.08.002
9. LaSarge CL, Santos VR, Danzer SC. PTEN deletion from adult-generated dentate granule cells disrupts granule cell mossy fiber axon structure. *NEUROBIOL DIS.* (2015) 75:142–50. doi: 10.1016/j.nbd.2014.12.029
10. Goldstein B, Macara IG. The PAR proteins: fundamental players in animal cell polarization. *Dev Cell.* (2007) 13:609–22. doi: 10.1016/j.devcel.2007.10.007
11. McCaffrey LM, Macara IG. Signaling pathways in cell polarity. *Cold Spring Harb Perspect Biol.* (2012) 4:a009654. doi: 10.1101/cshperspect.a009654
12. Thompson BJ. Cell polarity: models and mechanisms from yeast, worms and flies. *Development.* (2013) 140:13–21. doi: 10.1242/dev.083634
13. Shi SH, Jan LY, Jan YN. Hippocampal neuronal polarity specified by spatially localized mPar3/mPar6 and PI 3-kinase activity. *Cell.* (2003) 112:63–75. doi: 10.1016/S0092-8674(02)01249-7
14. Nishimura T, Kato K, Yamaguchi T, Fukata Y, Ohno S, Kaibuchi K. Role of the PAR-3-KIF3 complex in the establishment of neuronal polarity. *Nat Cell Biol.* (2004) 6:328–34. doi: 10.1038/ncb1118
15. Schwamborn JC, Puschel AW. The sequential activity of the GTPases Rap1B and Cdc42 determines neuronal polarity. *Nat Neurosci.* (2004) 7:923–9. doi: 10.1038/nn1295
16. Ohno S. Intercellular junctions and cellular polarity: the PAR-aPKC complex, a conserved core cassette playing fundamental roles in cell polarity. *Curr Opin Cell Biol.* (2001) 13:641–8. doi: 10.1016/S0955-0674(00)00264-7
17. Henrique D, Schweisguth F. Cell polarity: the ups and downs of the Par6/aPKC complex. *Curr Opin Genet Dev.* (2003) 13:341–50. doi: 10.1016/S0959-437X(03)00077-7
18. Ghosh S, Marquard T, Thaler JP, Carter N, Andrews SE, Pfaff SL, et al. Instructive role of aPKC zeta subcellular localization in the assembly of adherens junctions in neural progenitors. *Proc Natl Acad Sci USA.* (2008) 105:335–40. doi: 10.1073/pnas.0705713105
19. Parker SS, Mandell EK, Hapak SM, Maskaykina IY, Kusne Y, Kim J-Y, et al. Competing molecular interactions of aPKC isoforms regulate neuronal polarity. *Proc Natl Acad Sci USA.* (2013) 110:14450–5. doi: 10.1073/pnas.1301588110
20. Guglielmetti F, Rattray M, Baldessari S, Butelli E, Samanin R, Bendotti C. Selective up-regulation of protein kinase C epsilon in granule cells after kainic acid-induced seizures in rat. *Brain Res Mol Brain Res.* (1997) 3:1–2. doi: 10.1016/S0169-328X(97)00142-3
21. Gao R, Pratt CP, Yoon S, Martin-de-Saavedra MD, Forrest MP, Penzes P. CNTNAP2 is targeted to endosomes by the polarity protein PAR3. *Eur J Neurosci.* (2020) 51:1074–86. doi: 10.1111/ejn.14620
22. Rodenas-Cuadrado P, Ho J, Vernes SC. Shining a light on CNTNAP2: complex functions to complex disorders. *Eur J Hum Genet.* (2014) 22:171–8. doi: 10.1038/ejhg.2013.100
23. Thomas AM, Schwartz MD, Saxe MD, Kilduff TS. Cntnap2 knockout rats and mice exhibit epileptiform activity and abnormal sleep-wake physiology. *Sleep.* (2017) 40:zsw026. doi: 10.1093/sleep/zsw026
24. Bilder D, Li M, Perrimon N. Cooperative regulation of cell polarity and growth by Drosophila tumor suppressors. *Science.* (2000) 289:113–6. doi: 10.1126/science.289.5476.113
25. Zhang T, Hou C, Zhang S, Liu S, Li Z, Gao J. Lgl1 deficiency disrupts hippocampal development and impairs cognitive performance in mice. *Genes Brain Behav.* (2019) 18:e12605. doi: 10.1111/gbb.12605
26. Ravid S. The tumor suppressor Lgl1 regulates front-rear polarity of migrating cells. *Cell Adh Migr.* (2014) 8:378–83. doi: 10.4161/cam.29387
27. Wang T, Liu Y, Xu X, Deng C, Wu K, Zhu J, et al. Lgl1 Activation of Rab10 promotes axonal membrane trafficking underlying neuronal polarization. *Dev Cell.* (2011) 21:431–44. doi: 10.1016/j.devcel.2011.07.007
28. Betschinger J, Mechtler K, Knoblich JA. The Par complex directs asymmetric cell division by phosphorylating the cytoskeletal protein Lgl. *Nature.* (2003) 422:326–30. doi: 10.1038/nature01486

29. Racine RJ. Modification of seizure activity by electrical stimulation. II. Motor seizure. *Electroencephalogr Clin Neurophysiol.* (1972) 32:281–94. doi: 10.1016/0013-4694(72)90177-0
30. Cilio MR, Sogawa Y, Cha BH, Liu XZ, Huang LT, Holmes GL. Long-term effects of status epilepticus in the immature brain are specific for age and model. *Epilepsia.* (2003) 44:518–28. doi: 10.1046/j.1528-1157.2003.48802.x
31. Sloviter RS, Zappone CA, Harvey BD, Frotscher M. Kainic acid-induced recurrent mossy fiber innervation of dentate gyrus inhibitory interneurons: possible anatomical substrate of granule cell hyperinhibition in chronically epileptic rats. *J Comp Neurol.* (2006) 494:944–60. doi: 10.1002/cne.20850
32. Song M, Tian F, Wang Y, Huang X, Guo J, Ding D. Potential roles of the RGMa-FAK-Ras pathway in hippocampal mossy fiber sprouting in the pentylenetetrazole kindling model. *Mol Med Rep.* (2015) 11:1738–44. doi: 10.3892/mmr.2014.2993
33. Tauck DL, Nadler JV. Evidence of functional mossy fiber sprouting in hippocampal formation of kainic acid-treated rats. *J Neurosci.* (1985) 5:1016–22. doi: 10.1523/JNEUROSCI.05-04-01016.1985
34. Santhakumar V, Aradi I, Soltesz I. Role of mossy fiber sprouting and mossy cell loss in hyperexcitability: a network model of the dentate gyrus incorporating cell types and axonal topography. *J Neurophysiol.* (2005) 93:437–53. doi: 10.1152/jn.00777.2004
35. Shetty AK, Turner DA. Aging impairs axonal sprouting response of dentate granule cells following target loss and partial deafferentation. *J Comp Neurol.* (1999) 414:238–54.
36. Rao MS, Hattiangady B, Reddy DS, Shetty AK. Hippocampal neurodegeneration, spontaneous seizures, and mossy fiber sprouting in the F344 rat model of temporal lobe epilepsy. *J Neurosci Res.* (2006) 83:1088–105. doi: 10.1002/jnr.20802
37. Mathern GW, Babb TL, Leite JP, Pretorius K, Yeoman KM, Kuhlman PA. The pathogenic and progressive features of chronic human hippocampal epilepsy. *Epilepsy Res.* (1996) 26:151–61. doi: 10.1016/S0920-1211(96)00052-6
38. Song M, Tian F, Xia H, Xie Y. Repulsive guidance molecule a suppresses seizures and mossy fiber sprouting via the FAK-p120RasGAP-Ras signaling pathway. *Mol Med Rep.* (2019) 19:3255–62. doi: 10.3892/mmr.2019.9951
39. Paradiso B, Zucchini S, Su T, Bovolenta R, Berto E, Marconi P, et al. Localized overexpression of FGF-2 and BDNF in hippocampus reduces mossy fiber sprouting and spontaneous seizures up to 4 weeks after pilocarpine-induced status epilepticus. *Epilepsia.* (2011) 52:572–8. doi: 10.1111/j.1528-1167.2010.02930.x
40. Hapak SM, Rothlin CV, Ghosh S. PAR3-PAR6-atypical PKC polarity complex proteins in neuronal polarization. *Cell Mol Life Sci.* (2018) 75:2735–61. doi: 10.1007/s00018-018-2828-6
41. Buchser WJ, Slepak TI, Gutierrez-Arenas O, Bixby JL, Lemmon VP. Kinase/phosphatase overexpression reveals pathways regulating hippocampal neuron morphology. *Mol Syst Biol.* (2010) 6:391. doi: 10.1038/msb.2010.52
42. Yamanaka T, Tosaki A, Kurosawa M, Akimoto K, Hirose T, Ohno S, et al. Loss of aPKC lambda in differentiated neurons disrupts the polarity complex but does not induce obvious neuronal loss or disorientation in mouse brains. *PLoS ONE.* (2013) 8:e84036. doi: 10.1371/journal.pone.0084036
43. Hengst U, Deglincerti A, Kim HJ, Jeon NL, Jaffrey SR. Axonal elongation triggered by stimulus-induced local translation of a polarity complex protein. *Nat Cell Biol.* (2009) 11:1024–30. doi: 10.1038/ncb1916
44. Lin D, Edwards AS, Fawcett JP, Mbamalu G, Scott JD, Pawson T. A mammalian PAR-3-PAR-6 complex implicated in Cdc42/Rac1 and aPKC signalling and cell polarity. *Nat Cell Biol.* (2000) 2:540–7. doi: 10.1038/35019582
45. Plant PJ, Fawcett JP, Lin DCC, Holdorf AD, Binns K, Kulkarni S, et al. A polarity complex of mPar-6 and atypical PKC binds, phosphorylates and regulates mammalian Lgl. *Nat Cell Biol.* (2003) 5:301–8. doi: 10.1038/ncb948
46. Yamanaka T, Horikoshi Y, Izumi N, Suzuki A, Mizuno K, Ohno S. Lgl mediates apical domain disassembly by suppressing the PAR-3-aPKC-PAR-6 complex to orient apical membrane polarity. *J Cell Sci.* (2006) 119(Pt 10):2107–18. doi: 10.1242/jcs.02938
47. Joberty G, Petersen C, Gao L, Macara IG. The cell-polarity protein Par6 links Par3 and atypical protein kinase C to Cdc42. *Nat Cell Biol.* (2000) 2:531–9. doi: 10.1038/35019573
48. Wan Q, Liu J, Zheng Z, Zhu H, Chu X, Dong Z, et al. Regulation of myosin activation during cell-cell contact formation by Par3-Lgl antagonism: entosis without matrix detachment. *Mol Biol Cell.* (2012) 23:2076–91. doi: 10.1091/mbc.e11-11-0940
49. Bailey MJ, Prehoda KE. Establishment of par-polarized cortical domains via phosphoregulated membrane motifs. *J Neurochem.* (2015) 35:199–210. doi: 10.1016/j.devcel.2015.09.016
50. Yamanaka T, Horikoshi Y, Sugiyama Y, Ishiyama C, Suzuki A, Hirose T, et al. Mammalian LgI forms a protein complex with PAR-6 and aPKC independently of PAR-3 to regulate epithelial cell polarity. *Curr Biol.* (2003) 13:734–43. doi: 10.1016/S0960-9822(03)00244-6
51. Soriano EV, Ivanova ME, Fletcher G, Riou P, Knowles PP, Barnouin K, et al. aPKC inhibition by Par3 CR3 flanking regions controls substrate access and underpins apical-junctional polarization. *Dev Cell.* (2016) 38:384–98. doi: 10.1016/j.devcel.2016.07.018
52. Morais-de-Sa E, Mirouse V, St Johnston D. aPKC phosphorylation of bazooka defines the apical/lateral border in drosophila epithelial cells. *Cell.* (2010) 141:509–23. doi: 10.1016/j.cell.2010.02.040
53. Liu Z, Yang Y, Gu A, Xu J, Mao Y, Lu H, et al. Par complex cluster formation mediated by phase separation. *Nat Commun.* (2020) 11:2266. doi: 10.1038/s41467-020-16135-6
54. Baluchnejadmojarad T, Roghani M. Coenzyme Q10 ameliorates neurodegeneration, mossy fiber sprouting, and oxidative stress in intrahippocampal kainate model of temporal lobe epilepsy in rat. *J Mol Neurosci.* (2013) 49:194–201. doi: 10.1007/s12031-012-9886-2
55. Vivash L, Tostevin A, Liu DSH, Dalic L, Dedeurwaerdere S, Hicks RJ, et al. Changes in hippocampal GABA(A)/cBZR density during limbic epileptogenesis: relationship to cell loss and mossy fibre sprouting. *Neurobiol Dis.* (2011) 41:227–36. doi: 10.1016/j.nbd.2010.08.021
56. Schmeiser B, Zentner J, Prinz M, Brandt A, Freiman TM. Extent of mossy fiber sprouting in patients with mesiotemporal lobe epilepsy correlates with neuronal cell loss and granule cell dispersion. *Epilepsy Res.* (2017) 129:51–8. doi: 10.1016/j.eplepsyres.2016.11.011
57. Xie C, Sun J, Qiao W, Lu D, Wei L, Na M, et al. Administration of simvastatin after kainic acid-induced status epilepticus restrains chronic temporal lobe epilepsy. *PLoS ONE.* (2011) 6:e24966. doi: 10.1371/journal.pone.0024966

Conflict of Interest: The authors declare that the research was conducted in the absence of any commercial or financial relationships that could be construed as a potential conflict of interest.

Publisher's Note: All claims expressed in this article are solely those of the authors and do not necessarily represent those of their affiliated organizations, or those of the publisher, the editors and the reviewers. Any product that may be evaluated in this article, or claim that may be made by its manufacturer, is not guaranteed or endorsed by the publisher.

frontiers in Aging Neuroscience

REVIEW
published: 13 December 2021
doi: 10.3389/fnagi.2021.781174

Inflammation Mediated Epileptogenesis as Possible Mechanism Underlying Ischemic Post-stroke Epilepsy

*Anna Regina Tröscher[1], Joachim Gruber[1,2], Judith N. Wagner[1,2], Vincent Böhm[1,2], Anna-Sophia Wahl[3,4] and Tim J. von Oertzen[1,2]**

[1]Neurology I, Neuromed Campus, Kepler Universitätsklinikum, Linz, Austria, [2]Medical Faculty, Johannes Kepler University, Linz, Austria, [3]Brain Research Institute, University of Zurich, Zurich, Switzerland, [4]Central Institute of Mental Health, University of Heidelberg, Mannheim, Germany

Post-stroke Epilepsy (PSE) is one of the most common forms of acquired epilepsy, especially in the elderly population. As people get increasingly older, the number of stroke patients is expected to rise and concomitantly the number of people with PSE. Although many patients are affected by post-ischemic epileptogenesis, not much is known about the underlying pathomechanisms resulting in the development of chronic seizures. A common hypothesis is that persistent neuroinflammation and glial scar formation cause aberrant neuronal firing. Here, we summarize the clinical features of PSE and describe in detail the inflammatory changes after an ischemic stroke as well as the chronic changes reported in epilepsy. Moreover, we discuss alterations and disturbances in blood-brain-barrier leakage, astrogliosis, and extracellular matrix changes in both, stroke and epilepsy. In the end, we provide an overview of commonalities of inflammatory reactions and cellular processes in the post-ischemic environment and epileptic brain and discuss how these research questions should be addressed in the future.

Keywords: neuroinflammation, ischemia, post-stroke seizures, gliosis, BBB leakage

OPEN ACCESS

Edited by:
Diego Ruano, Sevilla University, Spain

Reviewed by:
Katja Kobow, University Hospital Erlangen, Germany
Hui-ling Zhang, Soochow University, China

****Correspondence:***
Tim J. von Oertzen
Tim.von_oertzen@jku.at

Specialty section:
This article was submitted to Neuroinflammation and Neuropathy, a section of the journal Frontiers in Aging Neuroscience

Received: *22 September 2021*
Accepted: *23 November 2021*
Published: *13 December 2021*

Citation:
Tröscher AR, Gruber J, Wagner JN, Böhm V, Wahl A-S and von Oertzen TJ (2021) Inflammation Mediated Epileptogenesis as Possible Mechanism Underlying Ischemic Post-stroke Epilepsy. Front. Aging Neurosci. 13:781174. doi: 10.3389/fnagi.2021.781174

INTRODUCTION

Ischemic strokes are among the most common causes of death and account for a large proportion of disabilities in Western societies (Deuschl et al., 2020). Importantly, cerebrovascular diseases are one of the main reasons for acquired epilepsy in adulthood, so-called post-stroke epilepsy (PSE; Pitkänen et al., 2016). With the rising number of geriatric patients worldwide, the number of stroke patients, and hence PSE patients, can be expected to rise significantly in the next decades (Deuschl et al., 2020). Although good descriptions and reviews of current clinical knowledge of PSE are available (Pitkänen et al., 2016; Feyissa et al., 2019; Xu, 2019; Zelano et al., 2020; Galovic et al., 2021), surprisingly little is known about the underlying pathomechanism that leads to PSE. Therefore, treatment and preventive actions are limited and speculative.

Common hypotheses for the post-ischemic epileptogenesis include gliosis, chronic inflammation, angiogenesis, neurodegeneration, altered synaptic plasticity, or synaptic sprouting (Li et al., 2010; Feyissa et al., 2019). Additionally, blood-brain-barrier (BBB) leakage during

stroke induces inflammation and pro-epileptogenic mechanisms (Vezzani et al., 2019). Mitochondrial dysfunction, edema, or ion gradient imbalances might contribute to stroke lesion size as well as to seizure generation. Moreover, seizure-like brain activity during ischemia also increases the infarct size and negatively impacts functional recovery (Williams and Tortella, 2002). This suggests that post-ischemic pathological changes and seizure generation are reciprocal processes which influence each other (Feyissa et al., 2019).

We here summarize clinical features of PSE and describe characteristics of neuroinflammation, blood-brain-barrier perturbations, gliosis, and changes in the extracellular matrix in stroke and epilepsy. Furthermore, we delineate similarities and possible interactions between the two pathologies and propose future directions for investigating the underlying pathomechanism in PSE in a preclinical and translational approach.

POST-STROKE EPILEPSY

Post-stroke seizures occur frequently and can be categorized into acute symptomatic (≤7 days post-stroke, ASS) and remote symptomatic seizures (>7 days post-stroke, RSS). ASS is considered to be the result of local metabolic imbalances (Feyissa et al., 2019). Although ASS drastically increases the risk for developing RSS, they do not contribute to the diagnosis of PSE. However, all patients who develop a single seizure more than 7 days after a stroke are classified as suffering from PSE as they have a 71.5% increased risk of developing further seizures within the next 10 years (Hesdorffer et al., 2009) and hence fall into the category of epilepsy according to the International League against Epilepsy (Fisher et al., 2014). Numbers of patients developing PSE vary due to different cohorts regarding the length of follow-up, stroke etiology, or varying definitions of early and RSS, but generally range from 3 to 25% (Galovic et al., 2018, 2021; Feyissa et al., 2019; Xu, 2019; Ferreira-Atuesta et al., 2021). Risk factors for PSE include strokes with cortical involvement, stroke severity, young age (below 65 years), or ASS (Galovic et al., 2018; Feyissa et al., 2019; Zelano et al., 2020; Ferreira-Atuesta et al., 2021).

Hemorrhagic strokes, which only make up about 5–10% of strokes, are more epileptogenic than ischemic ones (Caplan and Kase, 2016). ASS appears in between 2% and 4% of patients with ischemic strokes vs. 10% to 16% of patients with intracranial hemorrhages (Haapaniemi et al., 2014; Wang et al., 2017; Thevathasan et al., 2018). These numbers may be an under-estimate, as a study postulates that up to a fifth of patients showed electroencephalographic seizures in the acute phase after stroke (Bentes et al., 2017). The incidence of late-onset post-stroke seizures at a 5-year follow-up has been reported to be 9.5% for ischemic strokes and 11.8% for hemorrhagic strokes (Haapaniemi et al., 2014; Holtkamp et al., 2017).

Approximately 70% of PSE patients develop focal seizures, which occasionally generalize. The remaining 30% have bilateral tonic-clonic seizures only (Xu, 2019). PSE does not only lead to decreased quality of life, as does epilepsy in general, but it has also been linked with decreased post-stroke recovery, neurological deterioration, and poor functional outcomes (Graham et al., 2013; Baranowski, 2018; Feyissa et al., 2019). Seizures in PSE patients are often well manageable with anti-epileptic therapy (AED, anti-epileptic drugs), however, up to 40% of patients remain unresponsive to pharmacological intervention (Feyissa et al., 2019; Xu, 2019). General prophylactic AED treatment after stroke is not advisable, as this has been reported to decrease behavioral and motor recovery by inhibiting neural plasticity (Messé et al., 2009). Moreover, long-term AED usage may increase the risk of atherosclerosis, which would pose an additional risk for post-stroke patients (Tan et al., 2009). Although there are some clinical tools available to determine the risk of developing PSE after ischemic, hemorrhagic, or both stroke types (Strzelczyk et al., 2010; Haapaniemi et al., 2014; Galovic et al., 2018; Lekoubou et al., 2021), an easily measurable biomarker would ameliorate early diagnosis and facilitate preventive treatment even before the first seizure has occurred. In search of imaging biomarkers predicting the risk of poststroke seizures, a significant association between the incidence of PSE 2 years after the occurrence of hemorrhagic transformation post ischemic stroke in patients who underwent endovascular revascularization therapy was found (17.9% compared with 4.0%, $p = 0.001$; Thevathasan et al., 2018). In a recent study no impact of reperfusion techniques on the development of PSE was found (Ferreira-Atuesta et al., 2021).

Although RSS is significantly associated with stroke severity and stroke location in the middle cerebral artery territory among others (Galovic et al., 2018), no explicit information regarding more accurate stroke localization, infarct size, or concomitant cerebrovascular damages, for example microangiopathy, or loss in brain volume, is available.

Unfortunately, hardly anything is known about the pathomechanism of post-ischemic epileptogenesis on a cellular and molecular level. A better understanding of these processes would help to search for possible biomarker candidates in easily accessible compartments such as the blood and could identify patients at risk of developing PSE in a paraclinical setting.

Neuroinflammation as Possible Mechanism Underlying PSE

An ischemic insult induces a plethora of processes in the brain parenchyma, such as excitotoxicity, hypoxic injury, activation of the immune system, and BBB leakage (Wimmer et al., 2018; Jayaraj et al., 2019). Interestingly, similar mechanisms have been described to induce epileptogenesis (**Figure 1**; Bauer et al., 2017; Vezzani et al., 2019). Especially neuroinflammation-mediated epilepsy has become a focus of attention in recent years. Several immunological mediators have been shown to lower the seizure threshold. Innate as well as adaptive neuroinflammation has repeatedly been shown in the brain parenchyma in several forms of epilepsy (Vezzani et al., 2011a; Devinsky et al., 2013; Bauer et al., 2017).

Neuroinflammation in Stroke

Post-ischemic inflammation occurs rapidly after the event and is characterized by microglia activation, influx of peripheral immune cells, and BBB breakdown.

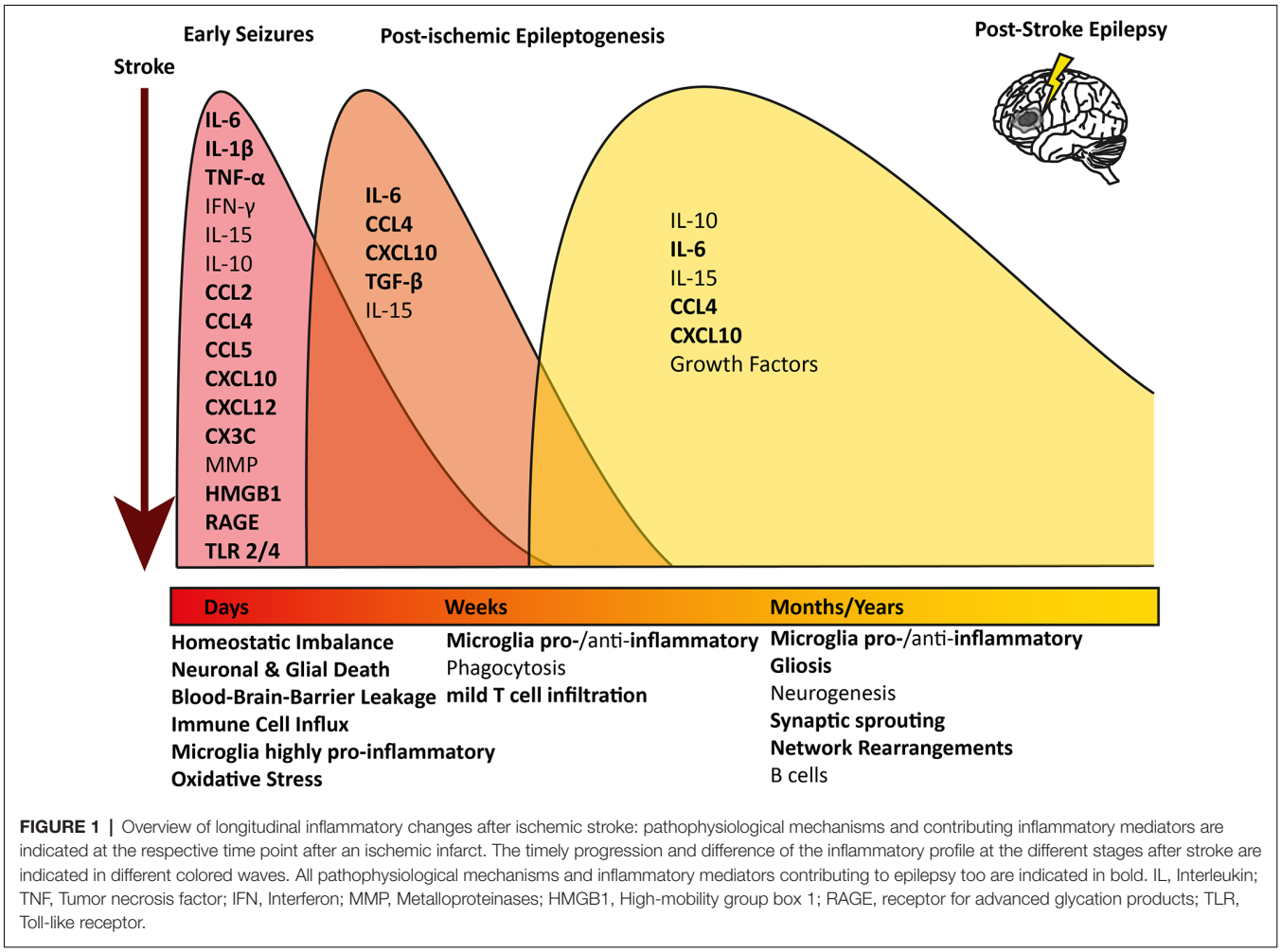

FIGURE 1 | Overview of longitudinal inflammatory changes after ischemic stroke: pathophysiological mechanisms and contributing inflammatory mediators are indicated at the respective time point after an ischemic infarct. The timely progression and difference of the inflammatory profile at the different stages after stroke are indicated in different colored waves. All pathophysiological mechanisms and inflammatory mediators contributing to epilepsy too are indicated in bold. IL, Interleukin; TNF, Tumor necrosis factor; IFN, Interferon; MMP, Metalloproteinases; HMGB1, High-mobility group box 1; RAGE, receptor for advanced glycation products; TLR, Toll-like receptor.

TABLE 1 | Summary of Inflammatory changes in stroke and epilepsy.

	Stroke	Epilepsy
Cell Loss	Neuronal and Glial Cell Death	Neuronal Loss (depending on etiology)
Immune Cells Involved	Macrophages, Neutrophils, Leukocytes, Lymphocytes, Microglia	Microglia, Lymphocytes
Microglia	First pro-inflammatory, then phagocytic, produce growth factors	Chronically pro-inflammatory, ramified morphology
Cytokines	IL-6, IL-1**β**, IL-15, IL-10, IFN-**γ**, TNF-**α**, TGF-**β**	IL-6, IL-1**β**, TNF-**α**, TGF-**β**
Chemokines	CCL1, CCL2, CCL4, CCL5, CCL22, CXCL10, CXCL12, CX3C	CCL2, CCL3, CCL4, CCL5, CXCL10, CX3CL1
Reactive Oxygen and Nitrogen Species	Plasma lipid peroxides and thiobarbituric acid in blood	Increased in blood, iNOS in post-mortem brains
Astrocytes	Hyperplasic, produce increased vimentin, GFAP, ephrin-A5, ECM molecules, CSPGs, nerve growth factors, BDNF, scar formation	Astrogliosis, ramified morphology
Blood-Brain Barrier	BBB breakdown (acute), HIF-1**α** induced MMP2 and MMP9, integrin breakdown, albumin leakage	BBB leakage (chronic), imbalance in brain homeostasis, albumin leakage
Alarmins	HMGB1, purins, peroxireduxins, RAGE, TLR2 and 4, S100B and Hsc70 downregulation in patients with a high probability of PSE	HMGB1, RAGE, TLR4
Network Rearrangements	Plasticity in the penumbra, axonal outgrowth through ECM proteins, neuroregeneration and rewiring (limited), synaptic sprouting	Synaptic sprouting in hippocampus

IL, Interleukin; TNF, Tumor necrosis factor; MMP, Metalloproteinases; HMGB1, High-mobility group box 1; RAGE, receptor for advanced glycation products; TLR, Toll-like receptor.

In the early stage after a stroke, acute neuronal and glial cell death occurs within the necrotic area. Peripheral immune cells, above all macrophages, neutrophils, and leukocytes, infiltrate the brain and migrate into the core lesion. Microglia in the surrounding areas increase in number and polarize towards a highly pro-inflammatory phenotype, expressing markers linked to oxidative stress, phagocytosis, and antigen presentation (Zrzavy et al., 2017; **Figure 1**, red wave). Pro-inflammatory cytokines are elevated in post-mortem tissue of stroke patients, such as interleukin (IL) 6, IL-1β, interferon (IFN) γ, tumor necrosis factor (TNF) α and IL-15 (Doll et al., 2014; Nguyen et al., 2016; Zrzavy et al., 2017; Wimmer et al., 2018). IL-1β

and TNFα levels in serum and plasma have been investigated and some studies reported an increase shortly after the stroke (Intiso et al., 2004; Sotgiu et al., 2006), whereas others did not (Tarkowski et al., 1995; Ormstad et al., 2011). However, due to the potent pro-inflammatory action of these cytokines and short half-life, a short-lived and locally restricted increase would be expected (Doll et al., 2014; Jayaraj et al., 2019). Further, many pro-inflammatory chemokines are upregulated in the brain, such as CCL1, CCL2, CCL4, CCL5, CCL22, CXCL10, and CXCL12, and some can be detected in serum or plasma (García-Berrocoso et al., 2014; Nguyen et al., 2016). On the other hand, anti-inflammatory cytokines such as IL-10 are highly upregulated in early stroke lesions and initially down-regulated in the serum, but levels increase later on (Ormstad et al., 2011; Nayak et al., 2012; Nguyen et al., 2016). Peripheral IL-6 and IL-10 levels were linked to worsened or improved stroke outcomes, respectively (Jiao et al., 2016; Nguyen et al., 2016). As microglia are polarized towards a pro-inflammatory phenotype, they can produce oxygen and nitrogen (ROS and NOS) species, which lead to BBB breakdown and act as neurotoxins (Seneş et al., 2007; Jayaraj et al., 2019). Astrocytes become hyperplasic and produce chemokines, cytokines, and astrocyte-specific proteins such as vimentin, or glial fibrillary acidic protein (GFAP), which contribute to scar formation (Wang et al., 2018; Pluta et al., 2021). Astrocytes also produce ephrin-A5, extracellular matrix molecules, and chondroit sulfate proteoglycans, which interfere with axonal sprouting, inhibit axonal growth and regeneration (Rolls et al., 2009; Overman et al., 2012; Huang et al., 2014). In the blood, increased levels of plasma lipid peroxides and thiobarbituric acids were found, a sign of ongoing oxidative stress and elevated levels of ROS and NOS (Alexandrova et al., 2003). Moreover, fraktalkine (CX3C), which can induce chemotaxis of leukocytes and microglia by binding to its receptor CX3CR1, seems to play a role in the post-ischemic outcome in an animal model, as CX3C knock-out animals had a nearly 30% reduction in infarct size and mortality (Soriano et al., 2002).

After the initial wave of inflammation, peripheral macrophages which have infiltrated the brain, together with brain-resident microglia, phagocytose debris of dead cells and shift towards either a mixed pro- and anti-inflammatory, or exclusively anti-inflammatory phenotype linked to the resolution of inflammation, removal of debris, and central nervous system (CNS) remodeling (Zrzavy et al., 2017). Pro-inflammatory mediators, such as IL-6, CXCL10, and CCL4, but also anti-inflammatory transforming growth factor (TGF) β are still significantly elevated (Nguyen et al., 2016; Jayaraj et al., 2019; **Figure 1**, orange wave). In post-mortem brains of patients, who died within 7 days after an ischemic infarct, astrocytes were shown to produce pro-inflammatory IL-15 *via* activating CD8+ T cells and natural killer cells (Li et al., 2017). Lymphocytes, especially CD8+ T cells, were increased in the ischemic lesion compared to healthy controls, although the number of T cells was about 10-fold lower compared to inflammatory conditions such as multiple sclerosis or encephalitis and did not show active proliferation as a sign of antigen recognition (Zrzavy et al., 2017).

In the late cystic or scar stage, an astrocytic scar has formed around the necrotic core. In this late phase after ischemic stroke, microglia reappear within the lesion core with a partly homeostatic, partly inflammatory phenotype (Zrzavy et al., 2017). Several pro- and anti-inflammatory cytokines and chemokines are still elevated and microglia produce increased levels of various growth factors, enhancing neurogenesis and plasticity within the penumbra (Nguyen et al., 2016; Jayaraj et al., 2019; **Figure 1**, yellow wave). B cells have been postulated to play a role in stroke recovery in the late stage. Increased numbers of regulatory B cells were shown to be beneficial, as they secret anti-inflammatory IL-10 (Offner and Hurn, 2012). On the other hand, in a mouse model for stroke, activated B cells infiltrated the brain weeks after a stroke and secreted immunoglobulin, leading to cognitive deficits. Post-stroke cognitive decline was decreased drastically upon depletion of B cells, indicating an active role of the activated B cells in the brain (Doyle et al., 2015).

Neuroinflammation in Epilepsy

In epilepsy, the temporal resolution of inflammatory processes is less well established. In humans, the epileptogenic processes leading to the first seizure can occur over years during which patients are free of symptoms. Most data on human patients derive from surgical resections of drug-resistant epilepsy patients, in whom epileptogenic activity has been ongoing for years. Hence, the pathological changes characterize a very late stage of the disease, and no conclusions regarding the initial events can be drawn. Results from both, human end-point analyses and animal studies, where clear time-course studies are feasible, revealed several pro-inflammatory mediators, which are involved in epileptogenesis. The most prominent one is IL-1β, which is produced in the brain of human patients with pharmaco-resistant epilepsy and was also shown to lower the seizure threshold in animals (Vezzani et al., 1999, 2000, 2011b). IL-1β leads to an altered phosphorylation of NMDA receptors, rendering them more permeable to calcium and therefore increasing neuronal firing or potentially even excitotoxicity (Viviani et al., 2003). Moreover, patients' serum IL-1β levels decrease after surgical resection of the epileptogenic foci (Pedre et al., 2018a). IL-6 is upregulated during epileptogenesis, decreases neurogenesis, and promotes gliosis (Minami et al., 1991; Ichiyama et al., 1998; Peltola et al., 2000; Valliéres et al., 2002; Liimatainen et al., 2009; Rana and Musto, 2018). Moreover, IL-6 serum levels were reduced after surgical resection of the epileptogenic foci and were significantly reduced in epileptic patients who became seizure-free after the surgery (Pedre et al., 2018a). Further, increased levels of oxidative stress markers as a possible sign for activated, pro-inflammatory microglia, were found in the blood of epilepsy patients, which decreased after surgery (López et al., 2007; Pedre et al., 2018b). Increased levels of inducible nitric oxide synthase (iNOS) were found in post-mortem tissue of epilepsy patients (Pauletti et al., 2019; Terrone et al., 2019). TNFα can exert various pro-epileptogenic properties in the brain (Minami et al., 1991; Ichiyama et al., 1998; Arulsamy and Shaikh, 2020). It is released from activated microglia upon extracellular glutamate detection and leads to an upregulation of synapses. *In vitro*, TNFα induces an upregulation of AMPA receptors and the endocytosis of GABA receptors (Stellwagen et al., 2005). Chemokines have also been

depicted to play a role in epileptogenesis. In human tissue resections CCL2, CCL3, CCL4, CCL5, and CXCL10 were highly upregulated (Wu et al., 2008; Tröscher et al., 2019). The same was found in animal models, where CCL2, CCL3, CCL4, and CCL5 have been involved in epileptic neuronal signaling (Fabene et al., 2008, 2010; Foresti et al., 2009; Xu et al., 2009; Cerri et al., 2017). Moreover, an endothelial upregulation of chemokines can lead to increased leukocyte influx, which has been shown to act pro-convulsively and induce an epileptogenic inflammatory milieu within the brain parenchyma in animals (Fabene et al., 2008, 2010; Cerri et al., 2017). In humans, T cell numbers were found to be uncorrelated with seizure frequency, making a direct link between T cells and epileptogenesis less likely (Tröscher et al., 2021). The neuronal chemokine fraktalkine (CX3CL1), which mediates neuronal-microglial interaction, has been shown to modulate $GABA_A$ currents in human temporal lobe epilepsy (Roseti et al., 2013; all inflammatory changes occurring in epilepsy in **Figure 1** in bold).

Astrogliosis and Glial Scar in Stroke and Epilepsy

The astrocytic scar formed in the late stage after stroke provides a scaffold for angiogenesis, modulates immune cells and prevents the uncontrollable spread of inflammation and cell damage to healthy areas, and maintains ion and fluid balance (Rolls et al., 2009). Moreover, astrocytes forming the scar produce nerve growth factors and brain-derived neurotrophic factors (Schwartz and Nishiyama, 1994), which facilitate survival and rewiring of surviving neurons in the penumbra (Rolls et al., 2009). Several extracellular matrix proteins have also been shown to aid axonal outgrowth (Dzyubenko et al., 2018). Although neuroregeneration and rewiring are difficult in the CNS, neuronal reorganization and repair occur post-ischemia and can be enhanced by glial-derived growth factors and stimulation (Zhang and Chopp, 2009; Wahl et al., 2014, 2017).

Astrogliosis is also a hallmark of medial temporal lobe epilepsy, where areas with or without neuronal loss can be affected (Thom, 2014; Blumcke et al., 2017). Moreover, it was shown that astrocytes can change the extracellular matrix in a TGFβ-dependent manner, leading to a breakdown of perineuronal nets around inhibitory neurons, triggering inhibition deficits (Kim et al., 2017). Disruption of the extracellular matrix leads to altered ion concentrations, osmolarity, and firing behavior in hippocampal neurons (Glykys et al., 2014). Astrocytes also play a critical role with respect to ion balancing, especially potassium buffering, and neurotransmitter homeostasis. These mechanisms have been shown to be altered in epilepsy surgical resections (Pekny et al., 2016).

Blood-Brain-Barrier Breakdown in Stroke and Epilepsy

Another hallmark of stroke is BBB breakdown. This is mainly mediated by proteinases such as metalloproteinases (mainly MMP2 and MMP9), which are induced by hypoxia-inducible factor (HIF) 1α or various pro-inflammatory cytokines. They directly decrease the expression of tight-junction proteins and shift their location. MMP9 levels were found to be increased after ischemic stroke and positively correlate with the severity of neurological deficits. Interestingly, MMP9 levels dropped after 72 h, except in patients with stroke progression (Brouns et al., 2011). Integrins, which under physiological conditions interact with the basement membrane to control BBB permeability, also break down, leading to edema and exacerbated inflammation (Yang and Rosenberg, 2011). In rodent stroke models, reactive oxygen species were shown to further enhance BBB leakage (Kim et al., 2001). Breakdown of the BBB leads to leakage of peripheral proteins such as albumin, which by itself acts highly pro-inflammatory within the brain parenchyma (Brouns et al., 2011; Altman et al., 2019; Yang et al., 2019).

BBB leakage also commonly occurs in epilepsy and also increases the risk of developing epilepsy after a precipitating incident (Marchi et al., 2007, 2010, 2012; van Vliet et al., 2007; Tomkins et al., 2008; Raabe et al., 2012). Peripheral proteins can induce seizures and lead to imbalances in brain homeostasis and trigger inflammation. Albumin was shown to decrease potassium buffering in a TGFβ-dependent manner (Schröder et al., 2000; Jauch et al., 2002; Cacheaux et al., 2009; Frigerio et al., 2012; Heinemann et al., 2012; Devinsky et al., 2013; Gorter et al., 2019). Moreover, seizures themselves can lead to increased BBB permeability (Marchi et al., 2007, 2012; van Vliet et al., 2007; Tomkins et al., 2008; Morin-Brureau et al., 2011; Devinsky et al., 2013; Vezzani et al., 2019). The importance of BBB leakage with respect to the development of PSE is further underlined by the fact that statins reduce the risk for hospitalization for epilepsy after stroke in a dose-dependent manner. Their effect is mainly ascribed to their anti-inflammatory and protective action on the BBB (Xu et al., 2020; Fang et al., 2021; Guo et al., 2021).

Alarmins in Stroke and Epilepsy

Inflammation in stroke as well as in epilepsy can be initiated, propagated, and maintained by the release of alarmins, which are mostly intracellular molecules released upon cellular stress or death. In stroke, various alarmins, such as the protein high-mobility group box 1 (HMGB1), purins, or peroxireduxins, are released and bind to various damage associated molecular pattern receptors (DAMPs), initiating an inflammatory cascade (Gülke et al., 2018). HMGB1 activates the receptor for advanced glycation products (RAGE) as well as toll-like receptor (TLR) 2 and 4, which are also activated by peroxiredoxins. Similar pathways, mediated *via* HMGB1, RAGE, and TLR4 were shown to be upregulated in epilepsy animal models and surgical resections of epilepsy patients (Zurolo et al., 2011; Paudel et al., 2019). HMGB1 was also found in the serum of stroke patients and high levels were linked to a worse outcome, indicated by higher follow-up modified Rankin scores at 1 year (Tsukagawa et al., 2017). Binding to these receptors initiates NF_KB signaling, which induces the transcription of several highly pro-inflammatory chemokines and cytokines (Liu et al., 2017) and was shown to be activated in hippocampal resections of medial temporal lobe epilepsy patients (Crespel et al., 2002). Purins, which are released from dying cells after seizures or ischemia, can activate the inflammasome *via* Nod-like receptor (NLRP) 3, which triggers the secretion of

IL1β and IL18 (Beamer et al., 2016; Gülke et al., 2018). The inflammasome or its products IL1β and IL18 have been shown to be upregulated in various epilepsies (Tröscher et al., 2019; Vezzani et al., 2019).

Commonalities in the Inflammatory Activation Between Epilepsy and Stroke

There is a significant overlap of inflammatory mechanisms after an ischemic infarct compared to findings in epilepsy patients. Pro-inflammatory cytokines, such as IL-6, IL-1β, and TNFα have been described in brains and in the blood of both, patients after stroke and in epilepsy (**Table 1**; Stellwagen et al., 2005; Doll et al., 2014; Nguyen et al., 2016; Zrzavy et al., 2017; Pedre et al., 2018a; Rana and Musto, 2018; Wimmer et al., 2018; Vezzani et al., 2019). Especially the pro-epileptogenic action of IL-1β and TNFα are well understood and their upregulation after ischemia could be a possible explanation for post-ischemic epileptogenesis (Stellwagen et al., 2005; Vezzani et al., 2019). Alarmins, secreted due to neuronal damage or cell death caused by the ischemia, may augment the inflammatory reaction and activate pro-epileptogenic pathways *via* pro-inflammatory cytokines (Vezzani et al., 2011b; Gülke et al., 2018). A recent study found downregulation of calcium-binding protein B (S100B) and heat-shock protein (Hsc70) as well as an upregulation of endostatin in patients directly after stroke, who had a high probability of developing PSE in the following months (Abraira et al., 2020). S100B and Hsc70 are DAMPs linked to BBB integrity, hence lower levels could point towards perturbed BBB function (Galovic et al., 2021). In addition, T cell and monocyte-attracting chemokines are expressed in the early, intermediate, and late stages after an ischemic infarct and in epilepsy resections (Fabene et al., 2010; García-Berrocoso et al., 2014; Cerri et al., 2017). How these chemokines act pro-epileptogenically is not yet fully understood, but T cells have been shown to infiltrate the brain in both epilepsy and after an ischemic stroke, albeit in low numbers (Zrzavy et al., 2017; Tröscher et al., 2021). However, a recent study showed that the number of T cells in medial temporal lobe epilepsy does not correlate with the seizure frequency. Therefore, parenchymal T cells are unlikely to be the key driver of post-ischemic epileptogenesis (Tröscher et al., 2021). However, so far little is known about the parenchymal inflammatory milieu in PSE brains.

Glial scar forming astrocytes are present around the lesion core after an ischemic infarct and are commonly found in epilepsy patients, for example in hippocampal sclerosis (Rolls et al., 2009; Robel and Sontheimer, 2015; Wang et al., 2018). Moreover, astrocytes play a key role in neurotransmitter homeostasis (Pekny et al., 2016). The glial scar and excessively produced extracellular matrix proteins around the lesion core may inhibit axonal regrowth and prevent physiological synaptic sprouting. Therefore, excessive scar formation around the lesion could potentially affect surviving neurons within the penumbra/scar area or neurons in the neighboring areas (Glykys et al., 2014; Robel and Sontheimer, 2015; Pekny et al., 2016; Wang et al., 2018). On the other hand, astroglial scars were also shown to produce neuronal growth factors and act beneficially in post-stroke rewiring (Schwartz and Nishiyama, 1994; Do Carmo Cunha et al., 2007; Rolls et al., 2009; Zhang and Chopp, 2009). In brain specimens of epilepsy patients, synaptic sprouting was also observed, where it was ascribed to inducing or facilitating seizure generation (Proper et al., 2000; Jarero-Basulto et al., 2018). Disturbances of previously functional networks have been shown by EEG recordings, where prolonged disturbed gamma oscillations were found in animal models and also correlated with stroke recovery in humans (Vecchio et al., 2019; Hazime et al., 2021).

Astrocytes play another critical role in post-ischemic parenchymal processes *via* their endfeet, constituting a part of the BBB (Alvarez et al., 2013). After ischemic infarcts, the BBB often breaks down leading to the influx of peripheral molecules and cells (Brouns et al., 2011). In epilepsy, BBB leakage is a commonly observed phenomenon and was repeatedly described as triggering or enhancing epileptic activity (Friedman, 2011). Therefore, chronic alterations in the BBB could be another mechanism by which PSE develops and how epileptic activity persists even months and years after the ischemic lesion occurred.

DISCUSSION AND FUTURE DIRECTIONS

Although PSE is one of the most common forms of acquired epilepsy in the elderly, surprisingly little is known about the underlying pathomechanisms. One of the most common theories for post-ischemic epileptogenesis is chronic inflammation, which can occur in stroke patients but also in patients suffering from epilepsy. Many studies have investigated the inflammatory cascades occurring after stroke (for review see Wimmer et al., 2018; Jayaraj et al., 2019). In epilepsy research chronic inflammation has been delineated as a potent driver of epileptogenesis as well (Wilcox and Vezzani, 2014; Bauer et al., 2017; Vezzani et al., 2019). However, hardly anything is known about the interaction of these two pathomechanisms.

In recent years, crucial scientific work has been done to pave the way for future studies, among them establishing a sensitive clinical screening tool for patients at high risk of developing PSE (Galovic et al., 2018). This will allow for designing studies to investigate possible pathomechanisms and therapeutic approaches for PSE by pre-selecting susceptible patients. Previously, designing prospective studies on PSE was hardly realistic due to the relatively low percentage of patients developing PSE. Using the SELECT score, a patient pool with patients at high risk for PSE can be generated and followed up. First investigations on blood biomarkers in PSE have recently been published and underline the fact, that inflammatory processes might be involved in the pathomechanism of PSE (Abraira et al., 2020). Furthermore, the recently published meta-analyses on the beneficial effect of statins on the development of PSE point towards a pro-inflammatory origin of RSS (Guo et al., 2015; Xu et al., 2020; Fang et al., 2021). As clinical research on PSE is very laborious and time-consuming, translational research would be very useful to understand the basic pathomechanisms. However, generating animal models is equally difficult, as mice and rats

also tend to develop seizures after stroke in relatively low numbers. Hence, high numbers of animals would be required for reliable and reproducible results. Moreover, the validity of results gained from young rodents for a human disease affecting the elderly is questionable (Reddy et al., 2017). *In vitro* approaches using human iPSCs or organotypic slices could lead to insights on basic molecular principles of post-ischemic epileptogenesis with human cells or tissues. However, most likely only combining results from all three approaches will lead to a better understanding of the underlying pathomechanism of post-ischemic PSE and thus help to identify targets for therapy and prophylaxis.

We summarized the key inflammatory mediators involved in both diseases and provided a broad overview on potential post-ischemic epileptogenic mechanisms. In the future, these questions have to be addressed in clinical as well as translational research to provide insights into the development of PSE. In animal models, the basic principles of post-ischemic inflammation and their potential to drive epileptogenesis can be studied in detail, allowing exactly timed disease course analyses and *in vivo* monitoring of neuronal activity. Moreover, in animal models confounding factors such as lesion size, age, and area of incident can easily be controlled for. In clinical research, the quest for biomarkers in easily accessible compartments, such as the blood, will be crucial. Moreover, electroencephalographic and imaging approaches can be used in human clinical research to identify key epileptogenic hubs and their specific firing properties during the latent phase of epileptogenesis. This will not only improve our basic understanding of post-ischemic brain physiology but also pave the way for potential prophylactic interventions, inhibiting epileptogenesis before the first seizure occurs.

AUTHOR CONTRIBUTIONS

AT and VB summarized the molecular biological aspects of stroke and epilepsy. JG and JW summarized the clinical aspects of PSE. A-SW contributed with her knowledge on stroke and stroke rehabilitation. AT wrote the manuscript. TO supervised the project. All authors contributed to the article and approved the submitted version.

FUNDING

AT was supported by the Austrian Epilepsy Association. A-SW was supported by the Dr. Hurka Foundation, Zurich. This work was supported by Johannes Kepler Open Access Publishing Fund.

REFERENCES

Abraira, L., Santamarina, E., Cazorla, S., Bustamante, A., Quintana, M., Toledo, M., et al. (2020). Blood biomarkers predictive of epilepsy after an acute stroke event. *Epilepsia* 61, 2244–2253. doi: 10.1111/epi.16648

Alexandrova, M. L., Bochev, P. G., Markova, V. I., Bechev, B. G., Popova, M. A., Danovska, M. P., et al. (2003). Oxidative stress in the chronic phase after stroke. *Redox Rep.* 8, 169–176. doi: 10.1179/135100003225001548

Altman, K., Shavit-Stein, E., and Maggio, N. (2019). Post stroke seizures and epilepsy: from proteases to maladaptive plasticity. *Front. Cell. Neurosci.* 13:397. doi: 10.3389/fncel.2019.00397

Alvarez, J. I., Katayama, T., and Prat, A. (2013). Glial influence on the blood brain barrier. *Glia* 61, 1939–1958. doi: 10.1002/glia.22575

Arulsamy, A., and Shaikh, M. F. (2020). Tumor necrosis factor-α, the pathological key to post-traumatic epilepsy: a comprehensive systematic review. *ACS Chem. Neurosci.* 11, 1900–1908. doi: 10.1021/acschemneuro.0c00301

Baranowski, C. J. (2018). The quality of life of older adults with epilepsy: a systematic review. *Seizure* 60, 190–197. doi: 10.1016/j.seizure.2018.06.002

Bauer, J., Becker, A. J., Elyaman, W., Peltola, J., Rüegg, S., Titulaer, M. J., et al. (2017). Innate and adaptive immunity in human epilepsies. *Epilepsia* 58, 57–68. doi: 10.1111/epi.13784

Beamer, E., Gölöncsér, F., Horváth, G., Beko, K., Otrokocsi, L., Koványi, B., et al. (2016). Purinergic mechanisms in neuroinflammation: an update from molecules to behavior. *Neuropharmacology* 104, 94–104. doi: 10.1016/j.neuropharm.2015.09.019

Bentes, C., Martins, H., Peralta, A. R., Casimiro, C., Morgado, C., Franco, A. C., et al. (2017). Post-stroke seizures are clinically underestimated. *J. Neurol.* 264, 1978–1985. doi: 10.1007/s00415-017-8586-9

Blumcke, I., Spreafico, R., Haaker, G., Coras, R., Kobow, K., Bien, C. G., et al. (2017). Histopathological findings in brain tissue obtained during epilepsy surgery. *N. Engl. J. Med.* 377, 1648–1656. doi: 10.1056/NEJMoa1703784

Brouns, R., Wauters, A., De Surgeloose, D., Mariën, P., and De Deyn, P. P. (2011). Biochemical markers for blood-brain barrier dysfunction in acute ischemic stroke correlate with evolution and outcome. *Eur. Neurol.* 65, 23–31. doi: 10.1159/000321965

Cacheaux, L. P., Ivens, S., David, Y., Lakhter, A. J., Bar-Klein, G., Shapira, M., et al. (2009). Transcriptome profiling reveals TGF-beta signaling involvement in epileptogenesis. *J. Neurosci.* 29, 8927–8935. doi: 10.1523/JNEUROSCI.0430-09.2009

Caplan, L. R. and Kase, C. S. (2016). "Intracerebral hemorrhage," in *Caplan's Stroke. A Clinical Approach*, ed L. R. Caplan (Cambridge University Press), 477–510. doi: 10.1017/CBO9781316095805.015

Cerri, C., Caleo, M., and Bozzi, Y. (2017). Chemokines as new inflammatory players in the pathogenesis of epilepsy. *Epilepsy Res.* 136, 77–83. doi: 10.1016/j.eplepsyres.2017.07.016

Crespel, A., Coubes, P., Rousset, M.-C., Brana, C., Rougier, A., Rondouin, G., et al. (2002). Inflammatory reactions in human medial temporal lobe epilepsy with hippocampal sclerosis. *Brain Res.* 952, 159–169. doi: 10.1016/s0006-8993(02)03050-0

Deuschl, G., Beghi, E., Fazekas, F., Varga, T., Christoforidi, K. A., Sipido, E., et al. (2020). The burden of neurological diseases in Europe: an analysis for the Global Burden of Disease Study 2017. *Lancet Public Health* 5, e551–e567. doi: 10.1016/S2468-2667(20)30190-0

Devinsky, O., Vezzani, A., Najjar, S., De Lanerolle, N. C., and Rogawski, M. A. (2013). Glia and epilepsy: excitability and inflammation. *Trends Neurosci.* 36, 174–184. doi: 10.1016/j.tins.2012.11.008

Do Carmo Cunha, J., De Freitas Azevedo Levy, B., De Luca, B. A., De Andrade, M. S. R., Gomide, V. C., and Chadi, G. (2007). Responses of reactive astrocytes containing S100β protein and fibroblast growth factor-2 in the border and in the adjacent preserved tissue after a contusion injury of the spinal cord in rats: implications for wound repair and neuroregeneration. *Wound Repair Regen.* 15, 134–146. doi: 10.1111/j.1524-475X.2006.00194.x

Doll, D. N., Barr, T. L., and Simpkins, J. W. (2014). Cytokines: their role in stroke and potential use as biomarkers and therapeutic targets. *Aging Dis.* 5, 294–306. doi: 10.14336/AD.2014.0500294

Doyle, K. P., Quach, L. N., Solé, M., Axtell, R. C., Nguyen, T. V. V., Soler-Llavina, G. J., et al. (2015). B-lymphocyte-mediated delayed cognitive impairment following stroke. *J. Neurosci.* 35, 2133–2145. doi: 10.1523/JNEUROSCI.4098-14.2015

Dzyubenko, E., Manrique-Castano, D., Kleinschnitz, C., Faissner, A., and Hermann, D. M. (2018). Role of immune responses for extracellular matrix remodeling in the ischemic brain. *Ther. Adv. Neurol. Disord.* 11:1756286418818092. doi: 10.1177/1756286418818092

Fabene, P. F., Bramanti, P., and Constantin, G. (2010). The emerging role for chemokines in epilepsy. *J. Neuroimmunol.* 224, 22–27. doi: 10.1016/j.jneuroim.2010.05.016

Fabene, P. F., Navarro Mora, G., Martinello, M., Rossi, B., Merigo, F., Ottoboni, L., et al. (2008). A role for leukocyte-endothelial adhesion mechanisms in epilepsy. *Nat. Med.* 14, 1377–1383. doi: 10.1038/nm.1878

Fang, J., Tuo, M., Ouyang, K., and Xu, Y. (2021). Statin on post-stroke epilepsy: a systematic review and meta-analysis. *J. Clin. Neurosci.* 83, 83–87. doi: 10.1016/j.jocn.2020.11.023

Ferreira-Atuesta, C., Döhler, N., Erdélyi-Canavese, B., Felbecker, A., Siebel, P., Scherrer, N., et al. (2021). Seizures after ischemic stroke: a matched multicenter study. *Ann. Neurol.* 90, 808–820. doi: 10.1002/ANA.26212

Feyissa, A. M., Hasan, T. F., and Meschia, J. F. (2019). Stroke-related epilepsy. *Eur. J. Neurol.* 26:18–e3. doi: 10.1111/ene.13813

Fisher, R. S., Acevedo, C., Arzimanoglou, A., Bogacz, A., Cross, J. H., Elger, C. E., et al. (2014). ILAE official report: a practical clinical definition of epilepsy. *Epilepsia* 55, 475–482. doi: 10.1111/epi.12550

Foresti, M. L., Arisi, G. M., Katki, K., Montañez, A., Sanchez, R. M., and Shapiro, L. A. (2009). Chemokine CCL2 and its receptor CCR2 are increased in the hippocampus following pilocarpine-induced status epilepticus. *J. Neuroinflammation* 6:40. doi: 10.1186/1742-2094-6-40

Friedman, A. (2011). Blood-brain barrier dysfunction, status epilepticus, seizures and epilepsy: a puzzle of a chicken and egg? in *Epilepsia*, 52, 19–20. doi: 10.1111/j.1528-1167.2011.03227.x

Frigerio, F., Frasca, A., Weissberg, I., Parrella, S., Friedman, A., Vezzani, A., et al. (2012). Long-lasting pro-ictogenic effects induced *in vivo* by rat brain exposure to serum albumin in the absence of concomitant pathology. *Epilepsia* 53, 1887–1897. doi: 10.1111/j.1528-1167.2012.03666.x

Galovic, M., Döhler, N., Erdélyi-Canavese, B., Felbecker, A., Siebel, P., Conrad, J., et al. (2018). Prediction of late seizures after ischaemic stroke with a novel prognostic model (the SeLECT score): a multivariable prediction model development and validation study. *Lancet Neurol.* 17, 143–152. doi: 10.1016/S1474-4422(17)30404-0

Galovic, M., Ferreira-Atuesta, C., Abraira, L., Döhler, N., Sinka, L., Brigo, F., et al. (2021). Seizures and epilepsy after stroke: epidemiology, biomarkers and management. *Drugs Aging* 38, 285–299. doi: 10.1007/s40266-021-00837-7

García-Berrocoso, T., Giralt, D., Llombart, V., Bustamante, A., Penalba, A., Flores, A., et al. (2014). Chemokines after human ischemic stroke: from neurovascular unit to blood using protein arrays. *Transl. Proteom.* 3, 1–9. doi: 10.1016/j.trprot.2014.03.001

Glykys, J., Dzhala, V., Egawa, K., Balena, T., Saponjian, Y., Kuchibhotla, K. V., et al. (2014). Local impermeant anions establish the neuronal chloride concentration. *Science* 343, 670–675. doi: 10.1126/science.1245423

Gorter, J. A., Aronica, E., and van Vliet, E. A. (2019). The roof is leaking and a storm is raging: repairing the blood-brain barrier in the fight against epilepsy. *Epilepsy Curr.* 19, 177–181. doi: 10.1177/1535759719844750

Graham, N. S. N., Crichton, S., Koutroumanidis, M., Wolfe, C. D. A., and Rudd, A. G. (2013). Incidence and associations of poststroke epilepsy the prospective South London stroke register. *Stroke* 44, 605–611. doi: 10.1161/STROKEAHA.111.000220

Gülke, E., Gelderblom, M., and Magnus, T. (2018). Danger signals in stroke and their role on microglia activation after ischemia. *Ther. Adv. Neurol. Disord.* 11:1756286418774254. doi: 10.1177/1756286418774254

Guo, J., Li, J., Zhou, M., Qin, F., Zhang, S., Wu, B., et al. (2015). Statin treatment reduces the risk of poststroke seizures. *Neurology* 85, 701–707. doi: 10.1212/WNL.0000000000001814

Guo, Y., Zhu, L. H., Zhao, K., Guo, X. M., and Yang, M. F. (2021). Statin use for the prevention of seizure and epilepsy in the patients at risk: a systematic review and meta-analysis of cohort studies. *Epilepsy Res.* 174:106652. doi: 10.1016/j.eplepsyres.2021.106652

Haapaniemi, E., Strbian, D., Rossi, C., Putaala, J., Sipi, T., Mustanoja, S., et al. (2014). The CAVE score for predicting late seizures after intracerebral hemorrhage. *Stroke* 45, 1971–1976. doi: 10.1161/STROKEAHA.114.004686

Hazime, M., Alasoadura, M., Lamtahri, R., Quilichini, P., Leprince, J., Vaudry, D., et al. (2021). Prolonged deficit of low gamma oscillations in the peri-infarct cortex of mice after stroke. *Exp. Neurol.* 341:113696. doi: 10.1016/j.expneurol.2021.113696

Heinemann, U., Kaufer, D., and Friedman, A. (2012). Blood-brain barrier dysfunction, TGFβ signaling and astrocyte dysfunction in epilepsy. *Glia* 60, 1251–1257. doi: 10.1002/glia.22311

Hesdorffer, D. C., Benn, E. K. T., Cascino, G. D., and Hauser, W. A. (2009). Is a first acute symptomatic seizure epilepsy? Mortality and risk for recurrent seizure. *Epilepsia* 50, 1102–1108. doi: 10.1111/j.1528-1167.2008.01945.x

Holtkamp, M., Beghi, E., Benninger, F., Kälviäinen, R., Rocamora, R., and Christensen, H. (2017). European Stroke Organisation guidelines for the management of post-stroke seizures and epilepsy. *Eur. Stroke J.* 2, 103–115. doi: 10.1177/2396987317705536

Huang, L., Wu, Z. B., ZhuGe, Q., Zheng, W. M., Shao, B., Wang, B., et al. (2014). Glial scar formation occurs in the human brain after ischemic stroke. *Int. J. Med. Sci.* 11, 344–348. doi: 10.7150/ijms.8140

Ichiyama, T., Nishikawa, M., Yoshitomi, T., Hayashi, T., and Furukawa, S. (1998). Tumor necrosis factor-alpha, interleukin-1 beta and interleukin-6 in cerebrospinal fluid from children with prolonged febrile seizures. Comparison with acute encephalitis/encephalopathy. *Neurology* 50, 407–411. doi: 10.1212/wnl.50.2.407

Intiso, D., Zarrelli, M. M., Lagioia, G., Di Rienzo, F., Checchia De Ambrosio, C., Simone, P., et al. (2004). Tumor necrosis factor alpha serum levels and inflammatory response in acute ischemic stroke patients. *Neurol. Sci.* 24, 390–396. doi: 10.1007/s10072-003-0194-z

Jarero-Basulto, J. J., Gasca-Martínez, Y., Rivera-Cervantes, M. C., Ureña-Guerrero, M. E., Feria-Velasco, A. I., and Beas-Zarate, C. (2018). Interactions between epilepsy and plasticity. *Pharmaceuticals (Basel)* 11:17. doi: 10.3390/ph11010017

Jauch, R., Windmüller, O., Lehmann, T. N., Heinemann, U., and Gabriel, S. (2002). Effects of barium, furosemide, ouabaine and 4,4'-diisothiocyanatostilbene-2,2'-disulfonic acid (DIDS) on ionophoretically-induced changes in extracellular potassium concentration in hippocampal slices from rats and from patients with epilepsy. *Brain Res.* 925, 18–27. doi: 10.1016/s0006-8993(01)03254-1

Jayaraj, R. L., Azimullah, S., Beiram, R., Jalal, F. Y., and Rosenberg, G. A. (2019). Neuroinflammation: friend and foe for ischemic stroke. *J. Neuroinflammation* 16:142. doi: 10.1186/s12974-019-1516-2

Jiao, J.-T., Cheng, C., Ma, Y.-J., Huang, J., Dai, M.-C., Jiang, C., et al. (2016). Association between inflammatory cytokines and the risk of post-stroke depression and the effect of depression on outcomes of patients with ischemic stroke in a 2-year prospective study. *Exp. Ther. Med.* 12, 1591–1598. doi: 10.3892/etm.2016.3494

Kim, G. W., Lewén, A., Copin, J. C., Watson, B. D., and Chan, P. H. (2001). The cytosolic antioxidant, copper/zinc superoxide dismutase, attenuates blood-brain barrier disruption and oxidative cellular injury after photothrombotic cortical ischemia in mice. *Neuroscience* 105, 1007–1018. doi: 10.1016/s0306-4522(01)00237-8

Kim, S. Y., Senatorov, V. V., Morrissey, C. S., Lippmann, K., Vazquez, O., Milikovsky, D. Z., et al. (2017). TGFβ signaling is associated with changes in inflammatory gene expression and perineuronal net degradation around inhibitory neurons following various neurological insults. *Sci. Rep.* 7:7711. doi: 10.1038/s41598-017-07394-3

Lekoubou, A., Debroy, K., Kwegyir-Aggrey, A., Bonilha, L., Kengne, A., and Chinchilli, V. (2021). Risk models to predict late-onset seizures after stroke: a systematic review. *Epilepsy Behav.* 121:108003. doi: 10.1016/j.yebeh.2021.108003

Li, M., Li, Z., Yao, Y., Jin, W. N., Wood, K., Liu, Q., et al. (2017). Astrocyte-derived interleukin-15 exacerbates ischemic brain injury *via* propagation of cellular immunity. *Proc. Natl. Acad. Sci. U S A* 114, E396–E405. doi: 10.1073/pnas.1612930114

Li, S., Overman, J. J., Katsman, D., Kozlov, S. V., Donnelly, C. J., Twiss, J. L., et al. (2010). An age-related sprouting transcriptome provides molecular control of axonal sprouting after stroke. *Nat. Neurosci.* 13, 1496–1504. doi: 10.1038/nn.2674

Liimatainen, S., Fallah, M., Kharazmi, E., Peltola, M., and Peltola, J. (2009). Interleukin-6 levels are increased in temporal lobe epilepsy but not in extra-temporal lobe epilepsy. *J. Neurol.* 256, 796–802. doi: 10.1007/s00415-009-5021-x

Liu, T., Zhang, L., Joo, D., and Sun, S. C. (2017). NF-κB signaling in inflammation. *Signal Transduct. Target. Ther.* 2:17023. doi: 10.1038/sigtrans.2017.23

López, J., González, M. E., Lorigados, L., Morales, L., Riverón, G., and Bauzá, J. Y. (2007). Oxidative stress markers in surgically treated patients with refractory epilepsy. *Clin. Biochem.* 40, 292–298. doi: 10.1016/j.clinbiochem.2006.11.019

Marchi, N., Angelov, L., Masaryk, T., Fazio, V., Granata, T., Hernandez, N., et al. (2007). Seizure-promoting effect of blood-brain barrier disruption. *Epilepsia* 48, 732–742. doi: 10.1111/j.1528-1167.2007.00988.x

Marchi, N., Granata, T., Ghosh, C., and Janigro, D. (2012). Blood-brain barrier dysfunction and epilepsy: Pathophysiologic role and therapeutic approaches. *Epilepsia* 53, 1877–1886. doi: 10.1111/j.1528-1167.2012.03637.x

Marchi, N., Teng, Q., Ghosh, C., Fan, Q., Nguyen, M. T., Desai, N. K., et al. (2010). Blood-brain barrier damage, but not parenchymal white blood cells, is a hallmark of seizure activity. *Brain Res.* 1353, 176–186. doi: 10.1016/j.brainres.2010.06.051

Messé, S. R., Sansing, L. H., Cucchiara, B. L., Herman, S. T., Lyden, P. D., and Kasner, S. E. (2009). Prophylactic antiepileptic drug use is associated with poor outcome following ICH. *Neurocrit. Care* 11, 38–44. doi: 10.1007/s12028-009-9207-y

Minami, M., Kuraishi, Y., and Satoh, M. (1991). Effects of kainic acid on messenger RNA levels of IL-1 beta, IL-6, TNF alpha and LIF in the rat brain. *Biochem. Biophys. Res. Commun.* 176, 593–598. doi: 10.1016/s0006-291x(05)80225-6

Morin-Brureau, M., Lebrun, A., Rousset, M. C., Fagni, L., Bockaert, J., de Bock, F., et al. (2011). Epileptiform activity induces vascular remodeling and zonula occludens 1 downregulation in organotypic hippocampal cultures: Role of VEGF signaling pathways. *J. Neurosci.* 31, 10677–10688. doi: 10.1523/JNEUROSCI.5692-10.2011

Nayak, A. R., Kashyap, R. S., Kabra, D., Purohit, H. J., Taori, G. M., and Daginawala, H. F. (2012). Time course of inflammatory cytokines in acute ischemic stroke patients and their relation to inter-alfa trypsin inhibitor heavy chain 4 and outcome. *Ann. Indian Acad. Neurol.* 15, 181–185. doi: 10.4103/0972-2327.99707

Nguyen, T. V. V., Frye, J. B., Zbesko, J. C., Stepanovic, K., Hayes, M., Urzua, A., et al. (2016). Multiplex immunoassay characterization and species comparison of inflammation in acute and non-acute ischemic infarcts in human and mouse brain tissue. *Acta Neuropathol. Commun.* 4:100. doi: 10.1186/s40478-016-0371-y

Offner, H., and Hurn, P. D. (2012). A novel hypothesis: regulatory B lymphocytes shape outcome from experimental stroke. *Transl. Stroke Res.* 3, 324–330. doi: 10.1007/s12975-012-0187-4

Ormstad, H., Aass, H. C. D., Lund-Sørensen, N., Amthor, K. F., and Sandvik, L. (2011). Serum levels of cytokines and C-reactive protein in acute ischemic stroke patients and their relationship to stroke lateralization, type and infarct volume. *J. Neurol.* 258, 677–685. doi: 10.1007/s00415-011-6006-0

Overman, J. J., Clarkson, A. N., Wanner, I. B., Overman, W. T., Eckstein, I., Maguire, J. L., et al. (2012). A role for ephrin-A5 in axonal sprouting, recovery and activity-dependent plasticity after stroke. *Proc. Natl. Acad. Sci. U S A* 109, E2230–E2239. doi: 10.1073/pnas.1204386109

Paudel, Y., Semple, B., Jones, N., Othman, I., and Shaikh, M. (2019). High mobility group box 1 (HMGB1) as a novel frontier in epileptogenesis: from pathogenesis to therapeutic approaches. *J. Neurochem.* 151, 542–557. doi: 10.1111/jnc.14663

Pauletti, A., Terrone, G., Shekh-Ahmad, T., Salamone, A., Ravizza, T., Rizzi, M., et al. (2019). Targeting oxidative stress improves disease outcomes in a rat model of acquired epilepsy. *Brain* 142:e39. doi: 10.1093/brain/awz130

Pedre, L. L., Chacón, L. M. M., Fuentes, N. P., De Los Robinson Agramonte, M. A., Sánchez, T. S., Cruz-Xenes, R. M., et al. (2018a). Follow-up of peripheral IL-1β and IL-6 and relation with apoptotic death in drug-resistant temporal lobe epilepsy patients submitted to surgery. *Behav. Sci. (Basel)* 8:21. doi: 10.3390/bs8020021

Pedre, L. L., Gallardo, J. M., Chacón, L. M. M., García, A. V., Flores-Mendoza, M., Neri-Gómez, T., et al. (2018b). Oxidative stress in patients with drug resistant partial complex seizure. *Behav. Sci. (Basel)* 8:59. doi: 10.3390/bs8060059

Pekny, M., Pekna, M., Messing, A., Steinhäuser, C., Lee, J. M., Parpura, V., et al. (2016). Astrocytes: a central element in neurological diseases. *Acta Neuropathol.* 131, 323–345. doi: 10.1007/s00401-015-1513-1

Peltola, J., Palmio, J., Korhonen, L., Suhonen, J., Miettinen, A., Hurme, M., et al. (2000). Interleukin-6 and interleukin-1 receptor antagonist in cerebrospinal fluid from patients with recent tonic-clonic seizures. *Epilepsy Res.* 41, 205–211. doi: 10.1016/s0920-1211(00)00140-6

Pitkänen, A., Roivainen, R., and Lukasiuk, K. (2016). Development of epilepsy after ischaemic stroke. *Lancet Neurol.* 15, 185–197. doi: 10.1016/S1474-4422(15)00248-3

Pluta, R., Januszewski, S., and Czuczwar, S. J. (2021). Neuroinflammation in post-ischemic neurodegeneration of the brain: friend, foe, or both? *Int. J. Mol. Sci.* 22:4405. doi: 10.3390/ijms22094405

Proper, E. A., Oestreicher, A. B., Jansen, G. H., Veelen, C. W. M. v., van Rijen, P. C., Gispen, W. H., et al. (2000). Immunohistochemical characterization of mossy fibre sprouting in the hippocampus of patients with pharmaco-resistant temporal lobe epilepsy. *Brain* 123, 19–30. doi: 10.1093/brain/123.1.19

Raabe, A., Schmitz, A. K., Pernhorst, K., Grote, A., Von Der Brelie, C., Urbach, H., et al. (2012). Cliniconeuropathologic correlations show astroglial albumin storage as a common factor in epileptogenic vascular lesions. *Epilepsia* 53, 539–548. doi: 10.1111/j.1528-1167.2012.03405.x

Rana, A., and Musto, A. E. (2018). The role of inflammation in the development of epilepsy. *J. Neuroinflammation* 15:144. doi: 10.1186/s12974-018-1192-7

Reddy, D. S., Bhimani, A., Kuruba, R., Park, M. J., and Sohrabji, F. (2017). Prospects of modeling poststroke epileptogenesis. *J. Neurosci. Res.* 95, 1000–1016. doi: 10.1002/jnr.23836

Robel, S., and Sontheimer, H. (2015). Glia as drivers of abnormal neuronal activity. *Nat. Neurosci.* 19, 28–33. doi: 10.1038/nn.4184

Rolls, A., Shechter, R., and Schwartz, M. (2009). The bright side of the glial scar in CNS repair. *Nat. Rev. Neurosci.* 10, 235–241. doi: 10.1038/nrn2591

Roseti, C., Fucile, S., Lauro, C., Martinello, K., Bertollini, C., Esposito, V., et al. (2013). Fractalkine/CX3CL1 modulates GABAA currents in human temporal lobe epilepsy. *Epilepsia* 54, 1834–1844. doi: 10.1111/epi.12354

Schröder, W., Hinterkeuser, S., Seifert, G., Schramm, J., Jabs, R., Wilkin, G. P., et al. (2000). Functional and molecular properties of human astrocytes in acute hippocampal slices obtained from patients with temporal lobe epilepsy. *Epilepsia* 41, S181–S184. doi: 10.1111/j.1528-1157.2000.tb01578.x

Schwartz, J. P., and Nishiyama, N. (1994). Neurotrophic factor gene expression in astrocytes during development and following injury. *Brain Res. Bull.* 35, 403–407. doi: 10.1016/0361-9230(94)90151-1

Seneş, M., Kazan, N., Coşkun, O., Zengi, O., Inan, L., and Yücel, D. (2007). Oxidative and nitrosative stress in acute ischaemic stroke. *Ann. Clin. Biochem.* 44, 43–47. doi: 10.1016/S2665-9913(21)00315-5

Soriano, S. G., Amaravadi, L. S., Wang, Y. F., Zhou, H., Yu, G. X., Tonra, J. R., et al. (2002). Mice deficient in fractalkine are less susceptible to cerebral ischemia-reperfusion injury. *J. Neuroimmunol.* 125, 59–65. doi: 10.1016/s0165-5728(02)00033-4

Sotgiu, S., Zanda, B., Marchetti, B., Fois, M. L., Arru, G., Pes, G. M., et al. (2006). Inflammatory biomarkers in blood of patients with acute brain ischemia. *Eur. J. Neurol.* 13, 505–513. doi: 10.1111/j.1468-1331.2006.01280.x

Stellwagen, D., Beattie, E. C., Seo, J. Y., and Malenka, R. C. (2005). Differential regulation of AMPA receptor and GABA receptor trafficking by tumor necrosis factor-α. *J. Neurosci.* 25, 3219–3228. doi: 10.1523/JNEUROSCI.4486-04.2005

Strzelczyk, A., Haag, A., Raupach, H., Herrendorf, G., Hamer, H. M., and Rosenow, F. (2010). Prospective evaluation of a post-stroke epilepsy risk scale. *J. Neurol.* 257, 1322–1326. doi: 10.1007/s00415-010-5520-9

Tan, T.-Y., Lu, C.-H., Chuang, H.-Y., Lin, T.-K., Liou, C.-W., Chang, W.-N., et al. (2009). Long-term antiepileptic drug therapy contributes to the acceleration of atherosclerosis. *Epilepsia* 50, 1579–1586. doi: 10.1111/j.1528-1167.2009.02024.x

Tarkowski, E., Rosengren, L., Blomstrand, C., Wikkelso, C., Jensen, C., Ekholm, S., et al. (1995). Early intrathecal production of interleukin-6 predicts the size of brain lesion in stroke. *Stroke* 26, 1393–1398. doi: 10.1161/01.str.26.8.1393

Terrone, G., Balosso, S., Pauletti, A., Ravizza, T., and Vezzani, A. (2019). Inflammation and reactive oxygen species as disease modifiers in epilepsy. *Neuropharmacology* 167:107742. doi: 10.1016/j.neuropharm.2019.107742

Thevathasan, A., Naylor, J., Churilov, L., Mitchell, P. J., Dowling, R. J., Yan, B., et al. (2018). Association between hemorrhagic transformation after endovascular therapy and poststroke seizures. *Epilepsia* 59, 403–409. doi: 10.1111/epi.13982

Thom, M. (2014). Review: hippocampal sclerosis in epilepsy: a neuropathology review. *Neuropathol. Appl. Neurobiol.* 40, 520–543. doi: 10.1111/nan.12150

Tomkins, O., Shelef, I., Kaizerman, I., Eliushin, A., Afawi, Z., Misk, A., et al. (2008). Blood-brain barrier disruption in post-traumatic epilepsy. *J. Neurol. Neurosurg. Psychiatry* 79, 774–777. doi: 10.1136/jnnp.2007.126425

Tröscher, A. R., Sakaraki, E., Mair, K. M., Köck, U., Racz, A., Borger, V., et al. (2021). T cell numbers correlate with neuronal loss rather than with seizure activity in medial temporal lobe epilepsy. *Epilepsia* 62, 1343–1353. doi: 10.1111/epi.16914

Tröscher, A. R., Wimmer, I., Quemada-Garrido, L., Köck, U., Gessl, D., Verberk, S. G. S., et al. (2019). Microglial nodules provide the environment for pathogenic T cells in human encephalitis. *Acta Neuropathol.* 137, 619–635. doi: 10.1007/s00401-019-01958-5

Tsukagawa, T., Katsumata, R., Fujita, M., Yasui, K., Akhoon, C., Ono, K., et al. (2017). Elevated serum high-mobility group box-1 protein level is associated with poor functional outcome in ischemic stroke. *J. Stroke Cerebrovasc. Dis.* 26, 2404–2411. doi: 10.1016/j.jstrokecerebrovasdis.2017.05.033

Valliéres, L., Campbell, I. L., Gage, F. H., and Sawchenko, P. E. (2002). Reduced hippocampal neurogenesis in adult transgenic mice with chronic astrocytic production of interleukin-6. *J. Neurosci.* 22, 486–492. doi: 10.1523/JNEUROSCI.22-02-00486.2002

van Vliet, E. A., Araújo, S. D. C., Redeker, S., van Schaik, R., Aronica, E., Gorter, J. A., et al. (2007). Blood-brain barrier leakage may lead to progression of temporal lobe epilepsy. *Brain* 130, 521–534. doi: 10.1093/brain/awl318

Vecchio, F., Tomino, C., Miraglia, F., Iodice, F., Erra, C., Di Iorio, R., et al. (2019). Cortical connectivity from EEG data in acute stroke: A study *via* graph theory as a potential biomarker for functional recovery. *Int. J. Psychophysiol.* 146, 133–138. doi: 10.1016/j.ijpsycho.2019.09.012

Vezzani, A., Balosso, S., and Ravizza, T. (2019). Neuroinflammatory pathways as treatment targets and biomarkers in epilepsy. *Nat. Rev. Neurol.* 15, 459–472. doi: 10.1038/s41582-019-0217-x

Vezzani, A., Conti, M., De Luigi, A., Ravizza, T., Moneta, D., Marchesi, F., et al. (1999). Interleukin-1beta immunoreactivity and microglia are enhanced in the rat hippocampus by focal kainate application: functional evidence for enhancement of electrographic seizures. *J. Neurosci.* 19, 5054–5065. doi: 10.1523/JNEUROSCI.19-12-05054.1999

Vezzani, A., French, J., Bartfai, T., and Baram, T. Z. (2011a). The role of inflammation in epilepsy. *Nat. Rev. Neurol.* 7, 31–40. doi: 10.1038/nrneurol.2010.178

Vezzani, A., Maroso, M., Balosso, S., Sanchez, M. A., and Bartfai, T. (2011b). IL-1 receptor/Toll-like receptor signaling in infection, inflammation, stress and neurodegeneration couples hyperexcitability and seizures. *Brain Behav. Immun.* 25, 1281–1289. doi: 10.1016/j.bbi.2011.03.018

Vezzani, A., Moneta, D., Conti, M., Richichi, C., Ravizza, T., De Luigi, A., et al. (2000). Powerful anticonvulsant action of IL-1 receptor antagonist on intracerebral injection and astrocytic overexpression in mice. *Proc. Natl. Acad. Sci. U S A* 97, 11534–11539. doi: 10.1073/pnas.190206797

Viviani, B., Bartesaghi, S., Gardoni, F., Vezzani, A., Behrens, M. M., Bartfai, T., et al. (2003). Interleukin-1β enhances NMDA receptor-mediated intracellular calcium increase through activation of the Src family of kinases. *J. Neurosci.* 23, 8692–8700. doi: 10.1523/JNEUROSCI.23-25-08692.2003

Wahl, A. S., Büchler, U., Brändli, A., Brattoli, B., Musall, S., Kasper, H., et al. (2017). Optogenetically stimulating intact rat corticospinal tract post-stroke restores motor control through regionalized functional circuit formation. *Nat. Commun.* 8:1187. doi: 10.1038/s41467-017-01090-6

Wahl, A. S., Omlor, W., Rubio, J. C., Chen, J. L., Zheng, H., Schröter, A., et al. (2014). Asynchronous therapy restores motor control by rewiring of the rat corticospinal tract after stroke. *Science* 344, 1250–1255. doi: 10.1126/science.1253050

Wang, H., Song, G., Chuang, H., Chiu, C., Abdelmaksoud, A., Ye, Y., et al. (2018). Portrait of glial scar in neurological diseases. *Int. J. Immunopathol. Pharmacol.* 31:2058738418801406. doi: 10.1177/2058738418801406

Wang, J. Z., Vyas, M. V., Saposnik, G., and Burneo, J. G. (2017). Incidence and management of seizures after ischemic stroke. *Neurology* 89, 1220–1228. doi: 10.1212/WNL.0000000000004407

Wilcox, K. S., and Vezzani, A. (2014). Does brain inflammation mediate pathological outcomes in epilepsy? *Adv. Exp. Med. Biol.* 813, 169–183. doi: 10.1007/978-94-017-8914-1_14

Williams, A. J., and Tortella, F. C. (2002). Neuroprotective effects of the sodium channel blocker RS100642 and attenuation of ischemia-induced brain seizures in the rat. *Brain Res.* 932, 45–55. doi: 10.1016/s0006-8993(02)02275-8

Wimmer, I., Zrzavy, T., and Lassmann, H. (2018). Neuroinflammatory responses in experimental and human stroke lesions. *J. Neuroimmunol.* 323, 10–18. doi: 10.1016/j.jneuroim.2018.07.003

Wu, Y., Wang, X., Mo, X., Xi, Z., Xiao, F., Li, J., et al. (2008). Expression of monocyte chemoattractant protein-1 in brain tissue of patients with intractable epilepsy. *Clin. Neuropathol.* 27, 55–63. doi: 10.5414/npp27055

Xu, M. Y. (2019). Poststroke seizure: optimising its management. *Stroke Vasc. Neurol.* 4, 48–56. doi: 10.1136/svn-2018-000175

Xu, J. H., Long, L., Tang, Y. C., Zhang, J. T., Hu, H. T., and Tang, F. R. (2009). CCR3, CCR2A and macrophage inflammatory protein (MIP)-1α, monocyte chemotactic protein-1 (MCP-1) in the mouse hippocampus during and after pilocarpine-induced status epilepticus (PISE). *Neuropathol. Appl. Neurobiol.* 35, 496–514. doi: 10.1111/j.1365-2990.2009.01022.x

Xu, T., Wang, Y., Yuan, J., Chen, Y., and Luo, H. (2020). Statin use and the risk of post-stroke seizures: a meta-analysis. *Seizure* 83, 63–69. doi: 10.1016/j.seizure.2020.10.004

Yang, C., Hawkins, K. E., Doré, S., and Candelario-Jalil, E. (2019). Neuroinflammatory mechanisms of blood-brain barrier damage in ischemic stroke. *Am. J. Physiol. Cell Physiol.* 316, C135–C153. doi: 10.1152/ajpcell.00136.2018

Yang, Y., and Rosenberg, G. A. (2011). Blood-brain barrier breakdown in acute and chronic cerebrovascular disease. *Stroke* 42, 3323–3328. doi: 10.1161/STROKEAHA.110.608257

Zelano, J., Holtkamp, M., Agarwal, N., Lattanzi, S., Trinka, E., and Brigo, F. (2020). How to diagnose and treat post-stroke seizures and epilepsy. *Epileptic Disord.* 22, 252–263. doi: 10.1684/epd.2020.1159

Zhang, Z. G., and Chopp, M. (2009). Neurorestorative therapies for stroke: underlying mechanisms and translation to the clinic. *Lancet Neurol.* 8, 491–500. doi: 10.1016/S1474-4422(09)70061-4

Zrzavy, T., Machado-Santos, J., Christine, S., Baumgartner, C., Weiner, H. L., Butovsky, O., et al. (2017). Dominant role of microglial and macrophage innate immune responses in human ischemic infarcts. *Brain Pathol.* 28, 791–805. doi: 10.1111/bpa.12583

Zurolo, E., Iyer, A., Maroso, M., Carbonell, C., Anink, J. J., Ravizza, T., et al. (2011). Activation of toll-like receptor, RAGE and HMGB1 signalling in malformations of cortical development. *Brain* 134, 1015–1032. doi: 10.1093/brain/awr032

Conflict of Interest: JW reports personal fees from UCB and Boehringer Ingelheim and non-financial support from Roche, outside the submitted work; TO reports personal fees and non-financial support from Eisai Pharma GmbH Vienna, grants, personal fees, and non-financial support from UCB Pharma GmbH Vienna, non-financial support from Medtronic Austria GmbH, grants, personal fees, and non-financial support from Novartis Pharma, personal fees from Roche Pharma, personal fees from Biogen Idec Austria, personal fees from Liva Nova, personal fees from Sanofi-Aventis GmbH, grants from Grossegger & Drbal GmbH, outside the submitted work.

The remaining authors declare that the research was conducted in the absence of any commercial or financial relationships that could be construed as a potential conflict of interest.

Publisher's Note: All claims expressed in this article are solely those of the authors and do not necessarily represent those of their affiliated organizations, or those of the publisher, the editors and the reviewers. Any product that may be evaluated in this article, or claim that may be made by its manufacturer, is not guaranteed or endorsed by the publisher.

frontiers in Cellular Neuroscience

MINI REVIEW
published: 24 March 2022
doi: 10.3389/fncel.2022.852151

The Potential of Circulating Cell-Free DNA Methylation as an Epilepsy Biomarker

Ricardo Martins-Ferreira[1,2,3,4], *Bárbara Guerra Leal*[2,3,4]* *and Paulo Pinho Costa*[2,3,4,5]

[1]*Epigenetics and Immune Disease Group, Josep Carreras Research Institute (IJC), Barcelona, Spain,* [2]*Immunogenetics Lab, Molecular Pathology and Immunology, Instituto de Ciências Biomédicas Abel Salazar—Universidade do Porto (ICBAS-UPorto), Porto, Portugal,* [3]*Autoimmunity and Neuroscience Group, Unit for Multidisciplinary Research in Biomedicine (UMIB), ICBAS-UPorto, Porto, Portugal,* [4]*Laboratory for Integrative and Translational Research in Population Health (ITR), Porto, Portugal,* [5]*Instituto Nacional de Saúde Dr. Ricardo Jorge, Department of Human Genetics, Porto, Portugal*

Circulating cell-free DNA (cfDNA) are highly degraded DNA fragments shed into the bloodstream. Apoptosis is likely to be the main source of cfDNA due to the matching sizes of cfDNA and apoptotic DNA cleavage fragments. The study of cfDNA in liquid biopsies has served clinical research greatly. Genetic analysis of these circulating fragments has been used in non-invasive prenatal testing, detection of graft rejection in organ transplants, and cancer detection and monitoring. cfDNA sequencing is, however, of limited value in settings in which genetic association is not well-established, such as most neurodegenerative diseases.Recent studies have taken advantage of the cell-type specificity of DNA methylation to determine the tissue of origin, thus detecting ongoing cell death taking place in specific body compartments. Such an approach is yet to be developed in the context of epilepsy research. In this article, we review the different approaches that have been used to monitor cell-type specific death through DNA methylation analysis, and recent data detecting neuronal death in neuropathological settings. We focus on the potential relevance of these tools in focal epilepsies, like Mesial Temporal Lobe Epilepsy with Hippocampal Sclerosis (MTLE-HS), characterized by severe neuronal loss. We speculate on the potential relevance of cfDNA methylation screening for the detection of neuronal cell death in individuals with high risk of epileptogenesis that would benefit from early diagnosis and consequent early treatment.

Keywords: cell-free DNA, DNA methylation, epilepsy, epileptogenesis, MTLE-HS, biomarker

OPEN ACCESS

Edited by:
Diana Cunha-Reis, University of Lisbon, Portugal

Reviewed by:
Ana Laura Márquez-Aguirre, CONACYT Centro de Investigación y Asistencia en Tecnología y Diseño del Estado de Jalisco (CIATEJ), Mexico

***Correspondence:**
Bárbara Guerra Leal
baguerraleal@gmail.com

Specialty section:
This article was submitted to Cellular Neuropathology, a section of the journal Frontiers in Cellular Neuroscience

Received: *10 January 2022*
Accepted: *24 February 2022*
Published: *24 March 2022*

Citation:
Martins-Ferreira R, Leal BG and Costa PP (2022) The Potential of Circulating Cell-Free DNA Methylation as an Epilepsy Biomarker. Front. Cell. Neurosci. 16:852151. doi: 10.3389/fncel.2022.852151

INTRODUCTION

The search for effective biomarkers is one of the most challenging tasks in epilepsy research. Epileptogenesis is now considered a progressive process, with seizure activity contributing to extensive damage and seizure recurrence (Pitkänen et al., 2015). Epilepsy diagnosis must thus be viewed as a race against the clock, aiming for the detection, as early as possible, of individuals

Abbreviations: cfDNA, cell-free DNA; DMP, differentially methylated position; DMR, differentially methylated region; HS, hippocampal sclerosis; MTLE, mesial temporal lobe epilepsy.

with a high risk of epilepsy development, that could be candidates for preventive pharmacological intervention. The search for novel viable biomarkers is considered crucial to improve the current hurdles to early diagnosis and prognostic monitoring in epileptic patients. A major issue continues to be the high refractoriness rates (estimated at 30%) across different types of epilepsy (Pitkänen et al., 2016). Epilepsy treatment is based on the control of ictogenesis. Current anti-seizure drugs target seizure control and are not directed to the whole epileptogenic landscape. Additionally, such biomarkers would facilitate economically feasible clinical trials for the development of new and more effective anti-epileptic therapies by allowing a more precise categorization of individuals with high probability of developing epilepsy (Engel and Pitkänen, 2020).

Nucleic acid-based disease biomarkers have represented one of the most exciting developments in recent years, with non-coding RNAs, specifically microRNAs, gaining center stage (Henshall et al., 2016). In this review, we consider the potential of the still largely unexplored circulating cell-free (cf) DNA. We will focus on cfDNA methylation and its ability to predict cell and tissue of origin in epilepsies with a histopathological phenotype of neuronal damage and death.

BIOGENESIS AND THE APOPTOTIC CASCADE

The first description of cfDNA in human plasma dates to 1948 (Mandel and Metais, 1948). Nowadays, it is broadly described as highly degraded DNA fragments circulating freely in the peripheral blood. However, the full spectrum of processes responsible for cfDNA production and release remains elusive. There is a perception that cfDNA may be originated from countless biological features, both physiological and pathological, such as inflammation, aging, exercise, or cancer. The main mechanisms of cfDNA release are considered to be active release or cellular breakdown (Aucamp et al., 2018). The overall conception, on which most of the studies in this field base their hypotheses, is that cfDNA originates predominantly from apoptosis. This relies on the matching sizes between cfDNA and DNA fragments resultant from the apoptotic cascade. Caspase-activated DNase is one of the main effectors of DNA fragmentation during apoptosis. It is a double-stranded endonuclease which lacks exonuclease activity, thus being only capable of fragmenting DNA in inter-nucleosomal linker regions (Heitzer et al., 2020). Human circulating cfDNA presents a predominant and consistent fragment length of approximately 167 bp (Snyder et al., 2016), which corresponds to the length of DNA wrapped around a nucleosome (∼147 bp) plus linker fragments (Heitzer et al., 2020).

GENETIC SEQUENCING AND LIQUID BIOPSIES

In practice, the study of cfDNA has consisted predominantly of its genetic characterization. Sequencing of cfDNA is nowadays routinely used in some clinic settings. Screening of fetal DNA circulating in the mother's bloodstream, non-invasive prenatal testing, is used to detect chromosomal abnormalities (Fan et al., 2012). Transplant graft rejection is also monitored by the detection of donor-derived cfDNA sequences (De Vlaminck et al., 2014). Throughout the last two decades, cfDNA sequencing has been increasingly applied to cancer detection (Chabon et al., 2020) and also in post-therapy prognosis (Nabet et al., 2020; Powles et al., 2021). These liquid biopsies provide for non-invasive detection of tumor DNA in biological fluids, also denominated as circulating tumor DNA.

The relevance and potential of cfDNA does not end in its genetics, though. The utility of nucleotide sequencing is narrow in non-mutation rich pathologies, meaning conditions in which a clear association with a mutated genetic profile is not observed. These include a considerable number of neurodegenerative diseases such as, in the interest of this review, different forms of epilepsy.

DECONVOLUTING CELL-OF-ORIGIN THROUGH DNA METHYLATION

The strong association between cfDNA and apoptosis suggests the occurrence of cell death somewhere in the organism. However, genetic screening of the circulating DNA is unable to specifically identify tissue or cell of origin. In this context, epigenetics and, specifically, DNA methylation have entered and significantly upgraded cfDNA research. DNA methylation consists of the covalent addition of a methyl group to cytosine residues in the genomic sequence. It occurs predominantly in CpG dinucleotides and is associated with transcriptional regulation. Certain patterns of DNA methylation are highly tissue and cell-specific and conserved in both physiologic and pathologic conditions (Dor and Cedar, 2018; **Figure 1**).

Alterations of DNA methylation in cfDNA may result from alterations in specific cells or tissue between the pathologic and disease-free settings. Additionally, it can also originate from changes in the composition of cfDNA due to differential cell death rates (**Figure 1**). The analysis of the cfDNA methylome has been conducted in two main lines of thought. The first opts for directly calculating differential methylation patterns, such as differentially methylated positions (DMPs) and differentially methylated regions (DMRs) between different conditions (Hatt et al., 2015; Jensen et al., 2015; Legendre et al., 2015; Xu et al., 2017; Gallardo-Gómez et al., 2018; Gordevičius et al., 2018). However, the direct usage of cfDNA profiles as predictors may be associated with an increased signal-to-noise ratio, since DMPs and even DMRs can be non-specifical and more difficult to interpret biologically. Cell or tissue-of-origin estimation may be considered as a reduction step, decreasing background noise, and increasing prediction accuracy (Feng et al., 2019). Prediction of cfDNA origin can be approached through two different strategies. The first consists of targeted DNA methylation analysis, that is predicting cell-of-origin by searching for previously identified specific DNA methylation alterations characteristic of a cell type (DMPs and DMRs). This approach has been applied throughout a wide spectrum of settings, including the detection of cfDNA derived from pancreatic β-cell in Type 1 diabetic patients

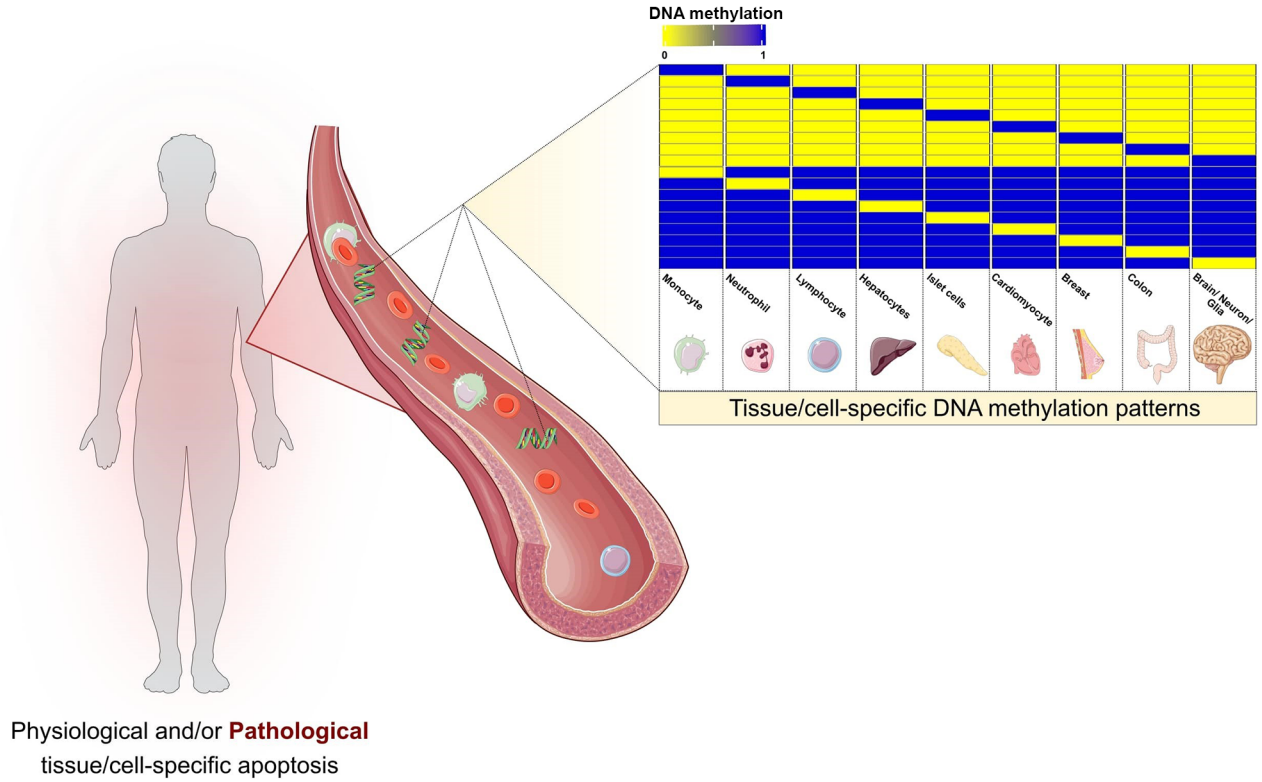

FIGURE 1 | Cell damage and apoptotic events during both physiological and pathological conditions are thought to release cell-free DNA (cfDNA) into the bloodstream. The pool of cfDNA in circulation present specific DNA methylation patterns that would allow the detection and localization of cell death, opening the doors for a wide spectrum of prospective clinical applications. The selected cell and tissue types are intended to be representative. Hematopoietic cells, the main contributors to cfDNA release, are depicted by monocytes, neutrophils, and lymphocytes. Hepatocytes, pancreatic islet cells, cardiomyocytes, breast, and colon are some examples of tissues with previous evidence on the estimation of cell/tissue of origin based on cfDNA methylation. Brain, neurons, and glia represent the potential of applying such pipelines in neurodegenerative diseases.

(Olsen et al., 2016a), cardiomyocytes in cardiac infarction and sepsis patients (Zemmour et al., 2018) and hepatocytes in liver transplant recipients, individuals who underwent hepatectomy and sepsis patients (Lehmann-Werman et al., 2018). The second approach consists of genome-wide deconvolution tools that have been developed to simultaneously estimate the percentages of the contribution of multiple tissue and cell types to circulating cfDNA. Deconvolution algorithms have been predominantly used in cancer DNA methylation research (Sun et al., 2015; Guo et al., 2017; Kang et al., 2017; Li et al., 2018). A study by Moss et al. (2018) developed a comprehensive reference-based deconvolution tool accounting for a total of 25 cell/tissue types obtained from 450k and EPIC arrays of primary tissue sources. They validated the previous conception that cfDNA in plasma of healthy individuals as originating predominantly from hematopoietic cells. Furthermore, the authors demonstrated promising results in pathological contexts, by detecting increased plasma cfDNA of pancreatic origin in islet transplant recipients, significant correlation of hepatocyte-derived cfDNA and clinical liver damage markers, and detection of tissue-specific cfDNA in three cancer settings (colon, lung, and breast). Interestingly, cfDNA estimated origin showed good prognostic ability in prostate cancer patients after treatment, and also showed promise in the prediction of tissue of origin in cancer patients with no clear primary (Cancer of Unknown Primary; Moss et al., 2018). An additional interesting aspect of this study is the fact that this deconvolution algorithm accounts for primary cortical neurons, thus allowing its usage in detecting neuronal cell death across neurodegenerative diseases.

BRAIN-DERIVED cfDNA IN NEURODEGENERATION

The application of cfDNA methylation-based analysis to neurodegenerative pathologies are still in their infancy. Research has consisted mostly of target-based studies, meaning that the detection of circulating brain-derived DNA relies on precisely measuring small regions, with specifically differential methylation behavior in the CNS in comparison to other tissues, mainly hematopoietic cells. A summary of the current data on CNS-derived cfDNA in a neurodegenerative context is presented in **Table 1**. The first such study that we are aware of is one by Lehmann-Werman et al. (2016), in which the authors first identified a pattern of clear demethylation in two clusters of CpGs in sorted oligodendrocytes' methylome (located at the *MBP3* gene and in an unannotated region). By

TABLE 1 | Evidence of CNS-derived cfDNA in neurodegenerative settings.

Condition	Cell or tissue of origin	DNA methylation pattern	Approach	Methodology	Reference
MS	Oligodendrocyte	Demethylation at *MBP3* and unannotated region (CG10809560, *Illumina annotation*)	Target-specific	Bisulfite sequencing	Lehmann-Werman et al. (2016)
Cardiac arrest with brain damage	Brain	Demethylation at unannotated region (CG09787504, *Illumina annotation*)	Target-specific	Bisulfite sequencing	Lehmann-Werman et al. (2016)
TBI	Brain	Demethylation at unannotated region (CG09787504, *Illumina annotation*)	Target-specific	Bisulfite sequencing	Lehmann-Werman et al. (2016)
MS	Oligodendrocyte	Demethylation at *MOG*	Target-specific	Methylation-specific PCR	Olsen et al. (2016b)
ALS	Brain	Increased methylation at *RHBDF* promoter	Target-specific	Bisulfite sequencing	Mendioroz et al. (2018)
AD	Brain	Increased methylation at *LHX2*	Target-specific	Bisulfite sequencing	Pai et al. (2019)
Explosive course trainees	Neuron and glia	Differential DNA methylation in 33 regions	Multi-targeted	Bisulfite amplicon sequencing	Chatterton et al. (2021)

AD, Alzheimer's disease; ALS, Amyotrophic lateral sclerosis; MS, Multiple Sclerosis; TBI, Traumatic Brain Injury.

bisulfite sequencing such regions, they described increased oligodendrocyte-derived cfDNA in serum or plasma of multiple sclerosis patients. Using the same strategy (known unmethylation of a cluster of nine CpGs of brain tissue), they observed an increase in brain-derived cfDNA in cardiac arrest patients with documented brain damage, and also in traumatic brain injury patients (Lehmann-Werman et al., 2016). In line with this, Olsen et al. (2016b) demonstrated increased demethylation of the *MOG* gene in sera of active multiple sclerosis patients. In amyotrophic lateral sclerosis patients, plasma cfDNA methylation levels of the *RHBDF* promoter were increased, relative to healthy controls (Mendioroz et al., 2018). Lastly, Alzheimer's patients have been shown to have higher levels of *LHX2* methylation in plasma-extracted cfDNA (Pai et al., 2019).

In a more technically evolved and encompassing study, Chatterton et al. (2021) achieved an interesting proof-of-concept in which they were able to detect neuron and glia-derived cfDNA in human plasma samples. They developed a bisulfite amplicon sequencing protocol of a total of 33 regions with neuron and glial-specific DNA methylation patterns identified with an in-house pipeline from 450k microarray profiles. In blood plasma samples of entry personnel during a training course using explosives, the authors report evidence of neuron and glial cfDNA. Furthermore, significantly increased levels of neuron-derived cfDNA were observed on the day of training in which exposure to higher pressures was experienced (Chatterton et al., 2021).

Tissue biopsies are extremely invasive and, in the case of neurologic conditions, particularly inaccessible. Cerebrospinal fluid (CSF) analysis is an option but still causes major discomfort to patients. Along the neurodegeneration spectrum, there are multiple profiles of neurotrauma and damage. One can infer that CNS-derived cfDNA shed into the bloodstream may become a more accessible and interpretable tool for neurodegenerative biomarker research.

POTENTIAL OF cfDNA METHYLOME PROFILING IN EPILEPSY

To the best of our knowledge, to date, there are only two studies on cfDNA studies in epilepsy. Both analyzing the concentration of cfDNA. Liimatainen et al. (2013) observed increased sera cfDNA concentration in 167 focal epilepsy patients vs. 250 healthy controls. Alapirtti et al. (2016) on the other hand, failed to verify differences between 52 refractory epilepsy patients (both focal and generalized) and 250 controls. One of the limitations of these studies is the heterogeneity of the studied populations, which include a large spectrum of epileptic syndromes. Given the variability within epilepsies and the increasingly evident differing etiopathogenic fingerprints between syndromes, more narrowly specified epilepsy cohorts would be of more relevance.

As for cfDNA methylation, nothing has, to the best of our knowledge, been reported yet. Nonetheless, altered DNA methylation patterns in brain tissue of epilepsy patients have been consistently described (Miller-Delaney et al., 2012; Liu et al., 2016; Wang et al., 2016; Zhang et al., 2021; Martins-Ferreira et al., 2022). Major efforts have been made for the use of DNA methylation as peripheral biomarkers, namely by demonstrating the correlation of DNA methylation patterns in brain tissue and peripheral tissues, such as blood, saliva, and buccal mucosa (Braun et al., 2019). Reinforcing the aforementioned idea, cfDNA methylation may be more representative of a specific pathological

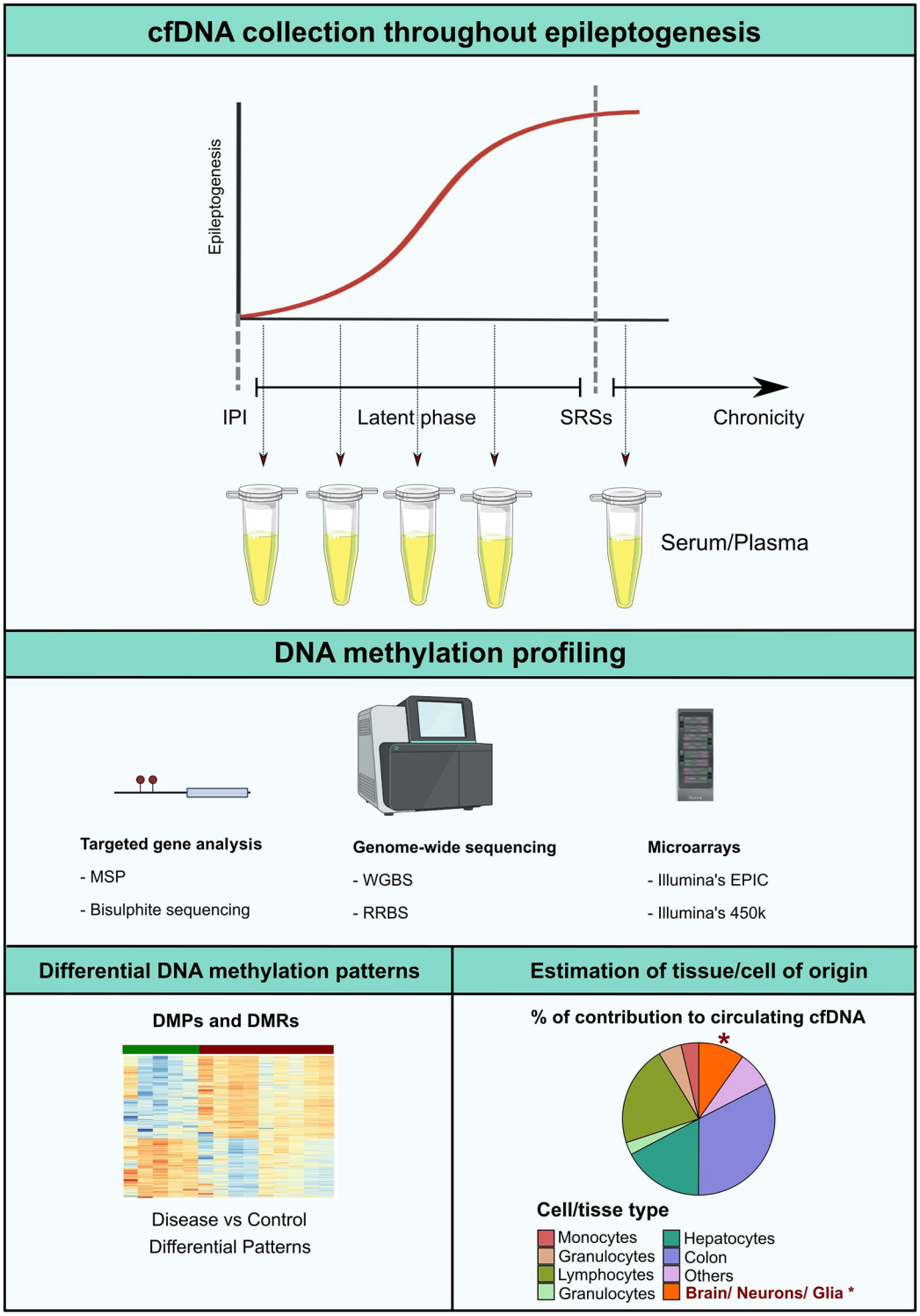

FIGURE 2 | Epileptogenesis is considered to follow a progressive model. After the initial precipitating injury (IPI), the brain parenchyma enters a latent phase in which the ability to generate spontaneous recurrent seizures (SRSs) is established. In the chronic stage, upon initiation of unprovoked seizure activity, epileptogenic molecular and structural remodeling progress with time. DNA methylation profiling along the different timeframes of epileptogenesis would potentially represent a valuable approach for the development of novel non-invasive biomarkers. Possible analytical strategies include detection of altered cfDNA methylation patterns in pathological settings in comparison to controls, or estimation of the percentage of tissue or cell type contribution to the circulating cfDNA pool, which potentially insights on occurring CNS-specific cell death in the early stages of the disease. MSP, Methylation-Specific PCR; RRBS, reduced representation bisulfite sequencing; WBGS, whole genome bisulfite sequencing.

phenotype due to the link between cfDNA methylome, differing of tissue/cell contribution, and pattern of cell death, as described throughout this review.

Mesial Temporal Lobe Epilepsy (MTLE) is one of the most studied epilepsies due to its high incidence (it is the most common focal epilepsy in adults) and its high refractoriness rates. Hippocampal sclerosis is the most prevalent histopathological feature in MTLE. It is characterized by an exacerbated state of gliosis and a severe neuronal death landscape in the mesial temporal regions (Blümcke et al., 2013). A pertinent question regarding MTLE's etiopathology is the time frame of HS occurrence. It has been considered a consequence of recurrent exposure to seizure activity. However, it can also be speculated that HS may have a role in promoting pro-epileptogenic activity onset and progression. This is, in part, due to the fact that the diagnosis often occurs in the chronic stage, upon the appearance of spontaneous recurrent seizures. The most recently reviewed definition of epileptogenesis describes it as a continuous event. After the initial precipitating injury, the brain undergoes a latent phase in which the ability to produce spontaneous recurrent seizures is acquired. The chronic stage, initiated upon the first unprovoked seizure, is no longer considered stationary, as was previously the case. It is rather a progressive phenomenon, with pathological molecular and cellular alterations extending as the disease progresses (Pitkänen et al., 2016). A recent study by our group has demonstrated major DNA methylation alterations in both hippocampus and anterior temporal neocortex of MTLE-HS patients in comparison to autopsied non-epileptic controls, with enrichment for a wide spectrum of epileptogenesis-related pathways. Additionally, we demonstrate a potential progressive remodeling of DNA methylation in inflammatory genes with increased disease duration (Martins-Ferreira et al., 2022).

The main argument of interest of this review focus on the fact that cell death occurs in the MTLE-HS brain. Despite the time-point at which it may be occurring. Thus, it is plausible that neuron- or glia-derived cfDNA may be released into the circulation during neuro damage. We call for novel cfDNA methylation screening studies in epileptic patients, from targeted approaches like bisulfite sequencing and methylation-specific PCR to genome-wide screenings using microarrays, whole-genome bisulfite sequencing, and reduced representation bisulfite sequencing. Such studies would be potentially helpful in all stages of the epileptogenic landscape. It could promote detection of patients at high risk of epileptogenesis after a brain trauma incident and during latency, facilitate earlier diagnosis and better monitoring, and provide for therapeutic outcome prediction (**Figure 2**).

CONCLUDING REMARKS

The research on circulating cfDNA has evolved exponentially during the last decades, from the proven clinical utility of genetic characterization to the emerging applications of DNA methylation. Identification of biomarkers is an urgent need across various pathologies, particularly in neurologic diseases in which tissue biopsies are extremely difficult to obtain or simply inaccessible. We propose that cfDNA methylation should be investigated in epileptic patients, as we consider it to be and intriguing and promising beam of light in what has been the gloomy field of epilepsy biomarker research.

AUTHOR CONTRIBUTIONS

All authors were responsible for the development of the conceptual map. RM-F performed literature search and drafted the manuscript. BL and PC were responsible for the critical revision and final approval of the final version to be published. All authors contributed to the article and approved the submitted version.

FUNDING

RM-F was funded by an FCT (Fundação para a Ciência e Tecnologia) fellowship (grant number SFRH/BD/137900/2018). Unit for Multidisciplinary Research in Biomedicine (UMIB) was funded by FCT Portugal (grant numbers UIDB/00215/2020 and UIDP/00215/2020), and Laboratory for Integrative and Translational Research in Population Health (ITR) (LA/P/0064/2020).

ACKNOWLEDGMENTS

We acknowledge Professor Berta Martins da Silva and the remaining members of the Immunogenetics Laboratory of the Molecular Pathology and Immunology Department of ICBAS-UP. We thank the Neurology, Neurophysiology and Neurosurgery Departments of *Hospital de Santo António—Centro Hospitalar e Universitário do Porto*. We also acknowledge Professor Esteban Ballestar and all members of Epigenetics and Immune Disease of the Josep Carreras Research Institute (IJC).

REFERENCES

Alapirtti, T., Jylhävä, J., Raitanen, J., Mäkinen, R., Peltola, J., Hurme, M. A., et al. (2016). The concentration of cell-free DNA in video-EEG patients is dependent on the epilepsy syndrome and duration of epilepsy. *Neurol. Res.* 38, 45–50. doi: 10.1080/01616412.2015.1127004

Aucamp, J., Bronkhorst, A. J., Badenhorst, C. P. S., and Pretorius, P. J. (2018). The diverse origins of circulating cell-free DNA in the human body: a critical re-evaluation of the literature. *Biol. Rev. Camb. Philos. Soc.* 93, 1649–1683. doi: 10.1111/brv.12413

Blümcke, I., Thom, M., Aronica, E., Armstrong, D. D., Bartolomei, F., Bernasconi, A., et al. (2013). International consensus classification of hippocampal sclerosis in temporal lobe epilepsy: a task force report from the ILAE commission on diagnostic methods. *Epilepsia* 54, 1315–1329. doi: 10.1111/epi.12220

Braun, P. R., Han, S., Hing, B., Nagahama, Y., Gaul, L. N., Heinzman, J. T., et al. (2019). Genome-wide DNA methylation comparison between live human brain and peripheral tissues within individuals. *Transl. Psychiatry* 9:47. doi: 10.1038/s41398-019-0376-y

Chabon, J. J., Hamilton, E. G., Kurtz, D. M., Esfahani, M. S., Moding, E. J., Stehr, H., et al. (2020). Integrating genomic features for non-invasive early lung cancer detection. *Nature* 580, 245–251. doi: 10.1038/s41586-020-2140-0

Chatterton, Z., Mendelev, N., Chen, S., Carr, W., Kamimori, G. H., Ge, Y., et al. (2021). Bisulfite amplicon sequencing can detect glia and neuron cell-free DNA in blood plasma. *Front. Mol. Neurosci.* 14:672614. doi: 10.3389/fnmol.2021.672614

Dor, Y., and Cedar, H. (2018). Principles of DNA methylation and their implications for biology and medicine. *Lancet* 392, 777–786. doi: 10.1016/S0140-6736(18)31268-6

Engel, J, Jr., and Pitkänen, A. (2020). Biomarkers for epileptogenesis and its treatment. *Neuropharmacology* 167:107735. doi: 10.1016/j.neuropharm.2019.107735

Fan, H. C., Gu, W., Wang, J., Blumenfeld, Y. J., El-Sayed, Y. Y., and Quake, S. R. (2012). Non-invasive prenatal measurement of the fetal genome. *Nature* 487, 320–324. doi: 10.1038/nature11251

Feng, H., Jin, P., and Wu, H. (2019). Disease prediction by cell-free DNA methylation. *Brief Bioinform.* 20, 585–597. doi: 10.1093/bib/bby029

Gallardo-Gómez, M., Moran, S., de la Cadena, M. P., Martínez-Zorzano, V. S., Rodríguez-Berrocal, F. J., Rodríguez-Girondo, M., et al. (2018). A new approach to epigenome-wide discovery of non-invasive methylation biomarkers for colorectal cancer screening in circulating cell-free DNA using pooled samples. *Clin. Epigenetics* 10:53. doi: 10.1186/s13148-018-0487-y

Gordevičius, J., Kriščiūnas, A., Groot, D. E., Yip, S. M., Susic, M., Kwan, A., et al. (2018). Cell-free DNA modification dynamics in abiraterone acetate-treated prostate cancer patients. *Clin. Cancer Res.* 24, 3317–3324. doi: 10.1158/1078-0432.CCR-18-0101

Guo, S., Diep, D., Plongthongkum, N., Fung, H.-L., Zhang, K., and Zhang, K. (2017). Identification of methylation haplotype blocks aids in deconvolution of heterogeneous tissue samples and tumor tissue-of-origin mapping from plasma DNA. *Nat. Genet.* 49, 635–642. doi: 10.1038/ng.3805

Hatt, L., Aagaard, M. M., Graakjaer, J., Bach, C., Sommer, S., Agerholm, I. E., et al. (2015). Microarray-based analysis of methylation status of CpGs in placental DNA and maternal blood DNA – potential new epigenetic biomarkers for cell free fetal DNA-based diagnosis. *PLoS One* 10:e0128918. doi: 10.1371/journal.pone.0128918

Heitzer, E., Auinger, L., and Speicher, M. R. (2020). Cell-free DNA and apoptosis: how dead cells inform about the living. *Trends Mol. Med.* 26, 519–528. doi: 10.1016/j.molmed.2020.01.012

Henshall, D. C., Hamer, H. M., Pasterkamp, R. J., Goldstein, D. B., Kjems, J., Prehn, J. H. M., et al. (2016). MicroRNAs in epilepsy: pathophysiology and clinical utility. *Lancet Neurol.* 15, 1368–1376. doi: 10.1016/S1474-4422(16)30246-0

Jensen, T. J., Kim, S. K., Zhu, Z., Chin, C., Gebhard, C., Lu, T., et al. (2015). Whole genome bisulfite sequencing of cell-free DNA and its cellular contributors uncovers placenta hypomethylated domains. *Genome Biol.* 16:78. doi: 10.1186/s13059-015-0645-x

Kang, S., Li, Q., Chen, Q., Zhou, Y., Park, S., Lee, G., et al. (2017). Cancerlocator: non-invasive cancer diagnosis and tissue-of-origin prediction using methylation profiles of cell-free DNA. *Genome Biol.* 18:53. doi: 10.1186/s13059-017-1191-5

Legendre, C., Gooden, G. C., Johnson, K., Martinez, R. A., Liang, W. S., and Salhia, B. (2015). Whole-genome bisulfite sequencing of cell-free DNA identifies signature associated with metastatic breast cancer. *Clin. Epigenetics* 7:100. doi: 10.1186/s13148-015-0135-8

Lehmann-Werman, R., Magenheim, J., Moss, J., Neiman, D., Abraham, O., Piyanzin, S., et al. (2018). Monitoring liver damage using hepatocyte-specific methylation markers in cell-free circulating DNA. *JCI Insight* 3:e120687. doi: 10.1172/jci.insight.120687

Lehmann-Werman, R., Neiman, D., Zemmour, H., Moss, J., Magenheim, J., Vaknin-Dembinsky, A., et al. (2016). Identification of tissue-specific cell death using methylation patterns of circulating DNA. *Proc. Natl. Acad. Sci. U S A* 113, E1826–1834. doi: 10.1073/pnas.1519286113

Li, W., Li, Q., Kang, S., Same, M., Zhou, Y., Sun, C., et al. (2018). Cancerdetector: ultrasensitive and non-invasive cancer detection at the resolution of individual reads using cell-free DNA methylation sequencing data. *Nucleic Acids Res.* 46:e89. doi: 10.1093/nar/gky423

Liimatainen, S. P., Jylhävä, J., Raitanen, J., Peltola, J. T., and Hurme, M. A. (2013). The concentration of cell-free DNA in focal epilepsy. *Epilepsy Res.* 105, 292–298. doi: 10.1016/j.eplepsyres.2013.03.005

Liu, X., Ou, S., Xu, T., Liu, S., Yuan, J., Huang, H., et al. (2016). New differentially expressed genes and differential DNA methylation underlying refractory epilepsy. *Oncotarget* 7, 87402–87416. doi: 10.18632/oncotarget.13642

Mandel, P., and Metais, P. (1948). [Nuclear acids in human blood plasma]. *Comptes rendus des seances de la Societe de biologie et de ses filiales* 142, 241–243.

Martins-Ferreira, R., Leal, B., Chaves, J., Li, T., Ciudad, L., Rangel, R., et al. (2022). Epilepsy progression is associated with cumulative DNA methylation changes in inflammatory genes. *Prog. Neurobiol.* 209:102207. doi: 10.1016/j.pneurobio.2021.102207

Mendioroz, M., Martínez-Merino, L., Blanco-Luquin, I., Urdánoz, A., Roldán, M., and Jericó, I. (2018). Liquid biopsy: a new source of candidate biomarkers in amyotrophic lateral sclerosis. *Ann. Clin. Transl. Neurol.* 5, 763–768. doi: 10.1002/acn3.565

Miller-Delaney, S. F. C., Das, S., Sano, T., Jimenez-Mateos, E. M., Bryan, K., Buckley, P. G., et al. (2012). Differential DNA methylation patterns define status epilepticus and epileptic tolerance. *J. Neurosci.* 32, 1577–1588. doi: 10.1523/JNEUROSCI.5180-11.2012

Moss, J., Magenheim, J., Neiman, D., Zemmour, H., Loyfer, N., Korach, A., et al. (2018). Comprehensive human cell-type methylation atlas reveals origins of circulating cell-free DNA in health and disease. *Nat. Commun.* 9:5068. doi: 10.1038/s41467-018-07466-6

Nabet, B. Y., Esfahani, M. S., Moding, E. J., Hamilton, E. G., Chabon, J. J., Rizvi, H., et al. (2020). Noninvasive early identification of therapeutic benefit from immune checkpoint inhibition. *Cell* 183, 363–376.e13. doi: 10.1016/j.cell.2020.09.001

Olsen, J. A., Kenna, L. A., Spelios, M. G., Hessner, M. J., and Akirav, E. M. (2016a). Circulating differentially methylated amylin DNA as a biomarker of β-cell loss in type 1 diabetes. *PLoS One* 11:e0152662. doi: 10.1371/journal.pone.0152662

Olsen, J. A., Kenna, L. A., Tipon, R. C., Spelios, M. G., Stecker, M. M., and Akirav, E. M. (2016b). A minimally-invasive blood-derived biomarker of oligodendrocyte cell-loss in multiple sclerosis. *EBioMedicine* 10, 227–235. doi: 10.1016/j.ebiom.2016.06.031

Pai, M.-C., Kuo, Y.-M., Wang, I.-F., Chiang, P.-M., and Tsai, K.-J. (2019). The role of methylated circulating nucleic acids as a potential biomarker in Alzheimer's disease. *Mol. Neurobiol.* 56, 2440–2449. doi: 10.1007/s12035-018-1229-z

Pitkänen, A., Löscher, W., Vezzani, A., Becker, A. J., Simonato, M., Lukasiuk, K., et al. (2016). Advances in the development of biomarkers for epilepsy. *Lancet Neurol.* 15, 843–856. doi: 10.1016/S1474-4422(16)00112-5

Pitkänen, A., Lukasiuk, K., Dudek, F. E., and Staley, K. J. (2015). Epileptogenesis. *Cold Spring Harb. Perspect. Med.* 5:a022822. doi: 10.1101/cshperspect.a022822

Powles, T., Assaf, Z. J., Davarpanah, N., Banchereau, R., Szabados, B. E., Yuen, K. C., et al. (2021). CtDNA guiding adjuvant immunotherapy in urothelial carcinoma. *Nature* 595, 432–437. doi: 10.1038/s41586-021-03642-9

Snyder, M. W., Kircher, M., Hill, A. J., Daza, R. M., and Shendure, J. (2016). Cell-free DNA comprises an *in vivo* nucleosome footprint that informs its tissues-of-origin. *Cell* 164, 57–68. doi: 10.1016/j.cell.2015.11.050

Sun, K., Jiang, P., Allen Chan, K. C., Wong, J., Cheng, Y. K. Y., Liang, R. H. S., et al. (2015). Plasma DNA tissue mapping by genome-wide methylation sequencing for noninvasive prenatal, cancer and transplantation assessments. *Proc. Natl. Acad. Sci. U S A* 112, E5503–5512. doi: 10.1073/pnas.1508736112

De Vlaminck, I., Valantine, H. A., Snyder, T. M., Strehl, C., Cohen, G., Luikart, H., et al. (2014). Circulating cell-free DNA enables noninvasive diagnosis of heart

transplant rejection. *Sci. Transl. Med.* 6:241ra77. doi: 10.1126/scitranslmed.3007803

Wang, L., Fu, X., Peng, X., Xiao, Z., Li, Z., Chen, G., et al. (2016). DNA methylation profiling revealss correlation of differential methylation patterns with gene expression in human epilepsy. *J. Mol. Neuroscience.* 59, 68–77. doi: 10.1007/s12031-016-0735-6

Xu, R.-H., Wei, W., Krawczyk, M., Wang, W., Luo, H., Flagg, K., et al. (2017). Circulating tumour DNA methylation markers for diagnosis and prognosis of hepatocellular carcinoma. *Nat. Mater.* 16, 1155–1161. doi: 10.1038/nmat4997

Zemmour, H., Planer, D., Magenheim, J., Moss, J., Neiman, D., Gilon, D., et al. (2018). Non-invasive detection of human cardiomyocyte death using methylation patterns of circulating DNA. *Nat. Commun.* 9:1443. doi: 10.1038/s41467-018-03961-y

Zhang, W., Wang, H., Liu, B., Jiang, M., Gu, Y., Yan, S., et al. (2021). Differential DNA methylation profiles in patients with temporal lobe epilepsy and hippocampal sclerosis ILAE type I. *J. Mol. Neurosci.* 71, 1951–1966. doi: 10.1007/s12031-020-01780-9

Conflict of Interest: The authors declare that the research was conducted in the absence of any commercial or financial relationships that could be construed as a potential conflict of interest.

Publisher's Note: All claims expressed in this article are solely those of the authors and do not necessarily represent those of their affiliated organizations, or those of the publisher, the editors and the reviewers. Any product that may be evaluated in this article, or claim that may be made by its manufacturer, is not guaranteed or endorsed by the publisher.

frontiers | Frontiers in Neurology

REVIEW
published: 28 June 2022
doi: 10.3389/fneur.2022.904225

Role of HMGB1/TLR4 and IL-1β/IL-1R1 Signaling Pathways in Epilepsy

Shaohui Zhang[1,2], *Feng Chen*[1], *Feng Zhai*[1]* *and Shuli Liang*[3]*

[1] Functional Neurosurgery Department, National Children's Health Center of China, Beijing Children's Hospital, Capital Medical University, Beijing, China, [2] Neurosurgery Department, People's Liberation of Army (PLA) General Hospital, Beijing, China, [3] Beijing Key Laboratory of Major Diseases in Children, Ministry of Education, Functional Neurosurgery Department, National Children's Health Center of China, Beijing Children's Hospital, Capital Medical University, Beijing, China

Epilepsy is a chronic disorder of the nervous system characterized by recurrent seizures. Inflammation is one of the six major causes of epilepsy, and its role in the pathogenesis of epilepsy is gaining increasing attention. Two signaling pathways, the high mobility group box-1 (HMGB1)/toll-like receptor 4 (TLR4) and interleukin-1β (IL-1β)/interleukin-1 receptor 1 (IL-1R1) pathways, have become the focus of research in recent years. These two signaling pathways have potential as biomarkers in the prediction, prognosis, and targeted therapy of epilepsy. This review focuses on the association between epilepsy and the neuroinflammatory responses mediated by these two signaling pathways. We hope to contribute further in-depth studies on the role of HMGB1/TLR4 and IL-1β/IL-1R1 signaling in epileptogenesis and provide insights into the development of specific agents targeting these two pathways.

Keywords: high mobility group box1, toll-like receptor, interleukin-1β, interleukin-1receptor1, high mobility group box1, epilepsy

OPEN ACCESS

Edited by:
Hua-Jun Feng,
Harvard Medical School,
United States

Reviewed by:
Fei Yin,
Xiangyang Central Hospital, China
Muhammad Ayaz Anwar,
Kyung Hee University, South Korea

***Correspondence:**
Feng Zhai
zhaifengyh5288@163.com
Shuli Liang
liangsl_304@sina.com

Specialty section:
This article was submitted to Epilepsy, a section of the journal Frontiers in Neurology

Received: *25 March 2022*
Accepted: *23 May 2022*
Published: *28 June 2022*

Citation:
Zhang S, Chen F, Zhai F and Liang S (2022) Role of HMGB1/TLR4 and IL-1β/IL-1R1 Signaling Pathways in Epilepsy. Front. Neurol. 13:904225. doi: 10.3389/fneur.2022.904225

INTRODUCTION

Epilepsy is a common chronic neurological disease, with a worldwide annual incidence and a prevalence rate of 50 in 100,000 and 700 in 100,000, respectively (1). Approximately 70 million people suffer from epilepsy (1, 2). Seizures seriously affect a patient's physical and mental health and create an economic burden on his family and society as a whole. Although anti-seizure medications have been widely used, approximately one-third of patients suffer from drug-refractory epilepsy. Surgery can be performed, but some patients still have poor postoperative outcomes (3). Based on the current situation, it is necessary to explore new mechanisms of epileptogenesis to develop novel therapeutic targets.

The mechanisms of epilepsy are complex, and the neuroinflammatory response is closely related to epilepsy. Inflammatory factors can affect the electrical activity of neurons and glial cells, in addition to causing local inflammatory reactions, while epileptic seizures also cause neuro-inflammatory reactions, further aggravating nerve cell damage, thus forming a vicious cycle involving immune inflammation, epileptic seizures, and brain injury (4, 5). Among the signaling pathways involved in inflammation, high mobility group protein B1 (HMGB1)/toll-like receptor 4 (TLR4) and interleukin-1β (IL-1 β)/interleukin 1 receptor (IL-1R) have received much attention. Here, HMGB1/TLR4 and IL-1β/IL-1R inflammasomes in the pathogenesis of epilepsy are reviewed and future perspectives are outlined.

STRUCTURE AND FUNCTION OF HMGB1/TLR4

HMGB1 is a non-histone protein located in the nucleus, which binds to DNA and is involved in DNA transcription, translation, and repair (6). HMGB1 is a chain-like structural protein made up of 215 amino acids, containing a sour tail (C-terminus) and two DNA-binding domains (box A and box B) located in the L configuration (N-terminus) (7). Box B, as a proinflammatory site, can be recognized by TLRs and the receptor for advanced glycation end products inducing HMGB1 to exhibit proinflammatory activity. Box A is an anti-inflammatory response site that can competitively inhibit the proinflammatory activity of HMGB1; however, both box B and box A can bind to DNA and play a role in folding and distorting the double-stranded DNA (8, 9). The two DNA binding boxes of HMGB1 contain three cysteines (cys23, cys45, and cys106). All three cysteines reside in a fully reduced state with thiol groups (all-thiol HMGB1) in normal cells. It is reported that HMGB1 exists in three isomers: fully reduced HMGB1, disulfide HMGB1, and sulfonyl HMGB1 (8). Fully reduced HMGB1 mainly exists in the nucleus in the form of non-acetylated thiol-HMGB1, which possesses cell migration-inducing activity but lacks cytokine-inducing activity. Fully reduced HMGB1 can be released into the extracellular space from damaged neurons and glial cells. In the extracellular space, non-acetylated thiol HMGB1 is partially oxidized to generate disulfide HMGB1 with a disulfide bond between Cys23 and Cys45; however, Cys106 remains in the reduced form. It is a TLR4 ligand that possesses cytokine-inducing activity but lacks cell migration-induced activity (9). Disulfide HMGB1 binds to TLR4 to initiate a neuroinflammatory response (**Figure 1**) (10). Complete oxidation of HMGB1 will produce sulfonyl HMGB1, lacking both cell migration-induced activity and cytokine-inducing activity. However, a new finding in tumor biology reveals that sulfonyl HMGB1 exerted anti-inflammatory effects *via* the RAGE signaling pathway, which can recruit immune-competent cells and inhibit cytotoxic cells (11). HMGB1 can be released into the extracellular space from neurons and glial cells in an active or passive manner. In the extracellular space, HMGB1 is mildly oxidized to generate disulfide HMGB1 with a disulfide bond between Cys23 and Cys45; however, Cys106 remains in the reduced form (9). Disulfide HMGB1 binds to TLR4 to initiate a neuroinflammatory response (**Figure 1**) (9, 10).

TLRs were first identified in 1988 in Drosophila melanogaster, followed by recognition of its homolog, TLR4, in humans in 1997. To date, 13 different types of TLRs (TLR1-TLR13) have been discovered in mammals, among which 10 are present in humans (TLR1-10), including both intracellular and extracellular members (12). They are members of the pattern recognition receptor family that bind to pathogen-associated molecular patterns to initiate innate immune responses. TLR4 is a receptor of innate immunity and a lipopolysaccharide (LPS) sensor that is widely expressed in several immune and non-immune cells of the mammalian host. Of note, both non-transformed cells (endothelial and epithelial cells, fibroblasts, glial cells, neurons, and neural progenitor cells) and transformed cells (neoplastic) in the body have been detected to express TLRs (8). It is widely expressed in the central nervous system, including microglia, astrocytes, and neurons (13). TLR4 contains intracellular, transmembrane, and extracellular domains. The intracellular transmembrane domain, also known as the Toll-IL-1R (TIR) domain, plays a role in signal transduction, and the extracellular domain consists of leucine-rich repeats (LRRs) (14). The main functions of TLR4 include the regulation of cytokine secretion and microglial phagocytic activity. TLR4 signaling in the brain drives autoimmune responses and initiates neuroinflammation, which plays an important role in a variety of brain disorders (e.g., cerebrovascular disease, brain tumors, and epilepsy) (15). HMGB1 is mainly involved in the pathophysiology of epilepsy by interacting with the primary receptor TLR4.

MECHANISMS UNDERLYING HMGB1/TLR4 MEDIATED NEUROINFLAMMATION IN EPILEPSY

HMGB1 plays a fundamental role in DNA repair, transcription, and replication. HMGB1 can be translocated to the cytosol, plasma membrane, and extracellular space in response to various stressors. When neurons, glial cells, and immune cells are stimulated by inflammatory factors (e.g., IL-1β and TNF-α) or activated in response to oxidative stress, HMGB1 is actively released from the intracellular space to the extracellular space. When an extrinsic factor (e.g., cerebral cortical dysplasia, tuberous sclerosis complex, trauma, tumor) causes cell damage or death, HMGB1 is passively released from the intracellular space to the extracellular space (16). The regulation of HMGB1 secretion is important for the regulation of HMGB1 mediated inflammation and is dependent on the corresponding factors, such as phosphorylation by calcium-dependent protein kinase C. Inflachromene is a microglial inhibitor that can bind to HMGB1, blocking its sequential cytoplasmic localization and extracellular release by perturbing the post-translational modification and downregulation of pro-inflammatory function (17). HMGB1 released extracellularly binds to TLR4 and receptors for advanced glycation end products (RAGE) on the surface of neurons and glial cells. The activated HMGB1/TLR4 signaling pathway delivers signals through protein myeloid differentiation factor 88 (MyD88) dependent and independent pathways and stimulates nuclear factors κB (NF-κB) transport into the nucleus, transcribing target genes responsible for neuroimmune inflammatory response (**Figure 1**) (6, 18). Upon activation by HMGB1/TLR4 signaling, phosphorylation of the NR2B subunit of the N-methyl-D-aspartic acid (NMDA) receptor leads to $Ca2^{+}$ influx, which renders neuronal cells hyperexcitable and ultimately induces epileptogenesis (17, 19). HMGB1, binds to TLR4, a member of the danger-associated molecular pattern family (15), an endogenous danger signal (16). Pattern recognition receptors present on various immune cells can recognize danger signals such as damage-associated molecular patterns, which in turn activate the innate immune system and initiate an immunoinflammatory response (20, 21).

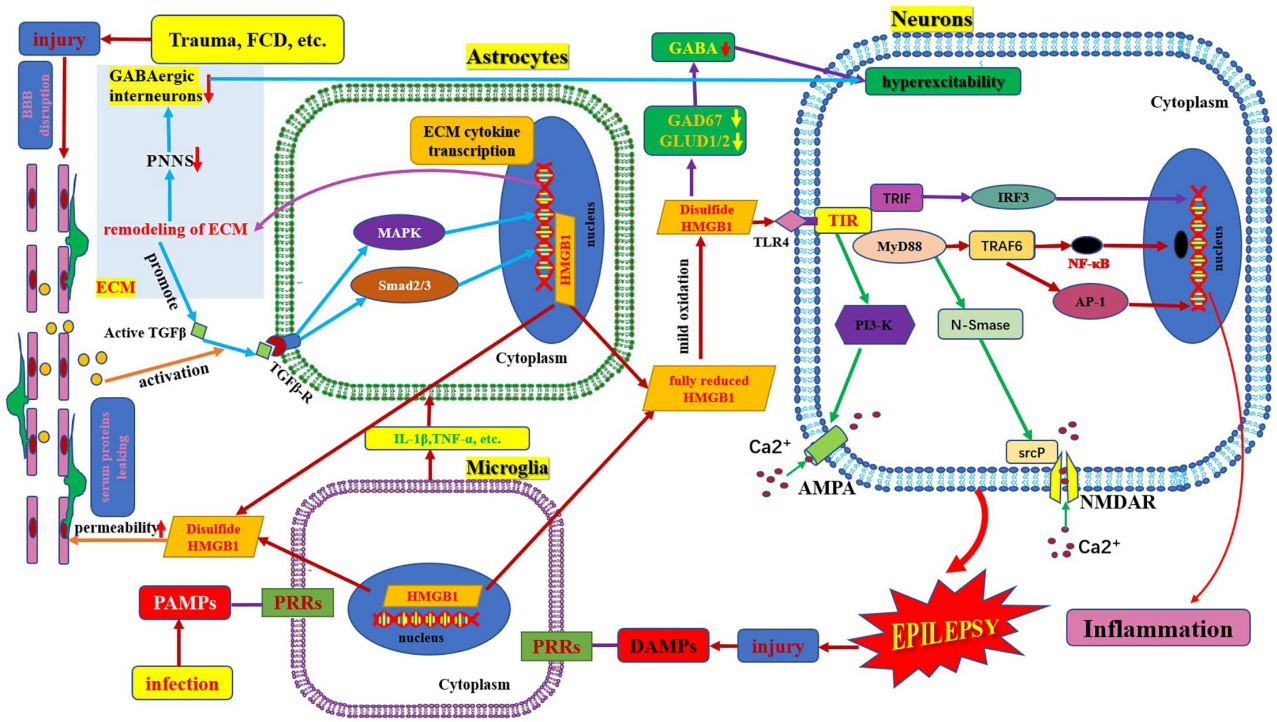

FIGURE 1 | Schematic of HMGB1/TLR-4 pathway and epilepsy. This figure shows the activation and secretion of HMGB1 and its epileptogenic mechanism, in combination with TLR4. AMPA, aminohydroxymethyloxazole propionic acid; BBB, blood–brain barrier; DAMP, danger-associated molecular patterns; FCD, focal cortical dysplasia; GAD 67, glutamate decarboxylase 67; GABA, γ- aminobutyric acid; GLUD, glutamate dehydrogenase; HMGB1, high mobility group box1; IL-1β, interleukin-1β; MyD88, myeloid differentiation factor 88; NMDAR, N-methyl-D-aspartic acid receptor; NF-κB, nuclear factors κB; PAMP, pathogen-associated molecular patterns; PRR, pattern recognition receptors; PI3K, phosphatidylinositol trihydroxykinase; TLR, toll-like receptor; TNF, tumor necrosis factor.

Neuroimmune responses lead to the production and release of active inflammatory factors (such as IL-1β and HMGB1). Extracellular HMGB1 binds to TLR4 on the surface of neurons and glial cells, which in turn leads to seizure precipitation. Seizures lead to brain cell damage, which in turn promotes the passive release of HMGB1. Proinflammatory cytokines, the release of which is induced by excess HMGB1 also in turn stimulate the release of more HMGB1, playing a key role in the occurrence and perpetuation of seizures (22). Several studies have found that in kainic acid-induced animal models, an increase in extracellular HMGB1 downregulated the expression of glutamate decarboxylase 67 and glutamate dehydrogenase 1/2 and increased intracellular glutamate concentration and major histocompatibility complex II (MHC II) levels. This leads to neuronal hyperexcitability and epileptogenesis (23). Terrone et al. reported that the activation of the HMGB1/TLR4 axis modulates glutamate receptor-mediated Ca^{2+} permeability in neurons by promoting NMDA-NR2B or α-aminohydroxymethyloxazole propionic acid-GluR2 receptor phosphorylation *via* PI3-kinase (19). Another mechanism by which HMGB1 may promote epilepsy is by the destruction of the blood–brain barrier (24). HMGB1 binding to TLR4 in BBB endothelial cells and perivascular astrocytes can alter the permeability function of BBB, leading to the extravasation of serum albumin. Extravasated serum albumin activates astrocytic transforming growth factor β signaling *via* transforming growth factor β receptor type I activin receptor-like kinase 5 (Alk5), and then leads to the activation of extracellular matrix genes through the downstream MAPK pathway and Smad2/3 pathway. The activation of the extracellular matrix gene can generate transcription and translation of extracellular matrix remodeling related molecules. These cytokines are released extracellularly and promote the persistent degradation of a protective extracellular matrix structure called the periglomerular neuronal network that surrounds inhibitory interneurons. Furthermore, remodeling of these extracellular matrices leads to dysfunction of interneurons, promoting excitation/inhibition (E/I) imbalance and ultimately epileptogenesis. However, seizures per se can also cause BBB dysfunction, forming a vicious circle (25).

ASSOCIATION BETWEEN HMGB1/TLR4 MEDIATED NEUROINFLAMMATION AND EPILEPSY

Several studies on acute injury-induced epilepsy animal models have shown that total HMGB1 increased in the blood before the onset of spontaneous seizures and during disease development and that both acetylated disulfide isoforms and disulfide isoforms

of HMGB1 progressively increased and constituted the majority of total HMGB1 in the blood. It is speculated that HMGB1 may be involved in the initiation of epilepsy after brain injury, and the level of HMGB1 in the blood might help to identify patients with a high risk of developing spontaneous seizures early after epileptogenic injury. In addition, the release of disulfide HMGB1 in the brain following status epilepticus may contribute to epileptogenesis and the consequent onset of spontaneous seizures. However, these changes persisted only in animals with active epilepsy, and disulfide HMGB1 was not detected in the blood of healthy individuals or those with well-controlled epilepsy. Thus, HMGB1 may be a useful predictive biomarker for seizure relapse and response to therapy (26, 27).

Animals with increased HMGB1 inflammatory subtypes in the blood before the onset may prospectively identify the possibility of epilepsy later. An increase in HMGB1 inflammatory subtypes persisted during active epilepsy in these animals. An early expression of the inflammatory, pathologic disulfide isoform of HMGB1 indicates the likelihood of experiencing further seizures in patients with newly diagnosed epilepsy. The drug-refractory epilepsy patients also invariably express significantly higher acetylated disulfide isoforms which are notably absent in patients with well-controlled epilepsy. The disulfide isoform of HMGB1, which seems to be the form most likely to promote seizure generation, is a potentially novel prognostic, diagnostic, and predictive biomarker of drug-resistant epilepsy in humans and highlights potential new targets for drug development (28). Pauletti et al. found that oxidative stress occurs in the brains of patients experiencing status epilepticus, as well as in patients with drug-resistant temporal lobe epilepsy, and this phenomenon is associated with the cytoplasmic translocation of HMGB1 in neurons and glia. Therefore, inhibiting the generation of disulfide HMGB1 by reducing oxidative stress may be a potential novel therapeutic approach (26).

A clinical study suggested that increased HMGB1 or TLR4 expression correlated with a higher risk and severity of epilepsy, as well as the increased possibility of anti-seizure medication resistance (22). Additionally, activation of the HMGB1/TLR4 axis has been demonstrated in surgically resected drug-refractory brain tissue (26). Kamaşsk et al. found that HMGB-1 and TLR4 levels in the severe epilepsy group were significantly higher than those in the control group or the mild epilepsy group, and the mild epilepsy group was significantly higher than those in the control group in the serum of children aged 4–17. It has been suggested that HMGB-1 and TLR4 expression levels correlate with epilepsy severity (29). Another clinical study demonstrated that the serum concentration of HMGB1 was negatively associated with patients' intelligence scores and positively associated with the frequency of seizures and the number of epileptiform discharges. These findings suggest that serum HMGB1 is potentially involved in the initiation and progression of epilepsy or epileptic lesions and is a potential predictive factor for epilepsy prognosis (30). A study on a rat model showed that the HMGB1/TLR4 axis was overexpressed in mesial temporal lobe epilepsy and could induce neuronal synaptic reconstruction and inflammatory responses in neurons *via* the p38MAPK signaling pathway (13). The HMGB1/TLR4 pathway was upregulated in neurons and astrocytes in the brain tissues of epileptic children with FCD-II, which led to an increase in the release of downstream pro-inflammatory cytokines (31). Therefore, the HMGB1/TLR4 axis plays a key role in FCD-II-related epilepsy and mesial temporal lobe epilepsy.

In animal models of pilocarpine-induced seizure, pharmacological inactivation of HMGB1 using a monoclonal antibody reduced seizure frequency and severity, and an anti-HMGB1 monoclonal antibody exerted protective effects on neuronal apoptosis and prevented epileptogenesis in association with inhibition of HMGB1 release (27). The reported anti-epileptic effect of the anti-HMGB1 monoclonal antibody might be due to inhibition of blood–brain barrier rupture, inflammatory responses, translocation of HMGB1, and neuronal cell death. Anti-HMGB1 monoclonal antibody therapy may be a novel strategy for preventing epileptogenesis (32). Another study has incorporated both acute and chronic seizure animal models. Anti-HMGB1 monoclonal antibody treatment attenuated electroshock and pentylenetetrazol-induced acute seizures, while anti-HMGB1 monoclonal antibody did not show any anti-seizure effect in TLR4 knockout mice, supporting the fact that HMGB1-TLR4 regulatory axis contributes to epileptogenesis (33). The anti-seizure effect of the anti-HMGB1 monoclonal antibody showed sufficient potential and specificity for treating kainic acid-induced seizures in an animal model and surgical tissue slices from patients with medically refractory temporal lobe epilepsy (33). Glycyrrhizin, a glycoconjugated triterpene extracted from licorice root and a natural anti-inflammatory compound, inhibits the function of HMGB1. It has a strong neuroprotective effect in mice with experimental autoimmune encephalomyelitis by reducing HMGB1 expression and release. Thus, it can be used to treat inflammatory diseases of the central nervous system (34). Glycyrrhizin can attenuate neuronal damage and alter the disease progression of post-status epilepticus by inhibiting HMGB1 activity and its translocation and protecting the blood–brain barrier permeability in a status epilepticus model induced by lithium-pilocarpine (35). However, the potential anti-epileptic mechanism of glycyrrhizin *via* HMGB1 is still unclear in seizure models and patients. A few studies have also identified other antiepileptic treatment schemes that act on the HMGB1/TLR signaling pathway. For example, epigallocatechin gallate can significantly attenuate the increase in TLR-4 and IL-1β levels in the hippocampus to achieve anti-epileptogenesis and neuroprotective effects in pilocarpine-induced epileptic rats (36, 37). In addition, micro-RNA plays a role in HMGB1-mediated epilepsy. Both miR-129-5p and miR-542-3p inhibit the development of epilepsy by suppressing HMGB1 expression and inhibiting the TLR4/NF-kB signaling pathway (38, 39). TLR4 agonists, LPS and MPL, can attenuate seizure severity in pilocarpine-induced rats with temporal lobe epilepsy (40), and pentoxifylline may represent a promising drug to inhibit epilepsy progression by targeting the HMGB1/TLR4/RAGE signaling pathway in pentylenetetrazol (PTZ)-kindling rats (41).

STRUCTURE AND FUNCTION OF IL-1β/IL-1R1

IL-1 was first identified in 1979. The IL-1 family includes three ligands, IL-1α, IL-1β, and IL-1Ra, all of which bind to the IL-1 receptor (42, 43). IL-1α is membrane-bound, whereas IL-1β is released into the extracellular space. IL1-Ra is a naturally occurring competitive inhibitor of both membrane-bound IL-1α and extracellular-released IL-1β, which acts as a brake to prevent the occurrence of excessive inflammation (44). IL1β is produced and secreted by several cell types. Although the vast majority of studies have focused on its production within cells of the innate immune system, such as monocytes and macrophages, it is mainly produced by activated microglia as well as neurons, astrocytes, and oligodendrocytes in the central nervous system (45). IL-1β is strongly induced in activated microglia and astrocytes during the acute phase of status epilepticus and in the chronic phase of spontaneous seizures in brain areas involved in seizure generation and propagation and is mainly sustained by astrocytes (4). IL-1β mainly binds to IL1R1 and activates NF-κB in target cells to induce and amplify the inflammatory response and plays an important role in injury and inflammation (**Figure 2**) (46).

The IL-1R family encompasses 10 type-1 transmembrane proteins with a similar architecture, which usually consist of an extracellular portion responsible for ligand binding, a transmembrane domain, and an intracellular portion where the TIR domain resides (toll IL1R homology region). IL-1R molecules can be divided into four subgroups based on their functions and differences in structural features (42). IL-1R1 is a biologically active type of IL-1R, formerly known as IL-1R type-I (47). When one of the agonist ligands, IL-1α or IL-1β, binds to IL-1R1 and changes its conformation, the complex forms of IL1-IL1R1 mediate IL-1-dependent activation (42). This complex recruits a number of intracellular adapter molecules, including myeloid differentiation factor 88, IL-1R-associated kinase, and tumor necrosis factor receptor-associated factor 6, to activate signal transduction pathways [such as nuclear factor-kB, activator protein-1, c-Jun N-terminal kinase, and p38 mitogen-associated protein kinase] and finally amplifies the inflammatory response (**Figure 2**) (47, 48).

MECHANISMS UNDERLYING IL-1β/IL-1R1-MEDIATED NEUROIMMUNE INFLAMMATION IN EPILEPSY

IL-1β is active only after it matures and is secreted from the cell. The process of maturation and secretion of IL-1β is roughly as follows: ① the cell is infected by bacteria or cell damage occurs; ② the pathogen-associated molecular patterns or damage-associated molecular patterns bind to the pattern recognition receptors and stimulate NF-κB transport into the nucleus and induce transcription of pre-IL-1β; ③ meanwhile, after pathogen-associated molecular patterns or damage-associated molecular patterns are recognized by pattern recognition receptors, the assembly and activation of inflammasomes (cytosolic multiprotein complexes) are triggered, which can promote the transformation of pro-caspase-1 into mature caspase-1 in the cytoplasm; ④ mature active caspase-1 causes cleavage of pro-IL-1β to mature IL-β; ⑤ finally, mature IL-1β is secreted through membrane pores *via* activated gasdermin D (49–51). The mechanism of epilepsy induced by IL-1β-mediated neuroimmune inflammatory responses is complex. IL-1β levels are significantly increased in the brain tissue and plasma samples from animal models of epilepsy and patients with temporal lobe epilepsy (45, 52). The IL-1β/IL-1R1 axis enhances NMDA receptor-mediated Ca^{2+} influx into neurons *via* phosphorylation of the NR2B subunit of the NMDA receptor *via* Src kinase, resulting in excitotoxicity and seizure (19, 43). IL-1β also affects neuronal excitability by increasing the extracellular glutamate concentration by inhibiting the astroglial glutamate transporter (19). IL-1β also inhibits GABA-mediated Cl^- influx into neurons, leading to increased neuronal excitability (19, 44). In addition, some studies have found indirect effects on neurons through the blood-brain barrier. IL-1β/IL-1R1 is expressed during epileptogenesis in both perivascular astrocytes and endothelial cells of the blood-brain barrier (4). IL-1β can affect blood-brain barrier permeability through disruption of tight-junction organization, nitric oxide production, or matrix metalloproteinase activation in endothelial cells. The brain barrier leakage promotes the exudation of inflammatory factors and neuronal damage. Moreover, these changes could lead to the infiltration of inflammatory cells from the periphery to the brain, which can aggravate inflammation and promote hyperexcitability, excitotoxicity, and epileptogenesis (**Figure 2**) (43). IL-1β can also stimulate synaptophysin expression and epileptiform discharges via the PI3K/Akt/mTOR signaling pathway to induce seizure generation in an animal model with temporal lobe epilepsy (53). Furthermore, the IL-1β/IL-1R1 signaling pathway promotes glial activation, proliferation, and cytokine release, which leads to an amplified inflammatory response and increases the risk of seizures and brain damage (54). However, after epileptogenesis, microglial activation produces large amounts of inflammatory factors (such as IL-1β). The massive release of IL-1β can lead to the production of adhesion molecules by endothelial cells, increasing leukocyte infiltration, which in turn produces more inflammatory mediators, leading to neuroimmune inflammatory responses and forming a vicious cycle (45, 55).

ASSOCIATION BETWEEN IL-1β/IL-1R1-MEDIATED NEUROIMMUNE INFLAMMATION AND EPILEPSY

Upregulation of IL-1β was found in the injured cortex, hippocampus, brain, and serum of a mouse model with post-traumatic epilepsy (54). In particular, the level of IL-1β expression in mice brains with status epilepticus was higher than that in control mice (19). Kostic *et al.* evaluated IL-1β levels in the cerebrospinal fluid and serum of 6 healthy dogs and 51 dogs with epilepsy (structural and idiopathic). IL-1β concentrations in the cerebrospinal fluid were not detectable.

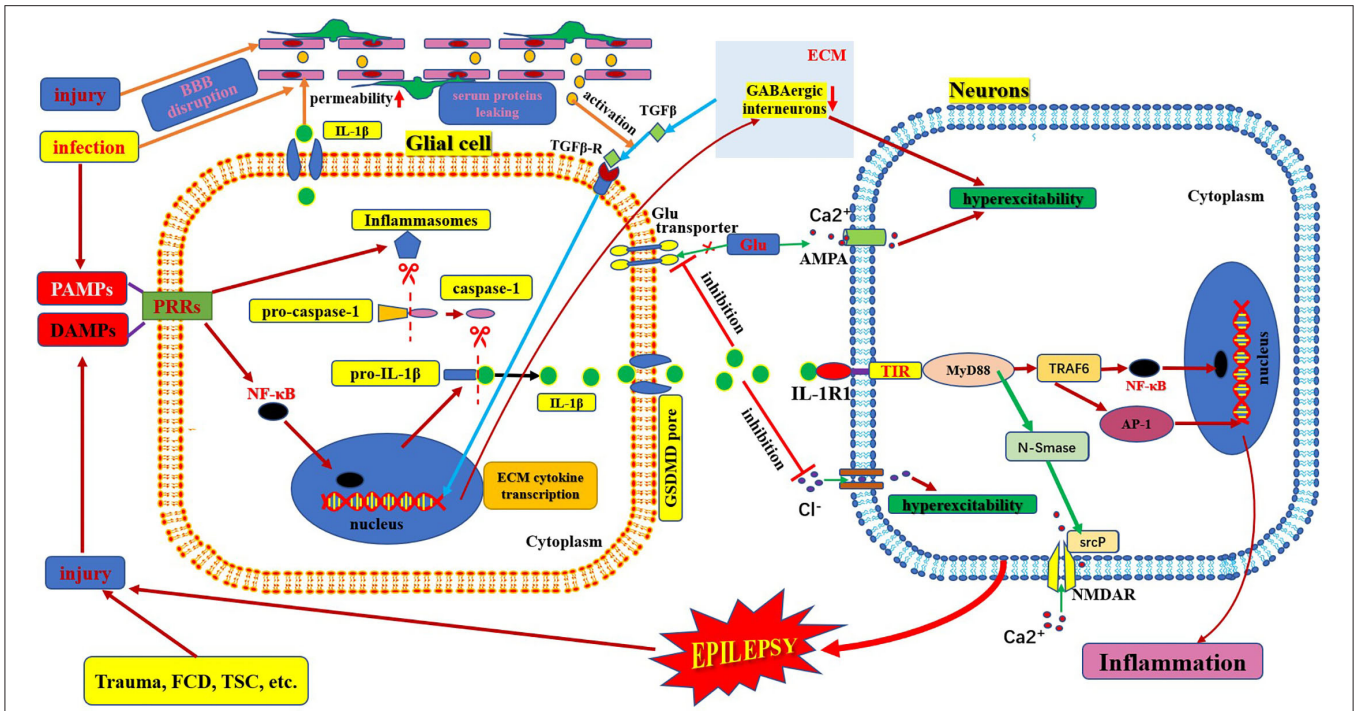

FIGURE 2 | Schematic of IL-1β/IL-1R1 pathway and epilepsy. This figure shows the activation and secretion of IL-1β and its epileptogenic mechanism in combination with IL-1R1. AMPA, aminohydroxymethyloxazole propionic acid; BBB: blood–brain barrier; DAMP, danger-associated molecular patterns; FCD, focal cortical dysplasia; GLU, glutamate; IL-1β, interleukin-1β; IL-1R, interleukin-1receptor; MyD88, myeloid differentiation factor 88; NMDAR, N-methyl-D-aspartic acid receptor; NF-κB, nuclear factors κB; PAMP, pathogen-associated molecular patterns; PRR, pattern recognition receptors; TSC, tuberous sclerosis complex.

However, dogs with epilepsy have increased serum IL-1β levels, regardless of the underlying cause of the disease (45). IL-1β levels were increased in the brain tissue samples of patients with TLE and displayed higher plasma levels of IL-1β (52). Another clinical study demonstrated that serum concentrations of IL-1β were negatively associated with patients' intelligence scores and positively associated with the frequency of seizures and number of epileptiform discharges. These findings suggest that IL-1β is potentially involved in the initiation and progression of epilepsy or epileptic lesions and is a potential predictive factor for epilepsy prognosis (30). Kamaşsk et al. found that IL-1β levels in the severe epilepsy group were higher than those in the control group or the mild epilepsy group ($P < 0.05$), and the level in the mild epilepsy group was higher than that in the control group ($P < 0.05$); in addition, the severe epilepsy group had higher IL-1R1 than the control group in the serum of children aged 4–17. It has been suggested that IL-1β/ IL-1R1 expression correlates with epilepsy severity (29). A prospective study of epilepsy outcomes showed that serum levels of IL-1β showed a significant correlation with the measures of disease severity and the number of anti-seizure medications used and a negative correlation with the age of disease onset in children with epilepsy. Thus, these data suggest that the serum levels of IL-1β are potential prognostic biomarkers for children with epilepsy (56). Moreover, the genotype frequency of rs1143627 TT of IL-1b-31 and the homozygous IL1RN*I were found to be more prevalent in patients with epilepsy, and the T allele of IL-1b-31 and IL1-RAI/I was substantially positively correlated with drug resistance in those who responded well to anti-seizure medications. The genotype of IL-1β/IL-1R1 could be a predictive marker for identifying individuals at risk of seizure and drug resistance development (47).

Anakinra, a human recombinant endogenous competitive antagonist of IL-1R1, is used to treat autoinflammatory and autoimmune disorders. Repetitive intracerebroventricular injections of anakinra after electrically induced status epilepticus in rats led to a decrease in spike frequency and reduced seizure generalization during convulsive status epilepticus (19). A child with febrile infection-related epilepsy syndrome (FIRES) showed improvement with anakinra and super-refractory status epilepticus (57). In addition, an adolescent female with a diagnosis of refractory epilepsy was treated with anakinra first and then with canakinumab, an IL-1β antibody, during a nonconvulsive status epilepticus, which resulted in complete resolution of clinical seizures (58). The IL-1 β/IL-1R signaling pathway might be a profoundly impactful adjunctive medication for certain refractory epilepsy syndromes.

ASSOCIATION OF HMGB1/TLR4 AND IL-1β/IL-1R

The HMGB1/TLR4 and IL-1β/IL-1R1 signaling pathways are key upstream generators of the neuroinflammatory response. HMGB1 can also bind to IL-1β to initiate an IL-1R1-mediated proinflammatory response (6, 17). There is a common crucial

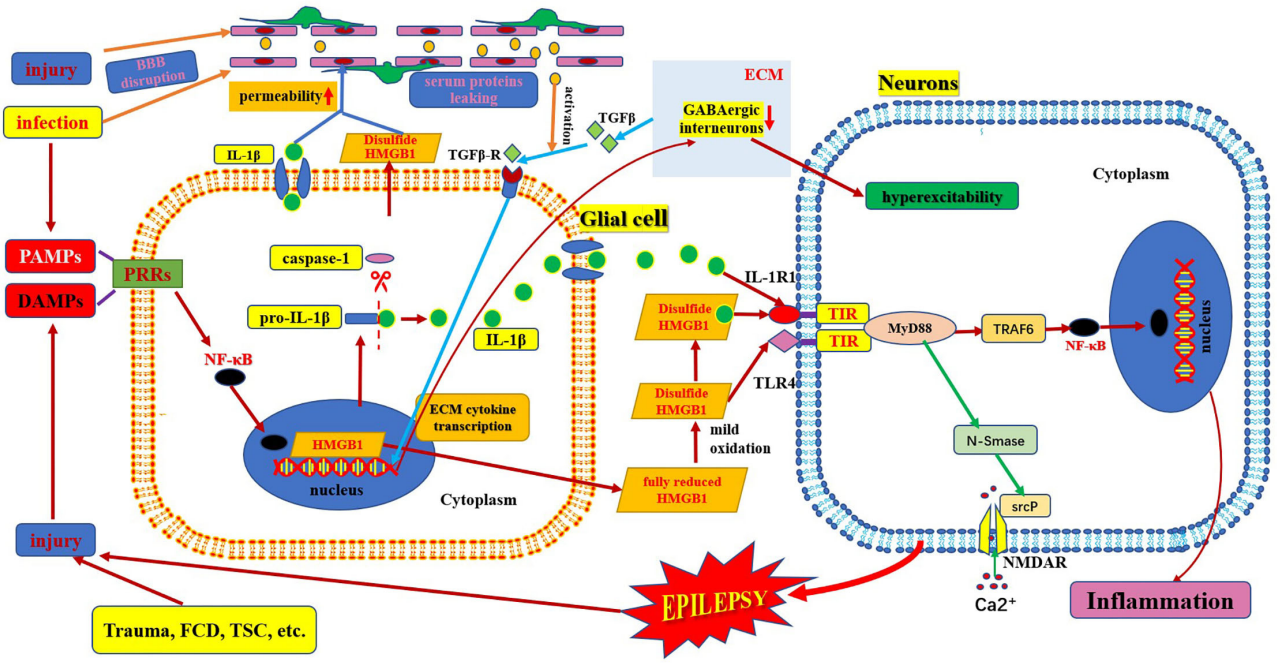

FIGURE 3 | Schematic of interaction of HMGB1/TLR-4 and IL-1β/IL-1R pathway in epilepsy. This figure shows the interaction between HMGB1/TLR-4 and the IL-1β/IL-1R pathway during their activation, secretion, and receptor combinations, and in the epileptogenic mechanism. BBB, blood–brain barrier; DAMP, danger-associated molecular patterns; FCD, focal cortical dysplasia; IL-1β, interleukin-1β; IL-1R, interleukin-1receptor; HMGB1, high mobility group box1; IL-1β, interleukin-1β; MyD88, myeloid differentiation factor 88; NMDAR, N-methyl-D-aspartic acid receptor; NF-κB, nuclear factors κB; PAMP, pathogen-associated molecular patterns; PRR, pattern recognition receptors; TLR, toll-like receptor; TSC, tuberous sclerosis complex.

signaling domain in both the IL-1 receptor and TLR4, designated as the toll interleukin-1 receptor homology region, which is now known as the TIR domain (42). Thus, the downstream signaling pathways activated by the TIR domain-containing receptor activation are very similar. First, several MyD88 molecules are recruited to the TIR domain to form MyD88 oligomers and then, IRAK-4, IRAK-1, and/or IRAK-2 are recruited. TRAF6 is recruited to hyperphosphorylated IRAK-1 oligomers and is activated. TAB2 and TAB3, ubiquitinated by TRAF6, enter the complex and associate with the TAK1/TAB1 complex, and undergo a conformational change resulting in TAK1 auto-phosphorylation and activation (**Figure 3**). Active TAK1 phosphorylates and activates the downstream protein kinase IKK, and NF-κB is then transported to the nucleus (14, 42). Eventually, their activation excited endogenous ligands leading to the transcriptional induction of NF-kB-regulated inflammatory genes, and, as a consequence, generating and rapidly amplifying the inflammatory cascade (46, 59). Activation of HMGB1/TLR4 and IL-1β/IL-1R1 axis-in depolarized neurons promotes excitotoxicity and seizures by enhancing Ca^{2+} influx *via* NMDA receptors (8). Another study showed that the activation of IL-1R1 and TLR4 signaling may induce acquired channelopathies by reducing the cyclic AMP-gated channel type 1 protein level and channel-mediated conductance on dendrites of hippocampal pyramidal neurons (60). Cyclic AMP-gated channel type 1 is a key regulator of the filtering properties of hippocampal pyramidal cell dendrites and their responses to excitatory inputs. They are involved in theta rhythms, which in turn are linked to cognitive functions. Cyclic AMP-gated channel type 1 is downregulated in animal models and human epilepsy and contributes to seizures and cognitive deficits (19). Moreover, both HMGB1/TLR4 and IL-1β/IL-1R signaling pathways are involved and contribute to the increased permeability of the blood–brain barrier (**Figure 3**). Leaky serum proteins induce transcription and translation of extracellular matrix-associated cytokines *via* transforming growth factors in astrocytes β signaling. These cytokines remodel the extracellular matrix. The ongoing degradation of perineuronal nets (a protective extracellular matrix) around GABAergic interneurons causes GABAergic interneuron dysfunction, which may contribute to hyperexcitability of brain tissue and provoke a long-lasting decrease in seizure threshold (25, 46).

FUTURE PERSPECTIVE AND CONCLUSION

Preclinical studies and clinical evidence show that HMGB1/TLR4 and IL-1β/IL-1R1 signaling pathways are involved in epileptogenesis caused by neuroimmune inflammatory responses and participate in the neuroinflammatory response of brain injury after epilepsy (**Table 1**). They are closely related to the

TABLE 1 | Summary of studies on the HMGB1/TLR4 and IL-1β/ IL-1R pathways and their association with epilepsy.

S.N.	Intervention	Experimental models	Pathway	Observations	References
1	HMGB1/TLR4	① Surgically removed brain sample of patients with intractable epilepsy ② Cell model of epilepsy induced by coriaria lactone (CL)	TLR4/NF-κB	① Increased expression of HMGB1 and NF-κB ② Translocation of HMGB1 from nuclear to cytoplasmic	(6)
2	HMGB1/TLR4	① Surgically removed brain tissue of children with drug-resistant MTLE ② Pilocarpine induced SE in rats	p38MAPK	① Overexpression of HMGB1 and TLR4 ② HMGB1 upregulated the protein level of p38MAPK	(13)
3	HMGB1/TLR4	Peripheral venous blood samples of patients with epilepsy	-	① Expressions of HMGB1 and TLR4 were higher in epilepsy patients ② Elevated HMGB1 and TLR4 expressions were both associated with longer seizure duration and increased seizure frequency ③ increased HMGB1 and TLR4 expressions were correlated with a higher possibility of anti-epilepsy drugs resistance	(22)
4	HMGB1	Primary rat neural cells (PRNCs) by KA administration	GAD67 and GLUD 1/2	① KA induced the translocation of HMGB1 from the nucleus to the cytosol ② PRNC cell viability and mitochondrial Activity ↓ ③ Expression of GAD67s and GLUD1/2 ↓	(23)
5	Anti-HMGB1 monoclonal antibody	① Acute seizure model induced by maximal electroshock or PTZ in rats ② chronic seizure model induced by KA in rats ③ Surgical specimens of patients with intractable epilepsy	-	① Acute seizures and translocation of HMGB1 ↓ ② The severity of chronic epilepsy ↓ ③ Spontaneous discharges ↓	(33)
6	Glycyrrhizin(GL)	Pilocarpine induced SE in rats	-	① HMGB1 expression in serum and hippocampus in the GL treatment group ↓ ② HMGB1 translocation from the nucleus to cytoplasm in hippocampal in the GL treatment group ↓ ③ Neuronal damage in the hippocampus in the GL treatment group ↓	(35)
7	Epigallocatechin-3-allate(EGCG)	Pilocarpine induced SE in rats	TLR4/NF-κB	① The frequency of spontaneous recurrent seizures and duration of seizures ↓ ② Level of TLR4 and NF-κB in the EGCG treatment group ↓	(37)
8	Lipopolysaccharides and Monophosphoryl lipid A	Pilocarpine induced seizure in rats	-	Early preconditioning with TLR4 agonists attenuates seizure severity	(40)
9	Pentoxifylline(PTX)	Pentylenetetrazole (PTZ)-induced seizure in rats	HMGB1/ RAGE/ TLR4	① Seizure severity score in the PTX treatment group ↓ ② Level of HMGB1, TLR4, RAGE, and NF-κB in the PTX treatment group ↓ ③ Cognition improved in the PTX treatment group ↑	(41)
10	IL-1β	Dogs with epilepsy (structural and idiopathic)	-	① Serum IL-1β was not elevated in dogs with TBI ② Increased serum IL-1β in dogs with epilepsy	(45)
11	IL-1β, caspase-1	① Hippocampal tissues from patients with MTLE ② Plasma of patients with MTLE	-	Both of them increased in tissue samples and plasma of patients with TLE	(52)
12	IL-1β	① Pilocarpine induced SE in rats ② Hippocampal neuronal model	PI3K/Akt/mTOR	IL-1β promoted SYN expression, and SYN expression is related to the PI3K/Akt/mTOR pathway	(53)
13	IL-1 receptor antagonist (IL-1Ra)	Pediatric mouse model with epilepsy after traumatic brain injury	-	① rIL-1Ra reduces subacute seizure susceptibility after pTBI ② rIL-1Ra reduces the chronic PTZ-evoked seizure response	(54)

(Continued)

TABLE 1 | Continued

S.N.	Intervention	Experimental models	Pathway	Observations	References
14	IL-1β	Peripheral venous blood samples of children with epilepsy	-	① Age at disease onset showed a significant correlation negatively with serum levels of IL-1β ② Serum levels of IL-1β showed a positive correlation with the measures of disease severity	(56)
15	Anakinra	A 13-year-old child with febrile infection-related epilepsy syndrome (FIRES)	-	Aanakinra reduces the relapse of highly recurrent refractory seizures at 1.5 years after FIRES onset	(57)
16	Anakinra canakinumab	A 14-year-old female with systemic autoinflammation with intractable epilepsy	-	Near-complete resolution of clinical seizures	(58)
17	Fisetin	① Acute seizure model induced by maximal electroshock or PTZ in rats ② chronic seizure model induced by PTZ in subconvulsive dose in rats	-	① delayed onset of seizures ② decreased the percentage of fully kindled mice ③ attenuated seizure severity score and mortality ④ decreased levels of HMGB1, TLR-4, IL-1β, and IL-1R1 in the hippocampus and cortex of the kindled mice	(59)

mechanism of epilepsy and the development of drug resistance and are important biomarkers for the occurrence, prognosis, and prediction of epilepsy. These two signaling pathways can induce neuroimmune inflammatory responses through multiple pathways, which is an important part of the neuroimmune inflammatory response theory in the pathogenesis of epilepsy. Notably, research on antibodies or inhibitors against these two signaling pathways has also made some progress and has shown good therapeutic effects. However, the complete upstream and downstream links of HMGB1/TLR4 and IL-1β/IL-1R1 signaling pathways, their complete mechanism of action in epilepsy of different etiologies, and the participation of genetic factors are still very limited. At present, there are few studies on the relationship between these two signaling pathways and their related antibodies or inhibitors, and there is a lack of in-depth experiments based on different etiologies and animal models. The clinical applications of these drugs require further exploration. Finally, it is expected that the IL-1β/Il-1R1 and HMGB1/TLR4 signaling pathways will provide more in-depth, scientific, and comprehensive research on the occurrence, prediction, prognosis, and treatment of epilepsy.

AUTHOR CONTRIBUTIONS

SL: conceptualization, writing—reviewing and editing, and funding acquisition. SZ and FC: writing—original draft preparation and investigation. FZ: writing—reviewing and editing. All authors contributed to the article and approved the submitted version.

FUNDING

This research was supported by the Beijing Nature & Science Foundation of China (7202045, SL) and the National Nature and Science Foundation of China (82071448, SL). The funders were not involved in the study design, data collection and analysis, interpretation of data, or writing of the report.

REFERENCES

1. Trinka E, Kwan P, Lee B, Dash A. Epilepsy in Asia: Disease burden, management barriers, and challenges. *Epilepssia.* (2019) 60(Suppl 1):7–21. doi: 10.1111/epi.14458
2. Thijs RD, Surges R, O'Brien TJ, Sander JW. Epilepsy in adults. *Lancet.* (2019) 393:689–701. doi: 10.1016/S0140-6736(18)32596-0
3. Wang S, Zhao M, Li T, Zhang C, Zhou J, Wang M, et al. Long-term efficacy and cognitive effects of bilateral hippocampal deep brain stimulation in patients with drug-resistant temporal lobe epilepsy. *Neurol Sci.* (2021) 42:225–33. doi: 10.1007/s10072-020-04554-8
4. van Vliet EA, Aronica E, Vezzani A, Ravizza T. Review: Neuroinflammatory pathways as treatment targets and biomarker candidates in epilepsy: emerging evidence from preclinical and clinical studies. *Neuropathol Appl Neurobiol.* (2018) 44:91–111. doi: 10.1111/nan.12444
5. Korff CM, Dale RC. The immune system in pediatric seizures and epilepsies. *Pediatrics.* (2017) 140:e20163534. doi: 10.1542/peds.2016-3534
6. Shi Y, Zhang L, Teng J, Miao W. HMGB1 mediates microglia activation via the TLR4/NF-κB pathway in coriaria lactone induced epilepsy. *Mol Med Rep.* (2018) 17:5125–31. doi: 10.3892/mmr.2018.8485
7. Yang L, Wang F, Yang L, Yuan Y, Chen Y, Zhang G, etal. HMGB1 a-box reverses brain edema and deterioration of neurological function in a traumatic brain injury mouse model cell. *Physiol Biochem.* (2018) 46:2532–42. doi: 10.1159/000489659
8. Paudel YN, Semple BD, Jones NC, Othman I, Shaikh MF. High mobility group box 1 (HMGB1) as a novel frontier in epileptogenesis: from

pathogenesis to therapeutic approaches. *J Neurochem.* (2019) 151:542–57. doi: 10.1111/jnc.14663
9. Andersson U, Tracey KJ, Yang H. Post-translational modification of HMGB1 disulfide bonds in stimulating and inhibiting inflammation. *Cells.* (2021) 10:3323. doi: 10.3390/cells10123323
10. Zhao L, Liu P, Kepp O, Kroemer G. Methods for measuring HMGB1 release during immunogenic cell death. *Methods Enzymol.* (2019) 629:177–93. doi: 10.1016/bs.mie.2019.05.001
11. Hubert P, Roncarati P, Demoulin S, Pilard C, Ancion M, Reynders C, et al. Extracellular HMGB1 blockade inhibits tumor growth through profoundly remodeling immune microenvironment and enhances checkpoint inhibitor-based immunotherapy. *J Immunother Cancer.* (2021) 9:e001966. doi: 10.1136/jitc-2020-001966
12. Vijay K. Toll-like receptors in immunity and inflammatory diseases: past, present, and future. *Int Immunopharmacol.* (2018) 59:391–412. doi: 10.1016/j.intimp.2018.03.002
13. Yang W, Li J, Shang Y, Zhao L, Wang M, Shi J, et al. HMGB1-TLR4 axis plays a regulatory role in the pathogenesis of mesial temporal lobe epilepsy in immature rat model and children via the p38MAPK signaling pathway. *Neurochem Res.* (2017) 42:1179–90. doi: 10.1007/s11064-016-2153-0
14. Fitzgerald KA, Kagan JC. Toll-like receptors and the control of immunity. *Cell.* (2020) 180:1044–66. doi: 10.1016/j.cell.2020.02.041
15. Paudel YN, Angelopoulou E, Akyuz E, Piperi C, Othman I, Shaikh MF. Role of Innate Immune Receptor TLR4 and its endogenous ligands in epileptogenesis. *Pharmacol Res.* (2020) 160:105172. doi: 10.1016/j.phrs.2020.105172
16. Wen Q, Liu J, Kang R, Zhou B, Tang D. The release and activity of HMGB1 in ferroptosis. *Biochem Biophys Res Commun.* (2019) 510:278–83. doi: 10.1016/j.bbrc.2019.01.090
17. Abg Abd Wahab DY, Gau CH, Zakaria R, Muthu Karuppan MK. A-Rahbi BS, Abdullah Z, et al. Review on cross talk between neurotransmitters and neuroinflammation in striatum and cerebellum in the mediation of motor behaviour. *Biomed Res Int.* (2019) 2019:1767203. doi: 10.1155/2019/1767203
18. Paudel YN, Shaikh MF, Chakraborti A, Kumari Y, Aledo-Serrano Á, Aleksovska K, et al. HMGB1: a common biomarker and potential target for tbi, neuroinflammation, epilepsy, and cognitive dysfunction. *Front Neurosci.* (2018) 12:628. doi: 10.3389/fnins.2018.00628
19. Terrone G, Balosso S, Pauletti A, Ravizza T, Vezzani A. Inflammation and reactive oxygen species as disease modifiers in epilepsy. *Neuropharmacology.* (2020) 167:107742. doi: 10.1016/j.neuropharm.2019.107742
20. Amarante-Mendes GP, Adjemian S, Branco LM, Zanetti LC, Weinlich R, Bortoluci KR. Pattern recognition receptors and the host cell death molecular machinery. *Front Immunol.* (2018) 9:2379. doi: 10.3389/fimmu.2018.02379
21. Mohseni-Moghaddam P, Roghani M, Khaleghzadeh-Ahangar H, Sadr SS, Sala C. A literature overview on epilepsy and inflammasome activation. *Brain Res Bull.* (2021) 172:229–35. doi: 10.1016/j.brainresbull.2021.05.001
22. Kan M, Song L, Zhang X, Zhang J, Fang P. Circulating high mobility group box-1 and toll-like receptor 4 expressions increase the risk and severity of epilepsy. *Braz J Med Biol Res.* (2019) 52:e7374. doi: 10.1590/1414-431X20197374
23. Kaneko Y, Pappas C, Malapira T, Vale FL, Tajiri N, Borlongan CV. Extracellular HMGB1 modulates glutamate metabolism associated with kainic acid-induced epilepsy-like hyperactivity in primary rat neural cells. *Cell Physiol Biochem.* (2017) 41:947–59. doi: 10.1159/000460513
24. Liebner S, Dijkhuizen RM, Reiss Y, Plate KH, Agalliu D, Constantin G. Functional morphology of the blood-brain barrier in health and disease. *Acta Neuropathol.* (2018) 135:311–36. doi: 10.1007/s00401-018-1815-1
25. Kim SY, Senatorov VV Jr, Morrissey CS, Lippmann K, Vazquez O, Milikovsky DZ, et al. TGFβ signaling is associated with changes in inflammatory gene expression and perineuronal net degradation around inhibitory neurons following various neurological insults. *Sci Rep.* (2017) 7:7711. doi: 10.1038/s41598-017-07394-3
26. Pauletti A, Terrone G, Shekh-Ahmad T, Salamone A, Ravizza T, Rizzi M, et al. Targeting oxidative stress improves disease outcomes in a rat model of acquired epilepsy. *Brain.* (2019) 142:e39. doi: 10.1093/brain/awz130
27. Walker LE, Frigerio F, Ravizza T, Ricci E, Tse K, Jenkins RE, et al. Molecular isoforms of high-mobility group box 1 are mechanistic biomarkers for epilepsy. *J Clin Invest.* (2019) 129:2166. doi: 10.1172/JCI129285
28. Auvin S, Walker L, Gallentine W, Jozwiak S, Tombini M, Sills GJ. Prospective clinical trials to investigate clinical and molecular biomarkers. *Epilepsia.* (2017) 58 Suppl 3:20–6. doi: 10.1111/epi.13782
29. Kamaşak T, Dilber B, Yaman SÖ, Durgut BD, Kurt T, Çoban E, et al. HMGB-1, TLR4, IL-1R1, TNF-α, and IL-1β: novel epilepsy markers? *Epileptic Disord.* (2020) 22:183–93. doi: 10.1684/epd.2020.1155
30. Zhu M, Chen J, Guo H, Ding L, Zhang Y, Xu Y. high mobility group protein B1 (HMGB1) and Interleukin-1β as prognostic biomarkers of epilepsy in children. *J Child Neurol.* (2018) 33:909–17. doi: 10.1177/0883073818801654
31. Zhang Z, Liu Q, Liu M, Wang H, Dong Y, Ji T, et al. Upregulation of HMGB1-TLR4 inflammatory pathway in focal cortical dysplasia type II. *J Neuroinflammation.* (2018) 15:27. doi: 10.1186/s12974-018-1078-8
32. Ravizza T, Terrone G, Salamone A, Frigerio F, Balosso S, Antoine DJ, et al. High Mobility Group Box 1 is a novel pathogenic factor and a mechanistic biomarker for epilepsy. *Brain Behav Immun.* (2018) 72:14–21. doi: 10.1016/j.bbi.2017.10.008
33. Zhao J, Wang Y, Xu C, Liu K, Wang Y, Chen L, et al. Therapeutic potential of an anti-high mobility group box-1 monoclonal antibody in epilepsy. *Brain Behav Immun.* (2017) 64:308–19. doi: 10.1016/j.bbi.2017.02.002
34. Sun Y, Chen H, Dai J, Wan Z, Xiong P, Xu Y, et al. Glycyrrhizin protects mice against experimental autoimmune encephalomyelitis by inhibiting high-mobility group Box 1 (HMGB1) expression and neuronal HMGB1 release. *Front Immunol.* (2018) 9:1518. doi: 10.3389/fimmu.2018.01518
35. Li YJ, Wang L, Zhang B, Gao F, Yang CM. Glycyrrhizin, an HMGB1 inhibitor, exhibits neuroprotective effects in rats after lithium-pilocarpine-induced status epilepticus. *J Pharm Pharmacol.* (2019) 71:390–99. doi: 10.1111/jphp.13040
36. Khalatbary AR, Khademi E. The green tea polyphenolic catechin epigallocatechin gallate and neuroprotection. *Nutr Neurosci.* (2020) 23:281–94. doi: 10.1080/1028415X.2018.1500124
37. Qu Z, Jia L, Xie T, Zhen J, Si P, Cui Z, et al. (-)-Epigallocatechin-3-gallate protects against lithium-pilocarpine-induced epilepsy by inhibiting the toll-like receptor 4 (TLR4)/nuclear factor-κB (NF-κB) signaling pathway. *Med Sci Monit.* (2019) 25:1749–58. doi: 10.12659/MSM.915025
38. Liu AH, Wu YT, Wang YP. MicroRNA-129-5p inhibits the development of autoimmune encephalomyelitis-related epilepsy by targeting HMGB1 through the TLR4/NF-kB signaling pathway. *Brain Res Bull.* (2017) 132:39–149. doi: 10.1016/j.brainresbull.2017.05.004
39. Yan Y, Xia H, Hu J, Zhang B. MicroRNA-542-3p Regulates P-glycoprotein expression in rat epilepsy via the toll-like receptor 4/nuclear Factor-kappaB signaling pathway. *Curr Neurovasc Res.* (2019) 16:433–40. doi: 10.2174/1567202616666191023160201
40. Hosseinzadeh M, Pourbadie HG, Khodagholi F, Daftari M, Naderi N, Motamedi F. Preconditioning with toll-like receptor agonists attenuates seizure activity and neuronal hyperexcitability in the pilocarpine rat model of epilepsy. *Neuroscience.* (2019) 408:388–99. doi: 10.1016/j.neuroscience.2019.04.020
41. Badawi GA, Shokr MM, Zaki HF, Mohamed AF. Pentoxifylline prevents epileptic seizure via modulating HMGB1/RAGE/TLR4 signalling pathway and improves memory in pentylenetetrazol kindling rats. *Clin Exp Pharmacol Physiol.* (2021) 48:1111–24. doi: 10.1111/1440-1681.13508
42. Boraschi D, Italiani P, Weil S, Martin MU. The family of the interleukin-1 receptors. *Immunol Rev.* (2018) 281:197–232. doi: 10.1111/imr.12606
43. Zhand A, Sayad A, Ghafouri-Fard S, Arsang-Jang S, Mazdeh M, Taheri M. Expression analysis of GRIN2B, BDNF, and IL-1β genes in the whole blood of epileptic patients. *Neurol Sci.* (2018) 39:1945–53. doi: 10.1007/s10072-018-3533-9
44. Barseem NF, Khattab ESAEH, Mahasab MM. IL-1β-31/IL1-RA genetic markers association with idiopathic generalized epilepsy and treatment response in a cohort of Egyptian population. *Int J Neurosci.* (2020) 130:348–54. doi: 10.1080/00207454.2019.1688809
45. Kostic D, Carlson R, Henke D, Rohn K, Tipold A. Evaluation of IL-1β levels in epilepsy and traumatic brain injury in dogs. *BMC Neurosci.* (2019) 20:29. doi: 10.1186/s12868-019-0509-5
46. Webster KM, Sun M, Crack P, O'Brien TJ, Shultz SR, Semple BD. Inflammation in epileptogenesis after traumatic brain injury. *J Neuroinflammation.* (2017) 14:10. doi: 10.1186/s12974-016-0786-1

47. Arend WP, Palmer G, Gabay C. IL-1, IL-18, and IL-33 families of cytokines. *Immunol Rev.* (2008) 223:20–38. doi: 10.1111/j.1600-065X.2008.00624.x
48. Chen L, Zheng L, Chen P, Liang G. Myeloid differentiation primary response protein 88 (MyD88): the central hub of TLR/IL-1R signaling. *J Med Chem.* (2020) 63:13316–29. doi: 10.1021/acs.jmedchem.0c00884
49. Voet S, Srinivasan S, Lamkanfi M, van Loo G. Inflammasomes in neuroinflammatory and neurodegenerative diseases. *EMBO Mol Med.* (2019) 11:e10248. doi: 10.15252/emmm.201810248
50. Zhou Z, Li H, Tian S, Yi W, Zhou Y, Yang H, et al. Critical roles of NLRP3 inflammasome in IL-1β secretion induced by Corynebacterium pseudotuberculosis in vitro. *Mol Immunol.* (2019) 116:11–7. doi: 10.1016/j.molimm.2019.09.016
51. Lopez-Castejon G, Brough D. Understanding the mechanism of IL-1β secretion. *Cytokine Growth Factor Rev.* (2011) 22:189–95. doi: 10.1016/j.cytogfr.2011.10.001
52. Cristina de. Brito Toscano E, Leandro Marciano Vieira É, Boni Rocha Dias B, Vidigal Caliari M, Paula Gonçalves A, Varela Giannetti A, et al. NLRP3 and NLRP1 inflammasomes are up-regulated in patients with mesial temporal lobe epilepsy and may contribute to overexpression of caspase-1 and IL-β in sclerotic hippocampi. *Brain Res.* (2021) 1752:147230. doi: 10.1016/j.brainres.2020.147230
53. Xiao Z, Peng J, Wu L, Arafat A, Yin F. The effect of IL-1β on synaptophysin expression and electrophysiology of hippocampal neurons through the PI3K/Akt/mTOR signaling pathway in a rat model of mesial temporal lobe epilepsy. *Neurol Res.* (2017) 39:640–48. doi: 10.1080/01616412.2017.1312070
54. Semple BD, O'Brien TJ, Gimlin K, Wright DK, Kim SE, Casillas-Espinosa PM, et al. Interleukin-1 receptor in seizure susceptibility after traumatic injury to the pediatric brain. *J Neurosci.* (2017) 37:7864–77. doi: 10.1523/JNEUROSCI.0982-17.2017
55. Lan X, Han X, Li Q, Yang QW, Wang J. Modulators of microglial activation and polarization after intracerebral haemorrhage. *Nat Rev Neurol.* (2017) 13:420–33. doi: 10.1038/nrneurol.2017.69
56. Choi J, Kim SY, Kim H, Lim BC, Hwang H, Chae JH, et al. Serum α-synuclein and IL-1β are increased and correlated with measures of disease severity in children with epilepsy: potential prognostic biomarkers? *BMC Neurol.* (2020) 20:85. doi: 10.1186/s12883-020-01662-y
57. Dilena R, Mauri E, Aronica E, Bernasconi P, Bana C, Cappelletti C, et al. Therapeutic effect of Anakinra in the relapsing chronic phase of febrile infection-related epilepsy syndrome. *Epilepsia Open.* (2019) 4:344–50. doi: 10.1002/epi4.12317
58. DeSena AD, Do T, Schulert GS. Systemic autoinflammation with intractable epilepsy managed with interleukin-1 blockade. *J Neuroinflammation.* (2018) 15:38. doi: 10.1186/s12974-018-1063-2
59. Khatoon S, Agarwal NB, Samim M, Alam O. Neuroprotective effect of fisetin through suppression of IL-1R/TLR axis and apoptosis in pentylenetetrazole-induced kindling in mice. *Front Neurol.* (2021) 12:689069. doi: 10.3389/fneur.2021.689069
60. Frigerio F, Flynn C, Han Y, Lyman K, Lugo JN, Ravizza T, et al. Neuroinflammation alters integrative properties of rat hippocampal pyramidal cells. *Mol Neurobiol.* (2018) 55:7500–11. doi: 10.1007/s12035-018-0915-1

Conflict of Interest: The authors declare that the research was conducted in the absence of any commercial or financial relationships that could be construed as a potential conflict of interest.

Publisher's Note: All claims expressed in this article are solely those of the authors and do not necessarily represent those of their affiliated organizations, or those of the publisher, the editors and the reviewers. Any product that may be evaluated in this article, or claim that may be made by its manufacturer, is not guaranteed or endorsed by the publisher.

frontiers | Frontiers in Cellular Neuroscience

ORIGINAL RESEARCH
published: 07 July 2022
doi: 10.3389/fncel.2022.910662

Mesial Temporal Lobe Epilepsy (MTLE) Drug-Refractoriness Is Associated With P2X7 Receptors Overexpression in the Human Hippocampus and Temporal Neocortex and May Be Predicted by Low Circulating Levels of miR-22

*Bárbara Guerra Leal[1,2,3], Aurora Barros-Barbosa[4], Fátima Ferreirinha[4], João Chaves[1,5], Rui Rangel[6], Agostinho Santos[7], Cláudia Carvalho[2], Ricardo Martins-Ferreira[1,2], Raquel Samões[5], Joel Freitas[8], João Lopes[8], João Ramalheira[8], Maria Graça Lobo[4], António Martins da Silva[1,3,8], Paulo P. Costa[1,3,9] and Paulo Correia-de-Sá[4]**

[1]Unit for Multidisciplinary Research in Biomedicine (UMIB), Instituto de Ciências Biomédicas Abel Salazar—Universidade do Porto (ICBAS-UP), Porto, Portugal, [2]Immunogenetics Laboratory, Molecular Pathology and Immunology Department, ICBAS-UP, Porto, Portugal, [3]Laboratory for Integrative and Translational Research in Population Health (ITR), Porto, Portugal, [4]Laboratório de Farmacologia e Neurobiologia—Center for Drug Discovery and Innovative Medicines (MedInUP), ICBAS-UP, Porto, Portugal, [5]Serviço de Neurologia, Hospital de Santo António—Centro Hospitalar e Universitário do Porto (HSA-CHUP), Porto, Portugal, [6]Serviço de Neurocirurgia, HSA-CHUP, Porto, Portugal, [7]Serviço de Patologia Forense, Instituto Nacional de Medicina Legal e Ciências Forenses—Delegação do Norte (INMLCF-DN), Porto, Portugal, [8]Serviço de Neurofisiologia, HSA-CHUP, Porto, Portugal, [9]Departamento de Genética, Instituto Nacional de Saúde Dr. Ricardo Jorge, Porto, Portugal

Objective: ATP-gated ionotropic P2X7 receptors (P2X7R) actively participate in epilepsy and other neurological disorders. Neocortical nerve terminals of patients with Mesial Temporal Lobe Epilepsy with Hippocampal Sclerosis (MTLE-HS) express higher P2X7R amounts. Overexpression of P2X7R bolsters ATP signals during seizures resulting in glial cell activation, cytokines production, and GABAergic rundown with unrestrained glutamatergic excitation. In a mouse model of status epilepticus, increased expression of P2X7R has been associated with the down-modulation of the non-coding micro RNA, miR-22. MiR levels are stable in biological fluids and normally reflect remote tissue production making them ideal disease biomarkers. Here, we compared P2X7R and miR-22 expression in epileptic brains and in the serum of patients with MTLE-HS, respectively.

Methods: Quantitative RT-PCR was used to evaluate the expression of P2X7R in the hippocampus and anterior temporal lobe of 23 patients with MTLE-HS and 10 cadaveric controls. Confocal microscopy and Western blot analysis were performed to assess P2X7R protein amounts. MiR-22 expression was evaluated in cell-free sera of 40 MTLE-HS patients and 48 healthy controls.

OPEN ACCESS

Edited by:
Pierre Szepetowski, INSERM U901 Institut de Neurobiologie de la Méditerranée, France

Reviewed by:
Tobias Engel, Royal College of Surgeons in Ireland, Ireland
Sylvian Bauer, Centre National de la Recherche Scientifique (CNRS), France

***Correspondence:**
Paulo Correia-de-Sá
farmacol@icbas.up.pt
orcid.org/0000-0002-6114-9189

Specialty section:
This article was submitted to Cellular Neuropathology, a section of the journal Frontiers in Cellular Neuroscience

Received: *01 April 2022*
Accepted: *07 June 2022*
Published: *07 July 2022*

Citation:
Guerra Leal B, Barros-Barbosa A, Ferreirinha F, Chaves J, Rangel R, Santos A, Carvalho C, Martins-Ferreira R, Samões R, Freitas J, Lopes J, Ramalheira J, Lobo MG, Martins da Silva A, Costa PP and Correia-de-Sá P (2022) Mesial Temporal Lobe Epilepsy (MTLE) Drug-Refractoriness Is Associated With P2X7 Receptors Overexpression in the Human Hippocampus and Temporal Neocortex and May Be Predicted by Low Circulating Levels of miR-22. Front. Cell. Neurosci. 16:910662. doi: 10.3389/fncel.2022.910662

Results: Nerve terminals of the hippocampus and neocortical temporal lobe of MTLE-HS patients overexpress ($p < 0.05$) an 85 kDa P2X7R protein whereas the normally occurring 67 kDa receptor protein dominates in the brain of the cadaveric controls. Contrariwise, miR-22 serum levels are diminished ($p < 0.001$) in MTLE-HS patients compared to age-matched control blood donors, a situation that is more evident in patients requiring multiple (>3) anti-epileptic drug (AED) regimens.

Conclusion: Data show that there is an inverse relationship between miR-22 serum levels and P2X7R expression in the hippocampus and neocortex of MTLE-HS patients, which implies that measuring serum miR-22 may be a clinical surrogate of P2X7R brain expression in the MTLE-HS. Moreover, the high area under the ROC curve (0.777; 95% CI 0.629–0.925; $p = 0.001$) suggests that low miR-22 serum levels may be a sensitive predictor of poor response to AEDs among MTLE-HS patients. Results also anticipate that targeting the miR-22/P2X7R axis may be a good strategy to develop newer AEDs.

Keywords: mesotemporal lobe epilepsy, hippocampus, microRNAs, P2X7 purinoceptor, miR-22, refractory epilepsy

INTRODUCTION

Mesial Temporal Lobe Epilepsy with Hippocampal Sclerosis (MTLE-HS) is the most frequent partial epilepsy in adults. Patients often present a history of Febrile Seizures (FS) in childhood and more than 80% are refractory to first-line anti-epileptic drugs (AEDs) requiring multiple drug regimens with limited success. In such cases, surgical ablation of the hippocampus and amygdala is the last resource to control epileptic seizures, yet this procedure may have devastating effects on patients' quality of life and constitutes a significant burden for national health care systems. Notwithstanding this, seizure recurrence may occur 10–18 years after surgery in 47% and 38% of the patients, respectively (Jeha et al., 2007; Hemb et al., 2013), and these patients remain with unmet clinical needs. While understanding the epileptogenic process is paramount to the development of newer AEDs, this task has been hampered because the mechanism(s) leading to MTLE-HS remain largely unknown.

Mounting evidence suggests a role for microRNAs (miRs) in the epileptogenic process (Henshall et al., 2016). These small non-coding RNA molecules function as post-transcriptional regulators of gene expression controlling biological processes, such as immune responses and neurotransmission. Different miR expression profiles have been described concerning epilepsy, with several miRs being up or downregulated after epileptic seizures, both in human patients and in animal models (Wang et al., 2015; Henshall et al., 2016). Interestingly, miRs are quite stable in biological fluids, such as plasma or serum, and normally reflect remote tissue production (Turchinovich et al., 2012), so circulating miRs have been proposed as promising novel biomarkers for diagnosis, prognosis and/or optimization of the anti-epileptic treatment (Wang et al., 2015; Henshall et al., 2016). In animal models, targeting specific miR molecules is associated with seizure reduction (Henshall, 2013). Circulating miR-22 is downregulated in an animal model of *status epilepticus* (Jimenez-Mateos et al., 2015). MiR-22 also displays a neuroprotective role in regulating neuronal death and apoptosis in a model of traumatic brain injury (Ma et al., 2016). It is also involved in the regulation of neuronal excitability, neuroinflammation, and aberrant neurogenesis, which are mechanisms tightly linked to ATP-mediated dangerous actions *via* P2X7 purinoceptors (P2X7R) activation (Jimenez-Mateos et al., 2015).

P2X7 purinoceptors are ligand-gated ion channels exhibiting low affinity for ATP, whose activation is only possible under conditions that favor extracellular ATP accumulation roughly to the millimolar concentration range (Rassendren et al., 1997; Sperlagh and Illes, 2014). Sustained extracellular ATP accumulation and subsequent P2X7 receptors activation are more likely during stressful conditions, such as a consequence of brain damage, hypoxia, and excessive neuronal activity during epileptic seizures. Yet, transient activation of this receptor may also be functionally relevant under physiological conditions, such as during synaptic plasticity phenomena triggered by high-frequency stimuli inherent to learning and memory processes (Campos et al., 2014). Once activated, the P2X7R behaves as a non-desensitizing cation channel involved in the long-lasting influx of Na^+ and Ca^{2+} and in the efflux of K^+, depending on ionic concentration gradients (Rassendren et al., 1997; Skaper, 2011). Prolonged P2X7R activation may lead to the formation of a reversible plasma membrane pore permeable to hydrophilic molecules up to 900 Da (Surprenant et al., 1996; Noronha-Matos et al., 2014). Using both human and animal preparations of the central nervous system (CNS), it has been demonstrated that the P2X7R is expressed in neurons, astrocytes, and microglia having pleiotropic effects modulating neuron-glia interaction, host defense, and neuroinflammation (Sperlagh and Illes, 2014). In microglial cells, the P2X7R has a trophic function modulating their activation and proliferation (Monif et al., 2009), which leads to the expression of pro-inflammatory cytokines, Il-1β and TNF-α, and reactive oxygen species (Ferrari et al., 1997; Skaper et al., 2010; Choi et al., 2012). Through this action, P2X7R may modulate neuronal cell death (Kanellopoulos and Delarasse, 2019). The presence of the P2X7R

in pre-synaptic nerve terminals and astrocytes explains its role in GABA and glutamate release (Marcoli et al., 2008). Our group has shown that P2X7R is overexpressed in neocortical nerve terminals of drug-resistant epileptic patients leading to down-modulation of GABA and glutamate uptake, which endures GABA signaling, increases GABAergic rundown, and, thereby, unbalances glutamatergic neuroexcitation (Barros-Barbosa et al., 2016). The presence of P2X7R in nerve terminals is controversial probably reflecting region-specific or pathology-associated neuronal expression. Upregulation of the P2X7R expression has also been verified in the hippocampus and cortex of animal models (Engel et al., 2012a; Jimenez-Pacheco et al., 2013, 2016; Barros-Barbosa et al., 2015, 2018; Morgan et al., 2020) contributing to resistance to pharmacotherapy during status epilepticus (Beamer et al., 2021). The neocortex of human patients with TLE also overexpress the P2X7R (Jimenez-Pacheco et al., 2013, 2016; Barros-Barbosa et al., 2016), but there is a gap in our knowledge concerning the location of this in the human hippocampus.

Recently, it was demonstrated that the P2X7R plasma levels were higher in rats with TLE than in control animals suggesting that it might have a putative role as a biomarker for the diagnosis and therapeutic follow-up of epilepsy (Conte et al., 2021). Interestingly, P2X7R antagonists reduce the number and duration of spontaneous seizures and gliosis, which effects are maintained beyond treatment cessation (Jimenez-Pacheco et al., 2013, 2016). The association between P2X7R antagonism and seizure suppression was confirmed by other research groups (Mesuret et al., 2014; Amhaoul et al., 2016; Amorim et al., 2017). Considering that increased expression of the P2X7R has been associated with down-modulation of the non-coding microRNA, miR-22, at the post-transcriptional level in a mouse model of status epilepticus (Jimenez-Mateos et al., 2015; Engel et al., 2017), we now set to compare the expression of P2X7R and miR-22 in epileptic brains and sera, respectively, of MTLE-HS patients.

MATERIAL AND METHODS

Brain Samples From Epileptic Patients and Cadaveric Controls

Resected fresh human brain samples were obtained from 23 MTLE-HS patients (13F/10M, 39.6 ± 9.8 years old; see **Table 1**) who underwent epilepsy surgical treatment (selective amygdalohippocampectomy or anterior temporal lobectomy) at the Neurosurgery Department of Hospital Santo António—Centro Hospitalar e Universitário do Porto (HSA-CHUP). The decision for surgery was taken by HSA-CHUP multidisciplinary epilepsy team incorporating neurologists, neurosurgeons, neuroradiologists, neurophysiologists, and neuropsychologists. All patients were resistant to maximal doses of two to four conventional AEDs used for more than two consecutive years (**Table 1**). Pre-surgical assessment was discussed by the team analyzing the results of brain MRI, prolonged video-EEG recording, ictal and interictal SPECT, neuropsychological assessment, and functional brain MRI, in order to determine the suitability of patients for surgical intervention.The antiepileptic drug therapy was not suspended before surgery; multi-AED combination regimens included 15 different drugs, most often comprising carbamazepine (n = 12), clonazepam (n = 11), levetiracetam (n = 8), topiramate (n = 6), valproic acid (n = 6) and oxcarbazepine (n = 5). The postoperative outcome was evaluated 7 years after surgery using the Engel Epilepsy Surgery Outcome Scale. The majority of patients were seizure-free (level I) or presented rare disability seizures (level II); only one patient showed no improvement after surgery (level IV).

TABLE 1 | Clinical and demographic data from MTLE-HS patients submitted to surgery.

Clinical/demographic data	MTLE-HS (n total = 23)
F/M	13 /10
Age at surgery ± SD, years (range)	39.6 ± 9.8 (24–60)
Age of onset ± SD, years (range)	10.3 ± 6.8 (1–28)
Disease mean duration ± SD, years (range)	29.3 ± 9.0 (10–49)
Number of antiepileptic drugs at surgery (AEDs = 2 / 3 / 4)	8 / 11 / 4
Hippocampal Sclerosis (Left /Right)	15 / 8
Febrile seizures antecedents (Yes / No)	15 / 8
Engel classification (I / II / III / IV)	16 / 2 / 4 / 1

AEDs, antiepileptic drugs; F, female; M, male; SD, standard deviation.

Surgical specimens of the hippocampus and anterior temporal lobe (neocortex) were collected. A complete coronal slice of 0.5 cm thickness was removed 3 cm posterior to the tip of the temporal pole. Samples were recovered in ice-cold artificial cerebrospinal fluid (CSF; 10 mM glucose, 124 mM NaCl, 3 mM KCl, 1 mM $MgCl_2$, 1.2 mM NaH_2PO_4, 26 mM $NaHCO_3$, 2 mM $CaCl_2$, pH = 7.40) and immediately cryopreserved in liquid nitrogen. The amount of tissue removed did not differ from the strictly necessary for successful surgical practice. Serum samples from the peripheral blood of nine out of the 23 MTLE-HS patients (4 F/5 M) were obtained for circulating miR-22 expression quantification (see below); three of these samples were collected at the time of surgery and the remaining were collected at the nearest blood test control. This study and all its procedures were approved by the Ethics Committees of HSA-CHUP and ICBAS-UP. All patients gave written informed consent, and the investigation conforms to the principles outlined in *The Code of Ethics of the World Medical Association* (Declaration of Helsinki).

Control brain samples were obtained using an identical procedure from 10 human cadavers (8 M/2 F, 67.0 ± 10.9 years old) with no previous history of neurologic disease, which were submitted to forensic autopsies performed within 4–7 h after post-mortem that corresponds to the tissue viability window for functional assays (see Barros-Barbosa et al., 2016). The indiscriminate occurrence of forensic autopsies to individuals meeting the inclusion criteria and the short post-mortem time-frame required to obtain good quality brain samples for functional and molecular assays are limitations difficult to overcome concerning sample size and matching of age/gender with the patients' group. Brain samples were discarded if post-collection assessment revealed active infectious or neoplastic diseases, chronic inflammatory conditions, neurologic poisoning, and/or past history of alcoholism and drug addiction.

TABLE 2 | Clinical and demographic data from MTLE-HS submitted to serum miR-22 determination.

Clinical/demographic data	MTLE-HS (n = 40)	
	Drug-refractory (n = 30)	Not refractory (n = 10)
F/M	23 / 17	7 / 3
Age ± SD, years (range)	43.0 ± 12.2 (24–68)	42.4 ± 12.3 (20–60)
Age of onset ± SD, years (range)	12.4 ± 9.8 (1–32)	12.8 ± 11.2 (1–51)
Disease mean duration ± SD, years (range)	30.7 ± 12.6 (6–56)	29.6 ± 13.9 (8–58)
Hippocampal Sclerosis (Left /Right / Bilateral)	18 / 11 / 1	7 / 3 / 0
Febrile seizures antecedents (Yes / No)	15 / 15	6 / 4
AED (0 / 1 / 2 / ≥ 3)	0 / 6 / 8 / 16	1 / 2 / 6 / 1

AEDs, antiepileptic drugs; F, female; M, male; SD, standard deviation.

Brain samples were made available by the Instituto Nacional de Medicina Legal e Ciências Forenses—Delegação do Norte (INMLCF-DN), according to Decree-Law 274/99, of 22 July, published in Diário da República—1st SERIE A, No. 169, of 22-07-1999, Page 4522, regarding the regulation on the ethical use of human cadaveric tissue for research. After collection, brain tissue was kept in cold artificial CSF (see above) until use.

Quantification of the P2X7R Gene Expression in Human Brain Tissue Samples

RNA was isolated from the fresh brain tissue, using the commercially available extraction kit RNeasy® Blood/Tissue kit (Qiagen, Germany) according to the manufacturer's instructions. RNA quantification and purity were evaluated using a Nanodrop Spectrophotometer (Thermo Scientific). Samples with an absorbance ratio at 260/280 nm between 1.5 and 2.0 were considered acceptable. RNA degradation was not assessed but according to previous reports, it remains stable for at least 36 h post-mortem (White et al., 2018). cDNA was synthesised with an available commercial kit (Nzy First-Strand cDNA Sunthesis Kit) in a BiometraAlfagene thermocycler, according to the manufacturer's instructions. P2X7R (hs0017521_m1) and the reference gene Ubiquitin C (UBC; hs00824723_m1) expression were quantified by Real Time PCR with specific primers and probes (Taqman® Kits, Applied Biosystems, USA) and a NzySpeedy qPCR mastermix (Nzytech, Portugal) in Corbett Rotor Gene 600 Real Time Thermocycler machine (Corbett Research, UK). UBC gene was chosen as the reference gene since its expression showed relatively low variability in expression levels in the regions studied (Trabzuni et al., 2011). Each reaction was performed in triplicate and the average Ct value was used in the analysis. The relative expression was calculated using the $2^{-\Delta\Delta CT}$ method.

Immunolocalization of P2X7R in the Human Hippocampus by Confocal Microscopy

Coronal sections of the hippocampus were fixed in 4% paraformaldehyde, cryopreserved in 30% sucrose, and stored in a tissue freezing medium at −80°C. Free-floating 30-μm hippocampal sections were incubated for 1 h, with blocking buffer (fetal bovine serum 10%, BSA 1%, triton X-100 0.5%, NaN_3 0.05%) and incubated overnight with the primary antibodies: rabbit anti-P2X7R (1:50, Alomone #APR-004, Jerusalem, Israel), goat anti-synaptic vesicle-associated membrane protein 1 (VAMP-1; 1:20, R&D Systems #AF4828, Minneapolis, MN, USA), and mouse anti-glial fibrillary acidic protein (GFAP, 1:200, Chemicon #MAB360, Temecula, CA, USA). Sections were rinsed and incubated for 2 h with species-specific secondary antibodies (donkey anti-rabbit Alexa Fluor 488, goat anti-mouse Alexa Fluor 633, and donkey anti-goat Alexa Fluor 633; Molecular Probes, Eugene, OR, USA). After mounting, sections were observed and analyzed with a laser scanning confocal microscope (Olympus FV1000, Tokyo, Japan). Co-localization was assessed by calculating the staining overlap and the Pearson's coefficient (ρ) for each confocal micrograph using the Olympus Fluoview 4.2 Software (Olympus FV1000, Tokyo, Japan), as previously described (Barros-Barbosa et al., 2016).

Immunoblot Analysis of the P2X7R Protein Amounts in Isolated Nerve Terminals of the Human Hippocampus

Total membrane lysates and nerve terminals of the hippocampus were isolated for immunoblot quantification of P2X7R protein amounts, as described previously (Bancila et al., 2009; see also Barros-Barbosa et al., 2016). Briefly, fragments of the hippocampus were gently homogenized in cold oxygenated (95% O_2/5% CO_2) Krebs solution (in mM: glucose 5.5, NaCl 136, KCl 3, $MgCl_2$ 1.2, Na_2HPO_4 1.2, $NaHCO_3$ 16.2, $CaCl_2$ 0.5, pH 7.40). The resulting homogenates were filtered through a nylon filter (mesh size 100 μm) to isolate nerve terminal membranes. The filtrate was left to sit until pellet formation, which was resuspended into Krebs solution and left at room temperature. The protein concentration was determined by the bicinchoninic acid method (Pierce, Thermo Scientific, Rockford, IL, USA) and was adjusted to 6.25 mg protein/mL. Membrane lysates and isolated nerve terminals were then homogenized in radioimmunoprecipitation assay buffer [Tris-HCl 25 mM (pH 7.6), NaCl 150 mM, sodium deoxycholate 1%, Triton-X-100 1%, SDS 0.1%, EDTA 5 mM, and protease inhibitors]. The samples were solubilized in SDS buffer [Tris-HCl 125 mM (pH 6.8), SDS 4%, bromophenol blue 0.005%, glycerol 20%, and 2-mercaptoethanol 5%], subjected to electrophoresis in SDS-polyacrylamide gels, and electrotransferred onto polyvinylidene difluoride (PVDF) membranes (Merck Millipore, Darmstadt, Germany). The

membranes were blocked in Tris-buffered saline [in mM: Tris-HCl 10 (pH 7.6), NaCl 150] containing Tween-20 0.05% and BSA 5% and incubated with the primary antibodies: mouse anti-GFAP (1:500, Chemicon, Temecula, CA, USA), mouse anti-synaptophysin (1:750, Chemicon, Temecula, CA), and rabbit anti-P2X7R (1:200; Alomone #APR-004, Jerusalem, Israel). Then, the membranes were washed and incubated with horseradish peroxidase–conjugated secondary antibody. For normalization purposes, the membranes were incubated with rabbit anti-β-actin antibody (1:1,000; Abcam, Cambridge, United Kingdom) or mouse anti-glyceraldehyde 3-phosphate dehydrogenase (GAPDH) antibody (1:200; Santa Cruz Biotechnology, Dallas, TX, USA) following the procedures described earlier. The antigen–antibody complexes were visualized using the ChemiDoc MP imaging system (Bio-Rad Laboratories, Hercules, CA, USA). Gel band image densities were quantified using Image J (National Institutes of Health, Bethesda, MD, USA). To test for specificity of the bands corresponding to P2X7R, the anti-P2X7R antibody was pre-adsorbed with a control peptide antigen corresponding to the amino acid residues 576–595 of the intracellular C-terminus of the P2X7R.

Quantification of the miR-22 Expression in the Human Serum

Serum samples were obtained from peripheral blood of 40 MTLE-HS patients (23 F/17 M, 43.0 ± 12.2 years old; 30 of them refractory to treatment; see **Table 2**) and 48 age-matched controls (28 F/20 M, 42.0 ± 10.8) without known neurological diseases. Patients were followed up at the Epilepsy Outpatient Clinic of the HSA-CHUP. All patients had MTLE-HS diagnosis based on clinical and electrophysiological studies (EEG and/or video-EEG monitoring) and on brain MRI (minimum 1.5 T) features. The definition of HS was based on brain MRI findings criteria which comprised atrophy, T2 hyperintensity signal, and altered internal structure on one or both hippocampi associated or not with other imaging criteria, like ipsilateral fornix atrophy, ipsilateral mamillary bodies atrophy, or ipsilateral entorhinal abnormalities. We excluded other MTLE-HS aetiologies like HS due to dual pathology. At the time of the study, 10 patients were not refractory to pharmacological treatment (**Table 2**). Data concerning FS antecedents was collected from patient medical records and 21 MTLE-HS patients had a history of FS (**Table 2**). Control individuals were voluntarily recruited among blood donors, ethnically matched, from the same geographic region.

Peripheral blood was collected in tubes without anticoagulant (Vacuette, GBO, Germany), centrifuged at 490 *g* and serum aliquots were stored at −20°C. RNA was extracted using the miRNeasy® Serum/Plasma Kit (Qiagen, Germany), according to the manufacturer's instructions. The synthesis of cDNA was performed with the Taqman® MicroRNA reverse Transcription-Applied Biosystems Kit (Applied Biosystems, USA) and a specific primer for miR-22 (Taqman® MicroRNA Assays, Applied Biosystems, USA). The reaction was performed in a BiometraAlfagene thermocycler accordingly to the manufacturer's instructions. The quantitative RT-PCR amplification was run with specific primers and probes for miR-22 (Taqman® MicroRNA Assays, Applied Biosystems, USA) and NzySpeedy qPCR mastermix (Nzytech, Portugal) in a Corbett Rotor Gene 600 Real Time Thermocycler (Corbett Research, UK). Each reaction was performed in triplicate and the average Ct value was used in the analysis. The relative expression was calculated using the $2^{-\Delta\Delta CT}$ method. MiR-22 level was evaluated in serum, a cell-free body fluid that is not known to have constant levels of a particular RNA species, hindering expression normalization by an endogenous control or housekeeping gene. To overcome this problem, the same serum volume was used for each subject and the same threshold was used so that expression levels could be compared between samples. Therefore, micro-RNA levels are expressed as 50-Ct (Wang et al., 2010).

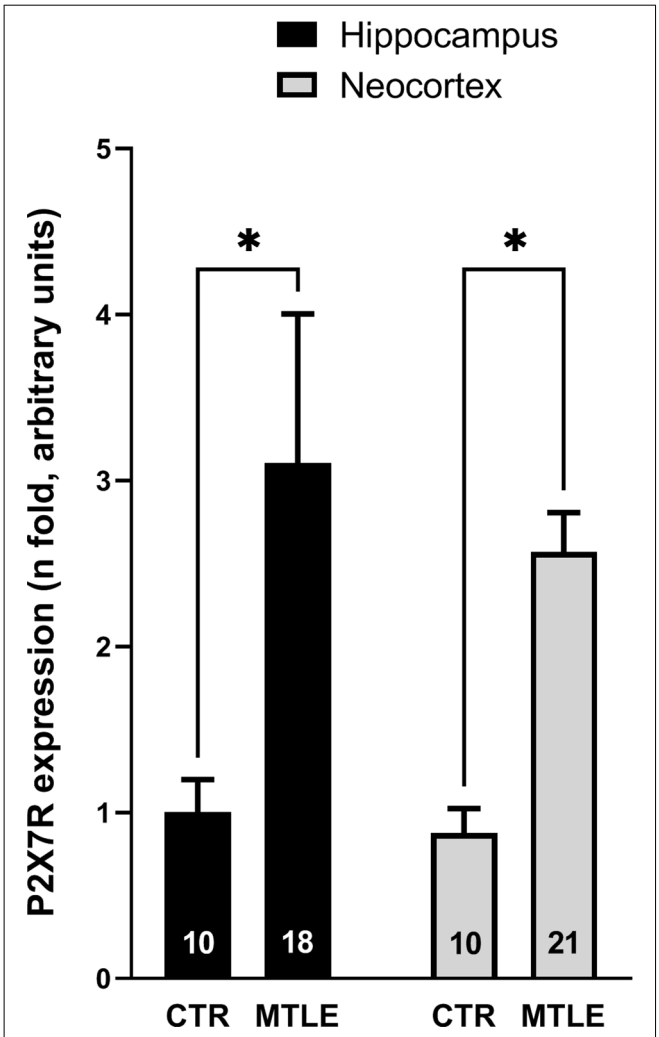

FIGURE 1 | The P2X7R mRNA is overexpressed in the hippocampus and temporal neocortex of drug-refractory MTLE-HS patients submitted to amygdalohippocampectomy compared to non-epileptic cadaveric controls (CTR). qPCR data are expressed as mean ± SD; *n* numbers inside each bar represent the number of individuals among 10 controls and 23 MTLE-HS patients in which quality assessment of retrieved RNA samples was suitable for quantification. *$p < 0.05$ (two-way ANOVA followed by Holm-Šídák's multiple comparisons test was used) represents significant differences when compared to control individuals.

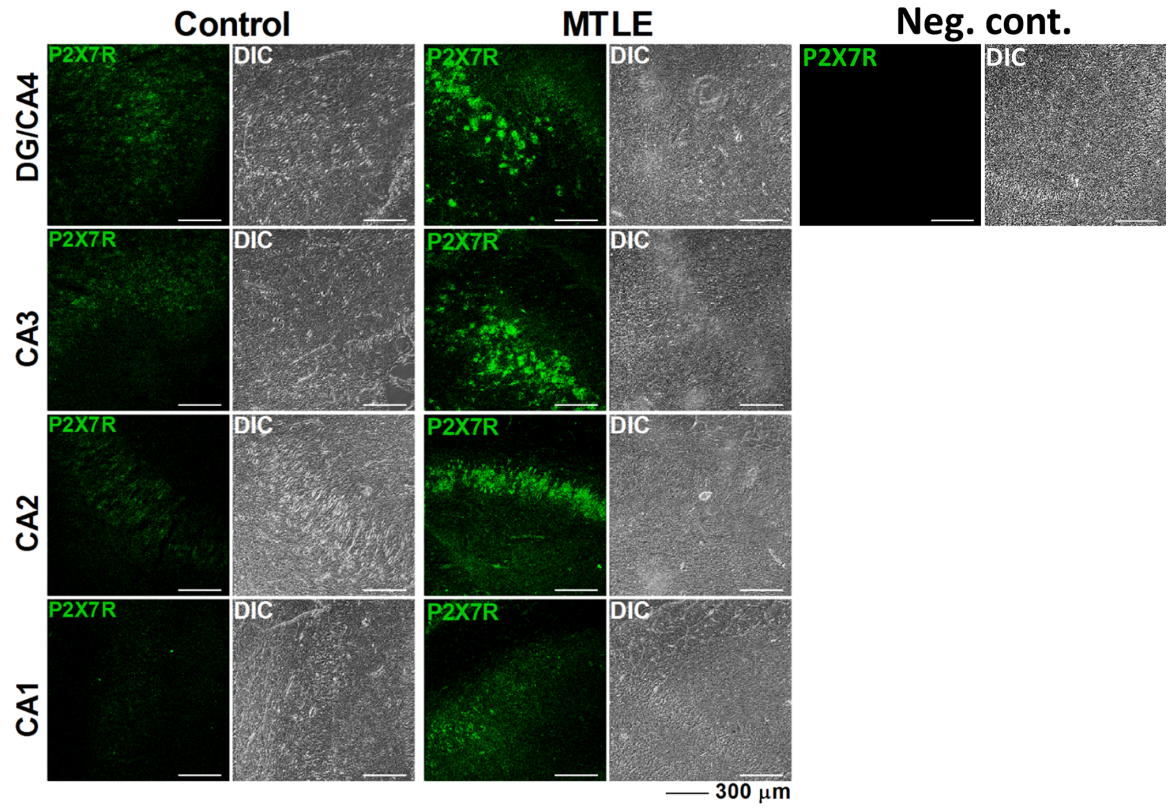

FIGURE 2 | Representative confocal micrographs of different sub-regions of the human hippocampus showing that the P2X7R immunoreactivity (green) is higher in the hippocampus of MTLE-HS patients than of non-epileptic cadaveric controls. A negative control resulting from incubation of the DG/CA4 hippocampal region of an MTLE-HS patient with the anti-rabbit secondary antibody without previous addition of the rabbit anti-P2X7R primary antibody (#APR-004) and differential interference contrast (DIC) images are shown for comparison; three confocal micrographs were obtained per individual; three individuals from each group (control and MTLE-HS) were analyzed showing similar results; scale bars = 300 μm.

Data Presentation and Statistical Analysis

P2X7R density was expressed as fold change of control individuals. Results are expressed as mean ± standard deviation (SD); "n" shown in graphs represents the total number of individuals. Normal distribution was evaluated with Kolmogorov-Smirnov test. Spearman's correlation coefficients were used to test interactions between age, age at onset, disease duration, and expression levels. Receiver Operator Characteristic (ROC) analysis was performed to investigate the ability of miR-22 serum levels to discriminate MTLE-HS patients, namely poorer responder to AEDs, from the control population. Statistical analysis was carried out using GraphPad Prism 9 software (La Jolla, CA, USA). Differences in ΔCt were evaluated using the unpaired Student's *t*-test with Welch correction. For multiple comparisons, one-way ANOVA with Dunnett's multiple comparison test or two-way ANOVA followed by Holm-Šídák's multiple comparison test was used, when indicated. $p < 0.05$ values were accepted as significant.

RESULTS

P2X7R mRNA transcripts are overexpressed in the hippocampus and temporal neocortex of MTLE-HS patients compared to that observed in control individuals (**Figure 1**). This was also observed at the P2X7R protein level in all sub-regions of the hippocampus, as demonstrated by immunofluorescence confocal microscopy (**Figure 2**). Increased P2X7R mRNA amounts in the hippocampus and temporal neocortex were not significantly ($p > 0.05$) correlated with gender, age of epilepsy onset, age at surgery, nor the duration of the disease condition (**Table 3**). Likewise, no significant differences ($p > 0.05$) were observed in the amount of P2X7R mRNA transcripts measured in the hippocampus and temporal neocortex among MTLE-HS patients' subgroups taking two, three, or four AED combinations at the time of surgery (data not shown). We also failed to detect differences ($p > 0.05$) in the amounts of P2X7R mRNA transcripts expressed in the hippocampus and temporal neocortex of MTLE-HS patients grouped by the three most prescribed AEDs, carbamazepine ($n = 12$), clonazepam ($n = 11$), and levetiracetam ($n = 8$), to ensure minimal statistical power.

Considering that epileptic patients submitted to surgery were significantly younger (39.6 ± 9.8 years old, $n = 23$) than the cadaveric controls (67.0 ± 10.9 years old, $n = 10$), and because aging can affect the expression of inflammasome components (Mawhinney et al., 2011), we asked whether age differences could account for increases in the P2X7R expression in the brain

TABLE 3 | Spearman's correlation analysis regarding the P2X7R expression.

	Age of onset	Disease duration	P2X7R Hip	P2X7R Ctx
Age of onset				
Correlation Coefficient	1	−0.311	0.326	−0.300
Sig (2-tailed)	- - -	0.148	0.187	0.186
Disease Duration				
Correlation Coefficient	−0.311	1	−0.017	−0.118
Sig (2-tailed)	0.148	- - -	0.948	0.609
P2X7R Hippocampus				
Correlation Coefficient	0.326	−0.017	1	0.383
Sig (2-tailed)	0.187	0.948	- - -	0.053
P2X7R Cortex				
Correlation Coefficient	−0.300	−0.118	0.383	1
Sig (2-tailed)	0.186	0.609	0.053	- - -

of epileptic patients. Using a Spearman's correlation analysis, we detected no significant correlation between the P2X7R expression and age of epileptic patients (**Figures 3B,D**), as well as of cadaveric controls (**Figures 3A,C**), both in the hippocampus (**Figures 3A,B**) and in the temporal neocortex (**Figures 3C,D**).

The confocal micrographs depicted in **Figure 4A** show that the P2X7R is predominantly overexpressed in VAMP-1-positive synaptic nerve terminals of all sub-regions of the epileptic hippocampus. Higher magnification images also show that the P2X7R co-localizes with the synaptic vesicle glicoprotein synaptophysin (Synapt), which is one of the most commonly used neuronal cell markers in neuropathology (**Figure 4E**). The P2X7R did not ($p > 0.05$) co-localize with the astrocytic cell marker, GFAP, despite the extensive astrogliosis existing in this epileptic brain area (**Figure 4B,F**; higher magnification images are shown in **Figure 4F**). Co-localization was assessed by evaluating the Pearson's coefficient (ρ) and staining overlap obtained by merging the two fluorescent channels (yellow staining; **Figures 4C,D**), as reported in a previous article (Barros-Barbosa et al., 2016).

Moreover, we show here that the P2X7R protein is enriched in isolated nerve terminals (**Figure 5A**) compared to total lysates of the hippocampus of MTLE-HS patients (**Figure 5B**), which is in agreement with that found in the human temporal neocortex (Jimenez-Pacheco et al., 2013; Barros-Barbosa et al., 2016). While the naturally occurring 67 kDa P2X7R protein predominates in the brain of non-epileptic controls (**Figures 5B,C**), a higher molecular weight (∼85 kDa) protein accounts more for the P2X7R overexpression in epileptic hippocampi (see e.g., Jimenez-Mateos et al., 2019; Mccarthy et al., 2019). Both P2X7R protein isotypes disappeared after pre-adsorption of the membranes with the control antigen peptide corresponding to amino acid residues 576–595 of the P2X7R intracellular C-terminus (**Figure 5B**, last lane).

Previous studies conducted in animal models suggest that miR-22 exerts a neuroprotective role in traumatic (Ma et al., 2016) and epileptic (Jimenez-Mateos et al., 2015) brain injuries by a mechanism tightly linked to P2X7R deactivation. Moreover, downregulation of circulating miR-22 was detected following *status epilepticus* in mice (Jimenez-Mateos et al., 2015). This prompted us to investigate if P2X7R overexpression in the hippocampus and temporal neocortex of drug-refractory MTLE-HS patients was associated with the downregulation of miR-22 serum amounts in these patients. An inverse relationship between miR-22 in the serum and the P2X7R mRNA expression in the hippocampus (**Figure 6A**) and temporal neocortex (**Figure 6B**) of epileptic patients was verified, i.e., low miR-22 in the serum corresponds to increases in P2X7R gene transcription in these two brain regions.

As a proof of concept, we also compared the miR-22 serum levels of 40 MTLE-HS patients (23 F/17 M; 43.0 ± 12.2 years old) followed at the Epilepsy Outpatient Clinic of HSA-CHUP with 48 age- and gender-matched blood donor controls (28 F/20 M; 42.0 ± 10.8 years old) with no known neurological disease condition. **Figure 7A** shows that MTLE-HS patients exhibit significantly lower ($p = 0.001$) miR-22 serum levels than the control population. This difference is even more evident in the subpopulation of epileptic patients requiring more than three different AEDs to control seizures ($p < 0.001$; **Figure 7B**). Like that observed concerning the P2X7R mRNA expression in the brain, no significant correlations ($p > 0.05$) were observed between mir-22 serum levels and gender, age of onset, age at surgery, and/or duration of the disease condition (**Table 4**).

The Receiver Operating Characteristics (ROC) graphs are commonly used in medical decision making. ROC graphs have long been used in signal detection theory to depict the trade-off between hit rates and false alarm rates of classifiers. A high area under the ROC curve (0.696; 95% CI 0.576–0.817; $p = 0.0023$) is consistent with low miR-22 serum levels being a sensitive biomarker for discriminating MTLE-HS patients (**Figure 7C**). The ROC curve analysis with an AUC of 0.777 (95% CI 0.629–0.925; $p = 0.001$) demonstrates that miR-22 serum expression levels (50-Ct) below 20 are highly specific (89%) and sensitive (69%) for discriminating healthy controls from poorer responders to anti-epileptic medication, i.e., MTLE-HS patients requiring more than three AEDs to control seizures (**Figure 7D**).

DISCUSSION

Our results show for the first time, that downregulation of miR-22 gene transcripts in the serum is inversely related to P2X7R overexpression in the hippocampus and temporal neocortex of human MTLE-HS patients, which is in agreement

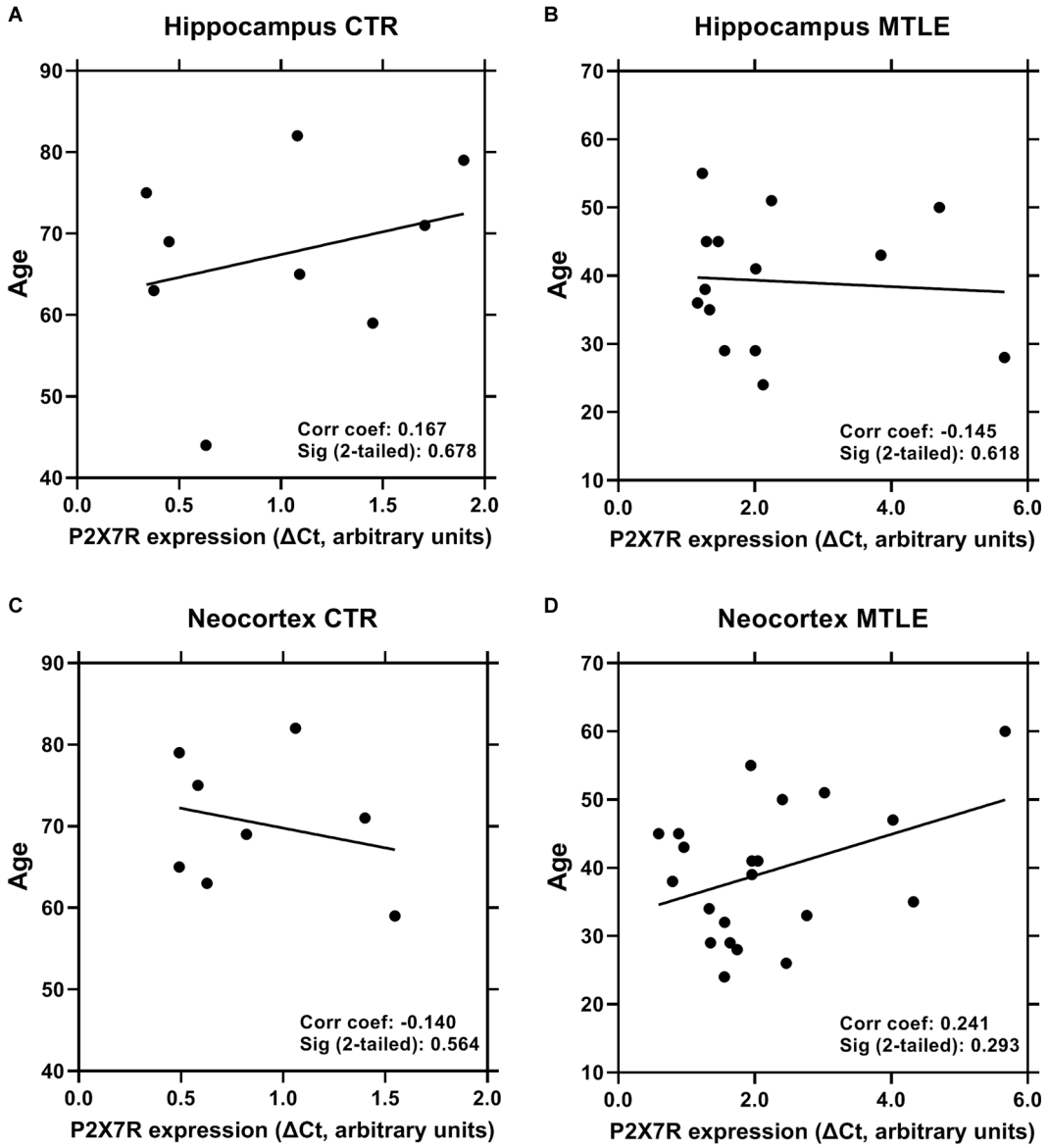

FIGURE 3 | No significant correlation was observed between the P2X7R expression and the age of epileptic patients (panels **B** and **D**) and non-epileptic cadaveric controls (panels **A** and **C**), both in the hippocampus (panels **A** and **B**) and in the temporal neocortex (panels **C** and **D**). Each point represents an individual sample among 10 controls and 23 MTLE-HS patients in which quality assessment of retrieved RNA samples was suitable for quantification. Spearman's correlation coefficients and significance *p* values (two-tailed) are shown inside each graph.

with the prediction made in the experimental TLE animal model (Jimenez-Mateos et al., 2015). Data also suggests that the inverse relationship between miR-22 and P2X7R gene transcription may occur soon after the epileptogenic trigger, but once established it is unlikely to be affected by the duration of the disease condition, as well as by the age of onset and gender. A high area under the ROC curve indicates that low miR-22 serum levels may be a highly specific biomarker to anticipate MTLE-HS patients with poor response to medication.

Brain damage and other stressful conditions, such as ischemia, trauma, or excessive neuronal activity, lead to a rapid upregulation of the P2X7R gene transcription and protein translation (North, 2002). This typically coincides with increases in extracellular ATP levels, thus favoring activation of low-affinity slow-desensitizing P2X7 receptors. Signaling through these receptors may affect both neuroinflammation and neurotransmission, which is associated with exacerbation and propagation of seizures throughout the brain. Upregulation of the P2X7R subtype in the temporal neocortex adjacent to the hippocampus, a region that is highly committed to seizure propagation, strengthens the overall pro-epileptic role of this ATP-sensitive receptor subtype predicted by several authors.

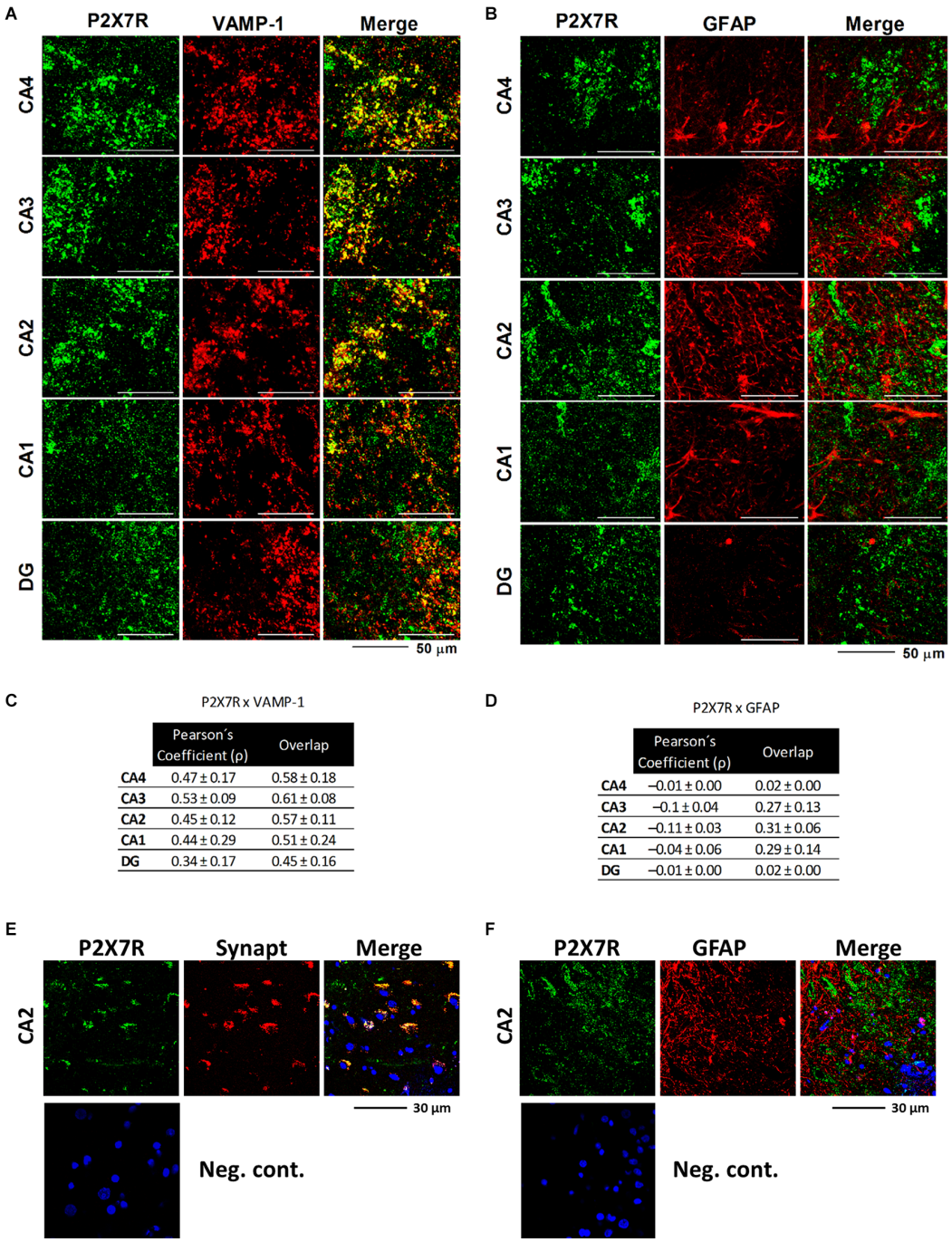

	Pearson´s Coefficient (ρ)	Overlap
CA4	0.47 ± 0.17	0.58 ± 0.18
CA3	0.53 ± 0.09	0.61 ± 0.08
CA2	0.45 ± 0.12	0.57 ± 0.11
CA1	0.44 ± 0.29	0.51 ± 0.24
DG	0.34 ± 0.17	0.45 ± 0.16

	Pearson´s Coefficient (ρ)	Overlap
CA4	−0.01 ± 0.00	0.02 ± 0.00
CA3	−0.1 ± 0.04	0.27 ± 0.13
CA2	−0.11 ± 0.03	0.31 ± 0.06
CA1	−0.04 ± 0.06	0.29 ± 0.14
DG	−0.01 ± 0.00	0.02 ± 0.00

FIGURE 4 | Representative confocal micrographs showing that the P2X7R immunoreactivity is located predominantly in nerve terminals, but not in glial cells, of all sub-regions of the hippocampus of MTLE-HS patients. Synaptic nerve terminals were identified with an antibody against the vesicle-associated membrane protein 1 (VAMP-1 or synaptobrevin 1), whereas astrocytes were stained with an antibody against the glial fibrillary acidic protein (GFAP). Note that VAMP-1-positive nerve terminals (red) are endowed with the P2X7R (green; panel **A**), but no significant co-localization was observed between P2X7R (green) and GFAP (red; panel **B**); scale bars = 50 μm. Data in panels **(C)** and **(D)** correspond to staining overlap and Pearson's Coefficient (ρ) parameters calculated from three to four confocal micrographs per individual; at least three individuals from each group, control, and MTLE-HS, were analyzed. These parameters were automatically calculated per image with Olympus Fluoview 4.2 Software (Olympus FV1000, Tokyo, Japan) and were used to estimate the co-localization of P2X7R and type-specific cell markers (yellow staining). Overlap between two colors gives values between +1 (total overlap) and 0 (no overlap); the Pearson's Coefficient (ρ) is a measure of the linear correlation between two variables (stainings), giving values between +1 and −1 inclusive, where 1 is total positive correlation, 0 is no correlation, and −1 is total negative correlation. Higher magnification images show that the P2X7R immunoreactivity also co-localizes with the synaptic vesicle glicoprotein synaptophysin (Synapt), which is one of the most commonly used neuronal cell markers in neuropathology (Panel **E**), but not with GFAP (Panel **F**). Nuclei are stained with DAPI; cross-reactivity for the secondary antibodies was tested in control experiments in which primary antibodies were omitted (negative controls).

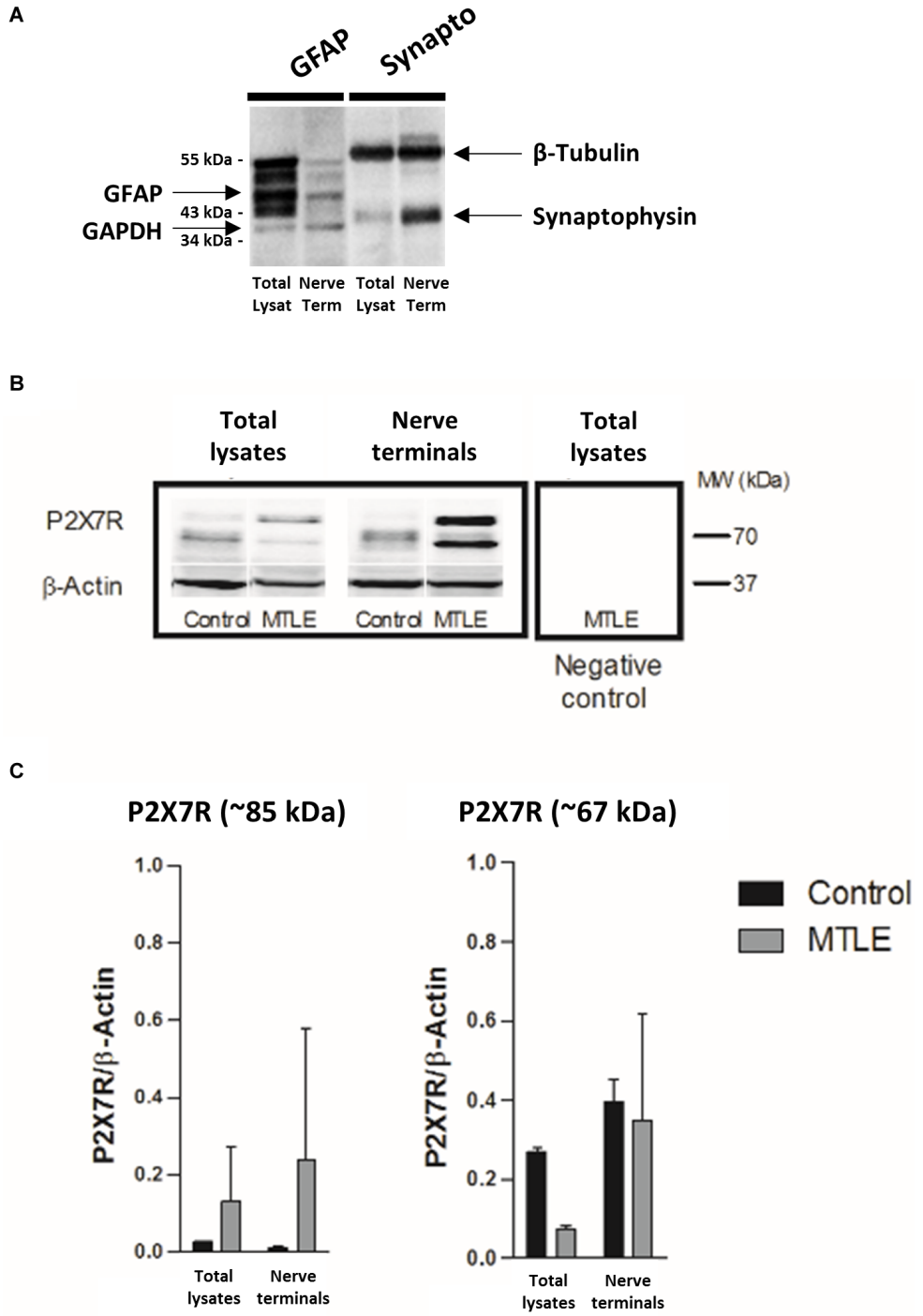

FIGURE 5 | The P2X7R protein is upregulated in nerve terminals of the hippocampus of drug-refractory MTLE-HS human patients. Panel **(A)** shows that using our methodology nerve terminals isolated from the hippocampus of MTLE-HS patients exhibit a higher density of the synaptic vesicle marker, synaptophysin (~34 kDa), compared to the astrocytic cell marker, GFAP, whilst the opposite was observed in total hippocampal lysates. In panel **(B)** are shown representative Western blots of the P2X7R immunoreactivity in total lysates and nerve terminals isolated from the human hippocampus of control individuals and MTLE-HS patients; gels were loaded with 100 μg of protein. Two protein species were recognized by the P2X7R antibody from Alomone (#APR-004, Jerusalem, Israel) corresponding to the naturally occurring 67 kDa receptor isoform and to a higher molecular mass (~85 kDa) P2X7R isotype; the latter is highly enriched in nerve terminals of the hippocampus of MTLE-HS patients compared to non-epileptic controls. Please note that the two bands corresponding to the P2X7R protein disappeared after pre-adsorption of the primary antibody with a control antigen peptide equivalent to the amino-acid residues 576–595 of the intracellular C-terminus of the P2X7R (negative control); β-Actin (38–41 kDa) was used as a reference protein. Panel **(C)** shows computed data obtained from immunoblot experiments; data are expressed as mean ± SD; each individual sample was processed in duplicate; at least three individuals from each group (control and MTLE-HS) were analyzed.

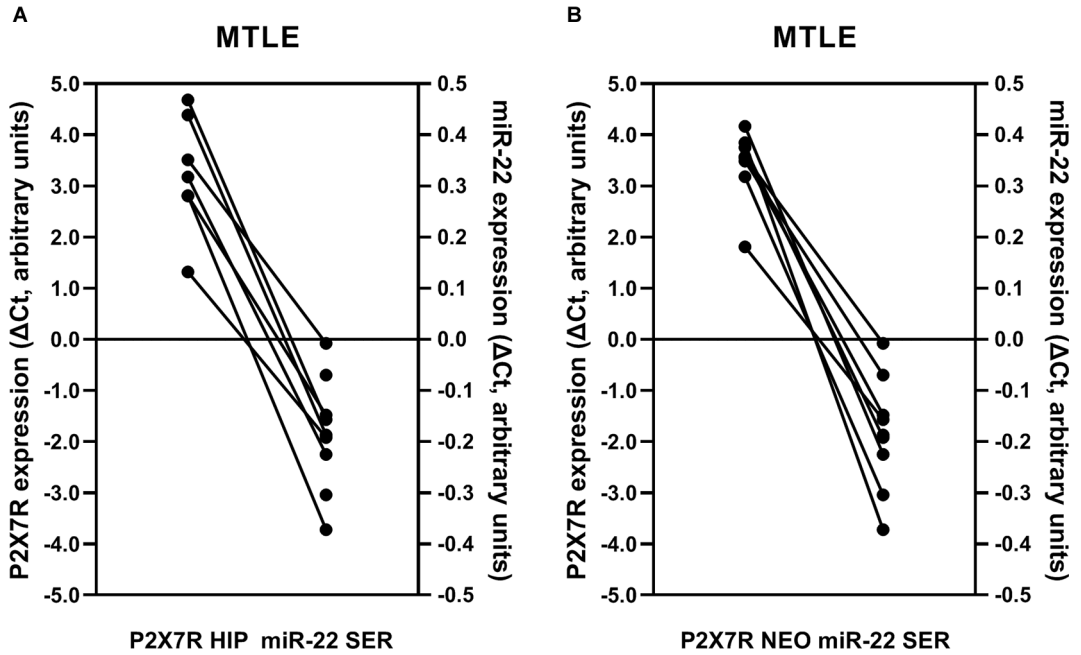

FIGURE 6 | The inverse relationship between miR-22 serum levels and the P2X7R expression in the hippocampus **(A)** and temporal neocortex **(B)** from drug-refractory MTLE-HS patients submitted to amygdalohippocampectomy. Ordinates represent ΔCt variation of P2X7R and miR-22 expression in epileptic patients compared to the corresponding median of non-epileptic controls; 0 represents null variation; positive and negative values correspond to increases and decreases relative to the control population, respectively. Please note that there is a mismatch between miR-22 serum quantifications and P2X7R mRNA determinations in the hippocampus (**A**, two patients missing) and temporal neocortex (**B**, one patient missing) because RNA samples were insufficient or did not pass the quality assessment.

Controversy exists regarding the cellular localization of P2X7R in the brain. Previous studies showed that P2X7R are predominantly located on glial cells, including microglia, oligodendrocytes, and astrocytes, although neuronal expression has also been described (Engel et al., 2012b; Barros-Barbosa et al., 2016). Differential cellular expression of the P2X7R seems to be highly dependent on the model and/or stage of the epileptic process under evaluation. For instance, in animal models of TLE or *status epilepticus* (Rappold et al., 2006; Dona et al., 2009; Jimenez-Pacheco et al., 2016), the P2X7R localizes predominantly in microglial cells of the CA3 hippocampal region, thus coinciding with major neuronal cell losses in this brain area (Engel et al., 2012a; Jimenez-Pacheco et al., 2013, 2016; Barros-Barbosa et al., 2016). This pattern dramatically changes in the CA1 and dentate gyrus regions where the P2X7R was found to be more abundant in neuronal cell populations (Dona et al., 2009; Engel et al., 2012a; Jimenez-Mateos et al., 2015). One may also argue that this may reflect different roles of the P2X7R according to distinct phases of epileptogenesis. *Ab initio*, the P2X7R upsurge may be relevant in order to negatively compensate for neuronal overexcitation (Armstrong et al., 2002) and to overcome cellular damage arising from excessive neuronal activity. As a consequence of this phenomenon, there is an increase in extracellular ATP levels with subsequent P2X7R overactivation, promoting proliferation and activation of microglial cells (Monif et al., 2009). This results in synchronous release of pro-inflammatory cytokines (Ferrari et al., 1997; Skaper et al., 2010; Choi et al., 2012), which are required for damaged cell repair. *In vitro* studies suggest the existence of a positive feedback loop between IL-1β and P2X7R (Narcisse et al., 2005), which may explain overexpression of both gene transcripts in the hippocampus and temporal neocortex of this MTLE-HS patients cohort (this study; see also Leal et al., 2017). In this situation of altered excitability, inflammatory microenvironment, and activated microglia, the extracellular levels of ATP continue to escalate and long-term P2X7R activation may lead to sustained and uncontrolled inflammatory reactions, cell death, and hyperexcitability (Sperlagh and Illes, 2014). Prolonged P2X7R activation rends cells more susceptible to ATP-induced death due to the formation of a plasma membrane pores resulting in intracellular Ca^{2+} overload and to the efflux of potassium and other relevant metabolites in a manner that is independent of inflammatory actions (Balosso et al., 2008; Skaper, 2011; Henshall, 2013). This scenario triggers synaptic neurotransmission deficiencies by interfering with glutamate homeostasis and ATP/adenosine metabolism (Barros-Barbosa et al., 2016, 2018). In addition, inflammatory cytokines may also interfere with neurotransmitter signaling, namely *via* NMDA receptors, resulting in neuronal hyperexcitability (Balosso et al., 2008). All these events aggravate neuronal network instability and dysregulation characterizing epilepsy, thus contributing to seizures prolongation and propagation to other brain regions.

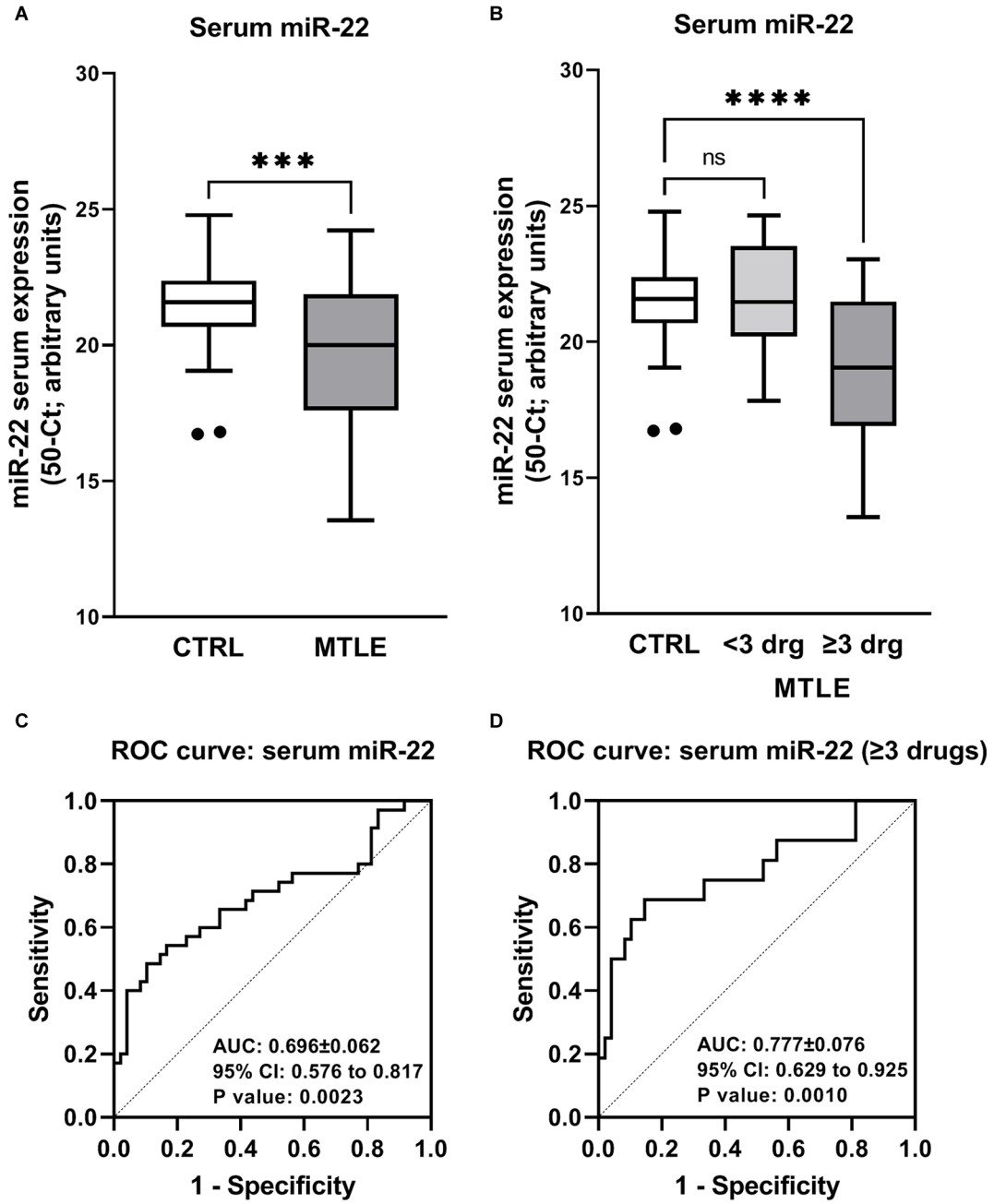

FIGURE 7 | Patients with drug-refractory MTLE-HS exhibit lower miR-22 serum levels than the control population (panel **A**). This difference is exaggerated when patients with poor response to medication (requirement of three or more AEDs) are considered (panel **B**). Boxes and whiskers (Tukey method) represent pooled data from 48 blood donor controls (CTRL) and 40 MTLE-HS patients (panel **A**); in panel **(B)** epileptic patients were subdivided into drug-resistant (≥3 AE Drugs) and non-drug-resistant (<3 AE Drugs). The values plotted individually are outliers according to the Grubbs test. In panel **(A)**, ***$p < 0.001$ (unpaired Student's *t*-test with Welch correction) represent significant differences compared to the control population; in panel **(B)**, ****$p < 0.0001$ (one-way ANOVA with Dunnett's multiple comparison test) represent significant differences compared to the control population. ns = non-significant. In panels **(C)** and **(D)**, represented are the receiver-operator characteristics (ROC) curves of miR-22 serum levels considering the whole MTLE-HS patients' population (panel **C**) or only patients from this cohort taking more than three AEDs (panel **D**). Please note that the area under de curve (AUC) increases considering MTLE-HS patients with poorer response to medication.

Using confocal microscopy for P2X7R protein co-localization with cell-type specific fluorescent markers (VAMP-1 and GFAP for nerve terminals and astrocytes, respectively), together with Western blot analysis to distinguish the P2X7R protein density in isolated nerve terminals *vis-a-vis* total cell membrane lysates, we show here for the first time that P2X7R is predominantly expressed in nerve terminals of the hippocampus of MTLE-HS human patients. Our findings agree with data obtained in

TABLE 4 | Spearman's correlation analysis for miR-22 serum expression.

	Age of onset	Disease duration	Circulating miR-22
Age of onset			
Correlation Coefficient	1	−0.89	0.207
Sig (2-tailed)	- - -	0.071	0.200
Disease Duration			
Correlation Coefficient	−0.89	1	0.269
Sig (2-tailed)	0.071	- - -	0.094

experimental TLE animal models, as well as in the temporal neocortex of epileptic patients (Armstrong et al., 2002; Vianna et al., 2002; Yu et al., 2008; Engel et al., 2012a; Jimenez-Pacheco et al., 2013, 2016; Barros-Barbosa et al., 2016). Mounting evidence suggests that neuronal P2X7R activation regulates the extracellular levels of GABA and glutamate (Khakh et al., 2003), indirectly by interfering with neuronal excitability, or more directly due to massive dysregulation of cytoplasmic ion homeostasis and consequent alteration of depolarization thresholds (Armstrong et al., 2002; Sperlagh et al., 2002). In this regard, our group showed that P2X7R activation downmodulates Na^+-dependent GABA and glutamate uptake in isolated nerve terminals from epileptic patients also contributing to the extracellular accumulation of these neurotransmitters (Barros-Barbosa et al., 2016). It seems that the P2X7R differentially regulates GABA and glutamate release depending on neuronal activity and microenvironment conditions (Barros-Barbosa et al., 2018).

Extracellular GABA accumulation caused by P2X7R over activation might not be protective as one would initially predict, since it may contribute to neuronal hyperexcitability due to paradoxical GABAergic "rundown" in the epileptic human brain (Barros-Barbosa et al., 2016). In line with these observations, it has been shown that overexpression of the P2X7R reduces responsiveness to anti-convulsants that may be overcome by P2X7R antagonists in animal models of *status epilepticus* (Beamer et al., 2021). Some authors claim that there is a reduction in seizure severity associated with reduced neuronal damage (Jimenez-Pacheco et al., 2013; Mesuret et al., 2014), while others argue that only the number and frequency of seizures are reduced (Jimenez-Pacheco et al., 2016). An interesting, yet puzzling, result is that the effect is maintained and sometimes even amplified when treatment with P2X7R antagonists is discontinued (Jimenez-Pacheco et al., 2016). Moreover, P2X7R antagonists have been shown to potentiate the anticonvulsant effects of lorazepam (Engel et al., 2012a) and carbamazepine (Fischer et al., 2016). Notwithstanding this, contradictory results regarding the P2X7R effect in seizure development have been reported using different animal models. For instance, while P2X7R inhibition leads to exacerbation of pilocarpine-induced chronic seizures, a situation that is commonly associated with high neuronal death and reduced astrocytic cell damage in the CA3 hippocampal area, blockage of P2X7R activation had no effect in seizures outcome of kainic acid-induced *status epilepticus* (Kim and Kang, 2011). As mentioned before, these idiosyncrasies may be justified taking into consideration the cellular type that is predominantly affected in each epilepsy model, as well as the mechanism and stage of the epileptogenic process being considered.

Remarkably, two protein species were recognized by the KO-validated P2X7R antibody (Apolloni et al., 2013). One corresponds to the naturally occurring (∼67 kDa) P2X7R isotype found in control brain specimens, while the other showing a higher molecular weight (∼85 kDa) identified a predominant P2X7R isoform in epileptic hippocampal nerve terminals. The putative clinical significance of the P2X7R enrichment in hippocampal nerve terminals *vis-a-vis* total lysates and the molecular mass gain of this receptor isoform cannot be answered by the present experimental setting, but it certainly deserves to be explored in future functional studies. Epileptogenesis may involve changes in the complex regulatory mechanisms that influence receptors expression, localization, and function, which include epigenetic DNA methylation, alternative splicing, microRNA interference, and post-translational modifications (e.g., phosphorylation, glycosylation, and palmitoylation) affecting receptors trafficking, assembly, and opening (see e.g., Jimenez-Mateos et al., 2019; Mccarthy et al., 2019). Despite AEDs can significantly influence epigenetics, as for instance chromatin-related epigenetic alterations (Navarrete-Modesto et al., 2019), we found any significant correlation between the number and type of combinatorial AED regimens at maximal therapeutic doses and the amount of P2X7R mRNA transcripts detected in the hippocampus and temporal neocortex of drug-refractory MTLE-HS surgical patients.

Mounting evidence suggests that acute and chronic P2X7R expression is tightly controlled in the CNS and that dysregulation of these mechanisms during epileptogenesis may affect disease severity and progression. Unilateral injection of kainic-acid induces P2X7R overexpression in the ipsilateral epileptogenic focus, but not in the contralateral hippocampus (Jimenez-Mateos et al., 2015). This was ascribed to post-transcriptional repression of the P2X7R in the contralateral hippocampus by a microRNA molecule, the miR-22 (Jimenez-Mateos et al., 2015). These authors also showed that miR-22 targeting of the P2X7 purinoceptor opposes seizure development. Coincidently or not, both P2X7R and miR-22 are regulated by the same transcription factor whose action is dependent on intracellular Ca^{2+} levels (Engel et al., 2017). The specificity protein 1 (Sp1) has been shown to induce P2X7R transcription *in vitro* and Sp1 occupancy of the miR-22 promoter region is blocked under conditions of high Ca^{2+} influx into neuronal cells, such as those occurring during excessive P2X7R activation driven by high ATP amounts released from cells during seizures. This calcium-sensitive feed-forward loop regulating the neuronal expression of the ATP-gated P2X7R is accompanied by a pro-convulsive downregulation of miR-22-mediated translational repression of the P2X7R protein synthesis leading to this receptor overexpression at the plasma membrane.

Our results strengthen this theory, since we observed that drug-refractory MTLE-HS patients possess higher than control levels of P2X7R in the hippocampus and adjacent temporal neocortex whilst miR-22 is downregulated in the serum. Our results are also in keeping with those obtained in the brain of epileptic animals used to validate serum

microRNA quantification. A similar relationship has also been observed in other neuroinflammatory disease conditions, such as amyotrophic lateral sclerosis (Parisi et al., 2013). One important limitation of our study is that due to technical reasons we were not able to measure miR-22 expression in the brain. For obvious reasons the amount of epileptic brain tissue available for the experiments was very limited, so we were only able to extract total RNA, which prevented the possibility of isolating and accurately quantifying the different RNA subtypes, including non-coding miRs (Brown et al., 2018). Having this in mind and knowing that miRs are very stable in biological fluids where they are thought to reflect remote tissue production (Turchinovich et al., 2012), we believe that serum miR-22 levels may be a clinical surrogate of its production in the brain whose levels may vary inversely to P2X7R expression in the cerebral tissue.

It is particularly interesting to note that MTLE-HS patients controlled with only one or, at least, two AEDs (good responders) had similar miR-22 serum expression levels as control individuals, whereas those requiring more than three AEDs to control seizures (poor responders) typically present low circulating amounts of this microRNA. In an animal model of traumatic brain injury, low miR-22 expression is associated with higher neuronal cell damage (Ma et al., 2016). Recently, it was also shown that miR-22 deficient mice have a more severe epilepsy phenotype, with seizures beginning earlier and being more frequent and longer than in wild-type littermates (Almeida Silva et al., 2020). Such differences are more prominent in early epilepsy stages and these animals overexpress the P2X7R in the brain. Genetic ablation of miR-22 blunted the inflammatory transcriptional response to *status epilepticus* and exacerbated epilepsy highlighting the putative dual role of inflammation in epileptogenesis. While this feature may be detrimental during later epileptogenesis stages when global cell dysregulation is observed, it may be beneficial at the initial inflammatory phase to remove cellular debris and to promote cell repair in order to recover homeostasis. In keeping with this, it has been demonstrated that miR-22 is an important regulator of morphogenesis of newly formed neurons in adults and it plays a role in suppressing aberrant neurogenesis associated with *status epilepticus* (Beamer et al., 2018).

Our results suggest that circulating miR-22 may be a promising biomarker of drug refractoriness in MTLE-HS patients. We are aware that changes in circulating levels of miR-22 may be produced by other (yet to resolve) clinical conditions besides MTLE-HS. Nevertheless, we anticipate that measuring serum miR-22 amounts might be useful if included with other putative biomarkers in epileptic patients' evaluation. In this regard, data from animal studies also point toward the quantification of P2X7R plasma levels as a useful biomarker for the diagnosis and therapeutic follow-up of epileptic individuals (Conte et al., 2021). Monocytes have been claimed as the main source of circulating PX7R, yet excessive brain production of this protein in epileptics cannot be excluded. Given the inverse relationship between circulating P2X7R and miR-22, it is tempting to speculate that both biomarkers possess the same neuronal origin in epileptics, and this deserves to be elucidated in future studies using larger multi-center cohorts.

Chronic epilepsy patients' refractory to multiple AED regimens, such as those referred to neurosurgical treatment in the present study, likely present seizures that are more frequent and severe. It is tempting to assume that, in these cases, sustained extracellular ATP accumulation together with the 85 kDa P2X7R protein overexpression, resulting in uncontrolled neuroinflammatory reaction and synaptic transmission dysregulation, may act as a positive feed-forward detrimental loop ending up in cellular damage and unrestrained seizures progression. Given the physiological role of the P2X7R to higher brain functions, like memory and cognition, the purinergic dysregulation may be more severe in predisposed individuals, who also may present more significant memory deficits as a co-morbid clinical condition. As a matter of fact, genetically predisposed individuals of the rs16944TT genotype displaying higher IL-1β (and P2X7) expression levels are more susceptible to developing MTLE-HS and seizure recurrence (Leal et al., 2018).

The mechanisms underlying P2X7R overexpression promoted by de-repression of miR-22-induced post-translational modifications may constitute novel molecular targets for the treatment of drug-refractory MTLE-HS patients. The timing of therapeutic intervention and whether it can effectively revert epileptogenesis and disease progression requires further investigations in animal models. Once proven, candidates for this putative novel therapeutic intervention may be selected by a simple blood test among drug-refractory epileptics exhibiting low miR-22 serum levels.

DATA AVAILABILITY STATEMENT

The raw data supporting the conclusions of this article will be made available by the authors, without undue reservation.

ETHICS STATEMENT

The studies involving human participants were reviewed and approved by Hospital de Santo António—Centro Hospitalar Universitário do Porto/Instituto de Ciências Biomédicas de Abel Salazar—Universidade do Porto. The patients/participants provided their written informed consent to participate in this study. Brain samples made available by the Instituto Nacional de Medicina Legal e Ciências Forenses—Delegação do Norte (INMLCF-DN) were obtained according to Decree-Law 274/99, of 22 July, published in Diário da República—1st SERIE A, No. 169, of 22-07-1999, Page 4522, regarding the regulation on the ethical use of human cadaveric tissue for research in Portugal.

AUTHOR CONTRIBUTIONS

BGL, and PC-S: conceptualization and writing—original draft preparation. BGL, AB-B, FF, MGL, JC, RR, AS, CC, RM-F, RS, JF, JL, and JR: methodology. BGL, AB-B, FF, MGL, JC, RR, and AMS: data curation. BGL, AMS, and PC-S: formal analysis. All authors: writing—review. BGL, JC, AMS, and PC-S: funding aquisition. AMS, PC, and PC-S: supervision. All authors contributed to the article and approved the submitted version.

FUNDING

This research was partial funded by a BICE Tecnifar Grant. The work performed in PC-S's Lab was partially supported by UP/Santander Totta and Fundação para a Ciência e Tecnologia (FCT, POCTI PTDC/SAU-PUB/28311/2017—EPIRaft grant and Fundo Europeu de Desenvolvimento Regional—FEDER funding and COMPETE—MedInUPprojectsPest-OE/SAU/UI215/2014, UID/BIM/4308/2016, UIDB/04308/2020 and UIDP/04308/2020). Unit for Multidisciplinary Research in Biomedicine (UMIB) is funded by the Foundation for Science and Technology (FCT) Portugal (grant numbers UIDB/00215/2020 and UIDP/00215/2020) and ITR—Laboratory for Integrative and Translational Research in Population Health (LA/P/0064/2020). RM-F was in receipt of an FCT PhD studentship (SFRH/BD/137900/2018). The funders had no role in study design, data collection and analysis or preparation of the manuscript.

ACKNOWLEDGMENTS

We acknowledge the participation of Dr. Marina Mendes, Ângela Oliveira and João Miguel Cordeiro in some of the experiments and the collaboration of nurses from the epilepsy outpatient clinic and from the surgical room in samples collection. We also acknowledge the helpful scientific discussions with Dr. Andreia Bettencourt. We also thank Mrs. M. Helena Costa e Silva, Helena Oliveira, Belmira Silva, Sandra Brás and Maria Rebelo for excellent technical assistance. The greatest acknowledgment is to the patients and their families, for their essential collaboration.

REFERENCES

Almeida Silva, L. F., Reschke, C. R., Nguyen, N. T., Langa, E., Sanz-Rodriguez, A., Gerbatin, R. R., et al. (2020). Genetic deletion of microRNA-22 blunts the inflammatory transcriptional response to status epilepticus and exacerbates epilepsy in mice. *Mol. Brain* 13:114. doi: 10.1186/s13041-020-00653-x

Amhaoul, H., Ali, I., Mola, M., Van Eetveldt, A., Szewczyk, K., Missault, S., et al. (2016). P2X7 receptor antagonism reduces the severity of spontaneous seizures in a chronic model of temporal lobe epilepsy. *Neuropharmacology* 105, 175–185. doi: 10.1016/j.neuropharm.2016.01.018

Amorim, R. P., Araujo, M. G. L., Valero, J., Lopes-Cendes, I., Pascoal, V. D. B., Malva, J. O., et al. (2017). Silencing of P2X7R by RNA interference in the hippocampus can attenuate morphological and behavioral impact of pilocarpine-induced epilepsy. *Purinergic Signal.* 13, 467–478. doi: 10.1007/s11302-017-9573-4

Apolloni, S., Amadio, S., Montilli, C., Volonte, C., and D'ambrosi, N. (2013). Ablation of P2X7 receptor exacerbates gliosis and motoneuron death in the SO D1–G93 A mouse model of amyotrophic lateral sclerosis. *Hum. Mol. Genet.* 22, 4102–4116. doi: 10.1093/hmg/ddt259

Armstrong, J. N., Brust, T. B., Lewis, R. G., and Macvicar, B. A. (2002). Activation of presynaptic P2X7-like receptors depresses mossy fiber-CA3 synaptic transmission through p38 mitogen-activated protein kinase. *J. Neurosci.* 22, 5938–5945. doi: 10.1523/JNEUROSCI.22-14-05938.2002

Balosso, S., Maroso, M., Sanchez-Alavez, M., Ravizza, T., Frasca, A., Bartfai, T., et al. (2008). A novel non-transcriptional pathway mediates the proconvulsive effects of interleukin-1β. *Brain* 131, 3256–3265. doi: 10.1093/brain/awn271

Bancila, V., Cordeiro, J. M., Bloc, A., and Dunant, Y. (2009). Nicotine-induced and depolarisation-induced glutamate release from hippocampus mossy fibre synaptosomes: two distinct mechanisms. *J. Neurochem.* 110, 570–580. doi: 10.1111/j.1471-4159.2009.06169.x

Barros-Barbosa, A. R., Fonseca, A. L., Guerra-Gomes, S., Ferreirinha, F., Santos, A., Rangel, R., et al. (2016). Up-regulation of P2X7 receptor-mediated inhibition of GABA uptake by nerve terminals of the human epileptic neocortex. *Epilepsia* 57, 99–110. doi: 10.1111/epi.13263

Barros-Barbosa, A. R., Lobo, M. G., Ferreirinha, F., Correia-De-Sa, P., and Cordeiro, J. M. (2015). P2X7 receptor activation downmodulates Na^+-dependent high-affinity GABA and glutamate transport into rat brain cortex synaptosomes. *Neuroscience* 306, 74–90. doi: 10.1016/j.neuroscience.2015.08.026

Barros-Barbosa, A. R., Oliveira, A., Lobo, M. G., Cordeiro, J. M., and Correia-De-Sa, P. (2018). Under stressful conditions activation of the ionotropic P2X7 receptor differentially regulates GABA and glutamate release from nerve terminals of the rat cerebral cortex. *Neurochem. Int.* 112, 81–95. doi: 10.1016/j.neuint.2017.11.005

Beamer, E., Morgan, J., Alves, M., Menéndez-Méndez, A., Morris, G., Zimmer, B., et al. (2021). Increased expression of the ATP-gated P2X7 receptor reduces responsiveness to anti-convulsants during status epilepticus in mice. *Br. J. Pharmacol.* 179, 2986–3006. doi: 10.1111/bph.15785

Beamer, E. H., Jurado-Arjona, J., Jimenez-Mateos, E. M., Morgan, J., Reschke, C. R., Kenny, A., et al. (2018). MicroRNA-22 controls aberrant neurogenesis and changes in neuronal morphology after status epilepticus. *Front. Mol. Neurosci.* 11:442. doi: 10.3389/fnmol.2018.00442

Brown, R. a. M., Epis, M. R., Horsham, J. L., Kabir, T. D., Richardson, K. L., Leedman, P. J., et al. (2018). Total RNA extraction from tissues for microRNA and target gene expression analysis: not all kits are created equal. *BMC Biotechnol.* 18:16. doi: 10.1186/s12896-018-0421-6

Campos, R. C., Parfitt, G. M., Polese, C. E., Coutinho-Silva, R., Morrone, F. B., Barros, D. M., et al. (2014). Pharmacological blockage and P2X7 deletion hinder aversive memories: reversion in an enriched environment. *Neuroscience* 280, 220–230. doi: 10.1016/j.neuroscience.2014.09.017

Choi, H. K., Ryu, H. J., Kim, J. E., Jo, S. M., Choi, H. C., Song, H. K., et al. (2012). The roles of P2X7 receptor in regional-specific microglial responses in the rat brain following status epilepticus. *Neurol. Sci.* 33, 515–525. doi: 10.1007/s10072-011-0740-z

Conte, G., Menendez-Mendez, A., Bauer, S., El-Naggar, H., Alves, M., Nicke, A., et al. (2021). Circulating P2X7 receptor signaling components as diagnostic biomarkers for temporal lobe epilepsy. *Cells* 10:2444. doi: 10.3390/cells10092444

Dona, F., Ulrich, H., Persike, D. S., Conceicao, I. M., Blini, J. P., Cavalheiro, E. A., et al. (2009). Alteration of purinergic P2X4 and P2X7 receptor expression in rats with temporal-lobe epilepsy induced by pilocarpine. *Epilepsy Res.* 83, 157–167. doi: 10.1016/j.eplepsyres.2008.10.008

Engel, T., Brennan, G. P., Sanz-Rodriguez, A., Alves, M., Beamer, E., Watters, O., et al. (2017). A calcium-sensitive feed-forward loop regulating the expression of the ATP-gated purinergic P2X7 receptor *via* specificity protein 1 and microRNA-22. *Biochim. Biophys. Acta Mol. Cell Res.* 1864, 255–266. doi: 10.1016/j.bbamcr.2016.11.007

Engel, T., Gomez-Villafuertes, R., Tanaka, K., Mesuret, G., Sanz-Rodriguez, A., Garcia-Huerta, P., et al. (2012a). Seizure suppression and neuroprotection by targeting the purinergic P2X7 receptor during status epilepticus in mice. *FASEB J.* 26, 1616–1628. doi: 10.1096/fj.11-196089

Engel, T., Jimenez-Pacheco, A., Miras-Portugal, M. T., Diaz-Hernandez, M., and Henshall, D. C. (2012b). P2X7 receptor in epilepsy; role in pathophysiology and potential targeting for seizure control. *Int. J. Physiol. Pathophysiol. Pharmacol.* 4, 174–187.

Ferrari, D., Chiozzi, P., Falzoni, S., Dal Susino, M., Melchiorri, L., Baricordi, O. R., et al. (1997). Extracellular ATP triggers IL-1 beta release by activating the purinergic P2Z receptor of human macrophages. *J. Immunol.* 159, 1451–1458.

Fischer, W., Franke, H., Krugel, U., Muller, H., Dinkel, K., Lord, B., et al. (2016). Critical evaluation of P2X7 receptor antagonists in selected

seizure models. *PLoS One* 11:e0156468. doi: 10.1371/journal.pone.0156468

Hemb, M., Palmini, A., Paglioli, E., Paglioli, E. B., Costa Da Costa, J., Azambuja, N., et al. (2013). An 18-year follow-up of seizure outcome after surgery for temporal lobe epilepsy and hippocampal sclerosis. *J. Neurol. Neurosurg. Psychiatry* 84, 800–805. doi: 10.1136/jnnp-2012-304038

Henshall, D. C. (2013). Antagomirs and microRNA in status epilepticus. *Epilepsia* 54, 17–19. doi: 10.1111/epi.12267

Henshall, D. C., Hamer, H. M., Pasterkamp, R. J., Goldstein, D. B., Kjems, J., Prehn, J. H., et al. (2016). MicroRNAs in epilepsy: pathophysiology and clinical utility. *Lancet Neurol.* 15, 1368–1376. doi: 10.1016/S1474-4422(16)30246-0

Jeha, L. E., Najm, I., Bingaman, W., Dinner, D., Widdess-Walsh, P., Luders, H., et al. (2007). Surgical outcome and prognostic factors of frontal lobe epilepsy surgery. *Brain* 130, 574–584. doi: 10.1093/brain/awl364

Jimenez-Mateos, E. M., Arribas-Blazquez, M., Sanz-Rodriguez, A., Concannon, C., Olivos-Ore, L. A., Reschke, C. R., et al. (2015). microRNA targeting of the P2X7 purinoceptor opposes a contralateral epileptogenic focus in the hippocampus. *Sci. Rep.* 5:17486. doi: 10.1038/srep17486

Jimenez-Mateos, E. M., Smith, J., Nicke, A., and Engel, T. (2019). Regulation of P2X7 receptor expression and function in the brain. *Brain Res. Bull.* 151, 153–163. doi: 10.1016/j.brainresbull.2018.12.008

Jimenez-Pacheco, A., Diaz-Hernandez, M., Arribas-Blazquez, M., Sanz-Rodriguez, A., Olivos-Ore, L. A., Artalejo, A. R., et al. (2016). Transient P2X7 receptor antagonism produces lasting reductions in spontaneous seizures and gliosis in experimental temporal lobe epilepsy. *J. Neurosci.* 36, 5920–5932. doi: 10.1523/JNEUROSCI.4009-15.2016

Jimenez-Pacheco, A., Mesuret, G., Sanz-Rodriguez, A., Tanaka, K., Mooney, C., Conroy, R., et al. (2013). Increased neocortical expression of the P2X7 receptor after status epilepticus and anticonvulsant effect of P2X7 receptor antagonist A-438079. *Epilepsia* 54, 1551–1561. doi: 10.1111/epi.12257

Kanellopoulos, J. M., and Delarasse, C. (2019). Pleiotropic roles of P2X7 in the central nervous system. *Front. Cell. Neurosci.* 13:401. doi: 10.3389/fncel.2019.00401

Khakh, B. S., Gittermann, D., Cockayne, D. A., and Jones, A. (2003). ATP modulation of excitatory synapses onto interneurons. *J. Neurosci.* 23, 7426–7437. doi: 10.1523/JNEUROSCI.23-19-07426.2003

Kim, J. E., and Kang, T. C. (2011). The P2X7 receptor-pannexin-1 complex decreases muscarinic acetylcholine receptor-mediated seizure susceptibility in mice. *J. Clin. Invest.* 121, 2037–2047. doi: 10.1172/JCI44818

Leal, B., Chaves, J., Carvalho, C., Bettencourt, A., Brito, C., Boleixa, D., et al. (2018). Immunogenetic predisposing factors for mesial temporal lobe epilepsy with hippocampal sclerosis. *Int J. Neurosci.* 128, 305–310. doi: 10.1080/00207454.2017.1349122

Leal, B., Chaves, J., Carvalho, C., Rangel, R., Santos, A., Bettencourt, A., et al. (2017). Brain expression of inflammatory mediators in mesial temporal lobe epilepsy patients. *J. Neuroimmunol.* 313, 82–88. doi: 10.1016/j.jneuroim.2017.10.014

Ma, J., Shui, S. F., Han, X. W., Guo, D., Li, T. F., Yan, L., et al. (2016). microRNA-22 attenuates neuronal cell apoptosis in a cell model of traumatic brain injury. *Am. J. Transl. Res.* 8, 1895–1902.

Marcoli, M., Cervetto, C., Paluzzi, P., Guarnieri, S., Alloisio, S., Thellung, S., et al. (2008). P2X7 pre-synaptic receptors in adult rat cerebrocortical nerve terminals: a role in ATP-induced glutamate release. *J. Neurochem.* 105, 2330–2342. doi: 10.1111/j.1471-4159.2008.05322.x

Mawhinney, L. J., De Rivero Vaccari, J. P., Dale, G. A., Keane, R. W., and Bramlett, H. M. (2011). Heightened inflammasome activation is linked to age-related cognitive impairment in Fischer 344 rats. *BMC Neurosci.* 12:123. doi: 10.1186/1471-2202-12-123

Mccarthy, A. E., Yoshioka, C., and Mansoor, S. E. (2019). Full-length P2X7 structures reveal how palmitoylation prevents channel desensitization. *Cell* 179, 659–670 e613. doi: 10.1016/j.cell.2019.09.017

Mesuret, G., Engel, T., Hessel, E. V., Sanz-Rodriguez, A., Jimenez-Pacheco, A., Miras-Portugal, M. T., et al. (2014). P2X7 receptor inhibition interrupts the progression of seizures in immature rats and reduces hippocampal damage. *CNS Neurosci. Ther.* 20, 556–564. doi: 10.1111/cns.12272

Monif, M., Reid, C. A., Powell, K. L., Smart, M. L., and Williams, D. A. (2009). The P2X7 receptor drives microglial activation and proliferation: a trophic role for P2X7R pore. *J. Neurosci.* 29, 3781–3791. doi: 10.1523/JNEUROSCI.5512-08.2009

Morgan, J., Alves, M., Conte, G., Menendez-Mendez, A., De Diego-Garcia, L., De Leo, G., et al. (2020). Characterization of the expression of the ATP-gated P2X7 receptor following status epilepticus and during epilepsy using a P2X7-EGFP reporter mouse. *Neurosci. Bull.* 36, 1242–1258. doi: 10.1007/s12264-020-00573-9

Narcisse, L., Scemes, E., Zhao, Y., Lee, S. C., and Brosnan, C. F. (2005). The cytokine IL-1beta transiently enhances P2X7 receptor expression and function in human astrocytes. *Glia* 49, 245–258. doi: 10.1002/glia.20110

Navarrete-Modesto, V., Orozco-Suarez, S., Feria-Romero, I. A., and Rocha, L. (2019). The molecular hallmarks of epigenetic effects mediated by antiepileptic drugs. *Epilepsy Res.* 149, 53–65. doi: 10.1016/j.eplepsyres.2018.11.006

Noronha-Matos, J. B., Coimbra, J., Sa-E-Sousa, A., Rocha, R., Marinhas, J., Freitas, R., et al. (2014). P2X7-induced zeiosis promotes osteogenic differentiation and mineralization of postmenopausal bone marrow-derived mesenchymal stem cells. *FASEB J.* 28, 5208–5222. doi: 10.1096/fj.14-257923

North, R. A. (2002). Molecular physiology of P2X receptors. *Physiol. Rev.* 82, 1013–1067. doi: 10.1152/physrev.00015.2002

Parisi, C., Arisi, I., D'ambrosi, N., Storti, A. E., Brandi, R., D'onofrio, M., et al. (2013). Dysregulated microRNAs in amyotrophic lateral sclerosis microglia modulate genes linked to neuroinflammation. *Cell Death Dis.* 4:e959. doi: 10.1038/cddis.2013.491

Rappold, P. M., Lynd-Balta, E., and Joseph, S. A. (2006). P2X7 receptor immunoreactive profile confined to resting and activated microglia in the epileptic brain. *Brain Res.* 1089, 171–178. doi: 10.1016/j.brainres.2006.03.040

Rassendren, F., Buell, G. N., Virginio, C., Collo, G., North, R. A., Surprenant, A., et al. (1997). The permeabilizing ATP receptor, P2X7. Cloning and expression of a human cDNA. *J. Biol. Chem.* 272, 5482–5486. doi: 10.1074/jbc.272.9.5482

Skaper, S. D. (2011). Ion channels on microglia: therapeutic targets for neuroprotection. *CNS Neurol. Disord. Drug Targets* 10, 44–56. doi: 10.2174/187152711794488638

Skaper, S. D., Debetto, P., and Giusti, P. (2010). The P2X7 purinergic receptor: from physiology to neurological disorders. *FASEB J.* 24, 337–345. doi: 10.1096/fj.09-138883

Sperlagh, B., and Illes, P. (2014). P2X7 receptor: an emerging target in central nervous system diseases. *Trends Pharmacol. Sci.* 35, 537–547. doi: 10.1016/j.tips.2014.08.002

Sperlagh, B., Kofalvi, A., Deuchars, J., Atkinson, L., Milligan, C. J., Buckley, N. J., et al. (2002). Involvement of P2X7 receptors in the regulation of neurotransmitter release in the rat hippocampus. *J. Neurochem.* 81, 1196–1211. doi: 10.1046/j.1471-4159.2002.00920.x

Surprenant, A., Rassendren, F., Kawashima, E., North, R. A., and Buell, G. (1996). The cytolytic P2Z receptor for extracellular ATP identified as a P2X receptor (P2X7). *Science* 272, 735–738. doi: 10.1126/science.272.5262.735

Trabzuni, D., Ryten, M., Walker, R., Smith, C., Imran, S., Ramasamy, A., et al. (2011). Quality control parameters on a large dataset of regionally dissected human control brains for whole genome expression studies. *J. Neurochem.* 119, 275–282. doi: 10.1111/j.1471-4159.2011.07432.x

Turchinovich, A., Weiz, L., and Burwinkel, B. (2012). Extracellular miRNAs: the mystery of their origin and function. *Trends Biochem. Sci.* 37, 460–465. doi: 10.1016/j.tibs.2012.08.003

Vianna, E. P., Ferreira, A. T., Naffah-Mazzacoratti, M. G., Sanabria, E. R., Funke, M., Cavalheiro, E. A., et al. (2002). Evidence that ATP participates in the pathophysiology of pilocarpine-induced temporal lobe epilepsy: fluorimetric, immunohistochemical and Western blot studies. *Epilepsia* 43, 227–229. doi: 10.1046/j.1528-1157.43.s.5.26.x

Wang, G., Tam, L. S., Li, E. K., Kwan, B. C., Chow, K. M., Luk, C. C., et al. (2010). Serum and urinary cell-free MiR-146a and MiR-155 in patients with systemic lupus erythematosus. *J. Rheumatol.* 37, 2516–2522. doi: 10.3899/jrheum.100308

Wang, J., Tan, L., Tian, Y., Ma, J., Tan, C. C., Wang, H. F., et al. (2015). Circulating microRNAs are promising novel biomarkers for drug-resistant epilepsy. *Sci. Rep.* 5:10201. doi: 10.1038/srep10201

White, K., Yang, P., Li, L., Farshori, A., Medina, A. E., Zielke, H. R., et al. (2018). Effect of postmortem interval and years in storage on RNA quality of tissue at a repository of the NIH neurobioBank. *Biopreserv. Biobank.* 16, 148–157. doi: 10.1089/bio.2017.0099

Yu, Y., Ugawa, S., Ueda, T., Ishida, Y., Inoue, K., Kyaw Nyunt, A., et al. (2008). Cellular localization of P2X7 receptor mRNA in the rat brain. *Brain Res.* 1194, 45–55. doi: 10.1016/j.brainres.2007.11.064

Conflict of Interest: The authors declare that the research was conducted in the absence of any commercial or financial relationships that could be construed as a potential conflict of interest.

Publisher's Note: All claims expressed in this article are solely those of the authors and do not necessarily represent those of their affiliated organizations, or those of the publisher, the editors and the reviewers. Any product that may be evaluated in this article, or claim that may be made by its manufacturer, is not guaranteed or endorsed by the publisher.

frontiers | Frontiers in Cellular Neuroscience

TYPE Mini Review
PUBLISHED 22 July 2022
DOI 10.3389/fncel.2022.931356

OPEN ACCESS

EDITED BY
Sandra Henriques Vaz,
Universidade de Lisboa, Portugal

REVIEWED BY
Marco I. Gonzalez,
University of California, Davis,
United States

*CORRESPONDENCE
Toni Christoph Berger
t.c.berger@medisin.uio.no
Kjell Heuser
dr.heuser@gmail.com

SPECIALTY SECTION
This article was submitted to Non-Neuronal Cells, a section of the journal Frontiers in Cellular Neuroscience

RECEIVED 28 April 2022
ACCEPTED 27 June 2022
PUBLISHED 22 July 2022

CITATION
Berger TC, Taubøll E and Heuser K (2022) The potential role of DNA methylation as preventive treatment target of epileptogenesis. *Front. Cell. Neurosci.* 16:931356. doi: 10.3389/fncel.2022.931356

The potential role of DNA methylation as preventive treatment target of epileptogenesis

Toni Christoph Berger[1]*, Erik Taubøll[1,2] and Kjell Heuser[1]*

[1]Department of Neurology, Oslo University Hospital, Oslo, Norway, [2]Faculty of Medicine, University of Oslo, Oslo, Norway

Pharmacological therapy of epilepsy has so far been limited to symptomatic treatment aimed at neuronal targets, with the result of an unchanged high proportion of patients lacking seizure control. The dissection of the intricate pathological mechanisms that transform normal brain matter to a focus for epileptic seizures—the process of epileptogenesis—could yield targets for novel treatment strategies preventing the development or progression of epilepsy. While many pathological features of epileptogenesis have been identified, obvious shortcomings in drug development are now believed to be based on the lack of knowledge of molecular upstream mechanisms, such as DNA methylation (DNAm), and as well as a failure to recognize glial cell involvement in epileptogenesis. This article highlights the potential role of DNAm and related gene expression (GE) as a treatment target in epileptogenesis.

KEYWORDS

epilepsy, epileptogenesis, DNA methylation, gene expression, therapy, epigenetics, glia, inflammation

Introduction

Epileptogenesis is the transformation of a physiologically functioning brain into an epileptic one, and the progression of manifested epilepsy (Pitkanen and Engel, 2014) (Figure 1). Although often initially not detectable clinically, this process is assumed to have a temporal and spatial starting point in the brain, involving an initial incident, such as trauma, hypoxia, infection, or complex febrile seizures. According to the current practical definition, this is followed by a latent phase devoid of clinical seizures, evolving to the chronic state that features the occurrence of spontaneous, and often progressive, epileptic seizures (Boison et al., 2013; Pitkanen and Engel, 2014). A prerequisite for the development of true anti-epileptogenic drugs preventing the emergence of clinical seizures, or stopping the worsening of chronic epilepsy, is to improve our understanding of the underlying pathological processes of epileptogenesis (Aronica and Gorter, 2007; Pitkanen and Lukasiuk, 2011; Loscher et al., 2013; Pitkänen et al., 2013; Löscher, 2020). Meanwhile, several pathological hallmarks of epileptogenesis are known. These are, for example, neuronal death, reactive gliosis, blood-brain barrier (BBB) disruption, axonal damage and sprouting, network reorganization, alteration of the extracellular

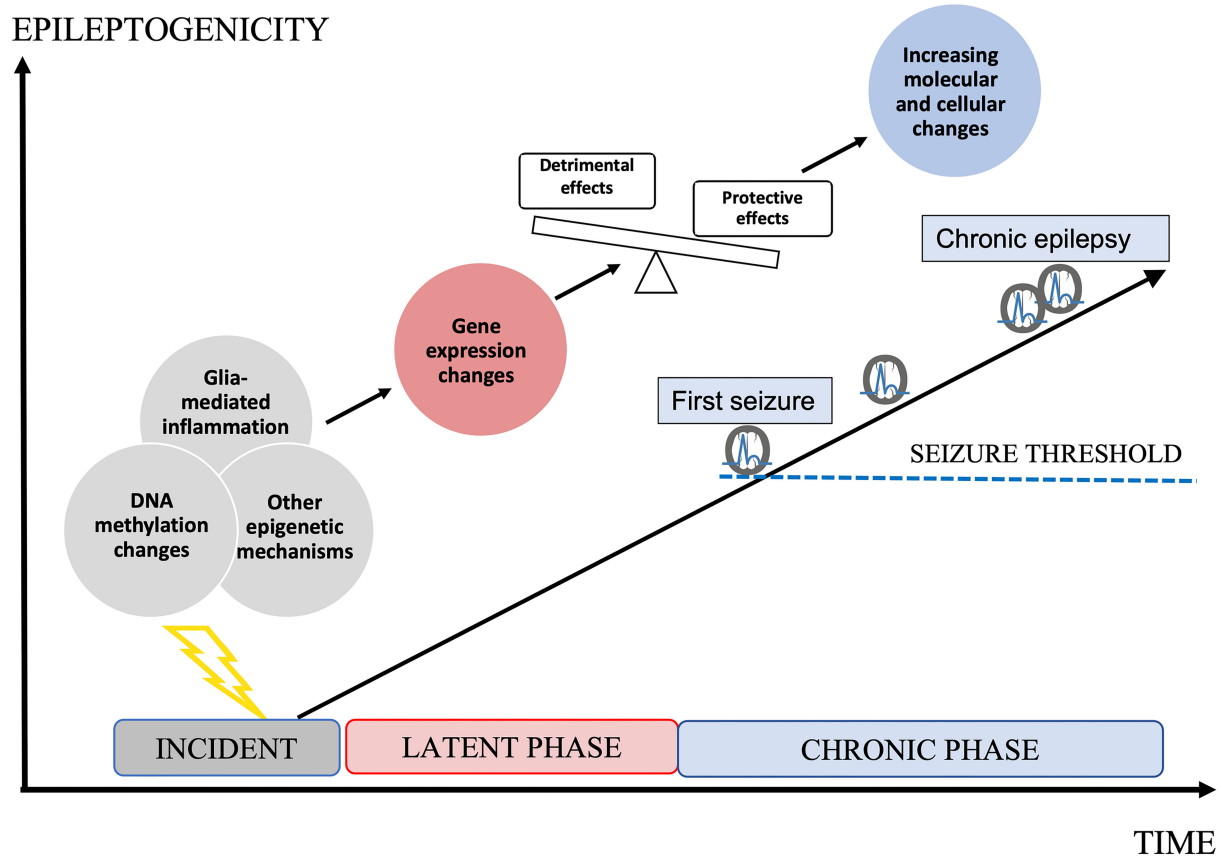

FIGURE 1
Epileptogenesis. Epileptogenesis describes the development of a brain becoming prone to generate epileptic seizures and further progression. An initial incident occurs to the brain, initiating the latent phase in which molecular and cellular changes increasingly develop. Epigenetic mechanisms, such as DNA methylation (DNAm) changes may determine changes in gene expression (GE) and by this cellular responses in both neurons and glial cells. Both protective and detrimental changes occur. Imbalance in favor to detrimental effects leads to increasing epileptogenicity up to the threshold of clinical seizures. During the chronic phase, epileptogenicity increases leading to the progression of clinical epilepsy, accompanied by increasing molecular and cellular changes. Both the latent phase and the chronic phase could be relevant to the development of anti-epileptogenic medication.

matrix (ECM), and astrocyte uncoupling, as well as substantial changes of the molecular architecture of both neurons and glial cells (Tauck and Nadler, 1985; de Lanerolle et al., 1989, 2012; Houser, 1990; Houser et al., 1990; Mathern et al., 1995; Eid et al., 2005, 2019; Vezzani and Granata, 2005; Dityatev, 2010; Blumcke et al., 2013; Bedner et al., 2015; Patel et al., 2019; Bruxel et al., 2021). What is more delicate is the lack of strategies for how to prevent the formation of these pathological features. Obvious shortcomings of novel preventive drug development are based on the lack of knowledge of molecular upstream mechanisms, such as DNA methylation (DNAm) or gene expression (GE) (Perucca et al., 2020), and also the neglect of the importance of glial cell involvement in the inflammatory processes accompanying epileptogenesis (Kalozoumi et al., 2018; Patel et al., 2019). The goal of this review is to discuss the significance of DNAm as a potential target for anti-epileptogenic treatment in the scope of novel knowledge of glial involvement in this process.

DNAm: Function and potential therapeutical target

After the human genome was deciphered in 2003, there were high expectations that pathological phenotypes would be linked to genomic variants (Collins et al., 2003; Green et al., 2015). However, the expectations did not come to fruition, and in the field of epilepsy, only a few genomic loci could be linked to epileptic conditions (International League Against Epilepsy Consortium on Complex Epilepsies, 2014; Abou-Khalil et al., 2018). The field of "epigenomics" arose with the hope to decipher the missing link between genotype and phenotype.

Today, epigenetics can be defined as mechanisms that largely determine the "transcriptome," meaning which genes are "used" to define a certain phenotype (Feinberg, 2007; McClung and Nestler, 2008; Gräff et al., 2011).

At the molecular level, epigenetics includes several mechanisms: DNAm, histone modifications, and non-coding RNAs are the most integral parts of this machinery (Gräff et al., 2011; Cavalli and Heard, 2019). These mechanisms are heavily interacted (Li et al., 2008; Cedar and Bergman, 2009; Wang et al., 2015). They determine chromatin accessibility, quality, and quantity of GE, and by this, tissue development in normal as well as pathological states. They can be altered by environmental factors (Danchin et al., 2011) and are mitotically inheritable (Cavalli and Heard, 2019). As such, they are potential upstream mechanisms for various molecular pathways, including those prompting pathological features of epileptogenesis. In the following, we will focus on DNA methylation in epileptogenesis.

DNA methylation is so far the most comprehensively studied epigenetic mechanism (Dor and Cedar, 2018) and is defined as the methylation (adding of a -CH3 group) of the DNA-base cytosine in a CpG (Cytosine – phosphate – Guanine) dinucleotide (CpG) (Luo et al., 2018). Oxidated variants of 5-methylcytosine (5-mC—in this review simply referred to as DNAm) include 5-hydroxymethylcytosine [5-hmC, relevant in post-mitotic neurons (Mellén et al., 2017)], 5-formylcytosine (5-fC), and 5-carboxylcytosine (5-caC), all of which potentially exert distinct effects on the GE and chromatin accessibility (Song and He, 2013). Other types of methylation include: non-CpG DNAm in, e.g., neurons (Kozlenkov et al., 2014), RNA methylation (Widagdo and Anggono, 2018), and mitochondrial DNAm (Cavalcante et al., 2020). In the central nervous system (CNS), DNAm has a major role in brain development, cell differentiation, and disease (Lister et al., 2013; Smith and Meissner, 2013; Sanosaka et al., 2017; Greenberg and Bourc'his, 2019). DNAm has been shown to influence the GE in a tissue-, context-, and cell-dependent manner (Smith and Meissner, 2013; Greenberg and Bourc'his, 2019), usually in a close interaction with transcription factors (Kribelbauer et al., 2019). How far DNAm states correlate with GE is still a matter of debate (Luo et al., 2018). GE is, on the other hand, regarded as an indicator of protein abundance and biological function, and provides a relevant estimate of downstream effects (Wang et al., 2009; Liu Y. et al., 2016; Silva and Vogel, 2016). Thus, DNAm might influence downstream molecular and cellular processes *via* GE regulation. DNAm is modifiable by environmental factors (Martin and Fry, 2018; Cavalli and Heard, 2019), hormones (Kovács et al., 2020), and even by neuronal activity (Guo et al., 2011). Recently, the site-specific modification of DNAm was shown to specifically alter GE (Liu X. S. et al., 2016; Liu and Jaenisch, 2019), which is especially interesting when it comes to novel therapeutic concepts. Further, disease-specific blood-DNAm pattern alterations have been reported in several pathological conditions (Fransquet et al., 2018; Agha et al., 2019; Henderson-Smith et al., 2019; Somineni et al., 2019) and proposed as possible biomarkers, with adjunct therapeutical implications (Kim et al., 2018; Berdasco and Esteller, 2019).

DNAm in epilepsy

Epilepsy-related alterations in DNAm have been shown in previous studies in both animal models (Miller-Delaney et al., 2012; Kobow et al., 2013; Machnes et al., 2013; Ryley Parrish et al., 2013; Williams-Karnesky et al., 2013; Li et al., 2015; Lusardi et al., 2015; Debski et al., 2016; Liu X. et al., 2016; Zybura-Broda et al., 2016) and in humans (Zhu et al., 2012; Miller-Delaney et al., 2015; Liu X. et al., 2016; Zhang et al., 2021) (Table 1). The most consistent finding is a state of DNA hypermethylation occurring in chronic-epilepsy states in both animal models (Kobow et al., 2013) and human hippocampal tissues (Miller-Delaney et al., 2015). Although some studies associate alterations in DNAm with GE changes (Kobow et al., 2009; Li et al., 2015; Debski et al., 2016), a recent study was more hesitant to reach this conclusion (Lipponen et al., 2018).

At the early stages of epileptogenesis, no changes (Ryley Parrish et al., 2013), or a slight tendency toward general DNA hypomethylation (Miller-Delaney et al., 2012), have been found. At single genes, DNAm changes have been recorded as soon as 1 h after status epilepticus (SE) initiation by intra-peritoneal (i.p.) kainate treatment in rats (Ryley Parrish et al., 2013). At chronic time points, a general tendency toward hypermethylation was found, and potential associations between DNAm and GE at specific genomic loci identified (Kobow et al., 2013). A follow-up study reanalyzed these results and compared them to two other murine models of focal epilepsy, traumatic brain injury (TBI) and amygdala stimulation, at chronic time points. This study found both a general tendency toward CpG hypomethylation (amygdala stimulation) and hypermethylation (pilocarpine, TBI) methylation and little overlap regarding DNAm between these models (Debski et al., 2016).

Some studies investigated both DNAm and GE changes to identify potential correlations. Although no general correlations between DNAm and GE were found, coincidental occurrences of these two phenomena were detected at some genomic loci (Kobow et al., 2013; Debski et al., 2016). Other studies have used more of a "black box" approach, investigating general methylation levels and testing interventions by means of DNA-methyl-transferase inhibitors—targeting the "hypermethylated" state in chronic epilepsy and potentially attenuating epileptogenesis. In one study (rat model, i.p. kainate) the application of a DNMT inhibitor did not significantly alter the disease course (some/despite of later onset of SE), but it did reduce the general hypermethylation state and also DNAm at one of the investigated genes (Ryley Parrish et al., 2013). Another group reported reversed hypermethylation, attenuated seizure severity, and later onset of epileptogenesis (kindling model in mice and rats using pentylenetetrazol) associated with both the application of a DNMT inhibitor and adenosine

TABLE 1 Relevant studies assessing DNA methylation (DNAm) in epileptogenesis.

Species	Tissue/ model	Methods	Results	Interpretation/conclusion	Reference chronol.
Mouse	Contralateral HC/ intracortical KA	Glial and neuronal nuclei sorted by flow cytometry. Alterations in GE and DNAm were assessed with RRBS and RNAseq. R package edgeR was used for statistical analysis	The CLH features substantial, mostly cell-specific changes in both GE and DNAm in glia and neurons. Changes in GE overlapped to a great degree between CLH and ILH; changes in DNAm did not. A significantly lower number of glial genes up- and downregulated compared to previous results from the ILH (Berger et al., 2019). Several genes and pathways potentially involved in anti-epileptogenic effects were upregulated in the CLH.	The CLH displays substantial changes in GE and DNAm. GE changes related to potential anti-epileptogenic effects seem to dominate compared to the pro-epileptogenic effects in the CLH.	Berger et al., 2020
Human	Hippocampal tissue resected from patients with TLE-HS	Genome-wide CpG-DNAm profiling and RNAseq to Dprofile global changes in promoter methylation and GE in HS patients. Real time PCR was performed to validate the findings of DNAm and RNAseq.	A total of 16040 sites showed altered DNAm in all the CpG islands. Of these, 3185 sites were in the promoter regions, of which 66 genes showed an inverse correlation between DNAm and expression. These genes are largely related to pathways predicted to participate in axon guidance by semaphorins, MAPK, ionotropic glutamate receptor pathway, notch signaling, regulatory activities related to TFAP2A and immune response, with the most distinct ones included TFAP2A, NRP1, SEMA3B, CACNG2, MAP3K11, and ADAM17.	Collectively, findings implicate DNAm as a critical regulator of the pathogenic mechanisms of epileptogenesis associated with HS.	Dixi et al., 2020
Mouse	Ipsilateral HC/ intracortical KA	Separation into neurons and glial nuclei was performed by flow cytometry. Changes in DNAm and GE were measured with RRBS and mRNAseq. R package edgeR for analysis.	Fulminant DNAm- and GE changes in both neurons and glia at 24 hours after initiation of status epilepticus were observed. The vast majority of these changes were specific for either neurons or glia. At several epilepsy-related genes, like *Hdac11, Spp1, Gal, Drd1 and Sv2c,* significant differential DNAm and differential GE coincided.	Neuron- and glia-specific changes in DNAm and GE in early epileptogenesis. Single genetic loci in several epilepsy-related genes, where DNAm and GE changes coincide, were detected.	Berger et al., 2019
Human	Focal cortical dysplasia (FCD)	DNA methylomes and transcriptomes were generated from massive parallel sequencing in 15 surgical FCD specimens, matched with 5 epilepsy and 6 non-epilepsy controls.	Differential hierarchical cluster analysis of DNAm distinguished major FCD subtypes (ie, Ia, IIa, and IIb) from patients with temporal lobe epilepsy patients and nonepileptic controls. Targeted panel sequencing identified a novel likely pathogenic variant in DEPDC5 in a patient with FCD type IIa. However, no enrichment of differential DNAm or GE was observed in mechanistic target of rapamycin (mTOR) pathway-related genes.	Evidence for disease-specific DNAm signatures toward focal epilepsies in favor of an integrated clinicopathologic and molecular classification system of FCD subtypes incorporating genomic DNAm.	Kobow et al., 2019
Human	Focal cortical dysplasia (FCD)	Genome-wide CpG-DNAm profiling by methylated DNA immunoprecipitation (MeDIP) microarray and RNAseq on cortical tissues resected from FCD type II patients.	A total of 19088 sites showed altered DNAm in all the CpG islands. Of these, 5725 sites were present in the promoter regions, of which 176 genes showed an inverse correlation between DNAm and GE. Many of these 176 genes were found to belong to a cohesive network of physically interacting proteins linked to several cellular functions. Pathway analysis revealed significant enrichment of receptor tyrosine kinases (RTK), EGFR, PDGFRA, NTRK3, and mTOR signaling pathways	The first study investigating the epigenetic signature associated with FCD type II pathology. Identified candidate genes may play a crucial role in the regulation of the pathogenic mechanisms of epileptogenesis associated with FCD type II pathologies.	Dixi et al., 2018

(Continued)

10.3389/fncel.2022.931356

TABLE 1 Continued

Species	Tissue/ model	Methods	Results	Interpretation/conclusion	Reference chronol.
Human	Blood	Comparison of blood whole genomic DNAm pattern in MTLE patients (n = 30) relative to controls (n = 30) with the Human DNAm 450 K BeadChip assay, exploring genes and pathways that are differentially methylated using bioinformatics profiling.	MTLE and control groups showed significantly different DNAm at 216 sites, with 164 sites involved hyper- and 52 sites hypo- DNAm. Two hyper- and 32 hypo-methylated sites were associated with promoters, while 87 hyper- and 43 hypo-methylated sites corresponded to coding regions. Differentially methylated genes were largely related to pathways predicted to participate in anion binding, oxidoreductant activity, growth regulation, skeletal development and drug metabolism, with the most distinct ones included *SLC34A2, CLCN6, CLCA4, CYP3A43, CYP3A4* and *CYP2C9*. Panels of genes also appeared to be differentially methylated relative to disease duration, resistance to anti-epileptics and MRI alterations of HS.	The peripheral epigenetic changes observed in MTLE could be involved in certain disease-related modulations and warrant further translational investigations.	Long et al., 2017
Human	Brain tissue from refractory epilepsy patients	Genome-wide DNAm and GE in brain tissues of 10 patients with refractory epilepsy using methylated DNA immunoprecipitation linked with sequencing and mRNAseq.	Diverse distribution of differentially methylated genes was found in X chromosome, while differentially methylated genes appeared rarely in Y chromosome. 62 differentially expressed genes, such as *MMP19, AZGP1, DES,* and *LGR6* were correlated with refractory epilepsy.	Findings provide a genome-wide profiling of DNAm and GE in brain tissues of patients with refractory epilepsy, which may provide a basis for further study on the etiology and mechanisms of refractory epilepsy.	Liu X. et al., 2016
Rat	3 models: - focal amygdala stimulation/ - systemic pilocarpine/ - lateral fluid-percussion (TBI)	DNAm and GE in the hippocampal CA3/dentate gyrus fields at 3 months following epileptogenic injury in three experimental models.	DNAm and GE profiles distinguished ctr. from injured animals. Consistent increased DNAm in gene bodies and hypoDNAm at non-genic regions. A common DNAm signature for all three different models was not found, and few regions common to any two models.	Evidence that genome-wide alteration of DNAm signatures is a general pathomechanism associated with epileptogenesis and epilepsy in animal models, but the broad pathophysiological differences between models are reflected in distinct etiology-dependent DNAm patterns.	Debski et al., 2016
Human	Brain tissue from epilepsy patients and ctr.	DNAm via methylated-cytosine DNA immunoprecipitation microarray chip. Differentially methylated loci validated by bisulfite sequencing PCR, and mRNA levels of candidate genes evaluated by RT-PCR.	224 genes showed differential DNAm between epileptic patients and ctr. Among the seven candidate genes, three genes (*TUBB2B, ATPGD1*, and *HTR6)* showed relative transcriptional regulation by DNAm. *TUBB2B* and *ATPGD1* exhibited hyper DNAm and decreased mRNA levels, whereas *HTR6* displayed hypo DNAm and increased mRNA levels in the epileptic samples.	Findings suggest that certain genes become differentially regulated by DNAm in human epilepsy.	Wang et al., 2016
Human	Resected HC tissue from TLE with- or without HS	DNAm analysis of all annotated CpG islands and promoter regions in the human genome. Comparative analysis of expression and promoter DNAm	146 protein-coding genes exhibited altered DNAm in TLE hippocampus (n = 9) when compared to ctr. (n = 5), with 81.5% of the promoters displaying hyper DNAm. Unique DNAm profiles were evident in TLE with or without HS, in addition to a common DNAm profile regardless of pathology grade.	The present study therefore reports select, genome-wide DNAm changes in human temporal lobe epilepsy that may contribute to the molecular architecture of the epileptic brain.	Miller-Delaney et al., 2015

(Continued)

10.3389/fncel.2022.931356

TABLE 1 Continued

Species	Tissue/ model	Methods	Results	Interpretation/conclusion	Reference chronol.
			GO terms associated with development, neuron remodeling and neuron maturation were over-represented in the DNAm profile of mild HS. In addition to genes associated with neuronal/synaptic transmission and cell death functions, differential hyperDNAm of genes associated with transcriptional regulation in TLE. A panel of 13, DNAm-sensitive microRNA are identified in TLE including *MIR27A*, miR-193a-5p (*MIR193A*) and miR-876-3p (*MIR876*), and the differential DNAm of long non-coding RNA.		
Mouse/ Rat	Transient kainic acid exposure using *in vitro* and *in vivo* rodent models.	Analysis of DNAm changes in the gria2 gene, which encodes for the GluA2 subunit of the ionotropic glutamate, alpha-amino-3-hydroxy-5-methyl-4-isoxazole proprionic acid receptor	KA exposure for 2 h to mouse hippocampal slices triggers DNAm of a 5' regulatory region of the gria2 gene. Increase in DNAm persists one week after removal of the drug, with concurrent suppression of gria2 mRNA expression levels. In a rat *in vivo* model of post kainic acid-induced epilepsy, we show similar hyperDNAm of the 5' region of gria2. Luciferase reporter assays support a regulatory role for DNAm of gria2 5' region. Inhibition of DNAm by RG108 blocked KA-induced hyperDNAm of gria2 5' region in HC slice cultures.	Our results suggest that DNAm of such genes as gria2 mediates persistent epileptiform activity and inter-individual differences in the epileptic response to neuronal insult and that pharmacological agents that block DNAm inhibit epileptiform activity raising the prospect of DNAm inhibitors in epilepsy therapeutics.	Machnes et al., 2013
Rat	Rat brain specimens	Methyl-CpG capture associated with massive parallel sequencing (Methyl-Seq) to assess the genomic DNAm. mRNAseq for GE analysis	Predominant increase of DNAm in chronic rat epilepsy. Aberrant DNAm patterns were inversely correlated with GE changes using mRNAseq from same animals and tissue specimens. Administration of a ketogenic, high-fat, low-carbohydrate diet attenuated seizure progression and ameliorated DNAm mediated changes in GE.	First report of unsupervised clustering of an epigenetic marker being used in epilepsy research to separate epileptic from non-epileptic animals as well as from animals receiving anti-convulsive dietary treatment.	Kobow et al., 2013
Rat	Experimental TLE provoked by kainic acid-induced SE	Bisulfite sequencing analysis; chromatin immunoprecipitation analysis	Increased glutamate receptor subunit epsilon-2 (*Grin2b/Nr2b*) and decreased *Bdnf* DNAm levels that corresponded to decreased *Grin2b/Nr2b* and increased *Bdnf* mRNA and protein expression in the epileptic hippocampus. Blockade of DNA methyltransferase (DNMT) activity decrease global DNAm levels and reduced *Grin2b/Nr2b*, but not *Bdnf* DNAm levels; and decreased *Grin2b/Nr2b* mRNA expression whereas GRIN2B protein expression increased in the epileptic hippocampus, suggesting that a posttranscriptional mechanism may be involved.	DNAm may be an early event triggered by SE that persists late into the epileptic hippocampus to contribute to GE changes in TLE.	Ryley Parrish et al., 2013

(Continued)

10.3389/fncel.2022.931356

TABLE 1 Continued

Species	Tissue/ model	Methods	Results	Interpretation/conclusion	Reference chronol.
Mouse	Hippocampus	Genome-wide DNAm analysis of 34,143 discrete loci representing all annotated CpG islands and promoter regions in the mouse genome	321 genes showed altered DNAm after status epilepticus alone or status epilepticus that followed seizure preconditioning, with >90% of the promoters of these genes undergoing hypo DNAm. These profiles included genes not previously associated with epilepsy, such as the polycomb gene *Phc2*. Differential DNAm events occurred throughout the genome, with the exception of a small region of chromosome 4, which was significantly overrepresented with genes hypomethylated. Gene ontology analysis emphasized the majority of differential DNAm events between the groups occurred in genes associated with nuclear functions, such as DNA binding and transcriptional regulation.	Evidence for genome-wide DNAm changes after status epilepticus and in epileptic tolerance, which may contribute to regulating the GE environment of the seizure-damaged hippocampus.	Miller-Delaney et al., 2012
Human	Hippocampus	DNA from 3 dissected HC regions from MTS specimens with granular cell dispersion (GCD), TLE samples without GCD, and autopsy ctrs. Promoter DNAm analyzed after bisulfite treatment, cloning, and direct sequencing	*Reelin* promoter DNAm was found to be greater in TLE specimens than in ctrs; promoter DNAm correlated with GCD among TLE. No other clinical or histopathological parameter (i.e. sex, age, seizure duration, medication or extent, of MTS) correlated with promoter DNAm.	These data support a compromised Reelin-signaling pathway and identify promoter DNAm as an epigenetic mechanism in the pathogenesis of TLE.	Kobow et al., 2009

(intracranial implants) (Williams-Karnesky et al., 2013). In our previous studies employing the intracortical kainate mouse model of mesial temporal lobe epilepsy, we observed vast and mainly cell-specific changes in DNAm in both the ipsilateral (Berger et al., 2019) and contralateral (Berger et al., 2020) hippocampi, with hypermethylation generally outweighing hypomethylation in both hippocampi. DNAm alterations near epilepsy-relevant genes and genes within epilepsy relevant Gene Ontology/Kyoto Encyclopedia of Genes and Genomes (GO/KEGG) pathways (Berger et al., 2019, 2020). However, we did not detect general correlations between DNAm and GE on genomic features (Berger et al., 2019, 2020). Nevertheless, at several potentially epileptogenesis-related genes, statistically significant alterations in DNAm and GE coincided (Berger et al., 2019). In summary, in this specific model, we were not able to conclude that DNAm facilitates a direct regulation of GE in early epileptogenesis. This conclusion concurs with results from work on the potential role of DNAm for GE in epileptogenesis (Lipponen et al., 2018) and the theory that DNAm mostly represents a secondary molecular marker of long-term gene silencing (Dor and Cedar, 2018; Luo et al., 2018; Greenberg and Bourc'his, 2019). In addition, prior studies investigating general methylation trends or associations have not demonstrated mechanistic correlations between DNAm and GE/protein alterations/epileptogenesis, but rather have shown co-incidences. Nevertheless, many previous studies and our data suggest wide-spread changes in DNAm in epileptogenesis. As the different epigenetic mechanisms (histone modifications and microRNA [miRNA]) are inter-linked (Li et al., 2008; Cedar and Bergman, 2009; Wang et al., 2015), DNAm may still affect downstream effects, not necessarily directly, but indirectly.

Increasing detection sensitivity by cell-specific approaches including focus on glial cells

Several recent studies have revealed a possible involvement of DNAm in both epileptogenesis and GE (Table 1). However, reports are not consistent and possible shortcomings may be associated with the widely used simultaneous bulk analysis of several different CNS cell types. The analysis of DNAm and GE in neurons and glia cells individually may rectify a crucial shortcoming of previous studies and be one prudent step toward deciphering the "DNA methylome." Neurons and glia facilitate mostly complementary tasks in physiological and pathological CNS states, such as epileptogenesis (Cahoy et al., 2008; Doyle et al., 2008; Zamanian et al., 2012; Patel et al., 2019), and exhibit different DNAm methylation profiles (Kozlenkov et al., 2014; Sanosaka et al., 2017). DNAm both in ways of 5hmC and non-CpG methylation are of a much higher significance in neurons than in glial cells (Kozlenkov et al., 2014; Mellén et al., 2017). Analyzing molecular mechanisms in these individual cell types

separately enhances resolution, and information can be obtained about the cellular origin of detected effects (e.g., changes in DNAm and GE, as well as their possible correlation). Further, the methylation of several genomic regions, such as regulatory elements exerts cell-specific effects (Li et al., 2021).

We recently introduced a more cell-specific methodology in 2 separate publications using cell sorting of brain tissue into neuronal and non-neuronal (glial) cells prior to DNAm and GE analysis (Berger et al., 2019, 2020). We found considerable changes in both DNAm and GE at 24 h post-initiation of SE in a mouse model of mesial temporal lobe epilepsy with hippocampal sclerosis (Berger et al., 2019, 2020). Most of these molecular alterations were specific to either neurons or glia. Further, GE changes uncovered a substantial involvement of glia cells in processes crucial to epileptogenesis, such as inflammation, neuronal death, neurogenesis, and Ca^{2+} signaling. Furthermore, we found a substantial overlap of genomic dysregulation with other epilepsy models, and even with other neurodegenerative diseases, such as Parkinson's disease or multiple sclerosis (Berger et al., 2019, 2020). These studies underscored our postulation that a cell-specific analysis of DNAm and GE in epileptogenesis provides deeper knowledge about the cellular origin of molecular mechanisms and by this, it provides a clearer view on putative upstream targets for drug development. This makes expressly sense in the scope of novel knowledge on glial cells as important orchestrators of brain inflammation and epileptogenesis. In the following, we focus on differentially regulated glial genes and their probable contribution to epileptogenesis.

Glial contribution to epileptogenesis

With our novel understanding of glial cells as central organizers of homeostatic functions and as major contributors to inflammation and brain excitability, we observe a paradigm shift where glial cells are included in the equation of epilepsy pathogenesis. Through this, we expect to approach novel curative treatment strategies for epilepsy (Heuser et al., 2021).

In the following, the most prominent hallmarks of epileptogenesis and specifically their glial contribution are discussed in detail, as alteration of glia-mediated downstream effects may represent novel treatment targets for anti-epileptogenic intervention.

Differentially regulated glial genes and their involvement in neuronal death

Death of pyramidal neurons in CA3/1 is a major hallmark of human mTLE-HS (Blumcke et al., 2013) and is reproduced in many animal models, including the intracortical kainic acid mouse model of mTLE-HS (Bedner et al., 2015). In this now widely used and well-characterized model, apoptosis is first detectable after 6 h post-injection (hpi)—but not at 4 h—in CA1 neurons (Bedner et al., 2015). At 24 hpi, both CA1 and CA3 exhibit apoptotic pyramidal neurons, and, from then on, a progressive neurodegeneration leads eventually to 90% neuronal death in CA1 and CA3 at 28 days post-injection (dpi), and a complete absence of hippocampal neurons at 9 months post-injection (mpi) (Bedner et al., 2015). Further, the majority of GABAergic interneurons in CA1 and the dentate gyrus responsible for tonic inhibition are diminished substantially already at 5 dpi (Müller et al., 2020). At 24 hpi, we detected that 8 genes related to the regulation of neuronal death were upregulated in glia, while 2 genes in this category were downregulated in neurons (Berger et al., 2019). Many of these glial genes are associated with tumor necrosis factor alpha (TNF-α), nuclear factor kappa-light-chain-enhancer of activated B cells (NF-kB), and interleukin 1 beta (IL-1β) related pathways (Berger et al., 2019) and have previously been shown to be upregulated to some extent in microglia, but mostly astrocytes, in reactive states (Schlomann et al., 2000; Almeida et al., 2005; Koyama and Ikegaya, 2005; Saha et al., 2006; Groves et al., 2018; Iughetti et al., 2018). Although these results do not necessarily imply a causal role, they at least indicate an important involvement of glia in general, and astrocytes in particular, for neuronal death and already in the early latent phase of epileptogenesis.

Differentially regulated glial genes and their involvement in reactive astrogliosis

Reactive astrogliosis is a common feature of various neurodegenerative states (Zamanian et al., 2012) and pathognomonic for several epileptic conditions, such as mesial temporal lobe epilepsy with hippocampal sclerosis (mTLE-HS) in humans, successfully mimicked in the i.c. mouse model of mTLE-HS (Blumcke et al., 2013; Bedner et al., 2015). In general, this phenomenon comprises morphological and molecular reshaping of astrocytes in response to an external stimulus, and it is associated with astrocyte proliferation, immune-cell recruitment, and scar formation (Escartin et al., 2021). These responses are not necessarily dichotomous as previously proposed (good vs. bad astrocytes) (Zamanian et al., 2012), but represent a continuum of various molecular responses, the cumulative consequences of which are at best unknown (Escartin et al., 2021).

In mTLE-HS, astrocytes undergo functional and morphological changes already in the early stages of epileptogenesis. As shown in the i.c. mouse model, already at 4 hpi, cell death (primarily *via* necroptosis and autophagy) is detectable in astrocytes and the number of astrocytes in the CA1 region is reduced (Wu et al., 2021). These structural alterations are accompanied by decreased coupling and impaired capability of K+ buffering (Bedner et al., 2015; Wu et al., 2021), which in

turn are associated with increased extracellular glutamate levels and epileptic seizures (Pannasch et al., 2011). Over the course of epileptogenesis, astrocytes proliferate, express more GFAP, and at 9 mpi, a time point relevant to findings in humans with mTLE-HS, clear structural integration into the surrounding tissue is absent (Bedner et al., 2015). Our data at 24 hpi in the ipsilateral hippocampus (Berger et al., 2019), reveal that *Serpina3n* is the most significantly differentially expressed gene in glia. This astrocytic gene is associated with inflammation (Takamiya et al., 2002) and neuronal damage (Gesase and Kiyama, 2007) and has previously been identified as one of the major molecular hallmarks of reactive astrogliosis (Zamanian et al., 2012). Other interesting genes upregulated at 24 hpi in the ipsilateral hippocampus are *Cox2* (*Ptgs2*) and *Cxcl10* (Berger et al., 2020), both of which are pro-epileptic and potentially pro-epileptogenic inflammatory agents (Nelson and Gruol, 2004; Sui et al., 2006; Rojas et al., 2014) that are dysregulated in reactive astrogliosis (Zamanian et al., 2012). Other potential pathways involved in functional astrocytic alterations, such as astrocyte uncoupling, are the upregulation of mitogen-activated protein kinase (MAPK) pathways observed at 24 hpi mainly in glia (Berger et al., 2019). Early astrocytic uncoupling has been linked to altered phosphorylation of Cx43 *via* MAPK (Deshpande et al., 2017). This potentially involves TNF-α and IL-1β (Retamal et al., 2007) [mostly increased in glia (Berger et al., 2019)], which have been previously shown to have a negative effect on astrocyte coupling in the i.c. mouse model of mTLE-HS (Bedner et al., 2015).

Differentially regulated glial genes and their involvement in brain inflammation

Inflammation is closely associated with epileptogenesis (Vezzani et al., 2011). Both astrocytes and microglia can initiate and modulate inflammatory responses (Aronica et al., 2012; Devinsky et al., 2013; Eyo et al., 2017; Liddelow et al., 2017) and orchestrate downstream alterations, such as neuronal death or reactive gliosis (Jha et al., 2019; Patel et al., 2019). Apart from the activation of astrocytes at early time points of epileptogenesis in the i.c. mouse model of mTLE-HS, microglia are both prone to necroptosis already at 4 hpi and activated (elevated Iba1) at 14 dpi (Deshpande et al., 2020; Wu et al., 2021). Elevations in the levels of both TNF-α and IL-1β have also been measured at the early stages of epileptogenesis in this model. At 24 hpi, we observed increased TNF-α and IL-1β pathways, mainly in glia (Berger et al., 2019). Both these cytokines effect glutamate uptake and release from astrocytes (Hu et al., 2000; Bezzi et al., 2001; Santello et al., 2011). They also affect astrocyte coupling and neuronal death. Inflammation is also connected to the disruption of the BBB, angiogenesis, alterations of the ECM, and aberrant neurogenesis, all important elements of epileptogenesis (Pitkanen and Lukasiuk, 2011; Patel et al., 2019).

In the i.c. kainic acid model of mTLE-HS, albumin extravasation is detected at 5 dpi and throughout epileptogenesis (3 and 9 mpi) (Deshpande et al., 2017). At 28 dpi, CD31 as a marker of endothelial cells, and as such of angiogenesis, is increased in the ipsilateral hippocampus 3-fold in both CA1 and DG (Deshpande et al., 2017). This is in line with our findings in the same model, where we at 24 hpi, detected a total of 19 glial genes and 11 neuronal genes involved in angiogenesis (Berger et al., 2019). Albumin extravasation is known to induce the activation of transforming growth factor beta (TGF-β) in astrocytes (Heinemann et al., 2012), which, in turn induces MAPKs potentially leading to Cx43 phosphorylation and uncoupling of astrocytes, a mechanism believed to be important in epileptogenesis (Deshpande et al., 2017). TGF-β further induces increased neuronal excitability *via* astrocyte-mediated reduction of Kir4.1, AQP channels, and glutamate transporters (Ivens et al., 2007; Kim et al., 2012). We found TGF-β pathways to be increased in both neurons and glia at 24 hpi (Berger et al., 2019).

Potential strategies and challenges of anti-epileptogenic intervention

Hypermethylation in chronic epilepsy states in both human and murine CNS tissue, represents the most consistent finding of DNAm alterations. Alas, the potential attenuation of epileptogenesis *via* DNAm inhibition could serve as an anti-epileptic or even anti-epileptogenic target (Ryley Parrish et al., 2013; Williams-Karnesky et al., 2013). Mechanistically, this may be linked to direct anti-epileptic/anti-epileptogenic effects of adenosine, as this molecule is metabolically connected to DNAm (Weltha et al., 2019).

Anti-epileptogenic therapy could either enforce endogenic homeostatic pathways or attenuate detrimental responses. Genes dysregulated in the latent phase but also in the early chronic state of epileptogenesis are potential upstream targets of anti-epileptogenic intervention. In general, all the above-mentioned genes with CpG islands in their promoters (possibly other genomic features also) could be targeted to alter GE *via* DNAm alteration [as shown feasible in ref. (Liu X. S. et al., 2016)]. Even if DNAm changes do not overlap with GE changes in different epilepsy models and at different specific time points, it may still be possible to alter the expression of crucial genes and pathways by means of epigenetic editing as described elsewhere (Liu X. S. et al., 2016; Holtzman and Gersbach, 2018; Liu and Jaenisch, 2019). To achieve this goal, an epigenetic tool, such as a modified CRISPR system with either a DNMT (to facilitate hypermethylation and potentially gene silencing) or a TET oxidase (to gain hypomethylation and gene activation), applicable both to the anatomical region and cell type of choice, would be necessary.

Further, specific post-transcriptional (Desi and Tay, 2019) or post-translational modifications (Wang et al., 2014) could

be employed to intervene between gene transcription and protein synthesis/downstream effects of the given target. As proposed by previous studies and supported by our findings (Berger et al., 2019, 2020), glia plays an important role in inflammatory pathways (Devinsky et al., 2013; Patel et al., 2019). Thus, the development of glia-specific drugs may lead the way to the next generation of anti-epileptogenic treatment. Nevertheless, a long way is ahead to reach these goals. One way to decipher the "epileptogenic code" would be to analyze all known molecular factors (e.g., DNAm, histone modifications, transcription factor binding, GE, proteomics, EEG, and clinical parameters) simultaneously and using comparable methods, crystalize patterns with the help of artificial intelligence, as has been performed with a fraction of parameters in ref. (Myszczynska et al., 2020). The next pragmatic steps toward this long-term goal include the assessment of cell-specific DNAm and throughout the whole process of epileptogenesis in animal models, with confirmation of results in human studies. Potential outcomes of such efforts include cell-specific molecular treatment targets and biomarkers for epileptogenesis. However, one of the most prominent challenges is the versatility of the epilepsies. Seizures are symptomatic manifestations of cerebral dysfunction and can be caused by a multitude of conditions, ranging from unknown idiopathic to the acquired causes, such as TBI, ischemic cerebral insults, infections, or hypoxia. Moreover, we must rely on simplified models restricted to only mimicking a certain group of the human epilepsies. Further, we must face concerns on comparability, interpretability, and translation of various research results based on diverse analytical tools (e.g., for GE—RNA-Seq or various kits) and bioinformatics processing.

Another important issue worth mentioning is the role of DNAm for diagnostic and prognostic approaches in epilepsy. As an example, the blood of patients with mTLE-HS has shown specific DNAm patterns (Long et al., 2017) and a concordant-twin study detected patterns that enabled distinction between focal and generalized epilepsy (Mohandas et al., 2019). These results suggest that blood-based DNAm could be a potential biomarker for epilepsy and epileptogenesis, paving the way to a more personalized management of people with epilepsy (PWE). Blood-based DNAm as a biomarker could also help to predict the patients risk for developing comorbidities, such as anxiety, depression, or cognitive decline and predict treatment response with existing anti-seizure medication (ASM).

Conclusions

Neurons and glia orchestrate epileptogenesis, with glia playing a crucial part in neuronal death, reactive gliosis, and inflammation in early epileptogenesis. Several, mostly inflammation-related and glia-derived genes may serve as targets for anti-epileptogenic intervention, potentially by means of epigenetic modification. Several recent studies have revealed widespread and cell-specific alterations in DNAm in epileptogenesis. To what extent and how exactly DNAm influences GE (and downstream effects) in epileptogenesis, is challenging to determine, and methodological shortcomings as well as inadequate processing of complex data seem to muddy the waters. We have yet to fathom the full complexity of interplay at various levels of molecular interactions in epileptogenesis. It is possible, or even likely, that not a single gene or pathway determines epileptogenesis, but rather the interaction of genes at a given time, the resulting levels of proteins, and cellular interactions that determine the epileptogenic phenotype.

Author contributions

KH and TB contributed to conception, design, writing, and revision of the article. ET contributed to the writing and revision of the article. All authors contributed to the article and approved the submitted version.

Funding

This work was supported by the European Commission (ERA-NET NEURON, Brain Inflammation, Glia and Epilepsy), the European Union's Horizon 2020 research and innovation program (Marie Sklodowska-Curie grant agreement No. 722053), and the South-Eastern Norway Regional Health Authority (No. 2014018).

Conflict of interest

The authors declare that the research was conducted in the absence of any commercial or financial relationships that could be construed as a potential conflict of interest.

Publisher's note

References

Abou-Khalil, B., Auce, P., Avbersek, A., Bahlo, M., Balding, D. J., Bast, T., et al. (2018). Genome-wide mega-analysis identifies 16 loci and highlights diverse biological mechanisms in the common epilepsies. *Nat. Commun.* 9, 5269. doi: 10.1038/s41467-018-07524-z

Agha, G., Mendelson, M. M., Ward-Caviness, C. K., Joehanes, R., Huan, T., Gondalia, R., et al. (2019). Blood leukocyte DNA methylation predicts risk of future myocardial infarction and coronary heart disease. *Circulation*. 140, 645–657. doi: 10.1161/CIRCULATIONAHA.118.039357

Almeida, R. D., Manadas, B. J., Melo, C. V., Gomes, J. R., Mendes, C. S., Grãos, M. M., et al. (2005). Neuroprotection by BDNF against glutamate-induced apoptotic cell death is mediated by ERK and PI3-kinase pathways. *Cell Death Differ*. 12, 1329–1343. doi: 10.1038/sj.cdd.4401662

Aronica, E., and Gorter, J. A. (2007). Gene expression profile in temporal lobe epilepsy. *Neuroscientist*. 13, 100–108. doi: 10.1177/1073858406295832

Aronica, E., Ravizza, T., Zurolo, E., and Vezzani, A. (2012). Astrocyte immune responses in epilepsy. *Glia* 60, 1258–1268. doi: 10.1002/glia.22312

Bedner, P., Dupper, A., Huttmann, K., Muller, J., Herde, M. K., Dublin, P., et al. (2015). Astrocyte uncoupling as a cause of human temporal lobe epilepsy. *Brain J. Neurol.* 138, 1208–1222. doi: 10.1093/brain/awv067

Berdasco, M., and Esteller, M. (2019). Clinical epigenetics: seizing opportunities for translation. *Nat. Rev. Genet.* 20, 109–127. doi: 10.1038/s41576-018-0074-2

Berger, T. C., Vigeland, M. D., Hjorthaug, H. S., Etholm, L., Nome, C. G., Tauboll, E., et al. (2019). Neuronal and glial DNA methylation and gene expression changes in early epileptogenesis. *PLoS ONE*. 14, e0226575. doi: 10.1371/journal.pone.0226575

Berger, T. C., Vigeland, M. D., Hjorthaug, H. S., Nome, C. G., Taubøll, E., Selmer, K. K., et al. (2020). Differential glial activation in early epileptogenesis-insights from cell-specific analysis of DNA methylation and gene expression in the contralateral hippocampus. *Front. Neurol.* 11, 573575. doi: 10.3389/fneur.2020.573575

Bezzi, P., Domercq, M., Brambilla, L., Galli, R., Schols, D., Clercq, D., et al. (2001). E, et al. CXCR4-activated astrocyte glutamate release via TNFalpha: amplification by microglia triggers neurotoxicity. *Nat. Neurosci.* 4, 702–710. doi: 10.1038/89490

Blumcke, I., Thom, M., Aronica, E., Armstrong, D. D., Bartolomei, F., Bernasconi, A., et al. (2013). International consensus classification of hippocampal sclerosis in temporal lobe epilepsy: a task force report from the ILAE commission on diagnostic methods. *Epilepsia* 54, 1315–1329. doi: 10.1111/epi.12220

Boison, D., Sandau, U., Ruskin, D., Kawamura, M., and Masino, S. (2013). Homeostatic control of brain function—new approaches to understand epileptogenesis. *Front. Cell. Neurosci.* 7, 109. doi: 10.3389/fncel.2013.00109

Bruxel, E. M., and Bruno, D. C. F., do Canto, A. M., Geraldis, J. C., Godoi, A. B., Martin, M., et al. (2021). Multi-omics in mesial temporal lobe epilepsy with hippocampal sclerosis: clues into the underlying mechanisms leading to disease. *Seizure* 90, 34–50. doi: 10.1016/j.seizure.2021.03.002

Cahoy, J. D., Emery, B., Kaushal, A., Foo, L. C., Zamanian, J. L., Christopherson, K. S., et al. (2008). A transcriptome database for astrocytes, neurons, and oligodendrocytes: a new resource for understanding brain development and function. *J. Neurosci.* 28, 264–278. doi: 10.1523/JNEUROSCI.4178-07.2008

Cavalcante, G. C., Magalhães, L., Ribeiro-Dos-Santos, Â., and Vidal, A. F. (2020). Mitochondrial epigenetics: non-coding RNAs as a novel layer of complexity. *Int. J. Mol. Sci.* 21, 1838. doi: 10.3390/ijms21051838

Cavalli, G., and Heard, E. (2019). Advances in epigenetics link genetics to the environment and disease. *Nature* 571, 489–499. doi: 10.1038/s41586-019-1411-0

Cedar, H., and Bergman, Y. (2009). Linking DNA methylation and histone modification: patterns and paradigms. *Nat. Rev. Genet.* 10, 295–304. doi: 10.1038/nrg2540

Collins, F. S., Morgan, M., and Patrinos, A. (2003). The human genome project: lessons from large-scale biology. *Science* 300, 286–290. doi: 10.1126/science.1084564

Danchin, É., Charmantier, A., Champagne, F. A., Mesoudi, A., Pujol, B., Blanchet, S., et al. (2011). Beyond DNA: integrating inclusive inheritance into an extended theory of evolution. *Nat. Rev. Genet.* 12, 475–486. doi: 10.1038/nrg3028

de Lanerolle, N. C., Kim, J. H., Robbins, R. J., and Spencer, D. D. (1989). Hippocampal interneuron loss and plasticity in human temporal lobe epilepsy. *Brain Res.* 495, 387–395. doi: 10.1016/0006-8993(89)90234-5

de Lanerolle, N. C., Lee, T. S., and Spencer, D. D. (2012). "Histopathology of human epilepsy," in *Jasper's Basic Mechanisms of the Epilepsies*, eds J. L. Noebels, M. Avoli, M. A. Rogawski, R. W. Olsen and A. V. Delgado-Escueta (Bethesda, MD: National Center for Biotechnology Information, US) Copyright ©. Michael A Rogawski, Antonio V Delgado-Escueta, Jeffrey L Noebels, Massimo Avoli and Richard W Olsen.

Debski, K. J., Pitkanen, A., Puhakka, N., Bot, A. M., Khurana, I., Harikrishnan, K. N., et al. (2016). Etiology matters - genomic DNA methylation patterns in three rat models of acquired epilepsy. *Sci. Rep.* 6, 25668. doi: 10.1038/srep25668

Deshpande, T., Li, T., Henning, L., Wu, Z., Müller, J., Seifert, G., et al. (2020). Constitutive deletion of astrocytic connexins aggravates kainate-induced epilepsy. *Glia* 68, 2136–2147. doi: 10.1002/glia.23832

Deshpande, T., Li, T., Herde, M. K., Becker, A., Vatter, H., Schwarz, M. K., et al. (2017). Subcellular reorganization and altered phosphorylation of the astrocytic gap junction protein connexin43 in human and experimental temporal lobe epilepsy. *Glia* 65, 1809–1820. doi: 10.1002/glia.23196

Desi, N., and Tay, Y. (2019). The butterfly effect of RNA alterations on transcriptomic equilibrium. *Cells* 8, 1634. doi: 10.3390/cells8121634

Devinsky, O., Vezzani, A., Najjar, S., De Lanerolle, N. C., and Rogawski, M. A. (2013). Glia and epilepsy: excitability and inflammation. *Trends Neurosci.* 36, 174–184. doi: 10.1016/j.tins.2012.11.008

Dityatev, A. (2010). Remodeling of extracellular matrix and epileptogenesis. *Epilepsia*. 51, 61–65. doi: 10.1111/j.1528-1167.2010.02612.x

Dixit, A. B., Sharma, D., Tripathi, M., Srivastava, A., Paul, D., Prakash, D., et al. (2018). Genome-wide DNA methylation and RNAseq analyses identify aberrant signalling pathways in focal cortical dysplasia (FCD) Type II. *Sci. Rep.* 8, 17976. doi: 10.1038/s41598-018-35892-5

Dixit, A. B., Srivastava, A., Sharma, D., Tripathi, M., Paul, D., Lalwani, S., et al. (2020). Integrated genome-wide DNA methylation and RNAseq analysis of hippocampal specimens identifies potential candidate genes and aberrant signalling pathways in patients with hippocampal sclerosis. *Neurol India* 68, 307–313. doi: 10.4103/0028-3886.280649

Dor, Y., and Cedar, H. (2018). Principles of DNA methylation and their implications for biology and medicine. *Lancet* 392, 777–786. doi: 10.1016/S0140-6736(18)31268-6

Doyle, J. P., Dougherty, J. D., Heiman, M., Schmidt, E. F., Stevens, T. R., Ma, G., et al. (2008). Application of a translational profiling approach for the comparative analysis of CNS cell types. *Cell* 135, 749–762. doi: 10.1016/j.cell.2008.10.029

Eid, T., Lee, T. S., Thomas, M. J., Amiry-Moghaddam, M., Bjornsen, L. P., Spencer, D. D., et al. (2005). Loss of perivascular aquaporin 4 may underlie deficient water and K+ homeostasis in the human epileptogenic hippocampus. *Proc. Natl. Acad. Sci. U.S.A.* 102, 1193–1198. doi: 10.1073/pnas.0409308102

Eid, T., Lee, T. W., Patrylo, P., and Zaveri, H. P. (2019). Astrocytes and glutamine synthetase in epileptogenesis. *J. Neurosci. Res.* 97, 1345–1362. doi: 10.1002/jnr.24267

Escartin, C., Galea, E., Lakatos, A., O'Callaghan, J. P., Petzold, G. C., Serrano-Pozo, A., et al. (2021). Reactive astrocyte nomenclature, definitions, and future directions. *Nat. Neurosci.* 24, 312–325. doi: 10.1038/s41593-020-00783-4

Eyo, U. B., Murugan, M., and Wu, L. J. (2017). Microglia-neuron communication in epilepsy. *Glia* 65, 5–18. doi: 10.1002/glia.23006

Feinberg, A. P. (2007). Phenotypic plasticity and the epigenetics of human disease. *Nature* 447, 433–440. doi: 10.1038/nature05919

Fransquet, P. D., Lacaze, P., Saffery, R., McNeil, J., Woods, R., Ryan, J., et al. (2018). Blood DNA methylation as a potential biomarker of dementia: a systematic review. *Alzheimers Dement.* 14, 81–103. doi: 10.1016/j.jalz.2017.10.002

Gesase, A. P., and Kiyama, H. (2007). Peripheral nerve injury induced expression of mRNA for serine protease inhibitor 3 in the rat facial and hypoglossal nuclei but not in the spinal cord. *Ital. J. Anat. Embryol.* 112, 157–168.

Gräff, J., Kim, D., Dobbin, M. M., and Tsai, L-., H. (2011). Epigenetic regulation of gene expression in physiological and pathological brain processes. *Physiol. Rev.* 91, 603–649. doi: 10.1152/physrev.00012.2010

Green, E. D., Watson, J. D., and Collins, F. S. (2015). Human genome project: twenty-five years of big biology. *Nature* 526, 29–31. doi: 10.1038/526029a

Greenberg, M. V. C., and Bourc'his, D. (2019). The diverse roles of DNA methylation in mammalian development and disease. *Nat. Rev. Mol. Cell Biol.* 20, 590–607. doi: 10.1038/s41580-019-0159-6

Groves, A., Kihara, Y., Jonnalagadda, D., Rivera, R., Kennedy, G., Mayford, M., et al. (2018). A Functionally defined *in vivo* astrocyte population identified by c-fos activation in a mouse model of multiple sclerosis modulated

by S1P signaling: immediate-early astrocytes (ieAstrocytes). *eNeuro* 5. doi: 10.1523/ENEURO.0239-18.2018

Guo, J. U., Ma, D. K., Mo, H., Ball, M. P., Jang, M. H., Bonaguidi, M. A., et al. (2011). Neuronal activity modifies the DNA methylation landscape in the adult brain. *Nat. Neurosci*. 14, 1345–1351. doi: 10.1038/nn.2900

Heinemann, U., Kaufer, D., and Friedman, A. (2012). Blood-brain barrier dysfunction, TGFβ signaling, and astrocyte dysfunction in epilepsy. *Glia* 60, 1251–1257. doi: 10.1002/glia.22311

Henderson-Smith, A., Fisch, K. M., Hua, J., Liu, G., Ricciardelli, E., Jepsen, K., et al. (2019). DNA methylation changes associated with Parkinson's disease progression: outcomes from the first longitudinal genome-wide methylation analysis in blood. *Epigenetics*. 14, 365–382. doi: 10.1080/15592294.2019.1588682

Heuser, K., de Curtis, M., and Steinhäuser, C. (2021). Editorial: glial dysfunction in epileptogenesis. *Front. Neurol*. 12, 716308. doi: 10.3389/fneur.2021.716308

Holtzman, L., and Gersbach, C. A. (2018). Editing the epigenome: reshaping the genomic landscape. *Annu. Rev. Genomics Hum. Genet*. 19, 43–71. doi: 10.1146/annurev-genom-083117-021632

Houser, C., Miyashiro, J., Swartz, B., Walsh, G., Rich, J., Delgado-Escueta, A., et al. (1990). Altered patterns of dynorphin immunoreactivity suggest mossy fiber reorganization in human hippocampal epilepsy. *J. Neurosci*. 10, 267–282. doi: 10.1523/JNEUROSCI.10-01-00267.1990

Houser, C. R. (1990). Granule cell dispersion in the dentate gyrus of humans with temporal lobe epilepsy. *Brain Res*. 535, 195–204. doi: 10.1016/0006-8993(90)91601-C

Hu, S., Sheng, W. S., Ehrlich, L. C., Peterson, P. K., and Chao, C. C. (2000). Cytokine effects on glutamate uptake by human astrocytes. *Neuroimmunomodulation* 7, 153–159. doi: 10.1159/000026433

International League Against Epilepsy Consortium on Complex Epilepsies (2014). Electronic address e-auea. Genetic determinants of common epilepsies: a meta-analysis of genome-wide association studies. *Lancet Neurol*. 13, 893–903. doi: 10.1016/S1474-4422(14)70171-1

Iughetti, L., Lucaccioni, L., Fugetto, F., Predieri, B., Berardi, A., Ferrari, F., et al. (2018). Brain-derived neurotrophic factor and epilepsy: a systematic review. *Neuropeptides* 72, 23–29. doi: 10.1016/j.npep.2018.09.005

Ivens, S., Kaufer, D., Flores, L. P., Bechmann, I., Zumsteg, D., Tomkins, O., et al. (2007). TGF-β receptor-mediated albumin uptake into astrocytes is involved in neocortical epileptogenesis. *Brain* 130, 535–547. doi: 10.1093/brain/awl317

Jha, M. K., Jo, M., Kim, J. H., and Suk, K. (2019). Microglia-astrocyte crosstalk: an intimate molecular conversation. *Neuroscientist* 25, 227–240. doi: 10.1177/1073858418783959

Kalozoumi, G., Kel-Margoulis, O., Vafiadaki, E., Greenberg, D., Bernard, H., Soreq, H., et al. (2018). Glial responses during epileptogenesis in Mus musculus point to potential therapeutic targets. *PLoS ONE*. 13, e0201742. doi: 10.1371/journal.pone.0201742

Kim, H., Wang, X., and Jin, P. (2018). Developing DNA methylation-based diagnostic biomarkers. *J. Genet. Genom*. 45, 87–97. doi: 10.1016/j.jgg.2018.02.003

Kim, S. Y., Buckwalter, M., Soreq, H., Vezzani, A., and Kaufer, D. (2012). Blood-brain barrier dysfunction-induced inflammatory signaling in brain pathology and epileptogenesis. *Epilepsia* 53, 37–44. doi: 10.1111/j.1528-1167.2012.03701.x

Kobow, K., Jeske, I., Hildebrandt, M., Hauke, J., Hahnen, E., Buslei, R., et al. (2009). Increased reelin promoter methylation is associated with granule cell dispersion in human temporal lobe epilepsy. *J. Neuropathol. Exp. Neurol*. 68, 356–364. doi: 10.1097/NEN.0b013e31819ba737

Kobow, K., Kaspi, A., Harikrishnan, K. N., Kiese, K., Ziemann, M., Khurana, I., et al. (2013). Deep sequencing reveals increased DNA methylation in chronic rat epilepsy. *Acta Neuropathol*. 126, 741–756. doi: 10.1007/s00401-013-1168-8

Kobow, K., Ziemann, M., Kaipananickal, H., Khurana, I., Mühlebner, A., Feucht, M., et al. (2019). Genomic DNA methylation distinguishes subtypes of human focal cortical dysplasia. *Epilepsia* 60, 1091–1103. doi: 10.1111/epi.14934

Kovács, T., Szabó-Meleg, E., and Ábrahám, I. M. (2020). Estradiol-induced epigenetically mediated mechanisms and regulation of gene expression. *Int. J. Mol. Sci*. 21, 3177. doi: 10.3390/ijms21093177

Koyama, R., and Ikegaya, Y. (2005). To BDNF or not to BDNF: that is the epileptic hippocampus. *Neuroscientist* 11, 282–287. doi: 10.1177/1073858405278266

Kozlenkov, A., Roussos, P., Timashpolsky, A., Barbu, M., Rudchenko, S., Bibikova, M., et al. (2014). Differences in DNA methylation between human neuronal and glial cells are concentrated in enhancers and non-CpG sites. *Nucleic Acids Res*. 42, 109–127. doi: 10.1093/nar/gkt838

Kribelbauer, J. F., Lu, X. J., Rohs, R., Mann, R. S., and Bussemaker, H. J. (2019). Toward a mechanistic understanding of DNA methylation readout by transcription factors. *J. Mol. Biol*. 432, 1801–1805. doi: 10.1016/j.jmb.2019.10.021

Li, H. J., Wan, R. P., Tang, L. J., Liu, S. J., Zhao, Q. H., Gao, M. M., et al. (2015). Alteration of Scn3a expression is mediated via CpG methylation and MBD2 in mouse hippocampus during postnatal development and seizure condition. *Biochim. Biophys. Acta*. 1849, 1–9. doi: 10.1016/j.bbagrm.2014.11.004

Li, X., Wang, X., He, K., Ma, Y., Su, N., He, H., et al. (2008). High-resolution mapping of epigenetic modifications of the rice genome uncovers interplay between DNA methylation, histone methylation, and gene expression. *Plant Cell* 20, 259–276. doi: 10.1105/tpc.107.056879

Li, Y. E., Preissl, S., Hou, X., Zhang, Z., Zhang, K., Qiu, Y., et al. (2021). An atlas of gene regulatory elements in adult mouse cerebrum. *Nature* 598, 129–136. doi: 10.1038/s41586-021-03604-1

Liddelow, S. A., Guttenplan, K. A., Clarke, L. E., Bennett, F. C., Bohlen, C. J., Schirmer, L., et al. (2017). Neurotoxic reactive astrocytes are induced by activated microglia. *Nature* 541, 481–487. doi: 10.1038/nature21029

Lipponen, A., El-Osta, A., Kaspi, A., Ziemann, M., Khurana, I., Kn, H., et al. (2018). Transcription factors Tp73, Cebpd, Pax6, and Spi1 rather than DNA methylation regulate chronic transcriptomics changes after experimental traumatic brain injury. *Acta Neuropathol. Commun*. 6, 17. doi: 10.1186/s40478-018-0519-z

Lister, R., Mukamel, E. A., Nery, J. R., Urich, M., Puddifoot, C. A., Johnson, N. D., et al. (2013). Global epigenomic reconfiguration during mammalian brain development. *Science* 2013, 341. doi: 10.1126/science.1237905

Liu, X., Ou, S., Xu, T., Liu, S., Yuan, J., Huang, H., et al. (2016). New differentially expressed genes and differential DNA methylation underlying refractory epilepsy. *Oncotarget*. 7, 87402–87416. doi: 10.18632/oncotarget.13642

Liu, X. S., and Jaenisch, R. (2019). Editing the epigenome to tackle brain disorders. *Trends Neurosci*. 42, 861–870. doi: 10.1016/j.tins.2019.10.003

Liu, X. S., Wu, H., Ji, X., Stelzer, Y., Wu, X., Czauderna, S., et al. (2016). Editing DNA methylation in the mammalian genome. *Cell* 167, 233–47.e17. doi: 10.1016/j.cell.2016.08.056

Liu, Y., Beyer, A., and Aebersold, R. (2016). On the dependency of cellular protein levels on mRNA abundance. *Cell* 165, 535–550. doi: 10.1016/j.cell.2016.03.014

Long, H-. Y., Feng, L., Kang, J., Luo, Z-, H., Xiao, W-., et al. (2017). Blood DNA methylation pattern is altered in mesial temporal lobe epilepsy. *Sci. Rep*. 7, 43810. doi: 10.1038/srep43810

Löscher, W. (2020). The holy grail of epilepsy prevention: Preclinical approaches to antiepileptogenic treatments. *Neuropharmacology*. 167, 107605. doi: 10.1016/j.neuropharm.2019.04.011

Loscher, W., Klitgaard, H., Twyman, R. E., and Schmidt, D. (2013). New avenues for anti-epileptic drug discovery and development. *Nat. Rev. Drug Discov*. 12, 757–776. doi: 10.1038/nrd4126

Luo, C., Hajkova, P., and Ecker, J. R. (2018). Dynamic DNA methylation: In the right place at the right time. *Science* 361, 1336–1340. doi: 10.1126/science.aat6806

Lusardi, T. A., Akula, K. K., Coffman, S. Q., Ruskin, D. N., Masino, S. A., Boison, D., et al. (2015). Ketogenic diet prevents epileptogenesis and disease progression in adult mice and rats. *Neuropharmacology* 99, 500–509. doi: 10.1016/j.neuropharm.2015.08.007

Machnes, Z. M., Huang, T. C., Chang, P. K., Gill, R., Reist, N., Dezsi, G., et al. (2013). DNA methylation mediates persistent epileptiform activity *in vitro* and *in vivo*. *PLoS ONE* 8, e76299. doi: 10.1371/journal.pone.0076299

Martin, E. M., and Fry, R. C. (2018). Environmental influences on the epigenome: exposure- associated DNA methylation in human populations. *Annu. Rev. Public Health*. 39, 309–333. doi: 10.1146/annurev-publhealth-040617-014629

Mathern, G. W., Babb, T. L., Vickrey, B. G., Melendez, M., and Pretorius, J. K. (1995). The clinical-pathogenic mechanisms of hippocampal neuron loss and surgical outcomes in temporal lobe epilepsy. *Brain J. Neurol*. 118, 105–118. doi: 10.1093/brain/118.1.105

McClung, C. A., and Nestler, E. J. (2008). Neuroplasticity mediated by altered gene expression. *Neuropsychopharmacology* 33, 3–17. doi: 10.1038/sj.npp.1301544

Mellén, M., Ayata, P., and Heintz, N. (2017). 5-hydroxymethylcytosine accumulation in postmitotic neurons results in functional demethylation of expressed genes. *Proc. Nat. Acad. Sci*. 114, E7812–E21. doi: 10.1073/pnas.1708044114

Miller-Delaney, S. F., Das, S., Sano, T., Jimenez-Mateos, E. M., Bryan, K., Buckley, P. G., et al. (2012). Differential DNA methylation patterns define status epilepticus and epileptic tolerance. *J. Neurosci*. 32, 1577–1588. doi: 10.1523/JNEUROSCI.5180-11.2012

Miller-Delaney, S. F. C., Bryan, K., Das, S., McKiernan, R. C., Bray, I. M., Reynolds, J. P., et al. (2015). Differential DNA methylation profiles of coding and non-coding genes define hippocampal sclerosis in human temporal lobe epilepsy. *Brain* 138, 616–631. doi: 10.1093/brain/awu373

Mohandas, N., Loke, Y. J., Hopkins, S., Mackenzie, L., Bennett, C., Berkovic, S. F., et al. (2019). Evidence for type-specific DNA methylation patterns in epilepsy: a discordant monozygotic twin approach. *Epigenomics* 11, 951–968. doi: 10.2217/epi-2018-0136

Müller, J., Timmermann, A., Henning, L., Müller, H., Steinhäuser, C., Bedner, P., et al. (2020). Astrocytic GABA accumulation in experimental temporal lobe epilepsy. *Front. Neurol.* 11, 1762. doi: 10.3389/fneur.2020.614923

Myszczynska, M. A., Ojamies, P. N., Lacoste, A. M. B., Neil, D., Saffari, A., Mead, R., et al. (2020). Applications of machine learning to diagnosis and treatment of neurodegenerative diseases. *Nat. Rev. Neurol.* 16, 440–456. doi: 10.1038/s41582-020-0377-8

Nelson, T. E., and Gruol, D. L. (2004). The chemokine CXCL10 modulates excitatory activity and intracellular calcium signaling in cultured hippocampal neurons. *J. Neuroimmunol.* 156, 74–87. doi: 10.1016/j.jneuroim.2004.07.009

Pannasch, U., Vargová, L., Reingruber, J., Ezan, P., Holcman, D., Giaume, C., et al. (2011). Astroglial networks scale synaptic activity and plasticity. *Proc. Natl. Acad. Sci. U.S.A.* 108, 8467–8472. doi: 10.1073/pnas.1016650108

Patel, D. C., Tewari, B. P., Chaunsali, L., and Sontheimer, H. (2019). Neuron–glia interactions in the pathophysiology of epilepsy. *Nat. Rev. Neurosci.* 20, 282–297. doi: 10.1038/s41583-019-0126-4

Perucca, E., Brodie, M. J., Kwan, P., and Tomson, T. (2020). 30 years of second-generation antiseizure medications: impact and future perspectives. *Lancet Neurol.* 19, 544–556. doi: 10.1016/S1474-4422(20)30035-1

Pitkanen, A., and Engel, J. (2014). Past and present definitions of epileptogenesis and its biomarkers. *Neurotherapeutics* 11, 231–241. doi: 10.1007/s13311-014-0257-2

Pitkanen, A., and Lukasiuk, K. (2011). Mechanisms of epileptogenesis and potential treatment targets. *Lancet Neurol.* 10, 173–186. doi: 10.1016/S1474-4422(10)70310-0

Pitkänen, A., Nehlig, A., Brooks-Kayal, A. R., Dudek, F. E., Friedman, D., Galanopoulou, A. S., et al. (2013). Issues related to development of antiepileptogenic therapies. *Epilepsia* 54, 35–43. doi: 10.1111/epi.12297

Retamal, M. A., Froger, N., Palacios-Prado, N., Ezan, P., Sáez, P. J., Sáez, J. C., et al. (2007). Cx43 hemichannels and gap junction channels in astrocytes are regulated oppositely by proinflammatory cytokines released from activated microglia. *J. Neurosci.* 27, 13781–13792. doi: 10.1523/JNEUROSCI.2042-07.2007

Rojas, A., Jiang, J., Ganesh, T., Yang, M. S., Lelutiu, N., Gueorguieva, P., et al. (2014). Cyclooxygenase-2 in epilepsy. *Epilepsia* 55, 17–25. doi: 10.1111/epi.12461

Ryley Parrish, R., Albertson, A. J., Buckingham, S. C., Hablitz, J. J., Mascia, K. L., Davis Haselden, W., et al. (2013). Status epilepticus triggers early and late alterations in brain-derived neurotrophic factor and NMDA glutamate receptor Grin2b DNA methylation levels in the hippocampus. *Neuroscience* 248, 602–619. doi: 10.1016/j.neuroscience.2013.06.029

Saha, R. N., Liu, X., and Pahan, K. (2006). Up-regulation of BDNF in astrocytes by TNF-alpha: a case for the neuroprotective role of cytokine. *J. Neuroimmune Pharmacol.* 1, 212–222. doi: 10.1007/s11481-006-9020-8

Sanosaka, T., Imamura, T., Hamazaki, N., Chai, M., Igarashi, K., Ideta-Otsuka, M., et al. (2017). DNA ethylome analysis identifies transcription factor-based epigenomic signatures of multilineage competence in neural stem/progenitor cells. *Cell Rep.* 20, 2992–3003. doi: 10.1016/j.celrep.2017.08.086

Santello, M., Bezzi, P., and Volterra, A. (2011). TNFα controls glutamatergic gliotransmission in the hippocampal dentate gyrus. *Neuron* 69, 988–1001. doi: 10.1016/j.neuron.2011.02.003

Schlomann, U., Rathke-Hartlieb, S., Yamamoto, S., Jockusch, H., and Bartsch, J. W. (2000). Tumor necrosis factor α induces a metalloprotease-disintegrin, ADAM8 (CD 156): implications for neuron–glia interactions during neurodegeneration. *J. Neurosci.* 20, 7964. doi: 10.1523/JNEUROSCI.20-21-07964.2000

Silva, G. M., and Vogel, C. (2016). Quantifying gene expression: the importance of being subtle. *Mol. Syst. Biol.* 12, 885. doi: 10.15252/msb.20167325

Smith, Z. D., and Meissner, A. D. N. A. (2013). methylation: roles in mammalian development. *Nat. Rev. Genet.* 14, 204–220. doi: 10.1038/nrg3354

Somineni, H. K., Venkateswaran, S., Kilaru, V., Marigorta, U. M., Mo, A., Okou, D. T., et al. (2019). Blood-derived DNA methylation signatures of crohn's disease and severity of intestinal inflammation. *Gastroenterology.* 156, 2254–65.e3. doi: 10.1053/j.gastro.2019.01.270

Song, C. X., and He, C. (2013). Potential functional roles of DNA demethylation intermediates. *Trends Biochem. Sci.* 38, 480–484. doi: 10.1016/j.tibs.2013.07.003

Sui, Y., Stehno-Bittel, L., Li, S., Loganathan, R., Dhillon, N. K., Pinson, D., et al. (2006). CXCL10-induced cell death in neurons: role of calcium dysregulation. *Eur. J. Neurosci.* 23, 957–964. doi: 10.1111/j.1460-9568.2006.04631.x

Takamiya, A., Takeda, M., Yoshida, A., and Kiyama, H. (2002). Inflammation induces serine protease inhibitor 3 expression in the rat pineal gland. *Neuroscience* 113, 387–394. doi: 10.1016/S0306-4522(02)00198-7

Tauck, D. L., and Nadler, J. V. (1985). Evidence of functional mossy fiber sprouting in hippocampal formation of kainic acid-treated rats. *J. Neurosci.* 5, 1016–1022. doi: 10.1523/JNEUROSCI.05-04-01016.1985

Vezzani, A., French, J., Bartfai, T., and Baram, T. Z. (2011). The role of inflammation in epilepsy. *Nat. Rev. Neurol.* 7, 31–40. doi: 10.1038/nrneurol.2010.178

Vezzani, A., and Granata, T. (2005). Brain inflammation in epilepsy: experimental and clinical evidence. *Epilepsia* 46, 1724–1743. doi: 10.1111/j.1528-1167.2005.00298.x

Wang, L., Fu, X., Peng, X., Xiao, Z., Li, Z., Chen, G., et al., (2016). DNA methylation profiling reveals correlation of differential methylation patterns with gene expression in human epilepsy. *J. Mol. Neurosci.* 59, 68–77. doi: 10.1007/s12031-016-0735-6

Wang, X., Zheng, G., and Dong, D. (2015). Coordinated action of histone modification and microRNA regulations in human genome. *Gene* 570, 277–281. doi: 10.1016/j.gene.2015.06.046

Wang, Y.-C., Peterson, S. E., and Loring, J. F. (2014). Protein post-translational modifications and regulation of pluripotency in human stem cells. *Cell Res.* 24, 143–160. doi: 10.1038/cr.2013.151

Wang, Z., Gerstein, M., and Snyder, M. (2009). RNA-Seq: a revolutionary tool for transcriptomics. *Nat. Rev. Genet.* 10, 57–63. doi: 10.1038/nrg2484

Weltha, L., Reemmer, J., and Boison, D. (2019). The role of adenosine in epilepsy. *Brain Res. Bull.* 151, 46–54. doi: 10.1016/j.brainresbull.2018.11.008

Widagdo, J., and Anggono, V. (2018). The m6A-epitranscriptomic signature in neurobiology: from neurodevelopment to brain plasticity. *J. Neurochem.* 147, 137–152. doi: 10.1111/jnc.14481

Williams-Karnesky, R. L., Sandau, U. S., Lusardi, T. A., Lytle, N. K., Farrell, J. M., Pritchard, E. M., et al. (2013). Epigenetic changes induced by adenosine augmentation therapy prevent epileptogenesis. *J. Clin. Invest.* 123, 3552–3563. doi: 10.1172/JCI65636

Wu, Z., Deshpande, T., Henning, L., Bedner, P., Seifert, G., Steinhäuser, C., et al. (2021). Cell death of hippocampal CA1 astrocytes during early epileptogenesis. *Epilepsia* 62, 1569–1583. doi: 10.1111/epi.16910

Zamanian, J. L., Xu, L., Foo, L. C., Nouri, N., Zhou, L., Giffard, R. G., et al. (2012). Genomic analysis of reactive astrogliosis. *J. Neurosci.* 32, 6391–6410. doi: 10.1523/JNEUROSCI.6221-11.2012

Zhang, W., Wang, H., Liu, B., Jiang, M., Gu, Y., Yan, S., et al. (2021). Differential DNA Methylation profiles in patients with temporal lobe epilepsy and hippocampal sclerosis ILAE Type I. *J. Mol. Neurosci.* 71, 1951–1966. doi: 10.1007/s12031-020-01780-9

Zhu, Q., Wang, L., Zhang, Y., Zhao, F. H., Luo, J., Xiao, Z., et al. (2012). Increased expression of DNA methyltransferase 1 and 3a in human temporal lobe epilepsy. *J. Mol. Neurosci.* 46, 420–426. doi: 10.1007/s12031-011-9602-7

Zybura-Broda, K., Amborska, R., Ambrozek-Latecka, M., Wilemska, J., Bogusz, A., Bucko, J., et al. (2016). Epigenetics of Epileptogenesis-Evoked Upregulation of Matrix Metalloproteinase-9 in Hippocampus. *PLoS ONE.* 11, e0159745. doi: 10.1371/journal.pone.0159745

frontiers | Frontiers in Cellular Neuroscience

TYPE Original Research
PUBLISHED 17 November 2022
DOI 10.3389/fncel.2022.1007458

OPEN ACCESS

EDITED BY
Diana Cunha-Reis,
University of Lisbon, Portugal

REVIEWED BY
Ajit Ray,
Carnegie Mellon University,
United States
Giulia Curia,
University of Modena and Reggio
Emilia, Italy

*CORRESPONDENCE
Shucui Li
lishucui929@163.com
Hongliu Sun
sun_china6@163.com;
sunhongliu@bzmc.edu.cn

†These authors have contributed equally to this work

SPECIALTY SECTION
This article was submitted to Cellular Neuropathology, a section of the journal Frontiers in Cellular Neuroscience

RECEIVED 30 July 2022
ACCEPTED 31 October 2022
PUBLISHED 17 November 2022

CITATION
Zhang M, Cheng Y, Zhai Y, Yuan Y, Hu H, Meng X, Fan X, Sun H and Li S (2022) Attenuated iron stress and oxidative stress may participate in anti-seizure and neuroprotective roles of xenon in pentylenetetrazole-induced epileptogenesis. *Front. Cell. Neurosci.* 16:1007458. doi: 10.3389/fncel.2022.1007458

Attenuated iron stress and oxidative stress may participate in anti-seizure and neuroprotective roles of xenon in pentylenetetrazole-induced epileptogenesis

Mengdi Zhang†, Yao Cheng†, Yujie Zhai, Yi Yuan, Haoran Hu, Xianfeng Meng, Xuemeng Fan, Hongliu Sun* and Shucui Li*

School of Pharmaceutical Sciences, Binzhou Medical University, Yantai, China

The previous studies have demonstrated the excellent neuroprotective effects of xenon. In this study, we verified the anti-seizure and neuroprotective roles of xenon in epileptogenesis and evaluated the involvement of oxidative stress and iron accumulation in the protective roles of xenon. Epileptogenesis was induced by pentylenetetrazole (PTZ) treatment in Sprague-Dawley rats. During epileptogenesis, we found increased levels of iron and oxidative stress accompanied by elevated levels of divalent metal transporter protein 1 and iron regulatory protein 1, which are closely associated with iron accumulation. Meanwhile, the levels of autophagy and mitophagy increased, alongside significant neuronal damage and cognitive deficits. Xenon treatment reversed these effects: oxidative stress and iron stress were reduced, neuronal injury and seizure severity were attenuated, and learning and memory deficits were improved. Thus, our results confirmed the neuroprotective and anti-seizure effects of xenon treatment in PTZ-induced epileptogenesis. The reduction in oxidative and iron stress may be the main mechanisms underlying xenon treatment. Thus, this study provides a potential intervention strategy for epileptogenesis.

KEYWORDS

epileptogenesis, neuronal injury, oxidative stress, iron stress, xenon

Introduction

Epilepsy is a chronic neurological disorder caused by abnormal neuronal discharges in the brain and is accompanied by recurrent spontaneous seizures (Dhir, 2012; Lignani et al., 2020). It has a high impact, with a global prevalence of 0.5–1% and lifetime incidence of 1–3% (Fauser and Tumani, 2017). Epilepsy can cause neuronal damage and cognitive deficits. Although many drugs exist for the clinical treatment of patients with epilepsy, drug resistance and serious side effects are non-negligible

(Schmidt and Loscher, 2005). Considering the unsatisfactory therapeutic effect of epilepsy, it is particularly important to explore potential protective strategies to prevent epileptic development.

Xenon is an inert gas that has been used in clinical practice as an anesthetic for more than 70 years (Maze and Laitio, 2020). Moreover, the safety of xenon has been verified through long-term clinical applications (Kulikov et al., 2019). In recent years, studies have demonstrated the excellent neuroprotective effects of xenon at sub-anesthetic doses (Metaxa et al., 2014; Yang et al., 2014; Lavaur et al., 2016a). For example, xenon promotes neuroprotection and repair by regulating glutamate metabolism in the cell culture and animal models of Alzheimer's disease (Lavaur et al., 2017). In addition, remarkable neuroprotective effects have been demonstrated in models of local and global ischemia and spinal cord ischemia/reperfusion (Cattano et al., 2011; Yang et al., 2012; Metaxa et al., 2014; Yang et al., 2014).

Neuronal damage and synchronous discharge are characteristics of epilepsy and epileptogenesis (During and Spencer, 1993; Chiu et al., 2016; Kim and Kang, 2018). Xenon can inhibit synchronous neuronal firing (Uchida et al., 2012) and reduce neuronal damage caused by hyperexcitability by regulating glutamate metabolism (Lavaur et al., 2016a,b). Our previous studies demonstrated that xenon can inhibit seizures, neuronal damage, and cognitive deficits in kainic acid-induced status epilepticus and hypoxia-induced seizures (Zhang et al., 2019; Zhang M. et al., 2020; Zhu et al., 2020). Our previous findings and results of other studies suggest that xenon may exert anti-seizure and neuroprotective effects during epileptogenesis.

Normal regulation of iron metabolism, including iron intake, storage, and transport, is essential for brain development and function (Chen et al., 2019). Disturbances in iron regulation are closely associated with neuronal damage and can lead to degenerative diseases (Chen et al., 2019). For example, when excess iron is ingested and little iron is excreted, iron accumulation exerts toxic effects (Allen et al., 2018) and predisposes patients to diseases such as epilepsy and Parkinson's disease (Jiang et al., 2010; Ayton et al., 2014).

Activation of the *N*-methyl-*D*-aspartate (NMDA) receptor critically contributes to epileptic hyperexcitability and hyperexcitability-induced neuronal injury. This activation can elevate the expression of divalent metal transporter protein 1 (DMT1), which is responsible for iron uptake and accumulation, and consequently leads to iron stress-induced apoptosis and neuronal injury (Cesar et al., 2012).

Additionally, the mutually reinforcing effects of iron stress and oxidative stress have been verified (Molinari et al., 2019). High iron levels can lead to oxidative stress through the Fenton reaction, and elevated levels of oxidative stress can further promote iron accumulation (Xu et al., 2008; Maremonti et al., 2020; Zhang M. et al., 2020). Hyperexcitability-induced oxidative stress is one of the main features of epilepsy and seizures (dos Santos et al., 2011). Thus, the simultaneous elevation of iron levels and oxidative stress caused by NMDA-regulated hyperexcitability may be associated with epileptogenesis and neuronal damage during this progression.

Xenon, an NMDA receptor antagonist, can also inhibit glutamate metabolism and eventually reduce hyperexcitability-induced damage (Lavaur et al., 2016a,b). Therefore, we hypothesized that xenon can inhibit seizures and neuronal injury during epileptogenesis by attenuating iron stress and oxidative stress.

We used the pentylenetetrazole (PTZ) kindling model to assess the differences in iron levels, oxidative stress, neuronal damage, cognitive deficits, and epileptogenesis between xenon-treated and non-xenon-treated rats to elucidate the protective effects of xenon and lay the foundation for future clinical applications.

Materials and methods

Animals

A total of 160 male Sprague–Dawley rats (220–250 g, 6-week old, no. SCXK2019-0003, provided by the Pengyue Experimental Animal Center, Jinan, China) were used in our experiments. The experiments were conducted in compliance with the National Institutes of Health Guide for the Care and Use of Laboratory Animals (NIH Publications No. 80-23, revised 1996) and ethical principles of the Binzhou Medical University Animal Experimentation Committee (approval no. 2020002). Each rat was housed in a separate cage. All animals had free access to food and water under a 12-h light-dark cycle. Efforts were made to reduce the number of animals and subsequent pain. All experiments were carried out between 8:00 and 17:00.

Pentylenetetrazole kindling

The rats were intraperitoneally injected with PTZ (40 mg/kg, 10 mg/ml, CAS 54-95-5, Sigma-Aldrich, Saint Louis, MA, USA) once every other day for a total of 15 days. The control group was injected with an equal volume of saline. Each rat was individually placed inside a clear resin for 2 h for behavioral observation and electroencephalography (EEG) recording (ADInstruments, Dunedin, New Zealand). According to Racine's seizure behavior standards (Racine, 1972), seizures were classified into stages 1–5.

Xenon intervention

The xenon mixture (70% xenon, 21% oxygen, and 9% nitrogen) was introduced into a closed transparent resin-viewing chamber with an air inlet at the bottom and an air outlet

at the top for 15 min at a controlled flow rate of 200 ml/min. The rats in the xenon group were then placed in the chamber and treated with the xenon mixture for 30 min immediately after the administration of each intraperitoneal PTZ injection. In total, there were 8 xenon treatments. The control group was treated with 21% oxygen and 79% nitrogen. After each PTZ injection, behavioral observations and EEG recordings were performed for 2 h.

Xenon treatment in our study was not sufficient to induce anesthesia, and the rats remained awake and were allowed to move freely throughout the experiment.

Cognitive and behavioral testing

The Morris water maze (XR-Xmaze; Xinruan, Shanghai, China) experiment was performed 24 h after the eighth PTZ injection (Day 16) to assess the learning and memory abilities of the rats (Morris, 1984). The rat water maze device consisted of a circular pool (150 cm in diameter and 60 cm in height), station (12 cm in diameter and 20–35 cm in height), and a camera device. The detection was persisted for 5 days and was divided into two sections: positioning navigation experiment (Days 1–4) and space exploration experiment (Day 5). During the positioning navigation experiment, the rats were allowed to swimming for 60 s in order to find the platform that was hidden under the water (Zhang et al., 2019). If the rats failed to find the platform, a tester would enable the rats to find and remain on the platform for 10 s. As previously described (Zhang M. et al., 2020), the learning and memory abilities of rats in each group were assessed by detecting the latency to find the platform, cumulative number of passages over the platform, and percentage of time spent in the target and alignment quadrant (Netto et al., 1993; Pereira et al., 2007).

After the detection of Morris water maze test, the rats were divided for the Western Blotting and immunohistochemistry experiments.

Reactive oxygen species assay

The oxidant-sensing fluorescent probe 2',7'-dichlorodihydrofluorescein diacetate (DCFH-DA) is a non-polar dye that is converted to highly fluorescent 2',7'-dichlorodihydrofluorescein (DCF) when oxidized by intracellular ROS (Rastogi et al., 2010). ROS levels were assessed by measuring DCF levels (Zhang M. et al., 2020).

As previously described (Zhang M. et al., 2020), DCF levels were evaluated at 24 h, 3 days, and 21 days (n = 5/group per time point) during PTZ-induced epileptogenesis. After administering pentobarbital sodium (50 mg/kg, intraperitoneally, CAS, 57-33-0, Xiya Reagent, Chengdu, China), the brain was quickly removed, and the cortex and hippocampus were separated on ice, following which 0.01M PBS (10 μL/mg) was added to the samples, which were then cut using scissors on ice. Sequentially, the cut issue was filtered through a stainless steel mesh (200 mesh/inch) for the single-cell suspensions (Cheng et al., 2021). In accordance with the instructions of the ROS Assay Kit (Beyotime, S0033, Shanghai, China), 500 μL DCFH-DA diluted with serum-free culture medium (1:1000, 10 μM/L) were added to the single cell suspensions (250 μL) for 40 min incubation at 37°C without daylight. After washing three times with 0.01M PBS, the fluorescence intensity of 200 μL samples was analyzed using a fluorescence microplate reader (Synery H1; Thermo, Waltham, MA, USA) at 488 nm (excitation wavelength) and 525 nm (emission wavelength).

Determination of mitochondrial reactive oxygen species

Similar to the ROS analysis, mito-SOX was detected at 24 h, 3 days, and 21 days (n = 5/group per time point) during epileptogenesis. After single-cell suspensions were prepared, 250 μL suspensions were added to 1 mL mito-SOX (M36008, 5 μM, Thermo Fisher, Waltham, MA, USA) and incubated for 10 min without light at 37°C. After three washing with 0.01M PBS, the fluorescence intensity was measured using a fluorescence microplate reader and a flow cytometer (BD FACSCantoTM; BD Biosciences, Piscataway, NJ, USA) at 510 nm (excitation wavelength) and 580 nm (emission wavelength).

Iron content detection

As previously described (Zhang M. et al., 2020), the cortex and hippocampus of each rat were isolated at 24 h, 3 days, and 21 days (n = 5/group per time point) during epileptogenesis. Subsequently, the iron content in the tissues was measured using an iron content detection kit (DIFE008, Bioassay Systems, NC, USA).

Fluoro-jade B staining

FJB staining was used to assess neuronal damage (Anderson et al., 2005). As previously described (Zhang M. et al., 2020), rats from each group were cardiac-perfused, and tissue slices were prepared at 24 h, 3 days, and 21 days (n = 5/group per time point) during epileptogenesis. The slices were stained using an FJB staining kit (AG310, Millipore, NC, USA). Positive signals of FJB were obtained through fluorescence microscopy (Olympus, Tokyo, Japan) and were manually counted.

Western blot analysis

As previously described (Zhang M. et al., 2020), the cortex and hippocampus of each rat were isolated on days 3

and 21 during epileptogenesis. Proteins were extracted using a reagent kit (P0012, Beyotime, China). Rabbit monoclonal antibodies against ferroportin 1 (FPN1, 1:2000, ab58695, Abcam, Cambridge, UK), iron regulatory protein 1 (IRP1, 1:1000, ab236773, Abcam, UK), microtubule-associated protein light chain 3beta (LC3B, 1:2000; ab48394, Abcam, UK), caspase-3 (1:1000, 9662, Cell Signaling Technology, Boston, MA, USA), activated caspase-3 (1:1000, ab2302, Abcam, UK), and glyceraldehyde 3-phosphate dehydrogenase (GAPDH, 1:3000, AB-P-R001, Kangcheng, Nanjing, China) were used for western blot analysis. Strip images were acquired using an image analyzer (ImageQuant LAS 500, GE Healthcare, Uppsala, Sweden). Grayscale analysis of target strips was performed using ImageJ V.1.37 software (National Institutes of Health, Bethesda, MD, USA).

Immunohistochemistry

As previously described (Zhang M. et al., 2020), tissue slices were obtained at 24 h, 3 days, and 21 days, and treated with IRP1/DMT1/4',6-diamidino-2-phenylindole

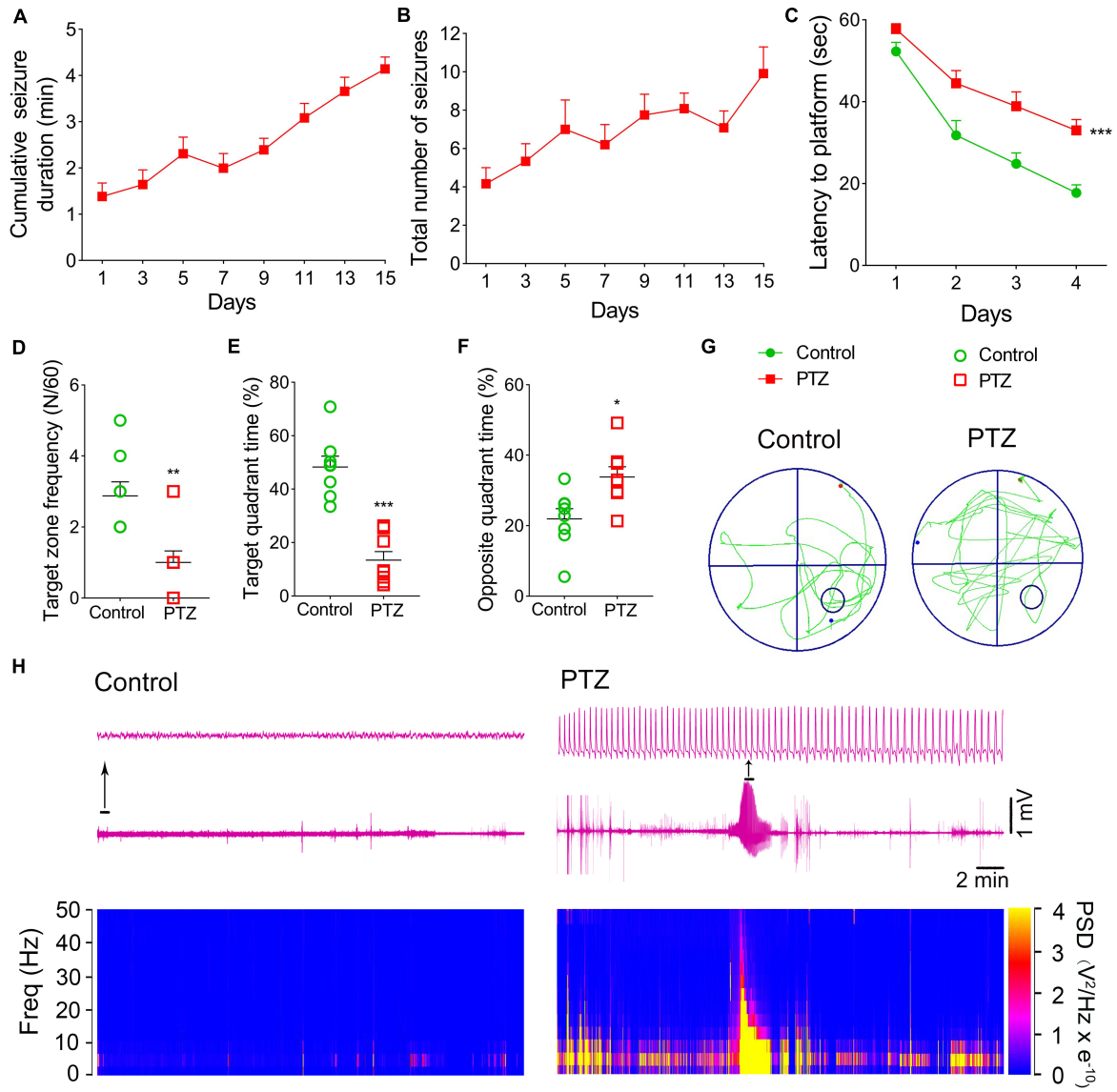

FIGURE 1
Pentylenetetrazole (PTZ)-induced epileptogenesis and cognitive deficits. **(A)** Cumulative seizure duration. **(B)** Total number of seizures. **(C)** Latency to the platform (two-way RM-ANOVA). **(D)** Frequency of platform crossings. **(E)** Target quadrant time (%). **(F)** Opposite quadrant time (%). **(G)** Representative platform exploration trajectories. **(H)** Representative EEGs and power spectrum density. Data are presented as mean ± SEM. $^{*}P < 0.05$, $^{**}P < 0.01$, and $^{***}P < 0.001$, compared with controls (unpaired *T*-tests).

(DAPI) and micro-tubule-associated protein light chain 3B (LC3B)/translocase of outer mitochondrial membrane 20 (TOMM20)/DAPI immunohistochemical staining. Rabbit monoclonal antibodies against IRP1 (1:200, ab236773, Abcam, UK) and LC3B (1:200, ab48394, Abcam, UK) and mouse monoclonal antibodies against TOMM20 (1:200, ab56783, Abcam, UK) and DMT1 (1:200, ab55735, Abcam, UK) were used for immunohistochemistry. Images were obtained using a fluorescence microscope (Olympus, Japan) and analyzed using ImageJ V.1.37 software (National Institutes of Health, USA).

Statistical analyses

Before the experiments, the number of rats in each group was estimated using a balanced one-way analysis of variance (ANOVA). All values are expressed as mean ± standard error of the mean (SEM), and statistical analysis of the data was performed using SPSS (Version 25.0; SPSS Inc., Chicago, IL, USA). The number and cumulative duration of seizures, and latency to reach the platform in the Morris water maze were analyzed using two-way RM-ANOVA. The difference in single variables between the two groups was analyzed by unpaired *t*-test, and the difference in single variables in multiple groups was analyzed using one-way ANOVA. In all analyses, statistical significance was set at $P < 0.05$.

Results

Pentylenetetrazole-induced epileptogenesis and cognitive deficits

Pentylenetetrazole (PTZ)-induced epileptogenesis and cognitive deficits were assessed in SD rats. In the PTZ group ($n = 12$), seizures (cumulative seizure duration, **Figure 1A**; total number of seizures, **Figure 1B**) were observed during epileptogenesis. The representative EEGs and analysis of the frequency spectrum and power spectrum density are shown in **Figure 1H**.

The Morris water maze experiment was performed on Day 16 to assess the learning and memory abilities of rats in PTZ-induced epileptogenesis. Compared to the control group ($n = 8$), the PTZ group ($n = 8$) had a longer latency to reach the platform ($P < 0.001$, **Figure 1C**), crossed the platform less frequently ($P = 0.003$, **Figure 1D**), spent lesser time in the target quadrant ($P < 0.001$, **Figure 1E**), and spent more time in the opposite quadrant ($P = 0.012$, **Figure 1F**). These results indicated that PTZ treatment leads to defects in learning and memory. The representative platform exploration trajectories for each group are shown in **Figure 1G**.

Iron levels significantly increased due to pentylenetetrazole treatment

The iron content and expression of iron-related proteins were detected in each group. The immunohistochemical results showed that the immunofluorescence intensity of hippocampus and cortex IRP1 was significantly higher in the PTZ-treated group than in the control group [e.g., dentate gyrus (DG), $P = 0.001$, **Figures 2A,C,D,F,G**, **Supplementary Figures 1A–F**]. The DMTI levels were also observed to increase ($P < 0.001$, **Figures 2B,E,H**). Western blotting results further confirmed that the levels of IRP1 were significantly higher in the PTZ group than in the control group (3 days, cortex, $P = 0.025$; hippocampus, $P = 0.011$; 21 days, cortex, $P < 0.001$; hippocampus, $P = 0.001$; **Figures 2I,J**). However, the expression of FPN1, which is responsible for iron outflow (Minor et al., 2019), was lower in the PTZ group than in the control group (**Figures 2I,K**). We also examined the iron content in the cortex and hippocampus and found that iron levels were significantly higher in the PTZ group than in the control group (24 h, 3 days, and 21 days, $P < 0.001$, **Figures 2L,M**).

Increased 2′,7′-dichlorodihydrofluorescein and mito-SOX levels during pentylenetetrazole-induced epileptogenesis

We also examined the DCF and mito-SOX levels in each group. The results showed that cortex and hippocampus DCF levels were significantly higher in the PTZ group than in the control group (24 h, cortex, $P = 0.004$; hippocampus, $P = 0.001$; 3 days, $P < 0.001$; 21 days, $P < 0.001$; **Figures 3A,B**). Similar increases in mito-SOX levels were also observed (cortex, $P < 0.001$; hippocampus, $P < 0.001$; **Figures 3C,D**). Representative mito-SOX flow cytometry results are shown in **Figure 3E**.

Increased autophagy/mitophagy and neuronal injury during pentylenetetrazole-induced epileptogenesis

LC3B is a marker of autophagosomes, which can initiate autophagy (Vives-Bauza and Przedborski, 2011). LC3B levels are clearly correlated with mitophagy (Nakatogawa et al., 2007; Weidberg et al., 2011; Klionsky et al., 2012). TOMM20 is a receptor on the outer mitochondrial membrane (Wu et al., 2018). Co-labeling of LC3B and TOMM20 indicates mitophagy

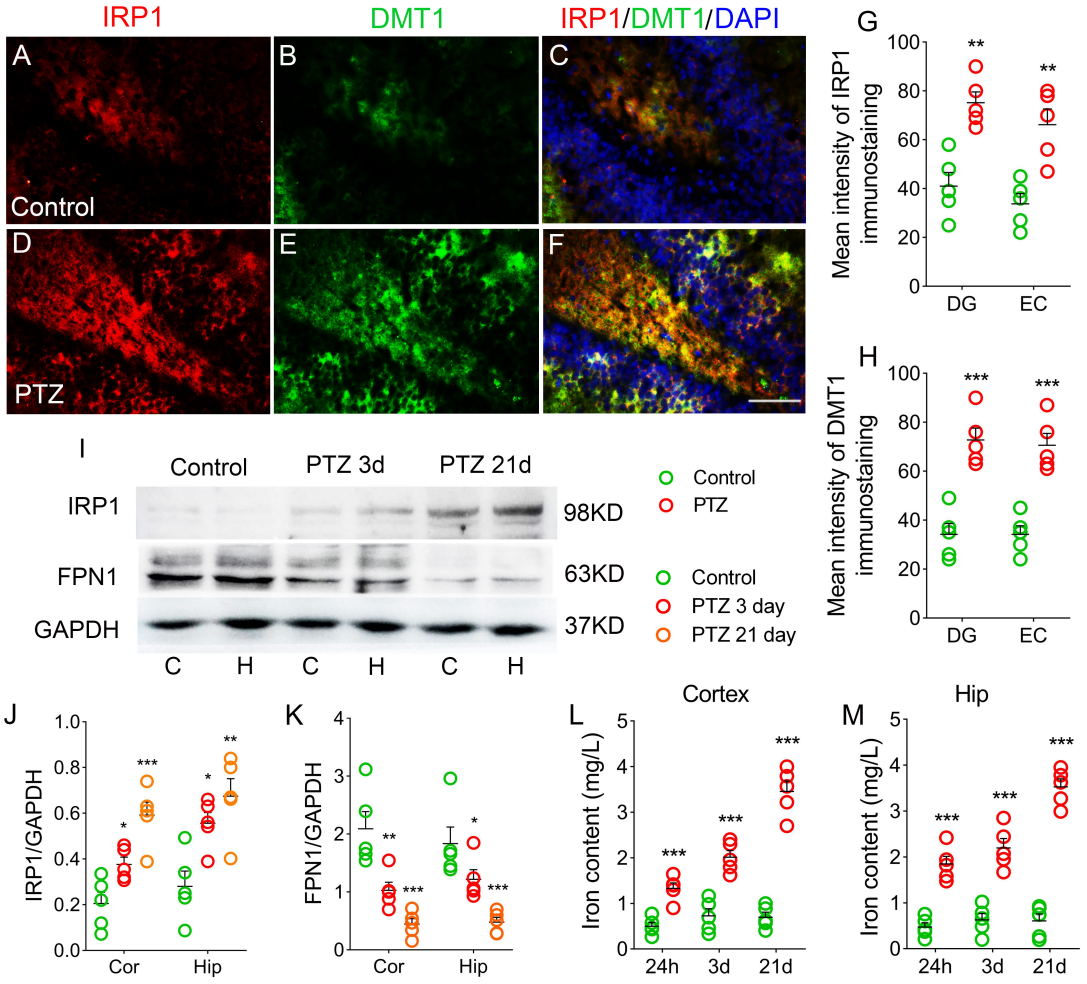

FIGURE 2
Pentylenetetrazole (PTZ) significantly increased iron levels. **(A–F)** Increased fluorescence intensity of IRP1 (red) and DMT1 (green) in the dentate gyrus (DG) region during PTZ-induced epileptogenesis (blue, DAPI). Bar = 80 μm. **(G,H)** Quantified changes in IRP1 and DMT1 (n = 5/group). **(I)** Expression of IRP1 and FPN1 in the hippocampus and cortex estimated by western blotting (n = 5/group). **(J,K)** Normalized intensity of IRP1 and FPN1 relative to GAPDH (one-way ANOVA). **(L,M)** Levels of iron (n = 5/timepoint). $^{**}P < 0.01$ and $^{***}P < 0.001$, compared with controls (unpaired T-tests).

(Wu et al., 2018). Counterstaining of LC3B and TOMM20 was performed to evaluate the mitophagy.

During epileptogenesis, we found a significant increase in the levels of LC3B and TOMM20 in the hippocampus and cortex ($P < 0.001$), and the majority of LC3B was co-labeled with TOMM20 (**Figures 4A–H**; **Supplementary Figures 1M–R**). Similar increases in LC3B levels were confirmed by western blotting ($P < 0.001$; **Figures 4I,J**).

In addition, in the PTZ group, the levels of activated caspase-3 were significantly higher (**Figures 4K,L**), and caspase-3 levels were decreased (**Figures 4K,M**) in the cortex and hippocampus compared with the control group. Neuronal damage was assessed using FJB staining (Anderson et al., 2005), which confirmed that FJB-positive signals were significantly increased by PTZ treatment ($P < 0.001$, **Figures 4N,O**).

Xenon treatment reduced severity of pentylenetetrazole-induced epileptic development and cognitive deficits

Rats in the xenon group (n = 16) received xenon treatment for 30 min immediately after PTZ injection, whereas the control group (n = 12) received 21% O_2/79% N_2 treatment. A comparison of seizure frequency and duration between PTZ and PTZ + 21% O_2 groups showed no significant difference (cumulative seizure duration, P = 0.841; total number of seizures, P = 0.824, **Supplementary Figures 2A,B**). The results showed that cumulative seizure duration ($P < 0.001$, **Figure 5A**) and total number of seizures ($P < 0.001$, **Figure 5B**) were significantly lower in the xenon group than in the control group.

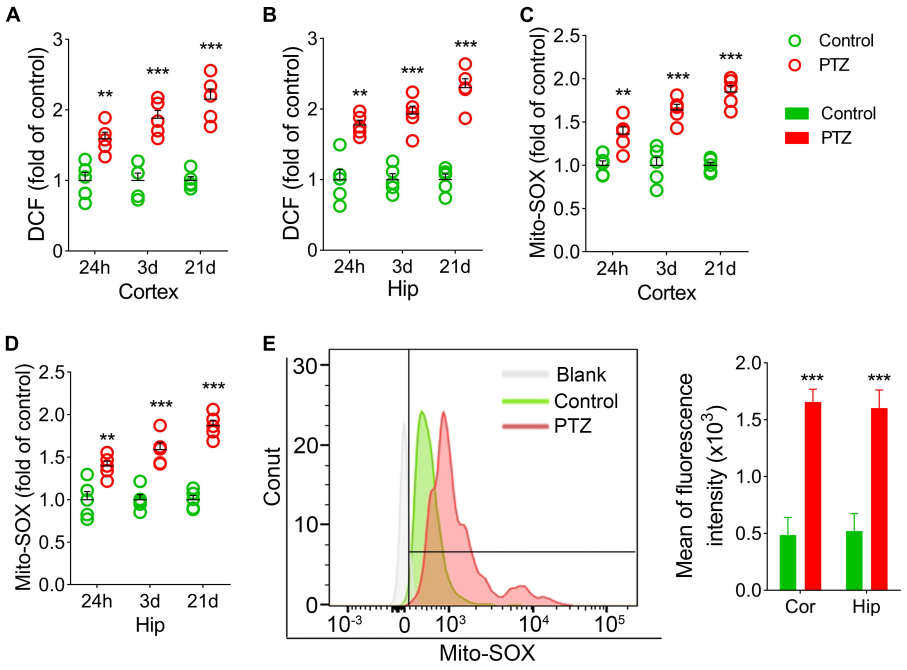

FIGURE 3
Increased 2′,7′-dichlorodihydrofluorescein (DCF) and mito-SOX levels during pentylenetetrazole (PTZ)-induced epileptogenesis. Increased DCF **(A,B)** and mito-SOX **(C,D)** levels in the hippocampus and cortex during epileptogenesis (n = 5/group). **(E)** Flow cytometry-based quantification of mito-SOX levels. $^{**}P < 0.01$ and $^{***}P < 0.001$, compared with controls (unpaired T-tests).

EEG analysis suggested a similar attenuation by xenon treatment (**Supplementary Figures 3A,B**).

The Morris water maze results indicated that xenon treatment attenuated learning and memory impairments induced by PTZ treatment. The xenon group showed shorter latency to reach the platform (P = 0.016, **Figure 5C**), crossed the platform more frequently (P = 0.016, **Figure 5D**), spent more time in the target quadrant ($P < 0.001$, **Figure 5E**), and spent less time in the opposite quadrant ($P < 0.001$, **Figure 5F**). While the difference between the naïve and xenon-treated rats indicated that xenon partly, but not completely rescued the cognition impairment induced by PTZ kindling (**Supplementary Figure 4**). The representative EEGs, analysis of the frequency spectrum and power spectrum density, and platform exploration trajectory of each group are shown in **Figures 5G,H**.

Xenon treatment reduced the iron accumulation caused by pentylenetetrazole treatment

The results of immunohistochemistry showed that the immunofluorescence intensity of IRP1 was significantly lower in the hippocampus and cortex (e.g., DG, P = 0.005; **Figures 6A,C,D,F,G**; EC, P = 0.003; **Figure 6G**) due to the xenon mixture inhalation. Similarly, decreased levels of DMT1 were observed (DG, **Figures 6B,E,H**, **Supplementary Figures 1G–L**; EC, **Figure 6H**) in xenon-treated rats. Western blotting results verified the decrease in IRP1 levels (3 days, cortex, P = 0.038; hippocampus, P = 0.046; 21 days, cortex, P = 0.042; hippocampus, P = 0.038; **Figures 6I,J**), while FPN1 levels were higher in the xenon group than in the control group (**Figures 6I,K**). The iron content results indicate that xenon treatment reversed PTZ-induced iron accumulation (24 h, cortex, P = 0.005; hippocampus, P = 0.012; 3 days, cortex, $P < 0.001$; hippocampus, P = 0.001; 21 days, $P < 0.001$; **Figures 6L,M**).

Xenon treatment reduced the elevated levels of 2′,7′-dichlorodihydrofluorescein and mito-SOX caused by pentylenetetrazole administration

The DCF results showed a significant reduction in the cortex (**Figure 7A**) and hippocampus (**Figure 7B**) in the xenon group compared with the control group. A similar decrease in mito-SOX levels was observed after xenon treatment (**Figures 7C,D**). Representative mito-SOX flow cytometry results are shown in **Figure 7E**.

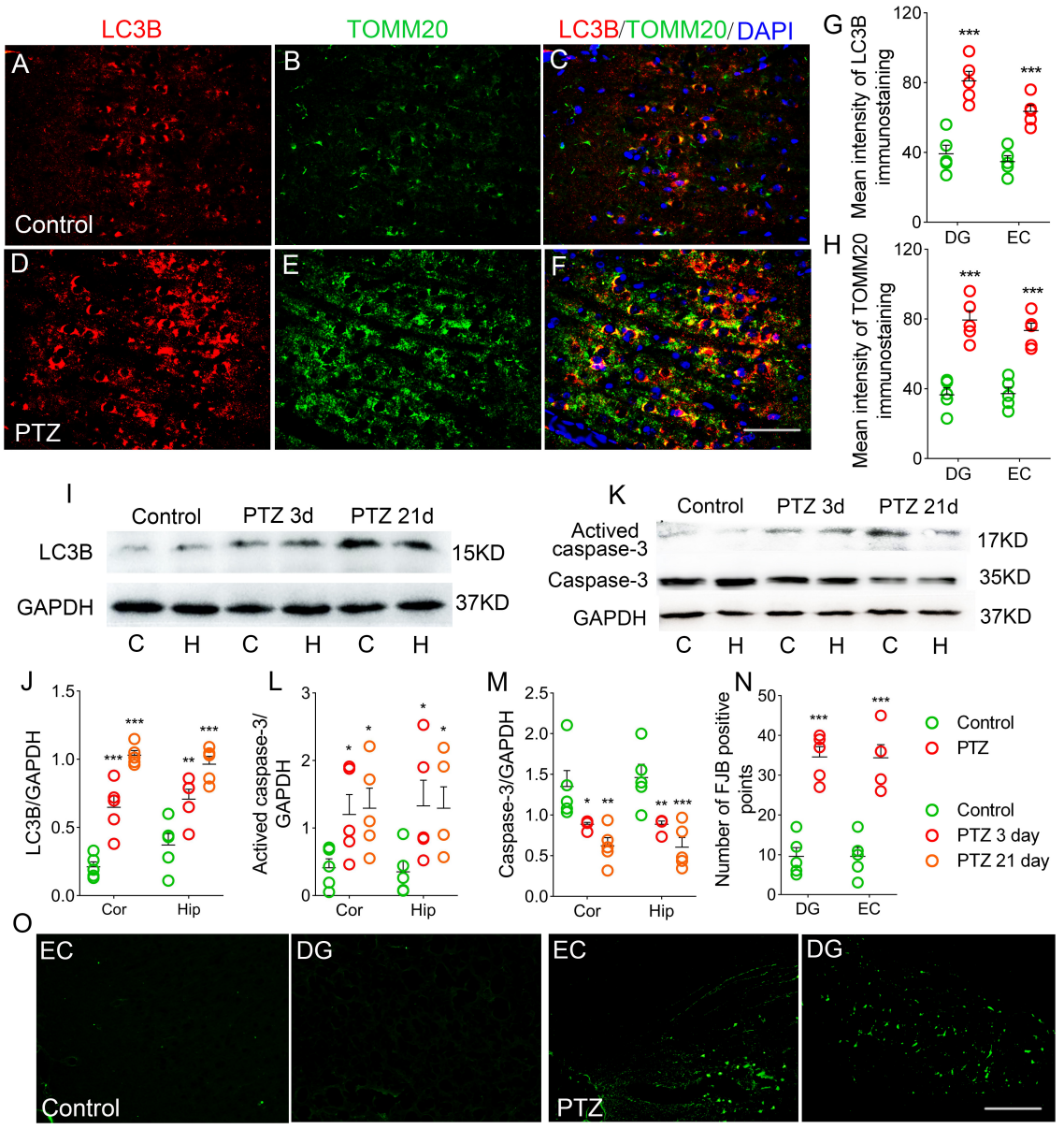

FIGURE 4
Increased autophagy/mitophagy and neuronal injury in pentylenetetrazole (PTZ)-induced epileptogenesis. **(A–F)** Increased fluorescence intensity of LC3B (red) and TOMM20 (green) in the EC region during epileptogenesis (n = 5/group; blue, DAPI). Bar = 60 μm. **(G,H)** Quantified changes in LC3B and TOMM20 (n = 5/group). **(I)** Expression of LC3B in the hippocampus and cortex estimated by western blotting (n = 5/group). **(J)** Normalized intensity of LC3B relative to GAPDH. **(K–M)** Levels of caspase-3 and activated caspase-3 in the hippocampus and cortex estimated by western blotting (n = 5/group). **(N,O)** Positive FJB signals counted in each group. *P < 0.05 and ***P < 0.001, all compared with controls (panels **J–M**, one-way ANOVA; the others, unpaired T-tests].

Xenon treatment prevented pentylenetetrazole-induced autophagy/mitophagy and neuronal injury

Immunohistochemical results showed that xenon treatment led to reduced levels of LC3B (DG, P < 0.001; EC, P < 0.001; Figures 8A,C,D,F,G; Supplementary Figures 1S–X) and TOMM20 (DG, P = 0.002; EC, P = 0.004; Figures 8B,E,H; Supplementary Figures 1S–X). Western blotting results further confirmed the significant a decrease in LC3B expression (3 days, cortex, P < 0.001; hippocampus, P = 0.001; 21 days, cortex, P < 0.005; hippocampus, P = 0.001; Figures 8I,J) after xenon treatment. Moreover, in the xenon group, the levels of activated caspase-3 were significantly lower and caspase-3

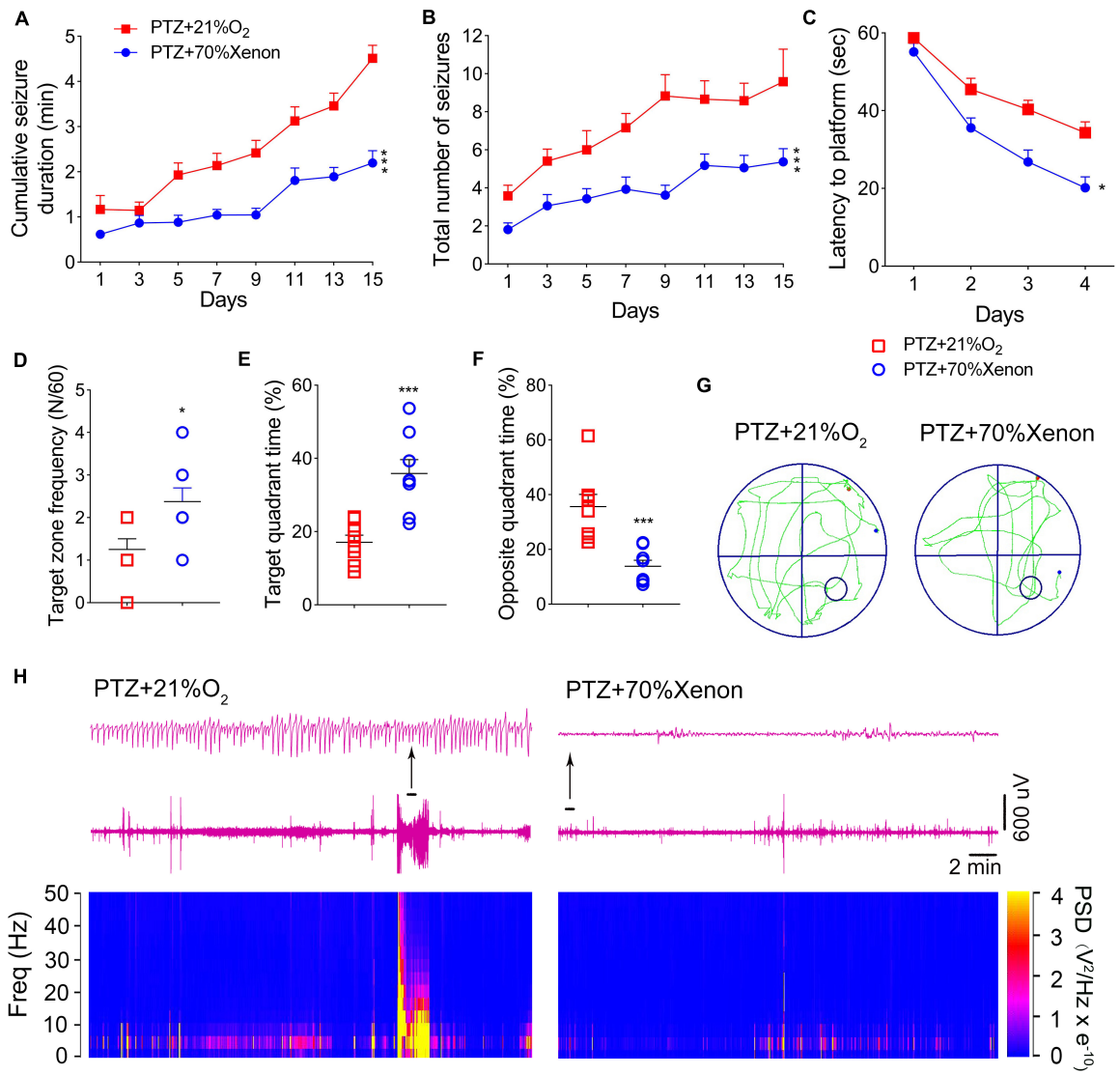

FIGURE 5
Xenon treatment reduced severity of pentylenetetrazole (PTZ)-induced epileptogenesis and cognitive deficits. **(A)** Cumulative seizure duration. **(B)** Total number of seizures. **(C)** Latency to the platform. **(D)** Frequency of platform crossings. **(E)** Target quadrant time (%). **(F)** Opposite quadrant time (%). **(G)** Representative tracking. **(H)** Representative electroencephalography (EEGs) and power spectrum density. Data are presented as mean ± SEM. $*P < 0.05$ and $***P < 0.001$, compared with controls (panels **A–C**, two-way RM-ANOVA; panels **D–F**, unpaired *T*-tests).

levels were higher than those in the control group at Days 3 and 21 (**Figures 8L–N**). Meanwhile, FJB-positive signals were significantly decreased (DG, $P = 0.033$; EC, $P < 0.001$; **Figures 8K,O**) in the xenon group compared with those in the control group.

Discussion

Our results demonstrate a strong link between oxidative stress, iron accumulation, and neuronal damage during PTZ-induced epileptogenesis. However, immediate xenon treatment following each PTZ injection significantly reduced PTZ-induced oxidative and iron stress, accompanied by neuronal damage, seizures, and cognitive dysfunction.

Epilepsy is a common nervous system disease. However, clinical therapy for epilepsy has limitations, and curative effects and adverse reactions tend to be unsatisfactory (Berg et al., 1996; Schmidt and Loscher, 2005). Moreover, partial cases of epilepsy may develop into refractory epilepsy (Perucca and Gilliam, 2012; Engel, 2017). Therefore, an effective and safe therapeutic strategy for preventing epileptic development is important.

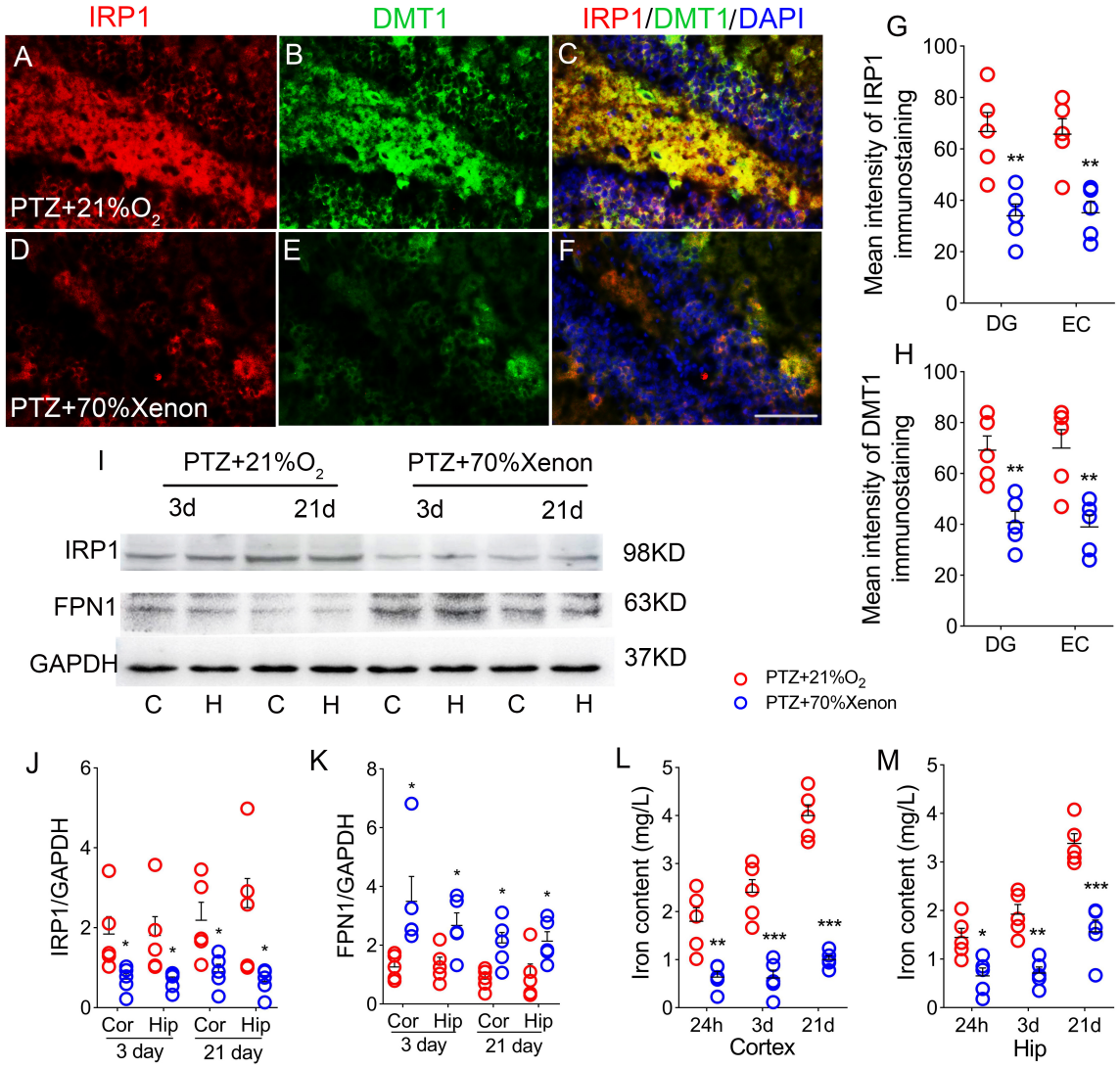

FIGURE 6
Xenon treatment reduced the iron accumulation caused by pentylenetetrazole (PTZ). **(A–F)** Increased levels of IRP1 (red) and DMT1 (green) in the dentate gyrus (DG) region caused by PTZ were attenuated by xenon treatment (blue, DAPI). Bar = 80 μm. **(G,H)** Quantified changes in IRP1 and DMT1 (n = 5/group). **(I)** Expression of IRP1 and FPN1 in the hippocampus and the cortex estimated by western blotting (n = 5/group). **(J,K)** Normalized intensity of IRP1 and FPN1 relative to GAPDH (one-way ANOVA). **(L,M)** Levels of iron (n = 5/timepoint). *P < 0.05, **P < 0.01, and ***P < 0.001, compared with controls (unpaired T-tests).

Pentylenetetrazole (PTZ) is a chloride channel antagonist of GABA-A receptor, which leads to injuries in the hippocampus and is widely used for kindling epileptic models (Ahmadi et al., 2017). During PTZ-kindling, seizures are induced by overexcitation (Schröder et al., 1993).

Elevated levels of glutamate-induced over-excitation and oxidative stress are vital characteristics of epileptic development (During and Spencer, 1993). During this progression, the overexcitation of NMDA receptors upregulates the expression of DMT1 (Wang et al., 2021), a protein that regulates iron influx, thereby increasing the level of cellular iron (Cesar et al., 2012). In addition, excess ROS further exacerbates iron accumulation by upregulating IRP1, which maintains intracellular iron homeostasis (Theil and Eisenstein, 2000), and further downregulates FPN1 (which is responsible for iron efflux) and upregulates DMT1 (which is responsible for iron influx) (Cesar et al., 2012). The iron content in the brain is regulated by iron-regulated proteins IRP1, DMT1, and FPN1 (Zhang et al., 2009; Song et al., 2010; Jiang et al., 2017). Eventually, iron accumulation-induced iron stress occurs following overexcitation and oxidative stress.

Iron metabolism in the brain is closely related to brain development and function. Past studies have confirmed a close relationship between iron levels and epilepsy

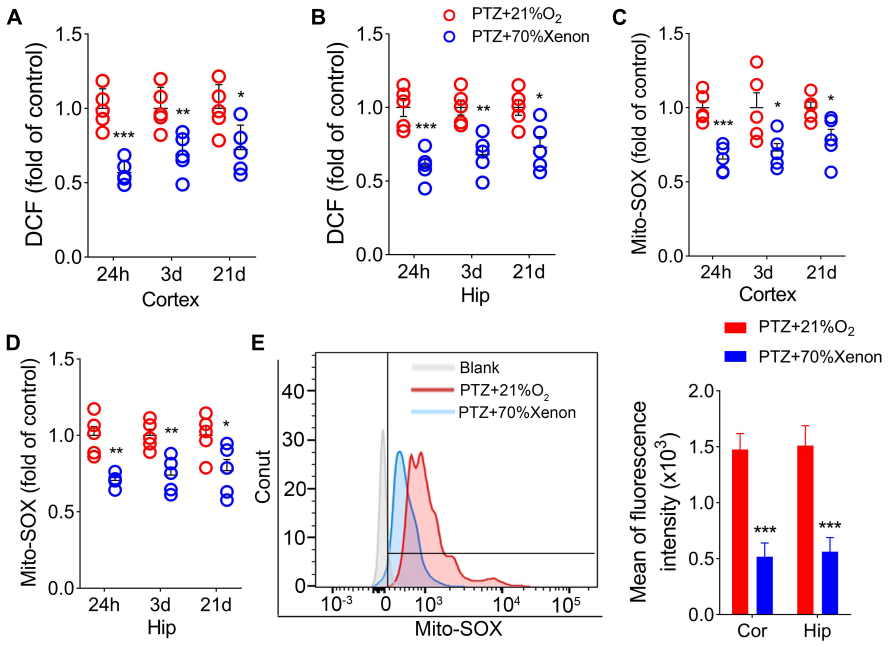

FIGURE 7
Xenon treatment reduced the elevated levels of 2′,7′-dichlorodihydrofluorescein (DCF) and mito-SOX caused by pentylenetetrazole (PTZ) administration. Decreased levels of DCF **(A,B)** and mito-SOX **(C,D)** in the hippocampus and cortex due to xenon treatment (n = 5/group). **(E)** Flow cytometry-based quantification of hippocampal mito-SOX levels. *$P < 0.05$, **$P < 0.01$, and ***$P < 0.001$, compared with controls (unpaired T-tests).

(Cai and Yang, 2021; Zimmer et al., 2021). Intracortical injections of Fe^{3+} can induce seizures (Das et al., 2017). High levels of iron generate several highly reactive hydroxyl radicals through the Fenton reaction (Nishizaki and Iwahashi, 2015), has a disruptive effect on lipids and proteins, and can trigger epilepsy and neuronal apoptosis by activating the calpain and caspase-3 pathways (Baudry and Bi, 2016). Obviously, there is a mutual promotion between iron accumulation and oxidative stress (Molinari et al., 2019).

Mitochondria are vital sites for ROS production, and approximately 90% of ROS are produced by mitochondria (Brand, 2010; Yan et al., 2013). In contrast, mitochondria are sensitive and vulnerable to ROS (Shimura, 2021) and produce antioxidant enzymes to clear excess ROS and maintain redox homeostasis. However, once this balance is disrupted and mitochondria are damaged, large amounts of ROS are produced, and triggering mitophagy (Sasaki et al., 2019). Mitochondrial dysfunction and mitophagy are of the main features of epilepsy (Chang and Yu, 2010). Immoderate mitophagy can change transient Ca^{2+} states and promote excess production of ROS (Han et al., 2011; Zhang Y. et al., 2020), ultimately triggering apoptosis by activating the calpain and caspase-3 pathways and aggravating neuronal injury (Baudry and Bi, 2016). In temporal lobe epilepsy, mitochondrial dysfunction-induced oxidative stress leads to increased neuronal excitation and promotes epileptogenesis (Rowley and Patel, 2013). Previous studies have suggested a possible contribution of oxidative stress, iron stress, and related apoptosis, neuronal injury, and mitophagy during epileptogenesis. Our results confirmed this hypothesis regarding PTZ-induced epileptic development.

According to our previous review (Zhang et al., 2021), xenon exerts neuroprotective effects involving not only the inhibition of *N*-methyl-daspartic acid (NMDA) receptors, attenuation of excitotoxicity, and NMDA receptor-related effects (Wilhelm et al., 2002), such as antioxidative effects, reduced activation of microglia, and Ca^{2+}-dependent mechanisms, as well as interaction with certain ion channels. Previous reports have confirmed the significant neuroprotective effects of xenon through antioxidant action (Yang et al., 2016). Xenon not only restores oxidative stress to basic levels, but also reduces mitochondrial damage mediated by oxidative stress through direct and indirect effects (Lavaur et al., 2017). Our results confirmed that xenon treatment could reduce the elevated levels of oxidative stress and iron, and the related apoptosis, neuronal injury, and mitophagy were attenuated, accompanied by relieved seizures and cognitive impairment in PTZ-kindling rats. These experiment results indicate that the reduction in closely related oxidative stress and iron stress may be vital contributors to protection underlying xenon treatment (**Supplementary Figure 5**).

Caspases are a family of proteins associated with inflammation and apoptosis (D'Amelio et al., 2010). Caspase-3

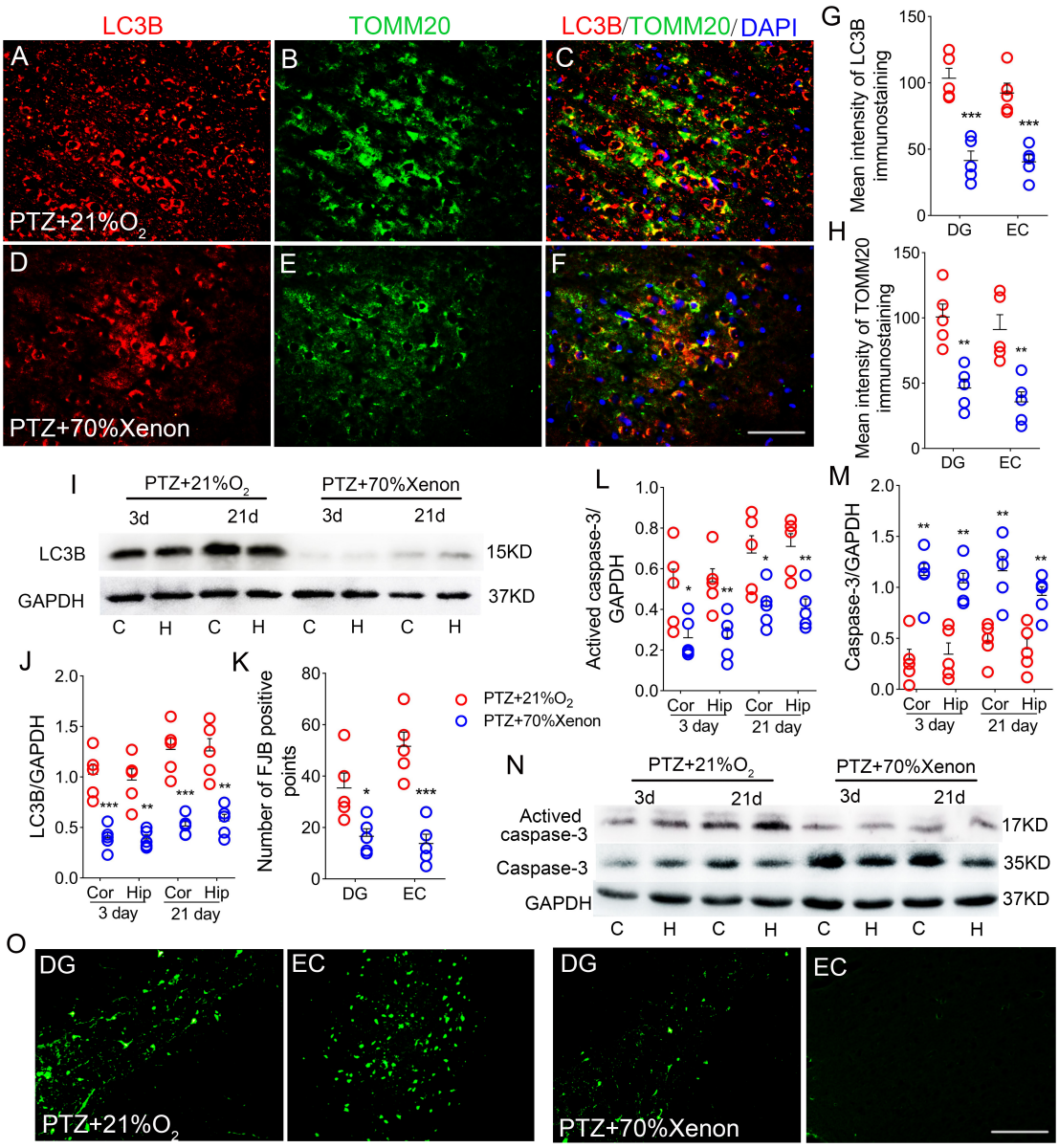

FIGURE 8
Xenon treatment prevented pentylenetetrazole (PTZ)-induced autophagy/mitophagy and neuronal injury. **(A–F)** Decreased fluorescence intensity of LC3B (red) and TOMM20 (green) in the EC region due to xenon treatment (n = 5/group; blue, DAPI). Bar = 60 μm. **(G,H)** Quantified changes in LC3B and TOMM20 (n = 5/group). **(I)** Expression of LC3B in the hippocampus and cortex estimated by western blotting (n = 5/group). **(J)** Normalized levels of LC3B relative to GAPDH. **(L–N)** Levels of caspase-3 and activated caspase-3 in the hippocampus and cortex estimated by western blotting (n = 5/group). **(K,O)** Positive FJB signals counted in each group. *P < 0.05, **P < 0.01, and ***P < 0.001, compared with controls (unpaired T-tests).

is considered a key member of the family that mediates the neuronal apoptosis pathway, and activated caspase-3 is thought to be an important indicator of neuronal apoptosis (D'Amelio et al., 2010; Zhao et al., 2021). According to the previous study, activation of caspase-3 was generally induced by oxidative stress injury (Kim et al., 2020). It has been reported that excessive production of ROS causes neuronal injury and then activates caspase-3 mediated apoptosis signaling pathways (Zhao et al., 2021). Our results showed that xenon treatment alleviated cell apoptosis, which may be related to the reduction in oxidative stress in PTZ-induced epileptogenesis.

The hippocampus and subregions of cortex are key brain regions that are closely related to epileptic development, and learning and memory (Lado et al., 2002; Coutureau and Scala, 2009; Vismer et al., 2015; Hainmueller and Bartos, 2020). It has been verified that EC is responsible

for receiving information and transmitting it to the DG, which is believed to be a vital region related to cognitive function (Hainmueller and Bartos, 2020). In our experiments, we found significant damage to these regions after successive PTZ injections, accompanied by seizures and cognitive defects. However, after xenon treatment, damage to the DG and EC was alleviated, seizures were attenuated, and cognitive functions were improved. The results indicated that reduced neuronal damage may contribute to anti-seizure effects and improvements of cognitive function caused by xenon (**Supplementary Figure 5**).

However, exposing epileptic patients to xenon-rich environments every time they develop an episode is impractical. Therefore, after determining the protective effects of xenon, the roles of xenon in more clinically relevant paradigms, for example, different time delays, or interictal treatment, are expected.

In summary, our study confirmed the significant anti-seizure and neuroprotective effects of xenon on PTZ-induced epileptogenesis. Furthermore, reducing iron stress and oxidative stress may be the potential mechanisms underlying xenon protection. Our study advances the application of xenon in prevention of epileptogenesis.

Data availability statement

The original contributions presented in this study are included in the article/**Supplementary material**, further inquiries can be directed to the corresponding authors.

Ethics statement

This animal study was reviewed and approved by Binzhou Medical University Animal Experimentation Committee (approval no. 2020002).

Author contributions

MZ and YC: study design, data acquisition, and analysis. HS and SL: study conception, design, data interpretation, and manuscript drafting. YZ, YY, HH, XM, and XF: PTZ-induced epileptogenesis model preparation and data acquisition. All authors contributed to the article and approved the submitted version.

Funding

This study was supported by the Natural Science Foundation of Nation (81573412) and Shandong Province (ZR2021MH034) and the Key Research and Development Plan of Shandong Province (2018GSF121004).

Acknowledgments

We would like to thank Editage for English language editing.

Conflict of interest

The authors declare that the research was conducted in the absence of any commercial or financial relationships that could be construed as a potential conflict of interest.

Publisher's note

All claims expressed in this article are solely those of the authors and do not necessarily represent those of their affiliated organizations, or those of the publisher, the editors and the reviewers. Any product that may be evaluated in this article, or claim that may be made by its manufacturer, is not guaranteed or endorsed by the publisher.

Supplementary material

The Supplementary Material for this article can be found online at: https://www.frontiersin.org/articles/10.3389/fncel.2022.1007458/full#supplementary-material

SUPPLEMENTARY FIGURE 1
The immunofluorescence in the dentate gyrus (DG) and EC (20× magnification images). **(A–L)** Fluorescence intensity of IRP1 (red) and DMT1 (green) in the DG region during pentylenetetrazole (PTZ)-induced epileptogenesis (blue, DAPI). Bar = 30 μm. **(M–X)** Fluorescence intensity of LC3B (red) and TOMM20 (green) in the EC region during epileptogenesis (blue, DAPI). Bar = 30 μ m.

SUPPLEMENTARY FIGURE 2
Comparison of seizure frequency and duration between pentylenetetrazole (PTZ) group and PTZ + 21% O_2 group. **(A)** Cumulative seizure duration and **(B)** total number of seizures in PTZ-treated group (two-way RM-ANOVA).

SUPPLEMENTARY FIGURE 3
The analysis of electroencephalography (EEGs) in rats treated with and without xenon. **(A)** Cumulative seizure duration, and **(B)** total number of seizures analyzed by EEGs (two-way RM-ANOVA). $^{**}P < 0.01$, and $^{***}P < 0.001$.

SUPPLEMENTARY FIGURE 4
Xenon treatment partially alleviated the cognition impairment induced by pentylenetetrazole (PTZ) kindling. **(A)** Latency to the platform (two-way RM-ANOVA). **(B)** Frequency of platform crossings. **(C)** Target quadrant time (%). **(D)** Opposite quadrant time (%). $^{*}P < 0.05$, compared with controls (unpaired *T*-tests).

SUPPLEMENTARY FIGURE 5
The roles and mechanisms of xenon in pentylenetetrazole (PTZ)-induced seizures and neuronal damage.

References

Ahmadi, M., Dufour, J. P., Seifritz, E., Mirnajafi-Zadeh, J., and Saab, B. J. (2017). The PTZ kindling mouse model of epilepsy exhibits exploratory drive deficits and aberrant activity amongst VTA dopamine neurons in both familiar and novel space. *Behav. Brain Res.* 330, 1–7. doi: 10.1016/j.bbr.2017.05.025

Allen, R. P., Picchietti, D. L., Auerbach, M., Cho, Y. W., Connor, J. R., Earley, C. J., et al. (2018). Evidence-based and consensus clinical practice guidelines for the iron treatment of restless legs syndrome/Willis-Ekbom disease in adults and children: An IRLSSG task force report. *Sleep Med.* 41, 27–44. doi: 10.1016/j.sleep.2017.11.1126

Anderson, K. J., Miller, K. M., Fugaccia, I., and Scheff, S. W. (2005). Regional distribution of fluoro-jade B staining in the hippocampus following traumatic brain injury. *Exp. Neurol.* 193, 125–130. doi: 10.1016/j.expneurol.2004.11.025

Ayton, S., Lei, P., Adlard, P. A., Volitakis, I., Cherny, R. A., Bush, A. I., et al. (2014). Iron accumulation confers neurotoxicity to a vulnerable population of nigral neurons: Implications for Parkinson's disease. *Mol. Neurodegener.* 9:27. doi: 10.1186/1750-1326-9-27

Baudry, M., and Bi, X. (2016). Calpain-1 and calpain-2: The yin and yang of synaptic plasticity and neurodegeneration. *Trends Neurosci.* 39, 235–245. doi: 10.1016/j.tins.2016.01.007

Berg, A. T., Testa, F. M., Levy, S. R., and Shinnar, S. (1996). The epidemlology of epilepsy. *Epileptic Disord.* 14, 383–398. doi: 10.1684/epd.2015.0751

Brand, M. D. (2010). The sites and topology of mitochondrial superoxide production. *Exp. Gerontol.* 45, 466–472. doi: 10.1016/j.exger.2010.01.003

Cai, Y., and Yang, Z. (2021). Ferroptosis and its role in epilepsy. *Front. Cell. Neurosci.* 15:696889. doi: 10.3389/fncel.2021.696889

Cattano, D., Valleggi, S., Cavazzana, A. O., Patel, C. B., Ma, D., Maze, M., et al. (2011). Xenon exposure in the neonatal rat brain: Effects on genes that regulate apoptosis. *Minerva Anestesiol.* 77, 571–578. doi: 10.1016/j.medin.2010.09.005

Cesar, M., Alexis, H., Andres, E., Alfredo, K., Cecilia, H., and Tulio, N. (2012). Iron mediates N-methyl-D-aspartate receptor-dependent stimulation of calcium-induced pathways and hippocampal synaptic plasticity. *J. Biol. Chem.* 286, 13382–13392. doi: 10.4161/cib.18710

Chang, S., and Yu, B. (2010). Mitochondrial matters of the brain: Mitochondrial dysfunction and oxidative status in epilepsy. *J. Bioenerg. Biomembr.* 42, 457–459. doi: 10.1007/s10863-010-9317-4

Chen, L. L., Huang, Y. J., Cui, J. T., Song, N., and Xie, J. (2019). Iron dysregulation in Parkinson's disease: Focused on the autophagy-lysosome pathway. *ACS Chem. Neurosci.* 10, 863–871. doi: 10.1021/acschemneuro.8b00390

Cheng, Y., Cui, Y., Zhai, Y., Xin, W., Yu, Y., Liang, J., et al. (2021). Neuroprotective effects of exogenous irisin in kainic acid-induced status epilepticus. *Front. Cell. Neurosci.* 15:738533. doi: 10.3389/fncel.2021.738533

Chiu, K. M., Lu, C. W., Lee, M. Y., Wang, M. J., Lin, T. Y., and Wang, S. J. (2016). Neuroprotective and anti-inflammatory effects of lidocaine in kainic acid-injected rats. *Neuroreport* 27, 501–507. doi: 10.1097/WNR.0000000000000570

Coutureau, E., and Scala, G. D. (2009). Entorhinal cortex and cognition. *Prog. Neuropsychopharmacol. Biol. Psychiatry* 33, 753–761. doi: 10.1016/j.pnpbp.2009.03.038

D'Amelio, M., Cavallucci, V., and Cecconi, F. (2010). Neuronal caspase-3 signaling: Not only cell death. *Cell Death Differ.* 17, 1104–1114. doi: 10.1038/cdd.2009.180

Das, J., Singh, R., and Sharma, D. (2017). Antiepileptic effect of fisetin in iron-induced experimental model of traumatic epilepsy in rats in the light of electrophysiological, biochemical, and behavioral observations. *Nutr. Neurosci.* 20, 255–264. doi: 10.1080/1028415X.2016.1183342

Dhir, A. (2012). Pentylenetetrazol (PTZ) kindling model of epilepsy. *Curr. Protoc. Neurosci.* Chapter 9:Unit9.37. doi: 10.1002/0471142301.ns0937s58

dos Santos, P. S., Costa, J. P., Tome Ada, R., Saldanha, G. B., de Souza, G. F., Feng, D., et al. (2011). Oxidative stress in rat striatum after pilocarpine-induced seizures is diminished by alpha-tocopherol. *Eur. J. Pharmacol.* 668, 65–71. doi: 10.1016/j.ejphar.2011.06.035

During, M. J., and Spencer, D. D. (1993). Extracellular hippocampal glutamate and spontaneous seizure in the conscious human brain. *Lancet* 341, 1607–1610. doi: 10.1016/0140-6736(93)90754-5

Engel, J. (2017). The current place of epilepsy surgery. *Curr. Opin. Neurol.* 32, 192–197. doi: 10.1097/WCO.0000000000000528

Fauser, S., and Tumani, H. (2017). Epilepsy. *Handb. Clin. Neurol.* 146, 259–266. doi: 10.1016/B978-0-12-804279-3.00015-0

Hainmueller, T., and Bartos, M. (2020). Dentate gyrus circuits for encoding, retrieval and discrimination of episodic memories. *Nat. Rev. Neurosci.* 21, 153–168. doi: 10.1038/s41583-019-0260-z

Han, Y., Lin, Y., Xie, N., Xue,Y., Tao, H., Rui, C., et al. (2011). Impaired mitochondrial biogenesis in hippocampi of rats with chronic seizures. *Neuroscience* 194, 234–240. doi: 10.1016/j.neuroscience.2011.07.068

Jiang, H., Song, N., Xu, H., Zhang, S., Wang, J., and Xie, J. (2010). Up-regulation of divalent metal transporter 1 in 6-hydroxydopamine intoxication is IRE/IRP dependent. *Cell Res.* 20, 345–356. doi: 10.1038/cr.2010.20

Jiang, H., Wang, J., Rogers, J., and Xie, J. (2017). Brain iron metabolism dysfunction in Parkinson's disease. *Mol. Neurobiol.* 54, 3078–3101. doi: 10.1007/s12035-016-9879-1

Kim, J. E., and Kang, T. C. (2018). Differential roles of mitochondrial translocation of active caspase-3 and HMGB1 in neuronal death induced by status epilepticus. *Front. Cell. Neurosci.* 12:301. doi: 10.3389/fncel.2018.00301

Kim, Y. H., Eom, J. W., and Koh, J. Y. (2020). Mechanism of zinc excitotoxicity: A focus on AMPK. *Front. Neurosci.* 14:577958. doi: 10.3389/fnins.2020.577958

Klionsky, D. J., Abdalla, F. C., Abeliovich, H., Abraham, R. T., Acevedo-Arozena, A., Adeli, K., et al. (2012). Guidelines for the use and interpretation of assays for monitoring autophagy. *Autophagy* 8, 445–544. doi: 10.4161/auto.19496

Kulikov, A., Bilotta, F., Borsellino, B., Sel'kov, D., Kobyakov, G., and Lubnin, A. (2019). Xenon anesthesia for awake craniotomy: Safety and efficacy. *Minerva Anestesiol.* 85, 148–155. doi: 10.23736/S0375-9393.18.12406-0

Lado, F. A., Laureta, E. C., and Moshé, S. L. (2002). Seizure-induced hippocampal damage in the mature and immature brain. *Epileptic. Disord.* 4, 83–97.

Lavaur, J., Le Nogue, D., Lemaire, M., Pype, J., Farjot, G., Hirsch, E. C., et al. (2017). The noble gas xenon provides protection and trophic stimulation to midbrain dopamine neurons. *J. Neurochem.* 142, 14–28. doi: 10.1111/jnc.14041

Lavaur, J., Lemaire, M., Pype, J., Le Nogue, D., Hirsch, E. C., and Michel, P. P. (2016a). Neuroprotective and neurorestorative potential of xenon. *Cell Death Dis.* 7:e2182. doi: 10.1038/cddis.2016.86

Lavaur, J., Lemaire, M., Pype, J., Le Nogue, D., Hirsch, E. C., and Michel, P. P. (2016b). Xenon-mediated neuroprotection in response to sustained, low-level excitotoxic stress. *Cell Death Discov.* 2:16018. doi: 10.1038/cddiscovery.2016.18

Lignani, G., Baldelli, P., and Marra, V. (2020). Homeostatic plasticity in epilepsy. *Front. Cell. Neurosci.* 14:197. doi: 10.3389/fncel.2020.00197

Maremonti, E., Eide, D. M., Rossbach, L. M., Lind, O. C., Salbu, B., and Brede, D. A. (2020). In vivo assessment of reactive oxygen species production and oxidative stress effects induced by chronic exposure to gamma radiation in *Caenorhabditis elegans*. *Free Radic. Biol. Med.* 152, 583–596. doi: 10.1016/j.freeradbiomed.2019.11.037

Maze, M., and Laitio, T. (2020). Neuroprotective properties of xenon. *Mol. Neurobiol.* 57, 118–124. doi: 10.1007/s12035-019-01761-z

Metaxa, V., Lagoudaki, R., Meditskou, S., Thomareis, O., Oikonomou, L., and Sakadamis, A. (2014). Delayed post-ischaemic administration of xenon reduces brain damage in a rat model of global ischaemia. *Brain Inj.* 28, 364–369. doi: 10.3109/02699052.2013.865273

Minor, E. A., Kupec, J. T., Nickerson, A. J., Narayanan, K., and Rajendran, V. M. (2019). Increased divalent metal ion transporter-1 (DMT1) and ferroportin-1 (FPN1) expression with enhanced iron absorption in ulcerative colitis human colon. *Am. J. Physiol. Cell Physiol.* 318, C263–C271. doi: 10.1152/ajpcell.00128.2019

Molinari, C., Morsanuto, V., Ghirlanda, S., Ruga, S., Notte, F., Gaetano, L., et al. (2019). Role of combined lipoic acid and vitamin D3 on astrocytes as a way to prevent brain ageing by induced oxidative stress and iron accumulation. *Oxid. Med. Cell. Longev.* 2019:2843121. doi: 10.1155/2019/2843121

Morris, R. (1984). Developments of a water-maze procedure for studying spatial learning in the rat. *J. Neurosci. Methods* 11, 47–60. doi: 10.1016/0165-0270(84)90007-4

Nakatogawa, H., Ichimura, Y., and Ohsumi, Y. (2007). Atg8, a ubiquitin-like protein required for autophagosome formation, mediates membrane tethering and hemifusion. *Cell* 130, 165–178. doi: 10.1016/j.cell.2007.05.021

Netto, C. A., Hodges, H., Sinden, J. D., Le Peillet, E., Kershaw, T., Sowinski, P., et al. (1993). Effects of fetal hippocampal field grafts on ischaemic-induced deficits in spatial navigation in the water maze. *Neuroscience* 54, 69–92. doi: 10.1016/0306-4522(93)90384-r

Nishizaki, D., and Iwahashi, H. (2015). Baicalin inhibits the fenton reaction by enhancing electron transfer from Fe (2+) to dissolved oxygen. *Am. J. Chin. Med.* 43, 87–101. doi: 10.1142/S0192415X15500068

Pereira, L. O., Arteni, N. S., Petersen, R. C., da Rocha, A. P., Achaval, M., and Netto, C. A. (2007). Effects of daily environmental enrichment on memory deficits and brain injury following neonatal hypoxia-ischemia in the rat. *Neurobiol. Learn. Mem.* 87, 101–108. doi: 10.1016/j.nlm.2006.07.003

Perucca, P., and Gilliam, F. G. (2012). Adverse effects of antiepileptic drugs. *Lancet Neurol.* 11, 792–802. doi: 10.1016/S1474-4422(12)70153-9

Racine, R. J. (1972). Modification of seizure activity by electrical stimulation. II. Motor seizure. *Electroencephalogr. Clin. Neurophysiol.* 32, 281–294. doi: 10.1016/0013-4694(72)90177-0

Rastogi, R. P., Singh, S. P., Hader, D. P., and Sinha, R. P. (2010). Detection of reactive oxygen species (ROS) by the oxidant-sensing probe 2',7'-dichlorodihydrofluorescein diacetate in the cyanobacterium *Anabaena variabilis* PCC 7937. *Biochem. Biophys. Res. Commun.* 397, 603–607. doi: 10.1016/j.bbrc.2010.06.006

Rowley, S., and Patel, M. (2013). Mitochondrial involvement and oxidative stress in temporal lobe epilepsy. *Free Radic. Biol. Med.* 62, 121–131. doi: 10.1016/j.freeradbiomed.2013.02.002

Sasaki, H., Hamatani, T., Kamijo, S., Iwai, M., Kobanawa, M., Ogawa, S., et al. (2019). Impact of oxidative stress on age-associated decline in oocyte developmental competence. *Front. Endocrinol.* 10:811. doi: 10.3389/fendo.2019.00811

Schmidt, D., and Loscher, W. (2005). Drug resistance in epilepsy: Putative neurobiologic and clinical mechanisms. *Epilepsia* 46, 858–877. doi: 10.1111/j.1528-1167.2005.54904.x

Schröder, H., Becker, A., and Lössner, B. (1993). Glutamate binding to brain membranes is increased in pentylenetetrazole-kindled rats. *J. Neurochem.* 60, 1007–1011. doi: 10.1111/j.1471-4159.1993.tb03248.x

Shimura, T. (2021). ATM-mediated mitochondrial radiation responses of human fibroblasts. *Genes* 12:1015. doi: 10.3390/genes12071015

Song, N., Wang, J., Jiang, H., and Xie, J. (2010). Ferroportin 1 but not hephaestin contributes to iron accumulation in a cell model of Parkinson's disease. *Free Radic. Biol. Med.* 48, 332–341. doi: 10.1016/j.freeradbiomed.2009.11.004

Theil, E. C., and Eisenstein, R. S. (2000). Combinatorial mRNA regulation: iron regulatory proteins and iso-iron-responsive elements (Iso-IREs). *J. Biol. Chem.* 275, 40659–40662. doi: 10.1074/jbc.R000019200

Uchida, T., Suzuki, S., Hirano, Y., Ito, D., Nagayama, M., and Gohara, K. (2012). Xenon-induced inhibition of synchronized bursts in a rat cortical neuronal network. *Neuroscience* 214, 149–158. doi: 10.1016/j.neuroscience.2012.03.063

Vismer, M. S., Forcelli, P. A., Skopin, M. D., Gale, K., and Koubeissi, M. Z. (2015). The piriform, perirhinal, and entorhinal cortex in seizure generation. *Front. Neural Circuits* 9:27. doi: 10.3389/fncir.2015.00027

Vives-Bauza, C., and Przedborski, S. (2011). Mitophagy: The latest problem for Parkinson's disease. *Trends Mol. Med.* 17, 158–165. doi: 10.1016/j.molmed.2010.11.002

Wang, Y., Tan, B., Wang, Y., and Chen, Z. (2021). Cholinergic signaling, neural excitability, and epilepsy. *Molecules* 26:2258. doi: 10.3390/molecules26082258

Weidberg, H., Shpilka, T., Shvets, E., Abada, A., Shimron, F., and Elazar, Z. (2011). LC3 and GATE-16N termini mediate membrane fusion processes required for autophagosome biogenesis. *Dev. Cell* 20, 444–454. doi: 10.1016/j.devcel.2011.02.0

Wilhelm, S., Ma, D., Maze, M., and Franks, N. P. (2002). Effects of xenon on in vitro and in vivo models of neuronal injury. *Anesthesiology* 96, 1485–1491. doi: 10.1097/00000542-200206000-00031

Wu, M., Liu, X., Chi, X., Zhang, L., Xiong, W., and Chiang, S. M. V. (2018). Mitophagy in refractory temporal lobe epilepsy patients with hippocampal sclerosis. *Cell. Mol. Neurobiol.* 38, 479–486. doi: 10.1007/s10571-017-0492-2

Xu, H. M., Jiang, H., Wang, J., Luo, B., and Xie, J. X. (2008). Over-expressed human divalent metal transporter 1 is involved in iron accumulation in MES23.5 cells. *Neurochem. Int.* 52, 1044–1051. doi: 10.1016/j.neuint.2007.10.019

Yan, M. H., Wang, X., and Zhu, X. (2013). Mitochondrial defects and oxidative stress in Alzheimer disease and Parkinson disease. *Free Radic. Biol. Med.* 62, 90–101. doi: 10.1016/j.freeradbiomed.2012.11.014

Yang, T., Sun, Y., and Zhang, F. (2016). Anti-oxidative aspect of inhaled anesthetic gases against acute brain injury. *Med. Gas Res.* 6, 223–226. doi: 10.4103/2045-9912.196905

Yang, T., Zhuang, L., Rei Fidalgo, A. M., Petrides, E., Terrando, N., Wu, X., et al. (2012). Xenon and sevoflurane provide analgesia during labor and fetal brain protection in a perinatal rat model of hypoxia-ischemia. *PLoS One* 7:e37020. doi: 10.1371/journal.pone.0037020

Yang, Y. W., Cheng, W. P., Lu, J. K., Dong, X. H., Wang, C. B., Zhang, J., et al. (2014). Timing of xenon-induced delayed postconditioning to protect against spinal cord ischaemia-reperfusion injury in rats. *Br. J. Anaesth.* 113, 168–176. doi: 10.1093/bja/aet352

Zhang, M., Cui, Y., Cheng, Y., Wang, Q., and Sun, H. (2021). The neuroprotective effect and possible therapeutic application of xenon in neurological diseases. *J. Neurosci. Res.* 99, 3274–3383. doi: 10.1002/jnr.24958

Zhang, M., Cui, Y., Zhu, W., Yu, J., Cheng, Y., Wu, X., et al. (2020). Attenuation of the mutual elevation of iron accumulation and oxidative stress may contribute to the neuroprotective and anti-seizure effects of xenon in neonatal hypoxia-induced seizures. *Free Radic. Biol. Med.* 161, 212–223.

Zhang, S., Wang, J., Song, N., Xie, J., and Jiang, H. (2009). Up-regulation of divalent metal transporter 1 is involved in 1-methyl-4-phenylpyridinium (MPP(+))-induced apoptosis in MES23.5 cells. *Neurobiol. Aging* 30, 1466–1476. doi: 10.1016/j.neurobiolaging.2007.11.025

Zhang, Y., Zhang, M., Liu, S., Zhu, W., Yu, J., Cui, Y., et al. (2019). Xenon exerts anti-seizure and neuroprotective effects in kainic acid-induced status epilepticus and neonatal hypoxia-induced seizure. *Exp. Neurol.* 322:113054. doi: 10.1016/j.expneurol.2019.113054

Zhang, Y., Zhang, M., Zhu, W., Yu, J., Wang, Q., Zhang, J., et al. (2020). Succinate accumulation induces mitochondrial reactive oxygen species generation and promotes status epilepticus in the kainic acid rat model. *Redox Biol.* 28:101365. doi: 10.1016/j.redox.2019.101365

Zhao, C., Yang, F., Wei, X., and Zhang, J. (2021). miR-139-5p upregulation alleviated spontaneous recurrent epileptiform discharge-induced oxidative stress and apoptosis in rat hippocampal neurons via regulating the notch pathway. *Cell Biol. Int.* 45, 463–476. doi: 10.1002/cbin.11509

Zhu, W., Zhu, J., Zhao, S., Li, J., Hou, D., Zhang, Y., et al. (2020). Xenon exerts neuroprotective effects on kainic acid-induced acute generalized seizures in rats via increased autophagy. *Front. Cell. Neurosci.* 14:582872. doi: 10.3389/fncel.2020.582872

Zimmer, T. S., David, B., Broekaart, D. W. M., Schidlowski, M., Ruffolo, G., Korotkov, A., et al. (2021). Seizure-mediated iron accumulation and dysregulated iron metabolism after status epilepticus and in temporal lobe epilepsy. *Acta Neuropathol.* 142, 729–759. doi: 10.1007/s00401-021-02348-6

frontiers | Frontiers in Cellular Neuroscience

TYPE Original Research
PUBLISHED 09 May 2023
DOI 10.3389/fncel.2023.1117697

OPEN ACCESS

EDITED BY
Hee Jung Chung,
University of Illinois Urbana-Champaign, United States

REVIEWED BY
Marilena Griguoli,
National Research Council (CNR), Italy
Gülcan Akgül,
Cornell University, United States

*CORRESPONDENCE
Diana Cunha-Reis
✉ dcreis@ciencias.ulisboa.pt

†These authors have contributed equally to this work

RECEIVED 06 December 2022
ACCEPTED 13 April 2023
PUBLISHED 09 May 2023

CITATION
Carvalho-Rosa JD, Rodrigues NC, Silva-Cruz A, Vaz SH and Cunha-Reis D (2023) Epileptiform activity influences theta-burst induced LTP in the adult hippocampus: a role for synaptic lipid raft disruption in early metaplasticity?
Front. Cell. Neurosci. 17:1117697.
doi: 10.3389/fncel.2023.1117697

Epileptiform activity influences theta-burst induced LTP in the adult hippocampus: a role for synaptic lipid raft disruption in early metaplasticity?

José D. Carvalho-Rosa[1,2†], Nádia C. Rodrigues[1,3†], Armando Silva-Cruz [2], Sandra H. Vaz [3,4] and Diana Cunha-Reis *

[1]Departamento de Química e Bioquímica, Faculdade de Ciências, Universidade de Lisboa, Lisbon, Portugal, [2]BioISI–Biosystems and Integrative Sciences Institute, Faculdade de Ciências, Universidade de Lisboa, Lisbon, Portugal, [3]Instituto de Medicina Molecular João Lobo Antunes, Faculdade de Medicina, Universidade de Lisboa, Lisbon, Portugal, [4]Instituto de Farmacologia e Neurociências, Faculdade de Medicina, Universidade de Lisboa, Lisbon, Portugal

Non-epileptic seizures are identified as a common epileptogenic trigger. Early metaplasticity following seizures may contribute to epileptogenesis by abnormally altering synaptic strength and homeostatic plasticity. We now studied how *in vitro* epileptiform activity (EA) triggers early changes in CA1 long-term potentiation (LTP) induced by theta-burst stimulation (TBS) in rat hippocampal slices and the involvement of lipid rafts in these early metaplasticity events. Two forms of EA were induced: (1) interictal-like EA evoked by Mg^{2+} withdrawal and K^+ elevation to 6 mM in the superfusion medium or (2) ictal-like EA induced by bicuculline (10 μM). Both EA patterns induced and LTP-like effect on CA1 synaptic transmission prior to LTP induction. LTP induced 30 min post EA was impaired, an effect more pronounced after ictal-like EA. LTP recovered to control levels 60 min post interictal-like EA but was still impaired 60 min after ictal-like EA. The synaptic molecular events underlying this altered LTP were investigated 30 min post EA in synaptosomes isolated from these slices. EA enhanced AMPA GluA1 Ser831 phosphorylation but decreased Ser845 phosphorylation and the GluA1/GluA2 ratio. Flotillin-1 and caveolin-1 were markedly decreased concomitantly with a marked increase in gephyrin levels and a less prominent increase in PSD-95. Altogether, EA differentially influences hippocampal CA1 LTP thorough regulation of GluA1/GluA2 levels and AMPA GluA1 phosphorylation suggesting that altered LTP post-seizures is a relevant target for antiepileptogenic therapies. In addition, this metaplasticity is also associated with marked alterations in classic and synaptic lipid raft markers, suggesting these may also constitute promising targets in epileptogenesis prevention.

KEYWORDS

seizures, epileptiform activity, bicuculline, low Mg^{2+}, long term potentiation (LTP), mesial temporal lobe epilepsy (MTLE), lipid rafts

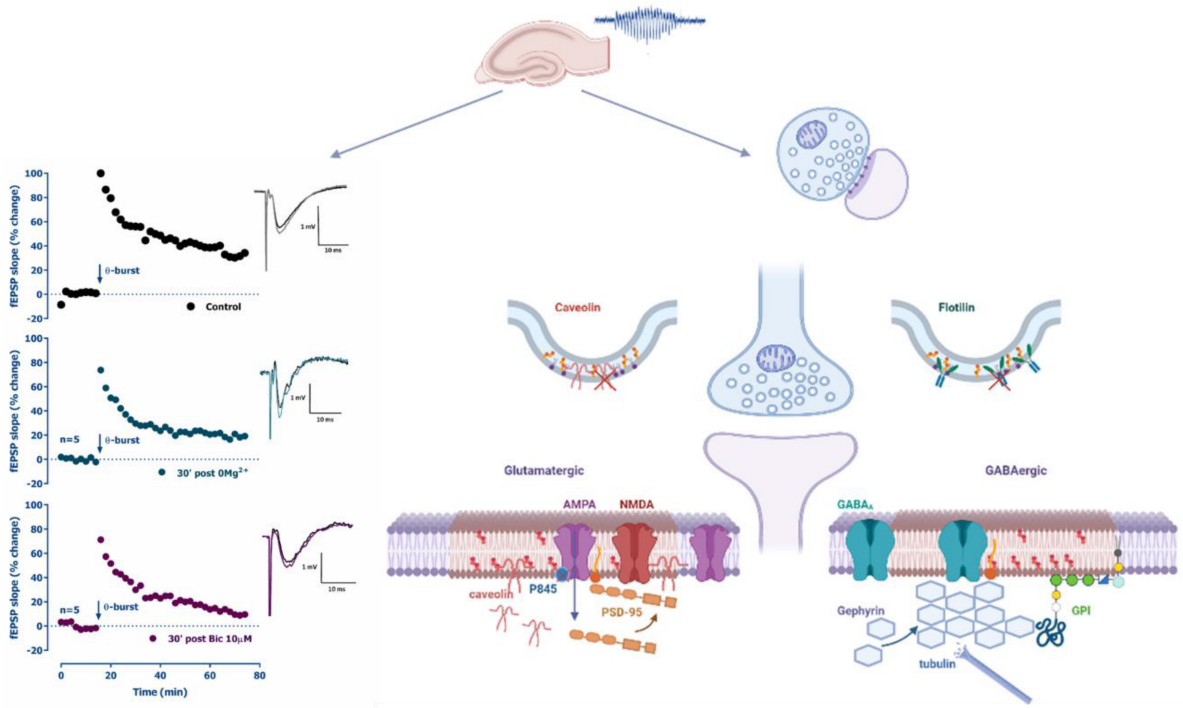

GRAPHICAL ABSTRACT
Altered long term potentiation (LTP) following *in vitro* epileptiform activity and major synaptic molecular alterations triggered.

Introduction

Epilepsy, a multifaceted disease characterized by the development of recurrent, unprovoked seizures, is a neurological disorder that affects over 65 million people worldwide. Its high-incidence and high-prevalence (6.4 cases per 1,000 persons) is nevertheless minored by its high mortality owing to accidents, *status epilepticus* or sudden unexpected death in epilepsy, often occurring during seizures (Devinsky et al., 2018). Being the most frequent, chronic, severe neurological disease it is a huge burden for public health systems (Moshé et al., 2015; Devinsky et al., 2018; Vezzani et al., 2019; Cunha-Reis et al., 2021) and since over one third of epilepsy cases are refractory to treatment with multiple antiseizure drugs (ASDs), it is imperative to identify new therapeutic targets.

Epileptogenesis, the process by which healthy brain networks develop enhanced susceptibility to generate spontaneous recurrent seizures leading to the development of epilepsy (Pitkänen et al., 2015; Vezzani et al., 2019), is currently perceived as a continuous and progressive process extending far beyond the latent period. Yet, the early pathophysiological mechanisms involved in epileptogenesis are still for the most part unknown and tackling epileptogenesis is an unmet clinical need (Pitkänen et al., 2015; Cunha-Reis et al., 2021). One key element is that different triggers likely lead to different seizure-onset, which will ultimately determine its first line of treatment (Sloviter, 2017). As such, establishing therapeutic targets in this early phase of epileptogenesis requires a better knowledge of these mechanisms.

Mesial temporal lobe epilepsy (MTLE) involves seizures typically arising in the hippocampus or other mesial temporal lobe structures. Only about 11–26% of patients with MTLE with hippocampal sclerosis achieve complete seizure control under pharmacological treatment with existing ASDs. As such, patients often require neurosurgical resection of the epileptic focus as a last resource to ameliorate seizure recurrence and to prevent fast worsening of the disease (Liu et al., 2012; Kuang et al., 2014; Thom, 2014). The etiology of MTLE epileptogenesis in still unknown, yet putative precipitating events such as trauma, complex febrile seizures, status epilepticus, inflammatory insults, or ischemia have been implicated. Such events may trigger epileptogenesis by generating aberrant synaptic plasticity/neuronal excitability, excitotoxicity, secondary non-convulsive *status epilepticus*, neuroinflammation and generation of reactive oxygen species that develop during a silent period, when spontaneous seizures do not occur (Thom, 2014; Gambardella et al., 2016; Sloviter, 2017), but their exact chronology it is not often easy to establish partly due to the multitude of putative epileptogenic events.

Within the first days of disease progression, enhanced neurogenesis and axonal sprouting accompany changes in neuronal excitability and synaptic plasticity driving the formation of novel synaptic connections and aberrant neural networks (Beck and Yaari, 2008). Synaptic plasticity, the ability of synapses to undergo long-lasting, activity-dependent bidirectional changes in

Abbreviations: $0Mg^{2+}$, modified aCSF containing $0Mg^{2+}$ and 6 mM elevated K^+; aCSF, artificial cerebrospinal fluid; AMPA, α-amino-3-hydroxy-5-methyl-4-isoxazolepropionic acid; ASDs, antiseizure drugs; *Bic*, bicuculline; EA, epileptiform activity; GPI, Glycosylphosphatidylinositol; MTLE, mesial temporal lobe epilepsy; NMDA, N-methyl-d-aspartate; TBS, theta-burst stimulation.

the strength of synaptic communication, can be mediated by altering the gain of stimulus-release coupling at the presynaptic component or by changes in the type, number, or properties of the neurotransmitter receptors and their coupling to the intracellular signaling machinery at the postsynaptic level (Bliss and Collingridge, 2019; Cunha-Reis and Caulino-Rocha, 2020). It has been hypothesized that such changes may occur maladaptively immediately following non-epileptic seizures, thus triggering epileptogenesis (Avanzini et al., 2014), but this has not so far been thoroughly investigated.

Lipid rafts are membrane microdomains involved in synaptic receptor clustering, synaptic signaling, synaptic vesicle recycling and neurotransmitter release (Allen et al., 2007) and may have a crucial role in both synaptic and homeostatic plasticity under such pathological conditions (Sebastião et al., 2013). Synaptic lipid raft markers include both classic raft-associated proteins like caveolin-1 and flotillin-1, characteristic of caveolae and planar lipid rafts, respectively, and structural postsynaptic receptor anchoring proteins like PSD-95, present at glutamatergic synapses, and gephyrin, distinctive of GABAergic synapses (Tulodziecka et al., 2016; Papadopoulos et al., 2017; Bai et al., 2021). The latter two are also recognized as important NMDA, AMPA, and $GABA_A$ membrane-anchoring proteins, respectively.

In vitro models of ictogenesis have provided important insights into the therapeutic potential of several candidate anti-seizure drugs (Gloveli et al., 1995; Debanne et al., 2006; Antonio et al., 2016; Dulla et al., 2018). In this paper we used such *in vitro* models of epileptiform activity to evaluate the time-course of changes in LTP occurring within 30 min to 1 h 30 m following seizures. LTP was evoked *in vitro* by theta burst stimulation (TBS), a sequence of electrical stimuli that mimic CA1 pyramidal cell burst firing as occurring during the hippocampal theta rhythm (4–10 Hz), an EEG pattern linked to hippocampal memory storage in rodents and involves the recruitment of GABAergic mechanisms (Vertes, 2005; Larson and Munkácsy, 2015; Artinian and Lacaille, 2018; Rodrigues et al., 2021). We characterized also the synaptic molecular alterations in AMPA receptors potentially underlying impaired LTP. In addition, its association with modified lipid raft dynamics, an important requirement for several molecular mechanisms involved in synaptic plasticity, was also investigated. A preliminary account of some of the results has been published as an abstract (Carvalho-Rosa and Cunha-Reis, 2019).

Materials and methods

All animal procedures and protocols were performed according to ARRIVE guidelines for experimental design, analysis, and their reporting. Animal housing and handing was performed in accordance with the Portuguese law (DL 113/2013) and European Community guidelines (86/609/EEC and 63/2010/CE). The experiments were performed on hippocampal slices (400 μm thick), cut perpendicularly to the long axis of the hippocampus, obtained from young-adult (6–7 weeks old) male outbred Wistar rats (Harlan Iberica, Barcelona, Spain) as previously described (Aidil-Carvalho et al., 2017). Female rats were not used due to hormonal influences on LTP (Warren et al., 1995; Good et al., 1999). Rats were anesthetized with halothane, decapitated, and both hippocampi were extracted in ice-cold artificial cerebrospinal fluid (aCSF), composition in mM: NaCl 124, KCl 3, NaH_2PO_4 1.25, $NaHCO_3$ 26, $MgSO_4$ 1, $CaCl_2$ 2, glucose 10, and oxygenated with a 95% O_2 - 5% CO_2 mixture.

This is known as paired-pulse facilitation (PPF) and is believed to result from the presence of residual calcium generated by the first stimulation in glutamatergic terminals, that results in an enhanced release of neurotransmitter in response to the second stimulation (Zucker, 2003) at CA3–CA1 synapses, where the release probability is low under the current stimulation conditions (Wu and Saggau, 1994; Debanne et al., 1996). PPF in the CA1 area of the hippocampus has also been attributed to paired-pulse depression in the fast inhibitory postsynaptic potential (IPSP) (Nathan and Lambert, 1991) believed to result from GABAB autoreceptor-mediated depression of neurotransmitter release at interneuron–pyramidal cell synapses (Davies et al., 1990; Lambert and Wilson, 1994).

Electrophysiological recordings and induction of epileptiform activity

Hippocampal slices (Aidil-Carvalho et al., 2017) were kept in a resting chamber in the same oxygenated aCSF at room temperature 22–25°C for at least 1 h for recovery, then one slice at a time was transferred to a submerged recording chamber of 1 ml capacity, where it was continuously superfused at a rate of 3 ml/min with the same oxygenated solution kept at 32°C. Stimulation (rectangular pulses of 0.1 ms, 100–260 μA) was delivered through a bipolar concentric wire electrode placed on the Schaffer collateral/commissural fibers in the *stratum radiatum*. Two separate sets of the Schaffer collaterals (S1 and S2) were stimulated alternately every 10 s, each pathway being stimulated every 20 s (0.05 Hz, **Figure 1A**). Extracellular recordings of field excitatory post-synaptic potentials (fEPSP) were obtained from CA1 *stratum radiatum* through micropipettes 4 M NaCl filled (2–4 MΩ resistance) using an Axoclamp-2B amplifier (10 Vm pre-amplifier, Axon Instruments, Molecular Devices, San Diego, CA, USA). fEPSPs were evoked on the two pathways, and the initial intensity of the stimulus, of comparable magnitude in both pathways, elicited a fEPSP of 600–1,000 μV amplitude (near 50% of the maximal response), yet avoiding signal contamination by the population spike. The fEPSPs signals were filtered at –3 bB with the inbuilt filter of the Axopatch 2-B, digitized at 20 kHz using a BNC-2110 (National Instruments, Austin, TX, USA) interface and acquired by a laboratory computer with the WinLTP software (Anderson and Collingridge, 2001, 2007). The averages of six consecutive evoked fEPSPs from each pathway were obtained, measured, graphically plotted, and recorded for further analysis. The fEPSPs were quantified as the slope of the initial phase of the potential.

Spontaneous epileptiform activity (EA) was induced after a stable fEPSP slope baseline was obtained for at least 20 min. Electrical stimulation was stopped during these EA induction protocols to allow for the monitoring of pure spontaneous activity. Interictal-like epileptiform activity was induced by removing Mg^{2+} from the superfusion media for 30 min ($0Mg^{2+}$) while increasing the K^+ concentration to 6 mM. These concentrations

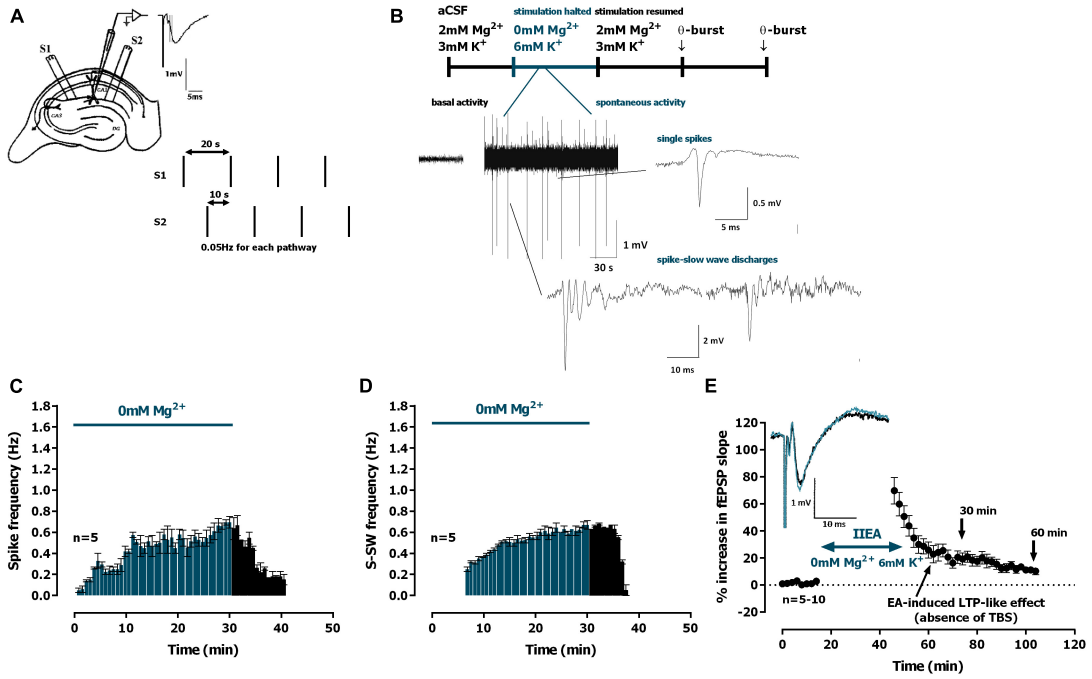

FIGURE 1
Interictal-like epileptiform activity induced by $0Mg^{2+}$ and long-term potentiation (LTP)-like effect. **(A)** Electrophysiological recordings of field excitatory post-synaptic potentials (fEPSPs) evoked by electrical stimulation in the CA1 area of hippocampal slices. The same recording configuration was used when monitoring spontaneous activity, but stimulation was halted during the 30 min perfusion with artificial cerebrospinal fluid (aCSF) lacking Mg^{2+} and containing 6 mM K^+ ($0Mg^{2+}$). **(B)** Time-course of a typical experiment showing the spontaneous activity recorded prior to $0Mg^{2+}$ arrival to the superfusion chamber (left) and during the 30 min $0Mg^{2+}$ perfusion. Traces of the two main types of epileptiform activity recorded, single *population spikes* and *spike-slow wave* activity, are shown at the millisecond scale. **(C,D)** Averaged time-course of the frequency of spontaneous *population spikes* **(C)** and *spike-slow wave* activity [**(D)**, n = 5]. **(E)** Averaged time-course of changes in fEPSP slope caused by $0Mg^{2+}$ perfusion. *Inset*: traces of fEPSPs obtained in the same experiment before (black) and 25–30 min after $0Mg^{2+}$ perfusion (blue). Electrophysiological recordings of fEPSPs evoked by electrical stimulation were performed in the CA1 area of hippocampal slices. Traces are the average of eight consecutive responses and are composed of the stimulus artifact, the presynaptic volley and the fEPSP. The mean ± S.E.M is depicted **(C,E)**.

were chosen to assure the short-term onset of EA (Gloveli et al., 1995; Antonio et al., 2016). Ictal-like EA was induced by perfusion with aCSF containing bicuculline (10 μM, *Bic*) for 15 min. Electrical stimulation was resumed when spontaneous activity halted. Analysis of spontaneous activity was performed by visual inspection of 10 s windows, identification, and manual recording of spontaneous events for all signals above 200 μV amplitude.

Influence of epileptiform activity on PPF and LTP

Altered synaptic properties following EA could involve changes in presynaptic regulation of neurotransmitter release. As such, we tested the influence of EA on PPF, a synaptic short-term synaptic plasticity property that could reveal such changes. PPF of fEPSP slope is believed to result from an enhancement in neurotransmitter release at CA3–CA1 synapses in response to the second stimulation due to the presence of residual calcium generated by the first stimulation in glutamatergic terminals (Zucker, 2003). This facilitation occurs because the release probability at these synapses is low under the current stimulation conditions (Wu and Saggau, 1994; Debanne et al., 1996). Although PPF in the CA1 area of the hippocampus has also been attributed to paired-pulse depression in the fast inhibitory postsynaptic potential (IPSP) (Nathan and Lambert, 1991), given that most synapses in the *stratum radiatum* are excitatory (Megías et al., 2001), PPF of fEPSP slope is mostly attributed to presynaptic changes in glutamate release.

To test the influence of EA on paired-pulse facilitation (PPF), PPF was elicited on the same pathway prior and 30 min after EA induced either by $0Mg^{2+}$ or *Bic* perfusion. The stimulation protocol used to induce PPF was the delivery of two consecutive pulses with 50 ms interpulse interval. The synaptic facilitation was quantified as the ratio P2/P1 between the slopes of the fEPSP elicited by the second P2 and the first P1 stimuli.

Long Term Potentiation (LTP) was induced by a mild theta burst stimulation (TBS) pattern (five trains of 100 Hz, four stimuli, separated by 200 ms) and was particularly chosen to avoid having a ceiling effect on LTP following EA. The TBS train used to induce LTP was delivered 30, 60, and 90 min after termination of EA induction protocols, provided a stable baseline was obtained for at least 16 min. LTP in control conditions (absence of prior EA) was time-matched to experiments performed 30 min after EA. Stimulus intensity was not altered during these stimulation protocols. LTP intensity was calculated as the % change in the average slope of the potentials taken from 50 to 60 min after TBS, compared to the average slope of the fEPSP measured during the 12 min that preceded TBS. Control and test conditions (for which epileptiform activity was induced prior to TBS) were tested in independent slices.

LTP induced at different time points following EA was in some (but not all) cases tested in independent pathways on the same slice. In all experiments S1 always refers to the first pathway (left or right, randomly assigned) to which TBS was applied. Each *n* represents a single LTP experiment) performed in one slice from an independent animal, i.e., *n* denotes the number of animals.

The independence of the two pathways regarding LTP expression was tested at the end of the experiments by studying paired-pulse facilitation (PPF) across both pathways. i.e., now the two Schaffer pathways were consecutively stimulated with 50 ms interpulse interval. The synaptic facilitation was quantified as the ratio P2/P1 between the slopes of the fEPSP elicited by the second P2 and the first P1 stimuli and less than 10% facilitation was observed.

Western blot analysis of synaptic lipid raft markers and AMPA receptor changes influencing synaptic plasticity, and GluA1 phosphorylation

Hippocampal slices were prepared as described above and allowed for functional recovery. Then four slices were introduced in placed in 100 μl Perspex chambers and superfused with oxygenated aCSF at 32°C at a flow rate of 3 ml/min. Field stimulation was delivered once every 15 s in the form of rectangular pulses (1 ms duration, and an amplitude of 8 V) through platinum electrodes located above and below the slices. The electrical pulses were continuously monitored with an oscilloscope. In test (but not in control) slices interictal-like and ictal EA was induced with $0Mg^{2+}$ and *Bic* perfusion as described above for electrophysiological experiments. Stimulation lasted for 30 min before induction of EA, it was halted during EA and was resumed for 30 min (average duration of an electrophysiological experiment until first TBS delivery), after which slices were collected. Hippocampal synaptosomes were isolated from hippocampal slices as previously described (Cunha-Reis et al., 2017). Briefly, at the end of stimulation, slices were collected in sucrose solution (320 mM Sucrose, 1 mg/ml BSA, 10 mM HEPES e 1 mM EDTA, and pH 7,4) containing protease (complete, mini, EDTA-free Protease Inhibitor Cocktail, and Sigma) and phosphatase (1 mM PMSF, 2 mM Na_3VO_4, and 10 mM NaF) inhibitors and homogenized with a Potter-Elvejham apparatus. Each sample (n = 1) was obtained from several slices (minimum four per condition) from 1 to 2 animals. The suspension was centrifuged at 3,000 g for 10 min, the supernatant collected and further centrifuged at 14,000 g for 12 min, and the pellet resuspended in 3 ml of a Percoll 45% (v/v) in modified aCSF (20 mM HEPES, 1 mM $MgCl_2$, 1.2 mM NaH_2PO_4, 2.7 mM NaCl; 3 mM KCl, 1.2 mM $CaCl_2$, 10 mM glucose, and pH 7.4). After centrifugation at 14,000 g for 2 min at 4°C, the top layer (synaptosome fraction) was washed twice with modified aCSF also containing protease and phosphatase inhibitors and hippocampal membranes were resuspended at a concentration of 1 mg/ml protein concentration (Bradford assay) in modified aCSF. Aliquots of this suspension of hippocampal membranes were snap-frozen in liquid nitrogen and stored at −80°C until Western-blot analysis. All samples were analysed in duplicate in western-blot experiments.

For western blot, samples were incubated for 5 min at 95°C with Laemmli buffer (125 mM Tris-BASE, 4% SDS, 50% glycerol, 0,02% Bromophenol Blue, and 10% β-mercaptoethanol), run on standard 10% sodium dodecyl sulphate polyacrylamide gel electrophoresis (SDS-PAGE) and transferred to PVDF membranes (Immobilon-P transfer membrane PVDF, pore size 0.45 μm, Immobilon) and blocked for 1 h with either 3% BSA or 5% milk (Caulino-Rocha et al., 2022). Membranes were incubated overnight at 4°C with mouse anti-gephyrin (#147011, Synaptic Systems, AB_2810214), rabbit anti-PSD-95 (#CST-2507, Cell Signaling Tech., AB_561221), mouse anti-caveolin-1 (#ab106642, Abcam, AB_10861399), mouse anti-flotillin-1 (#ab133497, Abcam, AB _11156367), rabbit antiphospho-Ser845-GluA1 (1:2500, Abcam #Ab76321; RRID:AB_1523688), rabbit antiphospho-Ser-831-GluA1 (1:2000, Abcam #Ab109464; RRID:AB_10862154), rabbit anti-GluA1 (1:4000, Millipore #AB1504; RRID:AB_2113602), rabbit anti-GluA2 (1:1000, Proteintech #11994-1-AP; RRID:AB_2113725), rabbit anti-alpha-tubulin (1:5000, Proteintech #11224-1-AP; RRID:AB_2210206) and rabbit anti-beta-actin (1:10000, Proteintech, Cat# 60008-1; RRID:AB_2289225) primary antibodies. After washing the membranes were incubated for 1 h with anti-rabbit or anti-mouse IgG secondary antibody both conjugated with horseradish peroxidase (HRP) (Proteintech) at room temperature. HRP activity was visualized by enhanced chemiluminescence with ECL Plus Western Blotting Detection System using a ImageQuant™ LAS imager (GE Healthcare, Portugal). Band intensity was estimated using the ImageJ software. β-actin or α-tubulin band density was taken as a loading control and used for data normalization. The % phosphorylation for each AMPA GluA1 subunit target was calculated normalizing the change in phosphorylated form band intensity by the change in band intensity of the total GluA1 immunostaining.

Materials

Bicuculline methochloride (Ascent Scientific, UK) was made up in 10 mM stock solutions in DMSO. Aliquots of the stock solutions were kept frozen at −20°C until use. An aliquot was diluted in aCSF for use in each experiment. The maximal DMSO concentration used (0.01% v/v, n = 4) was devoid of effects on fEPSP slope.

Data and statistical analysis

Long term potentiation (LTP) values are depicted as the mean ± S.E.M of n experiments. Each n represents a single experiment performed in slices obtained from one different animal for LTP experiments (i.e., n stands for the number of animals). For western blot experiments each sample was obtained from slices from 1 to 2 animals (i.e., each n stands for one or two animals combined). Statistical analysis was performed using GraphPad Prism 6.01 for Windows. In electrophysiology experiments, significance of the means of LTP-like effects was evaluated using Student's t-test. Significance of the differences between the LTP means was evaluated using one-way ANOVA with Sidak *post-hoc* test. Repeated measures ANOVA with Sidak's

post-hoc test (when F was significant) was used to evaluate group differences in western blot experiments. No outliers were identified in our data (ROUT method).

Results

To understand the impact of EA on the function of hippocampal synapses we studied its immediate influence on synaptic transmission in the CA1 area and early hour synaptic plasticity using electrophysiological recordings. We characterized spontaneous activity during seizure-inducing conditions, changes in electrically evoked synaptic transmission and LTP induced by mild TBS after EA.

Influence of interictal-like EA on basal synaptic transmission and LTP expression

The evoked fEPSPs recorded under basal stimulation conditions in the *stratum radiatum* of the CA1 area in hippocampal slices from young-adult rats (Figure 1A) had an average slope of 0.635 ± 0.026 mV/ms (n = 26), that represented 40–60% of the maximal response in each slice. Upon superfusion with modified aCSF lacking Mg^{2+} ($0Mg^{2+}$) for 30 min in the absence of electrical stimulation spontaneous activity started gradually with single spontaneous population spikes (Figure 1B, 0.7 to 1.2 mV amplitude, n = 5) and 6–8 min later larger amplitude (2.7 to 4 mV, n = 5) population spikes with wave reverberation (spike-slow wave discharges, *S-SW*, Figure 1B) were observed, as previously described (Gloveli et al., 1995). The maximum frequencies were reached near the end of the 30 min superfusion with $0Mg^{2+}$ and were of 0.695 ± 0.055 *spikes*/min (n = 5, Figure 1C) and of 0.670 ± 0.040 *S-SW*/min (n = 5, Figure 1D). All spontaneous activity was terminated within 8–12 min post $0Mg^{2+}$ washout. When resuming electrical stimulation an *LTP-like effect* was observed in the slope of the evoked fEPSPs (Figure 1E) with a remaining potentiation of 21.0 ± 4.7% (n = 10) 30 min after resuming electrical stimulation and of 10.7 ± 1.8% (n = 5) at 60 min.

We thus studied the influence of $0Mg^{2+}$-induced EA on LTP expression. When mild TBS was applied in control conditions the LTP magnitude corresponded to a 32.0 ± 1.3% enhancement of fEPSP slope 50–60 min after TBS (n = 13, Figure 2A), an effect that was absent when slices were stimulated in the presence of the NMDA receptor antagonist AP-5 (100 μM), as previously described

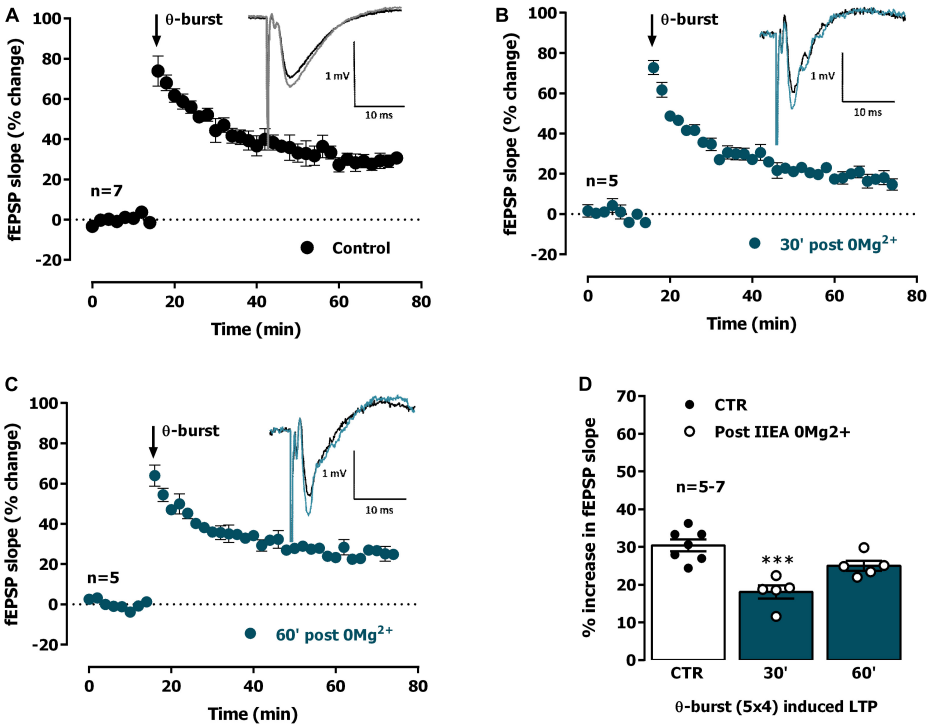

FIGURE 2
Interictal-like activity transiently impairs the expression of hippocampal CA1 long-term potentiation (LTP) of synaptic transmission. **(A)** Averaged time-course of changes in field excitatory post-synaptic potentials (fEPSP) slope (-●-) caused by theta-burst stimulation (TBS, five bursts at 5 Hz, each composed of four pulses at 100 Hz) in experiments in which a control slice was stimulated in the absence of added drugs. *Inset:* Traces of fEPSPs obtained in one of the same experiments before (black) and 50–60 min after TBS (gray). Traces are the average of eight consecutive responses and are composed of the stimulus artifact, the presynaptic volley and the fEPSP. **(B,C)** Averaged time-course of changes in fEPSP slope caused by TBS applied either 30 min **(B)** or 60 min **(C)** after interictal epileptiform activity induced by $0Mg^{2+}$ perfusion (-●-). **(D)** LTP magnitude estimated from the averaged enhancement of fEPSP slope observed 50–60 min after TBS in control slices (●, left open bar) or in slices previously experiencing interictal epileptiform activity induced by $0Mg^{2+}$ (○, blue bars). LTP was induced either 30 min (middle bar) or 60 min after epileptiform activity (right bar). *Inset:* Traces of fEPSPs obtained before (black) and 50–60 min after TBS (blue). Individual values and the mean ± S.E.M are depicted **(D)**. ***p < 0.001 (one-way ANOVA) as compared to LTP magnitude in control slices (○, in the left).

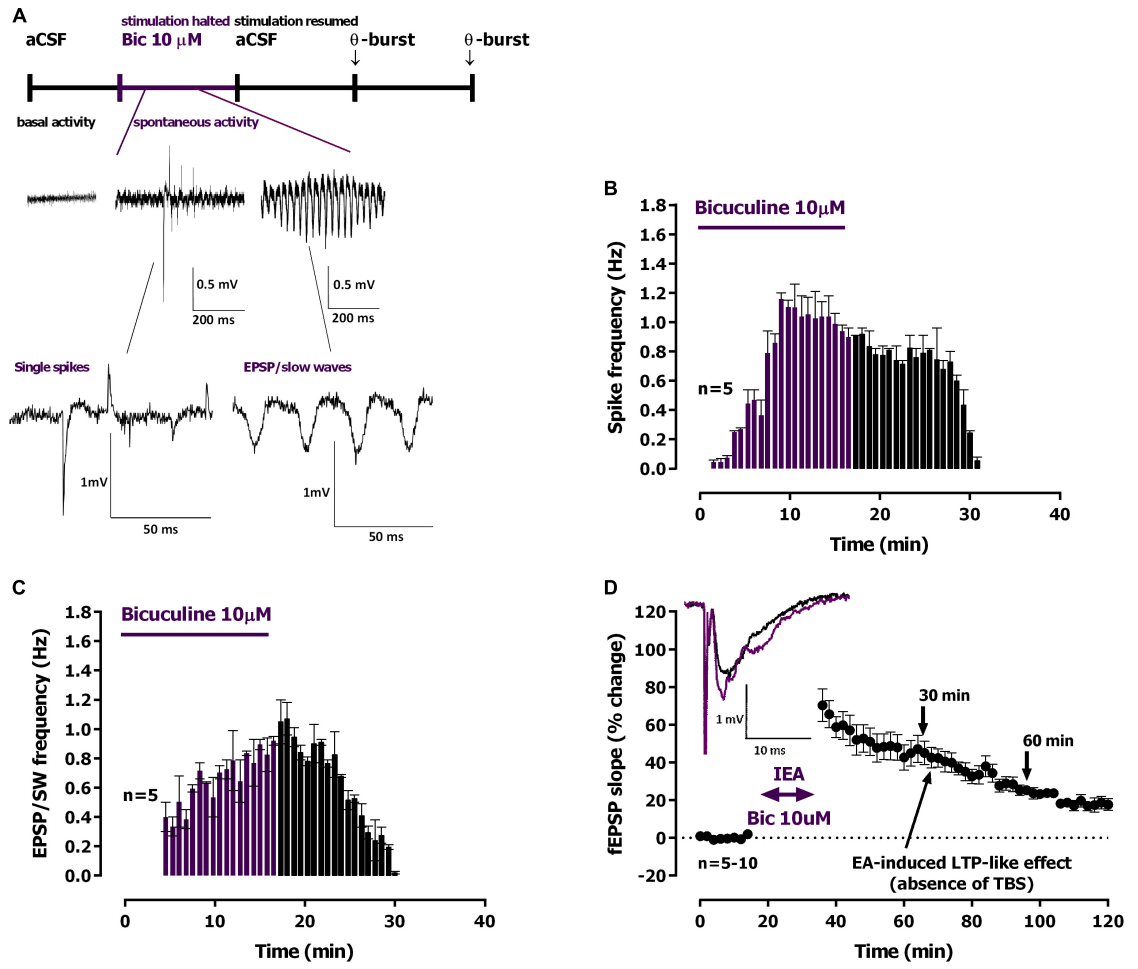

FIGURE 3
Ictal-like epileptiform activity induced by *Bicuculline* and long-term potentiation (LTP)-like effect. **(A)** Time-course of a typical experiment showing the spontaneous activity recorded prior to bicuculline (10 μM, *Bic*) delivery to the superfusion chamber (left) and during the 16 min *Bic* perfusion. Specific examples of the two main types of epileptiform activity recorded, single *population spikes* and *EPSP-slow wave* activity, are shown at the millisecond scale. Stimulation was halted during *Bic* perfusion. **(B,C)** Averaged time-course of the frequency of spontaneous *population spikes* **(B)** and *EPSP-slow wave* activity [**(C)**, *n* = 5]. **(D)** Averaged time-course of changes in eld excitatory post-synaptic potentials (fEPSP) slope caused by *Bic* perfusion. *Inset*: traces of fEPSPs obtained in the same experiment before (black) and 25–30 min after *Bic* perfusion (purple). Electrophysiological recordings of fEPSPs evoked by electrical stimulation were performed in the CA1 area of hippocampal slices. Traces are the average of eight consecutive responses and are composed of the stimulus artifact, the presynaptic volley and the fEPSP. The mean ± S.E.M is depicted **(B,D)**.

(Rodrigues et al., 2021). When a TBS train was delivered 30 min past interictal-like EA induced by $0Mg^{2+}$, LTP expression was impaired (% increase in fEPSP slope: 18.0 ± 1.8%, *n* = 5, Figure 2B). When delivered to the slices 60 min past interictal-like EA, the same TBS stimulation elicited a larger LTP, nearly as big as the one obtained in control slices, now increasing by 24.8 ± 1.1% (*n* = 5) the fEPSP slope 50–60 min post TBS (Figure 2C). This suggests interictal-like EA induced by $0Mg^{2+}$ does not promote marked or sustained changes in the LTP expressing ability of CA3 to CA1 synapses, that are only transiently affected by this type of EA.

Influence of ictal-like EA on basal synaptic transmission and LTP expression

Upon superfusion with modified aCSF containing bicuculline (10 μM, *Bic*) for 15 min spontaneous activity started with single isolated population spikes (Figure 3A, 0.51 to 0.89 mV amplitude, *n* = 7) that were increasingly more frequent, and more than the ones observed during $0Mg^{2+}$ perfusion (Figure 3B). Within 4–6 min of *Bic* superfusion slower waves of synchronous activity (0.29 to 0.68 mV, *n* = 7, Figure 3C) began to develop showing occasional (0.5 to 1 per min) high amplitude bursts (EPSP / slow-wave discharges, *EPSP-SW*, Figures 3A, C). The maximum EPSP-SW frequencies were reached by the end the 16 min superfusion with *Bic* and were of 1.070 ± 0.110 *S-SW*/min (*n* = 5, Figure 3C). The maximum spike frequencies were reached shortly (6–8 min) after beginning the 16 min superfusion with *Bic* and were of 1.040 ± 0.140 *spikes*/min (*n* = 5, Figure 3B). All spontaneous activity was terminated within 16–20 min of *Bic* washout. When resuming electrical stimulation an *LTP-like effect* was observed causing a potentiation of 45.1 ± 6.2% (*n* = 10) in the slope of the evoked fEPSPs (Figure 3D) obtained 30 min after resuming electrical stimulation,

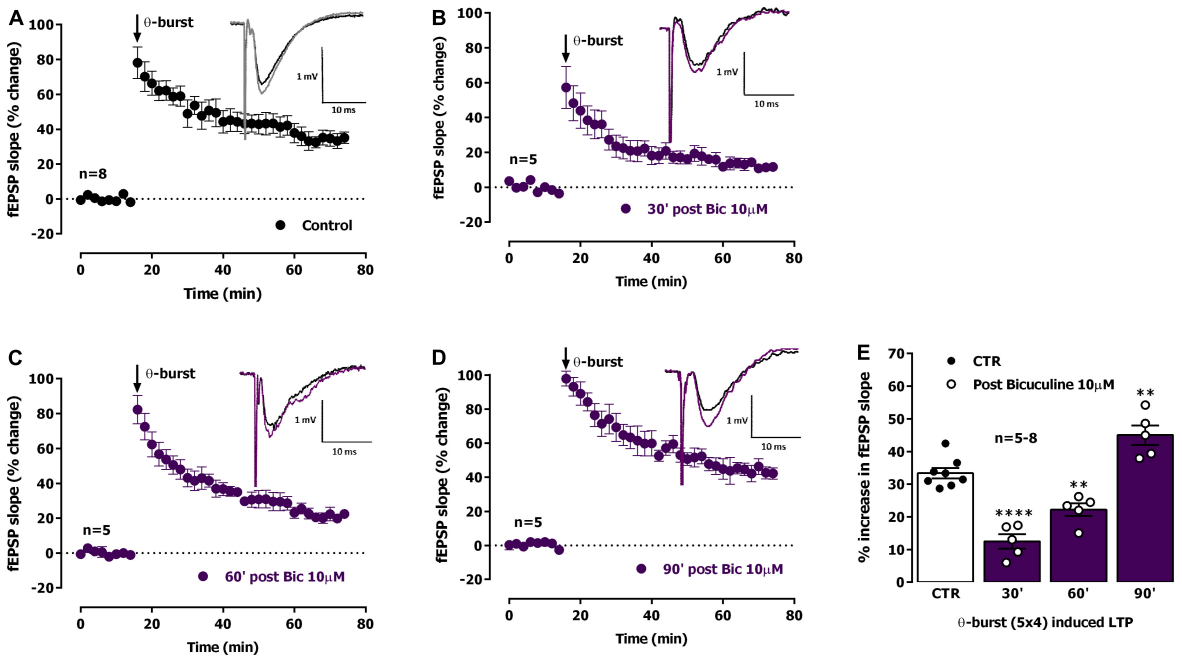

FIGURE 4
Ictal-like activity induces a biphasic alteration in the expression of hippocampal CA1 long-term potentiation (LTP) of synaptic transmission. **(A)** Averaged time-course of changes in fEPSP slope (-●-) caused by theta-burst stimulation (TBS, five bursts at 5 Hz, each composed of four pulses at 100 Hz) in experiments in which a control slice was stimulated in the absence of added drugs. *Inset:* Traces of field excitatory post-synaptic potentials (fEPSPs) obtained in one of the same experiments before (black) and 50–60 min after TBS (gray). Traces are the average of eight consecutive responses and are composed of the stimulus artifact, the presynaptic volley and the fEPSP. **(B–D)** Averaged time-course of changes in fEPSP slope caused by TBS delivered either 30 min **(B)**, 60 min **(C)** or 90 min **(D)** after ictal epileptiform activity induced by bicuculline 10 μM (*Bic*) perfusion (-●-). **(E)** LTP magnitude estimated from the averaged enhancement of fEPSP slope observed 50–60 min after TBS in control slices (●, left open bar) or in slices previously experiencing interictal epileptiform activity induced by *Bic* (○, purple bar). LTP was induced either 30 min (second bar), 60 min (third bar) or 90 min (last bar) after epileptiform activity. *Inset:* Traces of fEPSPs obtained before (black) and 50–60 min after TBS (purple). The mean ± S.E.M is depicted **(A–D)**. $^{**}p < 0.01$ and $^{****}p < 0.0001$ (one-way ANOVA) as compared to LTP magnitude in control slices (○, in the left).

of 25.3 ± 2.5% (n = 7) at 60 min and of 14.5 ± 1.3% (n = 5) at 90 min.

We thus studied the influence of *Bic*-induced EA on LTP expression. LTP induced by mild TBS 30 min following ictal-like EA elicited by *Bic* was strongly impaired (% increase in fEPSP slope: 12.5 ± 2.2%, n = 5, **Figure 4B**). TBS stimulation delivered to the slices 60 min past ictal-like EA, still elicited an impaired LTP, i.e., smaller than the one obtained in control slices, now increasing by 22.2 ± 1.9% (n = 5) the fEPSP slope 50–60 min post TBS (**Figure 4C**). When delivered to the slices 90 min past ictal-like EA, TBS stimulation now induced an LTP larger than the one obtained in control slices, thus increasing by 45.0 ± 3.0% (n = 5) the fEPSP slope 50–60 min post TBS (**Figure 4D**). As such, a biphasic change in the ability of TBS to induce LTP at CA1 hippocampal synapses occurs following ictal-like EA, first reflecting an impairment, then a mildly enhanced capacity to elicit LTP by TBS. This is likely an overshoot caused by recovery mechanisms (Russo et al., 2013).

Influence of EA on PPF

Altered LTP expression following EA could be due to changes in presynaptic regulation of neurotransmitter release. As such, we also investigated the influence of EA on PPF of the fEPSP slope, a synaptic short-term synaptic plasticity property of CA3–CA1 synapses, where the release probability upon basal stimulation is low, that results from an enhancement in neurotransmitter release in response to the second stimulation due to the presence of residual calcium generated by the first stimulation (Wu and Saggau, 1994; Debanne et al., 1996). PPF of fEPSP slope is mostly due to presynaptic changes in glutamate release.

When two consecutive stimulation pulses were delivered with a 50 ms interval to the Schaffer collateral/commissural pathway in the CA1 area, the slope of the fEPSP elicited by the second (test, S2) stimulation pulse was 1.4–1.8 times higher than the one evoked by the first (conditioning, S1) stimulation pulse (**Figure 5A**). Facilitation of glutamatergic transmission may play together with depression of GABAergic transmission in promoting PPF of fEPSP slope in hippocampal CA1. Most synapses in the *stratum radiatum* are excitatory (Megías et al., 2001), as such, changes in PPF of fEPSP slope are most likely predominantly due to presynaptic changes in glutamate release. Following interictal EA induced by $0Mg^{2+}$ PPF was enhanced (% increase in S_2/S_1 ratio was 15.0 ± 3.7% $n = 5$, $P < 0.05$, **Figures 5A, B**), suggesting that increased glutamate release probability is involved in the enhancement of synaptic transmission observed 30 min post interictal activity induced by $0Mg^{2+}$ in the CA1 area of the hippocampus. Conversely, after ictal activity induced by *Bic*, PPF was mildly reduced (% decrease in S_2/S_1 ratio was 11.0 ± 2.9% $n = 5$, $P < 0.05$, **Figures 5C, D**).

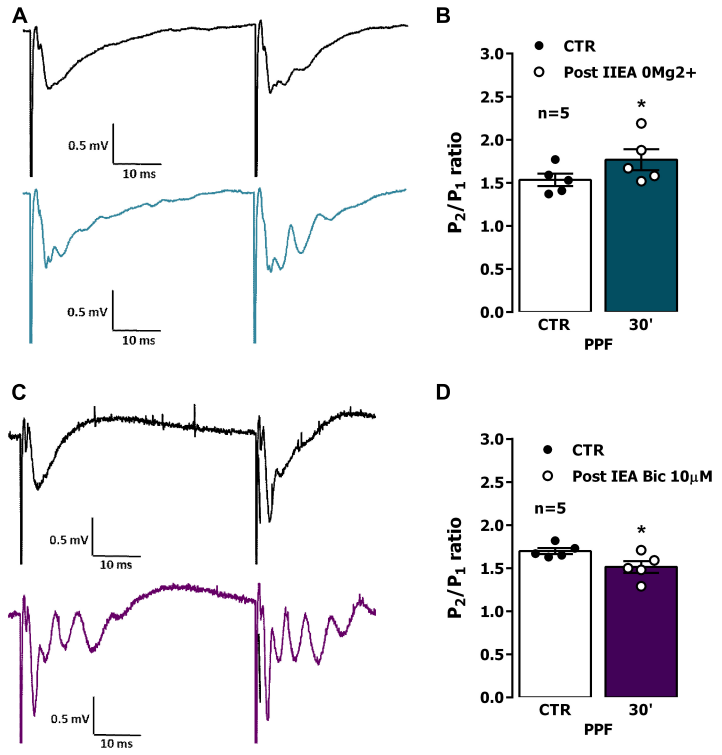

FIGURE 5
Impact of epileptiform activity on paired-pulse facilitation (PPF) of synaptic transmission in the CA1 area of the hippocampus. PPF was induced by applying two consecutive stimuli with 50 ms interval once every 20 s while recording field excitatory post-synaptic potentials (fEPSPs). **(A,C)** Representative recordings of fEPSPs pairs obtained when using the PPF paradigm before (top) and 30 min after interictal epileptiform activity induced by $0Mg^{2+}$ **(A)**, bottom, blue line or ictal epileptiform activity induced by *Bic* **(C)** bottom, purple line. Traces are the average of eight consecutive responses and are composed of the stimulus artifact, the presynaptic volley and the fEPSP. Influence of interictal epileptiform activity induced by $0Mg^{2+}$ **(B)** or of ictal epileptiform activity induced by *Bic* **(D)** on PPF magnitude estimated from change in the fEPSP slope ratio (S_2/S_1) between responses evoked by the first (conditioning) and the second (test) stimulation. In **(B,D)**, each bar represents the mean ± S.E.M of results obtained in five experiments. *$P < 0.05$ (paired Student's *t*-test) as compared with S_2/S_1 ratio prior to induction of epileptiform activity.

To further understand the molecular alterations at synapses that were underlying these changes in LTP expression we performed parallel experiments where hippocampal slices were also subjected to EA induced by $0Mg^{2+}$ or *Bic*, and 30 min later were processed for synaptosome isolation and analysis of synaptic proteins associated with altered synaptic plasticity. These included AMPA receptor subunits GluA1 and GluA2, GluA1 phosphorylation in Ser831 and Ser845, Kv4.2 potassium channels, synaptic structural and lipid raft markers such as PSD-95, gephyrin, caveolin-1, flotillin-1, α-tubulin, and synaptophysin-1.

Influence of interictal-like and ictal-like EA on AMPA receptor composition and phosphorylation supporting LTP expression

AMPA receptor subunit composition (GluA1-4) influences channel function and LTP outcomes (Chater and Goda, 2022), since AMPA receptors lacking GluA2 are Ca^{2+} permeable and when activated can further add to the postsynaptic Ca^{2+} rise and LTP levels. To elucidate the possible changes in synaptic AMPA receptor subunit composition that may impact its Ca^{2+} permeability and its contribution to altered LTP expression following EA we investigated changes in synaptic GluA1 and GluA2 levels and GluA1/GluA2 ratio. Following EA, the synaptic levels of AMPA GluA1 subunits (**Figure 6A**) were decreased to 77.1 ± 9.0% (n = 5) after $0Mg^{2+}$ exposure and to 72.0 ± 11.8% (n = 5) after *Bic* exposure. Opposingly, synaptic GluA2 subunits (**Figure 6D**) were increased to 127.3 ± 10.1% (n = 5) after $0Mg^{2+}$ exposure and to 152.8 ± 14.3% (n = 5) after *Bic* exposure. Consequently, GluA1/GluA2 ratios (**Figure 6E**) were also markedly reduced after $0Mg^{2+}$ and *Bic* exposure. No significant differences were found between $0Mg^{2+}$ or *Bic* exposure for both targets as well as GluA1/GluA2 ratios.

Long term potentiation (LTP) expression, and particularly mild TBS induced LTP, depends on the Ca^{2+}-dependent auto-phosphorylation of Ca^{2+}/calmodulin dependent protein kinase II (CaMKII), that influences the phosphorylation of AMPA GluA1 subunits and their synaptic recruitment (Appleby et al., 2011; Rodrigues et al., 2021). These are also targeted by other intracellular kinases like protein kinase A and C (PKA and PKC) affecting hippocampal LTP expression by supporting traffic or altering AMPA receptor opening probability (Lee et al., 2003). Although not directly involved in mild TBS-induced LTP (Rodrigues et al., 2021), altered PKA and PKC activity during EA could influence AMPA basal phosphorylation thus influencing subsequent TBS-induced LTP. We thus investigated if altered GluA1 phosphorylation levels

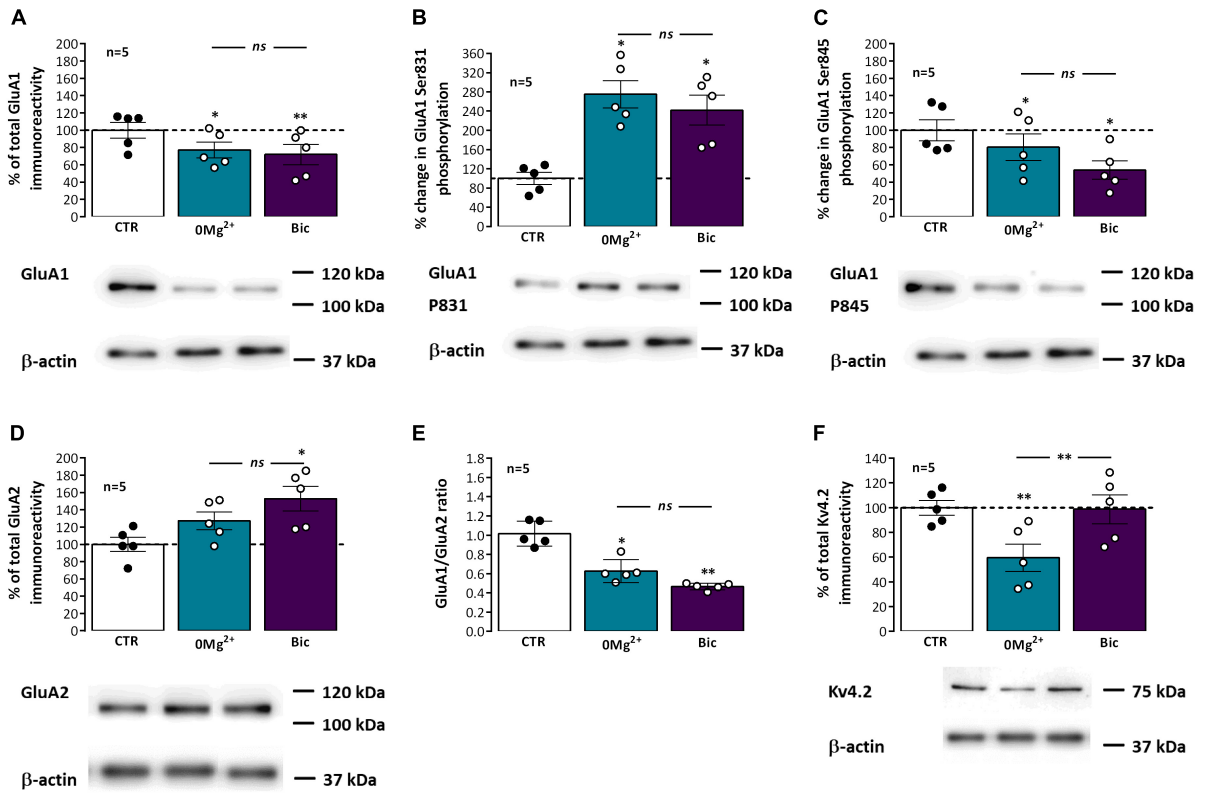

FIGURE 6
Impact of epileptiform activity on phosphorylation of synaptic hippocampal AMPA GluA1 subunits on Ser 831 and Ser 845, GluA1/GluA2 ratio and Kv4.2 levels. Each panel shows at the bottom the western-blot immunodetection of AMPA total GluA1 subunits **(A)**, its phosphorylated forms in Ser831 **(B)** and Ser845 **(C)**, total GluA2 subunits **(D)** and Kv4.2 potassium channels **(F)** obtained in one individual experiment where hippocampal slices underwent Schaffer collateral basal stimulation for 20 min and then were subjected either to interictal-like epileptiform activity (EA) induced by perfusion with $0Mg^{2+}$ for 30 min or ictal-like EA by exposure to bicuculine (10 μM, *Bic*) for 16 min, and then allowed to recover for 30 min before slice collection. Control slices were monitored for 70 min (the equivalent time of the EA protocol) before WB analysis. Western blot experiments were performed using synaptosome preparations obtained from these slices. Respective total GluA1 immunoreactivity **(A)**, % GluA1 phosphorylation in Ser831 **(B)** or Ser845 **(C)**, residues, total GluA2 immunoreactivity **(D)**, GluA1/GluA2 ratios **(E)** and total Kv4.2 potassium channel levels **(F)** are also plotted at the top for each panel. Individual values and the mean ± S.E.M of five independent experiments are depicted. 100% - averaged GluA1 or GluA2 immunoreactivity or GluA1 phosphorylation obtained in control conditions (CTR, absence of EA). *$P < 0.05$ and **$P < 0.01$ (*ANOVA*, Sidak's multiple comparison test) as compared to CTR; *ns* represents non -significant differences $P > 0.05$ (*ANOVA*, Sidak's multiple comparison test) between respective bars.

at Ser831, a prominent target of CaMKII and PKC, and Ser845, a main target of PKA were implicated in altered LTP responses following EA. Phosphorylation of GluA1 subunits in Ser831 (**Figure 6B**) was markedly increased to 275.0 ± 12.7% ($n = 5$) after $0Mg^{2+}$ induced EA and 241.9 ± 31.1% ($n = 5$) after *Bic* induced EA. Opposingly, phosphorylation of GluA1 subunits in Ser845 (**Figure 6C**) was decreased to 80.4 ± 15.4% ($n = 5$) after $0Mg^{2+}$ exposure and 53.9 ± 10.6% ($n = 5$) after *Bic* exposure. No significant differences were found between $0Mg^{2+}$ or *Bic* exposure for the phosphorylation on both targets.

Kv4.2 K^+ channels are important regulators of dendritic excitability by mediating the transient A-current. Its membrane levels and phosphorylation status are regulated by electrical activity patterns used in LTP induction (e.g., strong TBS), suggesting that the activity of the channel, contributes to LTP expression (Frick et al., 2004; Kim and Hoffman, 2008; Rodrigues et al., 2021). Following EA, Kv4.2 levels (**Figure 6F**) were reduced to 59.5 ± 11.1% ($n = 5$) after $0Mg^{2+}$ exposure but were not significantly altered (98.8 ± 11.7%, $n = 5$) after *Bic* induced EA.

Influence of EA on lipid raft associated proteins

Pre and postsynaptic membrane lipids differ substantially from the ones in the remaining neuronal membrane, hinting that synaptic signaling is strongly dependent on this specialization (Borroni et al., 2016; Flores et al., 2019) and different classes of membrane lipids integrate domains showing distinctive properties in terms of size, rigidity, and thickness (Wilson et al., 2020). Lipid rafts, liquid-ordered or gel-like membrane nanodomains segregated from the bulk membrane and enriched in cholesterol, sphingolipids and GPI-anchored proteins, are crucial for dynamic synaptic signaling. These comprise two main types of structure, caveolae, curved membrane domains, or planar lipid rafts (Allen et al., 2007; Borroni et al., 2016), characterized by the presence of the membrane proteins caveolins, a family of 22 kDa cholesterol-binding membrane proteins, and flotillins, a family of 49 kDa membrane proteins associated with the membrane inner leaflet, respectively. These play also an active role in promoting the

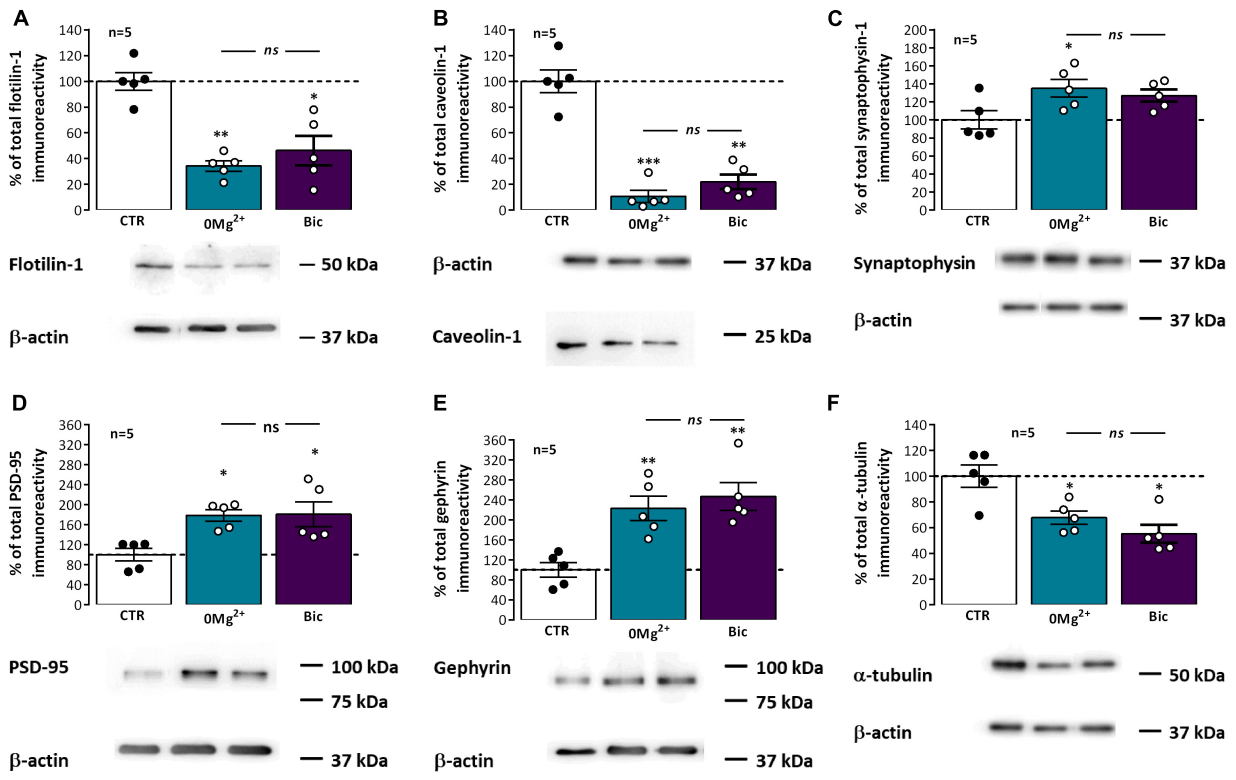

FIGURE 7
Impact of epileptiform activity on classic and synaptic lipid raft markers. Each panel shows at the bottom the western-blot immunodetection of flotillin-1 **(A)**, caveolin-1 **(B)**, synaptophysin-1 **(C)**, PSD-95 **(D)**, gephyrin **(E)**, and alpha-tubulin **(F)** obtained in one individual experiment where hippocampal slices underwent Schaffer collateral basal stimulation for 20 min and then were subjected either to interictal-like epileptiform activity (EA) induced by perfusion with $0Mg^{2+}$ for 30 min or ictal-like EA by exposure to bicuculline (10 μM, *Bic*) for 16 min, and then allowed to recover for 30 min before slice collection. Control slices were monitored for 70 min (the equivalent time of the EA protocol) before WB analysis. Western blot experiments were performed using synaptosome preparations obtained from these slices. Respective average change in total flotillin-1 **(A)**, caveolin-1 **(B)**, synaptophysin-1 **(C)**, PSD-95 **(D)**, gephyrin **(E)**, and alpha-tubulin **(F)** immunoreactivities are also plotted at the top in each panel. Individual values and the mean ± S.E.M of five independent experiments are depicted. 100% - averaged PSD-95, gephyrin, caveolin-1, flotillin-1, or synaptophysin-1 immunoreactivity in control conditions (CTR, absence of EA). *$P < 0.05$, **$P < 0.01$, and ***$P < 0.001$ (*ANOVA*, Sidak's multiple comparison test) as compared to CTR; *ns* represents non-significant differences $P > 0.05$ (*ANOVA*, Sidak's multiple comparison test) between respective bars.

phase separation within the membrane that maintains these lipid nanodomains at synapses (Allen et al., 2007; Frick et al., 2007). Synaptic lipid rafts can also be associated with synaptic lipid-raft nucleating/associated proteins like PSD-95 or gephyrin. Following EA, the synaptic levels of flotillin-1 (Figure 7A) were markedly reduced to 34.3 ± 4.1% (n = 5) after $0Mg^{2+}$ exposure and 46.3 ± 11.4% (n = 5) after *Bic* exposure while the levels of caveolin-1 (Figure 7B) were dramatically reduced to 10.6 ± 4.7% (n = 5) after $0Mg^{2+}$ exposure and 21.9 ± 5.6% (n = 5) after *Bic* exposure. Regarding the postsynaptic scaffolding protein of glutamatergic synapses PSD-95, after EA, it was observed an increase in PSD-95 levels to 178.6 ± 11.5% (n = 5) following $0Mg^{2+}$ exposure and to 180.8 ± 24.9% (n = 5) upon *Bic* exposure (Figure 7D). Gephyrin was also significantly altered 30 min next to EA, increasing to 222.9 ± 24.6% (n = 5) upon $0Mg^{2+}$ exposure and 246.8 ± 27.8% (n = 5) upon *Bic* exposure (Figure 7E). Only for PSD-95 was observed a significant difference in the EA response between $0Mg^{2+}$ and *Bic* exposure.

To understand the relation between the changes in these different proteins at synapses and overall synaptic alterations in this synaptosomal preparation we also evaluated the synaptic levels of synaptophysin-1, a synaptic vesicle associated glycoprotein. Synaptophysin-1 levels were mildly enhanced following exposure to both $0Mg^{2+}$ (135.1 ± 10.0%, n = 5) or *Bic* (126.9 ± 6.7%, n = 5). In addition, we investigated changes in the structural protein α-tubulin, since our preliminary studies using it as a western blot loading control suggested that the synaptic levels of this protein were also significantly changing after EA (Figure 7F). The synaptic levels of α-tubulin were decreased to 67.7 ± 5.1% (n = 5) following $0Mg^{2+}$ exposure and 55.0 ± 7.0% (n =5) after *Bic* exposure.

Discussion

In the present work we first describe that: (1) interictal-like EA induces a mild impairment in TBS-induced LTP observed 30 min after the insult that is fully recovered 1 h after; (2) ictal-like EA, in turn, induces a marked impairment in TBS-induced LTP within 30 min -1 h after the insult and this is reversed to a mild enhancement 1 h 30 m after; (3) Impairment of LTP induced by EA was globally associated to a decrease in AMPA GluA1 subunit

levels and an increase in GluA2 subunit levels, resulting in a marked decrease of the GluA1/GluA2 ratio, together with a marked increase in GluA1 P831 phosphorylation and a mild decrease in GluA1 P845 phosphorylation; (4) Kv4.2 K^+ channels levels were decreased following interictal-like EA but not following ictal-like EA; (5) EA also decreased the levels of classic lipid raft markers caveolin-1 and flotillin-1, while increasing synapse specific lipid raft markers PSD-95 and, most prominently, gephyrin.

In this work, the observed physiological alterations in LTP induction and expression, together with the alterations in the molecular composition of synapses, provide a good insight on the very early alterations of synaptic plasticity in adult rodents following two forms of epileptiform activity: (1) seizure-like activity (the one induced by bicuculline, 10 μM, *Bic*) and (2) neuronal interictal-like activity (induced by Mg^{2+} suppression, *0*Mg^{2+}), characteristic resting brain activity pattern of epilepsy patients, often observed in the latent period of epileptogenesis in animal models. The fact that LTP expression is influenced by previous neuronal and/or synaptic activity is not itself new (Abraham and Bear, 1996; Colgin et al., 2004; Zhang et al., 2005) and previous studies reported structural alterations in synapse architecture following seizures (Leite et al., 2005; Postnikova et al., 2017). Altered synaptic plasticity was also observed following numerous physiologic stress conditions, (Félix-Oliveira et al., 2014; Arias-Cavieres et al., 2021) and associated with the clustering of synaptic markers and altered synaptic morphology (Sebastian et al., 2013). Nonetheless, LTP changes occurring following *in vitro* events resembling seizure-like activity versus the ones caused by altered resting neuronal activity observed in epileptic patients was never investigated concomitantly in the same model. To this purpose, the use of the hippocampal slice *in vitro* system for seizure generation was preferred to the *in vivo* model of epilepsy also used by our research group (Serpa et al., 2022), since it allowed to assess LTP in the first hours following EA, thus avoiding the dissection and recovery time after slice preparation (usually 1 h– 1 h 30 m) that would expand the time window for LTP inspection. This is of particular interest to the development of early intervention therapies to prevent epileptogenesis.

Interictal-like EA, lasting for about 30 min, was characterized by spaced large amplitude burst of neuronal activity separated by more silent periods with occasional single spikes while ictal like activity, lasting for 20–25 min, was characterized by a continuous activity showing both population spikes and EPSP-SWs. As previously observed by many others (Gloveli et al., 1995; Debanne et al., 2006; Postnikova et al., 2020; Ergina et al., 2021), synaptic transmission was potentiated following both ictal-like and interictal-like EA (**Figures 1E**, **3D**), an LTP-like effect of EA that is similarly, dependent on NMDA receptor activation (Ben-Ari, 2001; Debanne et al., 2006). However, in this paper, we focused on the ability of EA to condition further LTP induction by mild TBS (five trains of four pulses delivered at 100 Hz with 200 ms interburst interval) in a time window from 30 min to 1 h 30 min post EA. Decreased LTP observed when induced 30 min following interictal-like EA (**Figure 2**), was virtually gone when LTP was induced 1 h after EA. In contrast, LTP impairment was much stronger when LTP was induced 30 min following ictal-like activity (**Figure 4**), and a milder impairment was still observed when LTP was induced 1 h following ictal-like EA. LTP induced 1 h 30 min after ictal-like activity was, however, slightly enhanced, suggesting an overshoot in synaptic recovery mechanisms (Russo et al., 2013). Previous studies addressed the alterations in LTP following *in vitro* 4-AP induced ictal-like EA in hippocampal slices or 3 h after Li^{2+}-pilocarpine-induced seizures in juvenile rats (Kryukov et al., 2016; Postnikova et al., 2020) and report a similar small reduction of LTP. Although this partially agrees with our observations, a slightly stronger TBS pattern was used, likely a requirement to induce a robust LTP in the juvenile rats (Rodrigues et al., 2021). LTP impairment after ictal-like EA was more pronounced in our work and was nearly recovered 1 h 30 m later, likely reflecting the shorter duration of the ictal-like EA in our work. The differences in the age, the LTP and EA induction methods and/or in the time frame of LTP evaluation after EA preclude a more elaborated discussion of all these findings. In this work, ictal-like activity, although shorter in duration than interictal-like activity, had a much greater impact on hippocampal LTP. This is in line with previous theories arguing that interictal-like activity is protective in epileptogenesis (Avoli, 2001; Avoli et al., 2006) and suggests that altered LTP mechanisms are not only important for epileptogenesis but also a relevant therapeutic target in its prevention (Albensi et al., 2004, 2007; Avanzini et al., 2014).

As previously mentioned, altered LTP expression following EA could be due to changes in presynaptic regulation of glutamate release, that could be assessed studying by PPF a synaptic short-term synaptic plasticity property that is influenced by such changes. In this work, PPF was mildly increased following *0*Mg^{2+} induced EA and was slightly decreased following *Bic*-induced EA, suggesting that each of the two types of EA have a different impact on presynaptic function. The reduction in PPF caused by *Bic*-induced EA, although not very pronounced, is consistent with an increased glutamate release probability and may reflect enhanced presynaptic Ca^{2+} post EA (Kovac et al., 2017). Conversely, the mild increase in PPF caused by *0*Mg^{2+}-induced EA is consistent with a decrease in glutamate release probability and with a putative neuroprotective role of this type of activity in epileptogenesis. Regarding its impacts on LTP expression following EA, it can be argued that enhanced glutamate release probability following ictal-like *Bic*-induced EA may somewhat contribute to enhanced LTP impairment by promoting glutamate depletion at CA3-CA1 synapses. However, it is likely that this is only a small contribution to this effect, given the small alteration in the PPF ratio.

Induction of CA1 LTP classically relies on the NMDA-mediated postsynaptic Ca^{2+} rise (Bliss et al., 2018), that follows primary AMPA receptor mediated postsynaptic depolarization. Yet, LTP outcomes are also dependent on AMPA receptor subunit composition, a variable tetrameric combination of GluA1-4 subunits influencing channel function (Wiltgen et al., 2010; Chater and Goda, 2022). In hippocampal synapses, GluA1/2 heterodimers are the most common, although GluA2/3 heterodimers are also present (Chater and Goda, 2022). Importantly, GluA2 containing AMPA Rs, being impermeable to Ca^{2+}, limit the contribution of AMPA Rs to the postsynaptic Ca^{2+} rise. Diminished levels of GluA2 containing AMPA receptors were linked to aging and pathological conditions such as brain lesions (Chater and Goda, 2022). In this work we found that synaptic GluA1 levels were decreased while GluA2 levels were increased in hippocampal slices exposed to EA (**Figures 5A, D**), an effect more pronounced following ictal-like activity. A concomitant decrease in GluA1/GluA2 ratio was observed for both conditions (**Figure 6E**). These findings suggest that epileptiform activity transiently reduces

the number of Ca^{2+}-permeable AMPA receptors at hippocampal synapses in adult rats, a likely endogenous neuroprotective measure. Interestingly, decreased AMPA Ca^{2+} permeability following $0Mg^{2+}$ induced EA was previously reported in mixed neuroglial cultures (Gaidin et al., 2019), which is consistent with our results. A recent work also implicates synaptic GluA2-lacking Ca^{2+} permeable receptors as the main event in the LTP-like effects of 4-AP induced EA in CA1 pyramidal neurons in juvenile rats (Postnikova et al., 2020). Given the different role played by AMPA subunits in synaptic plasticity at these young ages (Liu et al., 2020; Chater and Goda, 2022), it is likely that the AMPA glutamatergic component of this LTP-like effect may be distinct in adult circuitry (Goodkin et al., 2008; Avoli et al., 2022; Lévesque et al., 2022). Since the initiation of EA is itself dependent on GABAergic transmission (Avoli et al., 2022), the role of GABAergic transmission in the LTP-like effects of EA should also be elucidated. This would require a distinct approach to induce ictal-like activity than the one used in this study since direct effects of bicuculline on GABAergic receptors (Tang et al., 2023) may alter also the long-lasting response to EA.

The experimental approach used in this paper to monitor changes in synaptic AMPA receptors does not provide sufficient detail on their subsynaptic distribution (Chater and Goda, 2022), and the distinction between synaptic and perisynaptic AMPA receptors, or between pre- or postsynaptic receptors. In the context of seizure induced epileptogenesis, activation of extrasynaptic receptors by glutamate spillover from active synapses may be crucial to the establishment of metaplastic events contributing to maladaptive homeostatic plasticity such as changes in AMPA/NMDA ratio at glutamatergic synapses (Postnikova et al., 2020; Ergina et al., 2021; Chater and Goda, 2022). Future works should aim the elucidation of the exact changes occurring at synaptic and perisynaptic to clarify the contribution of AMPA receptors to early alterations in synaptic plasticity leading to epileptogenesis.

Long term potentiation (LTP) expression involves the phosphorylation of AMPA GluA1 subunits and their synaptic recruitment (Appleby et al., 2011; Park et al., 2021), a mechanism dependent on CamKII and intracellular kinases like PKA and PKC (Lee et al., 2003). Epileptiform activity could limit hippocampal LTP by inducing an activity-dependent enhancement in GluA1 phosphorylation status, thus generating a ceiling effect for LTP induction. In this work, the phosphorylation of AMPA GluA1 subunits at Ser831, a prominent target of CaMKII and PKC, was enhanced after both ictal-like and interictal like EA, an effect slightly more pronounced following interictal-like EA (**Figure 6B**). This suggests enhanced GluA1 phosphorylation at Ser831 contributes to the LTP-like effects of EA, likely by increasing channel conductance and promoting the recruitment of AMPA receptors to the synapse (Derkach et al., 1999, 2007). This may in turn impair LTP expression following EA, by limiting additional TBS-induced phosphorylation at Ser831. Thus, although the overall number of GluA1 subunits is decreased, the remaining GluA1 containing AMPA receptors are more likely found at synapses. Our observations early following EA contrast with the previously observed decrease in GluA1 Ser831 phosphorylation observed 3 h after pilocarpine induced seizures (Russo et al., 2013).

Phosphorylation of GluA1 at Ser845, a main target of PKA, was contrariwise decreased following both types of EA, and this decrease was more pronounced following ictal-like activity (**Figure 6C**). This change opposes the one observed after common TBS protocols *in vitro* (Park et al., 2021) but is consistent with our findings of decreased GluA1 containing receptors at synapses, an effect that may also reflect and endogenous neuroprotective measure against hyperexcitability induced by EA, as phosphorylation of GluA1 subunits at Ser845 drives AMPA receptor synaptic insertion, which could contribute to maladaptive homeostatic plasticity following seizures. This is fundamentally different from what is observed in the chronic period in the Li^{2+}-pilocarpine model of epilepsy, where both GluA1 P831 and P845 phosphorylation levels are increased (Serpa et al., 2022).

This work also found a decrease in synaptic Kv4.2 channels following interictal-like EA but not following ictal-like EA (**Figure 6F**). Expression of Kv4.2 channels is more prominent in dendritic spines vs. dendritic shafts, being largely responsible for the Ca^{2+}-activated delayed rectifying A-current (I_A) in CA1 pyramidal neuron distal dendrites, where it acts to control signal propagation and compartmentalization (Kim et al., 2007; Beck and Yaari, 2008; Kim and Hoffman, 2008). LTP induction with strong TBS stimuli reduces Kv4.2 dendritic membrane levels, leading to a shift in the voltage-dependence of I_A, and Kv4.2 channel activity contributes to LTP expression (Frick et al., 2004; Kim and Hoffman, 2008). Kv4.2 channels are responsible for the precision of the time window of pre and postsynaptic activity allowed for LTP induction (Zhao et al., 2011) and I_A activation also influences synaptic NMDA receptor composition at CA1 pyramidal neurons (Jung et al., 2008) and is synaptic morphology and seizure susceptibility (Tiwari et al., 2020). Altogether, our findings suggest that LTP will be easier to induce following interictal-like EA, resulting from an enlarged time window provided by Kv4.2 withdrawal from synapses. This may explain the lower impact and faster recovery of LTP expression following interictal-like vs ictal-like activity in our study, as this effect opposes the overall observed putative neuroprotective molecular remodeling at synapses (e.g., in AMPA receptor levels and phosphorylation). Being observed only following interictal-like (and not ictal-like EA), this effect is either not contributing to the putative protective effects of interictal-like EA (Avoli, 2001; Avoli et al., 2006) in epileptogenesis or reflects the ability of interictal-like activity to promote a faster synaptic recovery.

Synaptic α-tubulin levels were also altered in hippocampal slices following ictal-like and interictal-like EA (**Figure 7F**). As such, we could not use this protein as loading control for western blot analysis. Until recently the role of the microtubule cytoskeleton at synapses was not fully acknowledged but recent evidence has shed light on its importance in synaptic function, neurotransmitter release and synaptic plasticity (Waites et al., 2021). Decreased α-tubulin levels found in this work following EA likely indicate structural changes in synaptic morphology, as previously reported after seizures (Leite et al., 2005), and suggest that α-tubulin may undergo incorporation into microtubules following EA. Interestingly, the control of synaptic Ca^{2+} overload by microtubule dynamics has recently been reported (Vajente et al., 2019). Whether this mechanism may play a role endogenous neuroprotection against hyperexcitable states it remains to be established.

Chemical synapses are specialized structures composed of microdomains such as the presynaptic active zone and the postsynaptic density. Synaptic membranes, in turn, comprise nanodomains such as lipid rafts, liquid-ordered or gel-like membrane nanodomains segregated from the bulk membrane and

enriched in cholesterol, sphingolipids and GPI-anchored proteins, deemed essential for dynamic synaptic signaling in processes like neurotransmitter release and neurotransmitter receptor membrane cycling (Allen et al., 2007; Borroni et al., 2016). The membrane proteins caveolin-1 and flotillin-1 characterize the two main types of lipid rafts found at synapses, caveolae and planar lipid rafts (Allen et al., 2007; Borroni et al., 2016), and play an active role in promoting the phase separation that sustains these lipid nanodomains (Allen et al., 2007; Frick et al., 2007), yet, lipid domain stability is also regulated by its lipid composition and lipid leaflet distribution (Sodero et al., 2011). In this work we observed an extremely marked decrease in the synaptic levels of caveolin-1 and flotillin-1 (**Figures 7A, B**), suggesting that EA is a strong disruptor of normal lipid raft stability and of trafficking mechanisms regulated by these proteins. Previous studies showed that enhanced excitatory neurotransmission induces a massive cholesterol loss, and this was implicated in endogenous neuroprotection against oxidative stress (Iannilli et al., 2011; Sodero et al., 2011). Furthermore, the interaction of postsynaptic anchoring proteins like PSD-95 and gephyrin and neurotransmitter receptors, like AMPA receptor, with lipid raft domains is regulated by synaptic activity through post-translational modifications like palmitoylation or GPI anchoring (Papadopoulos et al., 2015; Tulodziecka et al., 2016; Itoh et al., 2018). This may in turn disrupt the normal synaptic signaling through AMPA, NMDA and $GABA_A$ receptors and impact synaptic plasticity mechanisms. Caveolin-1 was shown to enhance AMPA receptor binding capacity through direct inhibition of PLA2 activity (Gaudreault et al., 2004), thus suggesting that reduced caveolin levels may impair glutamatergic transmission and LTP expression. Caveolin-1 was also deemed essential in post-injury remodeling of the neuronal membrane following different insults (Gaudreault et al., 2005), such as brain injury by cerebral ischemia (Jasmin et al., 2007). Flotillin-1 in turn was implicated in glutamatergic synapse maturation, dendritic pruning and promotion of glutamate release. Flotillin is also involved in clathrin-independent endocytosis, by inducing membrane curvature and formation of plasma-membrane invaginations morphologically similar to caveolae (Frick et al., 2007) a process linked to neurotransmitter transporter internalization (Cremona et al., 2011). As such, decreased levels of flotillin-1 following seizures may contribute to decreased synaptic stability, impaired glutamatergic transmission and the impaired synaptic plasticity observed in this work. Altogether, this suggests that caveolins and flotillins are promising therapeutic targets to prevent epileptogenesis. The exact mechanism to be targeted requires still further investigation.

One possible explanation for the massive loss of some synaptic lipid raft markers could be the occurrence of massive synaptic protein internalization, degradation and autophagy in response to synaptic activity during hyperexcitable states (Li et al., 2012; Soykan et al., 2021). This would also imply a reduction in nerve terminal synaptic vesicles and its characteristic markers. Our observations that the synaptic vesicle marker synaptophysin is not significantly altered following both ictal-like and interictal-like EA (**Figure 7C**), suggests that these mechanisms are not likely contributing to reduce levels of synaptic proteins.

Distinct from classic lipid raft markers, the synaptic levels of postsynaptic scaffolding protein PSD-95, present at glutamatergic synapses, were moderately enhanced while the levels of gephyrin, present at GABAergic synapses, were massively enhanced following ictal-like and interictal-like EA (**Figures 7D, E**). PSD-95 is a lipid raft nucleating protein and plasma membrane cholesterol depleting was shown to reduce PSD-95 targeting to neuronal dendrites (Hering et al., 2003; Tulodziecka et al., 2016). Our results are in conflict with previous observations reporting that enhanced excitatory synaptic transmission causes cholesterol depleting (Sodero et al., 2011), expected to lower PSD-95 levels, and are also not in line with evidence in this work that synaptic lipid rafts are destabilized by EA and with reports that synaptic AMPA receptor levels, stabilized at synapses by palmitoylated PSD-95 (Han et al., 2015; Matt et al., 2019), are reduced following EA. However, this may reflect a specific response of the postsynaptic active zone to EA, since maintaining postsynaptic lipid rafts may be crucial to prevent epileptogenesis and abnormal spine growth by keeping together the molecular machinery allowing for AMPA receptor depalmitoylation and internalization (Han et al., 2015; Itoh et al., 2018).

GABAergic transmission and interneuron networks are key players in seizure initiation and in epileptogenesis (Magloire et al., 2019; Avoli et al., 2022). $GABA_A$ receptor postsynaptic recruitment to the inhibitory GABAergic synapses requires the scaffold protein gephyrin, that establishes a dynamic lattice-like structure with nanodomains of different size and density (Pizzarelli et al., 2020), and the action of the guanine nucleotide exchange factor collybistin through a PI3P dependent-process (Papadopoulos et al., 2017). Collybistin mutants with reduced lipid binding affinity disrupt GABAergic synapses by preventing gephyrin synaptic clustering and $GABA_A$ receptor targeting and this was in turn reported to trigger epilepsy (Papadopoulos et al., 2015). Gephyrin palmitoylation drives its membrane insertion and macromolecular clustering thus facilitating GABAergic transmission (Dejanovic et al., 2014; Matt et al., 2019). As such, the enhanced synaptic levels of gephyrin found in this work following EA may reflect its synaptic recruitment to reinforce GABAergic transmission, through $GABA_A$ recruitment, as an endogenous neuroprotective effort against hyperexcitability during ictal-like and interictal-like EA (Barberis, 2020). A similar response of GABAergic synapses was observed following anoxia (Lushnikova et al., 2011). This contrasts with the decreased levels of PSD-95 and gephyrin found in animal models and human MTLE (Sun et al., 2009; Fang et al., 2011; Bento-Oliveira, 2018), reinforcing the idea that acute and chronic synaptic responses to seizures are distinct.

Conclusion

Long term potentiation (LTP) expression is impaired following EA, and this impairment is stronger following ictal-like than after interictal-like activity. Altered LTP expression is accompanied by altered PPF, evidencing opposing presynaptic modifications of glutamate release, following ictal-like and interictal-like EA. In addition, we observed marked modifications in several synaptic proteins involved in synaptic plasticity mechanisms such as AMPA receptor subunits and its phosphorylation, and Kv4.2 channels. Furthermore, we detected altered synaptic membrane structure and domain regulating proteins like caveolin-1, flotillin-1, PSD-95 and gephyrin. Altogether, these results suggest that early changes in synaptic plasticity are a promising target for antiepileptogenic therapies and strategies focusing on modulation

of synaptic lipid raft domain dynamics may prove relevant to prevent epileptogenesis.

Data availability statement

The raw data supporting the conclusions of this article will be made available by the authors, without undue reservation.

Ethics statement

This animal study was reviewed and approved by the Ethics Committee of the Faculty of Medicine, University of Lisbon (Comissão de Ética para a Saúde do CHLN/FMUL). Approval was given in writing based on a detailed procedure report by the authors.

Author contributions

JC-R, NR, and AS-C: formal analysis and methodology. SV: methodology. DC-R: formal analysis, methodology, resources, supervision, funding acquisition, project administration, writing—original draft, review, and editing. All authors contributed to the article and approved the submitted version.

Funding

This work was supported by the national and international funding managed by the Fundação para a Ciência e a Tecnologia (FCT, IP), Portugal. Grants: FCT UIDB/04046/2020 and UIDP/04046/2020 to BioISI, PTDC/SAU-NEU/103639/2008; and FCT/POCTI (PTDC/SAU-PUB/28311/2017) EPIRaft grant to DC-R. Fellowships: SFRH/BPD/81358/2011 to DC-R and Researcher contract: Norma Transitória–DL57/2016/CP1479/CT0044 to DC-R.

Acknowledgments

The authors acknowledge the animal housing facilities of Instituto de Fisiología, Faculdade de Medicina de Lisboa, and Laia Amat-Garcia and Cidália Gaspar for technical contribution.

Conflict of interest

The authors declare that the research was conducted in the absence of any commercial or financial relationships that could be construed as a potential conflict of interest.

Publisher's note

All claims expressed in this article are solely those of the authors and do not necessarily represent those of their affiliated organizations, or those of the publisher, the editors and the reviewers. Any product that may be evaluated in this article, or claim that may be made by its manufacturer, is not guaranteed or endorsed by the publisher.

References

Abraham, W. C., and Bear, M. F. (1996). Metaplasticity: the plasticity of synaptic plasticity. *Trends Neurosci.* 19, 126–130. doi: 10.1016/S0166-2236(96)80018-X

Aidil-Carvalho, M. F., Carmo, A. J. S., Ribeiro, J. A., and Cunha-Reis, D. (2017). Mismatch novelty exploration training enhances hippocampal synaptic plasticity: a tool for cognitive stimulation? *Neurobiol. Learn. Mem.* 145, 240–250. doi: 10.1016/j.nlm.2017.09.004

Albensi, B. C., Ata, G., Schmidt, E., Waterman, J. D., and Janigro, D. (2004). Activation of long-term synaptic plasticity causes suppression of epileptiform activity in rat hippocampal slices. *Brain Res.* 998, 56–64. doi: 10.1016/j.brainres.2003.11.010

Albensi, B. C., Oliver, D. R., Toupin, J., and Odero, G. (2007). Electrical stimulation protocols for hippocampal synaptic plasticity and neuronal hyper-excitability: are they effective or relevant? *Exp. Neurol.* 204, 1–13. doi: 10.1016/j.expneurol.2006.12.009

Allen, J. A., Halverson-Tamboli, R. A., and Rasenick, M. M. (2007). Lipid raft microdomains and neurotransmitter signalling. *Nat. Rev. Neurosci.* 8, 128–140. doi: 10.1038/nrn2059

Anderson, W. W., and Collingridge, G. L. (2001). The LTP Program: a data acquisition program for on-line analysis of long-term potentiation and other synaptic events. *J. Neurosci. Methods* 108, 71–83. doi: 10.1016/s0165-0270(01)00374-0

Anderson, W. W., and Collingridge, G. L. (2007). Capabilities of the WinLTP data acquisition program extending beyond basic LTP experimental functions. *J. Neurosci. Methods* 162, 346–356. doi: 10.1016/j.jneumeth.2006.12.018

Antonio, L. L., Anderson, M. L., Angamo, E. A., Gabriel, S., Klaft, Z.-J., Liotta, A., et al. (2016). In vitro seizure like events and changes in ionic concentration. *J. Neurosci. Methods* 260, 33–44. doi: 10.1016/j.jneumeth.2015.08.014

Appleby, V. J., Corrêa, S. A. L., Duckworth, J. K., Nash, J. E., Noël, J., Fitzjohn, S. M., et al. (2011). LTP in hippocampal neurons is associated with a CaMKII-mediated increase in GluA1 surface expression. *J. Neurochem.* 116, 530–543. doi: 10.1111/j.1471-4159.2010.07133.x

Arias-Cavieres, A., Fonteh, A., Castro-Rivera, C. I., and Garcia, A. J. (2021). Intermittent Hypoxia causes targeted disruption to NMDA receptor dependent synaptic plasticity in area CA1 of the hippocampus. *Exp. Neurol.* 344:113808. doi: 10.1016/j.expneurol.2021.113808

Artinian, J., and Lacaille, J. C. (2018). Disinhibition in learning and memory circuits: new vistas for somatostatin interneurons and long-term synaptic plasticity. *Brain Res. Bull.* 141, 20–26. doi: 10.1016/j.brainresbull.2017.11.012

Avanzini, G., Forcelli, P. A., and Gale, K. (2014). "Are there really "Epileptogenic" mechanisms or only corruptions of "Normal" plasticity?," in *Issues in Clinical Epileptology: A View from the Bench. Advances in Experimental Medicine and Biology*, Vol. 813, eds H. Scharfman and P. Buckmaster (Dordrecht: Springer), 95–107. doi: 10.1007/978-94-017-8914-1_8

Avoli, M. (2001). Do interictal discharges promote or control seizures? Experimental evidence from an in vitro model of epileptiform discharge. *Epilepsia* 42, 2–4. doi: 10.1046/j.1528-1157.2001.042suppl.3002.x

Avoli, M., Biagini, G., and de Curtis, M. (2006). Do interictal spikes sustain seizures and epileptogenesis? *Epilepsy Curr.* 6, 203–207. doi: 10.1111/j.1535-7511.2006.00146.x

Avoli, M., de Curtis, M., Lévesque, M., Librizzi, L., Uva, L., and Wang, S. (2022). GABAA signaling, focal epileptiform synchronization and epileptogenesis. *Front. Neural Circuits* 16:984802. doi: 10.3389/fncir.2022.984802

Bai, G., Wang, Y., and Zhang, M. (2021). Gephyrin-mediated formation of inhibitory postsynaptic density sheet via phase separation. *Cell Res.* 31, 312–325. doi: 10.1038/s41422-020-00433-1

Barberis, A. (2020). Postsynaptic plasticity of GABAergic synapses. *Neuropharmacology* 169:107643. doi: 10.1016/j.neuropharm.2019.05.020

Beck, H., and Yaari, Y. (2008). Plasticity of intrinsic neuronal properties in CNS disorders. *Nat. Rev. Neurosci.* 9, 357–369. doi: 10.1038/nrn2371

Ben-Ari, Y. (2001). Cell death and synaptic reorganizations produced by seizures. *Epilepsia* 42, 5–7. doi: 10.1046/j.1528-1157.2001.042Suppl.3005.x

Bento-Oliveira, A. (2018). *Changes in Synaptic Plasticity and Lipid Raft Composition in a Rat Model of Temporal Lobe Epilepsy*. Lisbon: Universidade de Lisboa.

Bliss, T., and Collingridge, G. (2019). Persistent memories of long-term potentiation and the N -methyl-d-aspartate receptor. *Brain Neurosci. Adv.* 3, 1–10. doi: 10.1177/2398212819848213

Bliss, T. V. P., Collingridge, G. L., Morris, R. G. M., and Reymann, K. G. (2018). Long-term potentiation in the hippocampus: discovery, mechanisms and function. *Neuroforum* 24, A103–A120. doi: 10.1515/nf-2017-A059

Borroni, M. V., Vallés, A. S., and Barrantes, F. J. (2016). The lipid habitats of neurotransmitter receptors in brain. *Biochim. Biophys. Acta Biomembr.* 1858, 2662–2670. doi: 10.1016/j.bbamem.2016.07.005

Carvalho-Rosa, J. D., and Cunha-Reis, D. (2019). Endogenous VIP VPAC1 receptor activation during ictal and interictal-like activity induced in vitro by biccuculine and 0-Mg2+ modulates subsequent LTP expression in the rat hippocampus. *Front. Cell. Neurosci.* 13:28. doi: 10.3389/conf.fncel.2019.01.00028

Caulino-Rocha, A., Rodrigues, N. C., Ribeiro, J. A., and Cunha-Reis, D. (2022). Endogenous VIP VPAC1 receptor activation modulates hippocampal theta burst induced LTP: transduction pathways and GABAergic mechanisms. *Biology* 11:627. doi: 10.3390/BIOLOGY11050627

Chater, T. E., and Goda, Y. (2022). The shaping of AMPA receptor surface distribution by neuronal activity. *Front. Synaptic Neurosci.* 14:833782. doi: 10.3389/fnsyn.2022.833782

Colgin, L. L., Kubota, D., Jia, Y., Rex, C. S., and Lynch, G. (2004). Long-term potentiation is impaired in rat hippocampal slices that produce spontaneous sharp waves. *J. Physiol.* 558, 953–961. doi: 10.1113/jphysiol.2004.068080

Cremona, M. L., Matthies, H. J. G., Pau, K., Bowton, E., Speed, N., Lute, B. J., et al. (2011). Flotillin-1 is essential for PKC-triggered endocytosis and membrane microdomain localization of DAT. *Nat. Neurosci.* 14, 469–477. doi: 10.1038/nn.2781

Cunha-Reis, D., and Caulino-Rocha, A. (2020). VIP modulation of hippocampal synaptic plasticity: a role for VIP Receptors as therapeutic targets in cognitive decline and mesial temporal lobe epilepsy. *Front. Cell. Neurosci.* 14:153. doi: 10.3389/fncel.2020.00153

Cunha-Reis, D., Caulino-Rocha, A., and Correia-de-Sá, P. (2021). VIPergic neuroprotection in epileptogenesis: challenges and opportunities. *Pharmacol. Res.* 164:105356. doi: 10.1016/j.phrs.2020.105356

Cunha-Reis, D., Ribeiro, J. A., de Almeida, R. F. M., and Sebastião, A. M. (2017). VPAC1 and VPAC2 receptor activation on GABA release from hippocampal nerve terminals involve several different signalling pathways. *Br. J. Pharmacol.* 174, 4725–4737. doi: 10.1111/bph.14051

Davies, C. H., Davies, S. N., and Collingridge, G. L. (1990). Paired-pulse depression of monosynaptic GABA-mediated inhibitory postsynaptic responses in rat hippocampus. *J. Physiol.* 424, 513–531.

Debanne, D., Guérineau, N. C., Gähwiler, B. H., and Thompson, S. M. (1996). Paired-pulse facilitation and depression at unitary synapses in rat hippocampus: quantal fluctuation affects subsequent release. *J. Physiol.* 491, 163–176. doi: 10.1113/JPHYSIOL.1996.SP021204

Debanne, D., Thompson, S. M., and Gähwiler, B. H. (2006). A brief period of epileptiform activity strengthens excitatory synapses in the rat hippocampus in vitro. *Epilepsia* 47, 247–256. doi: 10.1111/j.1528-1167.2006.00416.x

Dejanovic, B., Semtner, M., Ebert, S., Lamkemeyer, T., Neuser, F., Lüscher, B., et al. (2014). Palmitoylation of gephyrin controls receptor clustering and plasticity of GABAergic synapses. *PLoS Biol.* 12:e1001908. doi: 10.1371/journal.pbio.1001908

Derkach, V., Barria, A., and Soderling, T. R. (1999). Ca2+/calmodulin-kinase II enhances channel conductance of alpha-amino-3-hydroxy-5-methyl-4-isoxazolepropionate type glutamate receptors. *Proc. Natl. Acad. Sci. U. S. A.* 96, 3269–3274. doi: 10.1073/pnas.96.6.3269

Derkach, V. A., Oh, M. C., Guire, E. S., and Soderling, T. R. (2007). Regulatory mechanisms of AMPA receptors in synaptic plasticity. *Nat. Rev. Neurosci.* 8, 101–113. doi: 10.1038/nrn2055

Devinsky, O., Vezzani, A., O'Brien, T. J., Jette, N., Scheffer, I. E., De Curtis, M., et al. (2018). Epilepsy. *Nat. Rev. Dis. Prim.* 4:18024. doi: 10.1038/nrdp.2018.24

Dulla, C. G., Janigro, D., Jiruska, P., Raimondo, J. V., Ikeda, A., Lin, C. C. K., et al. (2018). How do we use in vitro models to understand epileptiform and ictal activity? A report of the TASK1-WG4 group of the ILAE/AES Joint Translational Task Force. *Epilepsia Open* 3, 460–473. doi: 10.1002/epi4.12277

Ergina, J. L., Amakhin, D. V., Postnikova, T. Y., Soboleva, E. B., and Zaitsev, A. V. (2021). Short-term epileptiform activity potentiates excitatory synapses but does not affect intrinsic membrane properties of pyramidal neurons in the rat hippocampus in vitro. *Biomedicines* 9:1374. doi: 10.3390/biomedicines9101374

Fang, M., Shen, L., Yin, H., Pan, Y. M., Wang, L., Chen, D., et al. (2011). Downregulation of gephyrin in temporal lobe epilepsy neurons in humans and a rat model. *Synapse* 65, 1006–1014. doi: 10.1002/syn.20928

Félix-Oliveira, A., Dias, R. B., Colino-Oliveira, M., Rombo, D. M., and Sebastião, A. M. (2014). Homeostatic plasticity induced by brief activity deprivation enhances long-term potentiation in the mature rat hippocampus. *J. Neurophysiol.* 112, 3012–3022. doi: 10.1152/jn.00058.2014

Flores, A., Ramirez-Franco, J., Desplantes, R., Debreux, K., Ferracci, G., Wernert, F., et al. (2019). Gangliosides interact with synaptotagmin to form the high-affinity receptor complex for botulinum neurotoxin B. *Proc. Natl. Acad. Sci. U. S. A.* 116, 18098–18108. doi: 10.1073/pnas.1908051116

Frick, A., Magee, J., and Johnston, D. (2004). LTP is accompanied by an enhanced local excitability of pyramidal neuron dendrites. *Nat. Neurosci.* 7, 126–135. doi: 10.1038/nn1178

Frick, M., Bright, N. A., Riento, K., Bray, A., Merrified, C., and Nichols, B. J. (2007). Coassembly of flotillins induces formation of membrane microdomains, membrane curvature, and vesicle budding. *Curr. Biol.* 17, 1151–1156. doi: 10.1016/j.cub.2007.05.078

Gaidin, S. G., Zinchenko, V. P., Teplov, I. Y., Tuleukhanov, S. T., and Kosenkov, A. M. (2019). Epileptiform activity promotes decreasing of Ca2+ conductivity of NMDARs, AMPARs, KARs, and voltage-gated calcium channels in Mg2+-free model. *Epilepsy Res.* 158:106224. doi: 10.1016/j.eplepsyres.2019.106224

Gambardella, A., Labate, A., Cifelli, P., Ruffolo, G., Mumoli, L., Aronica, E., et al. (2016). Pharmacological modulation in mesial temporal lobe epilepsy: current status and future perspectives. *Pharmacol. Res.* 113, 421–425. doi: 10.1016/j.phrs.2016.09.019

Gaudreault, S. B., Blain, J.-F. F., Gratton, J.-P. P., and Poirier, J. (2005). A role for caveolin-1 in post-injury reactive neuronal plasticity. *J. Neurochem.* 92, 831–839. doi: 10.1111/j.1471-4159.2004.02917.x

Gaudreault, S. B., Chabot, C., Gratton, J.-P. P., and Poirier, J. (2004). The caveolin scaffolding domain modifies 2-amino-3-hydroxy-5-methyl-4-isoxazole propionate receptor binding properties by inhibiting phospholipase A2 activity. *J. Biol. Chem.* 279, 356–362. doi: 10.1074/jbc.M304777200

Gloveli, T., Albrecht, D., and Heinemann, U. (1995). Properties of low Mg2+ induced epileptiform activity in rat hippocampal and entorhinal cortex slices during adolescence. *Dev. Brain Res.* 87, 145–152. doi: 10.1016/0165-3806(95)00069-P

Good, M., Day, M., and Muir, J. L. (1999). Cyclical changes in endogenous levels of oestrogen modulate the induction of LTD and LTP in the hippocampal CA1 region. *Eur. J. Neurosci.* 11, 4476–4480. doi: 10.1046/J.1460-9568.1999.00920.X

Goodkin, H. P., Joshi, S., Mtchedlishvili, Z., Brar, J., and Kapur, J. (2008). Subunit-specific trafficking of GABA(A) receptors during status epilepticus. *J. Neurosci.* 28, 2527–2538. doi: 10.1523/JNEUROSCI.3426-07.2008

Han, J., Wu, P., Wang, F., and Chen, J. (2015). S-palmitoylation regulates AMPA receptors trafficking and function: a novel insight into synaptic regulation and therapeutics. *Acta Pharm. Sin. B* 5, 1–7. doi: 10.1016/j.apsb.2014.12.002

Hering, H., Lin, C. C., and Sheng, M. (2003). Lipid rafts in the maintenance of synapses, dendritic spines, and surface AMPA receptor stability. *J. Neurosci.* 23, 3262–3271. doi: 10.1523/jneurosci.23-08-03262.2003

Iannilli, F., Sodero, A. O., Ledesma, M. D., and Dotti, C. G. (2011). Oxidative stress activates the pro-survival TrkA pathway through membrane cholesterol loss. *Neurobiol. Aging* 32, 1033–1042. doi: 10.1016/j.neurobiolaging.2009.07.006

Itoh, M., Yamashita, M., Kaneko, M., Okuno, H., Abe, M., Yamazaki, M., et al. (2018). Deficiency of AMPAR–palmitoylation aggravates seizure susceptibility. *J. Neurosci.* 38, 10220–10235. doi: 10.1523/JNEUROSCI.1590-18.2018

Jasmin, J. F., Malhotra, S., Singh Dhallu, M., Mercier, I., Rosenbaum, D. M., and Lisanti, M. P. (2007). Caveolin-1 deficiency increases cerebral ischemic injury. *Circ. Res.* 100, 721–729. doi: 10.1161/01.RES.0000260180.42709.29

Jung, S.-C. C., Kim, J., and Hoffman, D. A. (2008). Rapid, bidirectional remodeling of synaptic NMDA receptor subunit composition by A-type K+ channel activity in hippocampal CA1 pyramidal neurons. *Neuron* 60, 657–671. doi: 10.1016/j.neuron.2008.08.029

Kim, J., and Hoffman, D. A. (2008). Potassium channels: newly found players in synaptic plasticity. *Neuroscience* 14, 276–286. doi: 10.1177/1073858408315041

Kim, J., Jung, S.-C. C., Clemens, A. M., Petralia, R. S., and Hoffman, D. A. (2007). Regulation of dendritic excitability by activity-dependent trafficking of the A-Type K+ channel subunit Kv4.2 in hippocampal neurons. *Neuron* 54, 933–947. doi: 10.1016/j.neuron.2007.05.026

Kovac, S., Kostova, A. T. D., Herrmann, A. M., Melzer, N., Meuth, S. G., and Gorji, A. (2017). Metabolic and homeostatic changes in seizures and acquired epilepsy—mitochondria, calcium dynamics and reactive oxygen species. *Int. J. Mol. Sci.* 18:1935. doi: 10.3390/ijms18091935

Kryukov, K. A., Kim, K. K., Magazanik, L. G., and Zaitsev, A. V. (2016). Status epilepticus alters hippocampal long-term synaptic potentiation in a rat lithium-pilocarpine model. *Neuroreport* 27, 1191–1195. doi: 10.1097/WNR.0000000000000656

Kuang, Y., Yang, T., Gu, J., Kong, B., and Cheng, L. (2014). Comparison of therapeutic effects between selective amygdalohippocampectomy and anterior

temporal lobectomy for the treatment of temporal lobe epilepsy: a meta-analysis. *Br. J. Neurosurg.* 28, 374–377. doi: 10.3109/02688697.2013.841854

Lambert, N. A., and Wilson, W. A. (1994). Temporally distinct mechanisms of use-dependent depression at inhibitory synapses in the rat hippocampus in vitro. *J. Neurophysiol.* 121, 121–130. doi: 10.1152/JN.1994.72.1.121

Larson, J., and Munkácsy, E. (2015). Theta-burst LTP. *Brain Res.* 1621, 38–50. doi: 10.1016/j.brainres.2014.10.034

Lee, H. K., Takamiya, K., Han, J. S., Man, H., Kim, C. H., Rumbaugh, G., et al. (2003). Phosphorylation of the AMPA receptor GluR1 subunit is required for synaptic plasticity and retention of spatial memory. *Cell* 112, 631–643. doi: 10.1016/S0092-8674(03)00122-3

Leite, J. P., Neder, L., Arisi, G. M., Carlotti, C. G., Assirati, J. A., and Moreira, J. E. (2005). Plasticity, synaptic strength, and epilepsy: what can we learn from ultrastructural data? *Epilepsia* 46, 134–141. doi: 10.1111/j.1528-1167.2005.01021.x

Lévesque, M., Wang, S., Etter, G., Williams, S., and Avoli, M. (2022). Bilateral optogenetic activation of inhibitory cells favors ictogenesis. *Neurobiol. Dis.* 171:105794. doi: 10.1016/j.nbd.2022.105794

Li, W., Liu, L., Liu, Y. Y., Luo, J., Lin, J. Y., Li, X., et al. (2012). Effects of electroconvulsive stimulation on long-term potentiation and synaptophysin in the hippocampus of rats with depressive behavior. *J. ECT* 28, 111–117. doi: 10.1097/YCT.0b013e31824a47ca

Liu, A., Ji, H., Ren, Q., Meng, Y., Zhang, H., Collingride, G., et al. (2020). The requirement of the C-terminal domain of GluA1 in different forms of long-term potentiation in the hippocampus is age-dependent. *Front. Synaptic Neurosci.* 12:588785. doi: 10.3389/fnsyn.2020.588785

Liu, J. Y. W., Thom, M., Catarino, C. B., Martinian, L., Figarella-Branger, D., Bartolomei, F., et al. (2012). Neuropathology of the blood-brain barrier and pharmaco-resistance in human epilepsy. *Brain* 135, 3115–3133. doi: 10.1093/brain/aws147

Lushnikova, I., Skibo, G., Muller, D., and Nikonenko, I. (2011). Excitatory synaptic activity is associated with a rapid structural plasticity of inhibitory synapses on hippocampal CA1 pyramidal cells. *Neuropharmacology* 60, 757–764. doi: 10.1016/j.neuropharm.2010.12.014

Magloire, V., Mercier, M. S., Kullmann, D. M., and Pavlov, I. (2019). GABAergic interneurons in seizures: investigating causality with optogenetics. *Neuroscientist* 25, 344–358. doi: 10.1177/1073858418805002

Matt, L., Kim, K., Chowdhury, D., and Hell, J. W. (2019). Role of palmitoylation of postsynaptic proteins in promoting synaptic plasticity. *Front. Mol. Neurosci.* 12:8. doi: 10.3389/fnmol.2019.00008

Megías, M., Emri, Z., Freund, T. F., and Gulyás, A. I. (2001). Total number and distribution of inhibitory and excitatory synapses on hippocampal CA1 pyramidal cells. *Neuroscience* 102, 527–540. doi: 10.1016/S0306-4522(00)00496-6

Moshé, S. L., Perucca, E., Ryvlin, P., and Tomson, T. (2015). Epilepsy: new advances. *Lancet* 385, 884–898. doi: 10.1016/S0140-6736(14)60456-6

Nathan, T., and Lambert, J. D. C. (1991). Depression of the fast IPSP underlies paired-pulse facilitation in area CA1 of the rat hippocampus. *J. Neurophysiol.* 66, 1704–1715. doi: 10.1152/JN.1991.66.5.1704

Papadopoulos, T., Rhee, H. J., Subramanian, D., Paraskevopoulou, F., Mueller, R., Schultz, C., et al. (2017). Endosomal phosphatidylinositol 3-phosphate promotes gephyrin clustering and GABAergic neurotransmission at inhibitory postsynapses. *J. Biol. Chem.* 292, 1160–1177. doi: 10.1074/jbc.M116.771592

Papadopoulos, T., Schemm, R., Grubmüller, H., and Brose, N. (2015). Lipid binding defects and perturbed synaptogenic activity of a collybistin R290H mutant that causes epilepsy and intellectual disability. *J. Biol. Chem.* 290, 8256–8270. doi: 10.1074/jbc.M114.633024

Park, P., Georgiou, J., Sanderson, T. M., Ko, K. H., Kang, H., Kim, J., et al. (2021). PKA drives an increase in AMPA receptor unitary conductance during LTP in the hippocampus. *Nat. Commun.* 12:413. doi: 10.1038/s41467-020-20523-3

Pitkänen, A., Lukasiuk, K., Edward Dudek, F., and Staley, K. J. (2015). Epileptogenesis. *Cold Spring Harb. Perspect. Med.* 5:a022822. doi: 10.1101/cshperspect.a022822

Pizzarelli, R., Griguoli, M., Zacchi, P., Petrini, E. M., Barberis, A., Cattaneo, A., et al. (2020). Tuning GABAergic inhibition: gephyrin molecular organization and functions. *Neuroscience* 439, 125–136. doi: 10.1016/j.neuroscience.2019.07.036

Postnikova, T. Y., Amakhin, D. V., Trofimova, A. M., and Zaitsev, A. V. (2020). Calcium-permeable AMPA receptors are essential to the synaptic plasticity induced by epileptiform activity in rat hippocampal slices. *Biochem. Biophys. Res. Commun.* 529, 1145–1150. doi: 10.1016/j.bbrc.2020.06.121

Postnikova, T. Y., Zubareva, O. E., Kovalenko, A. A., Kim, K. K., Magazanik, L. G., and Zaitsev, A. V. (2017). Status epilepticus impairs synaptic plasticity in rat hippocampus and is followed by changes in expression of NMDA receptors. *Biochemistry* 82, 282–290. doi: 10.1134/S0006297917030063

Rodrigues, N. C., Silva-Cruz, A., Caulino-Rocha, A., Bento-Oliveira, A., Alexandre Ribeiro, J., and Cunha-Reis, D. (2021). Hippocampal CA1 theta burst-induced LTP from weaning to adulthood: cellular and molecular mechanisms in young male rats revisited. *Eur. J. Neurosci.* 54, 5272–5292. doi: 10.1111/ejn.15390

Russo, I., Bonini, D., Via, L. L., Barlati, S., and Barbon, A. (2013). AMPA receptor properties are modulated in the early stages following pilocarpine-induced status epilepticus. *NeuroMol. Med.* 15, 324–338. doi: 10.1007/s12017-013-8221-6

Sebastian, V., Estil, J. B., Chen, D., Schrott, L. M., and Serrano, P. A. (2013). Acute physiological stress promotes clustering of synaptic markers and alters spine morphology in the hippocampus. *PLoS One* 8:e79077. doi: 10.1371/journal.pone.0079077

Sebastião, A. M., Colino-Oliveira, M., Assaife-Lopes, N., Dias, R. B., and Ribeiro, J. A. (2013). Lipid rafts, synaptic transmission and plasticity: impact in age-related neurodegenerative diseases. *Neuropharmacology* 64, 97–107. doi: 10.1016/j.neuropharm.2012.06.053

Serpa, A., Bento, M., Caulino-Rocha, A., Pawlak, S., and Cunha-Reis, D. (2022). Opposing reduced VPAC1 and enhanced VPAC2 VIP receptors in the hippocampus of the Li2+-pilocarpine rat model of temporal lobe epilepsy. *Neurochem. Int.* 158, 105383. doi: 10.1016/j.neuint.2022.105383

Sloviter, R. S. (2017). Epileptogenesis meets Occam's Razor. *Curr. Opin. Pharmacol.* 35, 105–110. doi: 10.1016/j.coph.2017.07.012

Sodero, A. O., Weissmann, C., Ledesma, M. D., and Dotti, C. G. (2011). Cellular stress from excitatory neurotransmission contributes to cholesterol loss in hippocampal neurons aging in vitro. *Neurobiol. Aging* 32, 1043–1053. doi: 10.1016/j.neurobiolaging.2010.06.001

Soykan, T., Haucke, V., and Kuijpers, M. (2021). Mechanism of synaptic protein turnover and its regulation by neuronal activity. *Curr. Opin. Neurobiol.* 69, 76–83. doi: 10.1016/j.conb.2021.02.006

Sun, Q.-J. J., Duan, R.-S. S., Wang, A.-H. H., Shang, W., Zhang, T., Zhang, X.-Q. Q., et al. (2009). Alterations of NR2B and PSD-95 expression in hippocampus of kainic acid-exposed rats with behavioural deficits. *Behav. Brain Res.* 201, 292–299. doi: 10.1016/j.bbr.2009.02.027

Tang, X. H., Diao, Y. G., Ren, Z. Y., Zang, Y. Y., Zhang, G. F., Wang, X. M., et al. (2023). A role of GABAA receptor α1 subunit in the hippocampus for rapid-acting antidepressant-like effects of ketamine. *Neuropharmacology* 225:109383. doi: 10.1016/j.neuropharm.2022.109383

Thom, M. (2014). Review: Hippocampal sclerosis in epilepsy: a neuropathology review. *Neuropathol. Appl. Neurobiol.* 40, 520–543. doi: 10.1111/nan.12150

Tiwari, D., Schaefer, T. L., Schroeder-Carter, L. M., Krzeski, J. C., Bunk, A. T., Parkins, E. V., et al. (2020). The potassium channel Kv4.2 regulates dendritic spine morphology, electroencephalographic characteristics and seizure susceptibility in mice. *Exp. Neurol.* 334:113437. doi: 10.1016/j.expneurol.2020.113437

Tulodziecka, K., Diaz-Rohrer, B. B., Farley, M. M., Chan, R. B., Di Paolo, G., Levental, K. R., et al. (2016). Remodeling of the postsynaptic plasma membrane during neural development. *Mol. Biol. Cell* 27, 3480–3489. doi: 10.1091/mbc.E16-06-0420

Vajente, N., Norante, R., Redolfi, N., Daga, A., Pizzo, P., and Pendin, D. (2019). Microtubules Stabilization by mutant spastin affects ER morphology and Ca2+ handling. *Front. Physiol.* 10:1544. doi: 10.3389/fphys.2019.01544

Vertes, R. P. (2005). Hippocampal theta rhythm: a tag for short-term memory. *Hippocampus* 15, 923–935. doi: 10.1002/hipo.20118

Vezzani, A., Balosso, S., and Ravizza, T. (2019). Neuroinflammatory pathways as treatment targets and biomarkers in epilepsy. *Nat. Rev. Neurol.* 15, 459–472. doi: 10.1038/s41582-019-0217-x

Waites, C., Qu, X., and Bartolini, F. (2021). The synaptic life of microtubules. *Curr. Opin. Neurobiol.* 69, 113–123. doi: 10.1016/j.conb.2021.03.004

Warren, S. G., Humphreys, A. G., Juraska, J. M., and Greenough, W. T. (1995). LTP varies across the estrous cycle: enhanced synaptic plasticity in proestrus rats. *Brain Res.* 703, 26–30. doi: 10.1016/0006-8993(95)01059-9

Wilson, K. A., MacDermott-Opeskin, H. I., Riley, E., Lin, Y., and O'Mara, M. L. (2020). Understanding the link between lipid diversity and the biophysical properties of the neuronal plasma membrane. *Biochemistry* 59, 3010–3018. doi: 10.1021/acs.biochem.0c00524

Wiltgen, B. J., Royle, G. A., Gray, E. E., Abdipranoto, A., Thangthaeng, N., Jacobs, N., et al. (2010). A role for calcium-permeable AMPA receptors in synaptic plasticity and learning. *PLoS One* 5:e12818. doi: 10.1371/journal.pone.0012818

Wu, L. G., and Saggau, P. (1994). Presynaptic calcium is increased during normal synaptic transmission and paired-pulse facilitation, but not in long-term potentiation in area CA1 of hippocampus. *J. Neurosci.* 14, 645–654. doi: 10.1523/JNEUROSCI.14-02-00645.1994

Zhang, L., Kirschstein, T., Sommersberg, B., Merkens, M., Manahan-Vaughan, D., Elgersma, Y., et al. (2005). Hippocampal synaptic metaplasticity requires inhibitory autophosphorylation of Ca2+/calmodulin-dependent kinase II. *J. Neurosci.* 25, 7697–7707. doi: 10.1523/JNEUROSCI.2086-05.2005

Zhao, C., Wang, L., Netoff, T., and Yuan, L. L. (2011). Dendritic mechanisms controlling the threshold and timing requirement of synaptic plasticity. *Hippocampus* 21, 288–297. doi: 10.1002/hipo.20748

Zucker, R. S. (2003). Short-term synaptic plasticity. *Annu. Rev. Neurosci.* 12, 13–31. doi: 10.1146/ANNUREV.NE.12.030189.000305

Frontiers in
Cellular Neuroscience

Leading research in cellular mechanisms underlying brain function and development

Part of the world's most cited neuroscience journal series that advances our understanding of the cellular mechanisms underlying cell function in the nervous system across all species.

Discover the latest Research Topics

See more →

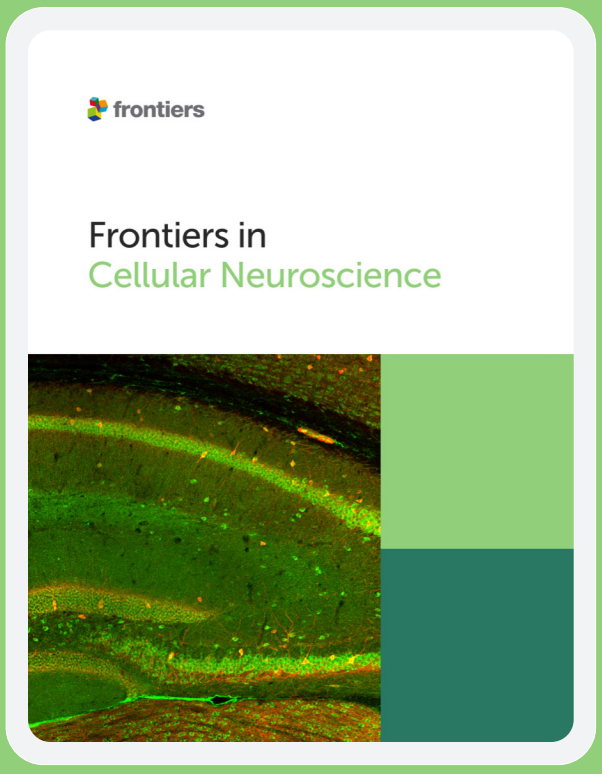

Frontiers

Avenue du Tribunal-Fédéral 34
1005 Lausanne, Switzerland
frontiersin.org

Contact us

+41 (0)21 510 17 00
frontiersin.org/about/contact